New Insights into Old Problems

The application of a multidisciplinary approach to the study of early Egyptian ceramic chronology, with a focus on luminescence dating

Amber Hood

Merton College

University of Oxford

A thesis submitted for the degree of

Doctor of Philosophy

April 2016

For Julie, Philip, and Edmund

Abstract

This thesis takes a multidisciplinary approach to the study of ancient Egyptian ceramics by applying scientific dating techniques alongside more traditional methods. It is the first study to apply OSL dating to an Egyptian ceramic assemblage, and it has done so by developing the minimum extraction technique (MET), which has made it possible to use OSL to sample, and thus analyse, ceramics housed in museums.

The MET is at present essential to the success of OSL dating of Egyptian ceramics, as the exportation ban on antiquities has prevented OSL analysis of field material.

For this thesis, using this new sampling technique, OSL has been applied to several assemblages from the Predynastic to the Early Dynastic period. Ceramics from Bêt Khallaf have been examined, with three phases being established: late Naqada III, First Intermediate Period, and the mediaeval Islamic period. Absolute dates have been determined for each phase and, where comparison is possible, have been found in good agreement with the historical chronology.

A set of vessels from Naqada, Ballas, and the Tomb of Djer at Abydos have been examined using OSL in conjunction with radiocarbon dating. Again, three phases of activity were discerned: late Naqada II, early Naqada III, and the first scientifically determined dates for a burning event in the Tomb of Djer (the New Kingdom).

The thesis also demonstrates how OSL can be used as a relative dating technique by analysing a collection of Wavy-Handled ceramics and wine jars from Turah, finding that the OSL results agree well with the established relative chronology.

Finally, this thesis has also examined the applicability of cladistic analysis to the study of Egyptian ceramics. Cladistics is a technique borrowed from the biological sciences which offers a complimentary way to examine the evolution of ceramic types and forms, in particular the development of beer and wine jars.

Acknowledgements

As a bright-eyed, first-year doctoral student, it is at first impossible to fully understand the enormity of the task ahead of you, or indeed, initially, to comprehend the vast support network that rapidly grows around you, lifting you up and getting you through to the very end. I have been immensely lucky to have had the best support network. From my supervisors and colleagues, to my friends and family, I am the first to admit that I could not have achieved this goal without each of you.

Essential to completing a thesis is having a thoughtful, generous-with-time, and supportive supervisor: one that is always there to answer your questions and coax you through the most difficult aspects of writing original research. I have been lucky in this respect three times over! To Jean-Luc Schwenninger, Christiana Köhler, and Christopher Bronk Ramsey, thank you a million times. I hope I have been one small part as good a student as you have been supervisors.

This project was made possible by the generous financial support provided by the G.A. Wainwright Fund, the Clarendon Fund, the Oxford Australia Scholarship Fund and Merton College. I am so grateful that these funds gave me the opportunity to pursue this research.

Equally, this project was only possible because of the generous help and assistance provided to me by the museum curators in charge of the ceramics sampled. Therefore, my deepest gratitude to Steven Snape, from the Garstang Museum, Jenn Houser-Wagner from the Penn Museum, Liam McNamara from the Ashmolean Museum, and to the staff of the Institute of Egyptology at the University of Vienna. Additionally, the samples from Petra, Jordan were incredibly useful, and many thanks to the BUPAP team for securing these for me, particularly Thomas Urban.

This project was truly a collaborative effort, and much work was put in by my colleagues. James Valentine, Mike Dee, and Marshall Woodworth: it has been a true pleasure working with each of you. I value the effort you have all put in to these projects and I look forward to continuing our collaborations, and friendship, in the future. Thanks also go to Phil Holdship and

Steve Wyatt from DESUO, who carried out the ICP-MS analyses presented here. Many thanks also to Löic Martin and Edmund Highcock for their invaluable assistance in using the DosıVox program. This thesis required me to delve into many areas of science I was not initially familiar with. For help with SEM analysis (as well as many long discussions on petrography and clay provenance), I must thank Chris Doherty for his constant patience and guidance.

Thank you to Miranda Bethell for doing such a wonderful job of proofreading this thesis, as always. I am blessed to have such a wonderful proofreader as part of my family.

I have also been blessed with a truly wonderful lab team. Many thanks to the Oxford luminescence group (Laine Clark-Balzan, Julie Durcan, Sallie Burrough, Abi Stone, Szilvie Bajkan, Catherine Buckland, Marine Frouin, Richard Bailey, Alex Rowell, and Dave Peat) whose friendship, support, guidance, advice, and encouragement has been invaluable. An extra big thank you, of course, must be given to Dave for doing so much of my sample prep so patiently.

My archaeology friends and my Helwan family also deserve a very warm mention, as it was beside them that I learned to love archaeology so much: thank you, Beverley Miles, Ben Franta, Tommy Urban, Mark Wheeler, Amanda Kiely, Aaron de Sousa, Natalie Barlow, and Jane Smythe.

Equally, my Merton family, and my adopted Pembroke family, have been central to my happiness and development throughout my time in Oxford. I will always cherish the love, support, and friendship of Stephanie Jones, Claire Higgins, Andrew Cichy, and Jon and Jenn Macdonald in particular.

To my wonderful family, both new and old, who have offered me unconditional support and encouragement from the outset, particularly my grandparents, and especially to Maeve Eason Hubbard, the closest to a sister that this only child can have!

I would never have made it to being a bright-eyed, first-year doctoral student without first having had the very best start to life. This was, of course, given to me by my parents, Philip and Julie, whom I love so very dearly. They have supported me unquestioningly through all my pursuits and dreams (from wanting to be an opera singer, an actor, a flight attendant, to, finally, the most fulfilling choice for me, an archaeologist), and this support is what has, ultimately, got me here. It is difficult to sum up just how essential they

have been to my happiness in life, and I will be forever grateful to them for all that they have done, but most especially, for always encouraging me to pursue and achieve my goals. This thesis belongs to them more than anyone else.

Finally, to Edmund. It is impossible to conceive how I would ever have made it through such a lengthy and often frustrating task without such a wonderful person by my side. Every day you have guided, supported, cared for and, most importantly of all, loved me. You said in your own acknowledgements that you hoped one day you could repay me in kind. It was never a debt, but you have repaid me more times over than you know. I love you with all my heart.

Post script: a loving thank you to Primrose, Wilfred, Inky, Snowy, and Buffy, for always lending their furry selves for cuddles when I needed them most!

Contents

List of Figures

List of Tables

Part I

Background

Chapter 1

Introduction and research objectives

1.1 Ceramics in Egyptian archaeology

Chronology is one of the most fundamental elements of archaeological enquiry. With a thorough understanding of chronology, archaeologists can piece together a history of events on local, regional, and interregional scales. Of all the archaeological material culture available for chronological study, pottery is arguably the most useful. Often considered the 'disposable waste' of the ancient world, pottery has two main benefits which make it particularly conducive to chronological enquiry. First, it is ubiquitous, and found at almost every archaeological site encountered. Secondly, pottery is a chronometer, and follows typological development—that is, the style and shape of a vessel is usually governed by the fashions in vogue at the time of production. This means that vessels with similar morphological and manufacturing characteristics are generally considered contemporary with one another. The study of typological development, typology, permits the recognition of diagnostic artefacts which are characteristic of a certain time period and allows the different forms and attributes of each type to be discerned (Renfrew and Bahn 2008:126–7).

Owing to these characteristics, ceramics are generally considered to be the 'backbone' of relative archaeological chronology. By understanding the development of ceramic styles, it is possible to understand the progression and development of other ma-

terial culture groups which are not as diagnostic as ceramic material, but are still found in association with various ceramic styles. Furthermore, by understanding the chronology of material culture it is possible to understand the development and progression of history itself—for example the emergence of societies, the development of states, the formation of trade networks, and the development of manufacturing process and skill-based production. In Egypt, ceramics are also a body of evidence that transcend social status, meaning that the age-old adage of archaeology being too often the study of the elite no longer applies: pottery represents the lives and death of individuals across social strata. When it comes to providing a greater understanding of the past, pottery is always more precious than gold.

1.2 Relative vs. absolute chronology of Egyptian ceramic material

The study of ceramic chronology has been invaluable in Egyptian archaeology. The first systematic and scientific study of a ceramic culture anywhere in the world was carried out by William Matthew Flinders Petrie in the late Victorian period on Egyptian ceramics. Petrie, generally considered the father of archaeology, attempted to classify and order the ceramics he encountered in his excavations at Predynastic Egyptian sites, and he later expanded his work to include additional Early Dynastic sites (Petrie 1899; Petrie 1921; Petrie et al. 1953). In his work, Petrie pioneered the technique of ceramic seriation in Egypt (known as 'sequence dating'), a methodology which allows the identification of diagnostic ceramic types within a given time period, and in turn enables the identification of distinct forms and attributes for each type (for further discussion see Section 2.1 below). Given that ceramics have been shown to change and develop temporally, with stylistic changes dictating their development, the concept of 'like goes with like', as developed by Petrie, forms the basis of relative dating in archaeology.

Relative dating is the establishing of a chronological sequence without being able

to anchor it to a fixed time scale. In contrast, absolute dating is the establishing of a chronological sequence with direct reference to a tangible calendar system (for example, years BC or years BP). There is often a discrepancy between the use of the terms 'relative' and 'absolute' chronology within Egyptology, and the main cause of confusion is governed by a distinction between the archaeological and historical chronologies. When discussing the historical chronology, 'relative' can be a term used to distinguish between the reigns of different kings, with the 'absolute' chronology being anchored to cosmological events, such as heliacal risings. In the archaeological chronology, 'relative' chronology is based upon the archaeological phases as distinguished, for example, by material culture and architecture, whereas 'absolute' refers to a date based on a known calendar system (e.g. years BC), determined by scientific dating methodologies e.g. radiocarbon dating, luminescence dating.

Fortunately, scientific study of Egyptian ceramics has achieved significant headway since the 1980s, and, as a result, much is known about manufacturing technology (e.g. Ownby and Griffiths 2009, Nicholson 1993; and often through ethnoarchaeology, e.g. Nicholson and Patterson 1989, Nicholson and Patterson 1985b, Nicholson and Patterson 1985a), clay/fabric and petrographic studies (Hartung et al. 2015, Ownby and Bourriau 2009, Mallory-Grennough and Greenough 1998, McGovern 1997), use history of vessels (see references in Chapter 9 and Appendix B), and to an increasing extent chemical analysis (e.g. Tobia and Sayre 1974, Morgenstein and Redmount 2005, Redmount and Morgenstein 1996). But in the field of ceramic chronology, while relative typological studies have previously formed the basis of understanding Egyptian ceramic chronology, and although Egyptian archaeologists have been at the forefront of relative dating research, the discipline has fallen dramatically behind with regard to scientifically obtained absolute dating. This is to its detriment, since by engaging in absolute dating, the archaeologist can obtain direct, calendar dates for ceramic material, thus complimenting and aiding a more comprehensive understanding of ceramic chronology than can be obtained by relative dating alone. The union of the disciplines can only benefit the study

of ancient Egyptian ceramics and the addition of a scientific basis to ceramic chronology of ancient Egypt would strengthen and enrich pre-existing relative chronologies.

1.3 Why has absolute dating not been applied more often to Egyptian ceramic material?

Given the benefits of coupling relative and absolute chronology in order to obtain the most comprehensive understanding for ceramic material, the first question that comes to mind is why has this not happened sooner in the case of Egyptian material?

In order to answer this question fully it is first necessary to understand the techniques available for absolute dating of ceramic material. There are two generally accessible, high-precision scientific techniques available to the archaeologist for the absolute dating of ceramics: radiocarbon dating and luminescence dating. The latter, in the case of ceramics, is the most beneficial. This is because radiocarbon dating is based upon the dating of organic compounds, whereas luminescence dating is based solely upon the dating of inorganic minerals. In the case of ceramics, radiocarbon dating can be useful for dating organic material stored within a vessel (thus only providing indirect dates for the presumed last use of a vessel), but luminescence dating can be used to date the vessel itself. This is because the main mineral used in luminescence dating is quartz, which—since it is a main component of the ceramic clay fabric in the form of sand—is abundant in Egyptian pottery.

Although radiocarbon dating has been applied for several decades, since the mid-1960s, and is now used with increasing frequency in the study of Egyptian material culture (e.g. Bronk Ramsey et al. 2010; Dee 2013d; Dee 2013b; Dee 2013a; Dee 2013c; Dee et al. 2009; Dee et al. 2012; Shortland and Bronk Ramsey 2013 and articles therein), luminescence dating has only been applied rarely to Egyptian ceramics. Furthermore, the limited number of studies incorporating luminescence dating in Egyptian archaeology used the thermoluminescence (TL) dating method, which although popular at its

inception in the 1960s is now supplanted by the newer optically stimulated luminescence (OSL) dating technique devised in the 1980s. Initially, when TL was a novel approach, several studies used TL to attempt to date Egyptian archaeological material, with varying success (e.g. Abdel-Wahab et al. 1996; Caton-Thompson and Whittle 1975; El-Fiki et al. 1994; Kroeper 2003; Riederer 1978; Sekkina et al. 2003; Whittle 1975; and see further discussion in Section 3.1.1). However, the introduction of OSL as a significant tool for dating archaeological materials coincided with the introduction of the Egyptian Law on the Protection of Antiquities (Law No. 117) enacted in 1983, which effected a ban on the export of archaeological material from Egypt, even for the purpose of scientific analysis (cf. Köhler 2011). Therefore, while archaeologists working in other regions were able to embrace this new luminescence dating technique, newly excavated Egyptian material was off-limits for OSL dating as well as other scientific dating and analytical techniques. Furthermore, as the necessary analytical facilities were unavailable, archaeologists could not carry out such investigations in Egypt either (a recent exception to this is the radiocarbon dating facility set up in Cairo at the Institut français d'archéologie orientale; however, this laboratory uses the older liquid scintillation technique, whereas accelerated mass spectrometry (AMS) radiocarbon dating is now the preferred method of choice). OSL dating remains unavailable to archaeologists working in Egypt, and, while OSL has continued to advance considerably in its archaeological application and methodology elsewhere (e.g. Lian and Roberts 2006, and references therein), there is still a conspicuous absence of OSL dating of Egyptian material. Excluded from this statement are OSL measurements done on non-archaeological material in Egypt (Bubenzer and Hilgers 2003), and measurements on geological samples found in association with archaeological sites (Bubenzer et al. 2007; Huyge et al. 2011; Liritzis et al. 2008; Liritzis et al. 2013;Vermeersch et al. 1998). The only Egyptian archaeological material available for OSL work since the introduction of OSL dating in archaeology has been museum material. Museum material is more difficult to work with for several reasons, not least because OSL is a destructive technique requiring the physical removal of a sample from

an artefact: there has been an understandable hesitation to subject museum specimens to a sampling protocol that has historically required a large (and often unsightly) sample for scientific analysis. This has caused OSL to be viewed unfavourably in many instances, resulting in museum material often being overlooked.

However, in order to progress with the application of scientific analysis of Egyptian material, it is essential to begin working with museum specimens, that is, artefacts legally exported from Egypt prior to the 1983 exportation ban, while recently excavated material remains off-limits (Hood and Schwenninger 2016). This thesis sets out to achieve this, by presenting a new OSL sampling technique, developed specifically with museum materials in mind, which requires only a small 2 mm $\times$ 4 mm sample to be extracted from the ceramic object. This new technique is the minimum extraction technique, or MET, a name which illustrates the minute quantity of sample needed. The MET (outlined in Section 4.1) is an innovative technique which has finally allowed the dating of museum material using luminescence (Hood and Schwenninger 2015). Thus, this thesis presents the first ever OSL results obtained for Egyptian ceramics and material culture, focusing on three main data sets all dating to the Predynastic and Early Dynastic period of ancient Egypt: ceramics from the sites of Bêt Khallaf, Turah and the Abydene region. At this stage, however, due to the limited scope of this thesis (i.e. only a relatively small number of samples could be incorporated into the study), a high-precision ceramic chronology using OSL dating on Egyptian ceramic cannot yet be achieved. This will require a more robust data set. However, by examining ceramic material from a broadly understood relative chronological period, this work clearly demonstrates the significant knowledge and benefits that OSL dating can provide for the field of Egyptian ceramic studies.

1.4 Research objectives: advocating a multidisciplinary approach to the study of ancient Egyptian ceramic chronology

Traditionally, the majority of studies on Egyptian ceramics have examined the material using one designated (usually relative) chronological technique (e.g. Hendrickx 1996; Jucha 2005; Kaiser 1957; Köhler 1998; Köhler 2014a; Petrie 1921; Petrie et al. 1953; Raue 1999). However, we are now in the position to broaden our scope of analysis and bring together a suite of analytical and chronological techniques available to archaeologists and engage in a more thorough examination of the ceramic assemblage. Indeed, by combining both relative and absolute dating methods, we can hope to achieve a broader and more comprehensive understanding of our subject matter. In the case of Egyptian ceramic material, by combining new OSL results with our prior understanding of more traditional ceramic analysis methods (i.e. ceramic typology and morphology), we can hope to add an entirely new body of information to the existing literature. Owing to the limited information and data available up till now for the absolute dating of Egyptian material, it is beneficial to adopt a multidisciplinary approach to widen the scope of new information and scholarship achievable for re-examining the ceramic assemblage of a period.

With such a multidisciplinary approach to the study of ancient Egyptian ceramic chronology, we have in hand a powerful tool to reassess and further define the chronological implications of a fascinating data set. Thus, in addition to pioneering the OSL method in Egyptian ceramics, this work also seeks to extend the scope of methodologies available for relative dating. First, the application of the MET and OSL dating as a relative dating technique, as well as an absolute dating technique, was examined by means of a case study conducted using material excavated from Turah and Hierakonpolis. Secondly, the application of cladistic analysis—a technique borrowed from the biological sciences which makes possible the tracing of the evolutionary development

of archaeological ceramics—could also be of immense benefit to this study as it would allow the 'fine-tuning' of some typological elements of Egyptian ceramic chronology. Preliminary results of the first steps in such an analysis are presented in Chapter 7.

To promote still further a multidisciplinary approach to the study of Egyptian ceramics, this thesis also presents a case study which illustrates how, by combining both OSL dating and radiocarbon dating, a more comprehensive and precise understanding of the absolute ceramic chronology can be achieved, while at the same time both techniques can be used as independent verification for the other. Establishing absolute chronologies by employing more than one method permits cross-checking and comparison of dating protocols and results. Furthermore, by using two independent absolute dating techniques which draw upon different materials, this case study also illustrates how, through a combination of techniques, a better and more thorough understanding of the archaeological history at a site can be determined.

1.5 Outline of this thesis

This thesis presents two separate, but complimentary, aims in its examination of Egyptian ceramic chronology: first, to introduce OSL dating to Egyptian ceramics using the MET and apply it to the study of early Egyptian ceramic material, and second, to use OSL dating alongside a multidisciplinary approach in order to achieve a more comprehensive understanding of ceramic history, examining not only chronology, but also ceramic manufacture, use history, and cultural formation processes affecting ceramic deposition in the archaeological record. Furthermore, this thesis will illustrate the benefits that OSL dating, used in conjunction with a multidisciplinary programme of analyses, can offer the future of ceramic studies in Egyptian archaeology.

This thesis comprises five parts. Part I (Chapters 1 to 3) presents the background of the project, with Chapter 1 providing an introduction to the thesis as well as presenting its research objectives. Chapter 2 presents the ceramic data set for this thesis and discusses the issues involved in the accessing of suitable material for analysis. Im-

portantly, it also introduces the data set in both its historical and archaeological context and provides a discussion on the scholarship which has been instrumental in identifying and analysing this archaeological culture. Chapter 3, the final chapter in Part I, briefly introduces the methodologies incorporated into this thesis.

Part II offers an overview of OSL dating and an introduction to it, and, in particular, introduces the reader to the minimum extraction technique (Chapter 4), discussing the development of the technique, and considerations which need to be taken into account when using it.

Part III examines OSL dating and its application to the main data set incorporated into this thesis, the ceramic assemblage recovered from the site of Bêt Khallaf. Chapter 5 presents the OSL results obtained for the Bêt Khallaf material as well as an in-depth examination of the OSL protocols used for analysis of this material. Chapter 6 considers the OSL results in relation to the existing relative ceramic chronology and typology, and presents newly determined chronological information for the assemblage, which includes a multi-period depositional history, based on the OSL evidence.

Part IV looks at further extending the study of early Egyptian ceramics by employing a multidisciplinary approach alongside OSL dating. Three case studies are presented to achieve this. The first, Chapter 7, examines the application of relative dating methods to the ceramic data set, specifically introducing cladistic analysis. It presents results of such analyses to date and discusses how cladistic analysis can continue to be applied to the study of Egyptian ceramics. Chapter 8 looks at using OSL as a relative dating technique, when the necessary information needed to achieved absolute dates using OSL is unobtainable. This chapter focuses on a data set obtained from the site of Turah and Hierakonpolis. Chapter 9 examines the application of OSL dating in conjunction with radiocarbon dating, working with a data set from the Abydene region, with six vessels from the sites of Naqada, Ballas, and the Tomb of Djer at Abydos.

The thesis concludes with Part V, where Chapter 10 summarises the results and findings, and makes concluding remarks on future directions for work in this field.

Chapter 2

The data set

The ceramic data examined in this thesis is primarily material that dates from the Naqada III archaeological phase of ancient Egypt, with two vessels dating to the late Naqada II period. Within the historical chronology, Naqada III lasts from the Late Predynastic period until around the beginning of the Old Kingdom, or alternatively, spans Dynasties 0–3. The period is divided into four phases, Naqada IIIA–D, which in turn are divided into seven sub-phases (see Table 2.2 below; Köhler in prep). With regard to the absolute chronology, it remains one of the more complicated periods of Egyptian history, the exact chronological sequence of which continues to be heavily debated (Köhler 2013: 224). The archaeologically-defined phases of the Naqada culture were initially synchronised to the elusive absolute chronology through the results of a century of research at Abydos. Identifying diagnostic artefact types within assemblages in the royal cemetery—thus tying these to the reigns of specific kings—enabled the typology to be anchored to the historical timeline.[1] This was achieved mainly through inscriptions bearing the names of the early kings on stone and ceramic vessels, and this made it possible for the Wavy-Handled[2] chronology, initially identified by Petrie (Petrie 1901a), to be built up through extensive observation across the royal tombs.

As already observed in Chapter 1, confusion often arises owing to the multitude of

[1] The historical timeline of the earliest dynasties is still a cause of historical uncertainty, especially given the uncertainty surrounding the precise succession of kings (Köhler 2013: 229–230).

[2] The use of term "Wavy-Handled" ware follows Petrie 1901a, who initially identified this ware type as one of nine main classes of the earliest known Egyptian ceramic styles.

terms in use for essentially the same period of early Egyptian history, based on discrepancies existing between the relative and absolute chronologies of early Egypt and the historical and archaeological definitions. In an attempt to clarify the situation, Table 2.1 presents a comprehensive overview of the different terminologies in common use for this period of Egyptian history. Within this thesis, the Hendrickx system of terminology will be used, alongside the historical dynastic system (highlighted in bold italics within the table).

The choice of time period and material for this study was both personal and practical. From a personal perspective, the author has worked with Naqada III material at the site of Helwan for six years and has, therefore, both a strong academic interest in the subject (including an Honours thesis based upon a reassessment of the Naqada IIID ceramic assemblage: Hood 2007) and the experience of working with material from this period in the field. Initially the Naqada IIID sub-phase of the Naqada III period presented itself as the most desirable focus for this project; however, the material eventually selected for analysis, and thus the material presented in this thesis, was heavily dictated by availability. Due to the destructive nature of OSL sampling, several museums initially approached were more hesitant than others, not allowing samples to be taken (see further discussion below), and other museums, while not having specific Naqada IIID material, were very willing to allow other Naqada III material in their collection to be sampled. Consequently, the selection of data for this project grew organically, and eventually comprised a selection of vessels from throughout the Naqada III period. Furthermore, the Naqada III period is an excellent choice for examining the application of a chronometric dating technique: this thesis seeks to address the common conception that OSL dating is not suitable for Egyptian material (see, for example, Goedicke 2006: 360) and to illustrate how OSL can be used as a chronological tool by Egyptian archaeologists.

Table 2.1: A correlation of the terminology of the Naqada culture (following: Hendrickx 2006: Table II.1.1 (pg. 56); Hendrickx 1996: Table 9; Köhler and Thalmann 2014). For more detailed comparisons of Kaiser and Hendrickx see Hendrickx 2011: 70. NB the absolute radiocarbon dates can vary between sources: these follow Köhler and Thalmann 2014.

Archaeological Chronology					**Historical Chronology**				
Relative Chronology				*Absolute Chronology*	*Relative Chronology*		*Absolute Chronology***		
Petrie (1896; 1901; 1953)	**Kaiser** (1957; 1990)	**Hendrickx** (1989; 1994; 1996)	**Hassan** (1988)	**Radiocarbon dating**	**Dynastic Division**	**King List**	**Hornung et al.** (2006)	**Shaw** (2000)	**Grimal** (1992)
Proto-dynastic (SD 76–86)		***Naqada IIID***	Terminal Predynastic	2850–2680 (2680–2620) BC	***Dynasty 2 (Dynasty 3)***	Hepetsekhemwy–Khasekhemwy (Djoser–)	2730–2590 (2592–2544) BC	2890–2686 (2686–2625) BC	2925–2700 (2700–2625) BC
Semainean (SD 60–75)	Stufen IIIa1–IIIc3	***Naqada IIIC1–3****		3100–2850 BC	***Dynasty 1***	Narmer–Qa'a	2900–2730 BC	3000–2890 BC	3150–2925 BC
		Naqada IIIB		3300–3100 BC	***Dynasty 0 (Abydos)/Protodynastic***	Iry–Hor/Ka			
		Naqada IIIA1–2			***Proto-Dynastic***	Scorpion I			
Gerzean (SD 38–60)	Stufen IIa–d	***Naqada IIC, IID1–2***	Late Predynastic		***Predynastic***				
Amratian (SD 30–37)	Stufen Ia–c	Naqada IIA–B IA–C	Middle Predynastic		Predynastic				

Notes: * Naqada IIIC3 has been added to the Hendrickx divisions by Köhler 2004 to differentiate the final stage of the cylindrical vessel as reflected in recent excavations at Helwan. ** Historical absolute dates are based upon historical sources such as cattle counts, king lists, and astronomical observations (see discussions in Köhler and Thalmann 2014 and Hornung et al. 2006 for additional information). Bold italic text denotes terminology used in this thesis. SD = sequence date (as determined by Petrie 1901a: 4–8; Petrie 1920: 3–4; and see Section 2.1). The data in this table appearing in brackets denotes the Third Dynasty, which is not always uniformly recognized as belonging to the Early Dynastic Period, thus here being presented in brackets alongside those periods which are universally accepted as Early Dynastic (i.e. Dynasties 0–2).

2.1 Historical context of the Naqada III period

Within the relative chronology of early Egypt, the Naqada III period is the last phase of the 'Naqada culture', a term first used by Scharff to describe the archaeological phase/-culture associated with Petrie's excavations at the sites of Naqada, Ballas, and Diospolis Parva in Upper Egypt (Scharff 1927, Petrie 1901a; Petrie and Quibell 1896; cf. Köhler in prep). At the time, the culture uncovered was unknown to archaeologists in Egypt, which initially led Petrie to consider the material as belonging to a 'New Race', although this surmise was quickly shown to be incorrect and the true Predynastic nature of the material was realised (Morgan 1896 cf.Hendrickx 2006: 60). Petrie's work on the Naqada culture focused mainly on the ceramic typology, and, as a result, Petrie characterised the development of the culture based on the emergence, occurrence, and evolution of distinct ceramic types.[3] He did this by organising them into what he called 'sequence dates' (SD) (Petrie 1901a: 4–8; Petrie 1920: 3–4; cf. Hendrickx 2006: 60) a system which is considered 'the first attempt at what is now known as seriation' (Hendrickx 1996: 36; Hendrickx 2006: 60). Starting at sequence date 30, Petrie initially divided the material into three groups, which were known as the Amratian (SD 30–37), Gerzean (SD 38–60) and Semainean (SD 60–75) (Hendrickx 2006: 62). Later, the SD system was extended to include what was considered 'Proto-dynastic' material, excavated primarily at the Tarkhan cemetery (Petrie et al. 1913), correlating to SD 76–86 (Hendrickx 2006: 62).

Although Scharff (Scharff 1927), and following him Baumgartel (Baumgartel 1947), tried to rework the definitions of Petrie's system, it was in 1957 that Petrie's sequence dating system was re-examined and modernised by Werner Kaiser (Kaiser 1957; cf. Köhler in prep). The impact of Kaiser's work was far-reaching and his contribution remains essential to the study of the period (Köhler in prep). Examining cemeteries 1400–1500 at Armant, Kaiser similarly distinguished three spatial zones within the cemetery based on distribution of ceramic types, which were considered to be of chronological signif-

[3] Whether the term 'culture' is appropriate or not to this situation is a topic that has recently been discussed elsewhere (Köhler in prep); however, for the purposes of this thesis, the term 'Naqada culture' is incorporated undisputed as the most straightforward terminological phrase in common use.

icance (Kaiser 1957 cf. Hendrickx 2006: 64). These three newly defined stages of the Naqada culture were further divided by Kaiser into sub-phases known as *Stufen* (singular Stufe), several of which were based upon additional ceramic material not seen in the Armant corpus, that is, to say that Kaiser knew of their existence based on additional archaeological evidence from other sites (Kaiser 1957 cf. Hendrickx 2006: 64). Although similar to Petrie's SD system, Kaiser's Stufen had the additional benefit of considering spatial distribution of the material (i.e. the horizontal stratigraphy within the cemetery) alongside the changes in ceramic style (Kaiser 1957 cf. Hendrickx 2006: 65, Table II.1.3). Kaiser's system also escaped the inherent problems of Petrie's tightly defined SDs in that by discussing three broadly defined periods, rather than three periods tightly restricted by specific SDs, Kaiser's Naqada culture division can be more readily expanded and added to with ease (Hendrickx 2006: 65).

Following Kaiser's redefinition of the Naqada culture, several further studies followed, concerning themselves primarily with computer seriation methods and distribution studies of the Naqada culture material. Computer seriation methods will be discussed in greater detail elsewhere (see Chapter 6). Of distribution studies carried out on this time period, there are two of particular interest: Friedman (Friedman 1981; cf. Hendrickx 2006: 68) was the first to engage in a study which focused primarily on the spatial distribution of the material culture (rather than the seriation method, which focuses on the presence/absence of ceramic types), in this case at cemetery 7000 at Naga ed-Der. Payne (Payne 1992; cf. Hendrickx 2006: 68) re-examined the Main Cemetery at Naqada in the light of Kaiser's revision of the Naqada culture and, in general, the similarity between the Armant and Naqada material was significant, thus further validating Kaiser's methodology.[4]

Thus far, discussion of the development of the Naqada culture has been presented without critique, as a simple linear narrative. However, this is not the case, and it is es-

[4] These additional studies have all been discussed and critiqued at length elsewhere and do not enhance the discussion surrounding the present work. The reader is referred to e.g. Hendrickx 1996, Hendrickx 2006 and Hood 2007 for a more comprehensive discussion of scholarship of the Naqada culture.

sential to note here that there are inherent problems with the scholarship of the culture (Köhler in prep; Köhler 2014b). For instance, the two major flaws in Petrie's original system were that it failed to truly distinguish between typology and chronology, and that he ignored the horizontal and spatial distribution of the material, which would have improved discussion of the chronological impact of the SD system (Hendrickx 2006: 63). Similarly, while considering the initial ceramic divisions of Petrie, Kaiser's Stufen chronology focuses primarily on a single cemetery, thus possibly restricting the applicability of the study to a broader geographical spread. Kaiser noted this problem, acknowledging that at the site of Mahasna, for example, regional differences are discernible (Kaiser 1957; cf. Hendrickx 2006: 65). Furthermore, although his Naqada chronology is based upon Armant, this cemetery only produces very scant evidence for several sub-phases of the culture (notably Stufen Ia, Ib, and IIIb), which thus renders them mostly theoretical rather than based on more solid evidence. Finally, Kaiser's large-scale study has never been published in full, and thus much of the methodological work and the more detailed descriptions of each sub-phase remain widely unknown. Although Kaiser also extended his original 1957 work in an additional article published in 1990, which extended his chronology into the First Dynasty, this also remains only partially published (Kaiser 1990).

In 1989 (and subsequently in 1994 and 1996) the most significant reworking of the phases of the Naqada culture, by Hendrickx, emerged in the literature, and it is this system which is the most favoured in today's scholarship (Hendrickx 1989; Hendrickx 1994; Hendrickx 1996). Hendrickx's work presented a study which incorporated a far wider corpus of material, from a multitude of sites across Egypt from which reliable archaeological evidence was available, and considered both the spatial distribution of the material and the assemblage of material culture associated with each context. While Hendrickx followed a similar methodology to Kaiser, the increased body of evidence permitted a more extensive understanding of the phases of the Naqada culture and therefore enabled Hendrickx to rework the definitions for each phase and sub-phase. In the litera-

ture, Hendrickx's divisions can be differentiated from Kaiser's by the replacement of the term Stufe for Naqada and by the capitalisation of the sub-phases (i.e. from Stufe IIIa2 to Naqada IIIA2). Two major additions to the Naqada chronology by Hendrickx are the newly defined Naqada IIID sub-phase (Hendrickx 1994), and the redefinition of Stufe IIIa2 as Naqada IIIA1, and of Stufe IIIa1/IId2 as Naqada IID (Hendrickx 2011: 72–73). Although his is the most methodologically sound of the Naqada culture chronologies, Hendrickx acknowledged that working with archaeological evidence from the Naqada period produces a conflict of interest: there is equal weight placed on identifying as large a number of individual vessel types as possible, but simultaneously a need for gaining further information on spatially distinct grave groups. The result is that individual researchers will often be governed by their own subjective views on how best to analyse and work with the data. Thus Hendrickx suggests that it may not ever be possible to establish clear and objective rules for defining the chronological phases of the Naqada culture (Hendrickx 2011: 71).

Finally, another issue which must be addressed when examining the history of the Naqada III period is the fact that much research needs to be conducted on material excavated over 100 years ago. This material is often poorly documented and, as a result, important information such as spatial distribution and exact depositional histories are often lacking, resulting in large gaps within the available data set. In addition, when considering a typological study, it is very important to work with good quality data, and sadly, when it comes to the ceramic material available from the turn of the twentieth century, one must often rely on poorly recorded drawings, with little diagnostic information. For example, in the case of Emery at Saqqara, the vessel types presented in the publications were not individual vessels but rather type designations, which were simply an amalgamation of various similar vessels (Emery 1949; Emery 1954; Emery 1958). It is often impossible to gain any further clarification for individual vessels as much of the pottery was left in the field, or found its way into private collections. Consequently, only the material given to museums is available for further study. This makes

much of the original work done on the Naqada culture unverifiable.

Table 2.2: Diagnostic features of the ceramic assemblage for each subdivision of the Naqada culture.

Naqada Sub-phase	Diagnostic ceramic features
IIIA1	• Black Topped Ware and Decorated Ware no longer present • Red Polished Ware now rare • Rough storage jars become more slender (form L30g/k; L31a) • Marl storage jars (form L36n/s) frequent • Late pottery classes increase in number of forms and quantity • Decorated Late Ware with less complex designs (forms D20–21; 24–25) • Wavy-Handled vessels become more slender (forms 49–50) and handles now a continuous band • Type 1 beer jar (Köhler and Smythe 2004)
IIIA2	• Quantity of Rough Ware significantly decreases (might possibly be due to regional variation, rather than being a specific typological marker, as the Naqada IIIB assemblage is dominated by material from the site of Tarkhan) • Quantity of Wavy-Handled ware increases (form W62) and Net Painted design emerges (W55, W58, W61, W62) • Marl storage jar L36n/s is replaced with a broader type (L36a/g2/k) • Rough Ware jars become increasingly slender (L31a) • Decorated pottery very rare • Type 1 beer jar (Köhler and Smythe 2004)
IIIB	• Slender Rough Ware jars become increasingly rare • Continued decrease in Rough Ware • Smaller marl storage jars become more common (form L36b, L38a) than their larger counterparts (L36a, L36k) • Wine jars with banded decoration begin to appear infrequently (SD 76), and have a vessel index of 2.5–2.6 (Köhler and Smythe 2004: 130) • Decorated pottery continues to be rare • Substantial decrease in Net Painted Wavy-Handled Ware • Wavy-Handled vessels become increasingly cylindrical and now have an incised continuous band • Type 1 and 2 beer jars (Köhler and Smythe 2004)
IIIC1	• Decorated vessels and Rough jars no longer present • Late Ware most represented ware group • Marl storage jars still present, Petrie's 65 group most frequent (Petrie 1921) • Increase in the quantity of wine jars with banded decoration which have a vessel index of 2.5–2.6 which increases to 2.8–3.0 in the later Naqada IIIC period (Köhler and Smythe 2004: 130) • Wavy-Handled vessels diminish in frequency and are now mostly cylindrical with no band decoration; they move towards being made predominately of Nile silt clay • Type 2 beer jars (Köhler and Smythe 2004)

Table 2.2: (continued)

Naqada Sub-phase	Diagnostic ceramic features
IIIC2	• Wavy-Handled vessels now a more degraded form, usually made of Nile silt, much narrower and straight-walled • Decrease in quantity of large marl storage vessels, but increase in both smaller varieties • Wine jars continue to be present, but now made almost always of Nile silt clay, (Köhler et al. 2011: 107) and a vessel index of 2.8–3.0 (Köhler and Smythe 2004) • Type 2 and 3 beer jars (Köhler and Smythe 2004)
IIIC3	• Degraded, small cylindrical vessel, made of Nile silt clay, narrow width and straight-walled—this degradation of the cylindrical was noted by Köhler at Helwan, who designates this final cylindrical vessel form as the Naqada IIIC3 sub-phase (Köhler 2004: 300–301; Köhler 2013; Köhler and Smythe 2004; Köhler et al. 2011: 107) • This phase is otherwise similar to Naqada IIIC2
IIID[5]	• Absence of Wavy-Handled/cylindrical vessels (Köhler and Smythe 2004) • Smaller marl storage jars still present • Wine jars become more elongated ('torpedo'-shaped), and have a vessel index of greater than 3.5 (Köhler and Smythe 2004: 130). However, it also appears that later in the Second Dynasty the wine jar becomes miniaturised and the vessel index is no longer a reliable date indicator, although the shape of these vessels remains 'torpedo' in style (Hartmann 2006; Hood 2010a). It also appears that these miniaturised vessels are increasingly made of a mixed marl-Nile clay • Type 4 beer jar (Köhler and Smythe 2004 • Types common in the Old Kingdom begin to emerge in their early stages of development: Internal Rim Bowl, Meydum Bowls, collared beer jar (which has also been designated 'Type 5 beer jar' by Hood and Valentine 2012 (cf. Köhler et al. 2011) • Commencement of the flared, restricted neck, flat-based, squat jar (early Naqada IIID) • Commencement of the restricted neck, flat-based jar (later Naqada IIID, likely a later form of the squat jar).

[5] Based upon the ceramic repertoire at Helwan, Köhler has further divided the Naqada IIID period into 5 date groups (Köhler 2004; Köhler 2014a). These date groups, although distinct, do contain several vessel types which appear across all groups which indicates a degree of continuity (or disturbance) within the archaeological record at this time. Therefore, precise and clear distinction between the five groups can be difficult (Köhler 2014a: 36). It is not yet clear how much these five groups are representative of the ceramic assemblage of Egypt as a whole, and to what extent some vessels present are local to the Helwan area. To summarise, (following Köhler 2014a: 37): the first group is Naqada IIIC3/IIID1 which is characterised by wine jars with a vessel index of ∼3, Type 2 beer jars and small barrel-shaped vessels. Group IIID2 is similar to Group IIIC3/IIID but also has wine jars with a slightly higher vessel index and the Type 3 beer jar, deep, polished bowls, and poorly made shallow plates and small ovoid vessels. Group IIID3 sees the introduction of the Type 4 beer jar and jars with a distinct shoulder ledge, and the deep, polished bowls become rare. Group IIID4 contains both Type 4 and Type 5 (i.e. collared) beer jars, bowls with flared profile, and the early development of the Internal Rim Bowls. Group IV continues to contain Type 4 and Type 5 beer jars, and Internal Rim Bowls (which show a continued development of the internal rim which is to become lower and wider, and significantly, it is this group that sees the introduction of the early Meydum carinated bowl).

Table 2.2 presents the main diagnostic features of the Naqada III ceramic assemblage. This table is based primarily upon the Naqada chronology of Hendrickx (Hendrickx 2006: 81–88, Table II.1.3), although it is further supplemented by additional research carried out since Hendrickx's publication, which is referenced accordingly.

2.1.1 Problems surrounding the Naqada III period

Although the Naqada culture has been known since Petrie's excavations in 1895, it is remarkable that this period of Egyptian history remains without a solid archaeological or historical chronology. This is owing in part to the limited number of excavations carried out at early sites, when compared to sites dating to the later Pharaonic periods (i.e. the Old, Middle, and New Kingdoms) which have historically attracted more archaeological attention. Indeed, it is only since the 1990s that there has been a significant increase in the number of excavations at Predynastic and Early Dynastic sites.

As a result, the Naqada III period has both an indeterminate ending and a poorly defined beginning. Irrespective of the misleadingly definitive nomenclature of the Naqada culture, the transitional phases between the three Naqada periods, and between the later Naqada III period and the Old Kingdom, remain elusive. A lack of archaeological evidence has resulted in a less robust data set available for examination and interpretation. Furthermore, although the nomenclature can often convey a false sense of chronological certainty, the fact remains that there is no single archaeological event or occurrence which demarcates the Naqada III period from its predecessor and successor: transitions are slow and gradual (Hendrickx 2006: 81). If we are to forcibly project certain chronological indicators onto the beginning of the Naqada III period, its two most defining features are first, that we see more uniformity in the spread of material culture across the country, with both northern and southern cultural traditions being seen along the length of the Nile (Köhler 2014b), and secondly, that it is around the beginning of the Naqada III period that the earliest forms of the Egyptian written language are observed, although to what extent this can be linked to the relative chronology at present remains

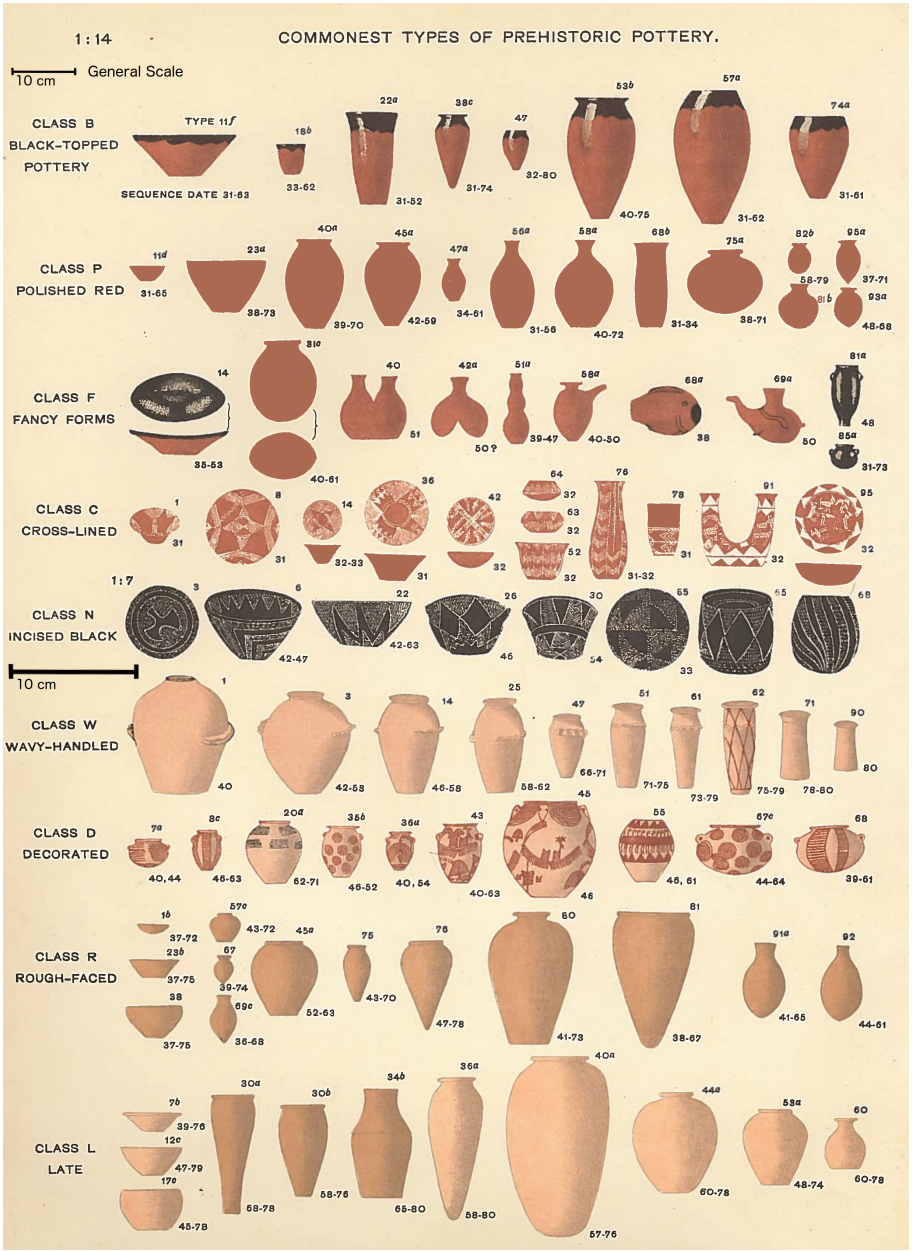

Figure 2.1: The most common types of early Egyptian pottery, as classified by Petrie. This figure accompanies Table 2.2, providing a illustrative guide to some of the most common ware types presented in this table. For the specific ceramic forms mentioned in Table 2.2 (e.g. L36b, W61), the reader is referred to Petrie 1921. This figure is taken from Petrie 1901a; the general scale applies to all vessels except to the black incised vessel class which has its own scale.

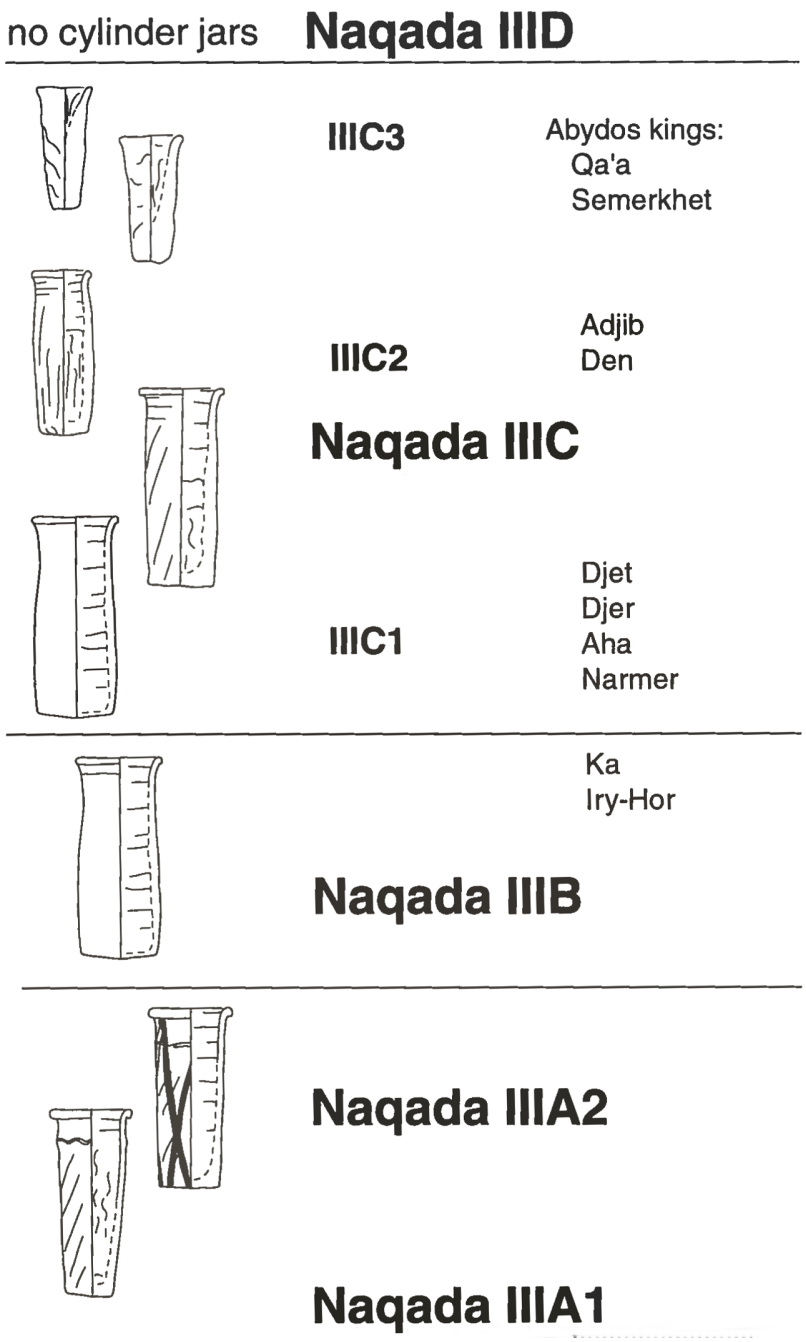

Figure 2.2: This figure presents the typology of cylindrical vessels (descending from Petrie's wavy handle vessel class) throughout the Naqada III period. This figure is an illustrative accompaniment to Table 2.2. This figure is taken from Köhler 2004. Figures not to scale.

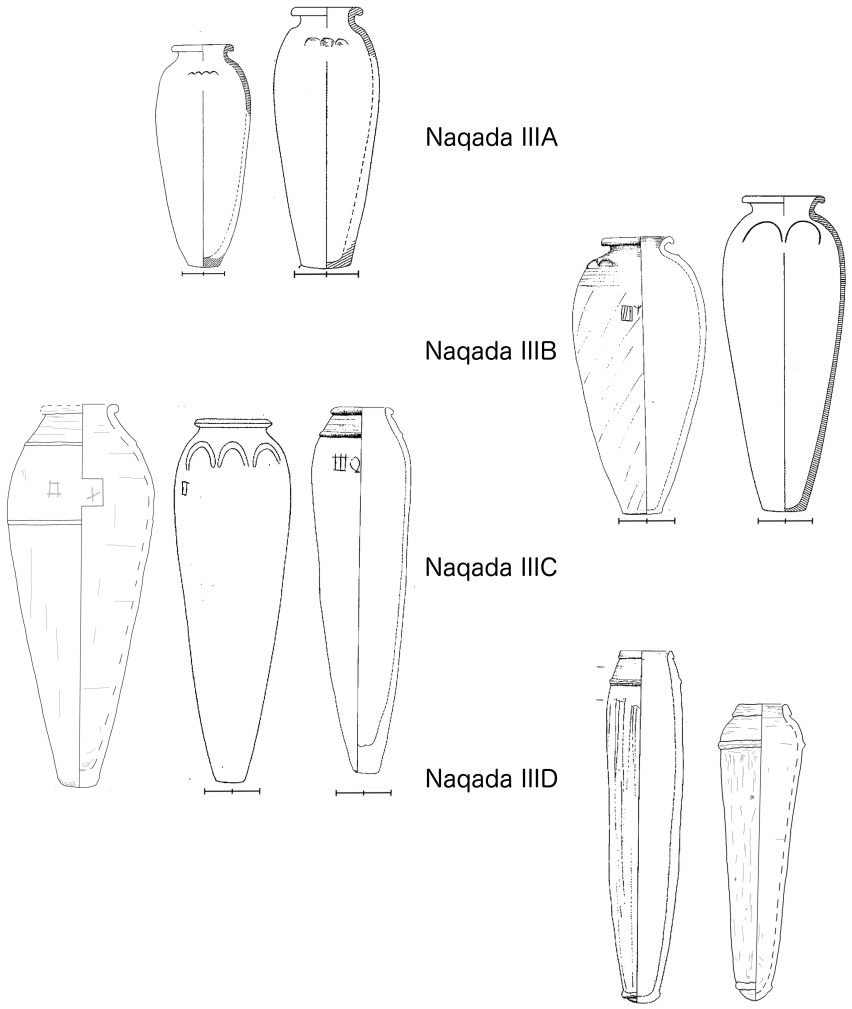

Figure 2.3: This figure presents the typology for wine jars (also descending from Petrie's wavy handle vessel class) throughout the Naqada III period. This figure is an illustrative accompaniment to Table 2.2. Line drawings taken from: Kroeper and Wildung 2000: 152, 154, 170; Köhler and Smythe 2004: Pl. 2, Pl. 3; Petrie et al. 1953: XXI; See also Appendix J (X5489) and Appendix C (X4116). See corresponding appendix for X4116 and X5489 for scaled images of these figures.

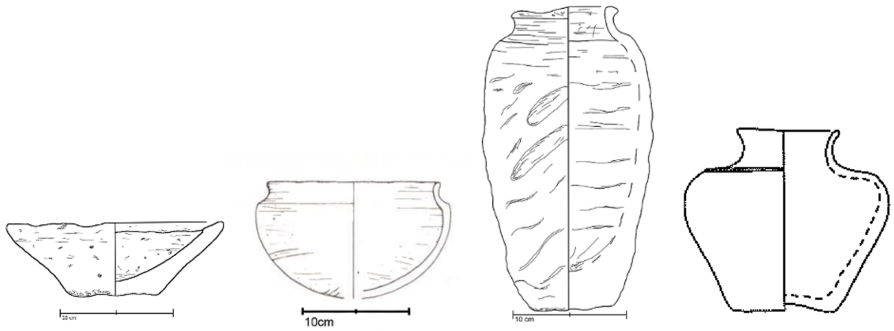

Figure 2.4: An illustration of Naqada IIID diagnostic vessel types to accompany Table 2.2. From left to right: internal rim bowl, Meydum bowl, flat based vessel, squat jar.

unknown (Hendrickx 2006: 82; Pers. Comm. E.C. Köhler, 2016). If we are to forcibly project certain chronological indicators onto the end of the Naqada III period, it would be the rise of the Old Kingdom and the commencement of monumental state architecture, most notably the occurrence of pyramid architecture. However, again it must be stressed that although these events could be used to draw a line around the term 'Naqada III', in no way do these events impact the material culture, which continues to evolve seamlessly between transitions—the ceramic assemblage is clear proof of this (Köhler 2011). Indeed, the concept of a clear-cut delineation between Naqada IIID and the Old Kingdom, is 'an entirely modern construct' (Köhler and Thalmann 2014: 182). In many respects the ceramics from the beginning of the Naqada III period are better understood than those from its end, a field of enquiry which in the early days of research had been largely ignored, insight into which can be gleamed by the words of Arthur Mace, an excavator at Naga ed-Der who said that the ceramic material retrieved from the later period was 'singularly dull and uninteresting' (Mace et al. 1909: 37).

Perhaps the largest corpus of early Naqada III ceramics comes from older excavations at around the turn of the twentieth century (i.e. Abydos, Naqada, Ballas, Turah, Naga ed-Deir, Tarkhan, Armant, Diospolis Parva). This lends this material the disadvantage of having generally poorer provenance. In many instances the find spots of individual objects were not fully recorded, or if they were, they were not always published, or even kept for posterity. For example, the vast majority of the Naqada material from

Petrie's excavation, although never published in full, was nevertheless thrown away as it was considered 'published' (Baumgartel 1970: 6). This means that the chronological studies of this material can never be reproduced. Further to this, because the original archaeological contexts are not preserved, it is almost impossible to accurately reconstruct depositional events. Many Wavy-Handled vessels (a common ceramic type and typological indicator) which were prevalent at many excavated sites in the early twentieth century, can no longer be associated with an exact tomb context, only a general site. This means that valuable information has been lost: the spatial distribution of tombs and their objects, and the occurrence frequency and distribution of different ceramic types in various contexts (i.e. elite or non-elite). Furthermore, almost nothing is known about their manufacture, whether they were produced in specific workshops, or which clay sources were exploited to make them.

In contrast to early Naqada III ceramics, when dealing with the later assemblage, the main problem is a singular lack of excavated material. At present, the 'official' end of the Naqada III period is the sub-phase Naqada IIID (corresponding to Petrie's Sequence Dates 83–87), first designated by Hendrickx (Hendrickx 1989; Hendrickx 1994; Hendrickx 1996: Table 7). The Naqada IIID period, until recently, remained largely defined either in negative terms (i.e. the absence of certain vessel types relative to the earlier assemblage) or based on the emergence of vessel types and forms known more frequently from the Old Kingdom. While recent scholarship (e.g. Köhler and Smythe 2004; Köhler 2014a; Köhler et al. 2011) is changing this view, it is this latter observation which has led many researchers to question the reasonable extent of the Naqada culture. Is the fact that Old Kingdom types are emerging during the Naqada IIID period a signal of the end of the Naqada culture, or, once again, is this trying too much to delineate a cultural marker which in actual fact is not represented in the continuous flow of material culture evolution? Alternatively, would further ceramic evidence eventually lead to the defining of Naqada IIIE or even Naqada V, that is, the point at which the Old Kingdom forms appear (Köhler and Smythe 2004: 136; Köhler in prep)? The verdict is still very much

out on this question, but it remains one of the most significant problems surrounding the end of the Naqada III period (Köhler 2011; Köhler 2013; Köhler et al. 2011; Köhler 2014a; Köhler and Thalmann 2014).

Another factor contributing to the lack of knowledge surrounding Naqada III is a significant bias in the available evidence towards material culture recovered from cemetery sites as opposed to settlement sites. With a small handful of exceptions (e.g. Buto, Elephantine, Tell el-Farkha, Adaïma), the majority of material dating to the late Naqada III period comes from cemeteries, and the early study of the Naqada chronology was based heavily on the evidence from Abydos, Elkab, and Armant (Köhler and Thalmann 2014: 185). Thus, although only a relatively small amount is known about Naqada III cemetery contexts in comparison to later historical periods, even less is known about settlement contexts. The tide is slowly turning, and since the mid-2000s, in the past several years, particularly in the Delta, a larger number of settlement sites are being recovered. However, it is likely that there will always be a bias towards cemetery data in the field of Egyptian archaeology as the cemeteries are located further out from the Nile river, in the low desert plateau. Although in modern times cemeteries are now at a greater risk of encroaching urban settlement, ancient settlement sites have already suffered this fate—being subjected to several thousands of years of continuous occupation which has all but destroyed the archaeology. It is for this reason that more cemetery sites are known than settlement sites (Köhler 2011). With regard to the ceramic assemblage this means that the current definitions of the phases and sub-phases of the Naqada culture are dictated primarily by the study of cemetery ceramics and this may not take into consideration likely variations within the two different ceramic assemblages: for example, a temporal lapse between the emergence of one form in a settlement context and its subsequent emergence in the cemetery assemblage. It also makes it difficult to discern chronological implications of vessels which may have been found exclusively in a settlement context rather than a cemetery context and vice versa. For instance, the wine jars, which follow a very clear typological sequence, are known almost exclusively

from cemetery contexts and do not appear in the settlement sites or, if so, only very rarely and in sherd form (Pers. Comm. E. C. Köhler and D. Raue, 2009; cf. Köhler et al. 2011: 108). It is essential, therefore, that the absence of a particular vessel type is not misidentified as a chronological marker when comparing settlement and cemetery sites.

Similarly, there is a stronger bias towards material excavated from sites within Upper Egypt as the majority of excavations carried out in the early to mid twentieth century were conducted south of the Cairo region, with only a few exceptions (e.g. Turah (Junker 1913), Abu Roash (Klasens 1957; Klasens 1958; Klasens 1957; Klasens 1960), Maassara (Larsen 1939; Larsen 1940), Saqqara (Emery 1949; Emery 1954; Emery 1958)). Although, again, this is something that has been changing since the 1990s (e.g. at sites such as Helwan (Köhler 2005; Köhler 2014a), Buto (Köhler 1998), Tell el-Farkha (Chłodnicki et al. 2012; Jucha 2001; Jucha 2003; Jucha 2005; Mączyńska 2004), new excavations at Saqqara (Hood 2010a)), this new research is still trickling down into the literature. Slow publication rates (and often the lack of discourse between investigators working across the field) mean that much of the new material is not yet available to all researchers and this results in the continued reliance upon older chronological systems, which do not include the most recent additions to the ceramic corpus. The main effect that this has had, and is continuing to have, naturally concerns the visibility of regional variation within the ceramic assemblage. While the Naqada III period does show a considerable degree of continuity across much of Egypt, preliminary publications of ceramic results often point to the occurrence of regional forms which occur at a single site or a cluster of sites within a designated area, but which are not known from elsewhere in the country. An example of this is the pedestal bowl known from later Naqada III contexts at Elephantine (e.g. Raue 1999: Abb 36.9), but which are seemingly completely absent from anywhere else within Egypt in ceramic form, although they are known elsewhere made of various types of stone (Pers. Comm. D. Raue 2009; cf. Pers. Comm. E. C. Köhler 2009). The understanding of regional variation in ceramics is extremely significant in archaeology as it often provides information on possibilities such as local workshop production and

manufacture, locally produced commodities, trade, insight into local traditions, and regional, economic, social, cultural, and religious differences. Once the Naqada III ceramic corpus is expanded to include all recently excavated material, it is likely that significant advances will be made in the interpretation of various elements of Egyptian society, culture, and chronology.

2.2 Museum material selected for OSL sampling

As already indicated, renewed academic interest in late Early Dynastic period has only come about since the mid 1980s, after the exportation ban enacted in Egypt. As a result, any new scientific analysis conducted on Naqada III ceramic material must rely solely upon museum material, mostly material excavated around the turn of the twentieth century and thus legally exported prior to the 1980s.

As already mentioned, the factors surrounding museum permission for sampling and OSL work heavily influenced the samples chosen within this thesis—in particular, the reluctance of curators to permit sampling. OSL sampling is destructive and even though the newly developed minimum extraction technique (MET) has significantly reduced the quantity of sample required, curators are often still wary of any technique which has the potential to cause damage to the artefact being analysed. This is particularly true in the case of Egyptian artefacts, given that, at present, the quantity of Egyptian material in a museum is finite, as the 1983 exportation ban does not permit further acquisition of recently excavated Egyptian objects. Furthermore, past studies which have engaged in thermoluminescence dating of Egyptian ceramics (Caton-Thompson and Whittle 1975; Kroeper 2003; Riederer 1978—on clay cores of bronze statuettes of the Late Period; Whittle 1975) used to require significant sample sizes which left a visible and prominent mark on the surface of the vessel, and generally only produced dates with large errors. There are two notable exceptions: first there is a group of three articles (El-Fiki et al. 1994; Abdel-Wahab et al. 1996; Sekkina et al. 2003) which, in general, presented positive results for the dating of Old Kingdom sherds. However, these articles have been criticised

(Goedicke 2006: 359) for both the instrumentation and the calculations used to obtain a very small error percentage. Secondly, TL dating has been used to examine the luminescence of Egyptian Blue pigment with some success (Schvoerer et al. 1988).

When requesting permission to work with museum material for this project, great care was taken to demonstrate in advance that the MET, unlike TL sampling techniques, would only leave a small surface mark on the vessel, and this was instrumental in seeking permission for destructive analysis for OSL sampling. While some museums were more eager to engage with a project using the novel MET, others were less so (in some cases taking two years to grant sampling permission) and some refused sampling permission entirely—understandably this resulted in initial delays in sampling for this project.

This project was fortunate to secure a total of 40 OSL samples from several museum collections. The material comes from the sites of Bêt Khallaf (24 samples), Turah (9 samples), Abydos, Naqada, and Ballas (6 samples) and Hierakonpolis (1 sample) (Figure 2.5).

These ceramics will be discussed more fully in the results and discussion section of this thesis (Parts III and IV). However, some introductory remarks about the material used in this thesis are presented below (in Section 2.2.1–2.2.3, and Section 2.3).

2.2.1 Ceramics from Bêt Khallaf (the Garstang Museum, the Penn Museum, and the Ashmolean Museum)

The 24 ceramics from Bêt Khallaf (excavated by Garstang at the beginning of the 20th century (Garstang and Sethe 1903)), form the largest and most significant data set for the project. From its inception, this project's aim was to focus primarily on the ceramics from Bêt Khallaf as it is arguably the most significant ceramic assemblage of late Naqada III (IIID) ceramics from a single site (among those housed outside Egypt). The site was excavated by Garstang in the early 1900s, and the intact ceramic material recovered from the site was removed from Egypt soon after excavation and dispersed across three museums: the Ashmolean Museum in Oxford, the Garstang Museum of Archaeology

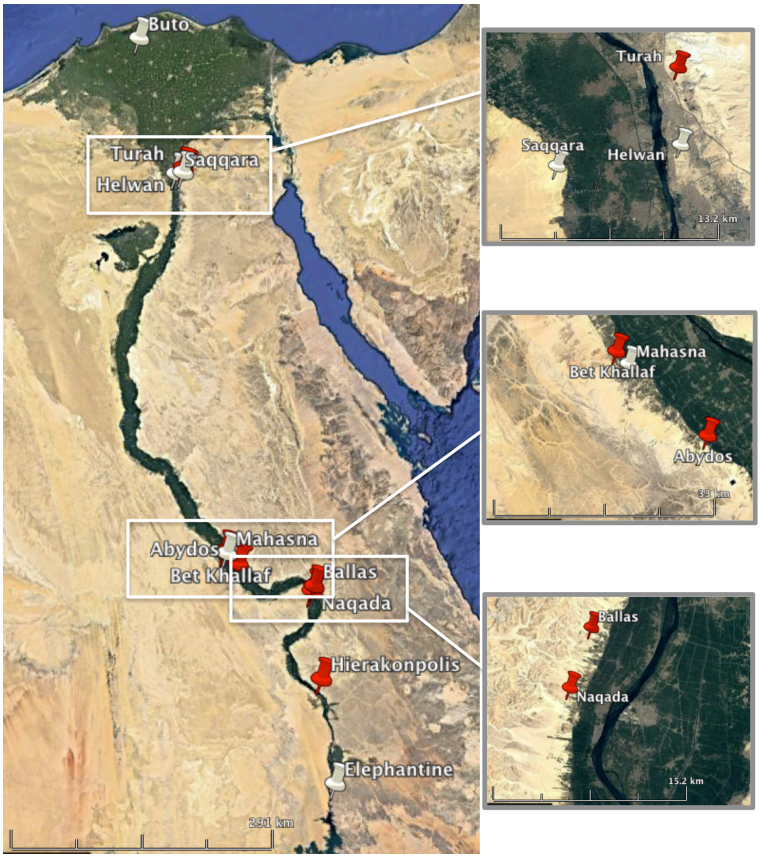

Figure 2.5: A map of Egypt showing all archaeological sites from which ceramic data was used in this thesis (red markers), along with those sites frequently mentioned within the text (white markers).

in Liverpool, and the University of Pennsylvania Museum of Archaeology and Anthropology in Pennsylvania (the Penn Museum). The assemblage was attributed to the early Third Dynasty by Garstang, although several of the vessels present in the assemblage are quintessentially late Naqada III forms which we see develop from the Second Dynasty onwards (i.e. the Internal Rim Bowl, the torpedo-shaped wine jar, the collared beer jar, and the restricted-neck, flat-based storage vessel).

The Bêt Khallaf assemblage is a perfect candidate for OSL dating as not only are many of the vessel types diagnostic (thus providing a perfect platform for using absolute dating to anchor the relative ceramic typology to a known calendrical system), but they also have a fairly good excavation record (by the standards of the time period in which they were excavated). The information present in the reports can be used to re-

duce errors associated with OSL dating. Although the calculation of an OSL date will be discussed in more detail below (Section 3.1.1.2), it is noted here that in order to calculate a date, three separate measurements are required. Of these three, the most difficult to obtain from museum materials is the 'external gamma dose rate', which relates to the rate at which a vessel has received a dose from its surrounding depositional environment. This essentially means that to calculate an OSL date, some original soil or sediment material from the original depositional environment is usually required. This can be extremely difficult to obtain from museum material: more often than not, the vessels are cleaned thoroughly before being put on display or into storage, meaning that soil or sediment material is unavailable for analysis. This can make the calculation of an OSL date extremely difficult and can increase the errors in the calculated dates significantly. Therefore, in order to achieve precise absolute dates for museum material using OSL, it is necessary to ensure that soil/sediment material is available prior to sampling. In the case of the Bêt Khallaf assemblage, such material was available because five of the vessels had a small quantity (less than 1 g) of original depositional material still adhering to both the interior and exterior of the vessel. The locations of this adhering sediment (under the rim of the vessel, and attached/moulded to the interior vessel wall), along with a visual analysis, suggested that this material was almost certainly original to the burial environment and/or the archaeological environment; thus, it was assumed that this material could be used in the calculation of the external dose rate (although of course such an assumption can never be fully verified regardless of how probable). The material from these vessels was used in order to determine the external dose rate for the entire assemblage (under the assumption that the assemblage comes from within a given context and from a particular site, it was possible to use the two samples as proxies for the other vessels).

By obtaining OSL dates for this assemblage, the Bêt Khallaf material will yield the first direct absolute dates achieved for an Egyptian ceramic assemblage and will assist in anchoring the relative ceramic typology of the late Naqada III period to an absolute

dating system.

2.2.2 Ceramics from Turah (Institute of Egyptology, Vienna)

The nine ceramics from Turah and sherd from Hierakonpolis form the second largest data set for the project, and are used in Case Study 2 (presented in Part IV of this thesis) which looks at furthering the application of OSL dating in Egyptian ceramics. Unlike the Bêt Khallaf material this material does not date to the late Naqada III period; rather, it comes from the early Naqada III archaeological phase (corresponding to the Late Predynastic and early Protodynastic/Early Dynastic periods). The material was sampled from the teaching collection at the Institute for Egyptology at the University of Vienna. This material was not selected in order to work on chronological questions surrounding the late Naqada III (IIID) period, but because of its capacity to illustrate the potential of OSL dating as a relative dating technique. OSL is primarily used as an absolute dating method, but it can also help answer chronological questions concerning the specific development of a ceramic type or form. This aids better understanding of the development of ceramic typology as well as of the individual vessel's temporal relationships within an assemblage or time period.

The site of Turah was excavated by Junker in the early 1900s, and the ceramic material recovered from the site was distributed across several museums worldwide. The ceramics sampled here are from the Institute of Egyptology in Vienna. Several of the vessels, in particular the varying forms of the Wavy-Handled/cylindrical vessel are particularly diagnostic and, given that a good understanding of their typological development already exists, the assemblage is well suited to illustrating the benefits of using OSL as a relative dating technique in addition to and in combination with using it as an absolute dating methodology. The Hierakonpolis sherd complimented the wine jars from Turah, and was excavated by Garstang (Garstang 1907).

2.2.3 Ceramics from Abydos, Naqada, and Ballas (Ashmolean Museum)

The four ceramics from Abydos, and the two from Naqada and Ballas (one from each of the two sites), are a collection of six vessels which are temporally similar and come from three individual sites in close proximity to one another. Chronologically, these six vessels are closer to the Turah assemblage than the Bêt Khallaf assemblage, and contain both Egyptian and imported vessels (found in Egyptian contexts), from the Predynastic and early First Dynasty. These six vessels form the data set for Case Study 3 (also presented in Part IV of this thesis) which examines the use of OSL dating alongside radiocarbon dating. These vessels were selected for analysis not for their chronological significance alone, but because they provided a perfect case study for illustrating the scope of archaeological science as applicable to Egyptian ceramic material, and because they are also an excellent example of applying a multidisciplinary approach to the study of a particular data set. The six vessels had already been selected for radiocarbon dating by the project 'Origins of Nationhood: A new chronology for the formation of the Egyptian State', (headed by C. Bronk Ramsey and M. Dee at the University of Oxford) as each of the six vessels had original pot contents within them. The benefits of also subjecting them to OSL dating were clear: by applying both OSL and radiocarbon dating to a single assemblage of vessels, it would be possible to cross-check and corroborate dates obtained by one technique against the other, thus producing a more robust dating programme. As OSL dating is done upon the vessel directly (i.e. the clay fabric itself) and radiocarbon dating, by contrast, is done on the organic material held within the vessel, both methodologies can determine whether the results from each subset of material correlate to one another. Where they do not, there is the possibility of learning more about the depositional history of the vessel. Furthermore, these six vessels are particularly interesting as the organic material within the vessels was found to have quite a significant quantity of non-organic, mineralogical material contained within it, and thus we were able to conduct OSL dating on the contents of the vessels as well as on

the vessel itself[6]. To our knowledge, applying such a comprehensive dating programme onto a single set of Egyptian vessels has never been done before. Finally, in the spirit of this thesis' advocation of a multidisciplinary approach to the study of Early Dynastic Egyptian material, it should also be noted that the work included gas chromatography mass spectrometry (GC-MS) analysis of the organic material to allow identification of the pot contents (presented in Appendix B).

2.3 Additional comparative ceramic material

This thesis presents the minimum extraction technique (MET), a new and novel sampling technique. As this technique was developed during the course of this project, and because experimentation was necessary during the initial development phase (in particular when determining necessary treatment protocols for the MET), it was necessary to work with plentiful material which was not from precious museum collections. The main reason for this was that the quantity of material required for experimental research and technique development was far greater than could be obtained from museum material. As already discussed, curators of Egyptian material prefer a minimal quantity of material to be extracted for analysis. Because Egyptian material is such a precious commodity in museums, none were willing to permit the extraction of more material than was necessary. The only exception to this was one vessel in the Bêt Khallaf assemblage held at the Penn Museum, which was not complete and had several sherds with it which had broken off from the main part of the vessel at an earlier date. It was agreed that in order to spare this vessel from further destructive analysis, a small disarticulated sherd would be collected instead. The quantity of material yielded by this sherd was far greater than what would be obtained by the MET, and thus we were able to use this sherd for

[6] It is of course possible the mineral component of the pot contents was post-depositional, but it is highly unlikely, as the material was recovered *in-situ*, and was extremely solid, not loose, and the sample was taken just under the exterior layer of the contents. Furthermore these vessels were excavated by Petrie, who noted the presence of the contents within the vessels. It is of course possible that the contents were added to the vessel after the vessel's first use, although absolute dating is able to shed light on these uncertainties.

perfecting some of the experimental analyses.

Although the additional sherd from the Penn Museum provided a good starting point, it was also necessary to have a larger data set of material in order to empirically determine a final and suitable 'recipe' for the MET. This material had to be from a recently excavated context, where there was no limit to the quantity of material obtainable, but it was also necessary to choose material that would be comparable mineralogically to Egyptian material (obviously, some degree of difference would be expected given that this material could not be sourced from Egypt). It should be noted here that the MET was first trialled prior to the commencement of this thesis, and the results were presented in a Masters thesis which focused on OSL dating of Madagascan ceramics (Hood 2010b). In order to use the MET for Egyptian material it was necessary to find material which was more mineralogically comparable. Fortunately, it was possible to obtain material from a site in Petra in Jordan, which was recently excavated by Brown University.[7] Material from Petra was suitable because several ceramics were obtained, all of which were large pieces of ceramic, which provided significant material for comparative tests, and they were considered to be similar mineralogically to the Egyptian material. The results of this experimental work will be discussed in Section 4.1.2.3.

[7] We are very grateful to the Brown University Project at Petra—in particular Tommy Urban, Emanuela Bocancea, and Sue Alcock—for allowing us to use this material.

Chapter 3

An introduction to the methodologies employed in this thesis

This chapter will present the multidisciplinary methodologies employed in this thesis. Although each method will be discussed in greater detail in the body of this work, this chapter provides an overview of each of the techniques, a history of their use in Egyptian archaeology, and a discussion of their benefits to this project.

3.1 Absolute dating methods

As already discussed, by employing absolute dating methods, and in particular OSL dating, this thesis is the first project to present absolute dates for an assemblage of ancient Egyptian ceramics. In addition, the relative chronology existing in the form of ceramic typology, is for the first time anchored to an absolute time frame, presented in the form of tangible calendar dates.

3.1.1 Optically stimulated luminescence dating

OSL dating belongs to the group of radiometric dating techniques known as radiation exposure dating or trapped charge dating. OSL is closely related to thermoluminescence (TL) dating although there are several key differences between the two techniques, dis-

cussed below in Section 3.1.1.1. The method is suitable for inorganic materials which contain minerals that can emit a luminescence signal, and it is generally useful for dating samples between the ages of *c.* 100 – *c.* 200 000 years (Walker 2005: 14; Fig 1.6).

OSL, like all luminescence techniques, is based upon the ability of naturally occurring radioisotopes to interact with mineral grains present within the fabric of ceramic material. The product of this interaction is what is measured to produce a date. Minerals naturally occurring in ceramic fabrics, especially quartz, act as a dosimeter and effectively record the amount of radiation which has been building up in the vessel since the last heating event, that is, firing. When a vessel is heated up to a temperature of approximately 400℃ and above, electron traps within the crystal structure of the quartz grains are 'reset'. The term 'reset' is used to mean that all the electrons within the crystal lattice structure of the quartz grains are returned to their state of minimum potential, that is, they are released from their traps. However, after the pot is fired and the traps are 'reset', naturally occurring radiation in the surrounding environment, particularly from Uranium (U), Thorium (Th), and Potassium (K), once again interacts with the crystal lattice and can excite electrons out of their state of minimum potential and up into electron traps. These electron traps then retain the excited electrons until they are subsequently released; electrons can be trapped for millions of years and an OSL signal can generally be measured up to about 300 000 years. It is the act of releasing these trapped electrons that produces a luminescence signal. By stimulating, or exciting, the electrons in a controlled laboratory environment, the electron traps are reset once again, and this act of controlled resetting creates a small burst of energy which is proportional to the amount of radiation the quartz grain has received over time, and more specifically, since it was initially reset during the firing process in antiquity. It is this burst of energy, which is emitted as light, that is measured and in turn provides the basis of an OSL date (see Aitken 1989: 148–149, Fig. 2, for a simplified illustration of and more detailed description of this process).

Luminescence dating was first considered as a potential chronometric dating tech-

nique after the observation of emitted luminescence of crushed pottery in the 1950s–1960s (Daniels et al. 1953; Grogler et al. 1960; Kennedy and Knopff 1960). Its true archaeological application to ceramic material was pioneered chiefly by Aitken from the 1960s to the 1980s (Aitken et al. 1964; Aitken et al. 1968; Aitken 1985; the reader is also referred to the following short selection of papers reviewing the application of luminescence dating to archaeology: Roberts 1997; Feathers 2003; Wintle 2008). Thermoluminescence (TL) dating was the original absolute dating methodology employed for archaeological ceramic material, noting that TL was developed post radiocarbon dating, but that TL offered a way to directly date the minerogenic material found in ceramics, unlike radiocarbon. It was not until 1985 that OSL made its way into the literature as a valid and promising luminescence-based dating technique, although it was initially only used for sediment dating (Huntley et al. 1985). While this remains the most common application of OSL, there has been an increase in the number of other applications of the method since *c.* 2000, including the dating of archaeological ceramic material (e.g. Atlıhan et al. 2012; Bailiff et al. 2010; Bailiff et al. 2013; Bailiff 2007; Barnett 2000; Benea et al. 2007; Blain et al. 2010; Brass and Schwenniger 2013; Feathers and Rhode 1998; Fitzpatrick et al. 2009; Guibert et al. 2009; Liritzis et al. 2001).

As already touched upon in Section 1.3, luminescence dating, and through association OSL, has often received rather negative feedback in Egyptian archaeology. This is probably due to the application of TL in a small number of early studies (Abdel-Wahab et al. 1996; Caton-Thompson and Whittle 1975; El-Fiki et al. 1994; Kroeper 2003; Riederer 1978; Sekkina et al. 2003; Whittle 1975) which were often unsuccessful or limited in dating ceramic material. This seems to have resulted in the subsequent absence of luminescence dating of Egyptian material from the literature for all but authenticity testing (Payne et al. 1977). Even a more recent communication, which discussed the legitimate limitations of luminescence dating in Egyptian archaeology, focused almost exclusively on TL, dismissing OSL without considering it in detail (Goedicke 2006: 360). Despite the fact that most past studies were carried out using what would now be considered out-

dated TL techniques, the general consensus remains the same: luminescence dating does not work in Egyptian archaeology (an exception to the general reticence about luminescence in Egyptian archaeology is Shortland (Shortland 2000: 93), who expressed the need for Egyptian archaeologists to understand and consider the scientific techniques now available and showed how they could improve current work and research; in this communication, Shortland offered an overview and brief discussion of the most common and generally applicable scientific techniques in Egyptian archaeology, including a discussion of the overall benefits of luminescence dating). Such an analysis fails to consider the significant watersheds in luminescence dating within other fields and the role it has played in revolutionising archaeological scholarship in other regions of the world. To name but a select few examples, OSL dating has been used: to help clarify the age range of *Homo floresiensis* in Indonesia (Morwood et al. 2004), to help identify the existence of pre-Clovis cultures in the Americas (Waters et al. 2011), to help date the earliest human remains found to date in Australia (Olley et al. 2006), to assist in the reassessment of controversial dates at the Jinmium rock shelter in Australia (Roberts et al. 1999), and to assist in the reassessment of the earliest human occupation in Australia (Gillespie 2002).[8]

This of course raises an important question: what is the difference between TL and OSL dating, and why can OSL be used more successfully on ceramic material, when the OSL technique was developed for sediments and TL was traditionally used for dating pottery?

3.1.1.1 What is the difference between TL and OSL dating?

The fundamental difference between TL and OSL is the way in which the electrons in the OSL/TL electron traps are stimulated in the laboratory. In TL dating, the electrons are stimulated in the laboratory by being heated up to approximately 400℃, whereas in OSL they are stimulated through exposure to light (generally blue light-emitting diodes).

[8] The reader is also referred to Feathers 2003 and Wintle 2008 for a more comprehensive overview of the application of OSL to archaeology and significant case studies.

Sunlight will also act as a stimulant to reset the electron traps, and hence an OSL sample needs to be extracted in specific lighting conditions (see sampling methodology below). More specifically, however, there are four main advantages to OSL over TL. First, TL generally requires a much larger sample size in order to prepare sufficient quantities of material for measurement, whereas OSL measurements can be performed on individual mineral grains.[9] Secondly, though other mineral components of the clay fabric may be used, OSL particularly favours the dating of quartz grains. Using pure quartz grains produces a clearer luminescence signal. In contrast, TL measurements are generally obtained from a fine-grained polymineralic fraction that produces a more complex signal, thus affecting the clarity of the analysis. Thirdly, an OSL signal is reset more readily than a TL signal, the latter originating from deeper, harder-to-bleach traps. Laboratory experiments have shown that for an OSL signal, exposure to sunlight of approximately 100 seconds bleaches the signal to less than 0.1% (Duller 2008: 7). In contrast, even after an exposure time of several hours, often over 30% of the TL signal remains (Godfrey-Smith et al. 1988). Since the traps are more likely to be fully reset at the time of solar exposure or during firing, the OSL method with its ability to almost completely empty the electron traps will be a more accurate representation of the levels of radiation accumulated in the quartz since firing (i.e. a more accurate date). The result of this is that an OSL signal generally produces more precise and accurate measurements. The final advantage of OSL over TL lies in the measurement protocol. In the single-aliquot regenerative-dose (SAR) protocol (Murray and Wintle 2000), the error of the equivalent dose (natural signal) measurement is reduced, because the signal is interpolated rather than extrapolated as in TL (Aitken 1998: 105; Murray and Wintle 2000; Lian and Roberts 2006; Wintle and Murray 2006)—the SAR protocol is further discussed in Section 5.2.2.

[9] It should be noted here that for authenticity testing, TL is conducted on a small sample size also. This is because the levels of precision required for a test of authenticity as opposed to obtaining an archaeological date are far lower, and therefore TL is suitable for determining artefact authenticity (Aitken 1989: 156).

3.1.1.2 How to obtain an OSL date

After sample extraction and preparation (Section 4.1), an OSL age is calculated using the following equation:[10]

$$Age\ (years) = \frac{equivalent\ dose\ (Gy)}{dose\ rate\ (Gy/year)} \tag{3.1}$$

where:

$$dose\ rate = internal\ dose\ rate + external\ dose\ rate. \tag{3.2}$$

Thus to calculate the age of a sample, we must calculate: the equivalent dose (D_e), the natural luminescence signal of the object, given in terms of the size of the radiation dose required to produce the measured luminescence; the internal dose rate ($\dot{D}_{int}$): radiation the sample receives from itself (i.e from the clay matrix of a vessel); and the external dose rate ($\dot{D}_{ext}$): radiation the sample receives from its burial environment (including cosmic dose rate ($\dot{D}_{cos}$)).

As discussed in Section 1.3 above, the OSL dating programme employed in this thesis seeks to obtain absolute dates directly from Egyptian ceramic material for the first time. Although it is unlikely that this work can achieve a high-precision dating programme (and indeed this is not the main focus of this project), through this work, it is hoped that the benefits of OSL dating can be clearly demonstrated. First, the research will provide an absolute date for the Bêt Khallaf ceramic assemblage and help anchor the early Third Dynasty to an absolute timescale; secondly it will illustrate the benefits of using OSL as a relative dating technique to better understand ceramic typology when absolute dates are unobtainable; and finally, it will illustrate how OSL can be used alongside other dating techniques, specifically radiocarbon dating, to provide a system for cross-checking and comparison of dating results.

[10] NB Absorbed radiation is measured in the SI (Système International) unit Gray or (Gy).

3.1.2 Radiocarbon dating

Radiocarbon dating is only employed in this thesis in a minor way, being used in Chapter 9 to illustrate the benefits of complimenting OSL dates with radiocarbon dates in instances where the same objects can be analysed by the two methods.

Radiocarbon dating is arguably the most well-known scientific dating method used in archaeology, perhaps owing to its being one of the first to be developed (Walker 2005: 17). In summary, a radiocarbon date is obtained by measuring the concentration of radiocarbon (^{14}C), an isotope of carbon which has a known half-life, that is, it decays at a constant measured rate. The measured quantity of radiocarbon found in archaeological material can then be used to deduce its age (Walker 2005: 18). The method is only suitable for organic material (i.e. material which contains the ^{14}C isotope) and it can be used to routinely date material up to an age of about 50 000 years (Walker 2005: 17).

Like luminescence dating, radiocarbon dating has a long but somewhat strained relationship with Egyptian archaeology. Egyptology's link with radiocarbon goes back to the origins of the method, when Libby, upon first devising the revolutionary technique, used a selection of Egyptian samples of apparently known age to demonstrate the applicability of radiocarbon to historical and archaeological questions (Arnold and Libby 1949: 678–680; Manning 2006: 327). However, although Egyptian data contributed positively to initial research into radiocarbon dating, it did not go unnoticed that inaccuracies and chronological discrepancies were frequent within the literature and a general consensus emerged that radiocarbon '[had] neither the accuracy nor precision to be of any real use to Egyptology' (Manning 2006: 328–329). From the late 2000s, this view has been changing, because more accurate, high-precision radiocarbon dates have been achieved using AMS (accelerated mass spectrometry) radiocarbon dating, and specifically through work carried out by the University of Oxford's Radiocarbon Unit (projects, led by C. Bronk Ramsey and M. Dee, include: Synchronising Absolute Scientific Dating and the Egyptian Historical Chronology; The Origins of Nationhood: A new chronology for the formation of the Egyptian state; Fractured Land: Drought and the fall of Old

Kingdom Egypt).

As discussed in Section 3.1.2 above, radiocarbon dating is only examined briefly in this thesis, presented as a case study which looks at a set of six vessels, to examine the benefits of using a comprehensive dating programme and of engaging in a suite of dating techniques to compliment and cross-check absolute dates obtained using other methodologies (i.e. OSL).

3.1.3 Bayesian modelling

Closely associated with radiocarbon dating is the use of Bayesian modelling to interpret and examine the archaeological data using mathematical and statistical analysis, specifically Bayes' theorem. This model-based approach allows known information to be incorporated into analyses and thus aid the interpretation process by building upon past research and drawing from known previous data (Buck 2005: 695). Specifically it allows other forms of archaeological data to be incorporated into the analysis and interpretation of absolute dates, such as known duration of archaeological phases or the certainty of phase-specific samples (Bronk Ramsey 2013: 33). Although Bayesian modelling has a well-established history within radiocarbon dating (e.g. Bronk Ramsey 2009; Bronk Ramsey et al. 2010; Dee et al. 2013; Needham et al. 1997; Savage 2001; Whittle et al. 2011), it is an approach that has only recently been utilised in OSL dating (e.g. Barton et al. 2009; Clark-Balzan et al. 2012; Cunningham et al. 2015; Guérin et al. 2015; Rhodes et al. 2003; Zink 2002; Zink 2013; Zink 2015), although this field is set to expand dramatically in the coming years.

In this project, for assessment of the OSL data from Bêt Khallaf and for the set of six vessels housed in the Ashmolean, we have engaged in multiphase Bayesian modelling to refine the (often broad) OSL dates by incorporating known relative chronological information, which has made it possible for improved chronological precision to be achieved for the two assemblages (see Section 5.4 and Section 9.5 for further details).

3.2 Relative dating methods

As already discussed, various methods of relative dating have been employed in Egyptian archaeology frequently and with great success. In the case of this thesis, which focuses on achieving the first absolute dates for Egyptian ceramic material, we have also employed relative dating techniques to cross-check and further understand absolute dates, and to be able to discuss these dates in their broader archaeological context. Further to applying OSL dating as a relative dating method as well as an absolute dating method, this thesis also employs morphological and typological assessment, and cladistic analysis.

3.2.1 Morphological and typological assessment

Morphological and typological assessment of artefacts is a valuable tool. It is a visual analysis used to examine the physical attributes and form of a vessel, as well as its clay characteristics, and compare it to other vessels that are similar, and hence likely to be its contemporaries. Such examination therefore seeks to find parallels for the object being discussed which cannot necessarily be examined through additional analyses, because the ceramic type being examined is rare and only known from a small number of contexts. As morphological assessment can be subjective, it is only employed as a complimentary element to other analyses and for discussion of results obtained using other methods.

3.2.2 Cladistic analysis

This thesis also employs cladistic analysis, a quantitative methodology used in the application of Darwinian evolutionary theory (i.e. using a phylogenetic approach) to the study of artefacts. Borrowed from the biological sciences, cladistics has been discussed and employed with increasing frequency over the past two decades as phenetic methods have now largely been abandoned (e.g. Barton and Clark 1997; Barton et al. 1997; Ly-

man and O'Brien 1997; Lyman and O'Brien 2006a; Lyman and O'Brien 2006b; Neff and Larson 1997; Broughton and O'Connell 1999; O'Brien and Lyman 1999; O'Brien and Lyman 2000; O'Brien and Lyman 2002; O'Brien and Lyman 2003; O'Brien and Lyman 2009; Preucel 1999; Collard and Shennan 2000; O'Brien 2001; Murray 2002; O'Brien, Lyman, and Darwent 2002; Gabora 2006; Lycett 2007; Buchanan and Collard 2008; see also Lipo et al. 2006 for an edited volume with select articles on this topic). Based on the concept of biological evolution that describes variation and changes in organisms through time via natural selection, cladistic analysis is a practical application of evolutionary archaeological theory that seeks to trace variations and changes in the archaeological record through time.[11]

In this thesis, cladistic analysis is applied to the study of Early Dynastic Egyptian ceramics to provide a more in-depth understanding of the developing ceramic corpus and to provide new insights into the features that signal gradual change in ceramic development. Cladistics here acts as another relative dating methodology which can assist in the fine-tuning of an absolute ceramic chronology achieved using scientific dating methods.

3.3 Chemical analysis

Two additional analyses are touched upon briefly in this thesis, although these were not central to the goals of this thesis but rather by-products of sampling protocols. GC-MS analysis, an elemental analysis used to discern the composition of organic material, was used to examine the contents of the ceramic vessels from the Tomb of Djer at Abydos, and of the two vessels from Naqada and Ballas. GC-MS analysis is considered a by-

[11] Evolutionary archaeology is a topic that has been and continues to be heavily debated and it is beyond the scope of this thesis to provide a comprehensive literature review on the subject. We refer the reader to the aforementioned references for a brief introduction to the concept of evolutionary archaeology and the surrounding debate. For the purposes of this thesis, we consider evolutionary archaeology to be identical to the theoretical approach used in the many works of O'Brien and Lyman, who in turn quote Endler 1986 in saying that evolutionary archaeology follows the concept of 'any net directional change or any cumulative change in the characteristics of organisms or populations over many generations—in other words, descent with modification' (O'Brien and Lyman 2000: 77).

product of OSL dating here as the contents of some vessels sampled were found to be a mixture of both inorganic and organic material. Therefore, when sampling the contents from the vessels for OSL dating, organic material suitable for GC-MS analysis was also procured. The results of GC-MS analysis are discussed in Appendix B. Additionally, ICP-MS analysis can be considered a by-product of OSL analysis (discussed further in Chapter 5) because a necessary component of the equivalent dose measurement, the internal dose rate, is determined by quantitative analysis of the elements of uranium, thorium and potassium, which are determined by ICP-MS. The results of ICP-MS analysis on clay samples can have implications for clay provenancing studies. Although these results are too preliminary to present in detail in this thesis, a brief communication can be seen in Appendix A.

Part II

Developing a new OSL sampling method for museum material

Chapter 4

The minimum extraction technique (MET)

4.1 What is the minimum extraction technique?

As already touched on in Section 1.3, the minimum extraction technique (MET) is a sampling protocol that was developed specifically to bring OSL dating to museum material, often the only material available for study, if the country of origin does not permit exportation of artefacts for scientific analysis or new excavations. The concept of the MET was briefly presented in a Master of Science thesis carried out at the Research Laboratory for Archaeology and the History of Art, University of Oxford (Hood 2010b), but is developed in full within this thesis, specifically for work on Egyptian ceramic chronology and now includes comprehensive MET sampling guidelines, validation of MET by comparing equivalent dose measurements on samples subjects to both MET and total extraction sampling techniques, and validation of the reduced reliance on a long HF etch time. This methodology has also recently been published in a peer-reviewed journal, see Hood and Schwenninger 2015.

4.1.1 Sample extraction

The minimum extraction technique is so called because of the very small sample size taken for measurement: it requires, in most circumstances, the removal of only a 2 mm $\times$ 4 mm core of material. When working on museum samples, it is of the upmost impor-

tance that sampling is done in a way which at all times upholds the aesthetic integrity of the vessel and the MET serves to ensure that damage to the vessel is kept to a strict minimum. The extraction of the sample results in only a very small hole (2 mm diameter) being created on the surface of the vessel (Figure 4.1).

Figure 4.1: Hole on the surface of a vessel resulting from MET sampling.

Furthermore, the sample can be taken from an inconspicuous area on the object, that is, from the base, under the rim, or from an exposed broken edge, further reducing its visibility. This hole can often be all but invisible, especially when drilled from a coarser fabric vessel, as it blends in with the natural blemishes present in the clay fabric. The unobtrusive sampling procedure of the MET has been met with approval by most museum curatorial and conservation staff approached during this project. In general, the base acts as a first choice for the drilling location as on the one hand, the base of the vessel is usually the most inconspicuous location for a sample to be removed, and on the other hand, the base of the vessel is usually its thickest part. Also, the base is often the preferred sample location for curatorial staff as the hole is not usually visible when on display. A visual depiction of the MET sampling procedure is presented in Figure 4.2.

The $\dot{D}_{int}$ sub-sample is extracted by a reusable 2 mm diameter ball diamond burr drill bit (Figure 4.3a) and should be stored in a gelatine capsule (for ease of weighing at a later stage for inductively coupled plasma mass spectrometry (ICP-MS) analysis—

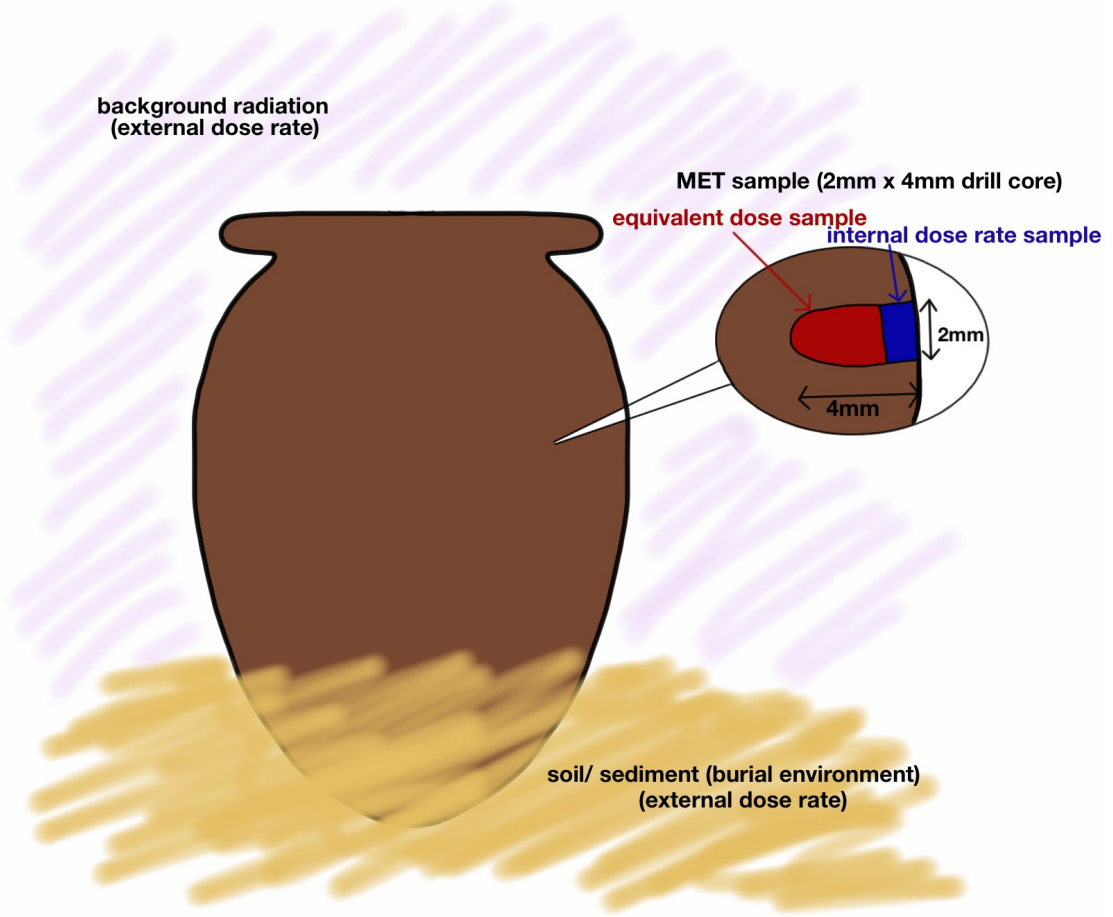

Figure 4.2: MET sampling schematic.

see Section 5.3.3).[12] The sub-sample used for the equivalent dose (D_e) measurement is then extracted using a 1.5 mm diameter diamond core drill bit (Figure 4.3b)—the smaller diameter ensures that no contamination occurs when drilling as the width of the drill bit is now smaller than the aperture of the sample location (1.5 mm instead of 2 mm). To avoid contamination, a new core drill bit is used for every sample. The extracted sample mainly constitutes a fine powder/dust and a small core that can be recovered from the interior of the drill head. The weight of the sample is usually 1–5 mg.

The drill heads are used in conjunction with a Dremel handheld Fortiflex drill for

[12] Initially the ICP-MS sub-sample was collected in small plastic bags, as is standard in regular OSL sampling. However, due to the very small sample yield of the MET, this method was found to be unsuitable. This was because the static charge and the porous interior of the plastic bag, meant the grains would adhere to the bag wall, making it almost impossible to extract and use. When extraction could be achieved, it usually resulted in some of the material being lost, and made it difficult to determine the exact weight of the sample for ICP-MS analysis. For this reason it is recommended to use a gelatine capsule.

ease of control and precision.

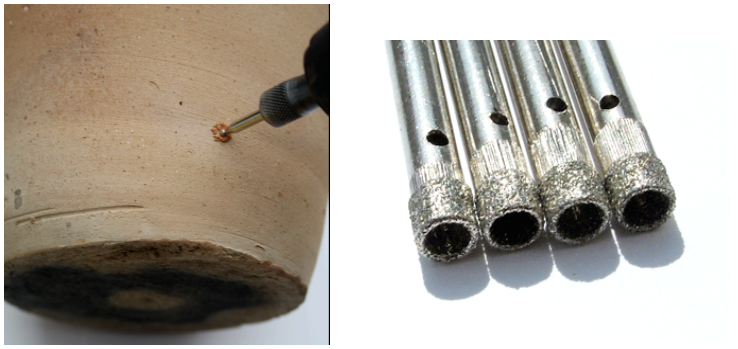

Figure 4.3: a) Diamond burr drill bit (left) and b) diamond core drill bits (right) used in MET sampling.

Sample extraction must always take place in conditions which prevent the exposure of the sample to light, usually in a darkroom-like environment with filtered red/yellow light only. An OSL laboratory is, of course, set up to meet these requirements. However, when sampling museum material it is usual to have to sample in the museum, owing to insurance concerns. Therefore, a suitable sampling location must be found prior to sampling, typically a small room which can be turned into a dark room, with subdued lighting conditions suitable for OSL sampling. In this study a portable filtered 590 nm LED strip was used for lighting once an area has been blacked out for sample preparation. Usually a small interior, windowless room or a storage cupboard was selected for this purpose.

Once drilled, samples are collected in small black opaque plastic vials, which in turn are double-bagged in black plastic opaque bags. This packaging protocol ensures that the MET samples are light-tight and can be transported safely for preparation and analysis in an OSL laboratory.

4.1.2 Coarse grains

Once the MET samples are collected, they are transported back to the luminescence laboratory, where sample preparation is carried out in subdued lighting conditions using yellow-orange light sources (filtered sodium lamps (588 nm) and LED lights (590

nm)). Furthermore, while sample preparation is carried out, unnecessary exposure even to subdued lighting is kept to a minimum, that is to say, samples are always kept in light-tight conditions when not being worked on. Although red/yellow light at a frequency of 588–590 nm will not readily affect (reset) the luminescence signal, prolonged or excessive exposure may affect the final measured signal.

Sample preparation essentially consists of the following: sorting of the grains by size, removal of the non-quartz component, and etching of the quartz grains.

4.1.2.1 Coarse grain sample preparation

Within the OSL laboratory, coarse grain sample preparation involves standard[13] treatment protocols, albeit slightly altered for the MET, using a five-step process in order to extract pure quartz for dating. Of these five steps, step three has been most significantly altered for the MET.

1. **Dry sieving**. The MET sample is initially sieved, using a small handheld test sieve, to isolate the following grain size fractions:

    - <90 μm
    - 90–180 μm [14]
    - 180–250 μm
    - >250 μm.

    The <90 μm fraction is reserved for sample preparation using the fine grain technique (Section 4.1.3). The >250 μm is kept, although is not used at present (it has been suggested that in future work, it might be possible to utilise the > 250 μm size fraction to undertake experiments in prolonged HF etching). It is possible that, by

[13] The term 'standard' in this context refers to those protocols used at the luminescence dating laboratory at the Research Laboratory for Archaeology and the History of Art (RLAHA), University of Oxford.

[14] With standard OSL protocols at RLAHA, it is usually typical to see the 90–180 μm fraction split between 90–12 μm and 125–180 μm. However, due to the tiny size of the MET sample, it is best to amalgamate these two size fractions together as the small quantity yielded across two individual fractions is often too small to work with efficiently.

subjecting large grain sizes to an etch time of several hours, both the alpha and beta attenuation layers might be removed from the grain, thus leaving only the gamma component to be determined (Pers. Comm. J.-L. Schwenninger, 2012).

2. **First HCl digestion**. The selected grain size fractions (usually 90–180 μm and 180–250 μm) are treated with hydrochloric acid (HCl, 10% concentration), until cessation of reaction. The purpose of this step is to remove any carbonates from the sample prior to subjecting the sample to the more vigorous hydrofluoric acid treatment. The HCl acid wash will dissolve any carbonates present.

3. **HF treatment**. The sample is then soaked in a solution of hydrofluoric acid (HF, 40% concentration) for ∼30 seconds, followed by four rinses in distilled water. It is this step where the MET sample preparation method varies most significantly from standard methodology as an etch time significantly less in duration is used for the MET as compared to standard OSL sample procedures. This is discussed in more detail below in Section 4.1.2.3.

4. **Second HCl digestion and final rinse**. After the HF wash, the sample is subjected to an additional HCl wash, which removes any fluoride precipitates. The sample is finally rinsed with distilled water and acetone.

5. **Drying**. Finally, the sample is placed in an oven until it is dried out (usually at an oven temperature of ∼30–∼50℃ for one day).

Upon the completion of these five steps, the sample is then ready to be prepared for sample measurement.[15]

[15] 'Drying' is the final step in MET sample preparation. However, it should be noted that the final step generally employed in standard OSL sample preparation is a final dry sieving in order to determine the size fractions of the initial sample after it has been subjected to an HF wash, thus allowing for the removal of any grains that have been fractured during the HF process.

4.1.2.2 Coarse grain aliquot preparation

After sample treatment, aliquots are made. An aliquot is the name given to the OSL sample once it is prepared and mounted on a small aluminium disc for machine measurement. In general, after treatment, the average grain yield for each MET sample was ∼20–∼40 grains. Of these, ∼10–∼30 are used to make between 2 and 4 multigrain aliquots and the remaining ∼10 grains are used for making single grain aliquots.

To make the aliquot, a small aluminium disc measuring 10 mm in diameter and 0.5 mm thick is used. A tiny drop of a silicon-oil is placed upon the middle of the disc. The grains from a sample are poured out onto a sterile piece of aluminium foil and are individually picked up using a tool made of a toothpick and a human eyelash. An eyelash is a perfect implement for picking up an individual grain of quartz both because it is supple and because it generally has a static charge which ensures a grain is picked up and adheres to the lash. Once isolated, the grain is transferred to the aluminium disc and placed within the silicon oil, to which it adheres. For multigrain aliquots, ∼5–∼10 grains are placed in the centre of the aluminium disc, whereas for a single grain aliquot a single grain is used (this way of preparing a single grain aliquot is unusual as it is more typical to use single grain discs, i.e. an aluminium disc with pits in the surface which can carry up to 100 single grains, rather than mounting a single grain on a standard aluminium aliquot disc).

Upon completion, the discs are transferred into a light-tight holder (which in turn is double-bagged in black opaque plastic), and can be stored until ready for measurement.

4.1.2.3 HF acid treatment protocol

As already mentioned, coarse grains are treated in hydrofluoric acid (HF). HF is used in sample preparation for three main reasons: first, it dissolves feldspar minerals within the samples, ensuring that, when measured, no luminescence signal is present for minerals other than quartz (Aitken 1985: 256); secondly, HF cleans the surface of the quartz grain and helps to remove impurities formed during the firing process (Aitken 1985: 256;

Fleming 1979). Finally, and most importantly, HF etches the quartz, which is thought to remove the exterior layer of the quartz which has absorbed an alpha dose (D_α) (Aitken 1998: 66–68). Of the three types of radiation naturally occurring, alpha, beta, gamma (excluding cosmic), each penetrates objects to different depths. With an individual coarse quartz grain, the beta, gamma and cosmic rays will go through the grain in its entirety, but in contrast D_α will only penetrate to a depth of ∼23–∼47 μm (Aitken 1985: 253). If this D_α layer can be etched away during an HF treatment, the alpha dose rate ($\dot{D}_\alpha$) can be factored out of the $\dot{D}$ calculation. That is, if the D_α contribution to the OSL signal is removed, only the beta ($\dot{D}_\beta$), gamma ($\dot{D}_\gamma$) and cosmic ($\dot{D}_{cos}$) dose rates need to be considered in the final age calculation.

As the MET sample is minute to begin with, it was quickly observed that standard HF protocols (i.e. 45 minutes in HF, 40%) are not appropriate for MET samples. This is because HF is so aggressive in its interaction with the sample material, that it often completely dissolves it. The net weight and volume of a standard OSL sample is often dramatically reduced during HF treatment, but in general the quantity of material being treated is around 1000–100 000 times larger than a MET sample (dependent upon sample type), and therefore far more material remains after etching. It is also possible that extracting the MET sample with a drill causes fractures in the crystalline structure of the quartz, which weakens the sample prior to the HF treatment. This may result in the quartz breaking up more readily, thus giving the HF more surface area upon which to work, resulting in more of the quartz being etched away.

Even for standard OSL samples, it has long been suggested that HF etching does not achieve isotropic removal of the outer surface of the quartz grain, 'because of the tendency of quartz to etch preferentially along dislocation lines in the crystal lattice structure' (Aitken 1985: 256; cf. Lang and Miuscov 1967). Therefore it is likely that, even with a standard sample, the alpha contribution will never be entirely removed and will always be a further consideration in dose rate calculations (Lang and Miuscov 1967; Bell and Zimmerman 1978). This has led to the general consensus that the effect of HF

protocols strongly depends on the characteristics of the quartz, and individual samples can act very differently from one another, depending on their geological provenance and even the behaviour and composition of individual quartz grains (see, for example, discussions presented in Sawakuchi et al. 2011; Pietsch et al. 2008; Preusser et al. 2006). Consequently, in some cases it can be justifiable to use reduced HF times or indeed remove the HF etch completely, choosing instead to determine the contribution of the alpha dose, as is standard practice in the fine grain technique (Adamiec and Aitken 1998: Table 7; Brennan et al. 1991; Brennan and Lyons 1989; Clark-Balzan 2012).

For the MET samples from Egyptian contexts examined for this project, it was decided that a significantly reduced HF treatment time would be beneficial, in order to prevent excessive sample loss, which would result in fewer OSL measurements. We did not wish to eliminate the HF step altogether, however, because it was observed that even a short HF wash can significantly improve the intensity of the OSL signal as the quartz grains were often covered in fine clay particles which impeded the OSL signal—a short HF time permitted the removal of such particles as well as generally 'cleaning' the sample. However, in order to validate the decision to eliminate a longer HF etching time, tests were conducted on both an Egyptian sample (sample X5460) and a sample from Petra, Jordan (sample X6307), to determine whether a reduced HF time would significantly affect the equivalent dose measurements obtained. It was hypothesised that a longer HF time would result in systematically lower D_e measurements as it would not include the alpha dose component of the dose.

Sample X5460, an Egyptian sherd from the University of Pennsylvania Museum of Anthropology and Archaeology, was used for this HF etch time experiment. This sherd had already become detached from the vessel, and was offered by the museum as a larger sample which could be used for additional experimentation. The sample was divided into three sub-samples, all of equal mass. Each of these samples was extracted according to standard protocols. At step three of the treatment process, each of the sub-samples were given three different treatments. The first sample was not subjected to any HF treatment

(i.e. it was mounted as it was). The second sub-sample was only subjected to an HCl wash. The final sample was washed in HCl and then etched in HF for 30 minutes.

After measurement, each sub-sample was examined under a scanning electron microscope (SEM) to assess the visible effects HF treatment had on the individual grains. Findings were in agreement with those discussed by Bell and Zimmerman (1978), in that etching had significantly altered the morphology of the surface of the grain. With no treatment or HCl wash only, the grains still had attached to them small clay particles and other debris. A 30 minute etching in HF resulted in grains with a more opaque, frosty surface which was heavily pitted. Thus, morphologically, the grains were visibly altered during the HF process. The change in surface morphology of the grains gave further weight to the theoretical assumption that a shorter HF treatment time would result in a systematically higher D_e being measured as the alpha dose contribution would be removed to a lesser extent. However, when measured, the aliquots made up of different sub-samples produced no statistically significant correlation between the HF treatment and the D_e measurement (Figure 4.4). Although in Figure 4.4 it appears that the aliquots etched for 30 minutes in HF mainly cluster at the top end of the graph, the reason we can state that there is no difference between the D_e based on HF time is that an HF treatment should remove a part of the dose contribution and thus would produce a D_e measurement of a lower value compared to those aliquots with no HF or reduced HF treatment. Therefore, these experiments illustrate that a prolonged HF treatment does not necessarily remove the expected dose contribution of the alpha dose and thus the assumption that a long HF etch will achieve this does not appear to be valid. While at this stage, with a limited dataset we can not make any statistically determined statements, future experiments and an increased dataset is likely to give support to the claims presented here that a prolonged HF etch does not remove in full the alpha dose contribution of the quartz grain. Indeed, the data indicates that there is no benefit from an increased HF etch time and that all D_e measurements were well within error, regardless of the time for which a sample was etched.

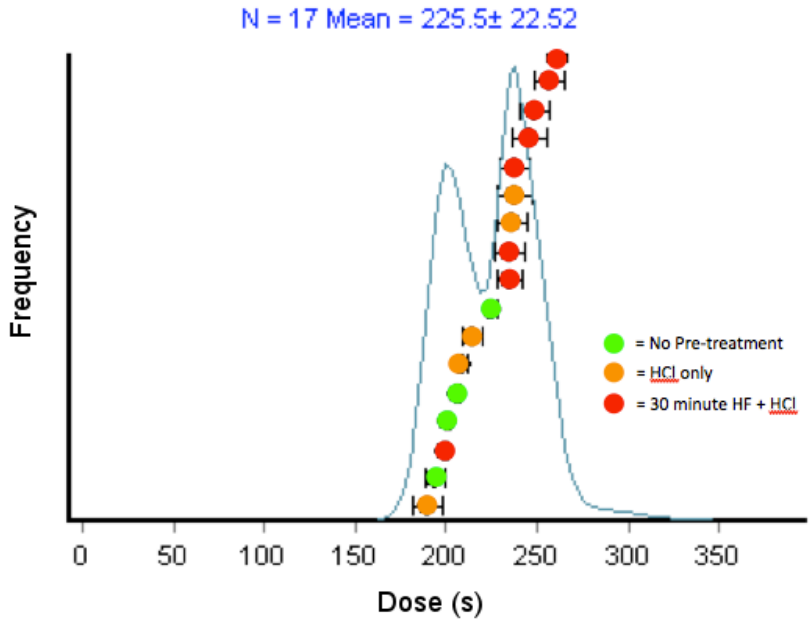

Figure 4.4: D_e measurements and their corresponding treatment times for sample X5460.

To further extend the data set for HF treatment times, it was decided to slightly alter the treatment protocols for each of the sub-samples of X6307 (a large sherd recently excavated from the Brown University excavations at Petra which could be used for multiple experimental analyses) so that they added to the data already collected from sample X5460. Sample X6307 was divided into five sub-samples. The first was subjected to HCl treatment only. The other four samples were washed in HCl initially, but they were also subjected to different HF etching times: the second sub-sample underwent a 5-minute HF wash, the third a 15-minute HF wash, the fourth a 30-minute HF wash and the fifth a 45-minute HF wash.

Again, we observed the same morphological surface changes in the samples: the HCl-only wash resulted in remnants of clay particles and debris still adhering to the surface of the grains. A 5-minute HF etch resulted in a 'clean' sample, and the grain surface was shiny and sharp. The increasing treatment times showed a steady progression of grains with a more pitted surface, which were increasingly opaque and increasingly rounded in grain shape, rather than the more sub-angular grains witnessed with a shortened HF time.

In keeping with the initial hypothesis, it was assumed that a shortened HF time would result in systematically higher D_e measurements. Yet once again, sample X6307 showed that this assumption was not valid: there was no correlation evident between HF treatment times and the corresponding D_e measurement (Figure 4.5).

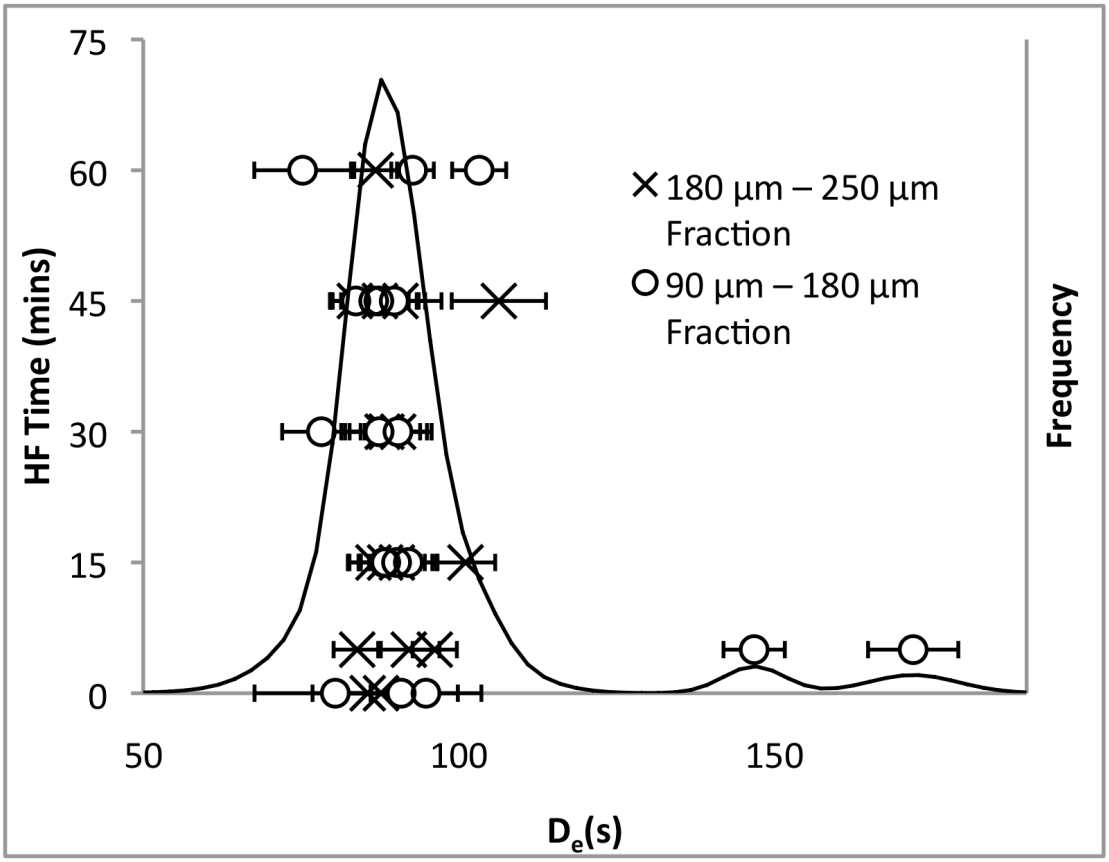

Figure 4.5: The effect of HF treatment time on the equivalent dose for two grain size fractions in sample X6307. No trend can be observed. The solid line is the probability distribution function (PDF) of the distribution of aliquots for the sample.

These experimental results obtained from samples X5460 and X6307 therefore support the discussions of Aitken 1985: 256, Lang and Miuscov 1967, Schultz 1980, and Bell and Zimmerman 1978, in which it was suggested that etching of the quartz grains did not always occur isotropically. If this is indeed the case, this means that previous assumptions of the $\dot{D}_\alpha$ contribution and its etching away by HF acid treatment require further, in-depth study in future work.

As these experiments on samples X5460 and X6307 indicate that there is no dis-

cernible difference between an increased HF time and no HF treatment, it was felt these results justified only using HF to clean the sample prior to measurement. A reduced HF time can result in non-quartz mineral contaminants such as feldspars still being present in a sample. It is possible to examine aliquots under an SEM after the OSL measurement to determine whether the signal is coming from quartz or other minerals within the sample. However, a less time-consuming practice is to use an infrared stimulated luminescence (IRSL) signal rejection criteria (e.g. Duller 2003; Mauz and Lang 2004) and/or determine an IRSL/OSL ratio, by using a post-IR blue OSL procedure (Banerjee et al. 2001). The latter was chosen in this thesis, and forms part of the aliquot rejection criteria outlined in Appendix D.

4.1.2.4 Validating the MET technique

In addition to examining the potential correlation between D_e values and HF etch time, it was also necessary to determine the reliability and validity of the MET protocol. Thus, the MET was also tested against standard ceramic OSL sample preparation in the Research Laboratory for Archaeology and the History of Art, University of Oxford. Measurements were carried out to determine whether the D_e measurements obtained from a sample using the MET protocol were statistically different from those obtained from a sample prepared using the traditional technique, referred to as 'total extraction' (TE). In the TE method, a sample size of $\sim$6 cm^2 is collected, comprising both the D_e and internal dose rate sample—this is approximately 500 times larger than an MET sample (i.e. $\sim$6000 mm^3 as opposed to $\sim$12 mm^3). For this experiment, sample X5460 was once again used for analysis.

In this experiment, aliquots were made for each of the following sub-samples of X5460 (the quantity of aliquots made was dependent upon sample yield after treatment):

- MET sample, 30–60 seconds HF treatment (8 aliquots, of which 2 are multigrain ($\sim$25 grains) and 6 are single grain)
- TE sample, no HF treatment (6 aliquots)

- TE, HCl treatment only (7 aliquots)
- TE sample, HCl + 30-minute HF treatment (18 aliquots, of which 1 is multigrain (∼30 grains) and 17 are single grain)

The results, presented in Figure 4.6 and Figure 4.7, show that there is no difference, outside normal expected errors, between those coarse grain samples extracted using MET sampling protocols and those obtained using TE sampling protocols, and again that no correlation is seen between different treatment protocols and D_e values. Again, it is felt that for museum samples requiring MET sampling, these experimental results illustrate the potential for the MET to be a beneficial and useful sampling protocol for museum specimens.

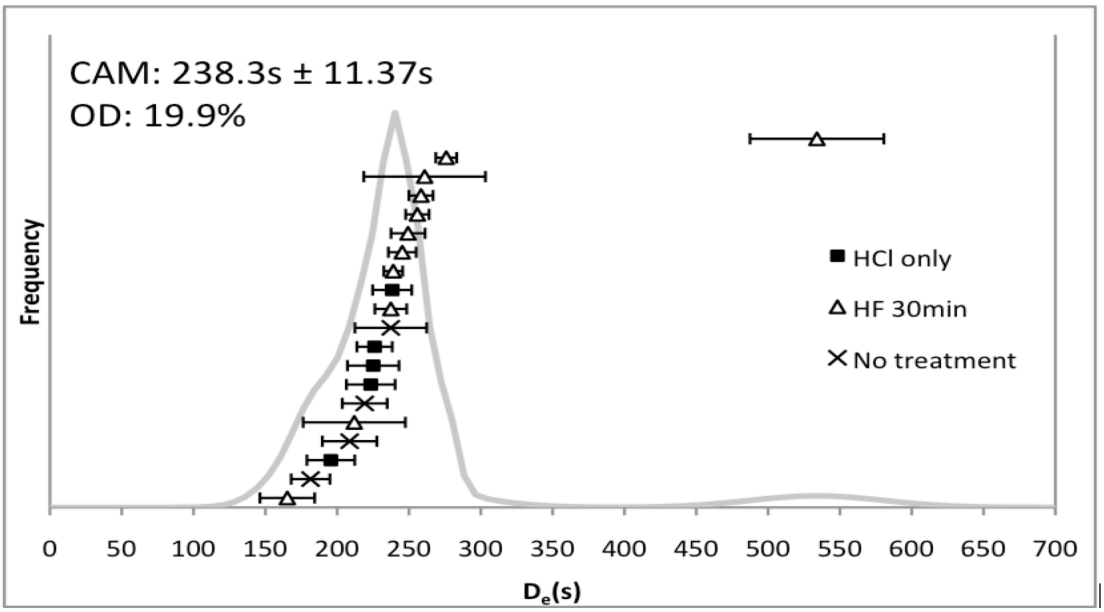

Figure 4.6: Probability distribution function (PDF) of multigrain D_e distribution for X5460, when sampled using the total extraction technique. Treatment type indicated on key. Multiple grain size fractions used (90–250 µm).

4.1.3 Fine grains

Owing to the considerations surrounding the coarse grain preparation using MET samples (i.e. a significantly reduced HF time), and to its being observed that several samples

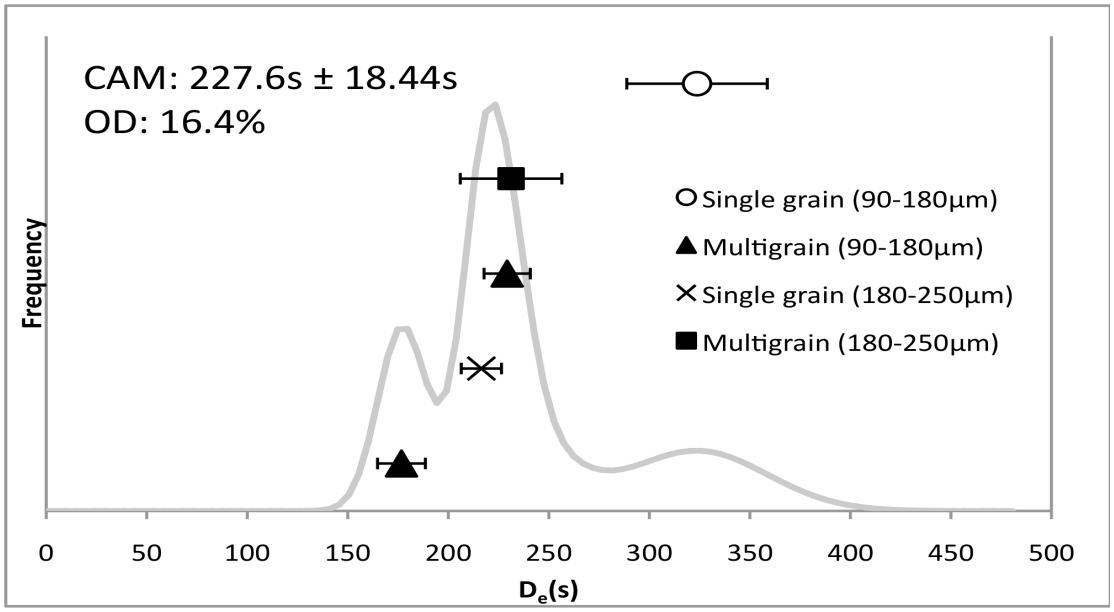

Figure 4.7: Probability distribution function (PDF) of aliquot distribution for sample X5460, when sampled using the minimum extraction technique. Treatment = ∼30 seconds HF + HCl. Grain size fraction indicated on key.

did not yield coarse grain results (particularly those samples made of fine material), the fine grain preparation method was also undertaken. This method compliments the MET protocol well. It completely negates the need for removing the alpha attenuation layer from the grains, since, for the grain size fraction that fine grains deal with, that is, 4 µm–11 µm, the alpha dose contribution is irrelevant. At this size, any alpha component irradiates the whole grain (Aitken 1985: 24). The fine grain method was first described by Zimmerman (Zimmerman 1967; Zimmerman 1971), although subsequent alterations have been made to the Zimmerman method (e.g. Frechen et al. 1996; Fleming 1975; Fleming 1979: 58–59).

4.1.3.1 Fine grain sample preparation

The fine grain sample preparation method used in this study was slightly altered from standard[16] preparation methods, owing to the small sample quantity of minerogenic material produced by the MET. Here we used a four-step process. Of these four steps,

[16] The term 'standard' in this context refers to those protocols used at the luminescence dating laboratory at the Research Laboratory for Archaeology and the History of Art (RLAHA), University of Oxford.

Steps 2 and 3 have been most significantly modified, because of the need to calculate accurate settling times to separate the 4 μm–11 μm grain size fraction.

1. **Dry sieving**. When the MET sample is initially sieved, as described above in Section 4.1.3.1, the < 90 μm grain size fraction is retained for the fine grain technique.

2. **First settling**. To isolate the 4–11 μm fraction, it is necessary to settle the grains in a water column, using Stokes' law to determine the correct settling times for procuring this size fraction. As the sample used for fine grain analysis is initially the < 90 μm fraction, the first settling step requires the removal of the 12–90 μm grain size fraction. Using Stokes' law (see, for example, Batchelor 2010: 230–235), a calculation was made to determine the time it would take grains larger than 11 μm to settle in a solution of deionised water, based on the density and viscosity of the water, the temperature of the water, and the height of the graduated cylinder in which they were being settled. For this work, we used a 10 mL graduated cylinder, for which the settling times are presented in Table 4.1. These settling times were based on the average ambient temperature of the deionised water stored in the RLAHA OSL laboratory, which fluctuates between 19℃–26℃ (the settling times presented in Table 4.1 and Table 4.2 are based on an average temperature of 19℃; however, the water used for each sample was measured prior to settling, and the exact temperature was used to calculate settling times).

   This first settling step therefore removes the grains larger than 11 μm. The water (which, after settling, now contains only grains smaller than 11 μm) is decanted into an identically sized graduated cylinder, leaving the settled material (i.e. the material remaining at the bottom on the cylinder was 12 μm–90 μm, which was then collected and stored).

3. **Second settling**. Once the water containing the <11 μm grain fraction is decanted into an identical cylinder at the end of Step 2: this commences Step 3. This step repeats the same process as described above, but as we are now isolating the 4 μm–

Table 4.1: Settling times (at 19℃) to remove the 12–90 μm grain size fraction.

Cylinder volume	Cylinder height	Drop height (average of cylinder height)	Settling time
25 mL	9.7 cm	4.85 cm	7 min 38 sec
10 mL	8.6 cm	4.3 cm	6 min 46 sec

11 μm grain size fraction, the settling times are adjusted accordingly (see Table 4.2).

Once the settling is achieved, the water suspension is discarded (since this only contains grains 3 μm or smaller).

Table 4.2: Settling times (at 19℃) to isolate the 4–11 μm grain size fraction.

Cylinder volume	Cylinder height	Drop height (average of cylinder height)	Settling time
25 mL	9.7 cm	4.85 cm	57 min 41 sec
10 mL	8.6 cm	4.3 cm	51 min 8 sec

4. **Preparation of liquid suspension**. The material left in the base of the cylinder after Step 3, that is, the 4 μm–11 μm grain size fraction, is carefully washed into a small glass vial using acetone and is then stoppered and kept in liquid suspension for aliquot preparation.

Upon the completion of these four steps, the sample is then ready to be mounted as fine grain aliquots (see Section 4.1.3.2).

The fine grain preparation process was first tested on a brick sample for which a large quantity of material was available for analysis. This made it possible to test the settling method, to ensure that the 4–11 μm fraction was being correctly isolated. Two test suspensions were measured, one using a 10 mL graduated cylinder and the other using a 25 mL. Once aliquots were prepared, they were examined under an SEM to determine whether the settling times accurately isolated the 4–11 μm grain size fraction.

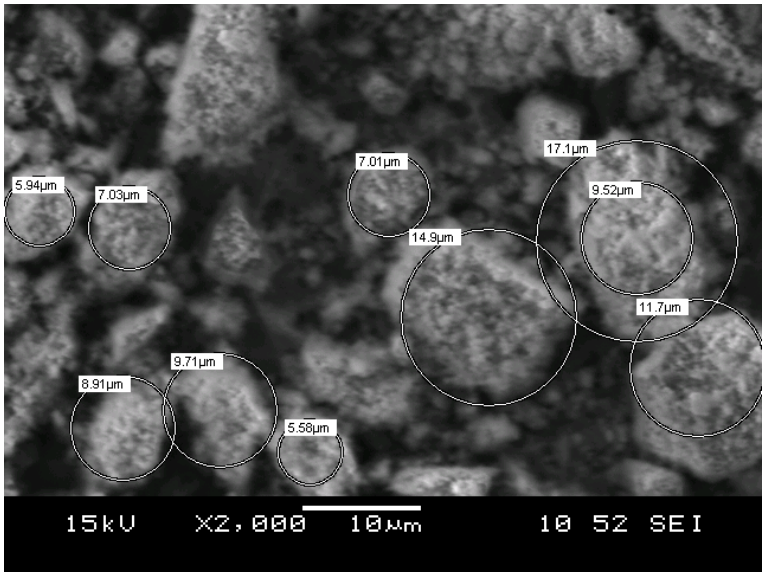

Figure 4.8: SEM image showing distribution of fine grain sizes for the brick test sample after settling to isolate the 4–11 µm fraction.

The SEM examinations showed that both the 25 mL cylinder and 10 mL cylinders were ideally suited to grain settling, with the large majority of grains being within the 4–11 µm fraction, although with some slightly smaller (∼3 µm) and some slightly larger (∼12–∼15 µm) grains occurring too (Figure 4.8). Given that this slightly increased grain size distribution is inevitable due to the use of average heights of water columns and assumption of spherical grain geometry upon which Stokes' law is based, it was considered that this methodology had worked sufficiently well for it to be used for fine grain preparation within this project. It was decided that the 10 mL cylinder would be used in sample preparation, however, as the smaller cylinder sizes made it easier to work with the small sample sizes provided by the MET.

4.1.3.2 Fine grain aliquot preparation

After isolating the 4 µm–11 µm grain size fraction, the fine grain aliquots are made. To make the aliquot, as with the coarse grain technique, a small aluminium disc 10 mm in diameter and 0.5 mm thick is used. The disc is placed in a small glass vial (measuring 12 mm diameter and 38 mm in height). It is essential that the disc is lying flat on the

base of the vial so that the fine grains can not become trapped under the disc, which would affect the preheating of the aliquots when being measured. This can be achieved by placing ∼0.25 mL of acetone in the vial and then placing the aluminium disc on top that (this creates a suction force and the disc remains at the bottom of the vial).

The glass vial containing the sample prepared in Step 4 above is then agitated (to ensure that all grains are once again in suspension) and, using a disposable pipette, ∼1 mL of liquid sample is added to the vial and is left to settle on to the disc.[17] This vial is then left open and placed in a fume cupboard so that the acetone can dry off. Once the acetone is evaporated, the disc can be removed from the vial—it should have upon it a thin monolayer of fine grains which have settled upon its surface during the evaporation process. The aliquot is then ready for measurement and should be stored in a light-tight disc holder until that time.

4.2 Summary remarks on the MET and its suitability

By using the MET, and combining both coarse and fine grain analyses, we have a powerful tool to determine D_e estimates for museum ceramics. Clearly, owing to the very small sample yield resulting from MET extraction, working with all grain size fractions produces a larger, and therefore more robust, data set for the OSL age determination. Furthermore, both coarse and fine grain analyses have distinct advantages and disadvantages. On the one hand, by working on the coarse grain fraction, we can work exclusively with pure quartz from the sample, and not rely solely upon a polymineralic fine grain fraction, which can potentially cause interference within the quartz luminescence signal. On the other hand, when measuring the fine grain fraction, it is not necessary to treat fine grains with HF or to take into account alpha attenuation in the grains. In addition, as $\dot{D}_{int}$ for fine grains includes a large alpha dose component (and is therefore

[17] In standard fine grain aliquot preparation, it is necessary at this step to be very careful not to use too much liquid and thus allow too many fine grains to adhere to the disc. It is often necessary, in standard methodology, to dilute the sample suspension. However, due to the very small amounts sampled using the MET, it has been observed that this quantity produces a good suspension for aliquot making (i.e. not too cloudy, that is, not too many grains present), which means it is not necessary to dilute the sample.

typically larger than for coarse grains), the relative contribution of $\dot{D}_{ext}$ to the total dose rate is diminished (Aitken 1985: 25). Since the error in $\dot{D}_{int}$ is generally lower than the error on $\dot{D}_{ext}$ (given the need to model $\dot{D}_{ext}$ to some extent, see Section 5.3.6), this can result in a lower error for the total $\dot{D}$. Thus, by using two methods—both fine grain and coarse grain analysis—which require differing assumptions, in particular about the nature of the process of irradiation during deposition in the archaeological record, the systematic errors resulting from these assumptions can be detected and reduced.

The MET is a suitable alternative sampling and measurement protocol for conducting OSL dating on museum material. While it cannot produce results with the same levels of accuracy as material obtained from recent excavations (due to a greater number of uncertainties in the calculation of the external and internal dose rates), the MET is a viable alternative for constructing absolute ceramic chronologies from museum specimens.

Part III

OSL dating of Early Dynastic Egyptian ceramics from Bêt Khallaf

Chapter 5

OSL results from Bêt Khallaf

5.1 An introduction to the OSL results

One of the main goals of this work is to examine how OSL dating can contribute to the discourse surrounding the ceramic chronology of the later Naqada III period. Although high chronological precision is not within the scope of this work, it is hoped that by incorporating OSL dating into the study of Egyptian ceramic chronology (working with museum material in particular), it will be possible to illustrate that OSL is a technique which can provide significant new information and can further our understanding of studied archaeological assemblages.

A data set of 24 ceramic vessels from Bêt Khallaf was chosen, the assemblage being representative of the transitional period between the late Naqada III period and the early Old Kingdom. Appendix C presents a catalogue of these 24 ceramics from Bêt Khallaf. As already discussed, there has been a recent renewal of interest in this traditionally understudied period, and the time is now ripe for examining what can be added to the current state of knowledge by absolute chronological and scientific methods.

However, prior to examining the OSL results from Bêt Khallaf in full, it is first necessary to discuss the measurements, procedures, and protocols used in this thesis for determining the equivalent dose (D_e) and the dose rate ($\dot{D}$), which jointly form the factors involved in determining a final age calculation—as discussed in Section 3.1.1.2—for

each ceramic sample.

5.2 Equivalent dose (D_e) measurement procedures

5.2.1 Equipment

All OSL measurements were carried out on a Risø automated TL/OSL DA-15 luminescence reader (Riso 2007) housed at the RLAHA luminescence dating laboratory, University of Oxford. Aliquots were analysed using the Analyst software package (Duller 1999).

Samples were measured using a post-IR blue OSL procedure. Developed by Banerjee et al. 2001, the post-IR blue OSL dating procedure ensures that the signal from any possible feldspar contaminates are depleted by an IR exposure prior to measurement of the OSL signal using blue light. Some feldspars were found to be present in the samples by SEM analysis; however, the IRSL luminescence signal from these could be sufficiently removed using the post-IR blue protocol. Optical excitation was done using filtered blue diodes (410–510 nm emission) and infrared stimulation was done using IR diodes (870 nm). The resulting luminescence signal for each aliquot was detected in the UV spectrum (370 nm) by an EMI 9635Q bialkali photomultiplier tube (PMT), which was fitted with a 7.5 mm Hoya U340 glass filter (Riso 2007). Irradiation of the sample was carried out with a sealed ^{90}Sr (strontium) beta source at a rate of $\sim$2.3Gy/min, with calibration carried out using Risø calibration quartz (Hansen et al. 2015), calibration being necessary to determine the correct dose rate the sample is receiving from the ^{90}Sr source at a given point in time (discussed further in Section 5.2.2).

5.2.2 D_e measurement

The luminescence of each sample is dependent upon the geological history of each grain contained within it and in order to accurately determine the natural luminescence response from a sample, the signal must be compared against a series of laboratory doses

given to the sample using the integrated ^{90}Sr source in the luminescence reader. This can be done by using either an additive dose method or a regeneration method (Duller 2008: 9). The latter is now the more routine, and this is the method that has been used for the determination of D_e in this project using the single aliquot regenerative dose (SAR) measurement protocol.[18]

The SAR protocol was developed in 2000, and further in 2006, and has been used routinely in OSL dating applications since this time (Murray and Wintle 2000; Wintle and Murray 2006). Its benefits over previous protocols are significant: first, it has been found that this protocol is applicable to many quartz samples and that OSL dating using this protocol has produced results in excellent agreement with pre-existing independent age controls (Duller 2008: 11; Rhodes 2011; Murray and Olley 2002; Rittenour 2008; Rhodes et al. 2003). Secondly, SAR applies a series of varying laboratory doses on a single aliquot, thus requiring a smaller sample size than other methods (and hence of particular importance to this project where we are dealing with museum material). Additionally, the natural OSL signal is interpolated from the regenerative dose response curve determined by a series of SAR cycles, rather than extrapolated as with other methods. Figure 5.1 shows a pictographic representation of the SAR protocol.

Although the SAR protocol has several benefits as outlined above, its main advantage lies in its ability to apply a quartz sensitivity correction to the measurement, by using a test dose step within each SAR cycle. Wintle and Murray showed that the heating of quartz can often change the luminescence properties as traps within its crystal lattice structure that give rise to luminescence are redistributed by each heating event (Wintle and Murray 1999). As heating is a vital component of each SAR cycle, using a test dose (Tx) and second OSL measurement (Lx) after the natural and each subsequent regenerative dose measurement allows a sensitivity correction to be made by using the ratio Lx/Tx. This normalises both measurements and determines the growth curve for

[18] The additive dose method, in contrast to the regenerative method works by giving the sample an additional dose on top of the already existing natural signal. Its primary disadvantage is that it requires multiple aliquots, which are not guaranteed to be identical to one another, and also that the equivalent dose is extrapolated, rather than interpolated.

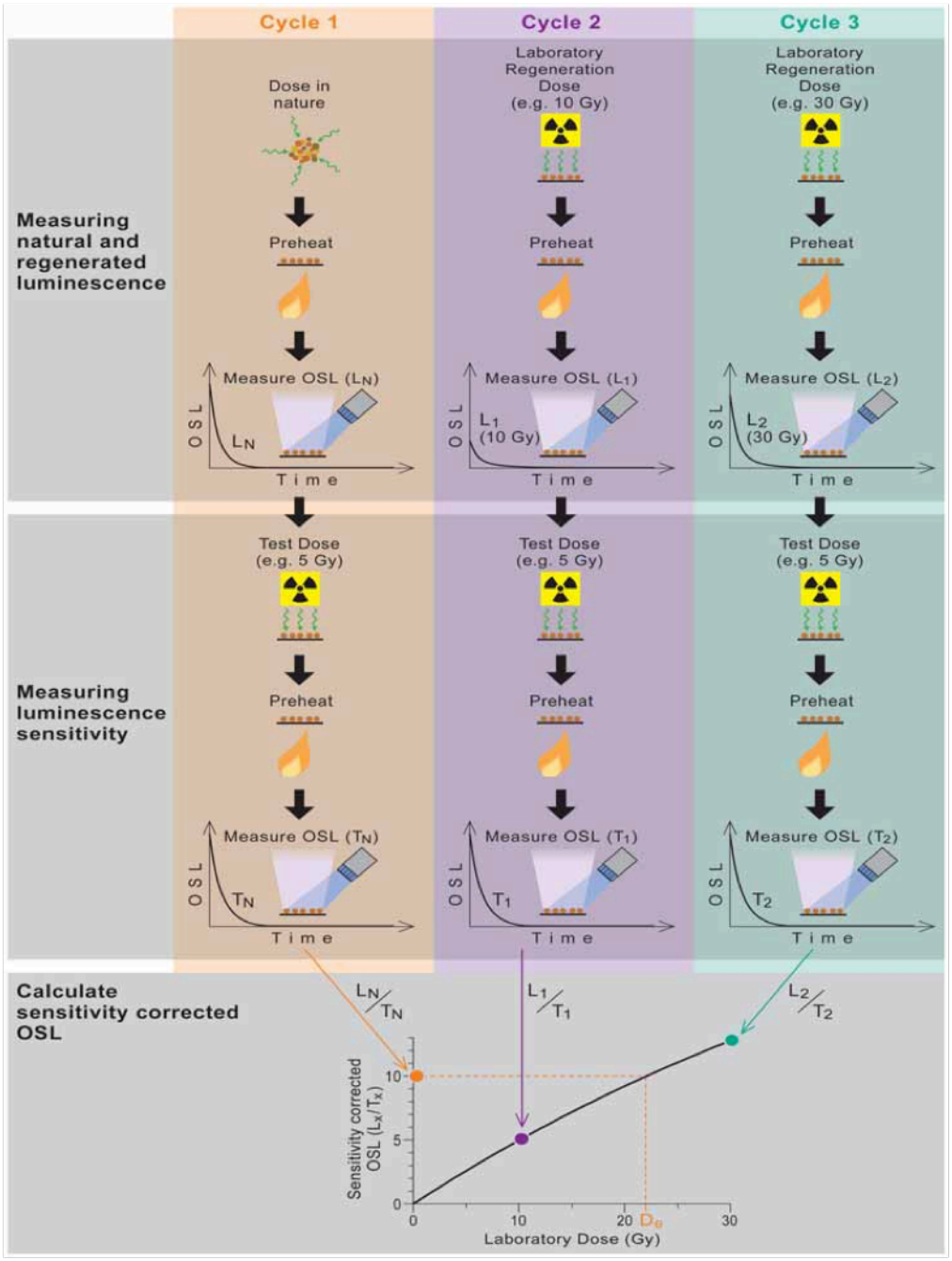

Figure 5.1: A step-by-step visual guide to the SAR protocol (taken from Duller 2008: 10).

each aliquot (Rhodes 2011: 471; Preusser et al. 2008: 112).

Additionally, prior to measurement of an entire data set, it is best practice to carry out two additional tests to ensure that the material being worked on is suitable for OSL measurement and that the characteristics of the quartz make it conducive to reliable dating. These tests are a preheat test and a dose recovery test.

The preheat test is carried out to ensure a correct temperature is selected prior to each OSL measurement. The preheat step rids the quartz of unstable signal components. To determine to what temperature the sample should be preheated, several aliquots for a sample are heated to a variety of temperatures ranging between 160℃ and 300℃, and the value at which the resulting D_e measurements remains constant is the temperature at which subsequent samples in the data set are preheated (Duller 2008: 12). Although in an ideal situation a preheat test would be carried out for each individual sample comprising a single data set this is not always possible due to machine time constraints and also, particularly in the case of this project, due to the very small quantity of material available for each sample. After a preheat test was conducted on Bêt Khallaf sample X5460, a preheat temperature was chosen of 240℃/220℃ (prior to the natural/regenerated luminescence measurement, and the luminescence sensitivity measurement, respectively). Figure 5.2 presents the results of this preheat test.

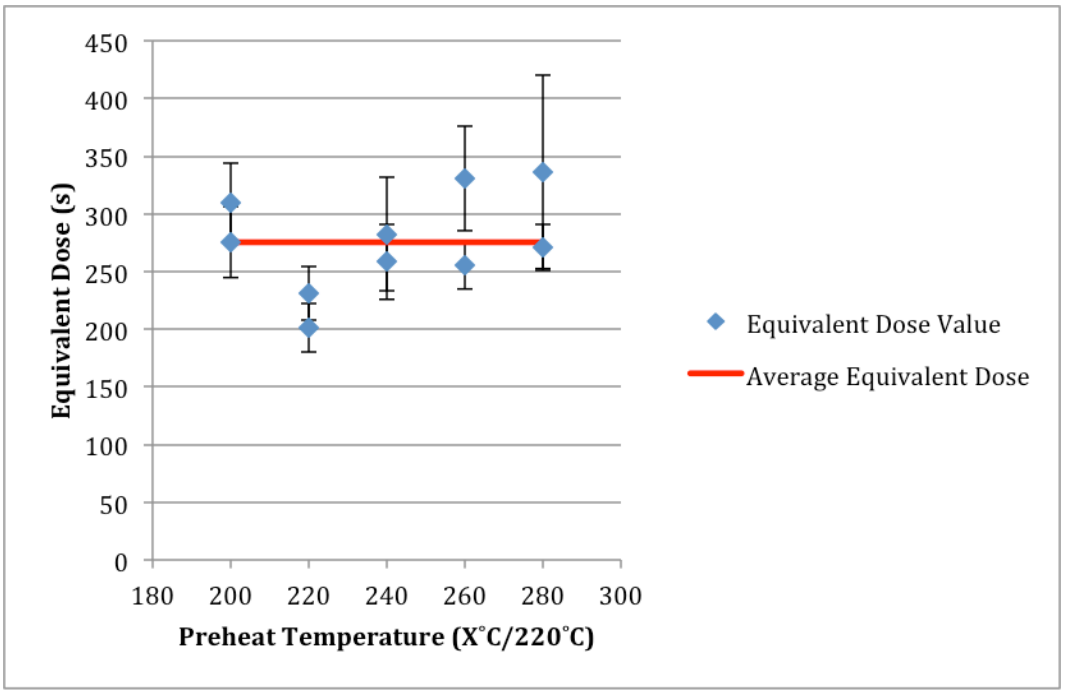

Figure 5.2: Preheat plot for sample X5460, showing the equivalent dose (and associated error) arising from varying preheat temperatures (220℃ up to 280℃ at 20℃ intervals). A preheat plateau is not strictly visible as all aliquots cluster around the average D_e value (∼275s); however, the 240℃/220℃ preheat provides the best unity for the known recovered dose (250s).

Table 5.1: Table showing data from preheat test (Figure 5.2). The equivalent dose and associated error from each pair of aliquots is given in seconds, along with the temperature in degrees Celsius and the difference between the two equivalent doses, again in seconds.

Preheat Temp	Aliquot A D_e	Aliquot A Err	Aliquot B D_e	Aliquot B Err	Difference
200	275.67	30.94	309.65	33.73	33.98
220	231.06	23.59	201.04	21.06	30.02
240	282.44	49.21	258.28	32.47	24.16
260	330.58	45.18	255.22	20.38	75.36
280	270.87	20.16	226.34	83.85	44.53

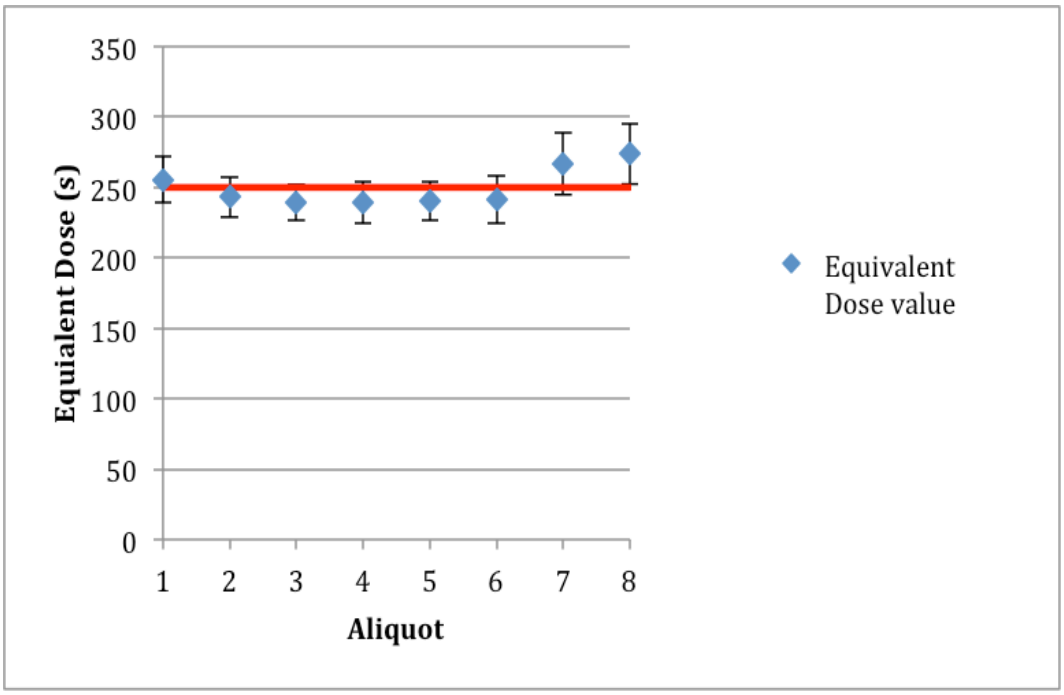

Figure 5.3: Dose Recovery plot showing that for all 8 aliquots measured after being given a known dose of 250s, the average recovered dose for the data set was 250.04±4.9 s and all aliquots were within error of this average (returning equivalent dose values within 10% of the known given dose), illustrating that the dose recovery test for sample X5460 was successful and that the quartz within the sample is behaving suitably for OSL dating. Note that the aliquot order is arbitrary.

The dose recovery test provides an excellent method for ensuring the suitability of the sample for OSL dating by retrieving a known laboratory dose given to the sample. On a series of aliquots for a single sample, the natural signal is bleached and a known dose (in seconds) is given to the aliquots. The standard SAR protocol is then carried out on each of the aliquots and it is expected that, if the luminescence properties of the sample are suitable for OSL measurement, the measured dose should return a signal within $\sim$10% of the given dose. As with the preheat test, ideally a dose recovery test would be conducted on each individual sample within a data set. However, owing to sample size, it is usually only possible to conduct a dose recovery test on a single representative sample. Once again, given the availability of additional material, sample X5460 was chosen to carry out a dose recovery test upon. Figure 5.3 presents these results.

In addition to incorporating a sensitivity correction and carrying out both dose recovery and preheat tests, the SAR protocol also includes several other quality controls to ensure appropriate measurement procedures for the SAR protocol. These include the recycling ratio test, recuperation, and an IRSL/OSL ratio check to determine if contamination by feldspars is present. For each of these tests and controls used in the SAR protocol, a standard set of 'rejection criteria' exists. It is good practice to follow these accepted criteria to ensure no subjective bias enters into the acceptance or rejection of individual aliquots being used to determine the final age estimate based upon the central age model.

The rejection criteria used in this project, to ensure reliable D_e determination, are described in Appendix D. In summary, aliquots are rejected if any of the following conditions occur: a test dose error of greater than 20%; a recycling ratio of greater than 20%; a recuperation value of greater than 5%; an IRSL/OSL ratio of greater than 15%.

After applying the rejection criteria, the central age model is used to calculate a single D_e estimate and corresponding error from the remaining (non-rejected) aliquots. In Appendix D these values are presented in seconds (s), being the length of time for which the samples were exposed to the source. However, these values must be converted

into Grays (Gy), that is, into an actual absorbed dose. In order to do this, the D_e (s) must be multiplied by the calibration factor (i.e. the dose rate) for the source at the time of measurement (cf. Section 5.2.1). This is seen in Appendix D, where the calibration dose rate for each sample is given alongside the machine-determined value in seconds.

Table 5.2 presents a summary of the D_e values obtained for each sample (after being converted into Gy) within the Bêt Khallaf data set. It is evident from Table 5.2 that not all of the 24 vessels from the Bêt Khallaf assemblage resulted in D_e determinations—indeed, as can be seen in Appendix D, X4119, X4120, X5469, X5471 produced no aliquots that passed the rejection criteria and therefore were excluded from further OSL analysis. Furthermore, X4113, although producing four aliquots which in themselves passed the rejection criteria, had too much over-dispersion among its 4 aliquots and did not produce a reliable D_e measurement.[19] Therefore Table 5.2 presents only the 19 (out of 24) samples which were accepted and deemed suitable for final OSL age calculation.

5.3 Measurement of the dose rate ($\dot{D}$)

Within luminescence dating, a vital component of the OSL age calculation is the measurement of $\dot{D}$ (the dose rate), which comprises $\dot{D}_{int}$ (the internal dose rate), $\dot{D}_{ext}$ (the external dose rate), and $\dot{D}_{cos}$ (the cosmic dose rate). Although measurement of D_e is often the main focus of a discussion on luminescence dating, it is the dose rate which can often contribute the most additional information to a luminescence date (i.e. about its depositional history) and it is also the dose rate which causes the most significant source of error in an age estimate (Durcan et al. 2015: 54). The following section exam-

[19] The over-dispersion (OD) value, calculated and presented in Appendix D for each sample, is a statistical representation of the variation occurring within the errors accompanying a D_e measurement. A standard OD rejection criteria does not exist in OSL dating (although many publications accept OD values of <20%). It has been discussed whether these values are too sample-dependent and whether it should be left to the discretion of the OSL practitioner to determine a suitable OD value for their sample population (Galbraith and Roberts 2012). With the exception of X4113, which had an OD value of >87%, the remainder of the Bêt Khallaf assemblage had OD values of <50% (with the majority of the values sitting below 20%). The spread in the data for X4113 clearly showed it to be an unreliable sample for OSL dating which is why this sample was rejected. All other samples, however, had OD values which were deemed suitable for further OSL analysis.

Table 5.2: Summary of the OSL D_e values for the Bêt Khallaf ceramic material (both fine and coarse grains)

Sample Number	Coarse grains (90–250 µm)		Fine grains (4–11 µm)	
	D_e (Gy)	D_e error (Gy)	D_e (Gy)	D_e error (Gy)
X4114	7.45	0.94	N/A	
X4115	7.31	0.25	8.33	0.74
X4118	12	0.46	11.59	1.04
X5460	9.98	0.6	10.79	0.75
X5461	10.56	0.4	9.02	1.17
X5462	8.37	0.9	N/A	
X5463	8.95	0.39	9.08	0.26
X5464	8.57	0.24	9.13	0.23
X5465	8.87	0.87	9.8	0.28
X5466	2.92	0.2	N/A	
X5467	8.1	0.47	6.84	1.13
X5470	8.114	0.44	9.87	0.93
X5472	9.25	0.2	10.19	1.78
X5473	8.35	1.21	9.39	0.35
X4116	6.66	1.31	N/A	
X4117	N/A		12.53	1.94
X5458	10.5	0.37	9.22	0.45
X5459	7.68	2.32	N/A	
X5468	8.65	0.55	9.37	0.35

ines the dose rate in detail, and specifically discusses its calculation within this project and how using the newly developed Dose Rate and Age Calculator (DRAC) program and the DosiVox program can assist in calculating and reconstructing the dose rate for a vessel.

5.3.1 DRAC (Dose rate and age calculator)

The five necessary measurements required to accurately determine $\dot{D}$ for each sample (the external dose rate ($\dot{D}_{ext}$), the internal dose rate ($\dot{D}_{int}$), the cosmic dose rate ($\dot{D}_{cos}$),

the radiation attenuation, and the moisture content) are discussed in greater detail below. In this project, final $\dot{D}$ calculation has been carried out by DRAC, a program which brings together each of the five $\dot{D}$ measurements, as well as the D_e estimate, to calculate a final age estimate for each sample by allowing direct input of D_e.

Developed by Durcan et al., DRAC is an open access, web-based program which permits fast and flexible $\dot{D}$ calculation and age estimation for each sample in a data set (Durcan et al. 2015). For each parameter, DRAC allows the user to define input values, and additionally allows the user to choose which values are used from the literature to determine aspects of the calculation such as radionuclide conversion factors, and attenuation factors. Further details about the functions used by DRAC and how the program works can be found in Durcan et al. 2015. DRAC input values used in the age calculation of the Egyptian ceramic material are discussed below and the final DRAC input and output tables for the Bêt Khallaf material are presented in Appendix E.

5.3.2 Calculation of $\dot{D}_{ext}$

In the case of dating ceramic material, $\dot{D}_{ext}$ comes from the radioactive isotopes of U, Th, and K naturally present in the sediment surrounding the vessel in its depositional environment (to a radius of 30 cm around the vessel). Under normal fieldwork conditions, when dating recently excavated material, it is possible to determine $\dot{D}_{ext}$ by one of two methods (or a combination of both): *in situ* gamma spectrometry (using a hand-held gamma spectrometer), or by collecting soil/sediment from the depositional environment of the sample and carrying out ICP-MS analysis (inductively coupled plasma mass spectrometry)—or NAA analysis, or ICP-AES/-OES analysis or by alpha/-beta counting[20]—on the sediment. All these methods produce an elemental analysis of

[20] Although ICP-MS analysis is the preferred method to work with for the MET, is should be noted that neutron activation analysis (NAA), inductively coupled plasma atomic/optical emission spectroscopy (ICP-AES/OES), or alpha/beta/gamma counting can also be used. However, with the small sample sizes resulting from extraction using the MET, alpha/beta and gamma-counting cannot be carried out within a feasible time frame. NAA is no longer routinely used, because it is now considered outdated compared to the ICP methods and requires a larger sample size. ICP-AES/OES, AAS or FES are considered by some to be preferable to ICP-MS (due to the problems surrounding the potential flooding of the K concentration by the Argon carrier gas used in ICP-MS (Preusser and Kasper 2001: 22; Bailey et al. 2003: 11). However,

the depositional environment, which allows the calculation of the concentrations of the three radioisotopes of interest.

One of the major considerations when working with museum material, and thus for this project, is accurate reconstruction of $\dot{D}_{ext}$, as without this, measurement of $\dot{D}_{ext}$ is likely to contribute the highest uncertainty in final $\dot{D}$ calculations for coarse grain material. In the absence of sediment/soil in direct association with the sample (which would be present with recently excavated material), it can be a challenge to reconstruct $\dot{D}_{ext}$ accurately. Museum material is routinely cleaned thoroughly prior to being put on display or into storage. This can therefore complicate the calculation of the external dose rate. In order to achieve an accurate estimation of the external dose rate, it is necessary to procure samples from museum material which still have some sediment material adhering to it. In this way, the material can be analysed by ICP-MS analysis to determine the concentrations of U, Th, and K in the sediment, which can act as a suitable alternative to soil material collected *in situ*. It is of course necessary to ensure that this material is indeed from the original depositional context, by visual and microscopic analysis.

In the absence of such material, there are two other possible options for reconstructing the external dose rate. The first is to go to the original excavation site and conduct *in situ* gamma spectroscopy in the approximate or exact location of the original find spot (i.e. the same methodology used for recently excavated material).[21] Alternatively, if this is not possible, one can estimate the external dose rate based upon careful reconstruction of the depositional environment using available environmental data. Environmental data for the surrounding region can often be found, and the reported findings can

which analysis is chosen is often entirely dependent upon resources available at the time. Any of the above methods can be considered suitable. For this project, ICP-MS is the method used for determining isotopic concentrations within the $\dot{D}_{ext}$.

[21] In theory gamma spectrometry is a distinct possibility for working on material within Egypt and something that would improve OSL dating on Egyptian material considerably. It was originally intended to carry out *in situ* measurements in the field (as the locations of most of the ceramic material sampled for OSL dating came from known contexts). However, travel to Egypt and carrying out such measurements in the field were not advisable in the current political instability in Egypt, from 2011 to the present. In the future, *in situ* gamma spectrometry should be used to verify $\dot{D}_{ext}$ measurements.

Table 5.3: Concentrations of radioisotopes in sediment samples in direct association with several Bêt Khallaf ceramic vessels.

Sample	Location of sample	Concentration of K (%)	Concentration of ^{232}Th (ppm)[22]	Concentration of ^{238}U (ppm)
X5458	Interior of vessel	1.38	4.4	1.3
X5459	Interior of vessel	0.88	3.9	1.5
X5463	Interior of vessel	0.88	4.6	1.8
X5467	Interior of vessel	0.41	1.38	0.45
X4120	Interior of vessel	0.81	3.2	2
X5458	Under rim	0.98	3.4	1.2
X5459	Under rim	0.71	3.2	1.4
Average		0.86±0.11	3.44±0.40	1.38±0.19

be used as a proxy for $\dot{D}_{ext}$. For example, this approach has been successfully applied elsewhere in the study of Iron Age pottery from South Africa (Zink et al. 2012) and for a luminescence study carried out upon a collection of Tanagra Terracotta figures (Zink and Porto 2005).

For the Bêt Khallaf material, it was noticed during the sampling process that several vessels had material adhering to their interior surface (vessels X5458, X5458, X5463, X5467, and X4120), or lodged tightly up under the rim of the vessel (vessels X5458 and X5459). It was possible therefore to collect this material for ICP-MS analysis and use the radionuclide concentrations as a proxy for the entire assemblage (see Table 5.3).

Although visual analysis (using a light microscope) of the material strongly indicates that the material came from the original depositional environment, there was a concern, particularly for the vessels from which the material was collected under the rim (X5458, X5459), that this may have been the remains of mud-sealings, commonly found upon vessels of the type yielding this material. However, it was noted that the ICP-MS analysis

[22]ppm = parts per million mass.

Table 5.4: Published dose rates for regions surrounding the Bêt Khallaf area and other archaeological sites across Egypt. NB Only research providing full disclosure of U, Th, and K values and how these were measured and obtained were used.

Site/location	Publication	Concentrations of K (%)	Concentration of ^{232}Th (ppm)	Concentration of ^{238}U (ppm)
Upper Egypt (greater region surrounding Bêt Khallaf)	Harb et al. 2008 (mean)	0.70	3.08	2.65
Giza, Egypt	Sekkina et al. 2003	0.93	4.77	2.67
Giza, Egypt	Abdel-Wahab et al. 1996	1.7	3.35	1.49
	Average	1.11	3.73	2.27
	Standard Deviation	0.52	0.91	0.68

across all six samples showed quite a strong degree of internal consistency (although less so for sample X5467). Furthermore, the literature also indicates that a fairly uniform natural dose rate is present in Egypt in the region surrounding Bêt Khallaf, and indeed across other archaeological sites throughout much of the country.[23] Table 5.4 illustrates these findings.

Given the results from ICP-MS analysis on the Bêt Khallaf material, alongside comparable results from the available literature, it can be assumed that a fairly accurate determination of the external dose rate from the surrounding sediment of the Bêt Khallaf assemblage has been achieved. However, here it is of course necessary to assume that the sediment adhering to the vessels in the Penn Museum collection is fully representative of the burial environment which would have surrounded the vessel during

[23] Literature exists on radionuclide concentrations from non-archaeological sites throughout Egypt, too, and over a larger geographical spread, such as along the Red Sea coast, and the Nile delta, as well as the Nile valley (see for example: El-Arabi 2005; El-Bahi et al. 2005; El-Gamal et al. 2013; El-Taher and Abbady 2012; Fahmi et al. 2011; Nada et al. 2009; Ramadan and El-Mongy 2001; Sroor et al. 2002; Uosif 2007; Uosif et al. 2013). However, a wider spread of radionuclide data is seen across this material, probably due to the geological spread of the data but also to the varying areas of sampling (that is, habitation sites or costal/desert zones as opposed to archaeological sites). For the purpose of this study we have only examined the data available from archaeological studies or studies based within the direct Bêt Khallaf region.

its deposition, to at least a radius of 30 cm. This is because it is the material contained within a sphere of radius 30 cm around the vessel which will govern its environmental (i.e. external) dose rate, as this is the typical penetration depth of gamma rays in burial contexts. Of course, such an assumption can never be fully verified. However, based on the good agreement between the literature and the ICP-MS results obtained from the Bêt Khallaf material, it can at least be assumed that there is a fair degree of consistency in the natural environmental dose rates in the region where Bêt Khallaf is located, and certainly within the direct area of the cemetery. Furthermore, Caton-Thompson and Whittle also illustrated that the radioactivity within the surrounding environs of eight pottery samples measured from Hemamieh, Egypt were comparable across several archaeological layers surrounding the sherds, again indicative of a fairly consistent soil matrix (Caton-Thompson and Whittle 1975: 96).

As such, the combination of the ICP-MS results obtained from the sediments adhering to vessels, and the available environmental data presented in the above-mentioned literature, allowed us to determine a good estimate for the external dose rate which would be used in our final age calculations. As the Bêt Khallaf ceramic collection was held in storage for ∼110 years prior to being sampled for OSL dating, it is possible to factor in an approximate contribution of background radiation in the museum environment to $\dot{D}_{ext}$ (following Castaing et al. 2004). However, due to the very small contribution to $\dot{D}_{ext}$ that this measurement is likely to have (and given that a proxy following Castaing et al. 2004 would have to be used rather than exact measurements from the Penn Museum, the Garstang Museum and the Ashmolean), it was decided that this factor could be removed from analysis of the Bêt Khallaf material without significantly affecting the final results.[24]

The ICP-MS values for this project which will be used to determine $\dot{D}_{ext}$ are presented in Table 5.3, with the average value being used. It was decided that an average

[24] In addition to this factor being only a small contribution to $\dot{D}_{ext}$, ICP-MS measurements indicate that $\dot{D}_{int}$ contributes significantly more to the total dose rate than $\dot{D}_{ext}$, further reducing the importance of this factor for the final age determination.

value would be the best value to use for $\dot{D}_{ext}$ calculation, even though the values varied slightly between the individual vessels yielding external sediment. This was because the long attenuation depth of the external gamma radiation means that $\dot{D}_{ext}$ is affected by a larger body of material than the sediment in direct contact with the vessel. In this case, an average value will be more representative than an individual measurement as it will compensate for the variation in composition of the surrounding sediment. How these values are used in final age calculation will be discussed below, when discussing the use of a radiation simulation software program, DosiVox, to calculate the external dose rate.

5.3.3 Calculation of $\dot{D}_{int}$

As already discussed, with the MET sampling protocol, the top ∼2 mm of the extracted sample (typically weighing ∼1–∼5 mg) is reserved for calculation of $\dot{D}_{int}$, the rate at which a vessel receives an annual dose from itself, owing to the presence of naturally occurring radioisotopes of U, Th, and K in the ceramic fabric. It is usually possible to calculate the concentrations of U, Th, and K using standard ICP-MS analysis.

It can, of course, often be difficult to accurately quantify the concentrations of radioisotopes when dealing with the minute sample sizes yielded for $\dot{D}_{int}$ calculation by the MET sampling method (in particular because the sample may be too small to contain a uniform distribution of the naturally occurring radioisotopes within the whole vessel). This can result in a larger-than-normal error range. However, these considerations are usually very dependent upon the individual assemblage being worked on. For example, it is sometimes possible to gain a better understanding of the internal dose rate for MET samples if the assemblage contains a number of vessels composed of the same material, or material similar enough to allow the results for ICP-MS analyses to be combined, resulting in a measurement based upon a larger sample size.

For this project, the ICP-MS analysis was carried out on the Bêt Khallaf samples by the Department of Earth Sciences, University of Oxford. Samples were prepared using

an acid digestion protocol: the samples were weighed into a Teflon beaker and then 3 mL of 27M HF and 1.5 mL of 16M HNO_3 were added to the beaker. The beakers were sealed and then heated at 90℃ overnight. Samples were then evaporated to dryness at 90℃. After evaporation, 2 mL of 16M HNO_3 was added to the sample and then evaporated to dryness (this step was repeated twice). Next, an additional 2 mL of 16M HNO_3 and of 18M-OHM water was added to the samples, following which the beaker was sealed and heated overnight. Finally, the sample was made-up to 10 mL with 18M-OHM water.[25]

After acid-digestion, all samples were run on a Thermo Finnigan Element 2 ICP-MS. After acid digestion was carried out, each sample was diluted using a 2% HNO_3 solution (prepared using in-house distilled nitric acid and 18.2M-OHM DI water). The analysis technique involved calibration using standard addition analysis, where a standard of a known K concentration was spiked onto replicates of selected samples at increasing ratios. Additional quality checks were conducted using an external standard (High Purity Standards 10ppm ICP-MS-68 A solution) and an internal standard (each sample, standard and blank, was additionally spiked with 1ng/g of Rhodium). All data were reported as elemental concentrations and were measured from a mass to charge ratio (m/z) of 39, 232, and 238 for K, Th, and U respectively.[26] These were then converted into ppm for ease of use in the DRAC program.

Table 5.5 shows the concentrations of U, Th, and K measured for each of the Bêt Khallaf samples, which were in turn used to calculate $\dot{D}_{int}$ in Gy/ka, using attenuation factors to account for grain size (Brennan 2003) and the infinite matrix assumption—an assumption commonly used to evaluate dose rates, which states that the radionuclide emissions in a matrix are equivalent to the amount absorbed (Guérin et al. 2012). For a ceramic object this assumes that the attenuation depth of both alpha and beta radiation is smaller than or comparable to the depth of the sample location within the vessel wall,

[25] The author is indebted to Steve Wyatt (Department of Earth Sciences, University of Oxford) for providing this description of the acid digestion process carried out upon these samples prior to ICP-MS analysis.

[26] The author is indebted to Phil Holdship and Steve Wyatt (Department of Earth Sciences, University of Oxford) for providing the information concerning the ICP-MS sample preparation and analysis protocols.

Table 5.5: Concentrations of U, Th and K (to three significant figures) for each Bêt Khallaf ceramic sample, measured using ICP-MS analysis, used to determine $\dot{D}_{int}$.

Sample	K (%)	^{232}Th (ppm)	^{238}U (ppm)
X4114	0.987	4.32	1.03
X4115	1.26	5.82	1.44
X4116	0.977	7.30	1.99
X4117	1.25	7.49	1.85
X4118[27]	1.42	5.79	1.48
X5458	0.972	6.70	1.82
X5459	1.01	7.69	2.45
X5460[27]	1.42	5.79	1.48
X5461	1.51	5.56	1.31
X5462	1.32	4.90	1.19
X5463	1.45	5.95	1.24
X5464	1.33	5.78	1.27
X5465	1.41	7.06	1.70
X5466	1.59	17.6	3.68
X5467	1.48	5.63	1.15
X5468	1.04	6.95	1.88
X5470	1.27	6.05	1.14
X5472	1.37	5.15	1.43
X5473	1.22	5.64	1.77

and this is true given that the depth of the sample is 2 mm–4 mm below the surface of the vessel wall and that the attenuation depth of beta particles is ∼2 mm and that the alpha attenuation depth is far smaller than this. A standard error of 5.6% was given to each sample when input into DRAC, based on the percent error calculated for the instrumentation process (2.5%) and approximated for the acid digestion process (5%), which were combined in quadrature, assuming the errors were independent (Pers. Comm. Phil Holdship and Steve Wyatt).

[27]X4118 and X5460 were measured by a commercial company at the very beginning of the project. The measurements for X4118 were %K=1.54; ^{232}Th (ppm)=6.3; ^{238}U (ppm)=2.3. The measurements for X5460 were %K=1.83; ^{232}Th (ppm)=6.2; ^{238}U (ppm)=1.9. The company measured four samples, but returned the remainder and said they were unable to process the rest of the sample set. This was because the sample size was too small for them to work with. While the remainder of the samples, upon re-sampling

5.3.4 Calculation of $\dot{D}_{cos}$

A small, yet integral part of $\dot{D}$ comes from cosmic rays and is known as the cosmic dose rate ($\dot{D}_{cos}$). As the name would suggest, this source of radiation comes from interstellar space and is calculated as a function of four primary factors: burial depth of a sample, the altitude of the find spot, its geomagnetic latitude as well as an average over-burden density (Prescott and Stephan 1982; Prescott and Hutton 1988; Prescott and Hutton 1994).

When working with museum materials, and in particular from excavations carried out over 50 years ago, it can often be difficult to determine these four factors, depending on how detailed the excavation reports for the site are. Although it is usually straightforward to determine the altitude and latitude of the site, the burial depth and over-burden density, if not recorded in the original excavation report, are more difficult to reconstruct.

For the Bêt Khallaf assemblage, the altitude and co-ordinates of the site were determined using Google Earth[28] as the satellite imaging accompanying this program allows ease of recognition of exact find locations, that is, the Bêt Khallaf mastabas (the superstructures above the burial location), from which the ceramic material studied in the project came, were easily identifiable in this program (Figure 5.4).

Excavation reports exist for the majority of the ceramics within this assemblage (Garstang and Sethe 1903), and therefore we can reconstruct a relatively good approx-

according to an improved sample storage protocol (gelatine capsules, as discussed above), were measured by the Department of Earth Sciences, University of Oxford (DESUO), who were confident in working with such small sample sizes (they are used to working with sub-milligram seawater material), X4118 and X5460 could not be re-sampled. X4114, however, was the single sample measured by both the commercial company and DESUO and the results between the two labs were vastly different. In contrast to the values produced by DESUO (see Table 5.5), the commercial company's values for X4114 were: %K=1.21; ^{232}Th (ppm=10.1); ^{238}U (ppm)=3.0. These values, particularly for ^{232}Th and ^{238}U are significantly higher than those produced by DESUO. Such occurrences have been discussed elsewhere and are not unusual (Preusser and Kasper 2001: 20). The fact that the laboratory felt they were not set up to deal with such small quantities of material indicates that these measurements were unreliable. So that these results did not adversely affect the $\dot{D}$ measurements and thus the age estimates for these two vessels, it was decided that an average value of the entire Bêt Khallaf Nile silt clay assemblage measured by DESUO would be used. It is this value that appears in Table 5.5. NB Table A.1, found in Appendix A presents all the ICP-MS values obtained for the entire assemblage independently upon each vessel, whereas Table 5.5 only presents those values corresponding to the ceramics from the assemblage which produced D_e measurements. Thus, it is Table A.1 that should be consulted for the calculation of the average elemental values for the assemblage.

[28] (Google Earth V 7.1.2.2041 (July 2013)), Bêt Khallaf, Egypt. Lat: 26.296983°, Long: 31.773725°, Eye alt 352 m, DigitalGlobe 2013. http://www.earth.google.com [July 17, 2015].

Figure 5.4: Satellite image of the Bêt Khallaf archaeological Site (Mastaba K1) taken from Google Earth, used to determine certain elements of the cosmic dose rate (elevation above sea-level, latitude/longitude co-ordinates).

imation of the over-burden density and burial depth. Similarly, Garstang's excavation reports allowed a fairly accurate reconstruction of the approximate location of the ceramic finds. Although specific vessels are not individually discussed, Garstang does mention the location of the ceramic finds in written description, which can in turn be located upon the plan and section drawings of each tomb. This then allows a decent reconstruction of the size of the chamber containing the pottery and its depth below the surface, all essential components in accurately reconstructing $\dot{D}_{cos}$.

DRAC allows a user-defined input for the factors contributing to $\dot{D}_{cos}$ as well as allowing user-defined error for each individual factor, which can be determined based on the confidence level in how accurately the excavation reports allow reconstruction and interpretation. Table 5.6 presents the user-defined input components for calculating $\dot{D}_{cos}$ for the Bêt Khallaf material (based upon Garstang and Sethe 1903). DRAC uses the seminal work of Prescott and Hutton to determine $\dot{D}_{cos}$ once the user-defined input parameters are established (Durcan et al. 2015: 58; cf. Prescott and Hutton 1994).

Table 5.6: Factors and accompanying measurements contributing to $\dot{D}_{cos}$ of the Bêt Khallaf assemblage

Tomb Number	Location of the tombs at Bêt Khallaf	Height above sea level of site surface	Burial chamber depth below the surface or below still-standing mastaba superstructure
Bêt Khallaf K1	Lat: 26.295483 Long: 31.7717979	94 m	27 m
Bêt Khallaf K2		94 m	12 m
Bêt Khallaf K3		94 m	12 m
Bêt Khallaf K5		94 m	11 m

5.3.5 Radiation attenuation

Radiation is attenuated, that is, absorbed, in both coarse and fine grains as the radiation interacts with the quartz crystal lattice. Thus, it is necessary to determine radiation attenuation factors in order to more accurately calculate $\dot{D}$ (i.e. from both internal and external sources), where $\dot{D}$ comprises $\dot{D}_{\alpha}$ (the alpha dose rate), $\dot{D}_{\beta}$ (the beta dose rate), and $\dot{D}_{\gamma}$ (the gamma dose rate). Factors to be considered here are: alpha efficiency, grain size attenuation, HF treatment (etching), and moisture content (Durcan et al. 2015: 56).

Alpha particles differ from beta and gamma particles in that they are highly ionising, which means that the deposited luminescence is proportional to the track length (the path made by the alpha particle) throughout the quartz crystal lattice. While beta and gamma particles deposit luminescence only at their final point of absorption, the alpha particles deposit energy along the whole track length. The alpha efficiency, or a-value, provides a way of determining the ratio of luminescence produced per unit of alpha track to the luminescence produced per unit absorbed beta dose (Durcan et al. 2015: 56). This is to say that it is necessary to convert the amount of alpha track to the amount of beta radiation that would give the same luminescence which is determined during D_e

measurement in the OSL/TL reader.[29] Within DRAC, a-values can be selected from the available literature (dependent upon grain size and mineral type) or can be user-defined if an alpha source has been used to determine the a-value for a specific sample. Given that an alpha source was not available to us for this study, the published values for quartz fine grains, 0.038 ± 0.002 (Rees-Jones 1995), and coarse grains, 0.10 ± 0.02 (Olley et al. 1998) were used, as recommended by Durcan et al. 2015: 56.

Grain size attenuation must also be considered as the differing sizes of grains used for OSL measurement will affect the extent to which the alpha and beta radiation penetrate the interior of the grain, and thus the overall quantity of radiation received by the grain. Within DRAC, grain size attenuation factors calculated by Brennan et al. 1991 have been used to determine this grain size attenuation (Durcan et al. 2015: 56–57; cf. Brennan et al. 1991). These attenuation factors relate the actual absorbed dose to the radiation which would be absorbed by a thin target, as calculated from the measurement of radionuclide concentrations provided by ICP-MS analysis of $\dot{D}_{int}$ and $\dot{D}_{ext}$.

As already discussed in Chapter 4.1.3.3, generally in OSL dating, a HF treatment is carried out in order to remove the alpha dose attenuation layer from the surface of a quartz grain. Given that for this project only a 30-second HF treatment was used, it must be assumed that etching did not occur and that, therefore, the contribution of the alpha dose to the OSL signal must still be included in the final age calculation. Following Brennan et al. 1991, DRAC provides the facility to specify the etch depth obtained during an HF treatment (in the case of the samples reported for this project, a depth of 0 μm was specified), which is used to calculate the resulting alpha contribution (Durcan et al. 2015: 56–57; cf. Brennan 2003).

The moisture content of a sample is another factor that influences radiation attenuation in the calculation of $\dot{D}$, because the presence of water causes a greater degree of attenuation within the object: a sherd that has been affected by water during deposition will produce systematically younger ages than expected. In the case of museum

[29] NB The luminescence produced per unit absorbed gamma dose is considered to be the same as that per unit absorbed beta dose.

material, where it is often impossible to accurately reconstruct the moisture content of a site over an object's often long-lived depositional history,[30] moisture correction factors (Aitken 1985) are used, which consider an average moisture content over the duration of burial. It has been noted that given the natural environmental conditions of many Egyptian sites, it may be possible to expect relatively low degrees of error due to the favourable climatic conditions (hot and dry), which limit the uncertainty of past variations in water on the environmental (external) dose rate (Shortland 2000: 93). Measured water contents for Egyptian material are found in the literature which can also assist in determining a water content for the Bêt Khallaf material. Sekkina et al. reported a 3.1±0.2% water content for Egyptian pottery at Giza, determined after water extraction was carried out by heating to 100℃ over 3 days (Sekkina et al. 2003: 98). This error is quite low, and elsewhere larger errors have been more routine. Bubenzer and Hilgers 2003 also presented data with very low moisture content (2%) due to hyperaridity for their examination of Holocene playa sediments in the Western dessert. Although the measured water content was 2%, when calculating the OSL ages a larger error factor was incorporated (up to 10%), to factor for wetter periods within the depositional history, as the timescales for dating were significantly broader, being geological rather than anthropogenic (Bubenzer and Hilgers 2003: 1083). Liritzis et al. reported a water uptake value of 0% for the environment in Abydos (Liritzis et al. 2013: Table 2). Finally, Hygue et al., who dated geological sediments in association with the Qurta petroglyphs, also recorded a soil water content of 3±1% (Huyge et al. 2011: 1188).

Based upon Bêt Khallaf's geographic position (positioned away from the cultivation area in the low desert plateau, in an hyperarid environment), it is expected that the ceramics from the assemblage will not have been exposed to excessive moisture throughout its depositional history. Given that these excavations were carried out before the

[30] When not working on museum material, it is possible to collect a sherd *in situ* and measure its water content directly under laboratory conditions; this was not possible for the Bêt Khallaf material as although a fragment of sample X5460 was given to us by the Penn Museum to carry out experimentations, this sherd had been out of its original depositional environment for over 100 years and thus the water content would have been negligible (i.e. it would have long since evaporated).

building of the Aswan High Dam this context is not affected by the rising water table. The Bêt Khallaf tombs are well above the water table (and no mention of damp conditions were mentioned by Garstang during excavation). When it came to determining a water content value for the Bêt Khallaf assemblage, it was considered acceptable to use a similar value to those found in the literature. Indeed, the several studies noted herein, although across a large geographic region, all produced very similar water content values for both pottery and soil sediments. Therefore, for the Bêt Khallaf material a standard moisture content value of 3±2% was used.

An additional factor that can affect the dose rate of a sample is the additional mineral components which may or may not be present in a vessel. In the case of this project it was concluded that additional minerals had very little effect upon the final dose rate calculation. This is presented briefly in Appendix F.

5.3.6 Modelling with DosıVox

Figure 5.5: Tomb 4/123 at Helwan, Egypt, providing an example of how a burial chamber is rarely filled with 100% fill. Photo courtesy of The Helwan Project ©.

We have already discussed the determination of $\dot{D}_{ext}$ using the U, Th, and K values

from ICP-MS analysis of the sediment material adhering to some of the Bêt Khallaf vessels. Once attenuated, these values can be converted into a dose rate (Gy ka^{-1}) and used to calculate a final OSL age. However, this initial value comes with the assumption of 100% geometry for $\dot{D}_\gamma$—that is, the assumption that the deposition environment of the vessel entirely surrounded by a sediment matrix of at least 30 cm on all sides, which is both homogenous and densely packed. For Egyptian tomb contexts this concept of being entirely buried to a depth of 30 cm on all sides is very rarely the true state of the depositional environment—Figure 5.5 presents a representation of a commonly encountered pottery deposit from chamber tombs. As discussed above, a major benefit of the Bêt Khallaf material is that Garstang's excavation records (Garstang and Sethe 1903) were of excellent quality for the early twentieth century and they allow us to reconstruct with a reasonable degree of confidence the exact burial environment of each vessel, which is further strengthened by finding parallels within the literature for similar temporal contexts. This research shows that the geometry of the Bêt Khallaf samples is unlikely to be 100% as these vessels were found in underground chamber tombs cut into the bedrock, which contained only a relatively small amount of fill.

Thus, the true $\dot{D}_\gamma$ is determined by a number of factors, some of which will require assumptions to be made; these are:

1. The orientation of the vessel: the pot can be either standing (upright or upside down), or lying on its side. Since the OSL sample is drilled from the base in all instances in this project, the orientation of the pot in its burial environment will affect $\dot{D}_\gamma$ (i.e. was the sample location submerged in fill or exposed to air?)

2. Whether standing or lying on its side, the pot can be buried from 0% to 100% in fill, with the remainder surrounded by air (or other material).

3. The vessels can be filled from 0% to 100% with either fill or other contents (e.g. organic bulk residue—it is unlikely that any of the Bêt Khallaf material contained contents: had the vessels been sealed with mud seals with intact contents,

Garstang would have felt that these were worthy of mention in his excavation report. It is, however, very possible that a small amount of debris or fill was found within the vessels).

4. The density of the vessel's clay matrix.

5. The density of the fill.

6. The vessel's proximity to the tomb walls, that is, its location within the tomb. Was it in the centre, corner, or along a side of the tomb?

7. The moisture content of the burial environment.

With regard to the position and burial situation of the vessels found within chamber tombs, to fully understand the likelihood of each possible scenario/assumption, it is first necessary to look at parallels for recently excavated material from the same historical period which have been well documented. We can find such parallels at the site of Helwan. Figures 5.6a–e show a variety of different depositional scenarios for ceramic vessels (see figure captions) and although all scenarios are in theory possible, it is more likely that the majority of large vessels are either standing upright with their bases in fill (e.g. Figure 5.6a), or that they are lying on their sides, either on or slightly within the surrounding fill (i.e. Figure 5.6a,c,d,e) (Pers. Comm. E.C. Köhler, 2015; and author's personal observations during excavation). For smaller vessels (i.e. bowls) it is most probable that they are resting, on their bases, on top of the fill, or slightly buried within that fill—this is because their dimensions would not allow them to rest on their sides naturally. In some cases it is likely that the bases of the storage vessels would not have been buried in fill, rather exposed to air and simply resting on the fill, that is, if the vessel was lying on its side, for example, wine, beer or storage jars (e.g. see Figure 5.6b).

With all these assumptions to consider when examining sample geometry, it is necessary to approximate a percentage of the sample geometry when calculating a final age estimate. Thus, for the gamma output of the DRAC program, although it gives a value

Figure 5.6: a–e): various, common depositional scenarios for vessels found within chamber tombs. All photos are courtesy of The Helwan Project ©.

for 4π (i.e. 100%) geometry, it would be necessary to scale this value in a way that accounts for the degree of burial of the vessel; given that, as described above, the vessels are unburied or only slightly buried one might consider a value of 2π (i.e. 50%) to be appropriate (following, for example, Rhodes et al. 2009). Of course, choosing a scaled figure for sample geometry is fraught with possible errors and is not an ideal solution for accurately determining the $\dot{D}_{\gamma}$, yet up until recently, such assumptions were necessary when working with complex depositional environments such as we see at Bêt Khallaf. Fortunately, new methods are now available which can overcome this problem.

With several possible scenarios for complex depositional geometries, traditionally it has been necessary to approximate the geometry of a pot's deposition by assigning a percentage multiplier to $\dot{D}_{ext}$. This produces significant errors attached to $\dot{D}_{ext}$ values,

yet has been standard practice until recently; however, from July 2015, the Luminescence Laboratory at the Université Bordeaux Montaigne, France has released an open-source software program, DosiVox, which allows the dose rate to be simulated for various depositional scenarios (Martin et al. 2015).

Although the DosiVox program has only just been released (and not yet in its final version (Pers. Comm. L. Martin, 2015)), the benefits of using this software to reconstruct the dosimetry of the Bêt Khallaf samples, even at this early stage of release, are significant. Therefore, it was decided in July 2015 that DosiVox would be used to examine the Bêt Khallaf material and to use a model of the reconstructed depositional environment to calculate $\dot{D}_{ext}$.[31] Thus, DosiVox was used to assess the varying scenarios discussed above and to determine which assumptions about the burial environment governed each vessel's final calculated dose rate.[32]

The excavation reports of Garstang provided us with a good starting point for reconstruction of the burial environment through DosiVox. Although the reports are far from being as comprehensive as a modern-day excavation report, Garstang does discuss the pottery and gives precise locations of the pottery deposit within each tomb, allowing an accurate find spot of the ceramics to be determined (Garstang and Sethe 1903: 8–16). In the case of Mastaba K1, it is even noted that 'the main passage hereabouts was strewn ... with large wine jars and pots' (Garstang and Sethe 1903: 10). This indicates that the vessels were visible to him upon entering the chamber, and thus not fully buried. Although some 'sifting of sand [fill]' was necessary (Garstang and Sethe 1903: 12), this only appears to be in context of small finds such as jewellery, not larger objects such as the ceramic vessels. This information allowed us to choose a 'most likely' base assump-

[31] It is beyond the scope of this thesis to present a full description of the DosiVox software and a discussion on its full potential as a tool in luminescence dosimetry. The reader is referred to Martin et al. 2015.

[32] The research carried out using DosiVox was a collaborative effort between the present author and E. Highcock. The present author would like to express her thanks to Dr Highcock for this help and for his assistance in compiling the following section. Furthermore, Dr L. Martin, the developer of the DosiVox software, has been of incredible help to the present author and Dr Highcock in learning to use this software in a very short period of time, and for this they extend their sincere thanks. The results of the DosiVox simulations employed in this thesis will be published jointly by the present author and Dr Highcock in the future.

tion for the burial environment: that the vessels were situated on top or only slightly buried in the tomb fill.

Owing to time constraints caused by the significant simulation time needed to test each case, this project limited itself to testing the first five assumptions listed above at high resolution, as these were deemed the most likely to affect $\dot{D}_{ext}$. Of the final two assumptions (assumptions 6–7), Assumption 6 was considered, but at low resolution (the attenuation of radiation through air with low moisture content is such that it should not matter where the vessel is located as it will, in theory, still receive radiation from all four walls of the tomb). Assumption 7 was not tested as the literature consulted seemed unanimous that the correct approximate value for water content within the burial environment was 3±2% (Sekkina et al. 2003; Bubenzer and Hilgers 2003; Liritzis et al. 2013; Huyge et al. 2011; see discussion above). One thing that can not be tested for is the proximity of other vessels to the case vessel. If a vessel was surrounded by other vessels in close proximity, it is likely that these will also contribute a $\dot{D}_{ext}$ to the case vessel. However, due to the nature of Garstang's publications, it is impossible to determine the order or arrangement in which the vessels were located in the tomb. Thus, each vessel was modelled to be the only vessel in the modelled tomb. Although it may be possible in future to include at least the vessels which were in the tomb within the simulation, as the DosiVox program is in its early stages of development and release, it is currently only possible to model a single pot (i.e. one sub-voxelised voxel) in each tomb. In the future, as the capabilities of DosiVox continue to expand, it will be possible to re-visit this assumption.

Even with the limited simulation time available, almost 550 simulations were carried out for this project (using approximately 5000 CPU hours). High-resolution simulations used 8 million particles; lower-resolution simulations used 2 or 4 million particles. For each case, six individual simulations were run in parallel (i.e. the same case, and hence the same input file, was run in parallel). As DosiVox uses a Monte Carlo method it was possible to take the mean of the 6 simulations and combine these to increase the

simulation resolution to 48 million particles per high-resolution case, that is, 6 parallel simulations × 8 million particles (Pers. Comm L. Martin, 2015).

The tomb shape and size was reconstructed using the figures provided by Garstang, and based on these figures, the tomb dimensions were replicated using voxels—a theoretical three-dimensional pixel (with user-defined x, y and z axes)—which can be combined with others in a three-dimensional grid that makes up the base structural component for a DosiVox radiation simulation model. Together, the voxels compose a dosimetric model. Each voxel (sized 30 cm × 30cm × 15 cm) within the model contains necessary information, mainly the material that it is modelling and this material's radionuclide data (Martin and Mercier 2015). The components of the tomb included air (within the tomb chamber), a sand-based fill (on the floor of the tomb), and gebel—Egyptian bedrock—which composed the walls and roof of the tomb. Although gebel would be the natural floor of the tomb, given that the excavation report states that fill was present, this has been used as a more accurate representation of the floor, because $\dot{D}_{ext}$ is determined by the solid material approximately 30 cm away from the sample site. Thus the gebel floor is likely to be too far away to affect the $\dot{D}_{ext}$ of the vessels when fill is present.

A single sub-voxelised voxel[33] in each simulation was used to represent the ceramic vessel. Each vessel was simulated using a simplified model of the vessel composed of 1cm × 1 cm × 1cm sub-voxels forming a regular rectangular shape (for the bowls and the pot stand other approximate shapes were used).[34] Within the sub-voxelised voxel the dose rate[35] is recorded separately for each sub-voxel, and average dose rates are

[33] A sub-voxelised voxel is a voxel that has been divided up into smaller sections (sub-voxels), allowing a higher spatial resolution in a given section of the tomb (i.e. the section that contains the vessel, without the cost of having such a high spatial resolution across the whole tomb (Martin and Mercier 2015).

[34] An upgrade to DosiVox is currently being developed that will make it possible to scan in a 3D image of the vessel (once reconstructed from a 2D line drawing) and upload the exact shape of the vessel into the model. However, although this will eventually lead to further refining of $\dot{D}_{ext}$, it is likely that this will not affect the $\dot{D}_{ext}$ results significantly (because the correct dimensions are already being used) and, almost certainly, any corrections will still remain within error. (Pers. Comm. L. Martin, 2015).

[35] Strictly speaking, DosiVox does not calculate dose rates but rather the total dose absorbed by a given sub-voxel during the simulation. This can be converted to a dose rate because DosiVox also records the total dose emitted by a sub-voxel during a simulation. The rate of emission is a known function of the concentrations of radionuclides (Guérin et al. 2011), and thus the recorded dose can be converted to a dose rate by multiplying by the ratio of the emission rate divided by the dose emitted during the simulation.

recorded for each material (air, clay, fill, and so on) The sub-voxels within the vessel were classified as two separate materials—'Clay' and 'ClayBase'—so that the average dose rate was recorded for the base (i.e. the OSL sample location) and the rest of the vessel separately. However, these two clay sub-voxel types were identical in their composition. Figure 5.7 presents a set of schematic representations of DosiVox simulation models used in this project.

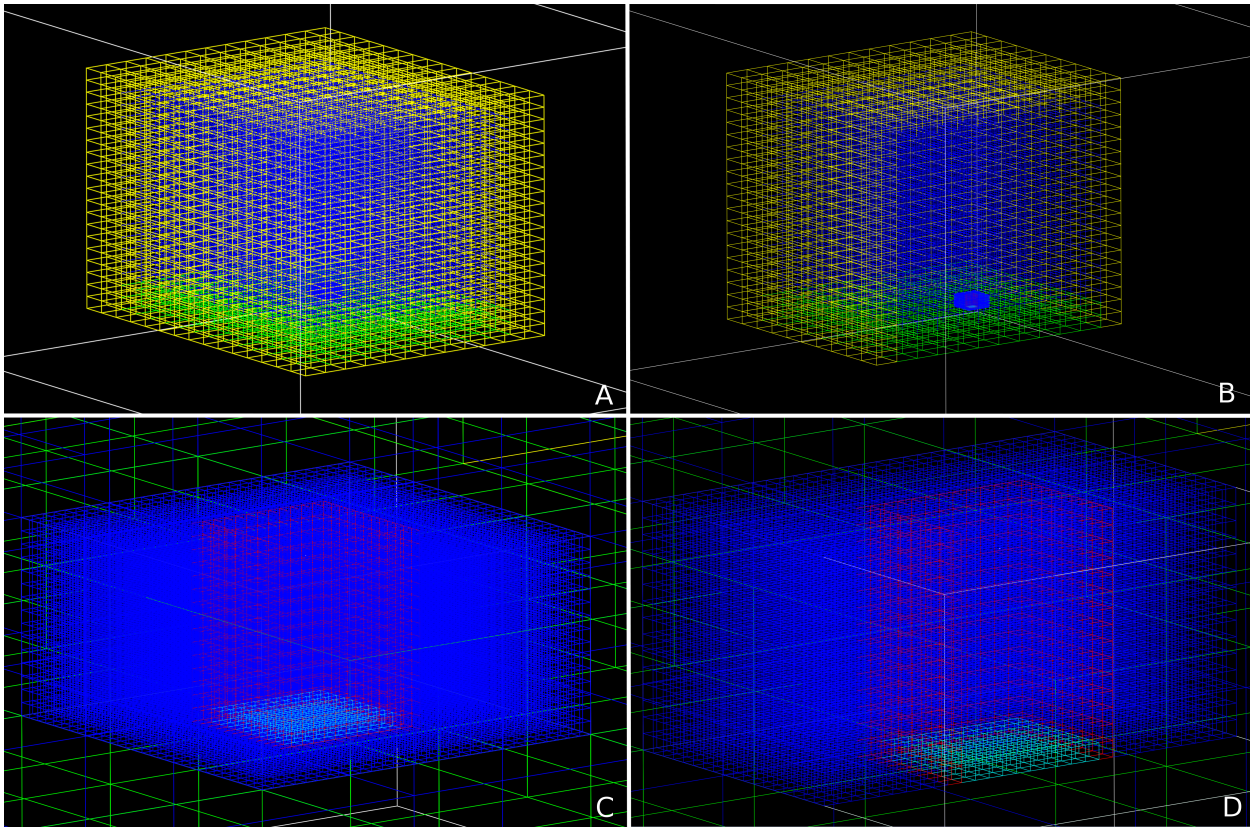

Figure 5.7: Wire frame representations of the DosiVox model for X5472. The whole tomb is subdivided into voxels which are filled with different components: yellow = gebel/bedrock, green = fill, blue = air, red = vessel walls, cyan = vessel base where the dose is recorded. A–D represent different views of the model: A) whole tomb; B) whole tomb cut away to reveal the detector (the sub-voxelised voxel which contains the vessel); C) close up view of the detector, D) detector cut away to reveal the vessel. NB these figures represent an unburied vessel.

DosiVox also requires the user to specify both the radionuclide concentrations in the clay, specifically the U, Th, and K quantities which were obtained by ICP-MS (see Table 5.5), and the chemical composition (i.e. the chemical compounds that make up the

Table 5.7: Chemical breakdown of five ceramic vessels from Bêt Khallaf obtained using ICP-MS

Sample	SiO_2	Al_2O_3	Fe_2O_3	MnO	MgO	CaO	Na_2O	K_2O	TiO_2	P_2O_5	Vacuum	Total
X5460	57.62	13.01	8.2	0.124	2.49	3.58	2.11	2.2	1.52	0.6	8.54	91.46
X4112	51.49	14.6	8.5	0.251	1.87	6.07	1.41	1.62	1.661	0.64	11.89	88.11
X4114	67.02	11.98	8.17	0.209	2.26	3.54	1.96	1.46	1.524	0.52	1.36	98.64
X4118	61.49	11.96	7.9	0.131	2.4	4.68	2.18	1.85	1.587	0.72	5.09	94.91
X4119	65.15	11.99	7.79	0.123	2.11	3.53	1.7	1.86	1.462	0.56	3.74	96.26
Mean Value	60.55	12.71	8.11	0.17	2.23	4.28	1.87	1.80	1.55	0.61	6.12	93.88

bulk of the clay, such as SiO_2 and Al_2O_3). For the latter, the data for the Nile silt clay was provided by five bulk samples initially tested by a commercial laboratory, which in addition to the elemental analysis provided a breakdown of the main components of the clay in percentages. With only five samples analysed it was not possible to know the specific chemical breakdown of each individual vessel from the Bêt Khallaf assemblage. Instead, based on these five samples, an average breakdown was determined (See Table 5.7). These values are well supported by Redmount and Morgenstein's values for Nile clay vessels (Redmount and Morgenstein 1996: Table 2). Unfortunately, no such chemical breakdown data was available for the marl clays within the assemblage. However, based on the comparability between the Bêt Khallaf results and the Redmount & Morgenstein results for the Nile clay, it was thought that the two marl clay values provided by the latter could be used as a proxy for the marl clay assemblage from Bêt Khallaf. Although this is not ideal—as marl clays show the most variability in composition and furthermore the two samples analysed by Redmount & Morgenstein are of Ballas clay, a very distinct clay type—the absence of raw data for this project, coupled with the absence of such data within the literature means that this is currently the only option available to us. It is generally accepted that these values are fairly standard across most specimens, so it was felt that this was an acceptable alternative. Table 5.8 gives the chemical composition breakdown of marl clay and Nile clay used in the DosiVox simulations (i.e.

Table 5.8: Chemical breakdown of Nile clay, take from Table 5.7, and marl clay, taken from Redmount and Morgenstein 1996, used in the DosiVox simulations.

Clay	SiO_2	Al_2O_3	Fe_2O_3	MnO	MgO	CaO	Na_2O	K_2O	TiO_2	P_2O_5	Vacuum	Total
Nile	60.55	12.71	8.11	0.17	2.23	4.28	1.87	1.80	1.55	0.61	6.12	93.88
marl	41.3	21.95	6.76	0.05	1.8	18.8	1.39	1.20	0.90	0.45	1.3	98.7

the mean value of the 5 bulk samples analysed from Bêt Khallaf for the Nile clay, and the mean value of the marl clay samples taken from Redmount & Morgenstein).

Earlier a list was given of seven properties of the burial environment which could affect $\dot{D}_\gamma$ and which cannot be conclusively determined from archaeological publications. Since these were not known, DosiVox simulations were carried out for various different assumptions for each of these unknowns and the effect on $\dot{D}_\gamma$ was assessed. A full description of these tests and the effect of their changes is given in Table 5.9 and illustrated in Figure 5.8.

Overall it was found that changing these assumptions only had a weak effect (i.e. if there was an effect its magnitude was lower than the error of the simulation result at the given resolution).[36] Thus, even though the incomplete archaeological literature produced unavoidable uncertainty in the model, this did not give rise to significant uncertainty in the calculated $\dot{D}_\gamma$.

[36] This somewhat unexpected result is certainly worthy of further study. It is likely to be a consequence of the particular circumstances being considered here (specific dosimetries and so on). However, it may be hypothesised that it could be due to the characteristics of the emission spectra of the radionuclides. The emission spectra of U and Th are dominated by lower-energy, short-range gamma rays. Since the concentrations of U and Th are larger in the clay than in the surrounding fill, it might be expected that the dose rate from these radionuclides is dominated by the dose rate coming from the clay of the vessel (effectively the internal gamma dose rate) and will thus be unaffected by most of the assumptions tested here. By contrast the K spectrum is dominated by one high-energy, long-range gamma emission, for which the attenuation rate in any of the components of the model of the tomb will be low. Therefore, whatever the orientation of the vessel or its immediate surroundings, the absorbed K dose rate will effectively be an average of the tomb as a whole, i.e. it will be affected by whatever material is within 30 cm of it, or 30 cm of the material which is separated from the pot by air (as the gamma radiation will travel directly through air with low moisture content).

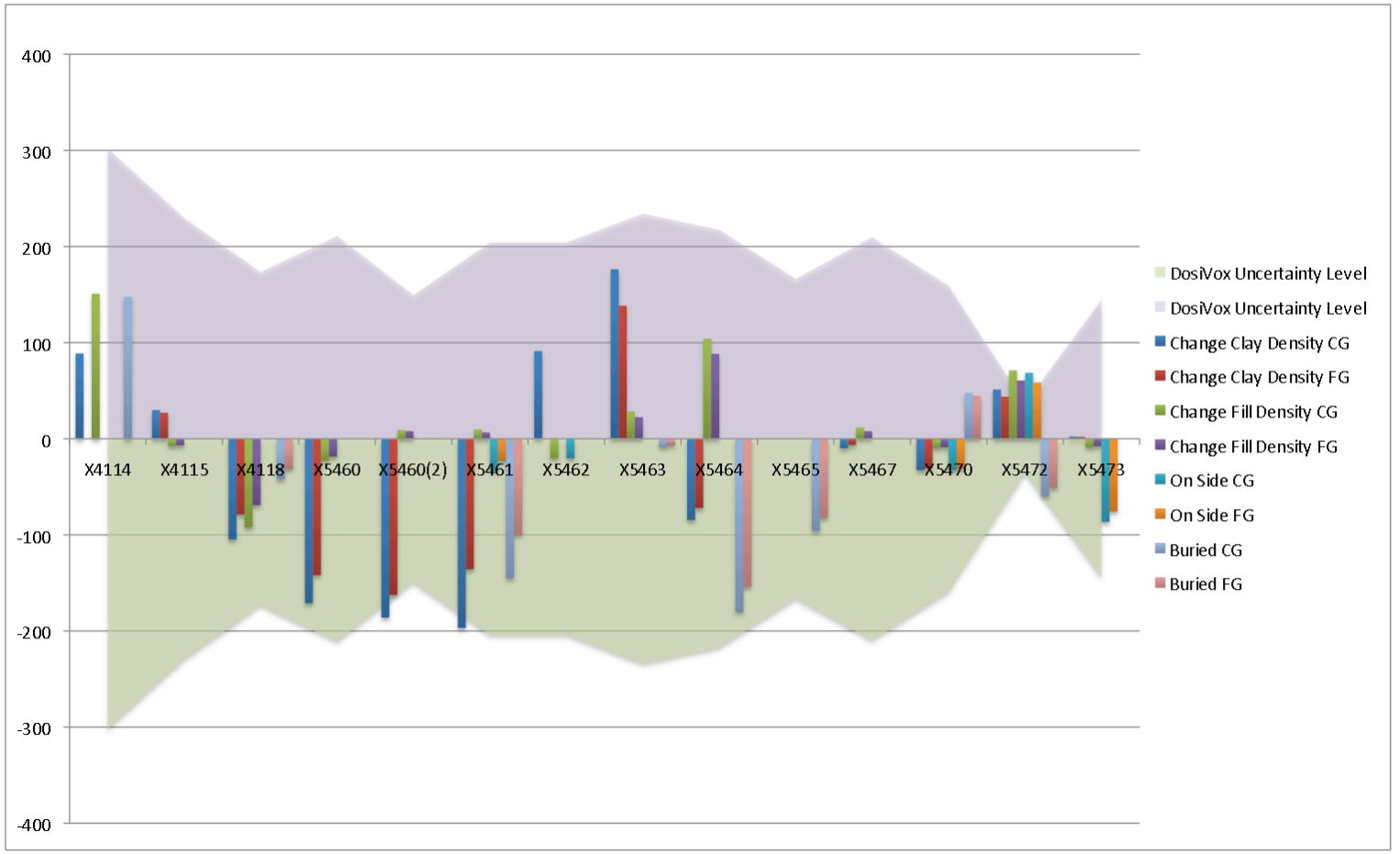

Figure 5.8: Graph depicting the effects of changes to the assumptions made in the DosiVox modelling. The change in the final age in years as a result of changing each assumption is plotted. The shaded area represents the error in years (1 sigma) resulting from the uncertainty in the DosiVox result for the reference case. It can be seen that changing all assumptions results only in errors which are comparable to or less than the typical error in the DosiVox simulations (which is itself small compared to the overall error). FG = fine grains, CG = coarse grains.

Table 5.9: The assumptions tested by DosiVox, illustrating the modelled cases whose outcome was initially unknown (left column) and the outcome of the DosiVox modelling which gives modelled answers for each assumption (right column).

Modelling Unknown	Effect on modelled dose rate of the Bêt Khallaf assemblage
1. The pot can be 1) standing (upright or upside down), or 2) lying on its side. Since the OSL sample is drilled from the base in all instances, it also matters whether the sample location was on the upper or lower side of the vessel (i.e. was the sample location submerged in fill or exposed to air)?	Two scenarios were considered: the pot standing on its base or lying on its side. These were considered the two limiting cases and as no measurable change was observed, it was concluded that the orientation of the pot and the location of the sample had no significant effect. To further examine the seeming minimal effect of vessel orientation on the measured D_e, it would be possible in the future to determine D_e for a set of samples taken from different locations on the same vessel.
2. Whether standing or lying on its side, the pot can be buried up to 100% in fill, or be unburied and thus exposed to air up to 100%.	Two scenarios were considered: the vessel lying on the surface of the fill or buried ∼15 cm, which for bowls means they are completely buried and for storage jars, they are buried up to half their height. Again, no measurable change was observed.
3. The vessels can be filled from 0% to 100% with either fill or other contents (e.g. organic bulk residue). NB No mention of organic residue was found in Garstang's report or present in the vessel today, so this was discounted as usually, if an ancient organic substance was recovered from a vessel during excavations in this era, these were left *in situ*.	Two scenarios were considered: the vessel was filled with fill or it had no fill inside it. Again, no measurable change was observed.

Table 5.9: (continued)

Modelling Unknown	Effect on modelled dose rate of the Bêt Khallaf assemblage
4. How does the density of the vessel's clay matrix affect the external $\dot{D}$?	Although we were not able to measure the clay density of all vessels, a single sherd (X5460) was measured as having a density of 1.4g/cm^3. In the visual analysis that accompanied each of the vessels the density of the vessels was determined as being 'high', 'medium', or 'low'. Independently of the density measurement carried out upon X5460, the vessel this sherd came from was deemed to have a 'low' density. Thus, based on this information, we were able to extrapolate that the density for vessels deemed to have a medium density was likely to be $\sim$1.6g/cm^3, and for vessels with a 'high' density, $\sim$1.8g/cm^3.[37] Two scenarios were considered: the clay density was either set to its known value or to a reference value of 1.8g/cm^3. No measurable change was observed between the two scenarios and thus it was concluded that although the clay densities are not known precisely for each vessel, variation within the likely range of values will not affect the result.
5. How does the density of the fill affect the external $\dot{D}$?	Two different fill densities were considered: 1.2g/cm^3 and 1.7g/cm^3 and no measurable change was observed. Thus while the density of the fill is very much an unknown quantity, given that the fill density is visibly less than that of the low density clay whose density was measured (as above), the value of 1.2g/cm^3 was used in final dose rate calculation. Thus, while the exact density of the Bêt Khallaf tomb fill can not be reconstructed accurately, simulation of two different scenarios illustrates that within the likely range of fill densities which could be present at Bêt Khallaf, variation within this range will not affect the modelled dose rate.

Table 5.9: (continued)

Modelling Unknown	Effect on modelled dose rate of the Bêt Khallaf assemblage
6. The vessel's proximity to the tomb walls, that is, its location within the tomb. Was it in the centre, corner, or along a side of the tomb?	A limited study of this was carried out at low resolution and no measurable changes were observed. Given the very low attenuation rates of gamma rays in air with low moisture content, this is to be expected.

As well as specifying the chemical composition and radionuclide concentrations for the pottery, it is also necessary to specify them for the fill and tomb walls, that is, the surrounding burial environment. For both the fill and the tomb walls we were able to use the radionuclide concentrations obtained directly from the seven samples of depositional material adhering to vessels from the Bêt Khallaf assemblage. These have been discussed and presented above in Table 5.3. As was mentioned above, an average value was calculated from all seven samples, because the long attenuation depth of gamma radiation means that it is more important to have a value which represents the entire burial environment rather than just the immediate surroundings of the vessel, considering complex geometries such as we see at Bêt Khallaf. Assuming the external dosimetries represent independent samples of the mean levels of radionuclide concentrations within the burial environment, we can estimate the error of this mean as the standard error of the seven samples (given in Table 5.3). It is assumed that this error will lead to an additional relative source of error in the dose rates calculated from the DosiVox simulations that is not more than the relative size of the error in the mean concentrations, and thus we include this error in quadrature with the relative error from the DosiVox simulations.

After these considerations were tested, final gamma dose rate calculations (composed of individual U, Th, and K simulated measurements) were obtained using DosiVox for each sample, and these are presented in Table 5.10.

[37] Ideally one would wish to measure the exact density of each vessel. However, given the restrictions on this (and the unlikelihood of museums permitting this measurement), for this project it was essential to extrapolate this information.

Table 5.10: Final dose rates determined by DosiVox for each Bêt Khallaf sample.

Sample ID	^{238}U (Gy ka^{-1})	^{238}U err (Gy ka^{-1})	^{232}Th (Gy ka^{-1})	^{232}Th err (Gy ka^{-1})	^{40}K (Gy ka^{-1})	^{40}K err (Gy ka^{-1})	Total (Gy ka^{-1})	Err (Gy ka^{-1})
X4114	0.125	0.02	0.152	0.06	0.230	0.04	0.507	0.099
X4115	0.180	0.08	0.166	0.04	0.254	0.06	0.600	0.132
X4116	0.166	0.04	0.183	0.02	0.233	0.03	0.582	0.091
X4117	0.163	0.02	0.171	0.03	0.241	0.03	0.575	0.087
X4118	0.131	0.03	0.171	0.04	0.249	0.02	0.551	0.088
X5458	0.150	0.07	0.166	0.04	0.230	0.01	0.546	0.107
X5459	0.152	0.03	0.172	0.02	0.232	0.03	0.556	0.085
X5460	0.120	0.03	0.162	0.05	0.244	0.03	0.526	0.094
X5461	0.156	0.07	0.157	0.02	0.278	0.06	0.591	0.121
X5462	0.155	0.04	0.150	0.03	0.260	0.02	0.565	0.090
X5463	0.134	0.02	0.164	0.02	0.262	0.04	0.560	0.086
X5464	0.108	0.02	0.205	0.06	0.211	0.04	0.524	0.100
X5465	0.147	0.04	0.169	0.02	0.243	0.03	0.559	0.089
X5466	0.169	0.05	0.197	0.05	0.272	0.02	0.638	0.109
X5467	0.159	0.04	0.169	0.03	0.245	0.02	0.573	0.091
X5468	0.172	0.03	0.163	0.02	0.229	0.04	0.564	0.090
X5470	0.157	0.05	0.152	0.04	0.229	0.04	0.538	0.102
X5472	0.144	0.03	0.135	0.05	0.273	0.03	0.552	0.096
X5473	0.133	0.03	0.169	0.02	0.235	0.04	0.537	0.087

These values were determined under the following assumptions (these are considered to be the 'best assumptions', though we note that since changing these assumptions produced negligible change it does not matter strongly which final assumptions we choose):

- Fill density: 1.2 g/cm^3
- Clay density: estimates of actual ceramic densities (see Table 5.9, point 4)
- Unburied and empty of fill
- Standing upright (tall vessels only) on their bases

Appendix G presents a sample input file for a DosiVox simulation.

Table 5.11: OSL ages calculated for each Bêt Khallaf sample, including alpha, beta, and cosmic dose rates calculated by DRAC, and gamma dose rates calculated by DosiVox.

Sample ID	Fine/ coarse grain	Alpha dose rate ($Gy\,ka^{-1}$)	Alpha dose rate error ($Gy\,ka^{-1}$)	Beta dose rate ($Gy\,ka^{-1}$)	Beta dose rate error ($Gy\,ka^{-1}$)	Gamma dose rate ($Gy\,ka^{-1}$)	Gamma dose rate error ($Gy\,ka^{-1}$)	Cosmic dose rate ($Gy\,ka^{-1}$)	Cosmic dose rate error ($Gy\,ka^{-1}$)	Total dose rate ($Gy\,ka^{-1}$)	Total dose rate error ($Gy\,ka^{-1}$)	D_e (Gy)	D_e error (Gy)	Age (ka)	Age err (ka)
X4114	CG	0.072	0.026	0.931	0.053	0.507	0.099	0.051	0.005	1.561	0.115	7.45	0.94	4.773	0.698
X4115	CG	0.110	0.030	1.239	0.064	0.600	0.132	0.051	0.005	2.000	0.150	7.31	0.25	3.655	0.301
X4115	FG	0.260	0.022	1.333	0.065	0.600	0.132	0.051	0.005	2.244	0.149	8.33	0.74	3.712	0.412
X4116	CG	0.143	0.039	1.133	0.054	0.582	0.091	0.056	0.006	1.914	0.113	6.66	1.31	3.480	0.715
X4117	FG	0.333	0.028	1.424	0.067	0.575	0.087	0.051	0.005	2.383	0.113	12.53	1.94	5.258	0.852
X4118	CG	0.108	0.030	1.397	0.074	0.551	0.088	0.056	0.006	2.112	0.119	12.00	0.46	5.682	0.388
X4118	FG	0.256	0.021	1.500	0.075	0.551	0.088	0.051	0.005	2.358	0.118	11.59	1.04	4.915	0.505

Table 5.11: (continued)

Sample ID	Fine/ coarse grain	Alpha dose rate ($Gy\,ka^{-1}$)	Alpha dose rate error ($Gy\,ka^{-1}$)	Beta dose rate ($Gy\,ka^{-1}$)	Beta dose rate error ($Gy\,ka^{-1}$)	Gamma dose rate ($Gy\,ka^{-1}$)	Gamma dose rate error ($Gy\,ka^{-1}$)	Cosmic dose rate ($Gy\,ka^{-1}$)	Cosmic dose rate error ($Gy\,ka^{-1}$)	Total dose rate ($Gy\,ka^{-1}$)	Total dose rate error ($Gy\,ka^{-1}$)	D_e (Gy)	D_e error (Gy)	Age (ka)	Age err (ka)
X5458	CG	0.131	0.035	1.091	0.053	0.546	0.107	0.018	0.002	1.786	0.124	10.50	0.37	5.879	0.459
X5458	FG	0.311	0.026	1.179	0.054	0.546	0.107	0.018	0.002	2.054	0.122	9.22	0.45	4.489	0.346
X5459	CG	0.147	0.052	1.201	0.062	0.556	0.085	0.018	0.002	1.922	0.117	7.68	2.32	3.996	1.231
X5460	CG	0.098	0.035	1.374	0.079	0.526	0.094	0.051	0.005	2.049	0.127	9.98	0.60	4.871	0.421
X5460	FG	0.256	0.021	1.500	0.075	0.526	0.094	0.051	0.005	2.333	0.122	10.79	0.75	4.625	0.402
X5461	CG	0.102	0.028	1.400	0.075	0.591	0.121	0.051	0.005	2.144	0.145	10.56	0.40	4.925	0.381
X5461	FG	0.241	0.020	1.502	0.076	0.591	0.121	0.051	0.005	2.385	0.144	9.02	1.17	3.782	0.541
X5462	CG	0.054	0.010	1.184	0.063	0.565	0.090	0.056	0.006	1.859	0.110	8.37	0.90	4.502	0.553

Table 5.11: (continued)

Sample ID	Fine/ coarse grain	Alpha dose rate ($Gy\,ka^{-1}$)	Alpha dose rate error ($Gy\,ka^{-1}$)	Beta dose rate ($Gy\,ka^{-1}$)	Beta dose rate error ($Gy\,ka^{-1}$)	Gamma dose rate ($Gy\,ka^{-1}$)	Gamma dose rate error ($Gy\,ka^{-1}$)	Cosmic dose rate ($Gy\,ka^{-1}$)	Cosmic dose rate error ($Gy\,ka^{-1}$)	Total dose rate ($Gy\,ka^{-1}$)	Total dose rate error ($Gy\,ka^{-1}$)	D_e (Gy)	D_e error (Gy)	Age (ka)	Age err (ka)
X5463	CG	0.094	0.034	1.334	0.077	0.560	0.086	0.051	0.005	2.039	0.121	8.95	0.39	4.389	0.323
X5463	FG	0.245	0.020	1.456	0.074	0.560	0.086	0.051	0.005	2.312	0.116	9.08	0.26	3.927	0.226
X5464	CG	0.103	0.029	1.267	0.067	0.524	0.100	0.051	0.005	1.945	0.124	8.57	0.24	4.406	0.307
X5464	FG	0.243	0.020	1.362	0.068	0.524	0.100	0.051	0.005	2.180	0.123	9.13	0.23	4.188	0.258
X5465	CG	0.131	0.036	1.408	0.072	0.559	0.089	0.051	0.005	2.149	0.120	8.87	0.87	4.128	0.466
X5465	FG	0.310	0.026	1.517	0.074	0.559	0.089	0.051	0.005	2.437	0.119	9.80	0.28	4.021	0.227
X5466	CG	0.278	0.102	1.991	0.101	0.638	0.109	0.051	0.005	2.958	0.181	2.92	0.20	0.987	0.091
X5467	CG	0.088	0.032	1.338	0.078	0.573	0.091	0.056	0.006	2.055	0.124	8.10	0.47	3.942	0.330

Table 5.11: (continued)

Sample ID	Fine/ coarse grain	Alpha dose rate ($Gy\,ka^{-1}$)	Alpha dose rate error ($Gy\,ka^{-1}$)	Beta dose rate ($Gy\,ka^{-1}$)	Beta dose rate error ($Gy\,ka^{-1}$)	Gamma dose rate ($Gy\,ka^{-1}$)	Gamma dose rate error ($Gy\,ka^{-1}$)	Cosmic dose rate ($Gy\,ka^{-1}$)	Cosmic dose rate error ($Gy\,ka^{-1}$)	Total dose rate ($Gy\,ka^{-1}$)	Total dose rate error ($Gy\,ka^{-1}$)	D_e (Gy)	D_e error (Gy)	Age (ka)	Age err (ka)
X5467	FG	0.229	0.019	1.458	0.075	0.573	0.091	0.056	0.006	2.316	0.119	6.84	1.13	2.953	0.511
X5468	CG	0.136	0.037	1.156	0.056	0.564	0.134	0.051	0.005	1.907	0.150	8.65	0.55	4.536	0.459
X5468	FG	0.323	0.027	1.250	0.058	0.571	0.086	0.051	0.005	2.195	0.108	9.37	0.35	4.269	0.263
X5470	CG	0.092	0.034	1.193	0.068	0.538	0.102	0.051	0.005	1.874	0.127	8.11	0.44	4.330	0.376
X5470	FG	0.238	0.020	1.304	0.065	0.538	0.102	0.051	0.005	2.131	0.123	9.87	0.93	4.632	0.511
X5472	CG	0.092	0.033	1.282	0.073	0.552	0.096	0.051	0.005	1.977	0.125	9.25	0.20	4.679	0.313
X5472	FG	0.242	0.020	1.398	0.070	0.552	0.096	0.051	0.005	2.243	0.121	10.19	1.78	4.543	0.830
X5473	CG	0.119	0.032	1.245	0.063	0.537	0.087	0.051	0.005	1.952	0.112	8.35	1.21	4.278	0.667

Table 5.11: (continued)

Sample ID	Fine/ coarse grain	Alpha dose rate ($Gy\,ka^{-1}$)	Alpha dose rate error ($Gy\,ka^{-1}$)	Beta dose rate ($Gy\,ka^{-1}$)	Beta dose rate error ($Gy\,ka^{-1}$)	Gamma dose rate ($Gy\,ka^{-1}$)	Gamma dose rate error ($Gy\,ka^{-1}$)	Cosmic dose rate ($Gy\,ka^{-1}$)	Cosmic dose rate error ($Gy\,ka^{-1}$)	Total dose rate ($Gy\,ka^{-1}$)	Total dose rate error ($Gy\,ka^{-1}$)	D_e (Gy)	D_e error (Gy)	Age (ka)	Age err (ka)
X5473	FG	0.283	0.024	1.341	0.064	0.537	0.087	0.051	0.005	2.212	0.111	9.39	0.35	4.245	0.265

Final age calculations were made by using the DosiVox gamma dose rates and the attenuated internal alpha and beta dose rate values obtained from using the DRAC program. The final age calculations, and the associated dose rate measurements, for the Bêt Khallaf assemblage are presented in Table 5.11.

Table 5.12: A comparison of the DosiVox gamma dose rate and the gamma geometries (50% and 100%) obtained using DRAC.

Sample ID	DRAC $\dot{D}_\gamma$ (100% geometry) (Gy ka^{-1})	DRAC $\dot{D}_\gamma$ error (100% geometry) (Gy ka^{-1})	DRAC $\dot{D}_\gamma$ (50% geometry) (Gy ka^{-1})	DRAC $\dot{D}_\gamma$ error (50% geometry) (Gy ka^{-1})	DosiVox $\dot{D}_\gamma$ (Gy.ka-1)	DosiVox $\dot{D}_\gamma$ error (Gy ka^{-1})
X4114	0.523	0.033	0.262	0.017	0.507	0.099
X4115	0.523	0.033	0.262	0.017	0.600	0.132
X4116	0.523	0.033	0.262	0.017	0.582	0.091
X4117	0.523	0.033	0.262	0.017	0.575	0.087
X4118	0.523	0.033	0.262	0.017	0.551	0.088
X5458	0.600	0.039	0.300	0.020	0.546	0.107
X5459	0.459	0.029	0.230	0.015	0.556	0.085
X5460	0.523	0.033	0.262	0.017	0.526	0.094
X5461	0.523	0.033	0.262	0.017	0.591	0.121
X5462	0.523	0.033	0.262	0.017	0.565	0.090
X5463	0.619	0.039	0.310	0.020	0.560	0.086
X5464	0.523	0.033	0.262	0.017	0.524	0.100
X5465	0.523	0.033	0.262	0.017	0.559	0.089
X5466	0.523	0.033	0.262	0.017	0.638	0.109
X5467	0.523	0.033	0.262	0.017	0.573	0.091
X5468	0.523	0.033	0.262	0.017	0.564	0.090
X5470	0.523	0.033	0.262	0.017	0.538	0.102
X5472	0.523	0.033	0.262	0.017	0.552	0.096
X5473	0.523	0.033	0.262	0.017	0.537	0.087

Table 5.12 shows the gamma dose rates calculated by DosiVox compared to those calculated by DRAC using an infinite matrix assumption and an assumption of either 2π or 4π geometry. As discussed above, prior to the incorporation of DosiVox into this project, the archaeological evidence indicated that a 2π geometry assumption would

be the most appropriate, following prior researchers (Rhodes et al. 2009), and that this would constitute the 'best guess' for the Bêt Khallaf geometry situation. However, it was also considered that given the lack of moisture present in the tomb, the radiation attenuation radius would be much larger than the standard, assumed 30cm radius; this is because the part of the pot unburied, and thus surrounded by air, would receive a dose from the closest radiation-emitting material that the vessel was separated from by air, in this case, the tomb walls. Due to the low levels of moisture, the radiation from the tomb walls would have passed straight through the air and thus would have also affected the radiation received by the vessel. In this case one could predict that a 4π geometry might be closer to the true radiation absorbed. The difference between a 2π and a 4π geometry would significantly alter the calculated ages, and thus, the benefit of the DosiVox program was again that it could accurately determine the gamma dose rate without having to rely upon assumed geometries based upon the infinite matrix assumption. Table 5.12 illustrates the significant difference of dose rate calculations determined by DosiVox as compared to using an infinite matrix assumption of 2π geometry: in fact, the DosiVox gamma dose rates are more similar to the figures for an assumption of 4π geometry. Thus, the use of a 2π geometry assumption, would have resulted in a significant error, although initially, prior to the application of DosiVox, this assumption would have been considered the most likely 'best guess' scenario.

It is clear therefore that the incorporation of DosiVox radiation transport modelling into this project has been of immense value. Without this program, the results generated would have been far more unreliable as they would have had to rely on educated guesswork, rather than direct modelling. Furthermore, DosiVox has allowed us to test a variety of assumptions and see how these affected the dose rate, something that would have been impossible when using approximate scaled geometries. This project has in fact been the first 'real-world' application of the DosiVox program to archaeological material and the results of this work presented here show very clearly the powerful potential this program can offer. This project has used DosiVox on a non-ideal situation (i.e. museum

material without detailed excavation accounts) with powerful results, so the benefits of using this program with ideal situations (i.e. recently excavated, well-documented contexts) would be significant. Based on the results of this project, we would strongly recommend DosiVox be used for all future luminescence dating projects which require the reconstruction of external dose rate calculations.

It is important to note that the values of the DosiVox dose rates are higher on average than the 100% geometry assumption (with a t-test confidence level of 95%), and, furthermore, that we are not asserting that the closeness of the DosiVox value to the 100% geometry value is a general result (see for example, the results from the Tomb of Djer given later in Chapter 8). The particular closeness for the tombs of Bêt Khallaf is likely to have resulted from two properties: first, that the walls and floor of the tomb are made uniformly from the local bedrock, and the fill is derived from it, and secondly that the air in the tomb has a low water content (3±2%) which limits the attenuation of the radiation originating from the tomb walls and ceiling. The fact that the DosiVox values are slightly higher is possibly a result of including the gamma radiation originating from the vessel, something which is not included in the DRAC calculation.

5.4 OSL age estimates for the Bêt Khallaf assemblage

As already discussed, Table 5.11 presents the OSL ages calculated for the Bêt Khallaf samples. Given the nature of the samples (i.e. very small sample sizes and thus a smaller number of accepted aliquots for each sample) it is very encouraging to see results which are in good agreement. We do, however, see in these results larger errors than is common in OSL dating of non-MET samples. It can also be seen that the main source of error in the Bêt Khallaf samples comes from the variations in D_e measurement, rather than dose rate calculations for $\dot{D}_{ext}$ or $\dot{D}_{int}$.

It has become common practice in radiocarbon dating (and increasingly in OSL dating too—see references provided in Section 3.1.3) to address the occurrence of measurement scatter and error by applying Bayesian modelling to the data. As already discussed

in Section 3.1.3, this technique employs mathematical models based upon Bayes' theorem, which allows one to infer the most likely age range of a set of archaeological dates based upon not only the measurements themselves, but *a priori* information from the archaeological record which may be able to inform further the likelihood of a specific date range.

Given the wide error ranges associated with the OSL dates for the Bêt Khallaf material, Bayesian modelling was applied to the data set, using the latest version (Version 4.2) of the OxCal program (Bronk Ramsey 1995; Bronk Ramsey 2009), in order to examine the most likely age range of the material.

The *a priori* assumptions used in the construction of this model were:

1. Based upon the architectural design of the tombs, the diagnostic ceramic assemblage, and the inscriptional material present in the tombs (i.e. seal impressions with the name of Djoser), we can assume that the Bêt Khallaf tombs from where the pottery comes (K1, K2, K3, and K5) are contemporary with one another (Garstang and Sethe 1903: 14,19).

2. Both the morphology of the ceramic assemblage, as well as the OSL data, suggest that three phases of ceramic material are present at Bêt Khallaf: a primary context of diagnostically distinct late Naqada III/early Old Kingdom ceramics; a secondary context of late First Intermediate Period material; and a tertiary context consisting of a single object whose OSL age suggested an mediaeval Islamic date. The multiphase model incorporated these three distinct phases seen in the OSL data, which were further supported by the observable ceramic typology.

   In general, it is not considered best-practice in Bayesian modelling to allow absolute dates to govern phase erection. However, in this case the majority of vessels in each phase were supported by *a priori* typological information. Only in a few cases do we allow an undiagnostic vessel to be clustered with a phase due to its date when it is typologically undiagnostic. This was considered acceptable in this

case given the absolute date is the only diagnostic information (furthermore, additional models were run excluding the undiagnostic vessels, and the results were essentially the same). Additionally, an overall boundary was assigned to the model to limit the model to search for solutions between 4000 BC and AD 500 (i.e. these boundaries were broad enough not to peremptorily truncate the errors associated with the OSL results, but limiting enough for the model to run more efficiently).

Table 5.13: The final OSL ages used in OxCal, based upon the combination of fine and coarse grain measurements from the same sample where applicable (i.e. where both grain types were present for a single sample)[38]. Where a combination of both fine and coarse grains were used, the robustness of combining both values was determined by a chi squared (χ^2) test, using the `R_combine` function in the OxCal programme. The degree of freedom for each sample was 1 and the 5% confidence threshold value is 3.8 (i.e. above this value, the χ^2 test fails.) [39]

Sample ID	Age (ka)	Err (ka)	Type	χ^2
X4114	4.773	0.698	CG	N/A
X4115	3.675	0.243	Combined	0.0
X4116	3.684	0.247	CG	N/A
X4117	5.258	0.852	FG	N/A
X4118	5.435	0.309	Combined	1.4
X5458	5.134	0.490	Combined	6.1
X5459	3.996	1.231	CG	N/A
X5460	4.747	0.291	Combined	0.2
X5461	4.639	0.316	Combined	2.8
X5462	4.502	0.553	CG	N/A
X5463	4.096	0.186	Combined	1.4
X5464	4.282	0.198	Combined	0.2
X5465	4.042	0.204	Combined	0.0
X5466	0.987	0.091	CG	N/A
X5467	3.732	0.281	Combined	2.5
X5468	4.340	0.228	Combined	0.3
X5470	4.443	0.303	Combined	0.2
X5472	4.663	0.293	Combined	0.0
X5473	4.250	0.246	Combined	0.0

[38]In this table the ages are presented in ka, as opposed to years BC because this is the input value

3. Fine grain aliquots and coarse grain aliquots from the OSL samples come from the same vessel and can therefore be considered to be the same age archaeologically. These two measurements were combined using kernel density estimation (KDE) using the R Luminescence Shiny package KDE function.[40] The final age results of the combined fine and coarse grain data can be seen in Table 5.13 and these values were used within the modelling program.

4. All vessels were assigned an outlier probability of 5%.

The first case model run in OxCal (Case 1, see Appendix H for the OxCal model input file), with the above-mentioned assumptions factored into a multiphase model, produced a model with an agreement index of 49.1, that is, just shy of the 60.0 agreement index which indicates a good model agreement and consistency (Bronk Ramsey 1995). However, vessel X4115 gave very poor agreement (10.0 agreement index) and from the OSL results it was seen to be of a much younger age than the rest of the assemblage. We know, however, that this vessel type (i.e. internal rim bowls with early rim development) is particularly diagnostic and is classically late Early Dynastic/early Old Kingdom in style. There is sufficient archaeological evidence (see discussion in Section 2.1 and Section 6.2) to indicate that this vessel type must be grouped with the Early Dynastic cluster. Upon further visual investigation of this vessel, it was realised that it had burn marks upon it which were consistent with a post-manufacture heating event. It is very likely therefore that the OSL measurement for X4115 is for a secondary firing event, that is, the OSL signal was reset at a later point in time (perhaps pertaining to secondary depositional activities occurring in the tomb). This phenomenon seems to be

required for the OxCal program.

[39]Of the samples presented here only X5458 failed to pass the χ^2 test. It would generally be deemed prudent to remove this sample from analysis. However, here we have retained this sample as there was no *a priori* archaeological or scientific reason to exclude this sample: we make a similar argument below for two vessels (X4116 and X4118) which show low agreement in our Bayesian model. It is worth noting that should this vessel be removed from the analysis or removed the coarse grain value for the vessel (i.e. if we deemed measurement error to be the cause of this discrepancy), this would improve the final analysis. However, for the sake of ensuring that excessive data-smoothing is not occurring at any stage in this project, we have made the decision to include this sample in the analysis at the expense of an increased degree of error in the final calculated ages.

[40] Available at: http://zerk.canopus.uberspace.de/R.Lum/

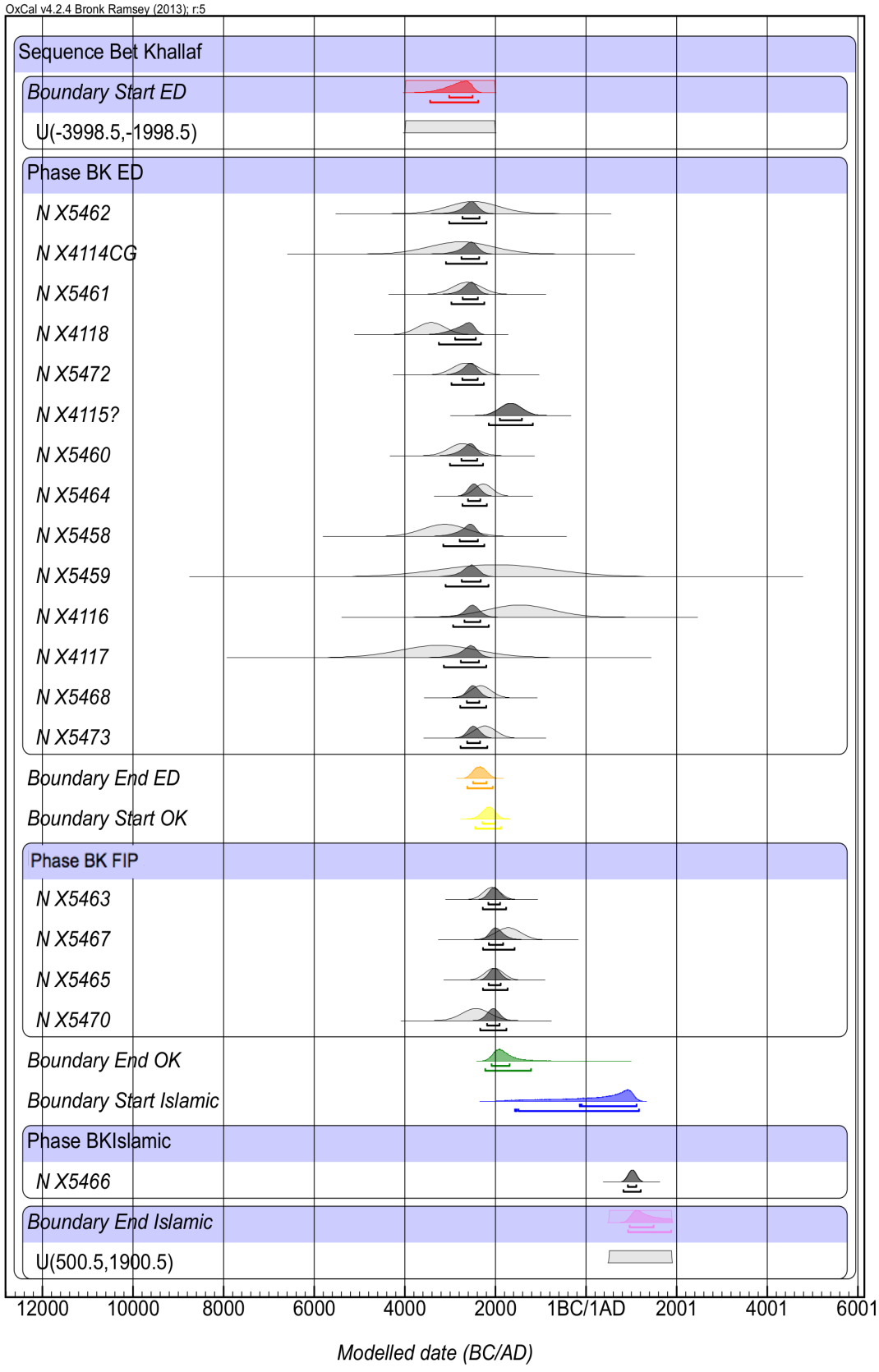

Figure 5.9: Multiphase plot showing the results of Bayesian modelling for Case 2. ED = Early Dynastic Period; FIP = First Intermediate Period.

Name Show all Show structure	Unmodelled (BC/AD)									Modelled (BC/AD)									Indices A_{model}=74.3 $A_{overall}$=73.4				Select All Visible	Page break
	from	to	%	from	to	%	μ	σ	m	from	to	%	from	to	%	μ	σ	m	A_{comb}	A	L	P	C	
Outlier_Model General										-136	134	68.2	-1146	572	95.4	-62	349	-1					99.9	34
T(5)	-1.135	1.135	68.2	-2.65	2.65	95.4	-2.26696e-8	1.29081	2.04945e-12							-0.0877439	1.21392	-0.085					98.4	35
U(0,4)	3.98986e-17	4	68.2	3.98986e-17	4	95.4	2	1.1431	2	5.37764e-17	2.904	68.1	5.37764e-17	3.66	95.4	1.82976	1.07475	1.82		100			99.1	2
Sequence Bet Khallaf																								3
Boundary Start ED	-4000	-2000	68.2	-4000	-2000	95.4	-3000	572	-3000	-3020	-2504	68.2	-3442	-2380	95.4	-2848	280	-2798		100			97.4	4
U(-3998.5,-1998.5)	-4000	-2000	68.2	-4000	-2000	95.4	-3000	572	-3000															5
Phase BK ED																								6
N X5462	-3052	-1924	68.2	-3594	-1382	95.4	-2488	553	-2488	-2728	-2352	68.2	-3021	-2197	95.4	-2577	198	-2557		133.4		95.9	99.9	7
N X4114CG	-3471	-2047	68.2	-4155	-1363	95.4	-2759	698	-2759	-2751	-2360	68.2	-3093	-2192	95.4	-2599	213	-2569		133		95.8	99.9	8
N X5461	-2947	-2303	68.2	-3257	-1993	95.4	-2625	316	-2625	-2723	-2388	68.2	-2973	-2246	95.4	-2584	177	-2565		124.3		96.2	99.8	9
N X4118	-3736	-3106	68.2	-4039	-2803	95.4	-3421	309	-3421	-2891	-2433	68.2	-3249	-2319	95.4	-2730	242	-2684		23.9		88.8	99.6	10
										Warning! Poor agreement - A= 23.9%(A'c= 60.0%)														
N X5472	-2948	-2350	68.2	-3235	-2063	95.4	-2649	293	-2649	-2731	-2391	68.2	-2972	-2257	95.4	-2590	175	-2570		121		96.2	99.9	11
N X4115	-1909	-1413	68.2	-2147	-1175	95.4	-1661	243	-1661	-1904	-1416	68.2	-2147	-1175	95.4	-1662	243	-1661				0.7	99.2	12
N X5460	-3030	-2436	68.2	-3315	-2151	95.4	-2733	291	-2733	-2752	-2402	68.2	-3005	-2274	95.4	-2611	181	-2589		112.5		96	99.8	13
N X5464	-2470	-2066	68.2	-2664	-1872	95.4	-2268	198	-2268	-2606	-2335	68.2	-2729	-2190	95.4	-2466	134	-2467		83.9		95.8	99.8	14
N X5458	-3620	-2620	68.2	-4100	-2140	95.4	-3120	490	-3120	-2790	-2388	68.2	-3152	-2246	95.4	-2643	222	-2604		85.6		95.6	99.8	15
N X5459	-3238	-726	68.2	-4444	481	95.4	-1982	1231	-1982	-2744	-2326	68.2	-3101	-2154	95.4	-2580	213	-2560		125.1		95.6	99.9	16
N X4116	-2195	-737	68.2	-2896	-36	95.4	-1466	715	-1466	-2684	-2334	68.2	-2935	-2148	95.4	-2529	184	-2520		48.7		95.1	99.9	17
										Warning! Poor agreement - A= 48.7%(A'c= 60.0%)														
N X4117	-4113	-2375	68.2	-4948	-1540	95.4	-3244	852	-3244	-2765	-2364	68.2	-3139	-2202	95.4	-2619	225	-2586		106.4		95.5	99.8	18
N X5468	-2559	-2093	68.2	-2782	-1870	95.4	-2326	228	-2326	-2632	-2356	68.2	-2778	-2203	95.4	-2493	141	-2493		100.6		96.1	99.8	19
N X5473	-2487	-1985	68.2	-2728	-1744	95.4	-2236	246	-2236	-2625	-2340	68.2	-2770	-2180	95.4	-2481	143	-2482		85.5		95.7	99.8	20
Boundary End ED										-2494	-2199	68.2	-2621	-2061	95.4	-2343	143	-2346					99	21
Boundary Start FIP										-2285	-2004	68.2	-2445	-1881	95.4	-2156	141	-2151					99.2	22
Phase BK FIP																								23
N X5463	-2272	-1892	68.2	-2454	-1710	95.4	-2082	186	-2082	-2157	-1898	68.2	-2280	-1764	95.4	-2023	128	-2025		114.6		96.3	99.8	24
N X5467	-2005	-1431	68.2	-2280	-1156	95.4	-1718	281	-1718	-2145	-1831	68.2	-2275	-1578	95.4	-1953	172	-1971		91.8		95.8	99.8	25
N X5465	-2236	-1820	68.2	-2436	-1620	95.4	-2028	204	-2028	-2150	-1885	68.2	-2276	-1732	95.4	-2008	135	-2013		119.8		96.3	99.8	26
N X5470	-2738	-2120	68.2	-3035	-1823	95.4	-2429	303	-2429	-2185	-1909	68.2	-2337	-1758	95.4	-2046	143	-2046		67		95.4	99.9	27
Boundary End OK										-2086	-1688	68.2	-2226	-1215	95.4	-1795	285	-1854					97.1	28
Boundary Start Islamic										-141	1116	68.3	-1570	1169	95.5	185	792	449					96.5	29
Phase BKIslamic																								30
N X5466	935	1121	68.2	846	1210	95.4	1028	91	1028	923	1110	68.2	827	1208	95.4	1015	98	1016		100		95.9	99.6	31
Boundary End Islamic	500	1900	68.2	500	1900	95.4	1200	400	1200	962	1493	68.2	930	1882	95.4	1313	263	1260		100			99.4	32
U(500.5,1900.5)	500	1900	68.2	500	1900	95.4	1200	400	1200															33

Figure 5.10: Table showing the multiphase model results for Case 2. ED = Early Dynastic Period; FIP = First Intermediate Period.

localised to this vessel only. It is interesting to note that the determined OSL date of this vessel (which is probably dating the secondary burning), seems consistent with the modelled ages of the second ceramic phase seen in the model (this will be discussed further in Chapter 6). To prevent the anomalous OSL age for X4115 skewing the model, a second case model was created (Case 2) in which X4115 was given an outlier probability of 100%, that is, it was considered an outlier (see Appendix I for the OxCal model input file).

This second model (Case 2, i.e. the model which saw the removal of X4115 from analysis) produced an overall agreement index of 74.3%. Within this second model vessels X4116 and X4118 showed poor agreement (with agreement indices of 48.7% and 23.9% respectively). However, as there was no archaeological reason for these vessels being given a 100% outlier probability the values were not rejected. As this second model produced an overall agreement index of 74.3%, this model was accepted and it is this model which provides this project with its final OSL ages and accompanying error estimates.

Figure 5.9 illustrates the multi-plot phase model for this project (based upon the second OxCal case model for Case 2) and Figure 5.10 presents the output table from OxCal which provides the accompanying data for Figure 5.9. A summary of Figures 5.9 and 5.10 is given in Table 5.14, which also provides the ages produced by the model to 1 and 2 σ (i.e. 68.2% and 95.4% probability).

From the OSL results and the Bayesian modelling of these results we see three clear chronological phases within the Bêt Khallaf assemblage. After modelling, the central age model (CAM)[41] was used to determine the most likely central age of each phase. Figures

[41] The central age model (CAM) is one of the most common ways in OSL dating to estimate the central age of a group of age values with associated individual errors. The CAM weighs the data points to take into account a natural phenomenon in luminescence dating which sees older ages systematically coupled with higher errors. In fact, for OSL it is the relative error which gives an indication of data quality, not the absolute error, and the CAM corrects for this. It does this by calculating the weighted mean of the logarithm of the D_e values (the absolute errors for the logarithms are in fact the relative errors for the actual D_e values). Thus, calculating the weighted mean of the logarithms uses the relative errors as weights as is most appropriate for luminescence analysis. The CAM also corrects for over-dispersion (which comes from underestimating associated errors) within the data set by adjusting all individual errors simultaneously, adding a correcting factor to these errors which is adjusted until the over-dispersion is removed (Galbraith and Roberts 2012).

Table 5.14: Summary of Figure 5.10. All ages are in BC (i.e. negative ages are AD dates).

		95.4% Probability		68.2% Probability			
		From	To	From	To	μ	σ
PHASE 1	Boundary Start	3442	2380	3020	2504	2848	280
	X4114	3093	2192	2751	2360	2599	213
	X4115	2147	1175	1904	1416	1662	243
	X4116	2935	2148	2684	2334	2529	194
	X4117	3139	2202	2765	2364	2619	225
	X4118	3249	2319	2891	2433	2730	424
	X5458	3152	2246	2970	2388	2643	222
	X5459	3101	2154	2744	2326	2580	213
	X5460	3005	2274	2752	2402	2611	181
	X5461	2973	2246	2723	2388	2584	177
	X5462	3021	2197	2728	2352	2577	198
	X5468	2778	2203	2632	2356	2493	141
	X5472	2972	2257	2731	2391	2590	175
	X5473	2770	2180	2625	2340	2481	143
	Boundary End	2621	2061	2494	2199	2343	143
PHASE 2	Boundary Start	2445	1881	2285	2004	2156	141
	X5463	2280	1764	2157	1898	2023	128
	X5465	2276	1732	2150	1885	2008	135
	X5467	2275	1578	2145	1831	1953	172
	X5470	2337	1758	2185	1909	2046	143
	Boundary End	2226	1215	2086	1688	1795	285
PHASE 3	Boundary Start	1570	−1169	141	−1116	−185	792
	X5466	−827	−1208	−923	−1110	−1015	98
	Boundary End	−930	−1882	−962	−1493	−1313	263

5.11 and 5.12 are Abanico plots[42] which illustrate the data and the calculation of the CAM for the first and second phases. Phase 1 produces a date which is consistent with the later phases of the historical Third Dynasty (according to the Shaw 2000 chronology) or the end of the Second Dynasty/beginning of Third Dynasty (following the Hornung et al.

[42]An albanico plot is a data visualization tool used in luminescence dating which incorporates both a radial plot and a histogram (Dietze et al. 2016).

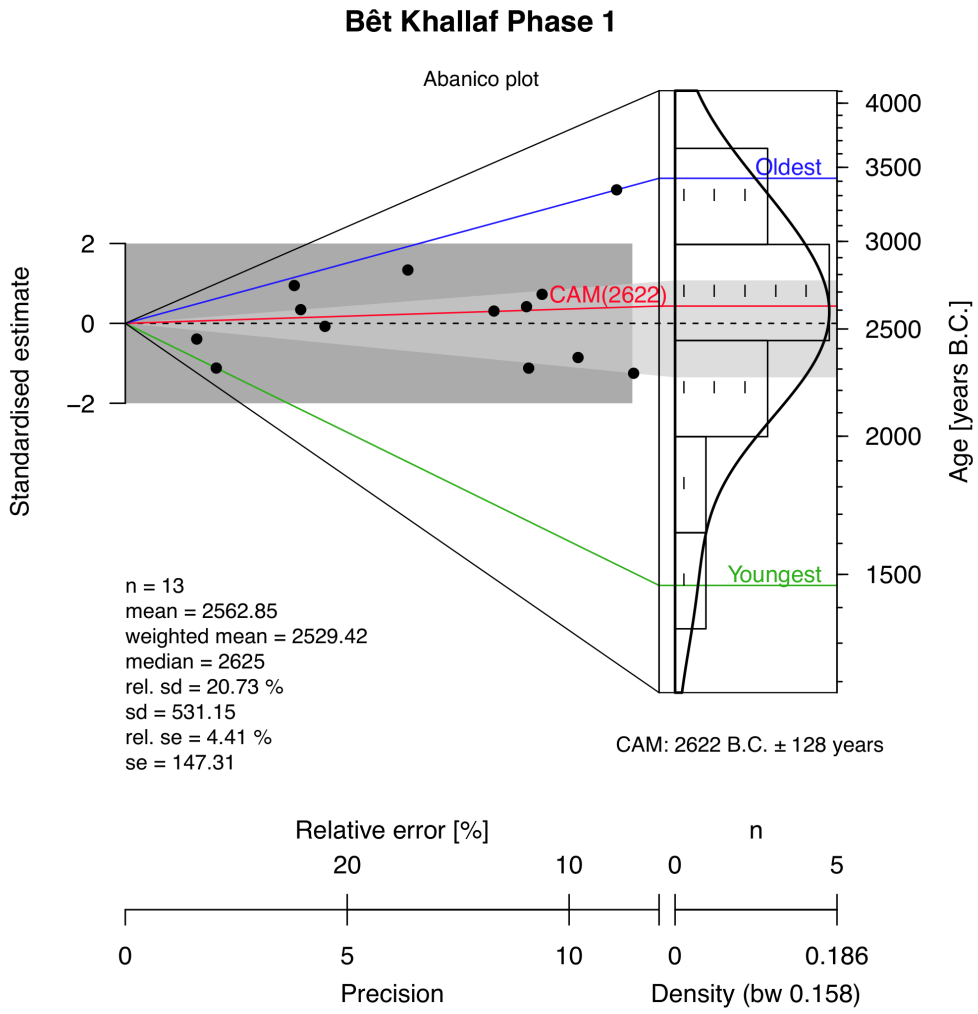

Figure 5.11: Abanico plot of the first phase of the Bêt Khallaf ceramic model. The central age model (CAM) is used to calculate the best estimate of the age of the assemblage.

2006 chronology; Table 2.1), with a central age of 2622 BC±128 years. Phase 2 produces an age cluster with a central age of 2082 BC±115 years, which corresponds to the late First Intermediate Period (Shaw 2000). Finally, Phase 3, which includes only one object is chronologically much later in date that the first two phases, being consistent with a mediaeval Islamic age of around AD 1000.

In Chapter 6, we will now discuss the archaeological significance and implications of these OSL results.

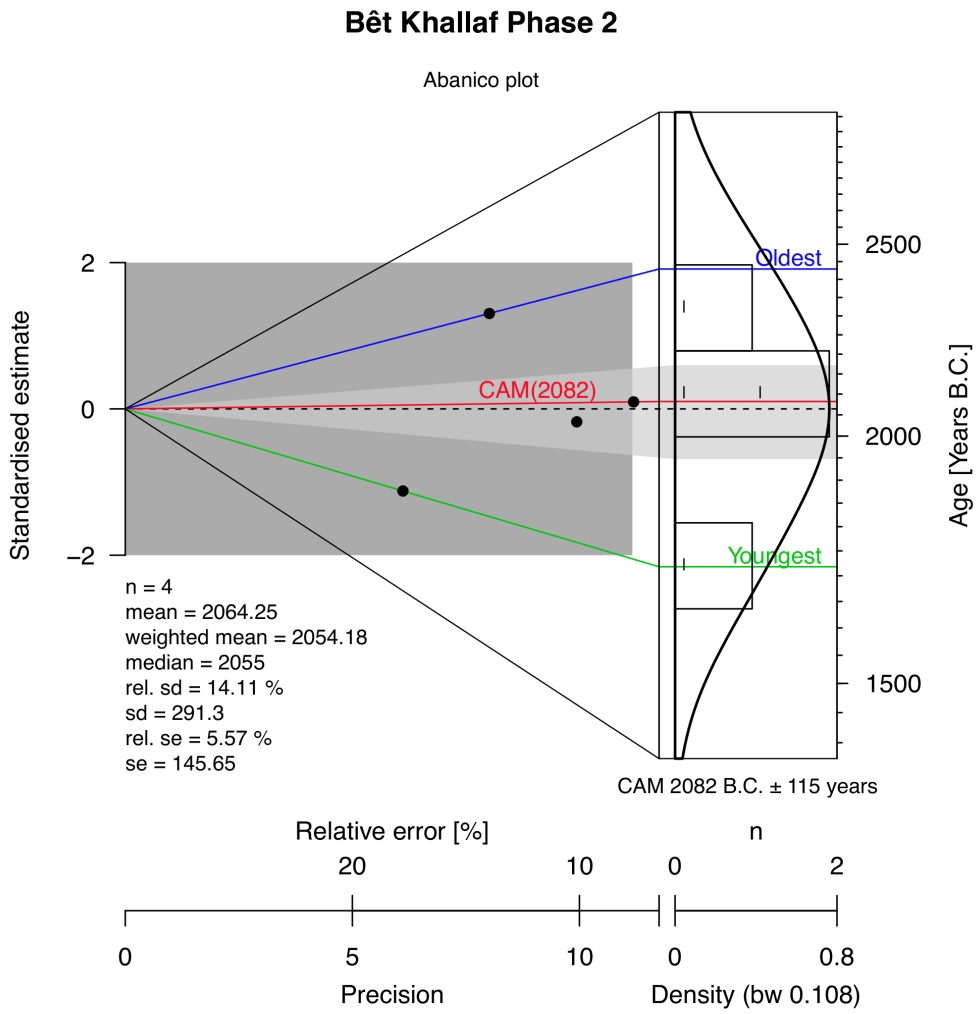

Figure 5.12: Abanico plot of the second phase of the Bêt Khallaf ceramic model. The central age model (CAM) is used to calculate the best estimate of the age of the assemblage.

Chapter 6

Comparison of the OSL dates with the relative ceramic chronology at Bêt Khallaf

The OSL results from the Bêt Khallaf assemblage, presented in Chapter 5, clearly illustrate three periods of archaeological activity at the cemetery site: the late Naqada III period/early Old Kingdom, the First Intermediate Period, and the Medieval Islamic period. This chapter will look at this assemblage, with its three represented archaeological periods, in more detail. It will examine how the archaeological record and material culture support the OSL measurements and lend to their interpretation. It will also offer a critique of the OSL measurements, leading to a discussion of the benefit of future OSL dating on similar material. This chapter will also examine how the OSL measurements compare to radiocarbon dates from material from the same relative chronological period. Finally, we will also discuss how these OSL results have contributed to our understanding of the Bêt Khallaf site, and the archaeological processes that formed its use history.

6.1 Assessment of the uncertainty of the OSL results when used in combination with Bayesian modelling and the relative chronology

Before comparing the OSL results to the relative chronology, it is necessary to discuss the implications of the Bayesian modelling for the Bêt Khallaf results. First, it is important to clarify the difference between the multiple individual events which comprise the final firing of each vessel, the three phases used in the Bayesian model, the three archaeological events whose properties we infer from the modelling and the three archaeological phases or periods in which we infer the events occurred. When we construct the Bayesian model, we group the individual events of each vessel being fired into three individual phases (i.e. we use a multiphase model) which are governed both by the OSL ages, and by the typological information assessed from the ceramic assemblage itself. However, at this stage, no assumptions are made about the duration of each of the three phases, simply that there are three phases, during which all of the vessel firings occurred, and that the three phases occurred in a particular order. Based on these model parameters, and additionally the OSL ages and errors, the Bayesian model gives probability distributions for the start and end date of each phase and probability distributions for the time of firing of each vessel.[43] In other words, if we consider, for example, the first phase, the Bayesian model has suggested that the most likely explanation of the OSL results (given the model parameters), is that the pots were fired over a period starting in 2848 BC $\pm$ 280 years and finishing in 2343 BC $\pm$ 143 years. It further suggests the most likely age of firing of each vessel from within that period, which is expressed by the modelled mean age, and associated error, for each pot. However, this is only the

[43] These probability distributions are characterised in this project by the 95.4% and 68.2% confidence intervals, as well as the mean and standard deviation (as can be seen in Table 5.14). In the following discussion, we generally use the 68.2% interval to discuss age ranges for individual vessels. This is justifiable in this case as we are relying on a small data set, and it is difficult at this stage to discuss the archaeological implications of the data using the 95.4% interval. It is hoped that in the future, with increased data, a 95.4% interval range can be used.

most likely scenario: if one considers the range associated with the start and end of the first phase, it is not inconsistent with the results to suggest that in fact the start and end of the phase occurred at the same time—that is, it is not inconsistent to suggest that all the pots were fired and buried at approximately the same time (i.e. a single burial event). Given prior knowledge of burial practices in ancient Egypt, it is more likely than not that the deposition of all vessels grouped together in a Bayesian phase happened at a single time (although not necessarily: as will be discussed below, the addition of more OSL dates in the future to this data set might indicate that the first phase represents a long or even additional depositional events) (e.g. Ikram 2015: 184, Grajetzki 2003:11, Baines and Lacovara 2002: 11). Thus it is possible to suggest that each Bayesian phase can be attributed to a single depositional event. In Section 5.4 the central age model (CAM) was used to calculate an estimate for the age of this depositional event and associated error. Finally, using archaeological evidence (in this case the relative ceramic typology), it is possible to place each of these events within an archaeological phase or period (and thus associate a calendar age with this phase or period).

It is also useful to present here a discussion of the accuracy achieved for OSL dates using the MET in combination with Bayesian modelling, prior to discussing the dates in relation to the relative ceramic typology. Here we demonstrate the effectiveness of combining *a priori* archaeological information in conjunction with OSL ages. Table 6.1 presents four estimates of the measurement error determined throughout the five stages of the modelling process, illustrating the improvement of error estimations achievable. The first error encountered with the OSL data is that associated with the equivalent dose and dose rate measurements. These errors are presented for each of the analysed vessels in Table 5.11. At this stage no prior information has been attached to the data and so significant errors are observable. The second stage is to determine the average modelled age of each individual vessel after multiphase modelling. At this stage we have included the information, coming from the relative ceramic typology, that the vessels can be loosely divided into three groups with a known chronological order. As a re-

sult of including this additional information we can achieve, for each individual vessel, a lower level of uncertainty (the second error in Table 6.1; of course, in general further improvements can be made if stratigraphic information is available in addition to ceramic morphology).

Table 6.1: Different measures of the error associated with the five stages of the modelling process. All values are in absolute years. In the first two rows of this table, OSL errors refer to the standard deviation of the ages given in Table 5.11 and modelled OSL errors refer to the standard deviation of the modelled OSL ages given in Table 5.14.

	Phase 1	Phase 2	Phase 3
Mean of OSL Errors	494	244	91
Mean of Modelled OSL Errors	188	145	98
Standard Deviation of the Unmodelled OSL Ages	531	291	N/A
Standard Error of the CAM	128	115	N/A

This can be resolved further by combining the data in the central age model, which assumes that each of the three phases represents a single depositional event, that is, the burial of the group of ceramic vessels, and therefore that all of the vessels in a phase have approximately the same age (while sometimes this assumption could be questioned with the inclusion of an ancestral ceramic form, for this assemblage, as it presently stands, no such indications for this assumption are present). This results in a single date—the central age—for this event. At this stage we are provided with a new way of determining the error of the OSL measurements. Since we have assumed that all vessels are the same age, the error in the individual measurements can now be estimated as the standard deviation of the unmodelled ages, which is an indication of how much the age of each individual vessel deviates from the central value. This gives an error closer to the initial error estimation in the OSL results (which in turn gives confidence to the original unmodelled error estimates). The final error is the standard error associated with the central age model. This gives a value—assuming that the age of the vessels in each phase is a single date—of the corresponding error in the date of the depositional event as a whole (as opposed to the error associated with each individual vessel). This provides an uncertainty which is in accordance with the best possible estimate for the

date of each of the three events seen in the Bêt Khallaf assemblage, and demonstrates the importance of having as many individual dates as possible for a given assemblage.[44]

To summarise, what we have demonstrated here is that while the error of OSL dating using the minimum extraction technique is large (i.e. up to 10%) when considering individual vessels, accuracy can be improved (i.e. to less than 3%) when considering multiple ages from a number of ceramics from a single assemblage or phase, using both the central age model and Bayesian analysis.

6.2 The late Naqada period: the primary context within the Bêt Khallaf assemblage

The first period of occupation at Bêt Khallaf illustrated in the OSL dates, and corresponding to Phase One in the Bayesian model, is the late Naqada III period, corresponding to the Third Dynasty within the historical chronology.[45] The OSL measurements, after analysis by the CAM, produce a central age of 2622 BC $\pm$128 years, indicating the date of the *most likely* age of the assemblage. This date is wholly expected as the archaeological material, since its excavation by Garstang in the early 1900s, was known to belong to this time period, evidenced by the similarities in both the material culture and the architectural features, seen between Bêt Khallaf and other comparable sites across Egypt from the same archaeological period. Additionally, in all five tombs that Garstang excavated, textual evidence exists at the site in the form of clay sealings which carry the name of 'Djoser', known historically to be the first king of the Third Dynasty, and builder of the Step Pyramid at Saqqara (Garstang and Sethe 1903). This archaeo-

[44] Of course, any systematic error will not be eliminated by any of these modelling steps. Examples of systematic error would be machine calibration error or erroneous assumptions in the DosiVox modelling. However, as already discussed above, the OSL reader was re-calibrated to minimise the chance of systematic error, and, as mentioned in Section 5.3.6 the effect of changing several important DosiVox assumptions was measured and found to be small. Of course, in the future this should be further clarified with complimentary *in situ* gamma spectroscopy readings.

[45] Remembering here that the late Naqada III period is generally considered to be the early Third Dynasty, but that the Third Dynasty in itself can be considered 'late Early Dynastic' or 'early Old Kingdom', depending on which chronological system is in use.

logical evidence, alongside radiocarbon dating and the absolute historical chronology, can provide age estimations for this period, and these ages are comparable to the results of the OSL measurements. Bronk Ramsey et al. 2010, who have arguably produced the most reliable radiocarbon dates for this period to date, place the accession of Djoser between 2691–2625 BC (95.4% confidence level). Of the two absolute historical chronologies in common use, the 'high-chronology' of Shaw 2000, which is the chronology most frequently cited by Egyptologists, places the reign of Djoser between 2667–2648 BC. In contrast, the 'low-chronology' of Hornung et al. 2006, places the reign of Djoser between 2592 and 2566 BC. Although the OSL results presented here seem to agree slightly more with the radiocarbon dates and the 'high-chronology', they really straddle both historical chronologies, and, with an error of $\pm$128 years, at present cannot robustly support one chronology over the other: this will be discussed further in Section 6.2.1. What we can say is that the absolute date range we see for Phase One in the OSL results is most likely contemporary with the construction of the tombs, and that the ceramics clustering around this date are probably part of the funerary deposit of the original tomb owner(s). While the OSL dates cannot yet achieve the same chronological precision as radiocarbon dating (and this is in part owing to the small number of samples we have in this project), it is still clear from these results, and their fit with already established absolute chronological dating methods, that the OSL technique has worked very well for the Bêt Khallaf material and can contribute to chronological discussion for this period.

With regard to the relative ceramic typology, the assemblage we see from the first phase at Bêt Khallaf is clearly diagnostic and typical of other late Naqada III assemblages known from elsewhere across Egypt. The most frequently occurring type within this assemblage is the so-called 'wine jar' (X4116, X4117, X5458, X5459, X5469). In this assemblage, these vessels are the elongated 'torpedo' shape which are indicative of a late Naqada IIID style, where we see a reversion of the wine jar vessel index. The wine jar vessel index is a concept introduced in Table 2.2, which demonstrates that the height to maximum width ratio is chronologically dependent for the wine jars from their first

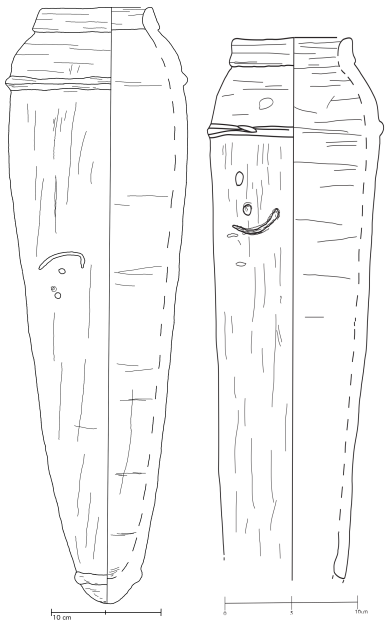

Figure 6.1: Two wine jars from the late Second Dynasty from the Early Dynastic tombs under the Tomb of Meryneith, Saqqara (Hood, unpublished data).

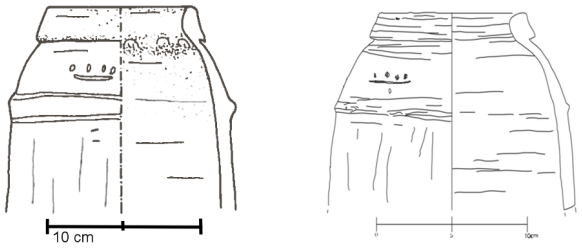

Figure 6.2: Two almost identical pot marks on wine jars from the late Second Dynasty from the Early Dynastic tombs under the Tomb of Meryneith, Saqqara (Hood 2010a) and from the Tomb of Khasekhemwy at Abydos (Engel 2000).

development up until the Naqada IIID period (Köhler and Smythe 2004), together with a slight tapering in of the vessel walls beneath the banded decoration (Köhler and Smythe 2004; Hendrickx 2006; Hartmann 2006), an observation made at Helwan (Köhler 2004; Köhler and Smythe 2004; Köhler 2014a), at Saqqara (in the Early Dynastic tombs beneath the Tombs of Meryneith and Maya (Hood 2010a), in the Tomb of Ninetjer (Lacher 2011: 218; Hartmann 2015, and author's personal observations in the field), Abydos in the Tomb of Peribsen (Petrie et al. 1953: Pl. XXIII; Hartmann 2006: 104), and in the Tomb of Khasekhemwy (Engel 2000), as well as at Bêt Khallaf. By contrast, during the

earlier stages of the Naqada III period, the wine jars follow a distinctive typological development, which sees the vessel with a more bulbous vessel wall profile, with a lower vessel index ratio (i.e. the maximum diameter is larger when compared to the height of the vessel), as opposed to the later stages of development which see a much higher vessel index (Köhler and Smythe 2004). The later Naqada IIID style of wine jar present at Bêt Khallaf is more often made of a marl, or at least a marl-Nile mixed clay, which is in contrast to the earlier types, which are more often made predominately of Nile clay (Köhler et al. 2011: 107). Additionally, it seems that another diagnostic feature of this style of wine jar is that it frequently displays a pot mark upon the shoulder of the vessel (above, or just below the banded decoration), and parallels exist at Helwan (Köhler 2014a: Tombs Op 4/ 8, 28; author's personal observations in the field), Saqqara (Hood 2010a; Hood unpublished data (Figure 6.1); Hartmann 2015), and Abydos (Engel 2000; Hartmann 2006).[46]

From a luminescence dating perspective, the wine jars present a challenge and it should be noted here that when considered individually, the wine jars do not lend them-

[46] A translation of these potmarks has yet to be achieved, although suggestions for their meaning include potter's marks, a distribution/counting mechanism, or a symbol depicting the commodities which they contained. From this author's point of view, for the wine jars she has observed, it is most likely that the potmarks are either a potter's sign or a distribution indicator. This is because distinct markings often appear on several vessels within a single assemblage (such as we see at Saqqara (Hood 2010a cf. Hood unpublished data, Figure 6.1), where it is likely the same potter (or workshop) was employed to manufacture or selected as supplier). Now it can also be observed that some identical potmarks can be found across regions: for example, the same potmark, Figure 6.2, is seen on two vessels, one from Saqqara (Hood 2010a: Fig. 14), and the other from the Tomb of Khasekhemwy at Abydos (Engel 2000: Fig. 6). While this may suggest that a traded commodity is present within the jars (and this observation is supported to a limited extent by Hendrickx et al. (Hendrickx et al. 2002), who observed a similarity between the later hieroglyphic symbol for milk '*mr*' being used as a potmark on small carinated jars at the site of Elkab; it was suggested that the potmarks, owing to their being incised prior to firing, were probably indicative of function (Hendrickx et al. 2002: 283–284)), but in that case, the symbols of these traded commodities would be more uniform and thus easier to decipher than they seem to be. Furthermore, the potmarks do not seem to offer a universality in their distribution, which one might expect should they be indicative of the contents of the vessels. Therefore, considering, the pot mark to be a symbol of the workshop/potter, interregional correlation of potmarks might indicate that a wide distribution network is in place, or may indicate patronage between the royal court and a provincial elite subject. (Of the matching potmarks at Abydos and Saqqara, one example is found in the tomb of a king, while the other is found in an elite tomb.) Indeed, Engel has suggested that such marks found in the Early Dynastic period may reflect a high degree of administration across the country (Engel 2015). The interpretation of potmarks on ceramic vessels in the late Naqada III period is still very much open to interpretation and indeed the most recent summary of potmark scholarship has indicated that all these options are plausible at this time and that exact meanings are most probably dependent on region and type of vessel (Budka and Engel 2015).

selves to precision OSL dating. As can be seen (Figure 5.9 and Table 5.11), the wine jars each yielded an age range which was far broader than those of the other vessels. Indeed, without using Bayesian modelling to mathematically project *a priori* information onto the age ranges of the wine jars, it would be difficult to assign a useful date range for these vessels. It is interesting that all five wine jars display this quality, and that it is only this type of vessel which displays a larger-than-expected age range in the OSL dates. The significant age ranges seen in all five of the wine jar vessels stems from the fact that we see a large error associated with the D_e measurement. This is not an uncommon observation in OSL dating, where some samples show low sensitivity and scatter in the D_e measurements. It is most likely that this is largely owing to the quartz sensitivity: not all quartz behaves in a manner conducive to OSL dating. The reason for this variation in quartz sensitivity remains unknown, although it is thought that it is an as-yet unquantified property of the quartz crystal lattice structure, the properties of which are largely governed by both depositional and sedimentary history (e.g. Duller 2004; Pietsch et al. 2008; Preusser et al. 2009; Sawakuchi et al. 2011). Given that we see low sensitivity and large sample scatter mainly within the marl clay wine jars, it is very possible that they share a similar clay source which has a depositional environment which has resulted in low sensitivity within the quartz found within the clay. It is unlikely that this variation and broad D_e range stems from the firing process, that is, that the OSL signal was not fully reset, because in all instances the ceramic material displays evidence of being fired at a high enough temperature to fully reset the OSL signal in sensitised quartz. Additionally, though the large scatter seen in the OSL ages of the wine jars could also be a result of the sampling method, this would not affect the observed low quartz sensitivity. It should be remembered that the age calculation and thus age range is derived using the central age calculation for all aliquots that yielded an OSL signal and cleared all rejection criteria (see Appendix D). It was noted during the drilling process that often, owing to the nature of the marl fabric, less sample was collected (even though the same size sample was taken) because some of the drilled ceramic fraction was so fine that it could

not be collected since it was dispersed during the drilling process. This means that less sample was available for aliquot preparation and this may have created a random error in sample age distribution. It is also possible that two types of quartz were found in the ceramic which had differing luminescence properties. For example, clay itself will generally contain a quartz component, but the potters may have chosen to add additional sand to the ceramic as temper. It might be that if two distinct geologically provenanced quartz samples were present, they may behave differently and give rise to a more complex luminescence signal than usual. Unfortunately, the scope of this project did not allow this to be examined further, although future work on this material may be able to shed light on this possibility. Finally, although more unlikely, it is possible that the light coloured clay fabric was more susceptible to light penetration, and thus some near-the-surface bleaching could have affected some of the quartz grains near the surface of the sample. This would have caused a similar bi-modal distribution as is seen in the aliquot data for each of the wine jars. This is an observation which is worth considering in future projects and the colour of the clay fabric should be examined to see whether any light penetration occurs in lighter coloured ceramics.

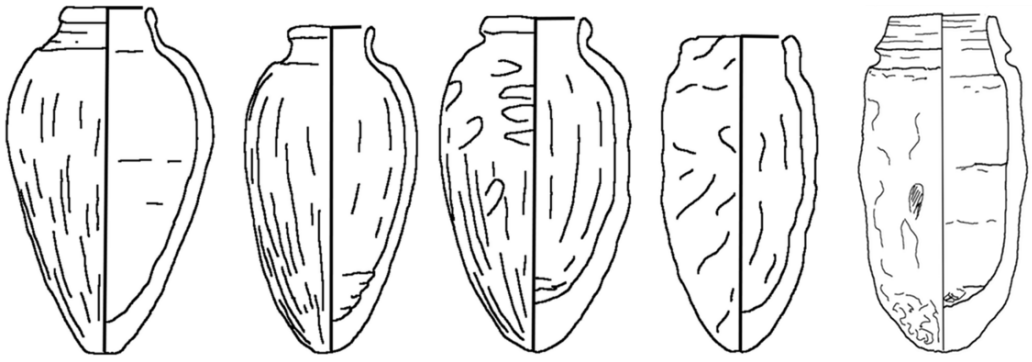

Figure 6.3: Beer jar typology, showing Types 1–5 following Köhler and Smythe 2004 and Hood and Valentine 2012. Figures not to scale.

After the wine jars, the most frequently occurring vessel type seen at Bêt Khallaf is the so-called 'beer jar', of which there are four present: X5461, X5462, X5471 and X5472. An Early Dynastic beer jar chronology was established (Köhler and Smythe 2004), which shows the development of this vessel form from the Naqada IIIA to Naqada IIID period,

over four identified ceramic types. An additional type, 'Type 5', was further discussed in Hood and Valentine 2012 where the typology is extended to include the beer jar with a distinct collared rim (cf. Köhler 2004: 306; Köhler 2014a: 37; Figure 6.3). From the available evidence, it would appear that Type 5 is present in the late Naqada IIID period and continues into the early Old Kingdom, and an increasingly developed collared rim form is identified at several sites (e.g. Helwan Tomb Op4/19, 32, 42, 44, 49, 50 (Köhler 2014a), Buto (Köhler 1998: Pl. 14), and Elephantine in a Third and Fourth Dynasty context (Raue 1999: 182, 184)). Of the four beer jars in the Bêt Khallaf assemblage, we see the latter half of the typology represented—a Type 3/4 vessel (X5472), two Type 4 vessels (X5471 and X5462) and a Type 4/5 which shows an early development of the collared rim (X5461)—indicative of a mid Second Dynasty to Third Dynasty date and thus typologically consistent with the OSL age of the Bêt Khallaf assemblage. Interestingly, the suggestion has been made that although the beer jar typology does have underlying chronological significance, there could also be a degree of ritual preference being observed, as often, when Type 4 vessels are observed in conjunction with Type 3, the latter are usually found in the burial chamber whereas the Type 4 are often found in associated offering deposits (Pers. Comm. E.C. Köhler, 2015). It is also possible that the Type 5 vessel serves a subtly different cultic function in the burial environment, although further examination of the archaeology and its interpretation are required before such a suggestion can be substantiated (Hood and Valentine 2012; Hood in press). The OSL ages associated with each vessel, although consistent with a late Early Dynastic/early Old Kingdom date, are not high-precision enough to examine the chronological implications of the beer jar typology at this point in time. However, in future studies, this would be a valuable question to consider, should additional data be available for OSL dating. Of the four vessels, X5471 did not yield an OSL date. Again, it appears that the fabric of the vessel did not yield quartz conducive to OSL dating, and interestingly, the fabric of this vessel was far more silty than was seen in the other vessel types. It had a finer, mud-like quality to it, which may indicate a very different clay provenance to

the other vessels.

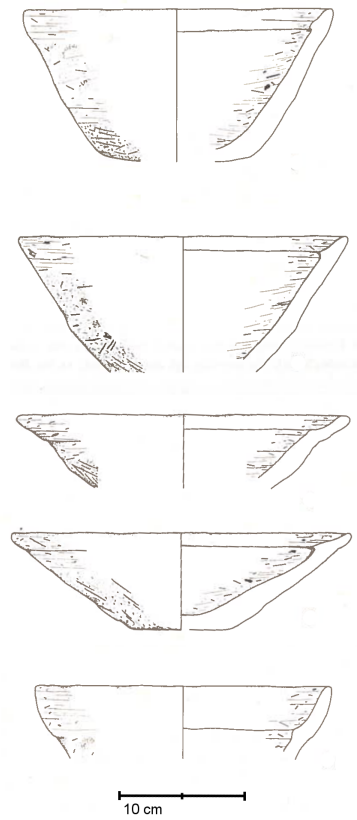

Figure 6.4: Illustrating the development of the Internal Rim Bowls at Elephantine, from a short shallow lip to a longer, deep lip. Figures taken from Raue 1999.

The Bêt Khallaf assemblage also includes two Internal Rim Bowls (X4115, X5464). The development of the Internal Rim Bowl is well documented across several Early Dynastic sites, notably Helwan (Köhler 2004; Köhler 2014a), Elephantine (Raue 1999; Hood in press; Köhler et al. 2011), and Buto (Köhler 1998). The vessel type also occurs in the Tomb of Khasekhemwy (Engel 1997). Considered to commence in the Second Dynasty, in the Naqada IIID period (Köhler 2004; Raue 1999; Hood 2007; Hendrickx 2006: 87) the typological development of this ceramic ware shows a clear stylistic change in the rim characteristics, namely that the rim is initially shallow (i.e. 2 cm) with a steep gradient, which then develops into a deeper rim with a lower gradient. A perfect example of this development, which spans the Second to Fourth dynasties, is illustrated at Elephantine (Figure 6.4). The Internal Rim Bowls at Bêt Khallaf are of an early form, that is,

with a shallow, short rim, and are most similar to those attributable to late Second/Third Dynasty contexts from other sites (e.g. in the Tomb of Khasekhemwy (Engel 1997), at Helwan (Köhler 2005; Köhler 2014a), and at Elephantine (Raue 1999)). The relative date attribution for this vessel type thus fits wells with the OSL dating for the Bêt Khallaf assemblage. With regard to the OSL ages of the two Internal Rim Bowls at Bêt Khallaf, one vessel, X5464, produces an OSL age range in good agreement with the relative age range assigned to the Bêt Khallaf assemblage (see Table 5.11). However, X4115, as already discussed in Section 5.4, has an OSL age which is much younger than the other measurements from Phase One of the Bêt Khallaf assemblage, even though typologically it is a perfect fit with the remainder of the assemblage. As discussed in Section 5.4, the reason for this is believed to be that, unlike other vessels in Phase One, this vessel has secondary burning marks upon it (visible in the photo appearing in the ceramic catalogue, Appendix C). It is likely therefore that the burning seen in this vessel is post-depositional and that the OSL measurement is representative of this secondary event, rather than the original manufacturing firing event. Interestingly, the OSL date range obtained for X4115, 1904–1416 BC at 68.2%, does not correspond very well to any of the absolute phases represented at Bêt Khallaf (although it is most comparable to the First Intermediate Period cluster) and thus might pertain to an additional archaeological event at the site—although an exact reconstruction of the events leading to this vessel's re-use is impossible to reconstruct, it is possible to hypothesise instances of cultic activity, curious exploration by later Egyptians, tomb robbing or secondary/tertiary burial. It has been observed that secondary contexts and deposits can contain ceramic vessels or fragments which show clear signs of post-manufacture heating (i.e. the presence of soot/ash on a vessel). It is impossible to know exactly the nature of this reuse (although prior examples indicate use in cooking or as a light source), however it is being increasingly observed in recent excavations (Köhler 2014a:43; Author's personal observations in Helwan and Saqqara; Pers. Comm. E.C. Kohler). Future excavations at Bêt Khallaf may shed light on additional phases of archaeological activity at the site which might

explain the D_e obtained for X4115.

We also see in Phase One a vessel type that is not yet regularly considered a diagnostic feature of the late Naqada III assemblage, yet it is the opinion of this author that it should be. This is the flat-based jar with restricted neck and high shoulder (hereafter called a 'flat-based jar') and it is found at Bêt Khallaf (X5460), but also at Saqqara (Hood unpublished data, Figure 6.5), at Elephantine (Hood in press), at Helwan in Tombs Op4/1, 10, (Köhler 2014a) and in the Tomb of Khasekhemwy (Engel 2000). It is possible that this form may derive from the earlier Second Dynasty flared rim squat jars (Figure 6.6), seen mainly at Helwan Tombs Op 4/7, 35 and 42 (Köhler 2005; Köhler 2014a), where it seems possible that there may be a visual transition present between the two vessels (author's personal observations in the field). This observation, however, must be more thoroughly examined before it can be stated with confidence, although this may soon be achievable with the application of cladistic analysis to the ceramic typology (see Section 7.2). That this vessel form belongs to the late Naqada III period is further evidenced by its OSL date, which places it securely within the age range for Phase One of the Bêt Khallaf assemblage, with an age range of 2752–2402 BC at 68.2% (mean: 2611 BC).

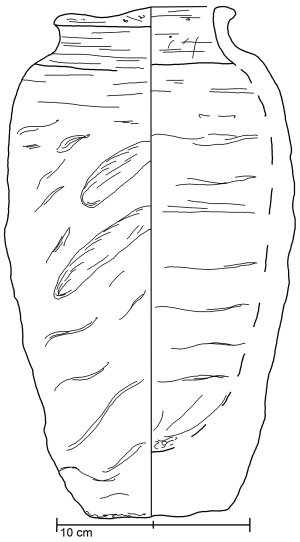

Figure 6.5: Flat-based jar from the late Second Dynasty from the Early Dynastic tombs under the Tomb of Meryneith, Saqqara (Hood, unpublished data).

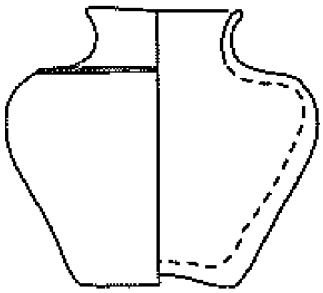

Figure 6.6: Squat vessel with flared rim found in early to mid Second Dynasty contexts at Helwan. Figure taken from Köhler 2004: 305.

Within the Bêt Khallaf Phase One assemblage there is a single example of an Early Dynastic bread mould, X5473, which produced an OSL date range of 2625–2340 BC at 68.2% confidence. Although it is likely that originally the offering deposit would have included many more of this vessel type, it is common that bread moulds do not survive deposition as well as other ceramic types. This is owing to their being often under-fired, with an exterior hardened shell giving way to a silty centre, which can often disintegrate during burial or upon excavation (author's personal observations in the field). However, X5473 is relatively well fired and has remained intact. In terms of bread mould typology, there is a significant degree of morphological variation seen in this vessel type in the earlier periods of Egyptian history, before the vessel type became more standardised in the Old, Middle and New Kingdoms. The variation in this vessel type is probably due to these vessels being locally produced, with many pottery workshops across the region producing similar, but varying, morphological forms. It thus appears unlikely at this stage that the variation seen across bread mould types during the late Naqada III period should be considered a chronological indicator, but rather a product of regional and/or workshop variation. Although a 'tentative bread mould typology was produced by Jacquet-Gordon 1981, the study lacked the quantity of data required for meaningful typological enquiry. A form similar to X5473 was not present (and indeed the study did not include late Naqada III material). Fortunately, parallels can be found outside this

study. From a comparison with the (limited) available literature, the form of X5473 is slightly less common, as it lacks the shorter neck coupled with a more distinctive sharp shoulder profile than appears to be most common for the late Naqada III period (e.g. such as can be seen in Helwan Tombs Op4/1, 7, 11, 15, 35, 42 (Köhler 2014a), at Tell el-Farkha (Chłodnicki 1995: 25) and at Buto (Köhler 1998: Pl. 43–46), and see Figure 6.7). Rather, X5473 has a slightly softer shoulder profile, with a much longer neck profile (and thus shorter conical base), and is most similar to a bread mould found at Maassara, Tomb 3, dating to the late Naqada III period (Larsen 1939: 195).

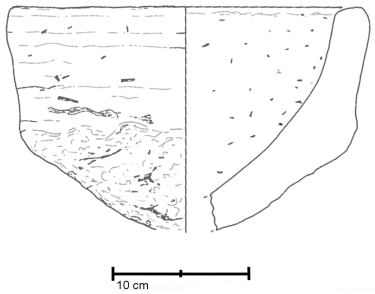

Figure 6.7: 'Typical' bread mould from the site of Helwan. Figure taken from Köhler and Smythe 2004: Plate 5.

In addition to the vessels already discussed, Phase One at Bêt Khallaf also included several undiagnostic vessel types, which although appearing Early Dynastic in character (based upon general morphology and clay type) are not of particular use as chronological indicators. For example, X4114 is a plate/bowl and X4118 is a pot stand, similar forms of which are seen throughout the Naqada III period (and beyond). It is their OSL ages and their clustering with Phase One at Bêt Khallaf which are their most diagnostic feature at this stage. However, it is intriguing to note that of all the assemblage, it is only these two vessels (with the exception of the wine jars as already discussed), which have a larger than typical error range, and whose final age range is more heavily influenced by the application of Bayesian modelling than the other vessels in the assemblage. It is possible that these vessels might be slightly older than the rest of the assemblage. At present there is no archaeological evidence to suggest a reason for this, which is why it was not justifiable to remove them from the analysis or to create another phase in

the model to account for their slightly older age spread than most of the rest of the assemblage. Another vessel, X5468, is difficult to place as no genuine parallels for it are known and it is an unusual vessel form: again, its most diagnostic feature is that it clusters well with the Phase One groups based upon its OSL date range, 2632–2356 BC at 68.2% probability. It is possible that this is a regional form, and it does show some similarities to the large egg-shaped, marl clay storage vessels known from Elephantine in Second and Third Dynasty contexts (Raue 1999; Hood unpublished data: Figure 6.8; and a specimen is also known from as far north as Saqqara, see Hood 2010a: Fig. 10). However, X5468 lacks the distinctive deep neck groove usually seen on this vessel type, and the clay type in X5468 is a Nile clay (although it is possibly mixed with a marl fabric too, which is supported by its ICP-MS analysis, see Appendix A). Furthermore, X5468 is also similar to a vessel recovered from the tomb of Khasekhemwy at Abydos (Köpp 2011: 88), although, again, it is difficult to call this vessel a direct parallel as there are distinct differences between the neck characteristics between the two vessels.

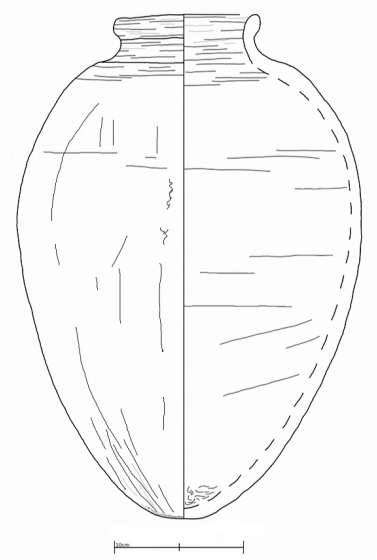

Figure 6.8: A marl storage jar, representative of those found frequently at Elephantine (Hood, unpublished data).

Another two vessels within the assemblage were also undiagnostic, and in addition failed to produce an OSL date: X4113 and X4120. X4113 was a simple plate/bowl, many

parallels of which can be found throughout many periods of Egyptian history. For the purposes of chronology, both in terms of its morphology and lack of OSL date, this vessel cannot contribute to the present discussion. X4120, a small, fine marl clay jar with remains of a bright red slip, could potentially be Early Dynastic in nature, but it could equally be part of an Old Kingdom or First Intermediate Period assemblage, based upon its fabric type and slip decoration, which are more reminiscent of the latter two periods. X4120 will be discussed in greater detail below in Section 6.3. Another vessel, X4119 also did not yield an OSL date. However, this vessel type does have a known parallel from the late Naqada III period, in the Tomb of Khasekhemwy (Engel 1997). It is unfortunate that an OSL date was not forthcoming for this piece. According to Garstang's publication (Garstang and Sethe 1903), two vessels of this type were found in the Bêt Khallaf assemblage. As this is an infrequent type from this period, although with a very informative parallel found in a royal tomb, it would be ideal to be able to find this second vessel from Bêt Khallaf and subject it to OSL analysis (its current whereabouts is unknown).

Thus far, the majority of the Phase One ceramics found at Bêt Khallaf and attributed to the early Third Dynasty by Garstang when first excavated have clearly reaffirmed this date, with both the OSL ages (CAM: 2622 BC$\pm$128 years) and the archaeological evidence illustrating a late Naqada III/early Old Kingdom date range. However, there are some vessel types which one would expect to find in an assemblage from this period which are absent. Notably, the Meydum bowl, a bowl with a distinct carinated rim (Figure 6.9), whose first occurrence dates to the mid Second Dynasty (Köhler 2004). The early form of the Meydum bowl, whose development continues well into the Old Kingdom, is a deeper vessel shape, with a more vertical rim, and indeed, its development can be related to a vessel index developed by Op de Beeck (Op de Beeck 2004), which illustrates that the rim width to vessel height increases over time. Many assemblages dating to this period feature this ceramic type and it is curious that no trace of them survive at Bêt Khallaf. As Garstang collected only intact vessels, it maybe that sherd evidence of this

vessel type still exists at the site to be recovered by future excavations.

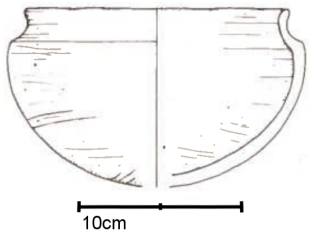

Figure 6.9: Illustration of a typical early Meydum bowl. Figure taken from Raue 1999.

Additionally, in Garstang's original publication of the Bêt Khallaf ceramic material (Figure 6.10 and Figure 6.11), the two pages on which illustrations of the vessels appear contain a total of 35 vessels, as opposed to the 24 we have sampled here. (One of the 24 vessels in this project, X5466—discussed below—was not included in Garstang's original publication as Garstang undoubtedly recognised the non-Early Dynastic nature of the piece; the situation is similar for X4120, which also does not appear in the book, and is also probably non-Early Dynastic, although an OSL date was not obtainable to verify this). An additional vessel is recorded as being stored at the Penn Museum; however, it was unavailable for OSL sampling because its current location within the museum is unknown. At this point in time, it remains unclear where the rest of the ceramic assemblage is stored, or indeed if it was ever removed from the site, or if it went into private collections. It appears that we are currently missing from our data set: an additional wine jar; a spouted bowl (which is of interest as chronologically it remains uncertain as to whether this is a late Naqada III form, see discussion below in Section 6.3); two additional beer jars; four additional assorted bowls (possibly including two more Internal Rim Bowls); and another spherical vessel. If access to this additional Bêt Khallaf ceramic material was possible, it would potentially refine the OSL date ranges further.

Indeed, what we see in the Bêt Khallaf OSL results is a high degree of spread in the data, although this spread can be compensated for through the application of Bayesian modelling. What this means, however, is that at present the dating results, while being

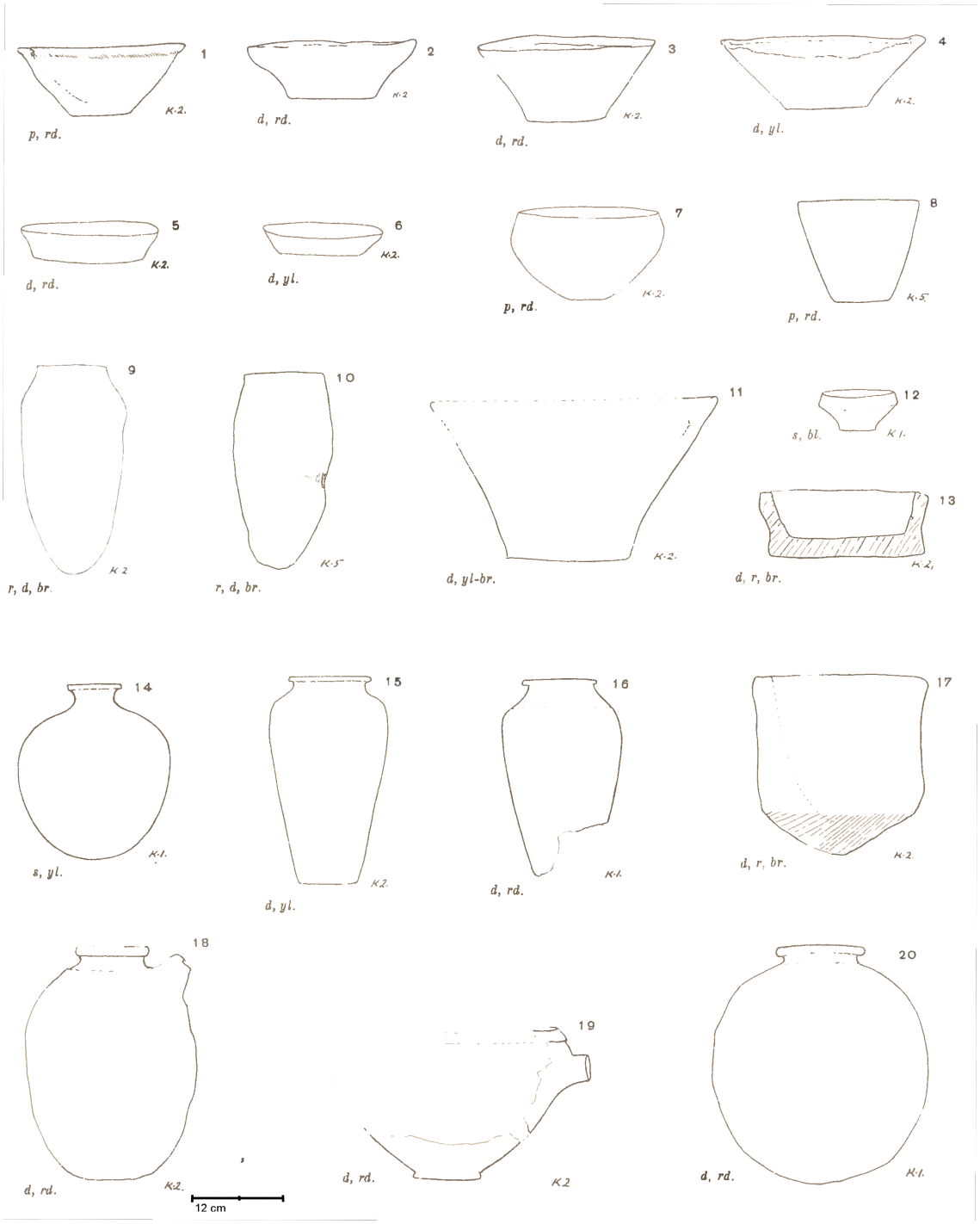

Figure 6.10: Plate XXX from Garstang and Sethe 1903, depicting the ceramic vessels excavated at the site of Bêt Khallaf.

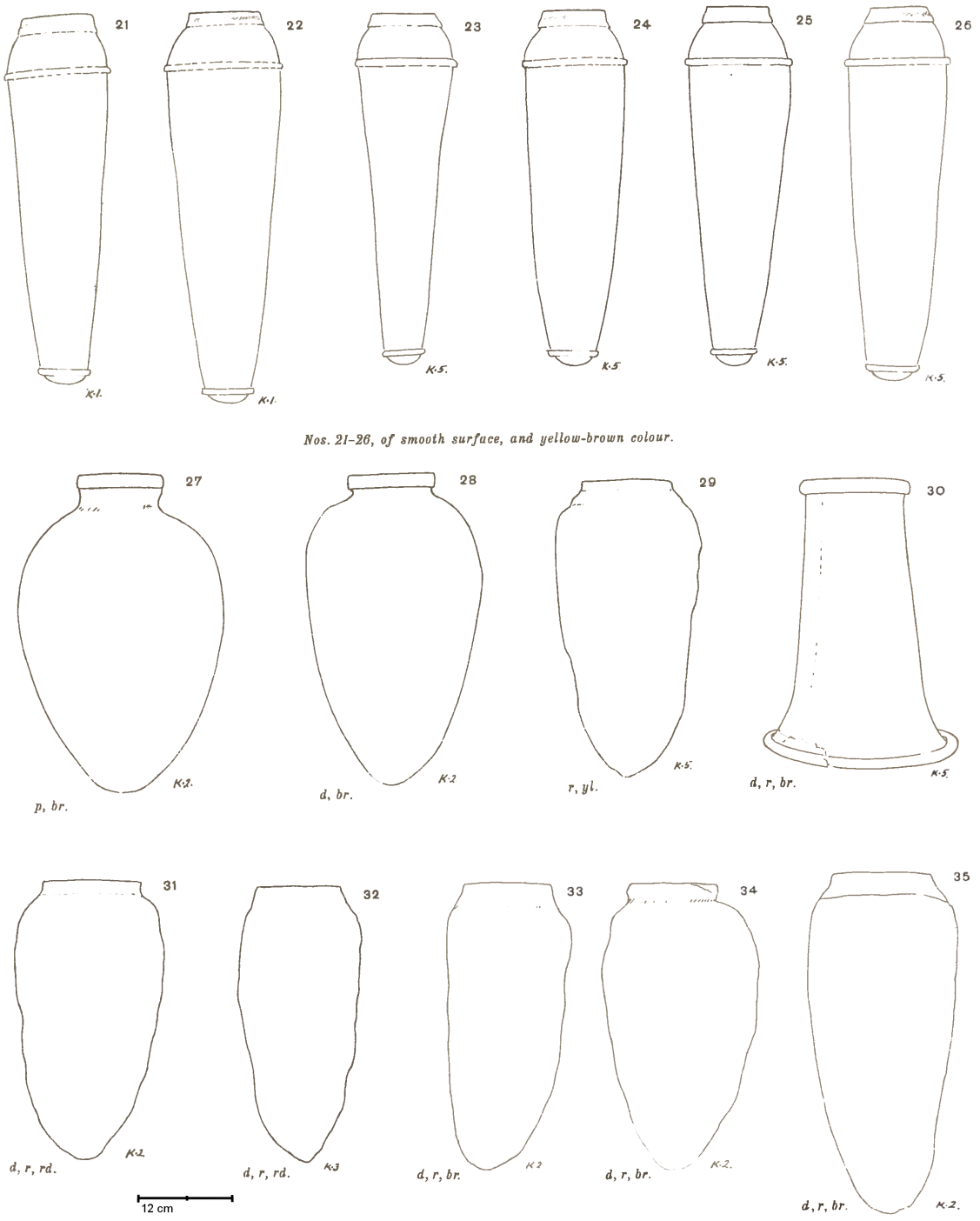

Figure 6.11: Plate XXXI from Garstang and Sethe 1903, depicting the ceramic vessels excavated at the site of Bêt Khallaf.

the first examples of the OSL technique used on Egyptian material, cannot yet improve upon the precision achieved by radiocarbon dating, or indeed by the relative historical chronology. However, it should be remembered that high chronological precision was not the goal of this project, rather it was to provide the first application of this technique to museum material and to illustrate the usefulness of the technique and advocate its inclusion in future chronological studies. Indeed, the Bêt Khallaf results have clearly demonstrated the benefits of applying OSL dating to Egyptian material, in order to assist in providing good (although not excellent) anchor points between an absolute and relative chronology. Additionally, the OSL results clearly illustrate how different chronological phases can be discerned between archaeological material at a particular site, which will be discussed further in Section 6.4. That we see a not-insignificant spread in the OSL data (see Table 5.2) is in part owing to the particularly wide spread we see in many of the marl clay (in particular wine jar) dates, which is attributable to the low sensitivity in the quartz contained in the pottery. Additionally, a reason for a broader age range than would be expected for a single use tomb could be that within the assemblage we are seeing a longer use history than a single burial (discounting, of course, Phase Two and Phase Three as discussed below), possibly a multi-generational family tomb. Neither the OSL results, nor the archaeology can suggest evidence of this at present, but it could be that future investigations, and with an increased data set from Bêt Khallaf, may find further evidence for this possibility.

6.2.1 Radiocarbon dating, the historical chronology and OSL dating: a common consensus among absolute dates?

It is also important to consider these OSL dates in their broader chronological framework. Above, we have discussed the ceramics themselves in detail, but it remains to be considered what this project has offered the broader absolute time frame established for this period, specifically its relevance, its comparison to radiocarbon dating, and how it ties in with the historical chronology. Of course, the OSL results are from a single

assemblage, from just one site, but it is an important one: it sits upon the cusp of the latest stages of the Naqada culture as it transitions into the Old Kingdom. Given the importance of this time period, our OSL results, while not being able to offer, at this stage, the high chronological precision seen in radiocarbon dating, can still contribute significantly to the general chronological discourse surrounding this period.

Prior to this project, the absolute dates for this transition from the Early Dynastic to the Old Kingdom (and consequently for the end of the Second Dynasty and beginning of the Third Dynasty), have traditionally been based on the historical chronology; more recently, AMS radiocarbon dates[47] have added significantly to the debate surrounding the absolute dates for this historical marker.

The historical 'absolute' chronology does not rely upon direct scientific analysis, but rather observations of historical records and reconstruction of astronomical events, thus its accuracy and interpretation can be—and frequently is—subject to much debate. As is generally known, the first major body of evidence for Egyptian chronology is Manetho, a Greek priest living in Egypt in the third century BC who wrote a history of ancient Egypt, including a record of the ruling pharaohs and the length of their reigns. It is assumed that Manetho was able to reconstruct a long chronology of Egypt given that his position would have given him access to temple records. Traditionally, Manetho has been used as a starting point for which to count backwards from his time, to the beginnings of pharaonic history, using additional sources along the way (e.g. Kitchen 1991). However, Manetho's *Aegyptiaca* is fraught with problems. First, the original document compiled by Manetho does not survive to modern day; only handwritten copies exist, which contain scribal errors: even contemporary versions of the text can vary between one another. Secondly, the historical texts of any civilisation are subject to political

[47] It should be noted here that initial radiocarbon dates for this period were obtained prior to the advent of AMS dating (e.g. Barker et al. 1969; Barker et al. 1971; Berger et al. 1965; Berger and Libby 1967; Hassan 1980; dates presented in Hendrickx 1999; Libby 1980, and see discussion in Rowland 2008). However, these have lacked the precision that more recent studies, since the 2000s, have achieved, specifically the work carried out by the Egyptian Chronology Project at the University of Oxford (e.g. Dee et al. 2013; Bronk Ramsey et al. 2010). Therefore, this discussion will only draw upon the most recent radiocarbon chronological work carried out on Egyptian material, following primarily Dee et al. 2013, Bronk Ramsey et al. 2010 and the radiocarbon date summary presented in Köhler and Thalmann 2014.

bias, and ancient Egypt is no exception to this, with unfavoured rulers—the classic case being that of Akhenaten—being erased from the common history and thus impacting adversely upon the reconstruction of a reliable historical chronology. Finally, not all periods of history are recorded equally, and records become lost, thus also affecting accurate reconstruction. In addition to Manetho's *Aegyptiaca*, there exist king lists from ancient Egypt, which can help confirm certain events and can add to history when they have recorded additional events. The major king lists surviving for ancient Egypt are the Palermo Stone, the Turin Canon and the inscribed texts on the wall of the Temple of Seti I at Abydos, the Hall of Records at Karnak, and the tomb chapel of Tjunuroy at Saqqara (e.g. Gardiner 1959; Redford 1986; Ryholt 2004; Shortland 2013; Wilkinson 1999: 218; Wilkinson 2000). Additionally, to help refine the information provided by Manetho and the king lists, there also exists for the reigns of certain rulers a 'fine-tuning' of sorts, in that regular events are recorded within a pharaoh's reign. One such example is the *heb-sed* festival which, theoretically, occurs after the first 30 years of king's reign and then every 3 years after the initial 30 years, although it is uncertain whether such festivals were carried out prior to the accepted 30-year period (Shaw and Nicholson 2002: 256; Murnane 1981). Other regular events included the burial of the Apis Bull, annual cattle counts and genealogical texts which discuss family chronology of priests and viziers under specific rulers (Shortland 2013: 23).

In order to anchor or pinpoint these events to an absolute timescale, 'dead-reckoning' is used: a known, observable event which can be dated to an exact year, is used as an anchor, and, based on evidence from written records, years of rulers can be counted back from that single point. In Egyptian history, there are three main 'dead-reckoning' events, albeit anchored late in Egyptian history. The first such date is in 664 BC, referring to the sacking of Thebes by Ashurbanipal and resulting in the establishing of the 26th Dynasty. The other two dates are both based upon observations of solar eclipses in 610 BC and in 763 BC (Shortland 2013). Theoretically, lunar and Sothic observations can also help refine the historical chronology, although these to date have had limited success (a

full discussion of astronomical events in relation to Egyptian Chronology can be found in Hornung et al. 2006, and a brief summary in Shortland 2013). With 'dead-reckoning' dates and their relevance to the study of the earliest dynasties, an immediate problem is observable: when counting back from 'dead-reckoning' events to the Old Kingdom, around 2000 years prior to these events, the inaccuracies in such a method accumulate and the final resulting date entails a degree of guesswork—educated guesswork, but guesswork none the less.

As discussed at the beginning of Section 6.2, the two most commonly accepted historical chronologies for ancient Egypt are those of Shaw 2000, referred to as the 'high chronology', and that of Hornung et al. 2006, referred to as the 'low chronology'. The names speak for themselves, as in general, the Shaw system results in higher absolute ages and the majority of events are considered to have taken place at an earlier time than the dates suggested by the 'low chronology'. With regard to the time period in history (i.e. the reign of Djoser) that the Bêt Khallaf ceramics are dated to, the 'low chronology' suggests 2592 BC as a date for the accession of Djoser (Hornung et al. 2006), whereas the 'high chronology' suggests a 2667 BC (i.e a difference of 75 years between the two proposed dating systems).

The results of the most recent (and in this author's opinion, most reliable) radiocarbon dates produce an accession date for Djoser between 2691 and 2625 BC at 95.4% probability (Bronk Ramsey et al. 2010), also reported as 2670 BC (Bárta 2013: 221), and 2680 BC (following the amalgamated radiocarbon dates presented in Köhler and Thalmann 2014, and Köhler 2013). All of these dates are more consistent with the 'high chronology' model of Shaw 2000. Additionally, in Dee's modelling work on the Old Kingdom, which examined four independent historical models and established chronologies, none supported the 'low chronology' system (Dee 2013c).

So where do the OSL results for Bêt Khallaf fit in to this discussion? First, it should be remembered that the 'high chronology', the 'low chronology' and the radiocarbon dates all discuss the most likely date for the accession of Djoser, that is, the beginning

of the Third Dynasty. We lack the archaeological precision to know exactly when in the reign of Djoser the Bêt Khallaf burials took place; all we know is that seals bearing the name of Djoser were placed in the tomb, which would indicate that they occurred at some point during Djoser's reign. The OSL results, after Bayesian modelling, suggest that the most likely date for the assemblage, following the CAM, is 2622 BC±128 years; in other words, a date almost exactly in-between the low and the high chronologies. One could deduce from these results that an agreement with the 'high chronology' is more likely than the low, by arguing that it is more probable that the Bêt Khallaf burials were during the reign of Djoser, rather than his year of accession, thus it would be expected that a plausible date for the Bêt Khallaf tombs would be slightly later than the accession date, as indeed 2622 BC is. However, the error of this date is broad, sitting at 128 years. Thus, we must reiterate here that OSL (at least using the MET method and with only a small number of samples), while adding significantly to our body of evidence and absolute chronological information for this period, lacks the chronological precision needed to resolve the debate between these two competing high and low chronologies. Nevertheless, it must be remembered that this project presents the first-ever attempt at using OSL dating in Egyptian archaeology and that high-precision dating in unlikely to be achieved in any such first attempt. The future is promising, however, and it is hoped that, when a larger data set becomes available, fine-tuned OSL chronologies can be determined. Such a larger data set could be achieved by incorporating more MET samples from museum collections. In addition, if samples can eventually be exported from Egypt, still more precision can be achieved using the larger sample sizes (and with a greater degree of certainty in the external dose rate calculations if *in situ* measurements are obtained), which would yield even more conclusive OSL data for this time period.

6.3 Two additional ceramic phases seen at Bêt Khallaf

Although Phase One, as determined by OSL dating, certainly represents the majority of the Bêt Khallaf ceramic assemblage, Bayesian modelling of the OSL results, alongside ceramic typology, clearly shows a multiphase occupation at the site, with two additional chronological phases being observed. The second depositional event, corresponding to Phase Two in the Bayesian model, is represented by four ceramic vessels: X5463, X5465, X5467 and X5470. The OSL dates associated with these four vessels produce a peak modal distribution of 2082 BC $\pm$115 years, which in contrast to Phase One, places these four vessels within late First Intermediate Period (FIP) following Shaw 2000, or the mid FIP following Hornung et al. 2006. When establishing the multiphase model in OxCal for the Bêt Khallaf material, in addition to the OSL ages which indicated a distinct chronological phase, the vessels in the Phase Two assemblage (with the exception of X5463) were recognised as being uncharacteristic of an Early Dynastic assemblage, based upon their morphology. X5463 was unfortunately an undiagnostic ceramic beer jar, which may indeed have dated to any time between the late Early Dynastic and First Intermediate Period, and it was the OSL date for this vessel which led to its inclusion in Phase Two over Phase One. Fortunately the three other vessels were more diagnostic, in particular X5470. X5470 was an interesting artefact as it has long been considered an Early Dynastic type. This is because it appeared in Petrie's Proto-dynastic Corpus as belonging to S.D. 87, that is, the late Naqada III period (Petrie et al. 1953: Pl. XXX). However, when this claim is investigated further, it is realised that seemingly the only reason it is incorporated into this sequence date is owing to its having been excavated alongside the late Naqada III assemblage at Bêt Khallaf. Petrie's inclusion of the form is based solely upon vessel X5470's inclusion within the Bêt Khallaf assemblage; it is thus a cyclical argument. It was therefore particularly interesting to observe its OSL date pointing to a later date that the Phase One group, but additionally that existing archaeological parallels

also firmly point to a First Intermediate Period date. Six vessels which are morphologically similar to X5470, albeit on a slightly smaller scale, are known from the sites of Qau (UC18033, UC18097, UC18099, and UC20500 from the Petrie Museum, London cf. Bourriau 1981: 53) and Mostagedda (MM10664 and MM10666, from the Medelhausmuseet, Stockholm), and have been dated to the First Intermediate Period. Additionally, the style of manufacture used in the construction of X5470 is possibly similar to that of UC20500, where 'the marks on the jar suggest ... the upper body was drawn on up on the wheel and joined to the lower body. This was modelled by hand and supported by three lines of rope where the join was made' (Bourriau 1981: 54). A corresponding rope imprint can be found on X5470. X5465 and X5467 additionally display what is considered a characteristic trait of First Intermediate Period pottery, in that they continued 'the Old Kingdom traditions of applying a red coat and polishing the surface' (Wodzińska 2009: 147). Red slip is not unknown in the Early Dynastic period, but it appeared to have lost its popularity at the end of the Naqada period and it was in the Old Kingdom onwards that it became increasingly popular once more (Hendrickx et al. 2002: 280). Given that vessels X5465 and X5467 also clearly cluster around a well-established First Intermediate Period ceramic type (X5470), their attribution to this date is reasonable and probable. It is difficult to find direct parallels for X5465 and X5467 as the number of ceramic types increases in the First Intermediate Period, due to the rise in the number of local ceramic production centres and the corresponding decrease in the centrally organised workshops of the Old Kingdom (Wodzińska 2009: 147; Bourriau 1981: 51). X4120, discussed above as being one of a small number of vessels not producing an OSL date, might also well fit in with the ceramics seen in this phase. The 'sealing-wax red' slip (Bourriau 1981: 51; cf. Wodzińska 2009: 113) on its surface is more similar to an Old Kingdom/First Intermediate Period style, and the morphology of the vessel is not typical of an Early Dynastic form. Of course, it is impossible to speculate further given the absence of an absolute date, and the absence of parallels for this vessel.

Finally, there is one vessel recorded in Garstang's catalogue, a spouted bowl (Figure

6.10, vessel 19), which, like X5470, is usually attributable to the Early Dynastic period based solely on the fact that Petrie included in it his Proto-dynastic Ceramic corpus based on Garstang's recovery of the vessel at Bêt Khallaf in 1903. The form itself is more similar to later Old Kingdom types, and it might be that this vessel too would more likely cluster with Phase Two, rather that the Early Dynastic assemblage. Once again, in the absence of an OSL age, this is based upon conjecture only. Unfortunately the whereabouts of this vessel is currently unknown, and thus an OSL date is currently unachievable.

The final depositional event, corresponding to Phase Three in the Bayesian model, is represented by a single ceramic object, X5466. When the assemblage was first assessed visually, it was immediately obvious that this piece was not consistent with an Early Dynastic assemblage, based upon its clay type and morphological characteristics. Additionally, the ICP-MS values for the clay of X5466 were significantly different to the other vessels within the assemblage (see Table 5.5, cf. Appendix A). However, no additional information for this vessel could be obtained, and thus the OSL results were relied upon to produce chronological information for this vessel. As can be seen from the OSL results (Table 5.14), this vessel is distinct chronologically from the rest of the assemblage and sees a OSL age of AD *c.*800–*c.*1200 (Table 5.11). Although broad, this date places this piece securely in the medieval Islamic period. Unfortunately, even though the OSL results were able to attribute this piece to a specific period of Egyptian history, no parallels could be found for this vessel. This is because non-decorated Islamic pottery remains very under-represented in the literature (Pers. Comm. G. Scanlon, 2006). It is therefore not possible to discuss X5466 in any further detail, but OSL dating has certainly been able to successfully illustrate that this vessel is an intrusive object in the Bêt Khallaf assemblage and shows that a degree of archaeological activity, however small, was present at the site of Bêt Khallaf in the medieval Islamic period.

6.4 The implications of the Bêt Khallaf OSL results and their impact on the existing ceramic chronology

The application of OSL dating to the Bêt Khallaf ceramic material has clearly demonstrated the usefulness of OSL dating in the study of Egyptian archaeology. Although luminescence dating in Egyptian archaeology has previously been considered of limited use (e.g. Goedicke 2006), it is hoped that the OSL work presented here for the Bêt Khallaf assemblage has demonstrated otherwise. While this is only a study carried out upon a single site, it is a proof of concept that this technique can be used on Egyptian material, even though at present legal requirements in place in Egypt (and given that an OSL facility is not available to archaeologists within Egypt) mean that only work upon ceramics housed in museums outside Egypt is possible. Indeed, if in the future such requirements are lifted, then the application of OSL dating to material within Egypt would be of even more benefit as it would allow a more controlled assessment of factors contributing to the final age calculation, in particular the external dose rate. Museum material is often overlooked for scientific analysis, but it is hoped that with the development of the MET technique, museum material will gain more interest for the application of OSL dating.

The research carried out upon the Bêt Khallaf material has added to the study of the late Naqada III ceramic assemblage by providing yet another independent chronometric dating technique (albeit one with a larger error range than is seen in radiocarbon dating) which has produced dates in good agreement with existing absolute chronologies, both radiometric and based upon the historical records from ancient Egypt itself. It is important to note that these OSL dates have been obtained directly from the ceramic material themselves, and not from material thought to be in association with the original depositional context. Furthermore, it has helped resolve inconsistencies within the original museum data set which had labelled all associated finds as 'Early Dynastic', whereas our results demonstrate that the use history of the tombs at Bêt Khallaf is more

complex, with three independent periods of occupation being represented within the burial complex. The Early Dynastic is certainly the dominant period of occupation (as would be expected), but there was also archaeological activity present during the First Intermediate Period and the Islamic period.

While we believe this study has added significantly to the discourse for the chronology of the late Naqada III period, it is also important to acknowledge where improvements could be made and address how future work should be directed.

6.5 Future directions

It would be ideal, in a future continuation of this project, to complete OSL analysis upon the 13 or so Bêt Khallaf ceramics which are currently unaccounted for (as discussed above). Additionally, these measurements would benefit from additional *in situ* measurements of the external dose rate at Bêt Khallaf, something which may be possible if permission is obtained to take a gamma spectrometer to the field.[48] By carrying out external dose rate measurements in the field, it is thought that a more accurate dose rate determination could be achieved than by ICP-MS analysis of soil sediment adhering to ceramic material throughout the storage period in museums. Another valuable measurement that could only be taken in the field is testing the density of the depositional matrix in which the ceramics were buried. This would impact dose rate estimations given by the DosiVox calculations (at present the density is an assumption, rather than a specific measurement).

Measurement of the equivalent dose could also be improved upon to some degree. When the MET was developed for this project, the sampling protocol was designed to ensure that museum curators would be willing to allow sampling to occur by keeping damage to the vessel through sampling to an absolute minimum. While the MET protocol has been shown to work well, in certain cases it is undeniable that additional sample

[48] It was originally hoped that such measurements could be carried out for this project, but given the political climate in Egypt between 2011 and 2015, this was decided against at the time.

material would have been of great benefit. This is particularly true for specimens where sample yield was low due to the loss of a super-fine drilled sample fraction. If it was possible to drill down to 5 mm or 6 mm (rather than 4 mm) in some instances this would probably double our aliquot yield and produce a more robust data set for a given sample. It is therefore important to continue to engage with museums and discuss methodological considerations and progress. This is likely to become an easier task now that this project presents a proof of concept and demonstrates that OSL dating can be successfully applied to museum ceramics. Additionally, further confidence in the sampling process might be gained if a new method was developed to help screen for samples which do not yield OSL results. As discussed, some vessels simply did not produce an OSL signal and thus no OSL measurement or age calculation was achievable. It might be possible to develop a technique by which individual quartz grains upon the surface of the vessel (which could be identified using a hand-held lens), were extracted and the sensitivity of the quartz could be assessed prior to a full MET sample being taken. This would mean that if the test sample indicated low or no sensitivity, it would not have to be subjected to unnecessary drilling. This test extraction would not have to be carried out in subdued lighting conditions as the sensitivity of the quartz can be determined using samples with a reset crystal lattice.

Finally, the site of Bêt Khallaf is only one late Naqada III site, and future work would ideally extend the scope of the dating programme to include other material from this period across the various sites which have material available in museum collections. It is of course also the logical progression of such a project to go beyond the time period of the late Naqada III period and conduct OSL analysis upon the wider Naqada culture. By extending research in such a manner, it would be possible to start using OSL dating (in conjunction with other techniques) to start examining regional variation with the ceramic assemblage.

Although the benefits of applying OSL dating have been demonstrated, OSL, like any other dating technique, should not be considered a stand-alone technique. Rather,

to achieve the most comprehensive understanding of a data set that is reasonably achievable, each technique should be used alongside additional methodologies. As this thesis has set out to apply a multidisciplinary approach to the study of Egyptian ceramics, the following part of this thesis will now further the application of a multidisciplinary analytical programme by examining additional techniques which can be used alongside OSL dating.

Part IV

Furthering the application of OSL dating: Additional case studies advocating a multidisciplinary approach to the study of Naqada III ceramics

Chapter 7

Cladistic analysis of Naqada III ceramics

OSL dating is a powerful tool in ceramic chronological studies, but its strength lies in being part of a multidisciplinary approach to these studies. We have already seen how OSL dating coupled with Bayesian modelling can bring new dimensions and greater clarity to our interpretations of the Bêt Khallaf results. However, scientific techniques must also continue to draw upon more established and traditional methods of ceramic studies, in particular relative dating techniques, which have always lent themselves to refining ceramic typology and chronology, in order to further increase the impact of absolute dating techniques.

7.1 Seriation analysis

One of the main relative dating methods used in archaeology is seriation analysis, a standard procedure in archaeology for simultaneously correlating artefact types with archaeological assemblages. It is based on the assumption that artefacts adhere to the 'like goes with like' principle, and thus it should be possible to arrange assemblages into typological or successive order based on the similarity or dissimilarity of type attributes (Orton et al. 1993: 190). Seriation also relies on a basic principle of archaeology: that a noticeable change in material culture is most likely to reflect the passing of time (Kemp 1975: 262).

Seriation is essentially a theoretical approach to typological and chronological studies, based on a number of assumptions which were largely established by Wilkinson in his seminal work on the topic (Wilkinson 1974).

Seriation was initially prominent in Egyptian archaeology, because the first attempt at seriation analysis performed on archaeological data was in Egypt, the work of Flinders Petrie, who established his corpus of early ceramics based on his findings at the Naqada and Ballas excavations in 1894–1895 (Petrie 1896). He ascertained that a relative sequence of excavated tombs could be established based on the contents of each tomb—essentially employing contextual seriation,[49] which is governed by the variation and continuation of artefact attributes over a period of time, which in turn can be placed into a sequence based on the aforementioned qualities (Kemp 1975: 259; Petrie 1899; Renfrew and Bahn 2008: 126–127).

In the case of the late Naqada III period only a small amount of research has focused upon seriation of the ceramic assemblage. This is primarily owing to the preliminary nature of most current research. However, the present author set out to achieve a preliminary seriation analysis of late Naqada III ceramics based upon published data, and Köhler has incorporated seriation analysis recently in her analysis of the ceramic material from the site of Helwan (Hood 2007; Köhler et al. 2011: 105; Pers. Comm. E. C. Köhler, 2013; Köhler 2014a: 36). Furthermore, the sequence date system established by Petrie (Petrie 1899; Petrie 1901a; Petrie 1921; Petrie et al. 1953; Petrie and Quibell 1896) is still useful up to a point, as are later assessments carried out by Kemp 1975, Kaiser 1957, Hendrickx 1989, Hendrickx 1994, Hendrickx 1996, and Wilkinson 1995, as discussed above in Section 2.1.

The application of seriation to this period has been extremely limited in part owing to the preliminary nature of the majority of ceramic studies produced for this period over the past decade. The study of late Early Dynastic culture has really only taken off since the late 1990s, and as the field generally experiences a significant time lag between

[49] Frequency seriation, in contrast, seeks to produce a typology through observing the frequency and abundance of artefact/attribute types over a period of time (Renfrew and Bahn 2008: 126–127).

excavation and publication, it is only now we are beginning to see in the literature more comprehensive reports and studies resulting from the ceramic finds. Seriation relies on a vaster body of data than is available at present (though this material will become available over the next decade). This is because seriation relies on metadata from complete publication of results relaying entire assemblage information, not just a select scattering of the more interesting finds published in preliminary reports. When such material becomes available, it will be possible to engage in a comprehensive analysis of the ceramic data from multiple regions across Egypt simultaneously looking at regional and inter-regional ceramic assemblages, and it is likely that such an endeavour will contribute greatly to the our present state of understanding of the late Naqada III period.

7.2 Cladistic analysis

Another method of analysis, based on a similar concept, which has been long overlooked in Egyptian archaeology (and indeed archaeology as a whole), is cladistic analysis. Borrowing from the biological sciences, cladistic analysis has the potential to significantly aid in artefact classification and typology. It can use all published data, even preliminary reports where only a selection of data is obtainable, as it relies only on the properties of the vessels themselves and not on the detailed contextual information that is required in seriation (this does not negate the value of seriation analysis: cladistics is useful in a different, yet complementary way to seriation).

Already briefly introduced in Section 3.2.2, cladistics is a well-developed method used in the biological sciences that establishes and studies evolutionary relationships between organisms, based on shared derived characters. Shared derived characters are features that occur in two or more taxa that have changed from the ancestral condition. Such characters can be physical (i.e. morphological), molecular (i.e. genetic), or behavioural, many of which have a genetic basis and are therefore inheritable. The result of a cladistic analysis is a branching, hierarchical tree, called a cladogram, that represents a hypothesis about the evolutionary relationships between the organisms included.

Given the potentially limitless number of hypotheses that could be generated to explain the evolutionary relationships between a group of organisms, the principle of parsimony (also known as Occam's razor) is employed, which advocates that the simplest hypothesis should be accepted. Based on this principle, cladograms are constructed to minimise the number of evolutionary transformations required to explain the variation between the organisms included. As a result, organisms that share many derived characters are grouped more closely together in a cladogram than those that do not (Wiley et al. 1991; Kitching et al. 1998, Lipscomb 1998).

Formulated by the German entomologist, Willi Hennig (Hennig 1950), cladistics did not become well known until translated into English (Hennig 1966), but has now become a common and widespread technique throughout palaeontological and biological disciplines. More recently, cladistics has also been successfully employed in other research areas including linguistics (e.g. Gray and Jordan 2000; Holden 2002; Rexová et al. 2003; Johnson 2008), textural criticisms (e.g. Robinson and O'Hara 1996), ethology (e.g. Proctor 1992; Paterson et al. 1995), and even business studies (e.g. McCarthy et al. 2000; Baldwin et al. 2005; McCarthy 2005).

The use of cladistics to explore phylogenetic trends in material culture, both in archaeology and anthropology, has been gaining momentum, particularly over the past decade. In this field, cladistics has been used to investigate hominin and human migration patterns based on assemblages of stone tools such as hand axes and projectile points (e.g. O'Brien et al. 2001; Darwent and O'Brien 2006; Buchanan and Collard 2007; Buchanan and Collard 2008; Lycett 2007; Lycett 2009), cultural evolution based on textile designs and weaving techniques (e.g. Tehrani and Collard 2002; Tehrani and Collard 2009), the influence of language and geographic proximity on California Indian basketry assemblages (Jordan and Shennan 2003), and the spread of Neolithic crop-based agriculture (e.g. Coward et al. 2008). However, only a small handful of examples of cladistics being applied to ceramics is known in the available literature (Cochrane 2008; Cochrane 2009; Cochrane and Lipo 2010; Collard and Shennan 2000;Hart and Engelbrecht 2012).

In 2009 a collaboration between the present author and a colleague, James Valentine, from the Department of Biological Sciences, Macquarie University, Sydney, began, which sought to assess the applicability of cladistics to Egyptian archaeology. It was thought that such a project could be of value to the study of late Naqada III ceramics, and could shed light upon the development of ceramic types. This was because cladistics holds the ability to fine-tune ceramic typology, uncovering stylistic changes and morphological variation that might not be immediately identified by the naked eye alone. The results of this project to date are presented below. First, a set of Egyptian beer jars are examined, followed by assessment of bowls and wine jars. These results are the first instance of cladistics being carried out upon Egyptian ceramic material. However, there are currently projects being carried out at Durham University by Michel de Vreeze who is looking at the application of cladistics to Tell el-Yahudiya ware (Vreeze 2016), as well as at Macquarie University and Charles Darwin University by Aaron de Souza and James Valentine who are looking at the application of cladistics to Nubian pottery.

7.2.1 Cladistic analysis of Naqada III beer jars

The most complete analyses carried out to date on Egyptian material are for the beer jar data set.[50]

The ceramic material used for the cladistic analysis of the late Naqada III beer jars is based primarily upon the ceramic assemblage from current excavations at Helwan, by the Helwan Project under the direction of E.C. Köhler. In particular, this work uses data from excavation area Operation 4, Tombs 1–50 (Köhler 2014a). The Helwan data was further supplemented with published material from Buto (Köhler 1998), Minshat Abu Omar (Kroeper and Wildung 2000) and Elephantine (Raue 1999). This combined data set ranges from the late First Dynasty through to the early Old Kingdom. The decision to focus this initial cladistic analysis on beer jars was for three main reasons. First, beer jars

[50] The following section on cladistic analysis for beer jars is a modified extract from Hood and Valentine 2012, which was jointly written by the present author and her colleague James Valentine from Charles Darwin University (formerly Macquarie University).

are a common component of the Early Dynastic ceramic assemblage, allowing a large data set for analysis to be established. Indeed, 123 complete beer jars are available from Helwan Operation 4, Tombs 1–50. Secondly, Köhler and Smythe 2004 had undertaken a preliminary typological assessment of Naqada IIIA/B to IIID beer jars from Helwan based on changes in morphology and surface features. Finally, chronological assessment for the typological sequence of Helwan beer jars (Köhler and Smythe 2004) provides a robust time frame against which the results of this cladistic analysis can be compared.

7.2.2 Establishing beer jar types and characters

In cladistic analysis, the description of ceramic objects is of paramount importance. Generally, description of ceramics in archaeology focuses upon documenting and describing the overall morphology, surface features and composition of individual vessels, rather than focusing on the specific morphological features of types of ceramic vessels. This situation is akin to describing the morphological features of each individual member of a species without establishing the common morphological feature or features that not only unite those individuals as members of the same species, but also separate them from closely related species. As cladistics determines evolutionary relationships between species (or higher taxonomic ranks) rather than individuals, the establishment of ceramic taxa is required. As described by O'Brien et al. (O'Brien, Lyman, Saab, et al. 2002), this is one of the greatest challenges in using cladistics to create phylogenetic histories of material culture.

To establish ceramic taxa or types (equivalent to the classes of O'Brien et al. (O'Brien, Lyman, Saab, et al. 2002) and the 'Operational Taxonomic Units' of Lycett 2007), a combination of 13 morphological characters were defined for each of the four main beer jar types identified by Köhler and Smythe 2004 which are referred to herein as type 1–4 beer jars (Figure 7.1; Table 7.1). Characters were defined primarily following Aston's descriptions of ceramic vessels (Aston 1998) and include those characters typically used to classify ceramic vessels, such as vessel shape (closed or open), rim type (modelled

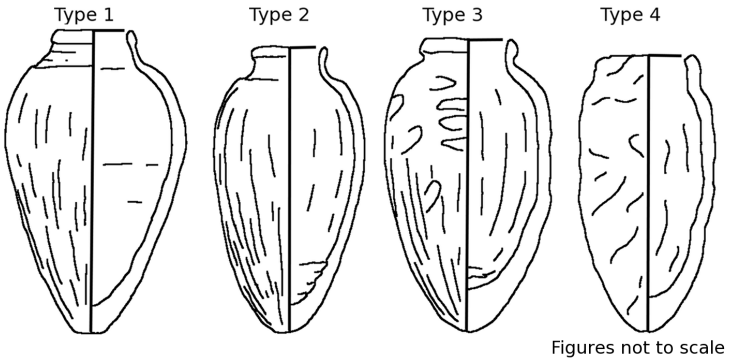

Figure 7.1: Early Dynastic beer jar typology (Types 1–4), taken from Köhler and Smythe 2004.

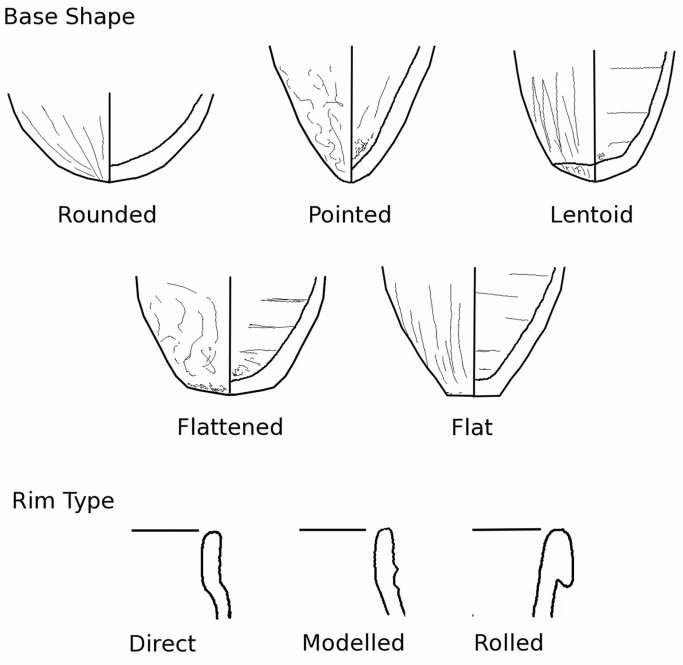

Figure 7.2: Base shape and rim type terminology based on Aston 1998.

Table 7.1: Distribution of morphological features across beer jar types and forms. The frequency of occurrence of each feature is indicated as a percentage.

		Type 1 beer jar (outgroup) (n=14)	Type 2 LSJ (n=2)	Type 1 LSJ (n=16)	Type 2 beer jar (n=27)	Type 3 beer jar (n=19)	Type 4, Form 1 beer jar (n=32)	Type 4, Form 2 beer jar (n=4)	Type 5 beer jar (n=9)
General vessel shape	**vessel shape**	closed	closed	closed	closed	closed	closed	closed	closed
	vessel index	1.34–1.90 (mean = 1.69)	1.61–1.73 (mean = 1.67)	1.54–1.82 (mean = 1.72)	1.66–2.29 (mean = 1.80)	1.57–2.01 (mean = 1.82)	2.01–2.42 (mean = 2.19)	1.92–2.15 (mean = 2.05)	1.64–2.38 (mean = 2.13)
	position of maximum diameter	high	middle	middle (81%); high (19%)	high (81%); middle (19%)	high (74%); middle (26%)	high (94%); middle (6%)	middle	high
	section profile	subangular	subangular	subangular	subangular	subangular	subangular (94%); rounded (6%)	subangular	subangular
	body surface	scraped	scraped	scrape	scraped	combined (scraped/wavy)	wavy	wavy	wavy
Rim	**rim type**	modelled (79%); rolled? (21%)	rolled	rolled (88%); modelled? (12%)	rolled (74%); modelled (26%)	rolled (63%); modelled (37%)	modelled (97%); rolled (3%)	modelled	modelled
	rim morphology	external	external	external	external	external	direct	direct	direct
	rim character	subangular (64%); rounded (29%); angular (7%)	angular (50%); subangular (50%)	subangular (75%); angular (25%)	subangular (59%): rounded (41%)	subangular (63%); rounded (32%); angular (5%)	subangular (56%); rounded (44%)	rounded (75%); subangular (25%)	rounded (56%); subangular (44%)
Neck	**neck profile**	straight (64%); convex (36%)	straight	straight (81%); concave (19%)	straight (70%); concave (26%); convex (4%)	concave (53%); straight (47%)	straight (94%); concave (6%)	straight	straight
	neck shape	convergent (93%); parallel (7%)	convergent	convergent (75%); parallel (25%)	convergent (52%); parallel (41%); divergent (7%)	convergent (89%); parallel (11%)	convergent (56%); parallel (44%)	convergent (75%); parallel (25%)	convergent (89%); parallel (11%)
	type of collar	collar absent	collar absent	collar absent	collar absent	collar absent	collar absent	collar absent	striated (44%); ridged (44%); ribbed (11%)
Shoulder	**shoulder profile**	angular (50%); subangular (50%)	angular	rounded (69%); subangular (31%)	rounded (70%); subangular (26%); angular (4%)	subangular (68%); rounded (16%); angular (16%)	subangular (59%); angular (25%); rounded (16%)	shoulder absent	subangular (67%); angular (33%)
Base	**base shape**	flat (86%); pointed (8%); rounded (8%)	lentoid	lentoid	rounded (63%); pointed (26%); flattened (7%); flat (4%)	rounded (47%); pointed (37%); flattened (11%); flat (5%)	pointed (53%); rounded (38%); flattened (9%)	pointed (75%); rounded (25%)	rounded (56%); pointed (44%)

or rolled), neck profile (straight, convex or concave), shoulder profile (angular, subangular or rounded) and base shape (rounded, flattened, flat, pointed or lentoid) (Figure 7.2; Table 7.1). Although fabric is an important component of all ceramic vessels, fabric type was not included as a character at this stage of analysis. At present, no correlation between fabric type and morphology is observable in our beer jar data set. When further material is collected for future studies, fabric will be assessed for its suitability for inclusion in future cladistic analyses. At present, however, fabric type appears to be more indicative of the region of manufacture rather than phylogeny, and so is unlikely to be a useful character in cladistics. Here it is also worthwhile remembering that Petrie observed that certain ceramic forms pass through several different fabric types (Petrie 1921: 6). As a result, Petrie did not always pay particular attention to the fabrics of early Egyptian ceramic assemblages during typological assessment. It must be understood that this does not in any way detract from the importance of fabric in the overall assessment and study of ceramics, but it does support an assertion that fabric type is not a useful character in cladistic analyses at this early stage.

The same 13 characters were then defined for all 123 beer jars in the data set, which allowed 96 to be identified as either a Type 1, 2, 3 or 4 beer jar. Additionally, through personal observation, Type 4 beer jars could be subdivided into two morphologically distinct form variants: those with a distinct shoulder (Type 4, Form 1) and those with the more traditional 'bullet' shape (Type 4, Form 2). The morphological features of the remaining 27 beer jars were considered sufficiently different to warrant two additional beer jar types being defined. The first, a fifth type of beer jar, the distinctive 'collared beer jar' (e.g. Köhler 2004), which exhibits a prominent collar, is named a Type 5 beer jar here for convenience (Figure 7.3). Type 5 beer jars appear to have developed directly from Type 4 beer jars and continue well into the Old Kingdom assemblage (Raue 1999; Köhler 2004; Köhler and Smythe 2004). Secondly, although not defined as a separate type or form within the cladistic analysis, two additional morphological form variants of Type 2 beer jar were discerned, both displaying a characteristic 'lentoid' base, here

called 'lentoid-based beer jar 1' (LSJ 1) and 'lentoid-based beer jar 2' (LSJ 2) (Figure 7.3(b)). It remains to be clarified whether this vessel is a type in its own right, or rather a form variant of Type 2 resulting from regional variation, form function or another cause (see below for further discussion).

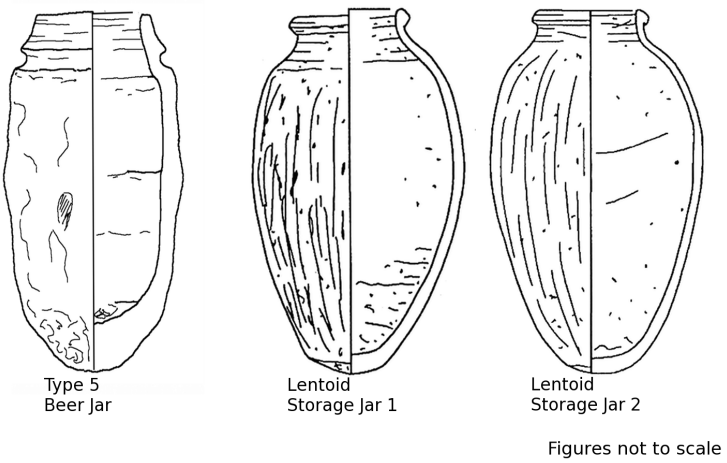

Figure 7.3: (Left to right): Type 5 beer jar; lentoid-based storage jar, Form 1 and lentoid-based storage jar, Form 2 (line drawings courtesy of the Helwan Project).

At the end of this process, eight morphologically distinct beer jar types and forms had been defined (Figure 7.4 and Table 7.1).[51]

The 13 characters described for each beer jar type and form indicated a high level of morphological variation in each one (i.e. interspecific variation or variation within types) (Table 7.1). This variation may be the result of 'mistakes' being made during the manufacturing process, or that there are additional beer jar type variations in the data set that have not been recognised. Furthermore, it is possible that these high levels of variation may result from the inclusion of transitional forms between types. For example, Type 1 beer jars are defined as having a flat base (Köhler and Smythe 2004), but several

[51] It is important to note here that although the variations or 'forms' are established as 'Types' for the purpose of the cladistic analysis in this chapter (i.e. LSJ 1, LSJ 2 and Type 4 Form 1 and Form 2), we do not believe that there is as yet sufficient evidence in the archaeological record or ceramic analysis to determine these forms as 'types' within the Egyptological literature. Indeed the lentoid-based vessels will need far more examination before they can be confidently defined in the literature as a distinct type. However, in the case of the Type 5 beer jar, we feel that it is now possible to start considering this an individual type in its own right.

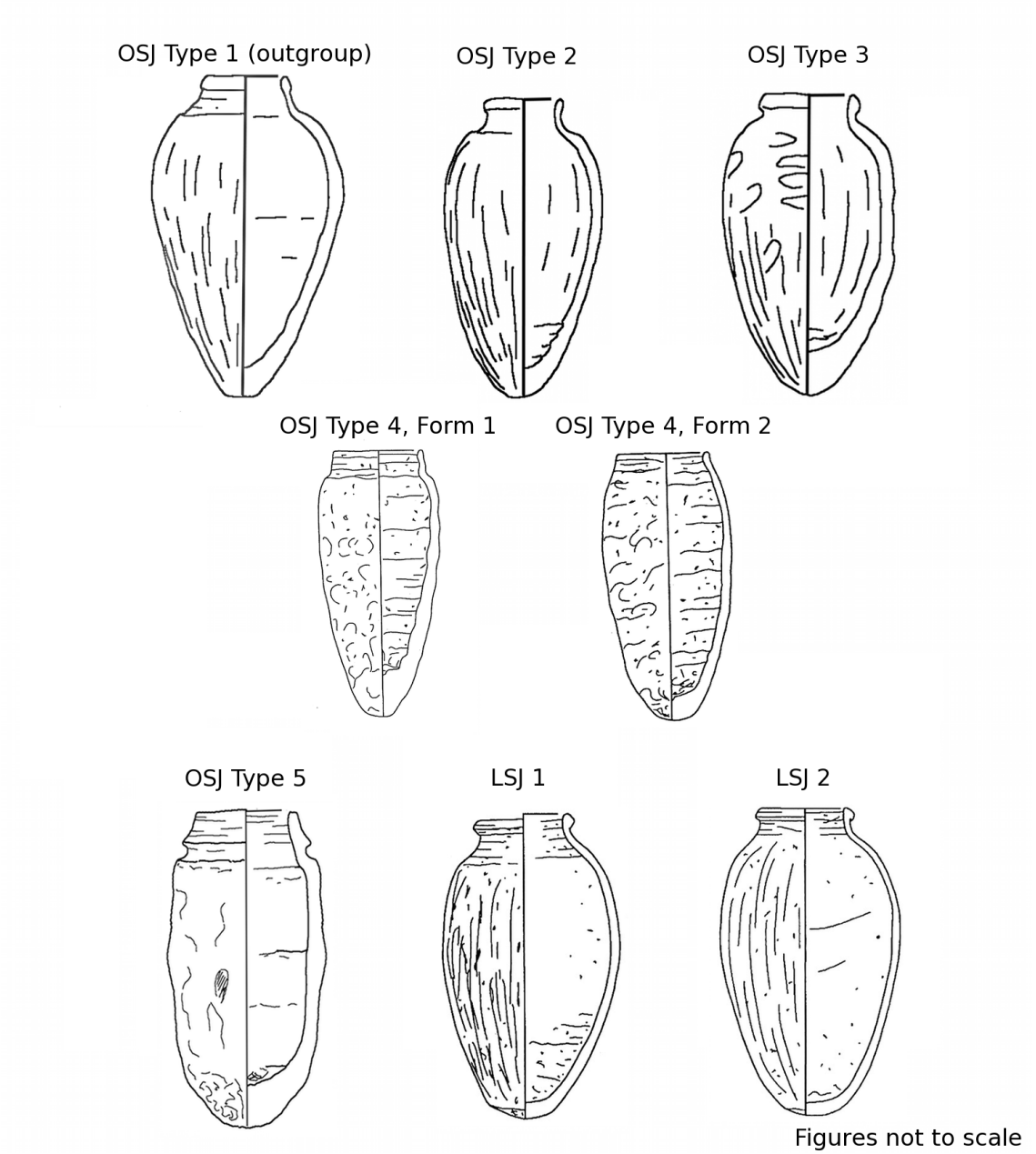

Figure 7.4: The eight morphologically distinct beer jar/LSJ types and forms identified in this study (line drawings: Types 1–3 taken from Köhler and Smythe 2004; LSJ 1, LSJ 2, Type 4 Form 1, Type 4 Form 2 courtesy of the Helwan Project). NB OSJ (ovoid storage jar) is an alternative designation for 'beer jar'.

vessels in our data set that have the overall body shape and general characters of a Type 1 beer jar display a rounded or pointed base. As a true Type 1 beer jar would only have a flat base, those with non-flat bases could be considered a transitional type in between Type 1 and Type 2. Such high levels of variation have the potential to collapse nodes

(the branching points in cladograms) due to the fact that too many potentially equally parsimonious evolutionary relationships can be established. To counter this, only those characters occurring with a frequency of more than 10% of individuals for each beer jar type in Table 7.1 were considered to be cladistically informative and included in the cladistic analysis. For instance an 'angular' shoulder profile of Type 2 was not considered to be cladistically informative since it only occurs in 4% of individual Type 2 beer jars. Since cladistics is based upon the presence of shared derived characters, only those characters presented in Table 7.1 that appear in two or more beer jar types are cladistically informative and included in the analysis. Although some ceramic vessels may have a highly distinctive and unique morphological feature, such as the striated, ridged or ribbed collar of Type 5 that allow it to be quickly and easily identified, unless such features are present in two or more vessels they do not provide any information on evolutionary relationships. The overall body shape is also cladistically uninformative since all beer jars in our data set have an oval body shape, apart from Type 1 which has an inverted triangle body shape. Such features (known as autapomorphies) evolve after the split from the common ancestor with the most closely related species. Likewise, morphological features common to all beer jars in Table 1, such as a closed vessel shape, do not shed any light on evolutionary relationships either. Such character states merely indicate the presence of an ancestral feature (called symplesiomorphies) retained within the group from the ancestral form and therefore were not included either. Such uninformative characters do not help establish evolutionary relationships. Ultimately, the characters considered to be cladistically informative in Table 7.1 were used to define 15 binary (e.g. absent/present) and one unordered, multistate character (e.g. absent/present, state 1/present, state 2) for each of the eight beer jar types and forms. These 16 characters derived from Table 7.1 define the list of characters and character states in Table 7.2, as well as a character matrix that shows the distribution of these character states across the eight beer jar types and forms (Table 7.3).

Table 7.2: List of characters and character states (derived from Table 7.1) that were used in the cladistic analysis of beer jar types and forms.

1. Mean vessel index: 0. 1.60–1.79 1. 1.80–1.99 2. >2.00	9. Concave neck: 0. absent 1. present
2. Middle maximum diameter: 0. absent 1. present	10. Parallel neck: 0. absent 1. present
3. High maximum diameter: 0. absent 1. present	11. Angular shoulder: 0. absent 1. present
4. Rolled rim: 0. absent 1. present	12. Subangular shoulder: 0. absent 1. present
5. External rim: 0. absent 1. present	13. Rounded shoulder: 0. absent 1. present
6. Direct rim: 0. absent 1. present	14. Rounded base: 0. absent 1. present
7. Angular rim: 0. absent 1. present	15. Pointed base: 0. absent 1. present
8. Rounded rim: 0. absent 1. present	16. Lentoid base: 0. absent 1. present

Table 7.3: Character state matrix of the 16 characters used in the cladistic analysis of beer jar types and forms. See Table 7.2 for character state definitions.

	1	2	3	4	5	6	7	8	9	10	11	12	13	14	15	16
Type 1 beer jar	0	0	1	1	1	0	0	1	0	0	1	1	0	0	0	0
Type 1 LSJ, Form 1	0	1	0	1	1	0	1	0	0	0	1	0	0	0	0	1
Type 1 LSJ, Form 2	0	1	1	1	1	0	1	0	1	1	0	1	1	0	0	1
Type 2 beer jar	1	1	1	1	1	0	0	1	1	1	0	1	1	1	1	0
Type 3 beer jar	1	1	1	1	1	0	0	1	1	1	1	1	1	1	1	0
Type 4, Form 1 beer jar	2	0	1	0	0	1	0	1	0	1	1	1	1	1	1	0
Type 4, Form 2 beer jar	2	1	0	0	0	1	0	1	0	1	0	0	0	1	1	0
Type 5 beer jar	2	0	1	0	0	1	0	1	0	1	1	1	0	1	1	0

7.2.3 Determining ingroup and outgroup beer jars

As discussed above, the beer jars from Helwan Op 4, particularly the material from Tombs 1–50 (Köhler 2014a), supplemented by additional material from Buto and Elephantine (Köhler 1998, Raue 1999, respectively) were chosen for cladistic analysis. These beer jars form the ingroup, or the group of ceramic vessels for which evolutionary relationships will be established. Another major challenge in using cladistics to establish a phylogenetic sequence of material artefacts is the selection of an appropriate outgroup (O'Brien, Lyman, Saab, et al. 2002). The role of the outgroup is to define ancestral and derived character states within the ingroup. To achieve this, the outgroup should be closely related to the ingroup and display the ancestral character states of that group (Smith 1994). As such, selection of an appropriate outgroup is an essential requirement of any cladistic analysis (Nixon and Carpenter 1993; Smith 1994, Lyons-Weiler et al. 1998). In this analysis, the Type 1 beer jar as described by Köhler and Smythe 2004 in their typological sequence of beer jars, supplemented by published material from Minshat Abu Omar (Kroeper and Wildung 2000), was selected as the outgroup. The Type 1 beer jar, whose first occurrence dates to Naqada IIIA/B, is not only absent in the Helwan Op 4, Tombs 1–50 material, but is also significantly older than any of the material in our data set (see discussion of chronological placing of this vessel type in Köhler 1998, Kroeper and Wildung 2000, Köhler and Smythe 2004). Although such a stratigraphic approach to outgroup selection is not without critics (e.g. Eldredge 1980; Aiello and Dean 1990; O'Brien and Lyman 2003), the stratigraphic position of individual taxa should not be ignored in phylogenetic analyses (e.g. Harper 1976; Gingerich and Schoeninger 1977; Fortey and Chatterton 1988). The Type 1 beer jar was therefore accepted as being the most likely candidate to represent the ancestral beer jar condition.

7.2.4 Beer jar results

The cladistic analysis was conducted using PAUP* (Phylogenetic Analysis Using Parsimony) version 4.0 beta 10 (Swofford 2002). The specific program parameters used in this

process can be found in Hood and Valentine 2012.

Cladistic analysis of the character matrix presented in Table 7.3 generated a single tree, 26 steps long, with a consistency index (CI) of 0.65 and an retention index (RI) of 0.68 (Figure 7.5), both 'goodness of fit' measures to assess cladogram robustness (as discussed in Hood and Valentine 2012: 52). Synapomorphic features supporting numbered internal nodes of the strict consensus tree (Figure 7.5) are listed in Table 7.4. Monophyly of the beer jars is not supported by this analysis and the preliminary typological sequence established by Köhler and Smythe 2004 of Naqada IIIA/B to IIID beer jars from Helwan is not entirely consistent with this analysis either. The evolutionary relationships at the base of the strict consensus tree between the Type 1 beer jar (outgroup), LSJ 1 and 2 and beer jar Types 2–5 are unclear. LSJ 1 and LSJ 2 form a clade supported by 93% of bootstrap replicates[52] (Figure 7.5 and Table 7.4). Synapomorphic features supporting this clade include an angular rim (character 7, state 1) and a lentoid base (character 16, state 1). Beer jar Types 2–5 form a clade supported by 87% of bootstrap replicates. Synapomorphic features supporting this clade include a vessel index of 1.88–1.99 (character 1, state 1), neck with parallel sides (character 10, state 1) and a rounded (character 14, state 1) or pointed (character 15, state 1) base.

The CI for the single most parsimonious cladogram (Figure 7.5) was 0.65 indicating a fairly high level of homology (i.e. similarity within the assemblage, owing to a shared ancestry between forms which indicates evolutionary relationships). Sanderson and Donoghue 1989 and Hauser and Boyajian 1997 have demonstrated that as the number of taxa and characters included in a cladistic analysis increase, the CI is reduced. Therefore the CI cannot be simply compared between different studies. The regression

[52]Bootstrapping (Efron 1979; Efron 1981; Efron 1982) is a heuristic tool which allows a test of robustness of branching points in a cladogram to be determined by subjecting a dataset to random resampling. Each time this happens the analysis is re-run (here, a total of 10,000 times) and a cladogram determined based on the randomly generated dataset. Although some character states may be eliminated from the dataset and others may be selected multiple times during the random resampling, the more character states supporting each branching point, the more likely that branching point will appear in a cladogram generated by random resampling. In each replicated analysis, we can compare what are the common branching points in each cladogram and from these, determine the bootstrapping value (the percentage of times when each individual replicate reproduces the same branching point in a cladogram).

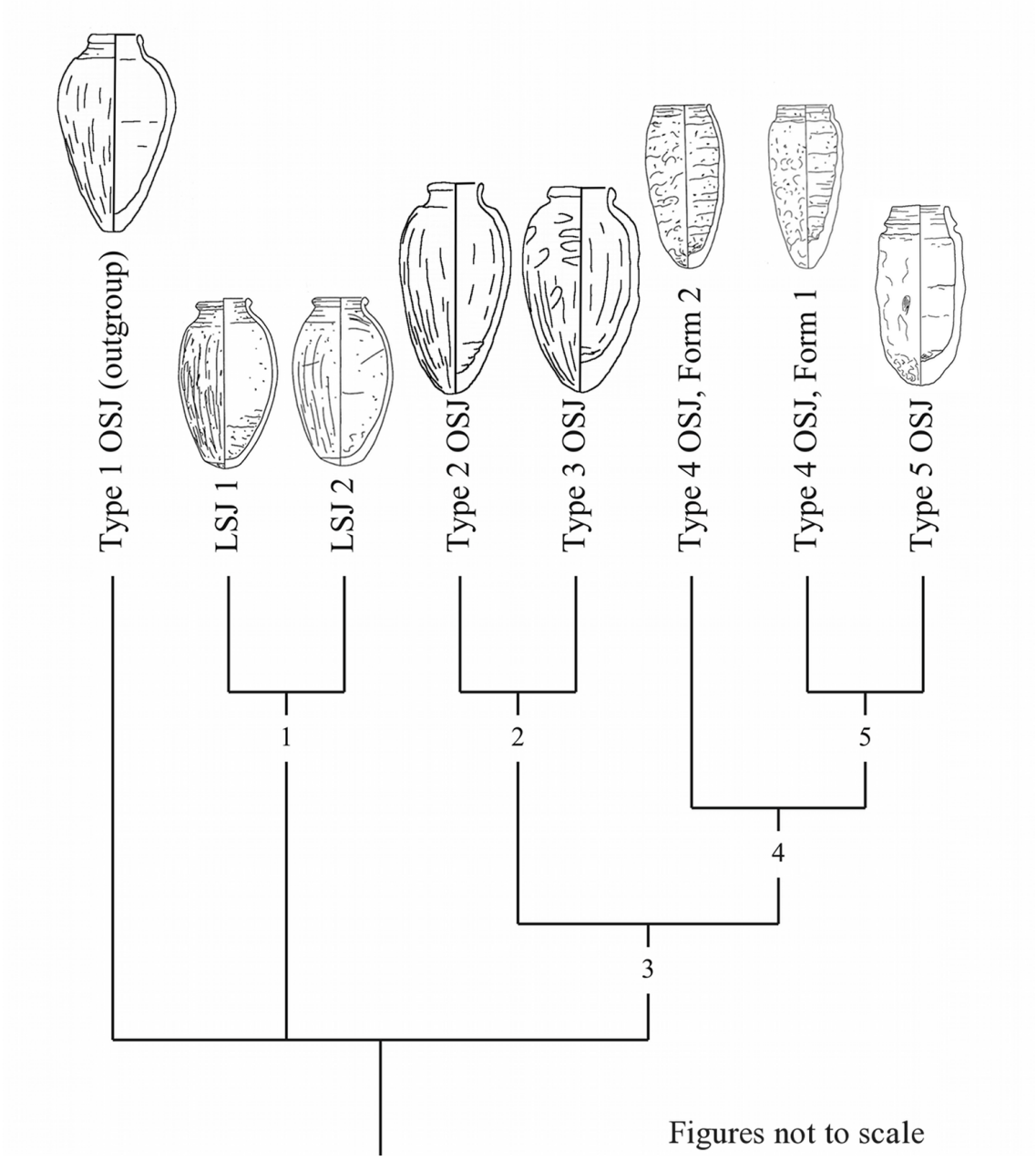

Figure 7.5: Single cladogram produced by cladistic analysis of the character matrix shown in Table 7.3. Synapomorphic characters and bootstrap support values for numbered internal nodes are presented in Table 7.4.

equation provided by Sanderson and Donoghue 1989 indicates that for eight taxa (as in this analysis), a CI of 0.73 is expected. This slight disparity can be explained by each beer jar in our data set possessing several character states for some characters such as rim type and base shape (Table 7.1). The retention index of 0.68 for the cladogram presented in Figure 7.5 falls within the range (and above the mean) of the RI values ob-

tained by Collard et al. 2006 for their biological and cultural based data sets. Based on the results of Collard et al. 2006, an RI of 0.68 for our data set indicates phylogenetic, rather than ethnogenetic, processes are responsible for the observed variation in the beer jars. That is, there is an inferred evolutionary relationship governing these observations, rather than external influences. The bootstrap support values indicate the percentage of times that a particular clade appears in a number of cladograms (in this case 10 000) constructed from randomly resampled versions of the character matrix presented in Table 7.3. The high bootstrap support values obtained here (Table 7.4) shows that each clade is supported by many characters and therefore remains relatively immune to the effects of random resampling. The bootstrap support values indicate that a strong phylogenetic signal occurs in the data set.

Table 7.4: Synapomorphic features and bootstrap support values for numbered internal nodes of the cladogram present in Figure 7.6.

Node	Bootstrap support values	Synapomorphic characters
1	93%	angular or rounded rim present; lentoid base present
2	85%	
3	87%	mean vessel index 1.80–1.99; rounded or pointed base present
4	94%	mean vessel index >2.00; rolled and external rims lost; direct rim present
5	57%	

7.2.5 Discussion of cladistic analysis of beer jars

According to the strict consensus tree, Type 4 and Type 5 beer jars are most derived relative to the outgroup (Type 1). This indicates that they have undergone the largest number of morphological changes from the ancestral condition as exemplified by Type 1 beer jars. Type 5 beer jars are most likely to be closely related to Type 4 beer jars, and Type 4, Form 1 in particular. Type 4, Form 2, although still closely related to Type

4, Form 1, are slightly less derived relative to the outgroup (i.e. they have undergone slightly fewer morphological changes than either Type 4, Form 1 or Type 5 relative to the outgroup). Types 2 and 3 beer jars appear to be more closely related to the outgroup, although they still show multiple derived morphological characters relative to the outgroup. Types 2 and 3 are clustered together as a result of their being morphologically more similar to each other than to the other Types (see Table 7.4 and Figure 7.5). It seems clear from the process of identifying characters during the initial stages of this study that a large amount of variation exists within many of the characters investigated. Only by including those characters that occur with a frequency of greater than 10% in each beer jar type was it possible to obtain a clear and strongly supported evolutionary signal. 'Noise' is generated by the large number of character states exhibited by each character. For example, the base shape of Type 1 can be flat, rounded or pointed (Table 7.1). However, each of these alternative character states for the base shape is treated as being of equal importance in a cladistic analysis, regardless of how frequently they occur. The inclusion of such 'noise' in the character matrix serves only to collapse nodes (branching points), reducing support and masking the evolutionary signal in the character matrix. A number of potential solutions exist to rectify this problem. Additional characters can be defined; however, given that this problem exists for many of the characters used in this analysis, defining additional characters will probably only increase the problem. Additional beer jar types could be established, but splitting them into finer and finer subdivisions, especially if such variations are attributable to mistakes made during the manufacturing process would result in the erection of potentially invalid types and forms. It is therefore essential to exercise caution when examining defining characteristics to avoid this problem.[53] It would, however, perhaps be possible to erect transitional types, which considered variation in characters (i.e. a variation of Type 1 beer jars would be those vessels, discussed above, with a rounded or pointed base,

[53] It is interesting to note here a study by Miller 1985. In his ethnographic account of contemporary ceramic production in India, Miller discusses the processes employed in ceramic manufacture and their impact upon the potters' and the archaeologists' classifications of type and form variation.

rather than a flat base, thus being 'Type 1/2 transitional beer jars' for example). Weighting characters (i.e. stating that some characters are more significant in the evolution of a group than others) can also be used to reduce the impact that such noise has in a cladistic analysis; however, selecting which characters to weight is frequently an arbitrary process (Felsenstein 1981; Suter 1994) and implies that both the phylogeny of the group and the significance of the characters used are already known (Smith 1994). By removing insignificant characters in large populations (i.e. those occurring less than 10% of the time) their impacts upon the outcome of the cladistic analysis are also removed, but all characters within small populations (i.e. those with less than 10 individuals) are retained since it is not possible to determine the dominance of a particular character state or states for such beer jars. Whether a 10% cut-off for character inclusion as used here is required for all types of ceramic vessels requires further investigation. Despite the overall success of the cladistic analysis in producing a robust cladogram, the evolutionary relationships between LSJ 1 and LSJ 2 and other beer jar types and forms are unclear. Revision of the characters and character states used in this analysis and/or the inclusion of additional characters and character states should help resolve the evolutionary relationships between these groups. However, this result could also indicate a previously unforeseen benefit of applying cladistics to Egyptian ceramics —the ability to identify anomalies within already established typological sequences that were not immediately apparent based upon visual analysis alone. Although the occurrence of a vessel with a lentoid base is unusual (Pers. Comm. E. C. Köhler, 2009), we maintain that LSJs are morphologically distinct and may, upon further study, represent a viable form variant or type. This illustrates that the situation for these vessels is more complex than previously conceived. Could the morphological differences in lentoid-based beer jars result from regional variation? Given the distinct fabric exhibited by LSJs compared to other beer jars types (Pers. Comm. E. C. Köhler, 2009) this is a distinct possibility. If so, what then is the origin of the LSJ? It is also important to note that these vessels are mostly clustered within three tombs. It may be possible that we are therefore seeing evidence of specific

workshop production or the work of a specific potter. Although these questions cannot be answered at present, it does suggest that cladistics can potentially identify anomalies within artefact typologies and aid in the identification of regional variation.

Unlike a traditional typological sequence that illustrates how one ceramic form evolves into another over time (i.e. a phylogenetic tree), cladograms do not show this type of information. For instance, the cladogram in Figure 7.5 does not say that Type 4, Form 1 beer jars evolved from Type 4, Form 2 beer jars. Instead, the cladogram indicates that these beer jars forms share a common ancestor that was neither a Type 2 nor Type 3 (although this is not supported by the archaeological evidence: there is much evidence in the archaeology for the development of Type 4 from Type 2 and Type 3). Despite this difference, an element of time is still implied from the base of the cladogram towards the top, but no specific length of time is indicated. Although the stratigraphic range of each beer jar and LSJ is relatively well constrained, this information was not included as a character in this analysis. Therefore, the robustness of the strict consensus tree can be further tested by attempting to correlate the first and last appearance datum of beer jars and LSJ, tomb assemblages, date group assemblages (Köhler 2004; Köhler 2014a) and association of types with their surrounding context.

The earliest type included in this analysis are Type 1 beer jars (the outgroup), which first appear during the Naqada IIIA/B period (Köhler 1998; Kroeper and Wildung 2000; Köhler and Smythe 2004). Type 2 vessels first appear during Naqada IIIB/C (Köhler and Smythe 2004), while Type 3 commenced during Naqada IIIC/D. Both Type 2 and Type 3 can occur concurrently with the Type 4 which seems to first appear no earlier than the mid Second Dynasty or Naqada IIID (Köhler 2004; Köhler and Smythe 2004; Pers. Comm. E. C. Köhler, 2009) (Figure 7.6). We also see this within the Bêt Khallaf assemblage, where X5462 and X5471, two Type 4 vessels, are found in association with a Type 3 beer jar (X5472). Given that these vessels occur concurrently and often in the same archaeological assemblages, it is possible that this results from a different function of each vessel (although collectively called 'beer jars', archaeological evidence remains

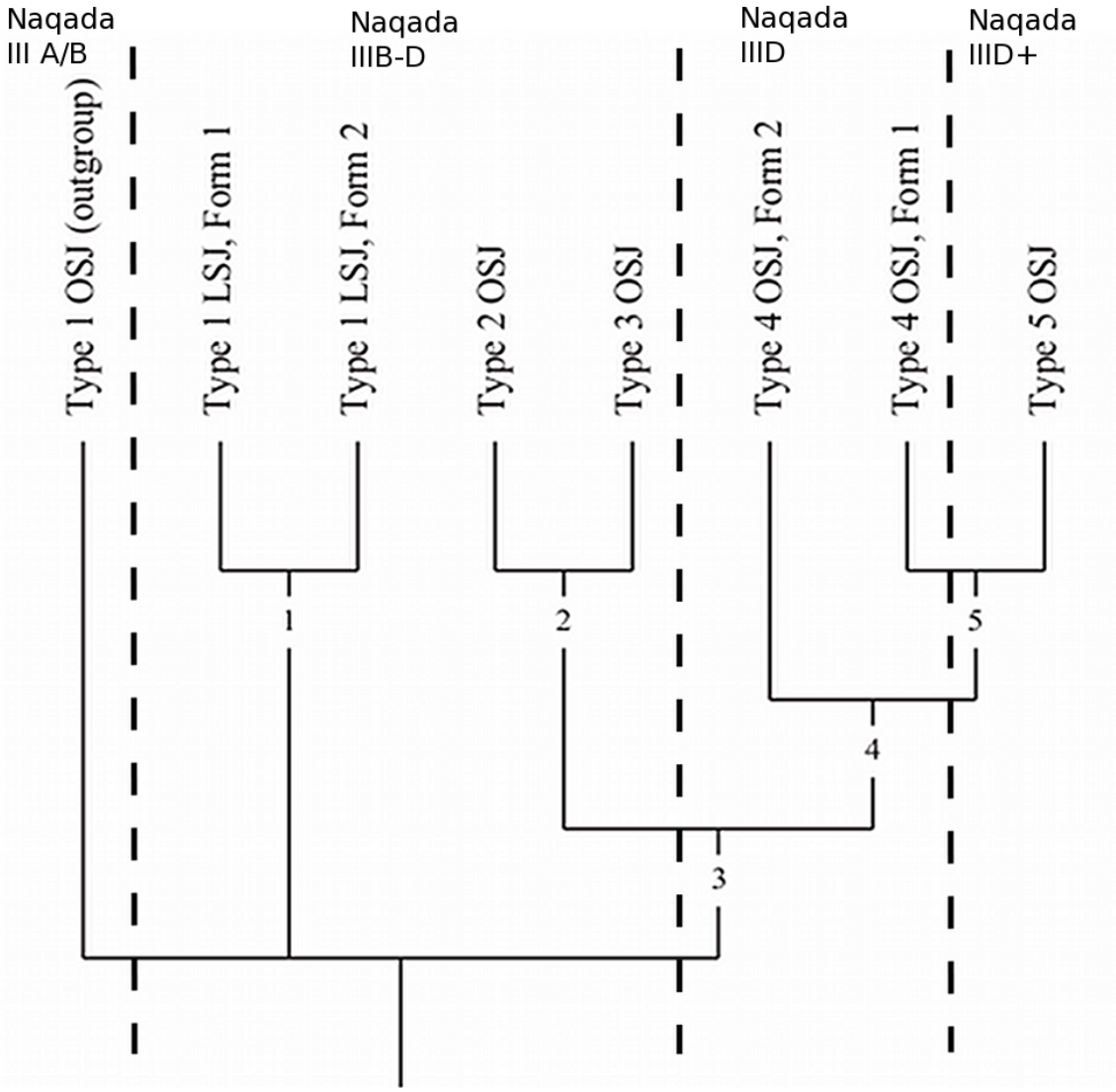

Figure 7.6: Single cladogram produced by cladistic analysis anchored to the proposed chronological time frame.

inconclusive as to their exact function). Further archaeological evidence is required to investigate this and at this stage we do not have enough data to determine the exact evolutionary developments illustrated here. The Type 5 beer jar is likely to emerge shortly after the Type 4 beer jar, although based on the archaeology it has been observed that in its early stages of development it is contemporaneous with Type 4. Indeed, within the Bêt Khallaf assemblage, vessel X5461 displays an early development of the collared rim, that is, the distinguishing feature of a Type 5 vessel, alongside the Type 3 and Type

4 beer jars. Again the possibility of a distinct form function arises. The Type 4 vessel continues well into the Old Kingdom and beyond and varies little in form over a long chronological period. At present it seems that the Type 5 beer jar commences with a slowly emerging collar and evolves into the more distinctive ledge collar seen in the early Old Kingdom. However, as yet, the archaeological evidence does not seem to indicate that Type 5 beer jars were long-lasting in the ceramic assemblage, rather they were eclipsed by the earlier Type 4 vessel and disappeared shortly after their initial occurrence (the brevity of this vessel's duration is not seemingly connected with it being produced in a single workshop, as the form is found throughout Egypt during the late Early Dynastic/early Old Kingdom periods).

In summary, although our cladogram can in many instances be successfully correlated with the existing preliminary stratigraphic and chronological information for the beer jars (Figure 7.6) observations resulting from both cladistic analysis and archaeological evidence illustrate the need for future work to be carried out on this data set, in which cladistics has the potential to play a vital role. However, when using this cladistic analysis alongside our OSL results for the Bêt Khallaf material, which included four Early Dynastic beer jars, we can begin to anchor our cladistic analysis to an absolute time frame as the Bêt Khallaf OSL results are the first absolute dates obtained directly from the ceramic material themselves. As discussed in the previous chapters, the age of the Bêt Khallaf assemblage is 2622 BC $\pm$128 years, which allows us to assume that the late Type 3, Type 4 and early Type 5 beer jars are chronologically placed around this time, and thus offer a *terminus post quem* and *terminus ante quem* date for the later Type 5 and earlier Type 1–Type 2 vessels respectively. In time, and both with further OSL dating and cladistic analysis, it is hoped that the chronological implications of cladistic analysis can be brought to light, and that cladistics can fine-tune ceramic development when high chronometric precision is lacking.

7.2.6 Cladistic analysis of Naqada III wine jars and bowls

In addition to the cladistic work carried out upon the beer jars as presented above, the author and her colleague have more recently started to examine other data sets from the late Naqada III repertoire, specifically looking at the so-called 'wine jars' and the assorted bowls known from this period. Unfortunately, as they presently stand, the results for analysis of the Naqada III bowls have been limited. Only 78 bowls were identified as suitable for analysis to date, and among these there was significant variation observed within the data, with 17 different vessel types being identified. Unfortunately, with so few examples of each vessel type, the robustness of the data is doubtful. A large part of the strict consensus tree remained unresolved and bootstrap analysis provides little support for the groupings present. This indicates the lack of a clear evolutionary signal in the data set. This does not mean that cladistic analysis has been unsuccessful here, but it does mean that more data is required, and it is likely that at least twice to three times the amount of already accumulated data is required to produce a meaningful analysis which can lend itself to the discussion of bowl typology during this period. It is hoped that this task can be completed over the next year or so, and with the publication of further data.

The wine jar data has produced very promising results, albeit results which would again benefit from an increased data set when such material becomes available. These results will therefore only be presented briefly here. The wine jar data set consisted of 126 individual vessels. The vessels used in this analysis were those wine jars presented in a series of published work (Köhler 2014a; Smythe 2004; Smythe 2008; Kroeper and Wildung 1994; Kroeper and Wildung 2000; Köhler and Smythe 2004) and unpublished data (collected by the present author, obtained from the Early Dynastic tombs beneath the Tombs of Meryneith and Maya, Saqqara, and the five wine jars from the Bêt Khallaf assemblage; and obtained from the Helwan Project, courtesy of E. C. Köhler). The methodology employed for analysis of the wine jars followed that for the beer jars, as presented above. Two main wine jar classes (WJ1 and WJ2) were identified following

Table 7.5: Distribution of morphological features across wine jar types. The frequency of occurrence of each feature is indicated as a percentage.

		WJ 1F1 (outgroup) (n = 18)	WJ 1F0 (n = 2)	WJ 1F2 (n = 7)	WJ 1F3 (n = 6)	WJ 1F4 (n = 8)	WJ 2F1 (n = 3)	WJ 2F2 (n = 37)	WJ 2F3 (n = 9)	WJ 2F4 (n = 10)	WJ 2F5 (n = 5)	WJ 1F1/F2 (n = 4)	WJ 1F2/F3 (n = 1)	WJ 1F3/F4 (n = 7)	WJ 2F2/F3 (n = 8)	WJ 2F3/F4 (n = 1)
General vessel shape	**vessel shape**	closed (100%)	closed (100%)	closed (100%)	closed (100%)	closed (100%)	closed (100%)	closed (100%)	closed (100%)	closed (100%)	closed (80.0%) unknown (20.0%)	closed (100%)	closed (100%)	closed (100%)	closed (100%)	closed (100%)
	vessel wall shape	straight (94.4%) curved (5.6%)	straight (50.0%) curved (50.0%)	straight (57.1%) curved (42.9%)	straight (50.0%) curved (50.0%)	straight (62.5%) curved (37.5%)	straight (100%)	straight (100%)	straight (100%)	straight (100%)	straight (100%)	straight (75.0%) curved (25.0%)	straight (100%)	straight (57.1%) curved (42.9%)	straight (100%)	straight (100%)
	position of maximum diameter	beneath rim (100%)	beneath rim (100%)	beneath rim (100%)	beneath rim (83.3%) unknown (16.7%)	beneath rim (100%)	beneath rim (100%)	beneath rim (94.6%) unknown (5.4%)	beneath rim (100%)	beneath rim (90.0%) unknown (10.0%)	beneath rim (40.0%) unknown (60.0%)	beneath rim (100%)	beneath rim (100%)	beneath rim (100%)	beneath rim (100%)	beneath rim (100%)
Rim	**rim morphology**	external (100%)	external (100%)	external (100%)	external (83.3%) unknown (16.7%)	external (100%)	external (100%)	external (97.3%) unknown (2.7%)	external (100%)	external (100%)	external (60.0%) unknown (20.0%)	external (100%)	external (100%)	external (100%)	external (100%)	external (100%)
	rim character	rounded (33.3%) subangular (55.6%) angular (11.1%)	rounded (50.0%) subangular (50.0%)	subangular (71.4%) angular (28.6%)	rounded (16.7%) subangular (66.7%) unknown (16.7%)	rounded (25.0%) subangular (62.5%) angular (12.5%)	subangular (66.7%) angular (33.3%)	rounded (51.4%) subangular (45.9%) unknown (2.7%)	rounded (22.2%) subangular (77.8%)	subangular (100%)	rounded (60.0%) unknown (20.0%)	rounded (50.0%) angular (50.0%)	subangular (100%)	rounded (28.6%) subangular (71.4%)	rounded (62.5%) subangular (37.5%)	subangular (100%)
	rim ridge on exterior	absent (100%)	absent (100%)	absent (100%)	absent (100%)	absent (100%)	absent (100%)	present (8.1%) absent (89.2%) unknown (2.7%)	present (44.4%) absent (55.6%)	present (90.0%) absent (10.0%)	absent (60.0%) unknown (40.0%)	absent (100%)	absent (100%)	absent (100%)	present (12.5%) absent (87.5%)	absent (100%)
	rim interior grooved	absent (100%)	absent (100%)	absent (100%)	absent (100%)	absent (100%)	absent (100%)	present (8.1%) absent (89.2%) unknown (2.7%)	present (44.4%) absent (55.6%)	present (10.0%) absent (90.0%)	absent (60.0%) unknown (40.0%)	absent (100%)	absent (100%)	absent (100%)	present (25.0%) absent (75.0%)	present (100%)

Table 7.5: Continued

		WJ 1F1 (outgroup) (n = 18)	WJ 1F0 (n = 2)	WJ 1F2 (n = 7)	WJ 1F3 (n = 6)	WJ 1F4 (n = 8)	WJ 2F1 (n = 3)	WJ 2F2 (n = 37)	WJ 2F3 (n = 9)	WJ 2F4 (n = 10)	WJ 2F5 (n = 5)	WJ 1F1/F2 (n = 4)	WJ 1F2/F3 (n = 1)	WJ 1F3/F4 (n = 7)	WJ 2F2/F3 (n = 8)	WJ 2F3/F4 (n = 1)
Neck	**neck profile**	concave (77.8%) straight (22.2%)	concave (100%)	concave (42.9%) straight (57.1%)	concave (83.3%) straight (16.7%)	concave (37.5%) straight (62.5%)	straight (33.3%) absent (66.7%)	straight (21.6%) absent (75.7%) unknown (2.7%)	absent (100%)	straight (60.0%) absent (40.0%)	straight (20.0%) absent (80.0%)	straight (50.0%) concave (50.0%)	straight (100%)	concave (71.4%) straight (28.4%)	straight (37.5%) absent (62.5%)	absent (100%)
	neck shape	parallel (33.3%) divergent (66.7%)	parallel (100%)	parallel (42.9%) dconvergent (57.1%)	parallel (50.0%) divergent (50.0%)	parallel (50.0%) divergent (12.5%) convergent (37.5%)	convergent (33.3%) absent (66.7%)	parallel (2.7%) convergent (18.9%) absent (75.7%) unknown (2.7%)	absent (100%)	convergent (60.0%) absent (40.0%)	convergent (20.0%) absent (80.0%)	parallel (50.0%) divergent (25.0%) convergent (25.0%)	parallel (100.0%)	parallel (42.9%) divergent (57.1%)	convergent (37.5%) absent (62.5%)	absent (100%)
	neck groove	absent (100%)	absent (100%)	absent (100%)	present (16.7%) absent (83.3%)	present (50.0%) absent (50.0%)	absent (100%)	absent (100%)	absent (100%)	absent (100%)	absent (100%)	absent (100%)	absent (100%)	absent (100%)	absent (100%)	absent (100%)
Shoulder	**shoulder profile**	curved (100%)	curved (100%)	curved (100%)	curved (83.3%) sharp (16.7%)	curved (100%)	curved (100%)	slight curve (55.6%) curved (70.3%)	slight curve (44.4%) curved (55.6%)	slight curve (20.0%) curved (80.0%)	slight curve (40.0%) curved (20.0%) unknown (40.0%)	curved (100%)	curved (100%)	curved (100%)	slight curve (50.0%) curved (50.0%)	slight curved (100%)
Base	**base shape**	flattened (27.8%) flat (50.0%) lentoid (22.2%)	flat (100%)	flattened (42.9%) flat (42.9%) lentoid (14.3%)	flattened (50.0%) flat (16.7%) rounded (33.3%)	flattened (12.5%) rounded (87.5%)	flattened (33.3%) lentoid (66.7%)	flattened (62.2%) flat (8.1%) lentoid (2.7%) rounded (24.3%) unknown (2.7%)	flattened (22.2%) rounded (77.8%)	rounded (90.0%) unknown (10.0%)	flattened (20.0%) flat (20.0%) rounded (60.0%)	flattened (75.0%) flat (25.0%)	flattened (100.0%)	flattened (57.1%) flat (42.9%)	flattened (62.5%) rounded (37.5%)	rounded (100%)

Table 7.5: Continued

		WJ 1F1 (outgroup) (n = 18)	WJ 1F0 (n = 2)	WJ 1F2 (n = 7)	WJ 1F3 (n = 6)	WJ 1F4 (n = 8)	WJ 2F1 (n = 3)	WJ 2F2 (n = 37)	WJ 2F3 (n = 9)	WJ 2F4 (n = 10)	WJ 2F5 (n = 5)	WJ 1F1/F2 (n = 4)	WJ 1F2/F3 (n = 1)	WJ 1F3/F4 (n = 7)	WJ 2F2/F3 (n = 8)	WJ 2F3/F4 (n = 1)
Decoration	**decoration method**	incised (83.3%) moulded (16.7%)	incised (100.0%)	incised (28.6%) absent (71.4%)	incised (66.7%) moulded (16.7%) absent (16.7%)	incised (25.0%) absent (75.0%)	incised (33.3%) applied (33.3%) absent (33.3%)	moulded (2.7%) applied (97.3%)	applied (100%)	applied (100%)	absent (40.0%) unknown (60.0%)	incised (50.0%) moulded (25.0%) absent (25.0%)	absent (100%)	incised (100%)	applied (100%)	applied (100%)
	decoration type	wavy (100%)	wavy (100%)	wavy (28.6%) absent (71.4%)	wavy (50.0%) 1 band (top) (16.7%) absent (16.7%) unknown (16.7%)	wavy (12.5%) 1 band (top) (12.5%) absent (75.0%)	1 band (top) (33.3%) 3 bands (top, max. diamater, bottom (33.3%) absent (75.0%)	1 band (top) (73.0%) 2 bands (top) (2.7%) 2 bands (top, bottom) (21.6%) 1 band (base) (2.7%)	1 band (top) (33.3%) 2 bands (top, bottom) (66.7%)	1 band (top) (20.0%) 2 bands (top, bottom) (80.0%)	absent (60.0%) unknown (40.0%)	wavy (75.0%) absent (25.0%)	absent (100%)	wavy (100%)	1 band (top) (100%)	2 bands (top, bottom) (100%)
	surface finish	absent (100%)	absent (100%)	burnished (14.3%) absent (100%)	absent (100%)	absent (100%)	absent (100%)	absent (100%)	absent (100%)	absent (100%)	absent (100%)	absent (100%)	absent (100%)	absent (100%)	absent (100%)	absent (100%)

Kaiser 1964, who discussed two wine jar classes occurring concurrently in Egypt: the first being those wine jars displaying crescent-shaped vestigial handles, and the second group supporting banded/rope decoration. The types were further defined based upon the wine jar vessel index as established by Köhler and Smythe 2004.[54] Table 7.5 defines 15 morphological features of wine jars. From this, 20 cladistically informative characters and character states were defined. This follows the same criteria for determining informative characters as described for the beer jars above. After this process was completed, 10 morphologically distinct wine jar types were identified and five transitional types were identified (i.e they were seen to be a combination of two distinct types)—for the purpose of the analysis, however, they have been considered as types on their own right, creating 15 types in the final analysis (Figure 7.7). The wine jar outgroup was defined as WJ1 F1, a wine jar dating to the Naqada IIIB period, and found exclusively at Minshat Abu Omar (Kroeper and Wildung 1994, Kroeper and Wildung 2000), which was identified as being the earliest wine jar type within the data set. The 15 characters described for each wine jar type indicate a high level of morphological variation exists in the data set, and as discussed for the beer jars, this is possibly owing to the vessels being handmade and subject to manufacturing imperfections and signature traits belonging to a single potter or workshop. Again, given that the presence of shared derived characters is necessary in cladistic analysis, only characters presented in Table 7.5 which were present in two or more vessels were included in analysis. The final characters and character states considered to be cladistically informative and used in final analysis are presented in Table 7.6 and the character matrix for the wine jar data set can be seen in Table 7.7.

The resulting cladogram produced after analysis can be seen in Figure 7.8. The CI for this analysis is 0.4651 and the RI is 0.7051 and a bootstrap analysis was carried out to assess the robustness of the data. Only four nodes on the produced cladogram gave bootstrap values of above 50% (Table 7.8 and Figure 7.8). Again, this indicated that the

[54] A more comprehensive discussion of the development of wine jars can be found in Section 6.2.

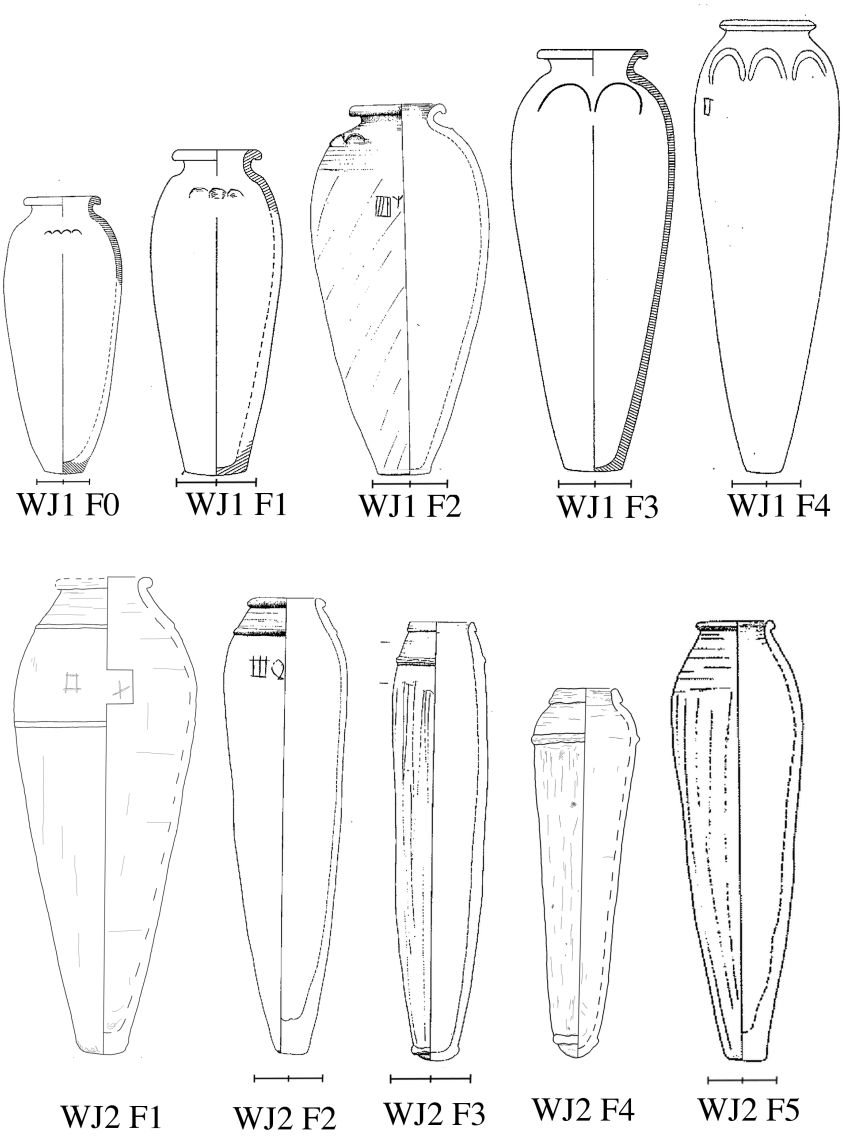

Figure 7.7: The 10 morphologically distinct wine jar types identified in this study. (The five transition forms are not illustrated here). Line drawings taken from: WJ1 F0 (Kroeper and Wildung 2000: 154), WJ1 F1 (Kroeper and Wildung 2000: 152), WJ1 F2 (Köhler and Smythe 2004: Pl. 2), WJ1 F3 (Kroeper and Wildung 2000: 170), WJ1 F4 (Petrie et al. 1953: XXI), WJ2 F1 (Turah, X5489), WJ2 F2 (Köhler and Smythe 2004: Pl. 3), WJ2 F3 (Köhler and Smythe 2004: Pl. 3), WJ2 F4 (Bêt Khallaf X4116), WJ2 F5 (Smythe 2008: 181)). NB. scales for X4116 and X5489 can be seen in Appendix J and Appendix C respectively.

Table 7.6: List of characters and character states (derived from Table 7.5) that was used in the cladistic analysis of wine jar types and forms.

1. Curved vessel wall: 0. absent 1. present	11. Flat base shape: 0. absent 1. present
2. Angular rim character: 0. absent 1. present	12. Flattened base shape: 0. absent 1. present
3. Subangular rim character: 0. absent 1. present	13. Rounded base shape: 0. absent 1. present
4. Rounded rim character: 0. absent 1. present	14. Lentoid base shape: 0. absent 1. present
5. Straight neck profile: 0. absent 1. present	15. Incised decoration method: 0. absent 1. present
6. Concave neck profile: 0. absent 1. present	16. Moulded decoration method: 0. absent 1. present
7. Parallel neck shape: 0. absent 1. present	17. Applied decoration method: 0. absent 1. present
8. Convergent neck shape: 0. absent 1. present	18. Wavy decoration method: 0. absent 1. present
9. Divergent neck shape: 0. absent 1. present	19. 1 band at top decoration method: 0. absent 1. present
10. Slight curve shoulder profile: 0. absent 1. present	20. 1 band at base decoration method: 0. absent 1. present

Table 7.7: Character state matrix of the 20 characters used in the cladistic analysis of wine jar types and forms. See Table 7.6 for character state definitions.

	1	2	3	4	5	6	7	8	9	10	11	12	13	14	15	16	17	18	19	20
WJ 1F1 (outgroup)	0	1	1	1	1	1	1	0	1	0	1	1	0	1	1	1	0	1	0	0
WJ 1F0	1	0	1	1	0	1	1	0	0	0	1	0	0	0	1	0	0	1	0	0
WJ 1F2	1	1	1	0	1	1	1	1	0	0	1	1	0	1	0/1	0	0	0/1	0	0
WJ 1F3	1	0	1	1	1	1	1	0	1	0	1	1	1	0	0/1	0/1	0	0/1	1	0
WJ 1F4	1	1	1	1	1	1	1	1	1	0	0	1	1	0	0/1	0	0	0/1	1	0
WJ 2F1	0	1	1	0	0/1	0	0	0/1	0	0	0	1	0	1	0/1	0	1	0	1	1
WJ 2F2	0	0	1	0	0/1	0	0	0/1	0	1	0	1	1	0	0	0	1	0	1	0
WJ 2F3	0	0	1	1	0	0	0	0	0	1	0	1	1	0	0	0	1	0	1	1
WJ 2F4	0	0	1	0	0/1	0	0	0/1	0	1	0	0	1	0	0	0	1	0	1	1
WJ 2F5	0	0	0	1	0/1	0	0	0/1	0	1	1	1	1	0	0	0	0	0	0	0
WJ 1F1/F2	1	1	0	1	1	1	0	1	1	0	1	1	0	0	1	1	0	1	0	0
WJ 1F2/F3	0	0	1	0	1	0	0	0	0	0	0	1	0	0	0	0	0	0	0	0
WJ 1F3/F4	1	0	1	1	1	1	0	0	1	0	1	1	0	0	1	0	0	1	0	0
WJ 2F2/F3	0	0	1	1	0/1	0	0	1	0	1	0	1	1	0	0	0	1	0	1	0
WJ 2F3/F4	0	0	1	0	0	0	0	0	0	1	0	0	1	0	0	0	1	0	1	1

data set is not particularly robust (here, we should remember that although the wine jar analysis had almost an identical number of vessels included for analysis as was seen for the beer jar data, only eight types were determined in the beer jar analysis, whereas the wine jar analysis has presented 15 types). This suggests that to ensure a more robust analysis is achieved, further data is required. Nevertheless, we can make several remarks for the wine jar data based on this preliminary analysis.

The strict consensus tree (Figure 7.8) shows that the WJ2 type wine jars are more derived relative to the outgroup than the members of the WJ1 group, and have thus undergone more evolutionary transformations. The most derived types relative to the outgroup are WJ2 F4 and the transitional type WJ2 F3/F4, the node for which is supported by a 64% bootstrap value. Given that these two vessel types are chronologically and typologically the latest wine jars known from existing sequences, this is in good agreement with the archaeology. It is the WJ2 F4 wine jars which are present at Bêt Khallaf. Also forming part of the same branch of the cladogram are WJ2 F1 and WJ2 F2, which are typologically similar to the WJ2 F4 and WJ2 F3/F4, and belong to the banded/rope decoration wine jar class. WJ2 F2, although continuing to be closely related to the most derived node, is slightly less derived relative to the outgroup, although the cladogram still indicated a degree of relatedness. The node separating the majority of the WJ2 types (with the exception of WJ2 F5 and WJ2 F2/F3) is supported by a bootstrap value of 46%. The node which includes WJ2 F2/F3 also, is supported by a bootstrap value of 58%. The WJ2 class are more closely related to one another than the WJ1 vessels and members of the WJ2 group form a monophyletic group—this indicates that the WJ2 vessels have a shared common ancestor, indicating a true evolutionary relationship between these vessels. The exception to this, however, is WJ2 F5, which was thought to be a variant of WJ2 F2, but insufficient information exists to discuss this further at this stage and it may be that archaeological information points to this vessel type being more similar to the WJ1 group (Pers. Comm. E. C. Köhler, 2016).

It is difficult to gain much meaningful information at this stage for the WJ1 class of

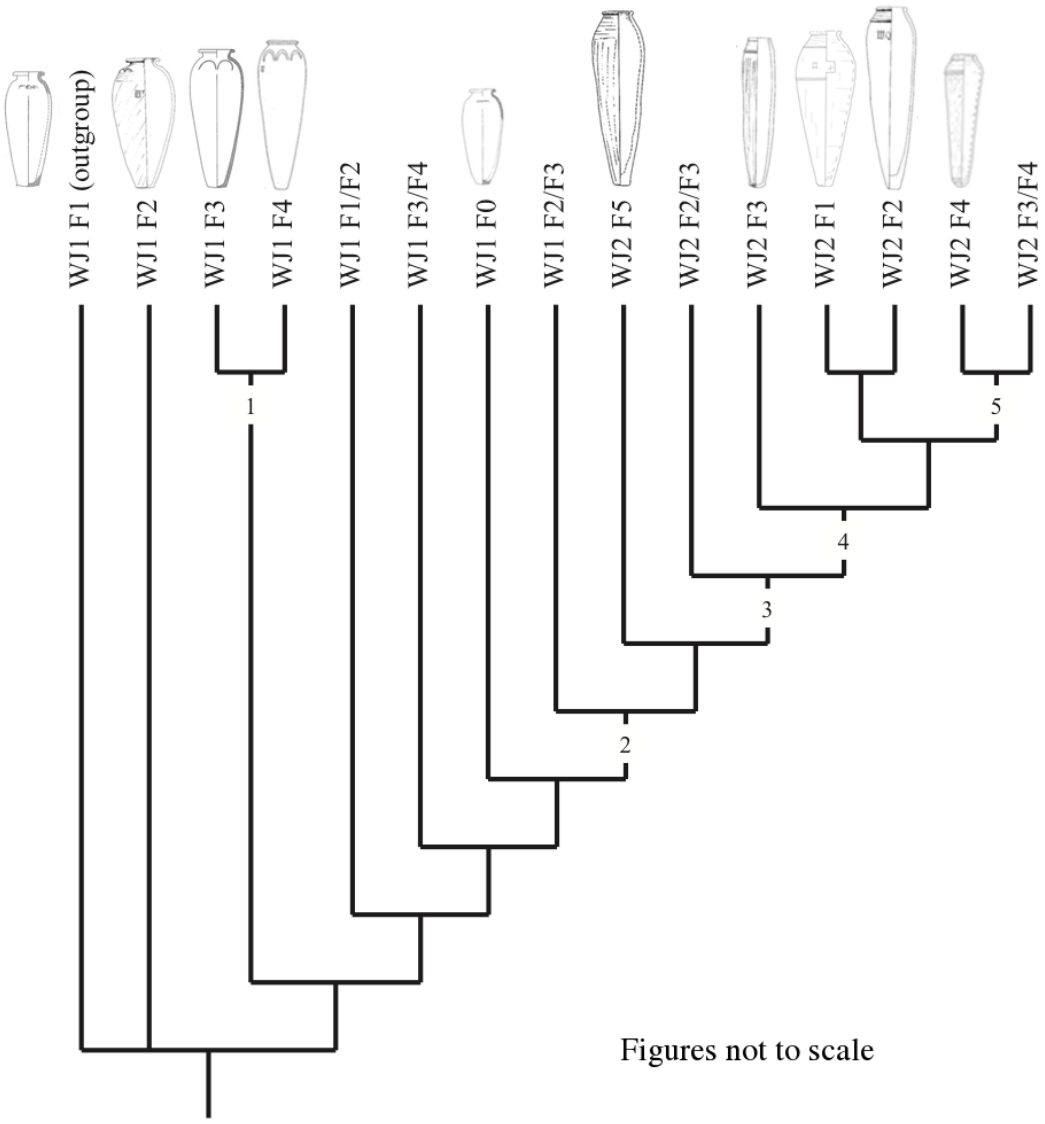

Figure 7.8: Single cladogram produced by cladistic analysis of the character matrix shown in Table 7.7. Synapomorphic characters and bootstrap support values for numbered internal nodes are presented in Table 7.8.

vessel as it is not possible to discuss relationships between the different classes based upon the cladogram: that is, members of the WJ1 group do not form a monophyletic group. However, WJ1 types are less derived from the outgroup than the WJ2 types. The relationships between WJ1 F1 and WJ1 F2 and the other wine jar types can not be verified at present. Furthermore, the results cannot yet lend weight to the idea that members of the WJ1 group form a separate and distinct grouping of wine jars, although the cladogram suggests that most types form sister groups to the WJ2 group. Indeed,

Table 7.8: Synapomorphic features and bootstrap support values for numbered internal nodes of the cladogram presented in Figure 7.8

Node	Bootstrap support values	Synapomorphic characters
1	51%	
2	69%	concave neck lost; incised decoration lost; wavy decoration lost
3	58%	applied decoration present
4	46%	1 band at base present
5	64%	

the WJ1 group appears to form a paraphyletic group, that is, they form a group that has had some descendant taxa (i.e. WJ1 class vessels) arbitrarily excluded. This means that all WJ2 types share more derived characters with each other than any of the WJ1 types, but the same is not true in reverse. That is, the WJ1 types do not, based on this analysis, appear to have a distinct evolutionary relationship. The exception to this is that WJ1 F3 and WJ1 F4 are separated from the majority of the clade and are shown to be least derived from the outgroup, an analysis which does agree to some extent with the archaeology given that these vessels are likely a direct typological continuation of WJ1 F1.

It might be possible to achieve a more robust analysis of this material in future when additional data are added, but also possibly by removing the transitional types. It does not seem at this stage that the transitional types add significantly to interpretation and it might be best to reassign the vessels to a non-transitional type (thus broadening the characters for those types, rather than allowing them to stand as a specific type). These results show that further work on the wine jar data set could be a lucrative line of further enquiry, and could help to fine-tune our understanding of current wine jar typologies.

7.2.7 Concluding remarks on the application of cladistic analysis to the study of Naqada III ceramics

The results presented here, particularly for the beer jars, indicate that cladistics has the potential to be a fruitful and insightful avenue of enquiry into Egyptian archaeology. Results to-date illustrate that, as a method designed to trace evolutionary development, cladistics can be used as a tool to confirm and refine existing typologies. We have seen this demonstrated herein, with cladistics in part supporting preliminary archaeological assessment for the beer jar data, and to a lesser extent for the wine jars. Cladistics can also be used to establish new typological sequences of material culture, which archaeological assessment on its own may overlook, and it can also be used as an independent method for providing a more refined assessment of morphological variation within a ceramic assemblage and shedding light on the possibility of new ceramic forms. Since cladistics does not in itself provide or include a chronological assessment of a data set, the resulting cladogram must be anchored to a chronological sequence through observation of the archaeological record and also, in the future, by anchoring absolute dates (i.e. OSL dates and radiocarbon dates) to the sequences established through cladistics—an initial step has been made here for the beer jar data, anchoring the late Type 3/Type 4/early Type 5 vessels to the absolute OSL-determined date obtained for Phase One of the Bêt Khallaf assemblage. To fully achieve this, further data would be required both for cladistics and OSL, but by developing both techniques independently, it will eventually prove possible to combine them, and achieve further understanding and chronological precision for the Naqada III ceramic data set. As this technique is a 'first attempt' within the field of Egyptian archaeology, we look forward to the future possibilities of its application and indeed of its potential impact upon the study of Early Dynastic ceramics.

7.3 Future directions

Ceramic studies can be greatly improved upon, and far more information from a single data set be achieved, when a multi- and interdisciplinary approach to their study is achieved. Although OSL dates can help anchor the chronology of a site, chronological information for individual ceramics is far more useful when the dates can be associated with a broader, more encompassing data set. Seriation can provide a backbone for the ceramic chronology by examining not just the typological development of a single vessel type, but by informing about the temporal relationships between different types, wares, and styles of pottery. Likewise, cladistics can help fine-tune seriation analysis by discerning more subtle changes in ceramic evolution which may not be identified within seriation analysis; this is because cladistics is focused more heavily upon individual characteristics for each individual vessel. In turn, OSL dating, although unlikely to ever be carried out upon all known ceramics, can be used to date individual vessels of typological significance, and anchor these to an absolute timeline. The scope for combining these techniques is vast and promising for the Naqada III period in Egypt. Although it is likely to take a lifetime's work to achieve such a broad-scale project, the work here presents the foundations for such an undertaking and demonstrates that the potential for such a study is significant and would greatly contribute to our knowledge of the Naqada III ceramic assemblage.

Chapter 8

OSL as a relative dating technique for late Predynastic and Early Dynastic Egyptian ceramics

8.1 Introduction

Up until this point, this thesis has focused on using OSL dating as an absolute dating method, specifically in order to produce the first absolute dates obtained directly from Egyptian ceramic vessels using the OSL technique. Yet OSL can also be used as a relative dating technique, although this is not routinely done for two reasons: first, in cases where access to recently excavated field material is forthcoming for OSL dating, using the technique as a relative dating method is not necessary; second, owing to the associated costs of OSL analysis as a relative dating technique, a no-cot relative dating technique, such as seriation, would generally be the more accepted option (the analysis cost for an OSL sample is £550.00 at RLAHA as of 2016). However, this thesis also focuses on applying OSL dating to ceramics held in museum collections, and it is here that using OSL as a relative dating technique comes into its own and can be of additional benefit to the archaeologist. In this instance, ceramic assemblages in museums whose provenance and chronology are uncertain, could well benefit from OSL dating being used as a rela-

tive dating technique to shed light upon their chronological implications. This chapter thus provides a proof-of-concept—that using OSL as a relative dating technique can be beneficial to understanding the chronology and typology of less well-studied ceramic assemblages—and illustrates the usefulness of OSL dating as a relative dating technique.

Many museum pieces were acquired in an era when detailed recording of provenance was rare, often with specimens being bought from antiquities dealers with no indication of the true find-spot of a piece, other than a broad regional location. Often this would happen to entire classes of vessels, which would be more prized above others, probably owing to a particular characteristic of the ware, and in turn significant information was lost. A particular case in point is the Predynastic Egyptian Decorated Ware, or D-Ware, one of nine ware types classified by Petrie in his Corpus of Prehistoric Pottery (Petrie 1921). Although Petrie (whose recording methods were arguably the best of his generation) along with his peers excavated a large number of such vessels for museum collections (at sites such as Naqada (Petrie and Quibell 1896), Gerzeh (Petrie et al. 1912), Mahasna (Ayrton and Loat 1911) and El Amrah (Randall-MacIver et al. 1902)), an equally large number were purchased by museums, from antiquities' dealers, to add to their collections, valued for their beautiful and highly stylised decoration (one of only several decorated wares known throughout Egyptian history). Without their origin being known (and having been well cleaned prior to display), these vessels lack a crucial piece of information for determining an absolute OSL date: determination of the external dose rate ($\dot{D}_{ext}$), which can be obtained using original soil adhering to the vessel. Without the $\dot{D}_{ext}$ measurement, only a relative date can be achieved; by taking the D_e measurement and dividing it by $\dot{D}_{int}$, rather than dividing it by the sum of $\dot{D}_{ext}$ and $\dot{D}_{int}$. While the lack of information about $\dot{D}_{ext}$ will mean that this relative date can deviate significantly from the true absolute age of the pot, the relative date may be used to determine the relative sequence of the ceramics in a manner similar to traditional relative dating techniques such as seriation, that is, these dates will help determine the sequence of the vessels. This relative date would depend on the assumption that $\dot{D}_{ext}$ is both small

compared to $\dot{D}_{int}$ and similar for all pots in a single assemblage; both assumptions are valid for Egypt at this point, based upon observed internal and external dose rates seen across the country. The use of OSL in this manner is useful where a group of ceramics is known, but no sequence has been ascertained. Similarly, OSL could be used in this manner for assemblages which are known to be from a particular location but where the internal chronology of the material is unknown. Lastly, once a relative OSL sequence has been calculated, if one member of the sequence has an associated absolute date calculated by other means (i.e. radiocarbon dating on vessel contents), the whole sequence is then anchored and the absolute ages of all the vessels are known (within error bars).

8.2 Data set

To illustrate how OSL can be used as a relative dating technique, and thus use the technique to further improve our understanding of the chronology of archaeological assemblages, two sets of objects were examined: a selection of Wavy-Handled vessels from Predynastic and Early Dynastic Egypt from the site of Turah, and three wine jars inscribed with *serekhs*, two from Turah and one from Hierakonpolis.

The Turah material was offered to this project by the University of Vienna, where an almost complete relative sequence of Wavy-Handled vessels was available for study with permission from the University to use MET sampling protocols. This assemblage is a prime set of material on which to demonstrate how OSL can be used as a relative dating technique, because, with regard to the relative chronology of ceramic typology, it is one of the most well-understood ceramic assemblages from this time period. The Wavy-Handled vessel provided the backbone of Petrie's ceramic sequencing system, being one of the longest-lived ceramic types. It was observed to continue across several archaeological phases spanning the Predynastic and Early Dynastic Periods. While other vessel types came and went, the Wavy-Handled vessel continued to develop and evolve. Petrie originally based his seriation of Predynastic and Early Dynastic Egyptian ceramics on this vessel type, noting the gradual change in vessel form from the bulbous vessel with

functional wavy handle (a style imported from the Levantine region), to the elongated cylindrical shape with a fine wavy decoration, which no longer served as a functional handle. Indeed, the final known stage of this vessel type no longer has a wavy decoration present at all (Köhler 2004). Figure 8.1 illustrates Petrie's sequence for this vessel type and the typological sequence of these vessels is discussed more fully below. The nine cylindrical vessels selected for OSL analysis at the University of Vienna represented an excellent typological assemblage of this particular ware, spanning the Naqada III A to Naqada IIIC2 periods.

Figure 8.1: Petrie's original sequencing of Wavy-Handled vessels (taken from Petrie, 1901: Front Plate)

In addition to the cylindrical vessels, three wine jars/sherds were also examined, two of which had an inscribed *serekh* (pre-fired engraved marks in the form of a rectangle, containing a symbol/name of historical figures). These vessels, owing to both their typology and their inscribed historical information (a *serekh* can often be directly linked to known figures or time period within the historical chronology), are prime candidates for illustrating the applicability of OSL as a relative dating technique. The two (almost complete) wine jars, also from the site of Turah, were made available for sampling by the University of Vienna and the wine jar sherd from the site of Hierakonpolis was offered by the Garstang Museum, Liverpool.

Appendix J presents the catalogue for the Turah ceramics sampled at the University of Vienna and the wine jar sherd sampled at the Garstang Museum, Liverpool. The vessels at the University of Vienna were excavated at the site of Turah, by Herman Junker, who worked at the site during the 1909/1910 excavation season. The results of the excavation were published in a single volume (Junker 1913). The majority of the material excavated from the site is now housed at the Kunsthistoriches Museum,

Vienna, although a teaching collection was also gifted to the University of Vienna, and it is from the latter that our samples have been collected.[55] Unfortunately, although it is known that all these ceramics come from the site of Turah, the exact provenance of each piece was not recorded and this information remains lost. No original depositional soil material was attached to the Turah material, and given that the site of Turah is now under military occupation (which makes the obtaining of *in situ* gamma spectroscopy measurements an impossibility), it is unlikely that absolute dates will be obtainable for this material in the future.

The wine jar sherd stored at the Garstang Museum was excavated by John Garstang in his 1905/1906 campaign at Hierakonpolis (Garstang 1907: 135, Pl. III; cf. Adams 1995: 123–124). Far more is known about the provenance of this sherd than those recovered from Turah as, owing to the nature of the *serekh* inscription, which possibly contains the name of Narmer, arguably Egypt's first Pharaoh, a rather detailed discussion of its find spot was noted in the publication. Unfortunately, no original depositional material was attached to the sherd, and thus at this stage it is only possible to provide a relative date for this sherd, and illustrate how this ties in to the historical chronology. It should be noted however that given the fairly detailed account of its location, in the future it might be possible to determine an absolute date for this piece by conducting *in situ* gamma spectroscopy measurements.

8.3 How to calculate a relative age using OSL dating

In this section we discuss how to calculate the relative ages of vessels using only the D_e and $\dot{D}_{int}$ measurements, as well as how to construct an estimate of the error associated

[55] The Kunsthistoriches Museum was also very helpful and supportive of this project, and permission was granted to do additional OSL sampling on their collection: the author extends her thanks to Regina Hölzl for her support of this project. However, prior to sampling, it was discovered that the collection is currently contaminated by a microspore which was considered a health and safety risk, unsuitable for samples requiring extraction by means of an electric drill. Therefore the collection could not be subjected to OSL analysis. It is hoped that in the future this unfortunate situation can be overcome and further work can be carried out upon this material.

with this calculation (which results from the fact that $\dot{D}_{ext}$ is not being considered in this determination).

The relative age of two vessels is defined as:

$$\frac{A_1}{A_2}, \tag{8.1}$$

where A_1 and A_2 are the absolute ages of two individual vessels respectively. Now,

$$A_1 = \frac{D_1}{I_1 + E_1} \tag{8.2}$$

and

$$A_2 = \frac{D_2}{I_2 + E_2}, \tag{8.3}$$

where D_1, I_1 and E_1 are the equivalent dose (D_e), the internal dose rate ($\dot{D}_{int}$) and the external dose rate ($\dot{D}_{ext}$), respectively, for the first vessel and likewise for the second vessel. Therefore,

$$\frac{A_1}{A_2} = \frac{D_1}{D_2}\frac{I_2 + E_2}{I_1 + E_1}. \tag{8.4}$$

If E_1 and E_2 (i.e. $\dot{D}_{ext}$) were known, we would know the exact relative age of the two vessels. However, even though these values are unknown, it is possible to calculate an approximate relative age for both of the vessels, and, additionally, an estimation of the error associated with that approximation.[56] There are three assumptions needed to determine this approximation: first, that $\dot{D}_{int}$ is similar for both vessels; secondly, that $\dot{D}_{ext}$ is similar for both vessels; thirdly, that for both vessels $\dot{D}_{ext}$ is smaller than $\dot{D}_{int}$.

More formally, we can define the parameters ϵ_I, ϵ_E and δ as follows:

$$\epsilon_I \equiv I_2 - I_1 \implies I_2 = I_1 + \epsilon_I, \tag{8.5}$$

$$\epsilon_E \equiv E_2 - E_1 \implies E_2 = E_1 + \epsilon_E, \tag{8.6}$$

$$\delta \equiv \frac{E_1}{I_1} \implies E_1 = \delta I_1, \tag{8.7}$$

and we further assume that these parameters are small, that is,

$$\left|\frac{\epsilon_I}{I_1}\right| \ll 1, \left|\frac{\epsilon_E}{E_1}\right| \ll 1, \delta \ll 1. \tag{8.8}$$

[56] The author would like to extend her sincere thanks to Edmund Highcock, who derived the final expression to determine expression for the error within the relative age calculation.

The meaning of these parameters, and the justification for assuming all three are small, will be discussed below.

Now ϵ_I and ϵ_E can be substituted directly into the equation for the relative age (8.4):

$$\frac{A_1}{A_2} = \frac{D_1}{D_2}\frac{I_1 + E_1 + \epsilon_I + \epsilon_E}{I_1 + E_1} \tag{8.9}$$

$$= \frac{D_1}{D_2}\left(1 + \frac{\epsilon_I + \epsilon_E}{I_1 + E_1}\right) \tag{8.10}$$

$$= \frac{D_1}{D_2}\left(1 + \frac{\epsilon_I}{I_1 + E_1} + \frac{\epsilon_E}{I_1 + E_1}\right). \tag{8.11}$$

Note that no approximations have been made up to this point, that is, the three assumptions have not yet been utilised.

At this point, it is possible to simply approximate the relative age as D_1/D_2, in which case the error would be given by the last two terms of equation (8.11), assuming, of course, that ϵ_I and ϵ_E are both small. However, is it possible to improve upon this estimate as follows.

First, the definition of δ is substituted into equation (8.11):

$$\frac{A_1}{A_2} = \frac{D_1}{D_2}\left(1 + \frac{\epsilon_I}{I_1\left(1+\delta\right)} + \frac{\epsilon_E}{I_1\left(1+\delta\right)}\right). \tag{8.12}$$

The ratio δ is now assumed to be small, which allows the following approximation to be made (using a Taylor series):

$$\frac{1}{1+\delta} \approx 1 - \delta \tag{8.13}$$

which means that

$$\frac{A_1}{A_2} \approx \frac{D_1}{D_2}\left(1 + \frac{\epsilon_I}{I_1}\left(1-\delta\right) + \frac{\epsilon_E}{I_1}\left(1-\delta\right)\right) \tag{8.14}$$

and therefore

$$\frac{A_1}{A_2} \approx \frac{D_1}{D_2}\left(1 + \frac{\epsilon_I}{I_1} - \frac{\epsilon_I}{I_1}\delta + \frac{\epsilon_E}{I_1}\left(1-\delta\right)\right). \tag{8.15}$$

However,

$$1 + \frac{\epsilon_I}{I_1} = \frac{I_2}{I_1}, \tag{8.16}$$

so

$$\frac{A_1}{A_2} \approx \frac{D_1}{D_2}\left(\frac{I_2}{I_1} - \frac{\epsilon_I}{I_1}\delta + \frac{\epsilon_E}{I_1}(1-\delta)\right). \tag{8.17}$$

It can be seen that the second term in this equation ($\epsilon_I\delta/I_1$) is second order, that is, it is the product of two small parameters and thus is smaller than the other two terms and can be neglected. Finally,

$$\frac{A_1}{A_2} \approx \frac{D_1}{D_2}\frac{I_2}{I_1}\left(1 + \frac{\epsilon_E}{I_1}\frac{I_1}{I_2}(1-\delta)\right). \tag{8.18}$$

Equation (8.18) demonstrates that the relative age can be approximated by

$$\frac{A_1}{A_2} \approx \frac{D_1}{D_2}\frac{I_2}{I_1} \tag{8.19}$$

with a relative error given by:

$$\frac{\epsilon_E}{I_2}(1-\delta). \tag{8.20}$$

Rearranging equation (8.19), it can be seen that

$$\frac{A_1}{A_2} \approx \frac{D_1/I_1}{D_2/I_2}, \tag{8.21}$$

and comparing this equation with (8.4), it can be seen that the approximation of the relative age of two vessels is simply effected by neglecting $\dot{D}_{ext}$, the external dose rate. However, the important point is that the relative error in this relative age is significantly smaller than the relative error in the individual absolute ages that could be calculated by neglecting $\dot{D}_{ext}$. The relative error (which results from neglecting $\dot{D}_{ext}$) in the absolute age (of, for example, the first vessel) is given by

$$\frac{D_1/I_1 - D_1/(I_1+E_1)}{D_1/(I_1+E_1)} \tag{8.22}$$

$$= \frac{1/I_1 - 1/(I_1(1+\delta))}{1/(I_1(1+\delta))} \tag{8.23}$$

$$\approx \frac{1-(1-\delta)}{1-\delta} \tag{8.24}$$

$$\approx \delta \tag{8.25}$$

where the second and third lines have used the definition of δ and the approximation (8.13).

The relative errors in the relative and absolute ages can now be compared by obtaining estimates for the values of δ and ϵ_E/I_2. It should be noted that though we are comparing the specific case of two vessels, in general ϵ_E can be thought of as the variation of $\dot{D}_{ext}$ within a studied ceramic assemblage, and I_2 can be considered as an order of magnitude estimate of $\dot{D}_{int}$, and δ is an estimate of the typical ratio between $\dot{D}_{ext}$ and $\dot{D}_{int}$. As no measurements for $\dot{D}_{ext}$ exist for these vessels, it is necessary here to approximate these based on existing values from the literature and from measurements taken from the Bêt Khallaf material (with the exception of I_2 which can be estimated as the mean of the $\dot{D}_{int}$ values of the Turah material). This is justifiable, because, as seen in Table 8.1, the values for $\dot{D}_{ext}$ measurements across a wide geographical region in the Nile valley are very similar to one another (noting however, that the literature suggests very different external dose rate measurements for regions within Egypt *outside* the Nile Valley, see discussion in Section 5.3.2). From Table 8.1 and Table 8.2 we can estimate $\epsilon_E \sim 0.108$, $I_2 \sim 1.61$ and $\delta \sim 0.726/1.61$, meaning that the relative error estimates are

$$\frac{\epsilon_E}{I_2}\,(1-\delta) \sim 3.6\% \tag{8.26}$$

for the relative ages and

$$\delta \sim 45\% \tag{8.27}$$

for the absolute ages.

In summary, this section shows that the relative age of two vessels is obtained by dividing D_e of one vessel by that of another, as well as dividing the associated $\dot{D}_{int}$ measurements for each vessel; effectively, this is calculating the ratio of the two absolute ages while neglecting $\dot{D}_{ext}$. Furthermore, it demonstrates that when neglecting $\dot{D}_{ext}$ the relative error in the *absolute* age for a given vessel is ∼45%, but the relative error in the *relative* age for a given vessel, is only ∼3.6% (an error which is small when added in quadrature to the relative error of the equivalent dose measurement). Thus, OSL

Table 8.1: The infinite matrix (4π) external gamma dose rate estimates for four different locations in the Nile Valley as well as their mean and standard deviation. The dose rate was calculated from measured radionuclide concentrations using the conversion factors in Guérin et al. 2011.

Source	Location	$\dot{D}_{ext}$ (Gy ka^{-1})
Section 5.3.2, Table 5.3	Bêt Khallaf	0.582
Harb et al. 2008	Upper Egypt (mean of 10 sites)	0.664
Sekkina et al. 2003	Giza	0.816
Abdel-Wahab et al. 1996	Giza	0.843
Mean (μ_E)		0.726
Standard Deviation (σ_E)		0.108

dating can be used as a relative dating method to establish relative chronology amongst a ceramic assemblage. In particular, it has further been demonstrated that this calculation can be used to examine the relative sequence of vessels across the Nile Valley where absolute ages have not been achieved, owing to a lack of $\dot{D}_{ext}$ measurements.

8.4 OSL results for the relative dating of cylindrical vessels and wine jars

The OSL samples and the D_e measurements were determined using the MET sampling protocol and the treatment procedures described in Section 4.1, on both fine and coarse grains. Appendix K presents the OSL data and measurements associated with each of the OSL samples taken from the cylindrical vessels and the wine jars, and also outlines the rejection criteria used for these samples (which were identical to those used for the Bêt Khallaf samples). Table 8.2 presents the final D_e measurements obtained for each vessel and the internal dose rate for each vessel using ICP-MS (refer to Section 5.3.3 for

Table 8.2: Relative ages of the cylindrical vessels and the wine jars from Turah and Hierakonpolis. The table shows the equivalent dose (D_e) and the total internal dose rate ($\dot{D}_{int}$) for both coarse grain (CG) and fine grain (FG) material as available. Also shown are the ages of each pot relative to a reference vessel (chosen to be X5486), again for CG and FG. Finally, the table also shows a combined age, which is either the CG or FG age if only one is available, or a combination of both CG and FG results made by using kernel density estimation. It is this combined age which is displayed in Figure 8.2.

Tomb	Vessel	D_e (CG) (Gy)	D_e (FG) (Gy)	$\dot{D}_{int}$ Dose Rate (CG) (Gy)	$\dot{D}_{int}$ Dose Rate (FG) (Gy)	Relative Date (CG) (Gy)	Relative Date (FG) (Gy)	Combined Relative Date (Gy)
Turah	X5482	N/A	12.05 ± 0.61	N/A	1.68 ± 0.07	N/A	1.18 ± 0.09	1.18 ± 0.09
Turah	X5484	8.09 ± 1.68	N/A	1.38 ± 0.07	N/A	0.86 ± 0.19	N/A	0.86 ± 0.19
Turah	X5486	9.60 ± 0.78	11.27 ± 0.40	1.41 ± 0.08	1.84 ± 0.07	1.00 ± 0.11	1.00 ± 0.07	1.00 ± 0.06
Turah	X5488	N/A	10.17 ± 1.36	N/A	1.63 ± 0.06	N/A	1.02 ± 0.15	1.02 ± 0.15
Turah	X5489	8.73 ± 0.32	10.05 ± 0.25	1.50 ± 0.08	1.81 ± 0.07	0.85 ± 0.06	0.91 ± 0.06	0.88 ± 0.04
Turah	X5490	N/A	9.81 ± 0.69	N/A	1.63 ± 0.06	N/A	0.98 ± 0.09	0.98 ± 0.09
HK	X4112	7.43 ± 0.48	N/A	1.65 ± 0.10	N/A	0.66 ± 0.06	N/A	0.66 ± 0.06

details on ICP-MS measurement).

8.5 Discussion of the results

8.5.1 Vessels not yielding an OSL signal

Prior to embarking on a discussion of the OSL results in relation to the relative ceramic typology, it is important to state that of the 10 vessels examined, all three wine jars produced OSL results, but three of the seven Wavy-Handled vessels did not yield an OSL result (X5483, X5485, X5487). This is a relatively high degree of failure. Of these three vessels, two were marl clay and, similarly to the Bêt Khallaf results (see discussion above), it is likely that the reason we see a higher degree of failed OSL measurements in marl clay vessels is that the quartz in the clay used in vessel production is characterised by low sensitivity. This is obviously not the case for all marl clays, but they do have a much higher failure rate than the Nile clays (see Section 6.2). However, of the three vessels which failed analysis, one was a Nile silt vessel (X5485). This is unusual as our observations suggest that Nile silt is usually well sensitised. It is impossible to determine exactly why this vessel failed to yield any OSL signal; it is likely to be a result of the clay source, although nothing from the visual analysis of the clay suggested a significant difference to regular 'medium' Nile clay fabric (i.e a type 21201 clay fabric according to the Köhler fabric warecode (Köhler 1998; Köhler 2005)).

It is unfortunate that X5483, X5485 and X5487 did not yield results as all three were particularly diagnostic: X5483 was a Naqada IIIA2 net painted cylinder, perhaps the most visually distinct and recognisable cylinder/Wavy-Handled form. Additionally, X5485 was a vessel type which correlates to the penultimate phase of the Wavy-Handled/cylinder typology, dating to Naqada IIIC2 and now made of Nile silt rather than marl clay (Köhler 2004: 301). Finally, X5487 is very unusual in its morphology, with a slightly convex lower vessel wall profile. It also bears a pot mark. The clay fabric type is also unusual for a cylindrical vessel and is more reminiscent of a late Naqada IIID wine

jar (Pers. Comm. E. C. Köhler, 2015). It is possible that this vessel may have been a later imitation of the earlier cylindrical vessel form (Pers. Comm. E. C. Köhler, 2015), but this cannot be determined owing to a lack of OSL measurements.

Regardless of the disappointment stemming from these three cylindrical/Wavy-Handled vessels not yielding an OSL signal, the seven OSL measurements obtained for the other vessels still allow us to examine the use of OSL as a dating technique and examine its correlation to the relative ceramic typology.

8.5.2 General discussion of the OSL results

Figure 8.2 presents the relative ages of the seven vessels for which OSL results were obtained. Before going on to discuss individual vessels it is important to make the following general remarks. First, there are two clear outliers, X5482 and X4112, whose relative ages of 1.15 and 0.7 would imply that they are roughly 700 years older and 1500 years younger than the rest of the group respectively, which is not consistent with known historical sequences. However, as detailed below, these outliers can be explained by problems with the measurement process.

Second, the errors associated with the remaining five vessels are broad compared to the difference in relative ages between them. This means that any statement about whether one vessel is older or younger than another must be treated with caution. However, as addressed in the discussion below, this in no way invalidates the usefulness of OSL dating as a relative dating tool, but rather means that more data (i.e. more vessels) are required than in this pilot study. If several examples of each vessel type were sampled, in combination with good statistical modelling and, even better, a technique such as cladistics, OSL as a relative dating technique would be a powerful tool. Even with the limited data available, we can make the following positive observations: that the five non-outlier ages are well clustered and could be considered consistent given errors with a spread in relative ages of around 5% (that is, roughly 250 years), and are consistent with the known historical chronology. Having made these observations, we now

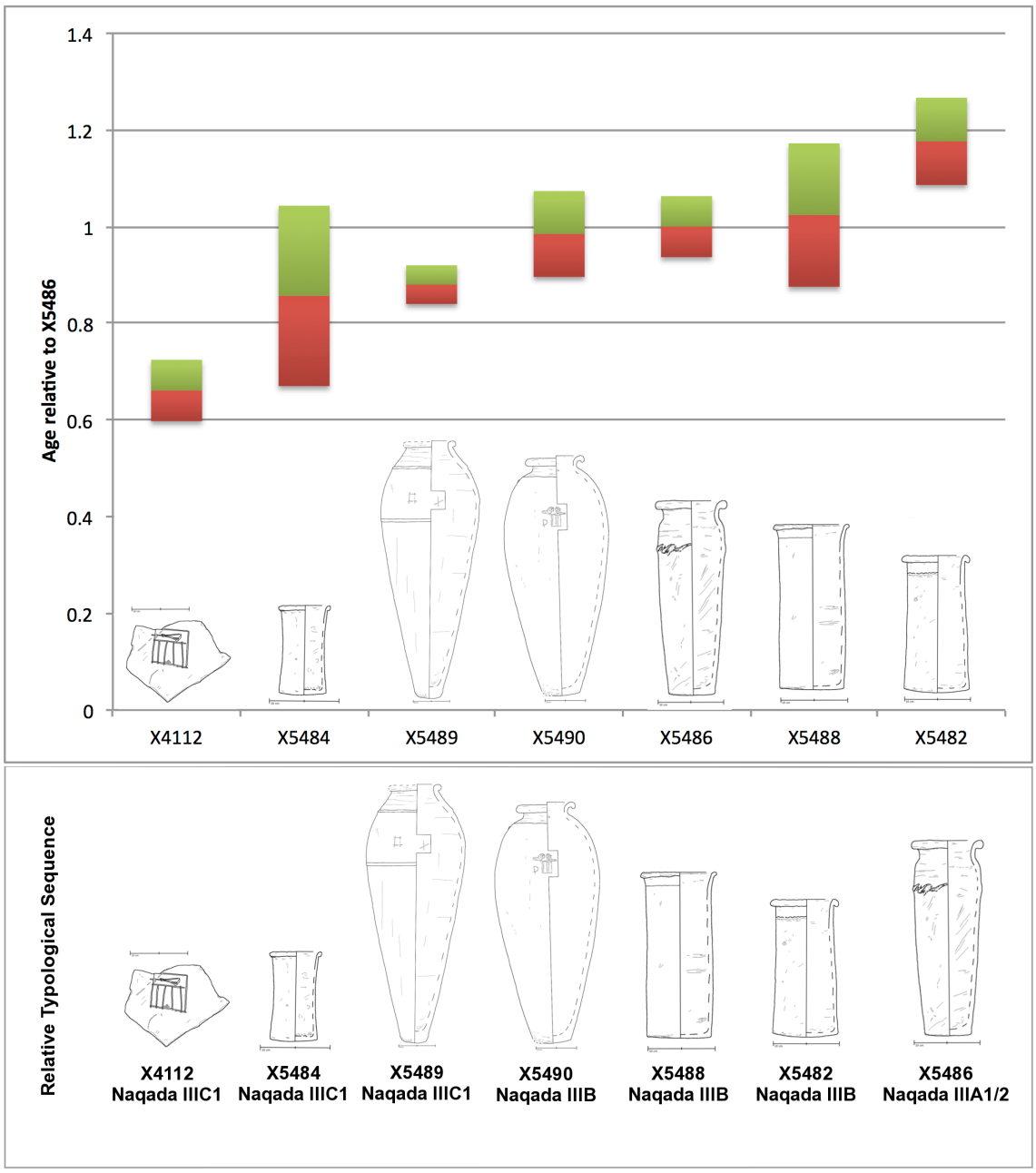

Figure 8.2: Upper: this graph shows the relative sequence of each vessel that produced a D_e measurement in the Turah/Hierakonpolis assemblage, based upon X5486 which acts as an anchoring reference point for the sequence (this vessel was chosen as both fine and coarse grain data was available for it). In turn, this graph therefore indicates the chronological progression of each vessel relative to X5486, with X4112 being the youngest in the assemblage. The red and green denote the upper and lower errors with the boundary between them being the central age value. Lower: in contrast with the upper figure, this figure depicts the known relative typological sequence for this material based upon archaeological evidence, and thus visually demonstrates the issues encountered with some of the OSL D_e measurements.

consider individual vessels, comparing them to established typology: a summary of this comparison is displayed in Figure 8.2.

8.5.3 Wavy-Handled vessel results in relation to the relative ceramic typology

The four Wavy-Handled vessels producing OSL results were: X5482, X5484, X5486, X5488. Of these, X5484 is the youngest within this assemblage, based upon the relative OSL dates, and this also fits well within the ceramic typology, which sees this vessel type as one of the latest stages of development in the Wavy-Handled/cylindrical vessel sequence, that is, a small cylinder with no wavy decoration upon it, corresponding to Naqada IIIC1. This vessel has a particularly large error associated with it, but this was to be expected—during the sampling process there was a small degree of contamination in the sample as the vessel base was very thin and the drill went through the base, which meant that some surface material ended up in the OSL sample. As a result, a larger than usual error was expected for this sample, but nonetheless, the majority of the sample was still conducted on non-contaminated material and this is evidenced by the fact we see a central D_e in agreement with the rest of the assemblage, and with the relative chronological indications of the assemblage.

The case of the other three cylindrical vessels is less straight forward. In relative archaeological terms, the order of these vessels would see X5486 as being the oldest in the assemblage, because this vessel type is assigned to the Naqada IIIA1/IIIA2 period. Morphologically, it is difficult to assign a definite IIIA1 or IIIA2 date to X5486 as the most diagnostic feature of such a designation here is the Wavy-Handled decoration. Indeed, it is that feature upon which Petrie originally placed the most importance when examining the Wavy-Handled sequence (Petrie et al. 1913); though this decision of Petrie's has been criticised by Hendrickx, who illustrates that the dependence upon the Wavy-Handled development was often to the exclusion of the overall development of the vessel shape and that the two characteristics should not be mutually exclusive when

considering chronology (Hendrickx 1996: 47). We see on X5486 a combination of an IIIA1-style band—a continuous modelled band around the vessel's maximum diameter (Petrie's band styles H/L/N, as seen in Petrie 1921: Pl. XXX), similar to Petrie's W56a and W56g (Hendrickx 2006: 83; Petrie 1921: Pl. XXX)—and an IIIA2-style band, which is a thinner, pinched or moulded crescent-shape decoration (Petrie's band styles O/Q/R, as seen in Petrie 1921: Pl. XXX) around the entire vessel, similar to Petrie's W55 and W61 types (Petrie 1921: Pl. XXX; Hendrickx 2006: 84).

Of X5488 and X5482, the latter is the older, displaying a wavy handle that is still 'wavy' in style (similar to Petrie's band style 47m and vessel type W71a (Petrie et al. 1913: Pl. XLIX; Hendrickx 2006: 86). X5488 is similar to Petrie's type W80/W85, with a band style 49l (Petrie et al. 1913: Pl. XLIX; Hendrickx 2006: 86).

Now, although X5486 dates to the Naqada IIIA1/IIIA2 period, it is placed in the OSL relative sequence as being younger than X5488 and X5482, which is not in keeping with the relative archaeological sequence, which places X5488 and X5482 within the Naqada IIIB period. Within the OSL relative sequence it is almost impossible to distinguish between X5486 and X5488, due to the significant errors associated with X5488. Indeed, this is the situation between all three vessels (X5482, X5486 and X5488): their associated errors make it difficult to distinguish a true chronological sequence here, except for confidently being able to state that all three vessels are chronologically older than X5484. This is a resolution error which would be resolved and thus further refined, should a larger data set be available. It should also be noted, however, that in the case of X5482, in absolute terms the discrepancy between the relative spread between it and X5486/X5488 is approximately 15% (see Figure 8.2), which in absolute years gives an error of $\sim$750 years. This is very unlikely and could be the result of a measurement error: a single aliquot within the OSL data (see Appendix K) produced a D_e measurement which, was significantly higher than the other measurements and is an outlier. However, as this aliquot could not be discounted based upon the standard rejection criteria applied, it was considered best practice to include this measurement even though it is likely to

produce an overestimation in the OSL measurement. Again, this is a issue which could be addressed by incorporating a larger primary data set.

8.5.4 Wine jar results in relation to the relative ceramic typology and historical chronology

All three wine jar samples (X4112, X5489 and X5490) yielded an OSL signal: the known relative typology for these three vessels (as well as their historical indicators, that is, a *serekh* in the case of both X4112 and X5490) was in good agreement with their relative OSL ages. Of the three, X5490 is likely to be the most ancient: excavated by Junker at Turah (Junker 1913: 47) it belongs to Van Den Brink's Type IIa (also Group 2.b.1), the *serekh*-incised wine jar group. X5490 is further distinguished by a double falcon incised above the *serekh* (Van Den Brink 1996: Table 1; cf. Van Den Brink 2001: 34), possibly associated with an unknown local ruler in the period just prior to the emergence of the First Dynasty kings, or, alternatively, a symbol of kingship per se, that is, not specifying a particular ruler (Kahl 2006: 96; cf. Engel 2005). This vessel type dates to the Naqada IIIB period. In addition to the *serekh* type-group designation, this wine jar is characterised by a flared rim and short, narrow neck and flattened base, which has two sets of three pushed-up, crescent-shaped residual wavy handles, that is, the handles are now decorative, not functional (Van Den Brink 1996: 144). Van Den Brink indicates that it is still not possible to assign a more definitive chronology to this vessel type (and he acknowledges that there are similarities between his Type II and Type III designations), although he notes that it is distinct from the Type I vessels from Naqada IIIA2 contexts, and from Type IV which are known from early First Dynasty (i.e. Naqada IIIC1) contexts (Van Den Brink 1996; Van Den Brink 2001). However, chronological overlap and regional variation between types is also acknowledged (Köhler and Van Den Brink 2002: 66). Thus, it is likely that a Naqada IIIB date is accurate for this vessel type.

Following X5490 in both typology and OSL relative date is X5489. X5489 can be assigned to the Naqada IIIC1 period. While these two wine jars are close in age (as in-

dicated by the relative age designations), they are two distinct wine jar varieties. It is most likely that the wine jar developed from the imported Wavy-Handled vessel type and its development split into two distinct forms: those with banded, rope-like decoration (i.e. X5489), and those with the crescent-shaped decoration, often in two groups of three crescents, like X5490 (Kaiser 1964; Van Den Brink 1992: 269–270). Wine jars with crescent-shaped decoration are also usually slightly more squat, with a flattened base, with a short, narrow neck and carry on the Wavy-Handled decoration, albeit in crescent-shaped vestigial handles. The pot mark found on X5489 is not a historical indicator like the *serekh* in X5490, and is currently, as with the vast majority of pot marks, undecipherable.

X4112 is chronologically later than the other two vessels, both from the OSL relative date and within the historical and archaeological chronology. Although only a sherd now remains, this would have originally belonged to a wine jar, as evidenced by the sherd morphology and fabric type (a fine Nile silt clay). The sherd retains an inscribed (pre-fired) *serekh* with the name of Narmer, the first king of the First Dynasty, seen within the *serekh*. This sherd has many parallels not only from Egypt (19 vessels or sherds as presented in Van Den Brink 2001: 57–67) but from the Levant, where two 'Narmer' sherds have been recovered. The latter have been discussed as chronological markers for interrelations between Egypt and her north-eastern neighbours during the Early Bronze Age II period (Braun 2004; Braun 2009). The 'Narmer' inscriptions have been found on vessels spanning Van Den Brink's Type II, III, and IV, which correlates to Naqada IIIB–Naqada IIIC2, although, of course, the reign of Narmer is securely placed in the Naqada IIIC1 period. It is felt that the longevity of the 'Narmer' designation is unlikely to be explained by attributing a particularly long reign-length to this king (Van Den Brink 2001: 57). To address this long-lasting *serekh* usage attributed to Narmer, Van Den Brink offers the suggestion that there were two kings who could be identified by the hieroglyphic signs usually read as 'Narmer'—Van Den Brink notes that on the Type II jars, often only the sign for *nr* appears on Type II jars, whereas later Type III and IV jars

have the full *nˁr mr* designation and these latter types are more often in association with the falcon symbol (Van Den Brink 2001: 57–58). Although this suggestion is offered by Van Den Brink, he feels that it is unlikely and that little evidence is available to support this, and thus continues to associate this *serekh* type with a single ruler. X4112 was further categorised by Van Den Brink as Narmer *serekh* Group 11.d.3, due to the name being designated with a single *nˁr* sign (Van Den Brink 2001: 66–67). Although X4112 is only a sherd and the vessel type is unknown, because of the character of the hieroglyphic sign, it is more probable that this sherd came from a Type II vessel, rather than a Type III or IV.

With regard to its relative OSL sequence, it should be noted that although fitting in with the relative sequence of the other two wine jars, on a relative scale the difference between the absolute ages of X4112 and X5489/X5490 sits at approximately 20% (see Figure 8.2). This is far too significant a discrepancy to fit with the relative sequence as it would place X4112 roughly 1 000 years later than the rest of the assemblage. However, as already discussed in the footnote accompanying Table 5.5, several samples for this project had their elemental concentrations determined by ICP-MS (to assist in calculation of the internal dose rate) at a commercial laboratory. This laboratory felt that they did not have the capability to deal with such small sample sizes, resulting in less confidence than in the subsequent measurements carried out at the Department of Earth Sciences, University of Oxford. Unfortunately, X4112 was one of those samples and, as observed with the other samples in the same situation, the ICP-MS for X4112 also produced elemental concentrations that were much higher, particularly for ^{238}U and ^{232}Th, which in turn results in internal dose rates that were exceedingly high compared to the other samples, which caused their ages to be underestimated. Thus, in the case of X4112 it would be ideal to remeasure the sample to re-quantify the elemental breakdown for the sample as this would decrease the absolute age difference between X4112 and the other samples within this assemblage.

8.6 Implications and future directions

This chapter has demonstrated that the application of OSL dating as a relative dating method has benefits for examining the relative typological sequence of ceramics. However, with the small data set and large errors on the dates presented, it is currently only possibly to demonstrate this technique as a proof-of-principle and to make broad statements when comparing the OSL vs. archaeological relative chronologies. Thus, while in itself it has not yielded new information (the relative sequences of the Wavy-Handled vessels and wine jars are well documented and well understood), this chapter has demonstrated that OSL dating can be of benefit to relative chronology as well as absolute. Although the Wavy-Handled/cylindrical vessels have proved problematic owing to issues surrounding a small data set, the wine jar assemblage demonstrates that the relative sequence of ceramics achieved through OSL dating of this assemblage, has been in full agreement with the pre-existing ceramic sequence described for the Naqada culture. Although this study has been limited in scope (only 10 vessels were used), increasing the number of vessels studied would further improve the reliability of using OSL as a relative dating method. In several instances, it might also be possible to anchor this sequence to an absolute timeline, should additional vessels studied yield original soil for $\dot{D}_{ext}$ analysis, or should other dates (e.g. radiocarbon dates on pot contents) become available for one or more of the vessels in the future. Additionally, in Chapter 7, we have already seen how the application of cladistics can improve upon and fine-tune relative sequences, and the combination of OSL dating and cladistics would provide a powerful tool indeed for a relative dating programme. In instances where only a small quantity of vessels are available for study, it would be possible to improve understanding of the relative OSL results by employing statistical modelling, in order to examine the likelihood of the ceramic sequencing. This, in combination with cladistic analysis, would provide an even stronger tool for future relative chronological work.

This technique would be of most benefit when working with museum contexts, when limited archaeological information is available. It could be of particular use for assem-

blages where little of the internal chronology of the group is understood. The two obvious examples in Egyptian history are the so-called 'Abydos Ware' and D-Ware (Decorated Ware) categories. If a large enough sample size was obtained, it is possible that using OSL as a relative dating tool would help shed light upon temporal elements of these wares, perhaps such as the relative sequence of decorated style. Of course, looking forward, such a technique is not only limited to Egyptian material, but also to a variety of ceramics found in museums world wide. For the purposes of museum specimens, such a study would also flag up the existence, or confirm suspicions, of vessels that may have been purchased but turn out to be modern forgeries (and, indeed, TL has a long history of being used in forgery and authenticity testing: see, for example Aitken 1985: 32; Fleming et al. 1970; Fleming et al. 1971; Junding 1993; Polikreti et al. 2002).

In summary, this chapter has provided a solid framework for implementing OSL dating as a relative dating method. While the usefulness of this technique will be heavily dependent upon individual assemblages and the quality of available relative dating methods, further potential for this technique is significant in the museum world and further advances in ceramic chronology can be made as a result.

Chapter 9

OSL used in conjunction with radiocarbon dating

9.1 Introduction

This thesis seeks to shed further light on the chronological implications of the ceramic data set spanning the Naqada III period. While OSL has been the primary focus of this thesis, additional methods have been touched upon which illustrate the benefits of a multidisciplinary approach to this study. Already in Section 6.2.1 we have discussed how the OSL results of the Bêt Khallaf material compare with existing radiocarbon results from the same time period. However, although these two different dating systems were cross-examined in relation to one another, the discussion could not benefit from the examination of the two sets of dating systems carried out upon the same material. Indeed, within chronological studies, where possible, it is ideal to use multiple methodological approaches upon a single data set in order to glean as much information as possible, and by carrying out a cross-comparison of results from the same material using differing techniques.

In archaeology, there are many examples where OSL dating has been used in conjunction with radiocarbon dating (e.g. Bishop et al. 2004; Lang et al. 2003; Long et al. 2011; Roberts et al. 1998). This is of significant benefit as it allows both inorganic and

organic material to be independently dated using both methods, which can be in turn used as a cross-checking mechanism for the internal chronology at a site. It some instances OSL can additionally be used to date material which surpasses the dating range of radiocarbon dating (radiocarbon can routinely date material back to 50 000 and sometimes as far back as 60 000 years, whereas OSL dating can easily extend to *c.* 200 000 years, and, non-routinely, even further than this (Walker 2005: 14; Olley et al. 2004)).

Within this project an exciting opportunity arose which allowed us to subject an assemblage of six ceramic vessels to both radiocarbon dating and OSL dating. The six vessels were selected initially for radiocarbon dating as they had been found to contain suitable organic material in the form of pot contents (Dee et al. 2016). Radiocarbon measurements obtained for the pot contents generated absolute dates for the last primary use of the pot, that is, the date of the deposition of the contents (Dee et al. 2016). Upon discussion with the radiocarbon project leader, Michael Dee, it was recognised that it would be beneficial to subject these six vessels to OSL analysis to directly date the pots themselves, not just their contents, and so a research collaboration was established to bring OSL dating to the study of these six vessels as well. Additionally, upon further examination of the vessels, it was realised that OSL dating could also be used to date the pot contents (as they contained a significant quantity of mineral material in addition to organic material), thus providing a cross-reference for the radiocarbon dates as well as an independent absolute age calculation.[57] Finally, a lump of sediment was found attached to the lug handle of one of the vessels which, being identified as original depositional material, was also deemed suitable for OSL analysis.

[57] Due to the organic nature of the vessel contents, it was felt that a reassessment of their contents should be undertaken also: the vessels had been previously analysed by GC-MS (Serpico and White 1996; Serpico and White 2000), but with the advancement of GC-MS techniques in the past decade, it was considered possible to improve upon the original analyses. The preliminary results of this analysis are discussed in Appendix B.

9.2 Data set: Abydos, Naqada, and Ballas ceramic assemblage

The six vessels examined in this study are housed in the Ashmolean Museum at the University of Oxford, and a catalogue of this material is presented in Appendix L. Of these, two vessels (X5474 and X5475) are of an early Wavy-Handled type, similar to Petrie's W41/W43 type designation, dating to the Naqada IIC/IID period. X5474 comes from Grave T5 at Naqada and X5475 was excavated from Tomb 588 at Ballas (Petrie and Quibell 1896). The other four vessels from this assemblage were recovered by Petrie from the Tomb of Djer (one of the First Dynasty kings of Egypt), Chamber 30,[58] at Abydos (Petrie 1900, Petrie 1901b). As already mentioned, the selection of these six vessels was carried out by Dr Dee, who chose them for their potential for radiocarbon dating. The radiocarbon sampling and measurement was carried out at the Oxford Radiocarbon Accelerator Unit (see Dee et al. 2016 for further radiocarbon sampling and measurement details).

As several different measurements were carried out upon the same vessel (i.e. radiocarbon analysis of the pot contents/residue, OSL analysis of ceramic material, OSL analysis of pot contents/residue and, in one case, OSL analysis of a sediment sample) several different sample numbers exist for a single vessel. Table 9.1 outlines the different sampling numbers (i.e. radiocarbon and OSL laboratory number) assigned to each vessel. Furthermore, it also outlines which samples were analysed successfully, which analyses failed (with these being discussed in further detail below), and also indicates when a sample was not taken.

[58] There remains slight confusion as to whether all four vessels from the Tomb of Djer discussed here were located in Chamber 30. Petrie's excavation report (Petrie 1901b), indicates that the four vessels were found together in Chamber 30, although he does not state this explicitly. The museum index cards, however, question (for undisclosed reasons) whether two vessels, AN1896–1908 E.4065 and AN1896–1908 E.4066, are from the Tomb of Djer. Nonetheless, based on Petrie's published evidence, it is felt that for the purpose of this project it is acceptable to assume that these vessels were found together in Chamber 30 as indicated in Petrie's original publication.

Table 9.1: Correspondence of the sample designations for the OSL ceramic samples, OSL residue samples and the Ashmolean Accession number. A sample was not collected from AN1896–1908 E.4065 as it was considered in every way identical to that of 1896–1908 E.4066. The 'X' numbers and Ashmolean accession numbers are used throughout this chapter to designate an OSL sample or a radiocarbon sample, respectively.

Site	Vessel (Ashmolean accession Number and radiocarbon sample number)	Vessel (project number)	Associated residue/sediment sample (project number)	Radiocarbon date (residue)	OSL date (ceramic)	OSL date (residue)
Naqada	AN1895.525	X5474	X6112	Yes	Failed	Failed
Ballas	AN1895.533	X5475	X6113	Yes	Failed	Failed
Tomb of Djer, Chamber 30	AN1896–1908 E.3158	X5476	X6114 (residue)	Failed	Failed	Yes
			X6120 (sediment)	N/A	N/A	Yes
Tomb of Djer, Chamber 30	AN1896–1908 E.4034	X5477	X6115	Yes	Yes	Yes
Tomb of Djer	AN1896–1908 E.4065	X5478	X6116	Yes	Yes	N/A
Tomb of Djer	AN1896–1908 E.4066	X5479	N/A	Yes	Yes	Yes

9.3 OSL dating of the Abydos, Naqada, and Ballas assemblage

9.3.1 OSL sampling and measurement

The OSL samples were collected in filtered lighting conditions in the Ashmolean Museum, and subsequently transferred to RLAHA for sample treatment and measurement. For the samples taken directly from the ceramic vessel, the MET sampling protocol was used and the treatment and measurement protocols followed for those samples were identical to those carried out for the Bêt Khallaf material, presented in Section 4.1 and Section 5.2. However, the pot contents and the sediment attached to the lug handle were sampled following more standard OSL sampling techniques carried out at RLAHA, that is, a $\sim$1 cm^2 sample was extracted from the surface of the contents and handle using a scalpel. This was then taken to the OSL laboratory at RLAHA and here 2 mm from each side of the sample was removed (to ensure the surfaces of the sample, which may have been exposed to light, were removed) and this was in turn analysed using ICP-MS analysis to determine $\dot{D}_{int}$. The contents samples were then washed in chloroform for one hour to remove any organic material, thus leaving only the mineral component for OSL analysis (note that it was not necessary to subject the sediment sample from the lug handle to a chloroform wash). The sample was then subjected to the treatment protocols as described in Chapter 5, although owing to the larger sample size, an HF time of 30 mins was used. Aliquots were prepared for OSL measurement and measurements were carried out on the TL/OSL Risø Reader at RLAHA, using a SAR protocol.

9.3.2 OSL results

Appendix M presents the OSL measurements obtained for these six vessels—from the ceramic material directly (X5474–X5479), from the minerogenic material contained within the pot contents (X6112–X6116), and from a lump of sandy sediment attached to the han-

Table 9.2: Summary of the OSL D_e values for the ceramic material from the Tomb of Djer (both fine and coarse grains).

Sample Number	Coarse grains		Fine grains	
	D_e (Gy)	D_e error (Gy)	D_e (Gy)	D_e error (Gy)
X5477	N/A		11.56	1.06
X5478	4.31	1.87	N/A	
X5479	N/A		4.37	1.53
X6114	3.87	1.13	N/A	
X6115	3.93	0.68	N/A	
X6116	4.59	0.14	N/A	
X6120	2.68	0.62	N/A	

dle of vessel X5476: sample X6120)—and presents the data post rejection criteria application. Of the samples analysed, X5474 and X5475 (from Naqada and Ballas respectively), did not meet rejection criteria. Of the OSL measurements made on the ceramic material, all aliquots from X5474 failed to produce an OSL signal. X5475 had two aliquots that yielded an OSL signal, but these two measurements varied so greatly from one another that confidence could not be held in the results. All aliquots for the pot contents (X6112 and X6113) failed to produce an OSL signal.

After calibration, the OSL measurements were converted into D_e measurements (i.e. in Gy; calibration dose rates for each sample can be found in Appendix M). Table 9.2 presents the summary of the D_e measurements for the Abydos, Naqada, and Ballas assemblage (calibration has been discussed previously in Section 5.2.2).

The measurement of the dose rate (comprising both the internal dose rate ($\dot{D}_{int}$), external dose rate ($\dot{D}_{ext}$) and cosmic dose rate ($\dot{D}_{cos}$)) was carried out in a manner identical to the Bêt Khallaf material, as outlined in Chapter 5. First, $\dot{D}_{int}$ was determined using DRAC (Dose Rate and Age Calculator, developed by Durcan et al. 2015) and the ICP-MS data obtained for each of the samples. The ICP-MS measurements were carried out by the Department of Earth Sciences, University of Oxford, and Table 9.3 presents the results. Next, $\dot{D}_{cos}$ was determined for those samples coming from the Tomb of Djer at

Table 9.3: Concentrations of U, Th, and K for each sample from the Tomb of Djer, measured using ICP-MS analysis, used to determine $\dot{D}_{int}$.

Sample	K (%)	^{232}Th (ppm)	^{238}U (ppm)
X5474	0.87	8.15	3.75
X5475	1.08	9.03	4.21
X5476	1.21	14.19	3.39
X5477	1.00	10.57	1.93
X5478	0.85	8.75	3.46
X5479	1.00	7.99	3.20
X6114	0.51	4.2	1.3
X6115	0.37	3.2	0.8
X6116	0.38	3.3	1.8
X6120	0.13	2.26	0.35

Table 9.4: Factors and accompanying measurements contributing to $\dot{D}_{cos}$ of the ceramic assemblage in the Tomb of Djer.

Tomb	Location of the tombs at Abydos	Height above sea level of site surface	Burial chamber depth below the surface
Tomb of Djer	Lat: 26.175379 Long: 31.967859	38 m	10 m

Abydos (the two vessels from Naqada and Ballas, X5474 and X5475, failed OSL analysis and thus determining $\dot{D}_{cos}$ for these two vessels was unnecessary). Table 9.4 presents the details used to calculate $\dot{D}_{cos}$ in DRAC. As for the Bêt Khallaf assemblage, a water content value of 3%$\pm$2% was assumed (following the discussion outlined in Section 5.3.5). Finally $\dot{D}_{ext}$ was determined as follows.

A single vessel within the Djer assemblage, X5476, had attached to its lug handle a small piece of sediment sample which was removed for ICP-MS analysis to help establish $\dot{D}_{ext}$ for the Djer vessels. Table 9.5 gives the details of the ICP-MS analysis for this sample. Initially, before the DosiVox program was released in July 2015, the only way to calculate $\dot{D}_{ext}$ was to use this sediment information to first determine a 4π geometry infinite matrix dose rate value in DRAC, and then to scale this according to the additional

Table 9.5: Concentrations of radioisotopes in sediment samples in direct association with the ceramic vessels in the Tomb of Djer.

Sample	Location of sample	Concentration of K (%)	Concentration of ^{232}Th (ppm)[59]	Concentration of ^{238}U (ppm)
X6120	Lug handle of vessel	0.131	2.26	0.35

archaeological information at hand. However, as is detailed in Section 5.3.6, the recent release of the DosiVox program has provided a more sophisticated alternative.

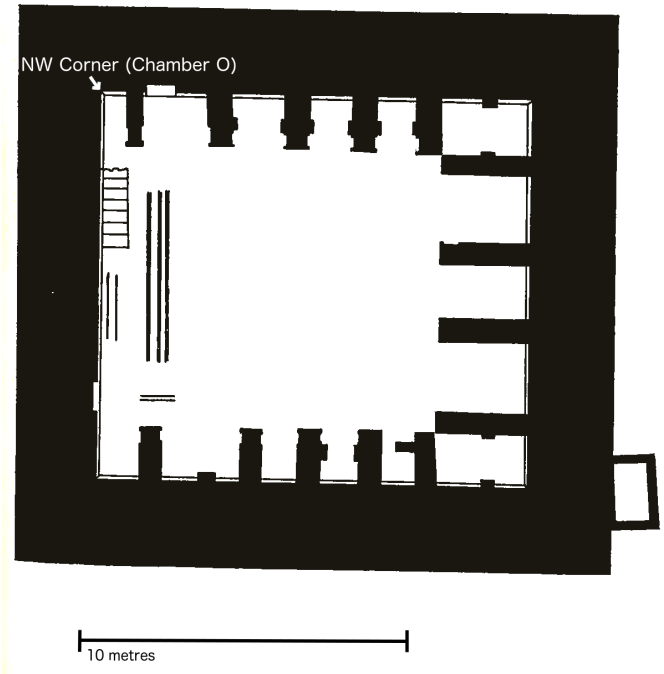

Figure 9.1: A schematic map of the burial chamber of the Tomb of Djer, which shows Chamber O, located in the north-west corner of the tomb.

In addition to the release of DosiVox, a more detailed description of the deposition environment was also available for the Tomb of Djer. The German Archaeological Institute has recently finished the re-mapping and reassessment of the architecture of the tomb, which up until this point, has only been recorded briefly in Petrie's early communications (Petrie 1901b: Pl. LVI, LVIII). The detailed recording and mapping of the tomb recently completed by the German team have provided this project with valuable

[59]ppm = parts per million mass.

Figure 9.2: A: An overview of the Tomb of Djer looking towards the NW corner where the vessels were buried. B: floor of the burial location of the four vessels (Chamber 30)—the circular depressions upon the floor are the pits created by the placement of the ceramic vessels. C: top of the burial location of the four vessels. D: plan view of the burial location of the vessels. These photos were generously provided, and permission for use granted, by M. Sählhof and are © The German Archaeological Institute.

Table 9.6: Final dose rates determined by DosiVox for each vessel in the Tomb of Djer.

Sample ID	^{238}U (Gy ka^{-1})	^{238}U err (Gy ka^{-1})	^{232}Th (Gy ka^{-1})	^{232}Th err (Gy ka^{-1})	^{40}K (Gy ka^{-1})	^{40}K err (Gy ka^{-1})	Total (Gy ka^{-1})	Err (Gy ka^{-1})
X5477	0.032	0.004	0.058	0.009	0.060	0.005	0.150	0.02
X5478	0.125	0.01	0.170	0.02	0.157	0.008	0.452	0.06
X5479	0.108	0.01	0.171	0.03	0.144	0.01	0.423	0.06
X6114	0.108	0.005	0.197	0.008	0.199	0.007	0.504	0.07
X6115	0.091	0.004	0.184	0.01	0.194	0.008	0.469	0.06
X6116	0.118	0.007	0.179	0.01	0.199	0.004	0.496	0.06
X6120	0.107	0.01	0.200	0.04	0.182	0.02	0.489	0.08

knowledge of the depositional environment of the four vessels from the Tomb of Djer (i.e. exact dimensions of the chamber), which in turn leads to a more accurate understanding of $\dot{D}_{ext}$ for the vessel.[60] Figure 9.1 presents a schematic map of the floor plan of the burial chamber of the Tomb of Djer. Figure 9.2 provides recent photographs of the north-west corner of the Tomb of Djer (Chamber 30). We can see from these photographs that the floor of Chamber 30 still retains small rounded pits; it is from these pits that the pottery vessels were recovered (more than four holes are present as many more vessels were recovered but only the four vessels used in this project were a) housed in the Ashmolean Museum and b) filled with contents for initial radiocarbon analysis). From the depths of these pits, we can determine that the vessels were half buried in the floor fill, up to about their mid-point, in an upright position (Pers. Comm. M. Sählhof, 2015).

In the absence of DosiVox a suitable *a priori* assumption would be that the sample geometry of the vessel, that is, the contribution of $\dot{D}_{ext}$ from different emitters surrounding the vessel, should comprise 3π fill/sediment and 1π residue (sample geometry has been discussed in detail above in Section 5.3.6). When modelling $\dot{D}_{ext}$ using DosiVox, the recent observations by the German Archaeological Institute of the Tomb of

[60] The author would like to extend her sincere thanks to the German Archaeological Institute, and especially to Martin Sählhof, for providing access to this as yet unpublished material. This material will shortly be available in a doctoral thesis being prepared by Mr Sählhof, *'Abydos, Umm el-Qaab: Die königliche Grabanlage O/Djer – Bauforschung und Baudokumentation'*.

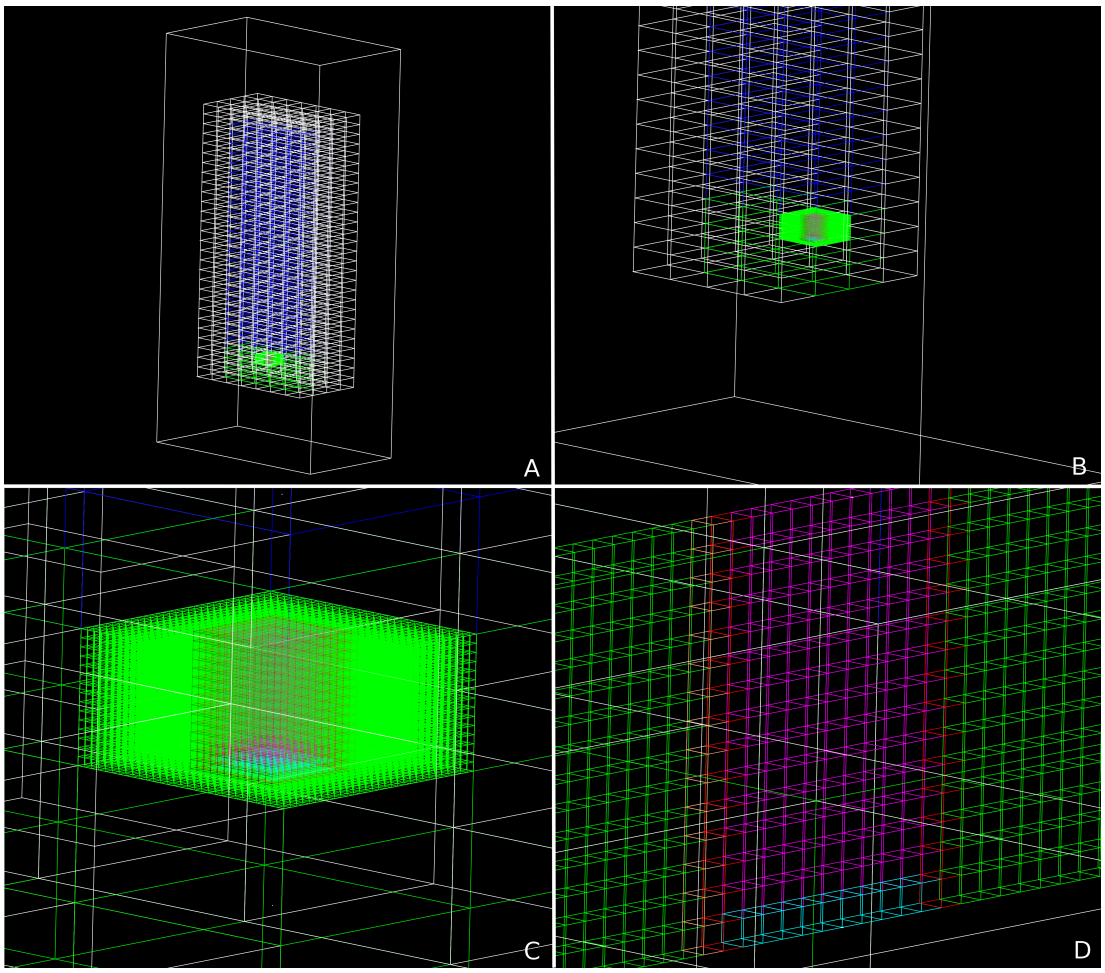

Figure 9.3: Wire frame representations of the DosiVox model for X5476 in the Tomb of Djer. The whole tomb is subdivided into voxels which are filled with different components: white = mudbrick, green = fill, blue = air, red = vessel walls, cyan = vessel base, orange = sediment attached to vessel wall (seen in D only), magenta = pot contents/residue. A–D represent different views of the model: A) whole tomb; B) whole tomb cut away to reveal the detector (the sub-voxelised voxel which contains the vessel); C) close up view of the detector, D) detector cut away to reveal a cross-section of the vessel and surrounding fill.

Djer mean that far fewer assumptions needed to be made, compared to what was necessary for Bêt Khallaf in Section 5.3.6. As already mentioned, it is known that the vessels were buried upright, half in fill; the dimensions of Chamber 30 are also known, as is the depth below the surface of the floor of the chamber. Additionally, it is known that the walls of the chamber are comprised of mudbrick, although it was necessary to assume that the chemical composition of the mudbricks was similar to clay as no sample of the wall fabric was available for study. It was further assumed that the composition

Table 9.7: A comparison of the DosiVox gamma dose rate and the gamma geometries (4π and scaled (3π+1π) obtained using DRAC for the Tomb of Djer.

Sample ID	DRAC $\dot{D}_\gamma$ (4π geometry) (Gy ka^{-1})	DRAC $\dot{D}_\gamma$ error (4π geometry) (Gy ka^{-1})	DRAC $\dot{D}_\gamma$ (scaled geometry) (Gy ka^{-1})	DRAC $\dot{D}_\gamma$ error (scaled geometry) (Gy ka^{-1})	DosiVox $\dot{D}_\gamma$ (Gy.ka-1)	DosiVox $\dot{D}_\gamma$ error (Gy ka^{-1})
X5477	0.174	0.012	0.212	0.01	0.15	0.02
X5478	0.174	0.012	0.212	0.01	0.452	0.06
X5479	0.174	0.012	0.212	0.01	0.423	0.06
X6114	0.458	0.029	0.229	0.015	0.504	0.07
X6115	0.324	0.021	0.162	0.011	0.469	0.06
X6116	0.439	0.028	0.220	0.014	0.496	0.06
X6120	0.174	0.012	0.158	0.008	0.489	0.08

of the floor fill could be represented by the sediment sample taken from the lug handle of X5476 (AN1896–1908 E.3158): sample X6120 (see Table 9.5 above). A representation of the DosiVox model is given in Figure 9.3. Table 9.6 gives the final gamma dose rates determined by DosiVox.

Table 9.7 shows a comparison between the gamma dose rates obtained using DosiVox, an infinite matrix dose rate (using 4π geometry), and an estimate based on the simple geometric assumptions detailed above (i.e. 3π fill and 1π residue). As can be seen, the DosiVox results clearly demonstrate that in the case of the Tomb of Djer, using standard or simplified geometric assumptions based on scalings of the infinite matrix dose rate produces significantly different results, which in turn affects the age determination of OSL samples by an appreciable amount. The example of the Tomb of Djer demonstrates this even more clearly than the Bêt Khallaf assemblage. This is because at Bêt Khallaf, the bedrock (gebel) which the tomb chamber was cut into was similar in composition to the fill on which the vessels were deposited. This, in combination with the low moisture content of the burial environment, meant that the vessel received a dose rate very close to 4π geometry as the low moisture content of the tomb resulted in the gamma radiation not being attenuated by the air; therefore the surrounding walls of the tomb also contribute to the dose received by the vessel. This essentially means that the vessel

is receiving a uniform radiation dose from its burial environment, that is, 4π geometry. In contrast, however, the Tomb of Djer has a chamber made of a fill floor, and walls made of mudbrick. The air, which is also considered of low moisture content, again prevents attenuation, and thus the vessels also receive a dose contribution from the mudbrick walls, as well as from the fill they are half buried in and from the residues/pot contents they contain. Once again, the *a priori* geometric assumptions failed to model $\dot{D}_{ext}$ but, unlike Bêt Khallaf, the more complicated environment of the tomb means that the DosiVox results can not be related *a posteriori* to any simple assumption either. Again, this project has demonstrated that for accurately reconstructing $\dot{D}_{ext}$ for archaeological samples with complex depositional environments, the application of a radiation transport modelling program, of which DosiVox is the only one currently available, is of paramount importance in accurately determining $\dot{D}_{ext}$ and thus the final age estimates for certain archaeological samples.

The final OSL ages are presented in Table 9.8. These ages were further modelled, alongside the radiocarbon dates produced by M. Dee, using Bayesian modelling to examine the chronological implications of the absolute dating of the Tomb of Djer (Dee et al. 2016). This will be discussed below in Section 9.5, after the radiocarbon results are presented.

Table 9.8: OSL ages calculated for each sample from the Tomb of Djer, including alpha, beta, and cosmic dose rates calculated by DRAC, gamma dose rates calculated by DosiVox.

Sample ID	Fine/ coarse grain	Alpha dose rate ($Gy\,ka^{-1}$)	Alpha dose rate error ($Gy\,ka^{-1}$)	Beta dose rate ($Gy\,ka^{-1}$)	Beta dose rate error ($Gy\,ka^{-1}$)	Gamma dose rate ($Gy\,ka^{-1}$)	Gamma dose rate error ($Gy\,ka^{-1}$)	Cosmic dose rate ($Gy\,ka^{-1}$)	Cosmic dose rate error ($Gy\,ka^{-1}$)	Total dose rate ($Gy\,ka^{-1}$)	Total dose rate error ($Gy\,ka^{-1}$)	D_e (Gy)	D_e error (Gy)	Age (ka)	Age err (ka)
X5477	FG	0.411	0.034	1.321	0.059	0.150	0.022	0.120	0.006	2.002	0.072	11.56	1.06	5.774	0.569
X5478	CG	0.208	0.055	1.253	0.057	0.452	0.062	0.120	0.006	2.033	0.101	4.31	1.87	2.120	0.926
X5479	FG	0.46	0.040	1.429	0.062	0.423	0.063	0.120	0.006	2.432	0.097	4.37	1.53	1.797	0.633
X6114	CG	0.079	0.028	0.621	0.030	0.504	0.065	0.124	0.012	1.328	0.078	3.87	1.13	2.914	0.868
X6115	CG	0.055	0.020	0.436	0.021	0.469	0.061	0.124	0.012	1.084	0.069	3.93	0.68	3.625	0.668
X6116	CG	0.085	0.031	0.568	0.027	0.496	0.064	0.124	0.012	1.273	0.077	4.59	0.14	3.606	0.245
X6120	CG	0.035	0.013	0.386	0.020	0.489	0.077	0.124	0.012	1.034	0.082	2.68	0.62	2.592	0.634

Table 9.9: Results of Radiocarbon samples as measured by Dee et al. 2016

Vessel	^{14}C sample number (OxA-)	Pre-treatment method	δ^{13}C	Radiocarbon measurement (Radiocarbon years (BP))	Radiocarbon measurement (Error in Radiocarbon years (BP))	Calibrated radiocarbon Date (BC) Type
AN1895.525	25417	ABA	−25.0	4577	35	3498–3106
AN1895.525	X-2446-41	CHCl3	−29.2	4543	31	3366–3103
AN1895.533	26091	ABA	−24.3	4625	31	3515–3349
AN1895.533	X-2473-57	CHCl3	−24.2	4582	29	3498–3119
AN1896–1908 E.3158	Failed					
AN1896–1908 E.4034	25595	ABA	−25.4	4344	32	3081–2896
AN1896–1908 E.4065	26044	ABA	−23.1	4307	33	3014–2884
AN1896–1908 E.4066	26091	ABA	−24.7	4397	29	3097–2917

Table 9.10: Side-by-side comparison of Radiocarbon and OSL results for the Tomb of Djer. NB This table presents age ranges prior to modelling; see Figure 9.4 for a comparison of modelled ages.

Ashmolean Number	OSL X-Number	14C Label (ABA/CHCl3)	14C Age Range (Residue/ABA)	14C Age Range (Residue/CHCl3)	OSL Age Range (Residue)	OSL Age Range (Vessel)	OSL Age Range (Sediment)
AN1895.525	X5474 (X6112,Res)	25417/ X-2446-41	3498–3106BC	3366–3103BC			
AN1895.533	X5475 (X6113,Res)	26091/ X-2473-57	3515–3349BC	3498–3119BC			
AN1896–1908 E.3158	X5476 (X6114,Res; X6120,Sed)	Failed			1767BC–31BC		1211BC–57AD
AN1896–1908 E.4034	X5477 (X6115,Res)	25595	3081–2896BC		2278–942BC	3190–4328BC	
AN1896–1908 E.4065	X5478 (X6116,Res)	26044	3014–2884BC		1836–1346BC	1031BC–821AD	
AN1896–1908 E.4066	X5479	26091	3097–2917BC			415BC– 851AD	

9.4 Radiocarbon dating of the Abydos, Naqada, and Ballas assemblage

9.4.1 Radiocarbon sampling and measurement

Radiocarbon dating was carried out on the organic contents of each of the six vessels. After sample extraction, two methods were used to prepare the samples: the Oxford Radiocarbon Accelerator Unit's (ORAU) standard Acid-Base-Acid (ABA) pretreatment procedure and a chloroform ($CHCl_3$) solvent extraction pretreatment method (Dee et al. 2016). Approximately 5 mg of each pretreated sample was combusted and the resulting carbon dioxide was retrieved cryogenically, graphitised and dated by accelerator mass spectrometry (AMS) at ORAU. A more comprehensive description for the pretreatment of these samples can be found in Dee et al. 2016.

9.4.2 Radiocarbon results

The radiocarbon results are presented in Table 9.9. As can be seen therein, all results obtained displayed excellent internal consistency (as well as good agreement with earlier radiocarbon dates and the historical ages attributed to the vessels; Dee et al. 2016). The single exception to this was vessel 1896–1908 E.3158 (OSL sample X5476), which yielded no organic material and thus failed radiocarbon analysis.

9.5 Bayesian modelling

Above, Table 9.8 and Table 9.9 have presented the OSL and radiocarbon results. As can be immediately seen, there is a large discrepancy between the radiocarbon results and the OSL results, although these dates come from the same vessels. As with the Bêt Khallaf material, Bayesian modelling has here been employed to further understand the complexities of this assemblage, using a combination of both the measured absolute dates alongside knowledge of the complex depositional history of the vessels to best

interpret these dates and to establish final ages for the assemblage. The final ages used in the Bayesian model are presented in Table 9.8.

Again, a multiphase model was used for this data and a set of *a priori* assumptions was established (using assumptions which were simple and based on archaeological evidence). These assumptions were:

1. Based upon the relative typology of the ceramics analysed, two relative ceramic stages are represented: The Naqada and Ballas vessels belong to the Naqada IID period (Hendrickx 2006: 78–81, Hendrickx 2011: 70), similar to Ware Type W41/W43 by Petrie (Petrie 1921: Pl. XXIX, cf. Hendrickx 2011: 70). The vessels from the Tomb of Djer are a collection of imported vessels (although see below in Section 9.6 for a discussion of the origin of two of the four vessels from the Tomb of Djer), and, while they do not fit into the well-established Egyptian ceramic typology, they are well known from other contexts and the reign of Djer is securely dated to the First Dynasty, both archaeologically and historically (i.e. the First Dynasty king lists are known, which securely place the reign of Djer within the early First Dynasty (Dreyer 1987: 36, Fig. 3, Dreyer 1996: 72, Fig. 26)). Based on this evidence, initially two phases are identified for the model.

2. The two vessels from Naqada and Ballas produced no OSL signals, and thus have been discarded from further OSL analysis. In the case of the four vessels from the Tomb of Djer, three of the four OSL dates are much later than the radiocarbon dates, with the radiocarbon dates being far more consistent with the expected age range for the assemblage based upon relative archaeological and historical data. However, it can be observed that these three vessels show very clear signs of burning, and that archaeologically it has been observed that a secondary firing event occurred at some stage after the original construction phase of the King's tomb. Given this, and the fact that an OSL signal can be reset upon being heated to ∼350℃, even though a vessel may have been manufactured in the Early Dynastic period, this initial signal resulting from the firing process will be erased by a

secondary burning event: the clock is reset to count forward from the date of the burning of the tomb. As the OSL results seem to cluster around a date much later in Egyptian history, and given that these three vessels are all significantly burned, it is likely that here the event that is being dated is the secondary firing event and thus this requires a third phase within the model.

3. Of the four vessels from Djer's tomb, one (X5477/AN1896–1908 E.4034) produced interesting results. The OSL date obtained from the ceramic material produced a date more consistent with the radiocarbon dates (and was thus included within the second phase of the model) but the date obtained from the residue was consistent with the secondary firing event (and was thus included in the third phase of the model). That a single vessel could provide two distinct OSL dates is very unusual, but not impossible given the archaeological evidence. This vessel, unlike the other three vessels in the assemblage, only showed burning over half its surface. Indeed, while one half was severely burnt and blackened, the other part showed no signs of being burnt even though the vessel was archaeologically intact. The OSL measurement from the ceramic sample, which produced an older OSL date consistent with Phase 2, was taken from a section of the vessel which had no evidence of burning. In contrast, the contents were all charred/burned and it was this sample that produced a date which was contemporary with Phase 3, the final phase which seems to demarcate a burning event within the tomb. It is difficult to suggest a reconstruction of events that would lead to a vessel being half burned, and thus a vessel being able to produce two very different OSL measurements. There are no detailed reports as to the exact deposition of the vessel as Petrie did not record the details of the context, although the German Archaeological Institute's recent work reveals that the vessels were sitting upright surrounded by fill (with depressions in the ground still present, indicating the location of the vessels). Therefore, it is possible that something was protecting the part of the pot not burned, either geological or another piece of material culture. It is unlikely that this mystery will

be solved, but nonetheless the two samples were grouped into Phase 2 and Phase 3 respectively so as to allow the raw data to govern the model.

Following these three *a priori* assumptions and using the data from Table 9.8, a three-phase model was produced using the OxCal program (Bronk Ramsey 2009). Modelled age results are presented in Figure 9.4, with a summary of these results presented in Table 9.11. A visual representation of the results of this model is given in Figure 9.5.

Name Show all Show structure	Unmodelled (BC/AD)									Modelled (BC/AD)									Indices A_{model}=91.2 $A_{overall}$=85.7					Select All Visible	Page break
	from	to	%	from	to	%	μ	σ	m	from	to	%	from	to	%	μ	σ	m	A_{comb}	A	L	P	C		
Outlier_Model General										-72	72	68.2	-827	1513	95.4	77	453	1					100	32	
T(5)	-1.135	1.135	68.2	-2.65	2.65	95.4	-2.26696e-8	1.29081	2.04945e-12							0.0553263	1.18234	0.05					99.7	33	
U(0,4)	3.98986e-17	4	68.2	3.98986e-17	4	95.4	2	1.1431	2	5.37764e-17	2.476	68.2	5.37764e-17	3.752	95.4	1.81327	1.11774	1.732		100			99.9	2	
Sequence Abydos																								3	
Boundary Start Naqada IIC or IID										-3396	-3353	68.2	-3583	-3344	95.4	-3404	83	-3375					98	4	
Phase Naqada IIC or IID																								5	
R_Date 525a	-3488	-3136	68.2	-3498	-3108	95.4	-3302	113	-3344	-3368	-3347	68.2	-3493	-3187	95.5	-3353	43	-3357		170.5		97.4	99.9	6	
R_Date 525b	-3362	-3122	68.1	-3366	-3104	95.4	-3232	85	-3207	-3365	-3339	68.2	-3485	-3183	95.4	-3340	45	-3351		115.3		96.8	99.9	7	
R_Date 533a	-3497	-3361	68.2	-3515	-3349	95.4	-3441	55	-3461	-3374	-3353	68.2	-3496	-3339	95.4	-3374	39	-3365		90.2		96.7	99.9	8	
R_Date 533b	-3488	-3196	68.2	-3498	-3119	95.4	-3332	105	-3356	-3367	-3350	68.2	-3488	-3197	95.4	-3357	39	-3358		157.7		97.6	99.9	9	
Boundary End Naqada IID										-3364	-3317	68.2	-3369	-3107	95.4	-3311	72	-3338					99.9	10	
Boundary Start Reign Djer										-3095	-2941	68.2	-3261	-2918	95.4	-3056	91	-3033					99.8	11	
Phase Reign of Djer																								12	
R_Date 4034	-3011	-2907	68.2	-3082	-2896	95.4	-2965	44	-2962	-3007	-2910	68.2	-3022	-2901	95.4	-2962	38	-2959		105.6		97	99.9	13	
R_Date 4066	-3085	-2930	68.2	-3096	-2917	95.4	-3012	66	-3006	-3015	-2922	68.2	-3083	-2914	95.4	-2981	45	-2973		104.7		96.7	99.9	14	
N 4034 (5477)pot	-4340	-3180	68.2	-4898	-2622	95.4	-3760	569	-3760	-3043	-2884	68.2	-3191	-2793	95.4	-2972	92	-2969		55		95.3	100	15	
										Warning! Poor agreement - A= 55.0%(A'c= 60.0%)															
R_Date 4065	-3002	-2888	68.2	-3012	-2884	95.4	-2930	40	-2914	-3008	-2892	68.2	-3014	-2888	95.4	-2943	41	-2928		82.8		96.7	99.9	16	
Boundary End Reign Djer										-2981	-2837	68.2	-3014	-2595	95.4	-2858	131	-2891					99.8	17	
Boundary FireStart										-1994	-1281	68.2	-2583	-1053	95.4	-1731	383	-1679					99.6	18	
Phase Tomb Fire																								19	
N 6115(4034)res	-2292	-930	68.2	-2947	-275	95.4	-1611	668	-1611	-1669	-988	68.2	-2070	-527	95.4	-1313	371	-1322		116.3		95.8	99.9	20	
N 6120(3158)sed	-1225	70	68.2	-1846	691	95.4	-578	634	-578	-1570	-771	68.2	-1849	-125	95.4	-1072	432	-1133		92.6		95.6	99.8	21	
N 6116(4066)pot	-1842	-1342	68.2	-2082	-1102	95.4	-1592	245	-1592	-1669	-1191	68.2	-1917	-966	95.4	-1434	239	-1434		92.6		95.3	99.9	22	
N 6114(3158)res	-1785	-15	68.2	-2636	837	95.4	-900	868	-900	-1652	-836	68.2	-1990	-159	95.4	-1164	439	-1218		122.2		95.7	99.9	23	
N 5478	-1047	836	68.2	-1952	1741	95.4	-106	923	-106	-1611	-744	68.2	-1916	42	95.4	-1053	489	-1132		80.7		95.4	99.8	24	
N 5479	-429	864	68.2	-1049	1484	95.4	218	633	218	-1541	-572	68.2	-1787	170	95.4	-920	509	-1009		39.5		93	99.8	25	
										Warning! Poor agreement - A= 39.5%(A'c= 60.0%)															
Boundary FireEnd										-1401	-246	68.2	-1676	672	95.4	-632	641	-743					98.4	26	
Fire										-1520	-929	68.2	-1787	-532	95.4	-1181	315	-1205					99.4	27	

Figure 9.4: OxCal output table for the Naqada, Abydos (Tomb of Djer), and Ballas ceramic assemblage showing multiphase model results.

As can be seen in Table 9.11, Figure 9.4, and Figure 9.5, the model supports the as-

Table 9.11: Summary of Oxcal Results for the Tomb of Djer (as seen in Figure 9.4). All ages are in BC (i.e. negative ages are AD dates).

		95.4% Probability		68.2% Probability			
		From	To	From	To	μ	σ
PHASE 1	Boundary Start	3882	3351	3574	3369	3534	154
	1895.525a	3493	3187	3368	3347	3353	43
	1895.525b	3485	3183	3365	3339	3340	45
	1895.533a	3496	3339	3374	3353	3374	39
	1895.533b	3488	3197	3367	3350	3357	39
	Boundary End	3369	3107	3364	3317	3311	72
PHASE 2	Boundary Start	3261	2918	3095	2941	3056	91
	1896-1908 E.4034	3022	2901	3007	2910	2962	38
	1896-1908 E.4066	3083	2914	3015	2922	2981	45
	X5477	3191	2793	3043	2884	2972	92
	1896-1908 E.4065	3014	2888	3008	2892	2943	41
	Boundary End	3014	2595	2981	2837	2858	131
PHASE 3	Boundary Start	2583	1053	1994	1281	1731	383
	X6115	2070	527	1669	988	1313	371
	X6120	1849	125	1570	771	1072	432
	X6116	1917	966	1669	1191	1434	239
	X6114	1990	159	1652	836	1164	439
	X5478	1916	−42	1611	744	1053	489
	X5479	1787	−170	1541	572	920	509
	Boundary End	1676	−672	1401	246	632	641

sumptions governing a three-phase model, with an overall model agreement index of 91.2 (Appendix N presents the OxCal code used in the model). Although one vessel in Phase 2 (X5477) and one in Phase 3 (X5479) showed poor internal consistency within the model, their agreement indices of 55 and 39.5 respectively were still accepted as no archaeological evidence suggested that these vessels were inconsistent with the rest of the assemblage (additionally the model was run excluding these vessels but the results were essentially the same). Furthermore, it can be seen from the OSL data (Table 9.8) that vessel X5477 had a very wide error range resulting from the measurement procedure and this uncertainty is adequate explanation of the discrepancy. While X5479 had a relatively small error attached to the OSL measurement (in comparison to other ves-

sels within the assemblage), archaeologically the vessel is identical to X5478 (the vessels are identical in form and clay fabric and are very likely to have been made in the same workshop) and therefore although the agreement index was fairly low for this vessel, it cannot be discarded from the analysis. This model is thus accepted as the final age model for this ceramic assemblage.

While Table 9.11 presents the age ranges for each individual date in each model phase, for ease of discussion central ages within each phase, that is, the most likely mid-point of the age determination, are best visualised by graphically. Figure 9.6 illustrates the calculation of the mid-point for Phase 1 using the weighted mean[61], producing a mid-point date of 3363 BC±44 years for the phase, which correlates well with the historical absolute date of the late Predynastic, Naqada IIC/IID period of *c.*3500–*c.*3200 BC (Shaw 2000: 481). Figure 9.7 produces a CAM central age for Phase 2 of 3085 BC±70 years, which again is in good agreement with the radiocarbon age associated with Djer in the most recent radiocarbon dating programme: 3130–3021 BC, at 95.4% confidence (Dee et al. 2013). While the radiocarbon dates included in this model were taken from Dee et al. 2016, the final ages presented here vary slightly to Dee's. This is because Dee's model was based solely upon the radiocarbon dates, whereas this project's model also includes the results of OSL dating, which will impact the modelled radiocarbon dates. Additionally, due to an OSL age being also included in this plot, the CAM has again been used to determine the central age of this data. This had an insignificant effect, with only a 10-year difference between the CAM and the weighted mean.

Phase 3 examines a dating horizon which seems to mark the fire/burning event that took place later in the history of the Tomb of Djer. Figure 9.8 illustrates the OxCal model produced for the modal peak distribution of the most likely date for this fire event, and is complimented by Figure 9.9 which gives the CAM date as 1307 BC ±205 years, which correlates to the historical late 18th Dynasty, that is, the New Kingdom (Shaw 2000).

[61] Unlike the case of the Bêt Khallaf material, for Phase 1 the weighted mean has been used to calculate the mid-point, rather than the central age model (CAM). This is because Phase 1 consists entirely of radiocarbon ages, not OSL ages. Phase 2 and 3, however, have been analysed using the CAM, as was outlined in Section 5.4.

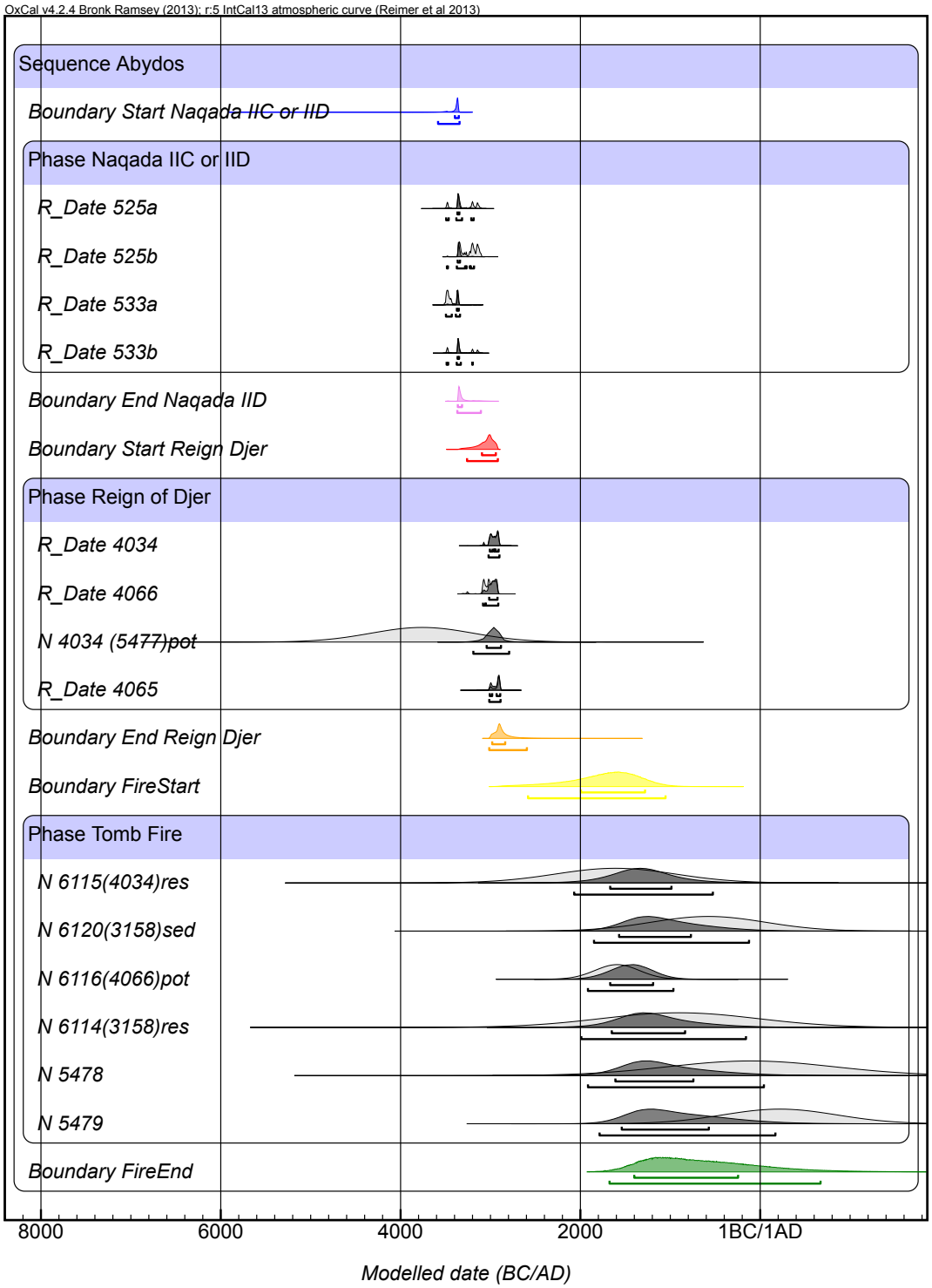

Figure 9.5: OxCal multiphase model of the ceramic assemblage at Naqada, Ballas, and the Tomb of Djer.

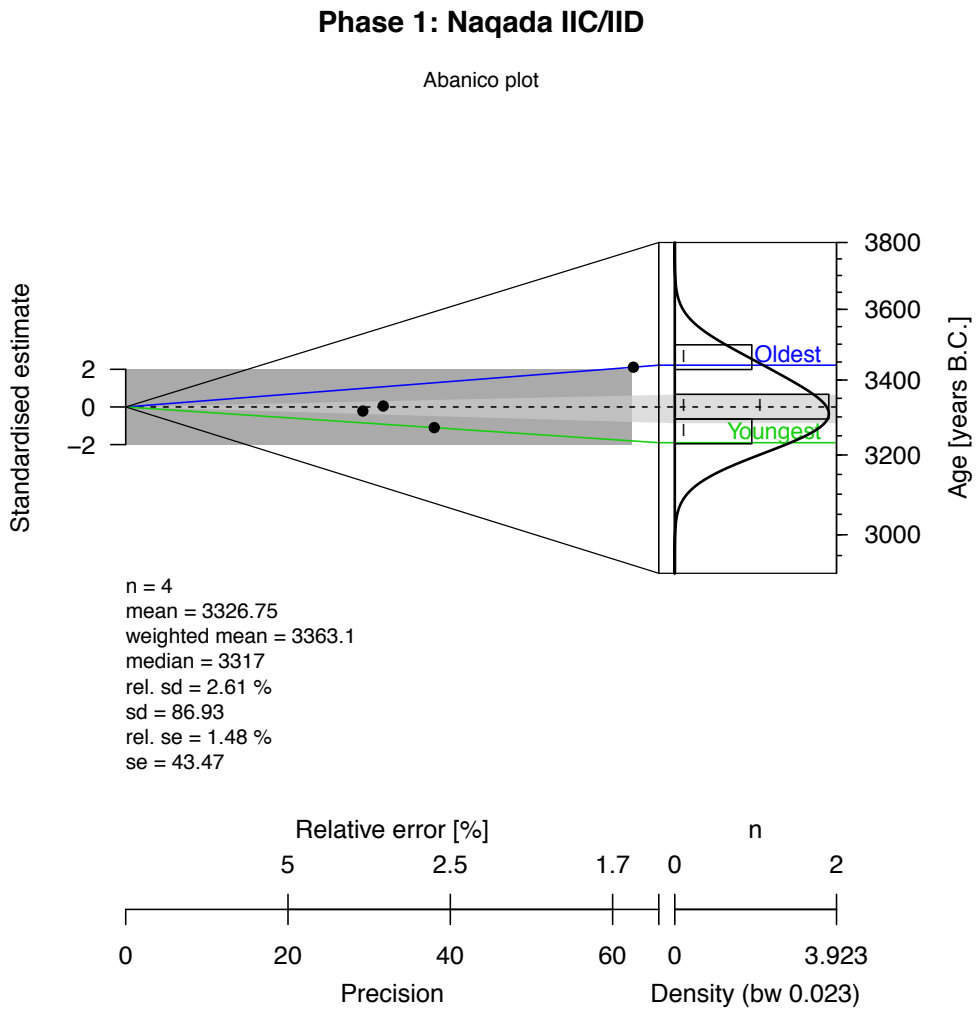

Figure 9.6: Abanico plot illustrating the ages and central value (weighted mean, dashed line) of Phase One, the Naqada IIC/IID vessels from Naqada and Ballas.

9.6 Discussion of results in relation to the ceramic typology

Of the three phases determined through both radiocarbon and OSL measurement, the first two phases are well corroborated within the archaeological relative chronology and Phase 3 provides a new interpretation of the chronological history of the Tomb of Djer.

Phase 1 comprises two vessels only, which although from two different locations (Naqada and Ballas), are similar in type, both belonging to Petrie's W class, most comparable to type W41/W43 (Petrie 1921: Pl. XXIX; Hendrickx 2011: 70). This type is

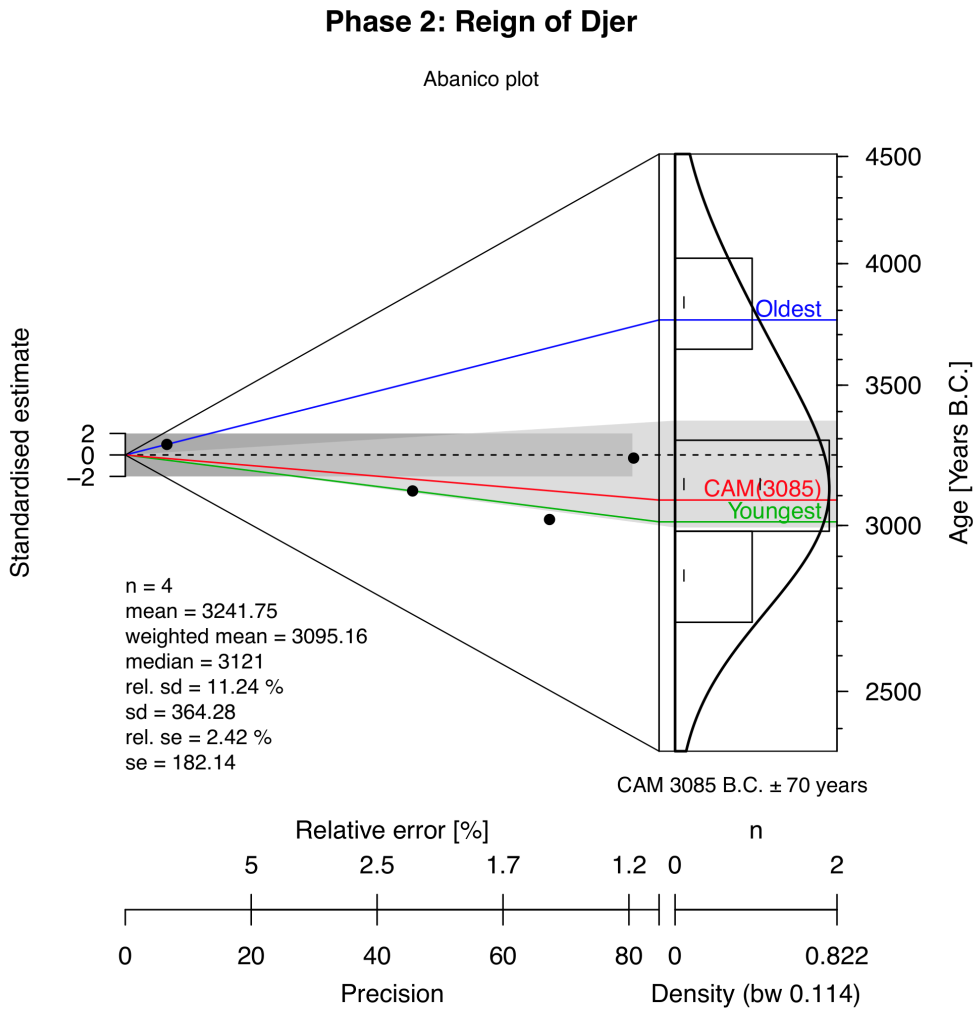

Figure 9.7: Abanico plot illustrating the central age model of Phase Two, the four vessels dating to the reign of Djer.

firmly placed in the literature as belonging to the Naqada IIC/IID period (Hendrickx 2006; Hendrickx 2011; Kaiser 1957), although their size and wall profile would suggest they belong to the later stage of this relative division, that is, Naqada IID (Hendrickx 2011: 70). There has been considerable debate in recent years over the internal chronology of the late Naqada II period, and this has influenced discussion surrounding the correct relative designation for this Wavy-Handled vessel type. Hendrickx began such a debate by questioning Kaiser's decision to impose a division between Stufe II and Stufe III even though his own definition of the material culture included W41, W43 and W47 ware in both the last phase of Stufe II (Stufe IId2) as well as in Stufe IIIa1 (Kaiser 1957).

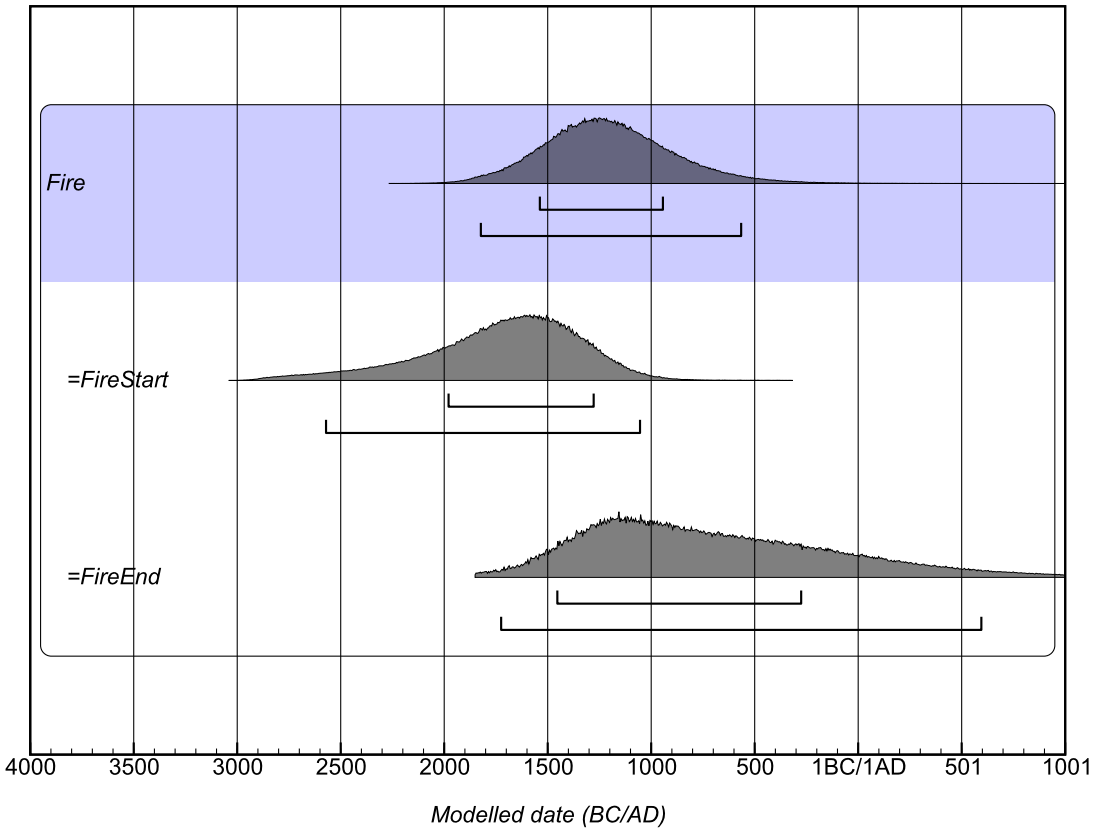

Figure 9.8: OxCal model of the peak distribution of the most likely date for the firing event at the Tomb of Djer.

Hendrickx felt that having this vessel type in both archaeological phases undermined the legitimacy of dividing the boundary between the two phases at this point, and thus determined that this vessel type belonged to the late Naqada II phase (Hendrickx 2006; Hendrickx 2011). The subdivision of Naqada IID into sub-phases Naqada IID1 and IID2 (a system followed by both Kaiser and Hendrickx) has likewise recently come under review. Evidence from the site of Adaïma in Upper Egypt strongly suggests that this division is not supported by the archaeological evidence, and that indeed the concept of both Naqada IIC and Naqada IID as two distinct cultural phases is difficult to justify based on the most recent archaeological evidence (Buchez 2007; Buchez 2011). This discussion is further complicated by recent radiocarbon results, which indicate on, the one hand, that it is impossible to distinguish dates taken from material usually assigned a Naqada IIIA1 date and those assigned to Naqada IID, but, on the other hand, it is possible

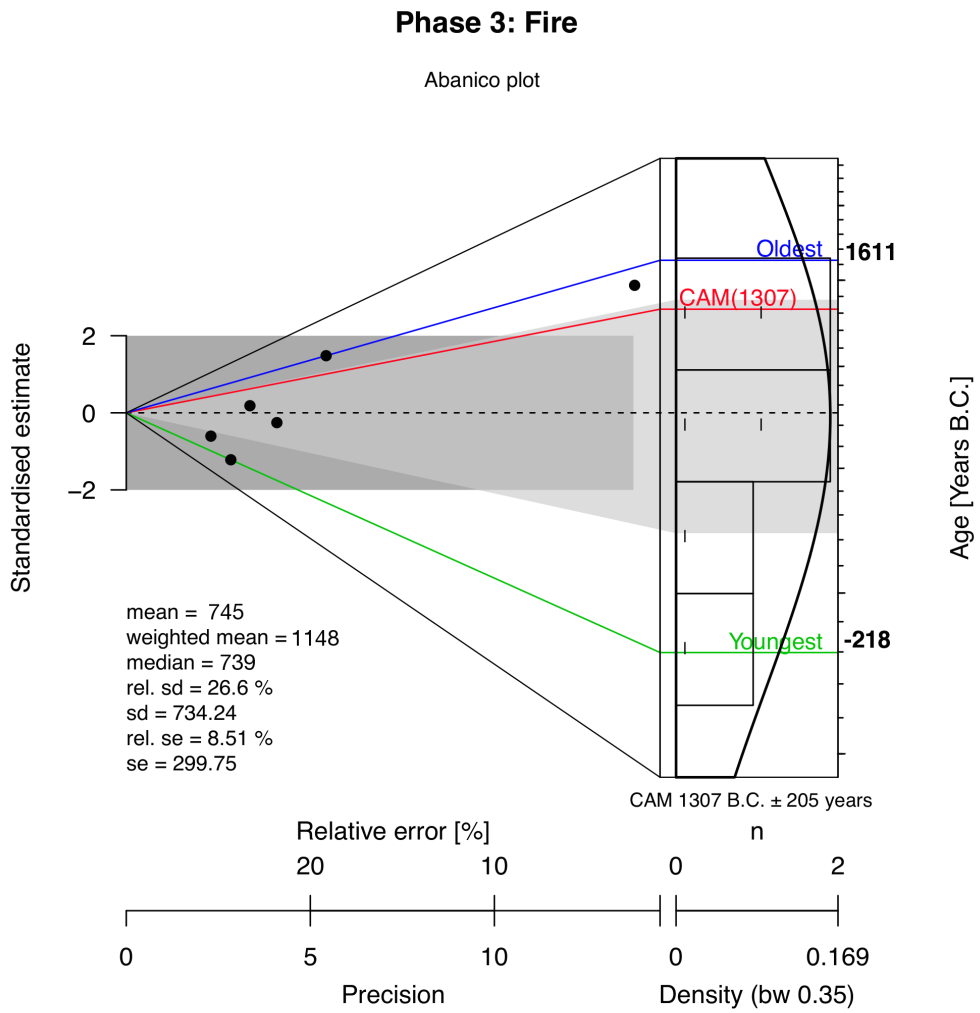

Figure 9.9: Abanico plot illustrating the central age of Phase 3, the firing event within the Tomb of Djer.

to distinguish between Naqada IIC and Naqada IID (Dee et al. 2014).

Although essential in the understanding of the relative Naqada culture, the discussion of whether Naqada IIC and IID are classified as distinct chronological phases, or are eventually to be amalgamated into a single phase, is not critical to our discussion of Phase 1 in the assemblage presented here. At this point in time, high chronological precision in absolute dating cannot rival the fine-tuning possible by extensive relative typological sequencing within the ceramic assemblage of the Naqada culture. This is because not enough absolute dates currently exist for vessels from the Naqada IIC or IID period and as such, a tight absolute chronology cannot assist in the debate as to

whether a single phase or two distinct phases should be considered for the late Naqada II period. What the radiocarbon evidence presented here for Phase 1 does show is that the contents from these two vessels date to 3363 BC ±44 years, which falls well within the date range given to the Naqada II period following the historical chronology of Shaw 2000 (3500–3200 BC). However, this date is closer to the younger end of the historical date range, possibly supporting morphological observations that these two vessels best fit a Naqada IID date, rather than Naqada IIC. Additionally, radiocarbon/modelled dates obtained recently on other late Naqada II material are also in good to reasonable agreement with the four radiocarbon dates presented here (e.g. Bard 2003; Dee et al. 2013; Hassan 1985; Mindant-Reynes and Sabatier 1999: 95; Savage 2001).

Of course, a date obtained from the contents of a vessel is not necessarily a date for the vessel itself. It is here that an OSL date can assist in providing an independent verification of the radiocarbon dates of associated material, if an OSL date is obtained directly from the ceramic fabric itself. It is very unfortunate that, in this instance, the OSL measurements on both vessels did not yield results and cannot be included in the age determination for Phase 1. Thus, in theory, the residue/pot contents dated here by radiocarbon could demonstrate the age of a secondary use event, if the vessels were re-used at another point during history (Dee et al. 2016). However, given the excellent agreement with the relative and historical ages for these two vessels, this is unlikely, and furthermore, it would be difficult to determine such a slight age difference between a vessel and its secondary use, if both events were in close proximity to one another, without a significantly larger body of evidence for more fine-tuned absolute dates.

As already discussed, Phase 2 has a central age of 3085 BC ± 70 years. This date is is good agreement with the published radiocarbon dates existing for the reign of Djer (i.e. 3130–3021 BC, following Dee et al. 2013, cf. Dee et al. 2016), although it is slightly later than the broad historical dates (*c.* 3500 – *c.* 3200 BC) assigned to this period by Shaw 2000, and older than the dates assigned by Hornung et al. 2006 (2870–2823 BC). Phase 2 is represented by four vessels excavated from the Tomb of Djer, historically considered

the third king of the First Dynasty. As a whole, the four vessels are often given the designation 'Abydos Ware'[62], owing to their being imported into Egypt (their origins are generally assumed to be the southern Levant, although recent evidence suggests Lebanon as another possible point of origin (Hartung et al. 2015)). The imports, while not part of a tight relative typological sequence such as the Egyptian Wavy-Handled ware, are still archaeologically attested to the Early Bronze II Phase in the Levant (Braun 2009: 27), and are somewhat frequent in royal contexts within the early dynasties (Wilkinson 1999: 158).

Of the four vessels, all four produced a radiocarbon date from the organic pot contents. In contrast, the OSL was not successful on the ceramic fabric as only one sample produced an OSL measurement, and the measurement on this sample was accompanied by an extremely large error, that without the assistance of Bayesian modelling, would have been difficult to interpret. It is unknown why these OSL samples were unsuccessful, but, as already discussed, the success of an OSL date is very often attributable to the quartz within the ceramic fabric. Not all quartz behaves in a manner conducive to OSL dating. The reason for this is unknown, although it is assumed it has to do with an as yet unquantified property of the quartz crystal lattice structure, and the depositional and sedimentological history of present quartz sources (e.g. Duller 2004; Pietsch et al. 2008; Preusser et al. 2006; Sawakuchi et al. 2011). It is very likely that the clay of the Djer vessels is made of a raw clay fabric which contains very different quartz to others examined throughout this project. This is probably owing to their being imported wares. However, of the four vessels in Djer's tomb, this author believes that only two are imported wares. AN1896–1908 E. 4034 and E. 3158 have very clear morphological traits which are readily identified as imported styles that vary significantly from the local Egyptian assemblage: the flat base, and lug handles. Given than the vessels are so

[62] The term 'Abydos Ware' is a misleading one, which recently has been much debated. The origin of this term comes from the fact that many of the royal tombs of the First Dynasty at Abydos contain these imported wares (Wilkinson 1999: 158). However, criticism of the term arises from the fact that it is essentially an uninformative umbrella term used for any non-Egyptian ceramics found during the Early Dynastic Period, probably imported from the north-east Levant/Syrio-Palestine region (Braun 2009: 27–28; Braun 2011: 977–978; Hartung et al. 2015: 295).

badly burnt, it is not possible to visually examine the clay fabric, but further evidence of their being imports can be obtained through observation of their concentrations of U and Th radionuclides: as can be seen in Table 9.3, the concentration of Th in both vessels (samples X5476 and X5477) is significantly higher than the known Egyptian samples (cf. Appendix A). Likewise, the concentrations of U are significantly lower. Such significant discrepancies within the elemental breakdown of a clay source indicate that the clay source is not likely to be from the same locality.

Indeed, the two imported vessels discussed in this thesis display very different elemental concentrations compared to the Egyptian assemblage, as seen in Table 9.3 and presented briefly in Appendix A. While these two vessels are clearly imported wares, in contrast, the other two vessels in the Tomb of Djer (X5478 and X5479)—although attributed variously as imported wares by Petrie (Petrie 1901b: Pl. VIII), and as Nile silt vessels in the original museum acquisition records—are morphologically much more Egyptian in nature. They have a rounded base, and although not intact, they are similar to Petrie's Late Ware L37 (Pers. Comm. E.C. Köhler, 2015). It is possible, however, and the belief of this author, that these vessels (which are identical to one another, probably made from the same source material and even by the same potter/workshop, given their comparable morphology and contents), might be made of marl clay. This is supported by the preliminary ICP-MS data (see Appendix A). It is again not possible to confirm this at this stage as these vessels were so badly burnt that no reliable visual analysis could be carried out, although examination of the drilled sample indicated that the fabric was more likely a marl than a Nile clay.

Phase 3, although chronologically distinct, is, in contrast to Phases 1 and 2, not based on the ceramic typology. As already discussed, the dates within this phase also come from the pot contents of the vessels from the Tomb of Djer, but are determined using OSL rather than radiocarbon dating, and are very different to the corresponding radiocarbon ages. This is because the radiocarbon age is dating the death of the organic material contained within the residue in the pots whereas the OSL age is dating the last resetting

of the OSL signal within the residues; this last resetting is in all probability a secondary burning event. That the vessels were severely burned in a secondary event (that is, after their initial manufacture date) is evident through the blackened colour encasing the vessels (Adams and Porat 1996: 106; Petrie 1901b: 8–9). It is also supported by further archaeological evidence which has led scholars since the days of Petrie to discuss a fire event which occurred in the tomb. The date of this fire has previously been based upon speculation only, although the most commonly held hypothesis is that the fire predates the Middle Kingdom and possibly dates to the First Intermediate Period. It has been assumed that a burning event in the tomb would have predated the archaeological evidence that suggests that the tomb underwent restoration in the Middle Kingdom (evidence for this exists in both the Tombs of Djer and Den) as the recovered material culture from the Middle Kingdom onwards shows no signs of having been burnt. Furthermore, the staircase that covered the north-west chamber where these vessels were found was considered to have been built around the same time (Dreyer et al. 2003; Dreyer 2010; Dreyer et al. 2013; Effland and Effland 2006; Müller 2004; Petrie 1901b: 8–9). A First Intermediate Period date for the burning is traditionally conjectured on the basis that the First Intermediate Period is a period in history when Egypt saw political strife and upheaval, and this might act as an explanation for why a tomb of a (then ancient) king was burned.

This argument is speculative at best: there is much archaeological evidence that now suggests that the First Intermediate Period was not a time of significant political or economic strife, but rather that the archaeological changes seen in material culture and central organisation come from a time of decentralised power and more local epicentres of culture and authority, rather than significant, country-wide political disruption.

Richards (who also quotes G. Dreyer) offers the explanation that the *Teachings for Merikare*—a text written in the Middle Kingdom, but in the voice of a First Intermediate Period king—might refer to the burning of the Early Dynastic and Old Kingdom tombs at Abydos, and this includes the Tomb of Djer (Richards 2002: 100). The text states that 'Egypt will fight in the necropolis, destroying tomb-chambers in a destruction of deeds

. . . a vile deed happened in my time; the nome of Thinis was destroyed. It happened . . . I knew of it only after it was done' (translation: Parkinson 1997: 221–222, 225). However, this explanation, although plausible, remains circumstantial: there is no archaeological evidence that links this text to a First Intermediate Period date, and textual evidence can be a poor proxy for scientifically or archaeologically determined dating criteria.

Furthermore, we must remember that archaeological activity at the Tomb of Djer was common throughout much of Egyptian history, from the initial burial of Djer, to the Egyptian Middle and New Kingdoms, and the Late Period, throughout which the Tomb of Djer was considered as the Tomb of Osiris by the ancient Egyptians. In essence, the date of the fire event that blackened much of the Tomb of Djer, and presumably these four vessels as well, is still open to conjecture and interpretation.

The OSL dates obtained in Phase 3 from the pot contents all systematically point to a burning event in a much later phase of Egyptian history than the First Intermediate Period or the Early Dynastic Period. The CAM date for this phase is 1307 BC ±205 years. Although the date range on this age is broad, the resulting age range of 1512–1102 BC is not consistent with a date prior to the Middle Kingdom. In fact, it is entirely in keeping with a New Kingdom date, with the central age favouring a late 18th Dynasty date, based on Shaw 2000's chronology. If we consider the Bayesian model rather than the CAM, the boundary start age at 95% probability is 2583–1053 BC and it is 1994–1281 BC at 68% probability, with the mean age for this boundary sitting at 1731 BC ± 383 years (see Table 9.11). So while this does allow an earlier date to be possible (i.e. 2583 BC at the earliest—4th Dynasty according to Shaw 2000), it renders it highly unlikely.

Phase 3 presents us with the first empirically based evidence for the date of the fire in the Tomb of Djer, and this contributes significantly to our understanding of the depositional history of the tomb. The central age of 1307 BC ± 205 years contradicts the preconception that the fire occurred during the First Intermediate Period or at least prior to the Middle Kingdom, and rather suggests a New Kingdom date.

Although these results are both exciting and promising, there is still the need to exer-

cise caution in their interpretation. This phase is based only on six dates, and the spread in the OSL age estimates is significant, although they are improved by the Bayesian modelling. The six dates cluster well around the New Kingdom but more confidence in these results would be achievable using additional measurements from other vessels from the tomb, and, if available, from the mudbrick walls of the tomb itself. This would provide a more robust dating programme. Furthermore, an assumption of the mudbrick composition was necessary in using DosiVox modelling for this assemblage, since no chemical or elemental breakdown was available for a mudbrick from the Tomb of Djer (or indeed any chronologically or regionally comparable mudbrick) within the literature (and no sample was available for analysis as it is likely that no mudbricks from this tomb exist in museum collections outside Egypt). The chemical composition and density of the mudbrick chamber structure in the DosiVox model was based therefore on the assumption that the mudbrick would be very similar in composition to Nile silt clay from the region, which could be deduced from the Bêt Khallaf assemblage. This assumption is a valid one, and examination of the DosiVox assumptions from the Bêt Khallaf assemblage suggests that the difference would not be significant when considered in relation to the errors already associated with the OSL data (see Section 5.3.6). However, to improve even further and to ensure an even more precise dating programme, it would be ideal to have additional and more accurate information in the future for the mudbricks in the Tomb of Djer, if any should ever become available for analysis.

Finally it is essential to also work with the archaeology alongside the absolute dates. Archaeologically speaking, it makes very good sense to attribute the burning event to before the Middle Kingdom, given that no material culture recovered in the tomb from this period onwards displays evidence of being burnt. It may be that the burning event we are dating, that is, in the north-west corner of the tomb, in Chamber 30, was a localised event, and does not relate to the wider tomb burning. Though there are many possible causes of a localised burning, at this stage they are all pure conjecture. Nonetheless, localised burning must still be noted as a possibility and would help explain why

earlier material elsewhere in the tomb was not also burnt. Therefore, without corroborative OSL dates from across the tomb, it is possible that the fire event in this chamber is not a representative date for a larger-scale fire event for the tomb as a whole. A more comprehensive OSL dating programme would allow these questions to be considered further.

It is also essential to re-stress that the OSL date measured in a sample records the *last* firing event of the vessel. The first firing event, which gives rise to the first OSL signal, in the case of pottery, is the date of manufacture (i.e. the firing of the vessel). However, any subsequent, significant heating event will again reset the OSL signal and the radiometric clock will be reset to zero. Theoretically, there is no limit to the number of times a vessel can be fired. But the OSL signal measured in the laboratory will be the last of such events. Thus, it is possible that the Tomb of Djer was set on fire several times throughout Egyptian history, and that the late New Kingdom is simply the last time such an event occurred. Indeed, it may be that the blackened walls visible sporadically throughout the tomb represent a tertiary firing, that is, that the secondary firing simply caused the mudbricks to fire to their current red colour, but that a subsequent, tertiary firing event caused the now red bricks (and at the same time, the ceramic vessels observed here) to blacken further. Further investigation is required.

9.7 The benefits of using OSL and radiocarbon dating in tandem

The six vessel assemblage discussed in this chapter has clearly demonstrated the significant benefits of applying a combination of chronometric dating techniques to a single artefact or assemblage. The combination of radiocarbon and OSL dating on this assemblage of six vessels from the Ashmolean Museum demonstrates how individually these techniques can only tell part of the story, but together they can go even further.

The most obvious benefit is that not all samples are conducive to all chronometric

dating techniques. For example, one vessel in this assemblage (1896–1908 E.3158/X5477) failed to produce a radiocarbon date as the contents of the vessel did not contain retrievable organic material, but was instead minerogenic in nature. Although failing to produce a radiocarbon result, the minerogenic nature of this material meant that it was suitable for OSL dating. Thus, by using both techniques, additional information was yielded by these artefacts. The date of a third phase (depositional event) was deduced using the OSL results: specifically the date of a fire event within the Tomb of Djer. So while the OSL date could not be used as an independent verification for the radiocarbon date in this instance, additional archaeological information was determined through OSL which might otherwise have remained unknown. Similarly, as for the two vessels in Phase 1, OSL dating could not be carried out on the ceramic material or vessel contents (again, most likely due to the nature of the quartz, but, additionally in the case of AN1895.525, because the pot contents yielded no mineral material and was found to be composed of a fatty material only). Thus, while no OSL date was achievable for Phase 1, the phase could still be defined through radiocarbon dating alone, where four measurements were carried out upon two samples using two different pretreatment protocols (Dee et al. 2016).

It is perhaps Phase 3 that best illustrates the benefits of using a multi-method dating programme. By using radiocarbon dating alone (albeit in conjunction with the relative ceramic typology), a date is achievable for the most likely original use-event for this assemblage, based upon the dating of the contents. However, the OSL results provide another chapter in the story, by dating the additional tomb firing event, which was known to have occurred, based on additional archaeological evidence, but which had not yet been dated by independent, empirical means. Thus, once again this assemblage has illustrated the scope achievable for complex depositional histories, which may otherwise have continued to be based upon theoretical speculation, rather than scientific analysis.

9.8 Future directions

These results from the Tomb of Djer present an exciting new step for scientific investigation of Predynastic and Early Dynastic Egyptian material and this project clearly demonstrates the untapped potential of applying a suite of scientific analyses to archaeological assemblages held in museum collections.

However, this research could be further improved upon in order to ensure more robustness within the data set. At present, the Tomb of Djer is only represented here by four vessels. However, more vessels from this context are held within museum collections and it is possible that permission may be granted for further OSL and radiocarbon analysis, particularly considering the initial success of the findings presented here. Indeed, curators at the Ashmolean Museum have already expressed their interest in continuing with this project (Pers. Comm. L. McNamara, 2015). It is thought that at least 10 additional vessels may be available for further analysis, which would more than double the current data set. With an increased set of results, the modelling of this assemblage would be more fine-tuned and produce results which had an even higher confidence level.

As already mentioned above, a necessary assumption was made in the DosiVox modelling of the mudbrick walls within the Tomb of Djer. Although this assumption is unlikely to affect the dating results significantly, it would be best practice to confirm this by obtaining a compositional and elemental analysis of a mudbrick from the Tomb of Djer. How possible this will be in the future is uncertain: initial enquiries have indicated that it is likely that no mudbricks from the tomb were removed from Egypt prior to the exportation ban on antiquities in 1983. Thus it may be impossible to carry out the measurements required on a short-term timescale. Of course, in the future, the antiquities law may become less strict for cases of scientific analysis that cannot be carried out in Egypt, but that remains unpromising at this stage.

It must also be acknowledged that the ceramic material of the 'Abydos Ware' and the two vessels from Naqada and Ballas were made of ceramic fabrics which were only

partially conducive to OSL dating: as can be seen above, several OSL analyses failed. Again, it would be beneficial here to perhaps develop a pre-sampling screening method that would allow us to test the sensitivity of the quartz prior to sample extraction in order to prevent samples from being drilled from vessels which are unlikely to produce tangible results.

In conclusion, this chapter has demonstrated the benefits of subjecting ceramic data sets to multiple chronometric dating techniques. This chapter thus advocates such an approach to the study of all Egyptian ceramic assemblages, not just the example presented here. Although there are future steps that must be taken to ensure the continued improvement of the study of this particular data set, this study has enabled new, and previously unknown, data to be determined for this data set, particularly in the case of the Tomb of Djer. It is hoped that this project will be seen as one which has contributed significantly to the understanding of this area of Egyptian history.

Part V

Conclusion

Chapter 10

Concluding remarks

10.1 Summary of findings

The current restrictions placed on the scientific analysis of ancient Egyptian material have meant that since its inception, OSL dating has been of limited use in Egyptian archaeology. Owing to the ban on the exportation of archaeological material from the country, in combination with the large sample sizes historically needed from museum specimens, this has meant that while other disciplines have benefited from what OSL dating can bring to their field, Egyptology has had to do without it. It is hoped, however, that this thesis has clearly demonstrated that this need no longer be the case, and that the time is ripe for reintroducing OSL dating as a viable and productive avenue of enquiry for Egyptian ceramic studies.

This thesis, which has focused on the ceramic assemblage of the Naqada III period, has shown that through application of the minimum extract technique (MET), OSL dating can now be more sensitively carried out upon museum specimens, requiring only a small quantity of sample material and causing only minimal damage to the sampled vessel. The main body of ceramic material examined by this thesis was from the site of Bêt Khallaf, and, as laid out in Chapters 5 and 6, the OSL work carried out upon the 24 vessels (housed in the Penn Museum, the Ashmolean Museum, and the Garstang Museum) illustrated that OSL dating (using the MET sampling protocol) of Egyptian material was

not only possible, but undeniably beneficial to the study of the late Naqada III ceramic assemblage. Indeed, this thesis presents the first OSL dates obtained for ancient Egyptian ceramic material. Although we cannot yet hope to achieve high chronological precision (this is currently hampered by having to reconstruct much of the dose rate and by a restricted data set), the OSL date for the main ceramic phase at Bêt Khallaf was in good agreement with corresponding radiocarbon measurements, and additionally, although we could not confidently distinguish between Hornung et al.'s 'low' or Shaw's 'high' chronologies (while favouring the latter slightly), the OSL results were consistent with the historical absolute dating regimes within error, producing a date range of 2622 BC $\pm$ 128 years. Thus, these results provide another, independent means of verification for the beginning of the Third Dynasty of Ancient Egypt. The OSL dating programme was also able to offer valuable insight into a multiphase archaeological record at Bêt Khallaf. In addition to the original late Naqada III/early Old Kingdom activity at the tombs, the cemetery of Bêt Khallaf also witnessed additional archaeological activity in the late First Intermediate Period and the medieval Islamic period. Through OSL dating, used in conjunction with existing ceramic typology, it was demonstrated that the ceramic assemblage recovered by Garstang was not solely Early Dynastic in nature, but rather came from several additional periods of activity. This has allowed us to re-evaluate the inclusion of at least one vessel (X5470) in Petrie's Early Dynastic corpus (Petrie et al. 1953) and it further demonstrates the power of OSL as a dating tool to discern different periods of occupation at a single site.

This thesis has also endeavoured to illustrate how the application of a multidisciplinary approach to the study of Egyptian ceramic material can assist in achieving a more detailed and thorough understanding of this material. OSL dating, while of benefit when used independently, can achieve more informative results when used alongside other methods. Accordingly, it should not be considered a stand-alone technique, but rather a single item in a toolbox of analytical techniques available to the archaeologist. Thus, the Bêt Khallaf OSL results were improved significantly by the application of

Bayesian modelling. Additionally, the introduction of cladistic analysis to the Early Dynastic data set, recounted in Chapter 7, although still a 'work-in-progress', illustrates the degree of additional information that can be gleaned from borrowing a technique traditionally used in another discipline (in this case the biological sciences) and applying it to ceramic data sets. Indeed, this technique, of which this project is the first application to an Egyptian data set, has the potential to allow us to fine-tune our understanding of ceramic development, and in the case of the beer jars, we have already begun to ascertain variations in the ceramic assemblage (i.e the lentoid-based vessels), which were not previously identified, and which may lead to a detailed discussion on ceramic provenance and manufacture, and regional variations.

OSL dating has also been shown to lend itself to relative dating, in cases where the required information for achieving an absolute OSL date is not forthcoming (that is, when the environmental dose rate cannot be determined). In Chapter 8, the Turah data set provided a proof of concept for using OSL as a relative dating tool, and this could be of use to many museum assemblages for which no external dose rate information is achievable.

This thesis has also demonstrated the benefits of using OSL alongside other forms of scientific dating. We saw in Chapter 9 how by subjecting a single data set to both OSL dating and radiocarbon dating, each technique was able to provide insight into the history of the vessels that the other could not: radiocarbon dating provided an age for the original use of the vessel, whereas OSL dating was able to shed light upon a previously undated burning event in the Tomb of Djer. Although earlier scholarship had discussed this event as being during the First Intermediate Period, the OSL results pointed towards a New Kingdom date, that is, significantly later than originally thought. It is evident in the case of this assemblage at the least that a more complete and complex archaeological history of a data set can be ascertained by using OSL and radiocarbon dating in tandem. Similarly, this chapter also demonstrated the future potential of the application of GC-MS analysis to the study of pot contents and residues to help shed

light on the use history of the vessels.

10.2 Future priorities and directions

In concluding a large body of work, it is essential to discuss the future potential of the research and directions which further research could take. In many ways, this thesis has uncovered more questions than it has answered, offering insight into a multitude of new research avenues, all of which would be of ongoing benefit to the study of Egyptian ceramics.

Perhaps the most pressing priority of future research is to clearly demonstrate to a wider audience the significant benefits that the application of OSL dating can lend to the study of Egyptian ceramics. As was noted at the beginning of this thesis, the last mention of OSL dating in Egyptology was by Goedicke (Goedicke 2006), where a dismissive summary of the technique was presented with an air of finality as to its (lack of) usefulness to Egyptian archaeology. There remains today a dubiousness associated with luminescence dating of Egyptian material, as well as a near-constant confusion surrounding the differences between OSL dating and thermoluminescence dating. It is essential to begin to change this misconception, and to establish a new dialogue, disseminating the usefulness of OSL to future studies. While it is unlikely that the antiquities law of Egypt will change in the near future, it remains crucial to promote the ability to work with museum material and illustrate clearly the benefits of doing so.

Beyond the specific case of luminescence dating, there has traditionally existed a general lack of communication between Egyptologists and archaeological scientists, which has been of benefit to no one—indeed, in many ways it has been detrimental to the discipline. This has recently begun to change, although it still requires work on both sides (and the works discussed throughout this thesis do provide exceptions to such a general statement, particularly the works of Bourriau, Dee and Bronk Ramsey, Köhler, Nicholson, and Shortland). For their part, more Egyptian archaeologists should be willing to engage in discussions to ensure they are aware of the variety of options available

to them and their material, and be willing to enhance their field research with museum studies in which scientific analyses can be carried out. The archaeological scientists likewise should be willing to accept that the results of scientific analysis are essentially meaningless unless carried out alongside stringent and informed archaeological research of a more traditional nature. Cooperation and a willingness to engage on both sides can only be of benefit to the future of Egyptology. Manning wrote of this situation, allegorising Jane Austen's *Pride and Prejudice* that 'this failure to get along has a veritable history of nearly six decades! The fault of pride could undeniably be placed at the door of the scientists; look at much literature, and the fault of prejudice could be suggested when reading some publications by archaeologists' (Manning 2010: 11).

To continue this train of thought, it should also be discussed more frequently that a multidisciplinary approach to a particular field of study is likely to bring significant progress to scholarship in that field. Therefore, communication once again is vital and a dialogue must exist that can inform practitioners as to the techniques available to them and their research. It is also important for individual researchers to acknowledge that a multidisciplinary approach requires a cross-collaboration with many experts across several fields. The complexity and level of knowledge required for an individual to be considered an expert in a single field means that a single researcher (archaeologist or archaeological scientist) cannot achieve everything on their own. The future of Egyptian archaeological enquiry should lie in collaborations which seek to obtain as much information as possible from a data set, and engaging with a multitude of researchers, each of whom can bring to a project something of benefit.

Given that the application of OSL dating is now possible for museum materials, the present author feels strongly that current fieldwork should be complimented by museum research and analysis. The natural progression of this project is to improve upon the results presented here by expanding the data sets presented in this thesis and eventually achieving a higher degree of precision in OSL dating on museum materials. For the Bêt Khallaf assemblage, it is hoped that the remainder of the assemblage can be located and

analysed. It is also hoped that the Bêt Khallaf data will be complemented by additional ceramic material from other sites (which are typologically comparable to the Bêt Khallaf material) so that the dating programme for late Naqada III ceramics could be extended. Furthermore, the application of OSL dating to museum material need not be limited to the Naqada III period. Indeed, many ceramic typologies from across Egypt would benefit from OSL dating of their assemblages and it is likely that such research would lead to chronological questions being resolved. Similarly, the scope of relative dating using OSL dating could be improved by an increased data set from Turah, and again, other ceramic assemblages from Egypt could benefit from relative dating, even when an absolute dating programme cannot be carried out in full.

This thesis has also clearly demonstrated the exciting possibilities that the application of cladistic analysis offers to a multidisciplinary approach to the study of Egyptian ceramics. It is hoped that future work in cladistics will be expanded to included larger, more comprehensive datasets. In turn, this will allow the evolutionary relationship between types in a ceramic assemblage to be more fully established, with further, direct comparisons able to be made between the known archaeological record and the resulting cladograms. The use of cladistics is of significant benefit to the study of Egyptian ceramics as it provides archaeologists with a way to fine-tune and correctly ascertain the nuances of change in ceramic morphology which are not always directly discernible through visual analysis alone. It provides a way of assessing, computationally, a significant quantity of data throughout which there is much variation, and as the ceramic record in Egypt is so substantial, cladistics as an additional method of analysing the data will be a welcomed addition to the field.

With regard to chemical analysis, as seen in Appendix A and Appendix B, this thesis was only able to begin to demonstrate the potential power of ICP-MS analysis in the provenancing of raw clay materials, and of GC-MS analysis in the study of the use history of ceramics during the Naqada III period. However, plans are already laid to continue this project and the first steps taken will be to extend the scope of current analyses

upon the data set used in this thesis. It is intended to carry out a full elemental analysis of the ceramic fabric using ICP-MS, and thus extend the discussion of the concentrations of U, Th, and K to include all detectable elements, and then to subject the pot contents from Abydos, Naqada, and Ballas vessels to GC-C-IRMS analysis.

Although there is still much work to be done, and there is a long way to go in unveiling all the secrets Egyptian ceramics have to offer, the multidisciplinary approach to the study of ancient Egyptian ceramics has a bright and promising future. This thesis, within its limitations, has shown what it is possible to achieve when engaging in a multidisciplinary analysis of ceramic material, and has demonstrated the benefits of using traditional and modern scientific methods in combination. It is hoped that this research will pave the way for further studies and that, in turn, the application of OSL dating in conjunction with multidisciplinary studies of ceramic material will lead to a more informed understanding of ceramic history, use, and chronology.

Glossary, Acronyms and Selected Symbols

$\dot{D}_{\alpha}$ (alpha dose rate) is the dose a sample receives from alpha radiation.

$\dot{D}$ (dose rate) is the total amount of radiation that an OSL sample has been exposed to since depostion. This is comprised of $\dot{D}_{ext}$, $\dot{D}_{int}$ and the $\dot{D}_{cos}$.

$\dot{D}_{\beta}$ (beta dose rate) is the dose a sample receives from alpha radiation.

$\dot{D}_{cos}$ (cosmic dose rate) is the rate at which an OSL sample has received a radiation dose from naturally occurring cosmic rays within the atmosphere.

$\dot{D}_{ext}$ (external dose rate) is the rate at which an OSL sample has received a radiation dose from its external environment.

$\dot{D}_{\gamma}$ (gamma dose rate) is the dose a sample receives from gamma radiation.

$\dot{D}_{int}$ (internal dose rate) is the rate at which an OSL sample has received a radiation dose from itself (internally).

D_e (equivalent dose rate) is the amount of radiation an OSL sample has received since it was deposited.

Autapomorphies is a classification based upon overall similarity rather than evolutionary relationships.

Bootstrapping is a heuristic tool for testing robustness of a data set based on random sampling with substitution.

C.I. (consistency index) is a measure of fit which shows homology due to shared ancestry (i.e. there is one evolutionary pattern and characters do not appear more than once).

Cladistics is an approach to classification developed for biological sciences, based upon shared derived characters. Originally used for organism classification it can be used in archaeology for artefact classification.

Cladogram is a branching hierarchical tree resulting from cladistic analysis.

GC-C-IRMS (gas chromatography-combustion-isotope ratio mass spectrometry) is similar to GC-MS, but is a gas chromatograph with an isotope ratio mass spectrometer. This technique can produce more sensitive analyses and better detection levels than GC-MS.

GC-MS (gas chromatography – mass spectrometry) is a technique used to determine the chemical composition of an organic sample.

Gy (grays) is the international unit for absorbed radiation.

ICP-MS (inductively-coupled plasma – mass spectrometry) is a technique used to determine the elemental composition of a sample

Ingroup is all other data (i.e. taxa/vessels) used in the cladistic analysis which are not part of the outgroup.

LA-ICP-MS (laser ablation inductively-coupled plasma mass spectrometry) is an analytical technique that is used to determine elemental composition of a sample, but can be used on solid samples.

Monophyly occurs when all taxa are descendant from the ancestral form and all descendant taxa form a group.

ORAU is the Oxford Radiocarbon Accelerator Unit, University of Oxford.

OSL (optically stimulated luminescence dating) is a chronometric dating technique which exploits the natural emission of light from certain minerogenic materials (e.g. quartz), which occurs when the mineral is exposed to certain light frequencies

OUES is the Department of Earth Sciences, University of Oxford.

Outgroup is an organism (type of vessel) which defines the ancestral and derived character states within the ingroup.

Paraphyly occurs when all taxa are descendant from the ancestral form but not all taxa are found in final group.

Parsimony is a principal which states that, all things being equal, the simplest hypothesis should be accepted.

Phenetics is a classification based upon overall similarity rather than evolutionary relationships.

Phylogeny is the evolutionary relationship of a group of organisms based on observed evolutionary, hierarchical traits

R.I. (retention index) is a measure of robustness which indicates phylogenetic, rather than ethnogenetic processes have taken place.

RLAHA is the Research Laboratory for Archaeology and the History of Art, University of Oxford.

SAR (single aliquot regenerative-dose protocol) is a commonly used set of laboratory measurements used to measure the D_e for an aliquot of an OSL sample.

SD (sequence date) is a numerical system devised by Petrie which places the ceramics of the Pre- and Early Dynastic periods of Egypt into a typological sequence.

Symplesiomorphies is an ancestral feature retained within the ingroup of a cladistic analysis.

Synapomorphic is a character present in an ancestral form and shared with descendants.

TL is thermoluminescence – as for OSL, but the light is emitted from a crystal when heated, rather than when exposed to light.

Part VI

Bibliography

Abdel-Wahab, M.S., S.A. El-Fiki, M.A. El-Fiki, M. Gomaa, S. Abdel-Kariem, and N. El-Faramawy (1996), 'Annual Dose Measurements and TL-dating of Ancient Egyptian Pottery', in *Radiation Physics and Chemistry* 47.5, pp. 697–700.

Adamiec, G. and M.J. Aitken (1998), 'Dose-Rate Conversion Factors: Update', in *Ancient TL* 16.2, pp. 37–50.

Adams, B. (1995), *Ancient Nekhen: Garstang in the City of Hierakonpolis* (New Malden: SIA Publishing).

Adams, B. and N. Porat (1996), 'Imported pottery with potmarks from Abydos', in *Aspects of Early Egypt*, ed. J. Spencer (London: British Museum Press), pp. 98–107.

Aiello, L.C. and C. Dean (1990), *An Introduction to Human Evolutionary Anatomy* (Oxford: Academic Press).

Aitken, M.J. (1985), *Thermoluminescence Dating* (London: Academic Press).

Aitken, M.J. (1989), 'Luminescence Dating: A Guide for Non-Specialists', in *Archaeometry* 31.2, pp. 147–159.

Aitken, M.J. (1998), *An Introduction to Optical Dating: The Dating of Quaternary Sediments by the Use of Photon-Stimulated Luminescence* (Oxford: Oxford University Press).

Aitken, M.J, M.S. Tite, and J. Reid (1964), 'Thermoluminescent Dating of Ancient Ceramics', in *Nature* 202, pp. 1032–1033.

Aitken, M.J., D.W. Zimmerman, and S.J. Fleming (1968), 'Thermoluminescent Dating of Ancient Pottery', in *Nature* 219, pp. 442–444.

El-Arabi, A.M. (2005), 'Gamma Activity in Some Environmental Samples in South Egypt', in *Indian Journal of Pure and Applied Physics* 43.6, pp. 422–426.

Arnold, J.R. and W.F. Libby (1949), 'Age Determinations by Radiocarbon Content: Checks with Samples of Known Age', in *Science* 110.2869, pp. 678–680.

Aston, D. (1998), *Die Keramik des Grabungsplatzes Q1: Tiel 1 Corpus of Fabrics, Wares and Shapes* (Mainz: Verlag Philipp von Zabern).

Atlıhan, M Altay, Eren Şahiner, and Feriştah Soykal Alanyalı (2012), 'Dose Estimation and Dating of Pottery from Turkey', in *Radiation Physics and Chemistry* 81.6, pp. 594–598.

Ayrton, E.R and W.L.S. Loat (1911), *Pre-dynastic Cemetery at El Mahasna* (London: The Egypt Exploration Fund).

El-Bahi, S.M., N.W. El-Dine, F. Ahmed, A. Sroor, and M.A. Abdl Salaam (2005), 'Natural Radioactivity Levels for Selected Kinds of Egyptian Sand', in *Isotopes in Environmental Health Studies* 41.2, pp. 161–168.

Bailey, R.M., S. Stokes, and H. Bray (2003), 'Inductively-Coupled Plasma Mass Spectrometry (ICP-MS) for Dose Rate Determination: Some Guidelines for Sample Preparation and Analysis', in *Ancient TL* 21.1, pp. 11–15.

Bailiff, I.K. (2007), 'Methodological Developments in the Luminescence Dating of Brick from English Late-Medieval and Post-Medieval Buildings', in *Archaeometry* 49.4, pp. 827–851.

Bailiff, I.K., S. Blain, C.P. Graves, T. Gurling, and S. Semple (2010), 'Uses and Recycling of Brick in Medieval and Tudor English Buildings: Insights from the Application of Luminescence Dating and New Avenues for Further Research', in *Archaeological Journal* 167.1, pp. 165–196.

Bailiff, I.K., H.R. Lacey, R.A.E Coningham, P. Gunawardhana, G. Adikari, C. E. Davis, M.J. Manuel, and K.M. Strickland (2013), 'Luminescence Dating of Brick Stupas: An Application to the Hinterland of Anuradhapura, Sri Lanka', in *Antiquity* 87.335, pp. 189–201.

Baines, J. and P. Lacovara (2002), 'Burial and the Dead in Ancient Egyptian Society: Respect, Formalism, Neglect', in *Journal of Social Archaeology* 2.1, pp. 5–36.

Baldwin, J.S., P.M. Allen, B. Winder, and K. Ridgway (2005), 'Modelling Manufacturing Evolution: Thoughts on Sustainable Industrial Development', in *Journal of Cleaner Production* 13.9, pp. 887–902.

Banerjee, D., A.S. Murray, L. Bøtter-Jensen, and A. Lang (2001), 'Equivalent Dose Estimation Using a Single Aliquot of Polymineral Fine Grains', in *Radiation Measurements* 33.1, pp. 73–94.

Bard, Kathryn A (2003), 'Radiocarbon dates from Halfiah Gibli (Abadiyeh), a predynastic settlement in Upper Egypt', in *Radiocarbon* 45.1, pp. 123–130.

Barker, H., R. Burleigh, and N. Meeks (1969), 'British Museum Natural Radiocarbon Measurements VI', in *Radiocarbon* 11.2, pp. 278–294.

Barker, H., R. Burleigh, and N. Meeks (1971), 'British Museum Natural Radiocarbon Measurements VII', in *Radiocarbon* 13.2, pp. 2157–188.

Barnard, H. (2008), 'Eastern Desert Ware: Traces of the Inhabitants of the Eastern Desert in Egypt and Sudan During the 4th-6th Centuries CE', PhD thesis, Faculty of Archaeology, Leiden University.

Barnett, S.M. (2000), 'Luminescence Dating of Pottery from Later Prehistoric Britain', in *Archaeometry* 42.2, pp. 431–457.

Bárta, M. (2013), 'Radiocarbon Dates for the Old Kingdom and their Correspondences', in *Radiocarbon and the Chronologies of Ancient Egypt*, ed. A.J. Shortland and C. Bronk Ramsey (Oxford: Oxbow Books), pp. 218–223.

Barton, C.M. and G.A. Clark (1997), 'Evolutionary Theory in Archaeological Explanation', in *Rediscovering Darwin: Evolutionary Theory and Archaeological Explanation*, vol. 7, Archaeological Papers of the American Anthropological Associations 1 (Virginia: American Anthropological Association), pp. 3–15.

Barton, C.M., G.A. Clark, and D.B. Bamforth, eds. (1997), *Rediscovering Darwin: Evolutionary theory and archeological explanation*, vol. 7, Archaeological Papers of the American Anthropological Association 1 (Virginia: American Anthropological Association).

Barton, R.N.E., A. Bouzouggar, S.N. Collcutt, J.-L. Schwenninger, and L. Clark-Balzan (2009), 'OSL Dating of the Aterian Levels at Dar es-Soltan I (Rabat, Morocco) and Implications for the Dispersal of Modern Homo Sapiens', in *Quaternary Science Reviews* 28.19, pp. 1914–1931.

Batchelor, G.K. (2010), *An Introduction to Fluid Dynamics* (Cambridge: Cambridge University Press).

Baumgartel, E.J. (1947), *The Cultures of Prehistoric Egypt* (Oxford: Oxford University Press).

Baumgartel, E.J. (1970), *Petrie's Naqada Excavation: A Supplement* (London: Quaritch).

Bell, W.T. and D.W. Zimmerman (1978), 'The Effect of HF Acid Etching on the Morphology of Quartz Inclusions for Thermoluminescence Dating', in *Archaeometry* 20.1, pp. 63–65.

Benea, V., D. Vandenberghe, A. Timar, P. van Den Haute, C. Cosma, M. Gligor, and C. Florescu (2007), 'Luminescence Dating of Neolithic Ceramics from Lumea Nouă, Romania', in *Geochronometria* 28.1, pp. 9–16.

Berger, R., G.J. Fergusson, and W.F. Libby (1965), 'UCLA radiocarbon dates IV.', in *Radiocarbon* 7.1, pp. 336–371.

Berger, R. and W.F. Libby (1967), 'UCLA Radiocarbon Dates VI', in *Radiocarbon* 9, pp. 477–504.

Bishop, P., D.C.W. Sanderson, and M.T. Stark (2004), 'OSL and Radiocarbon Dating of a Pre-Angkorian Canal in the Mekong Delta, Southern Cambodia', in *Journal of Archaeological Science* 31.3, pp. 319–336.

Blain, S., I.K. Bailiff, P. Guibert, A. Bouvier, and M. Baylé (2010), 'An Intercomparison Study of Luminescence Dating Protocols and Techniques Applied to Medieval Brick Samples from Normandy (France)', in *Quaternary Geochronology* 5.2, pp. 311–316.

Bourriau, J. (1981), *Umm el-Ga'ab: Pottery from the Nile Valley before the Arab conquest* (Cambridge: Cambridge University Press).

Brass, M. and J-L. Schwenniger (2013), 'Jebel Moya (Sudan): New Dates from a Mortuary Complex at the Southern Meroitic Frontier', in *Azania: Archaeological Research in Africa* 48.4, pp. 455–472.

Braun, E. (2004), 'Egypt and the southern Levant: Shifting Patterns of Relationships during Dynasty 0', in *Egypt at its Origins: Studies in Memory of Barbara Adams. Proceedings of the International Conference "Origin of the State. Predynastic and Early Dynastic Egypt", Kraków, 28th August–1st September 2002*, ed. S. Hendrickx, R.F. Friedman,

K.M. Ciałwicz, and M. Chłodnicki, vol. 138, Orientalia Lovaniensia Analecta (Leuven: Peeters), pp. 507–517.

Braun, E. (2011), 'South Levantine Early Bronze Age Chronological Correlations with Egypt in Light of the Narmer Serekhs from Tel Erani and Arad: New Interpretations', in *Egypt at its Origins 3: Proceedings of the Third International Conference "Origin of the State. Predynastic and Early Dynastic Egypt", London, 27th July–1st August 2008*, ed. R.F. Friedman and P.N. Fiske, vol. 205, Orientalia Lovaniensia Analecta (Leuven: Peeters), pp. 975–1001.

Braun, Eliot (2009), 'South Levantine Early Bronze Age Chronological Correlations with Egypt in Light of the Narmer serekhs from Tel Erani and Arad: New interpretations', in *British Museum Studies in Ancient Egypt and Sudan* 13, pp. 25–48.

Brennan, BJ (2003), 'Beta doses to spherical grains', in *Radiation Measurements* 37.4, pp. 299–303.

Brennan, B.J. and R.G. Lyons (1989), 'Ranges of Alpha Particles in Various Media', in *Ancient TL* 7.2, pp. 32–37.

Brennan, B.J., R.G. Lyons, and S.W. Phillips (1991), 'Attenuation of Alpha Particle Track Dose for Spherical Grains', in *International Journal of Radiation Applications and Instrumentation. Part D. Nuclear Tracks and Radiation Measurements* 18.1, pp. 249–253.

Bronk Ramsey, C. (1995), 'Radiocarbon Calibration and Analysis of Stratigraphy: The OxCal Program.', in *Radiocarbon* 37.2, pp. 425–430.

Bronk Ramsey, C. (2009), 'Bayesian Analysis of Radiocarbon Dates', in *Radiocarbon* 51.1, pp. 337–360.

Bronk Ramsey, C. (2013), 'Using Radiocarbon Evidence in Egyptian Chronological Research', in *Radiocarbon and the Chronologies of Ancient Egypt*, ed. A.J. Shortland and C. Bronk Ramsey (Oxford: Oxbow Books), pp. 29–39.

Bronk Ramsey, C., M.W. Dee, J.M. Rowland, T.F.G. Higham, S.A. Harris, F. Brock, A. Quiles, E.M. Wild, E.S. Marcus, and A.J. Shortland (2010), 'Radiocarbon-based Chronology for Dynastic Egypt', in *Science* 328.5985, pp. 1554–1557.

Broughton, J.M. and J.F. O'Connell (1999), 'On Evolutionary Ecology, Selectionist Archaeology, and Behavioral Archaeology', in *American Antiquity* 64.1, pp. 153–165.

Bubenzer, O. and A. Hilgers (2003), 'Luminescence Dating of Holocene Playa Sediments of the Egyptian Plateau, Western Desert, Egypt', in *Quaternary Science Reviews* 22.10, pp. 1077–1084.

Bubenzer, O., A. Hilgers, and H. Riemer (2007), 'Luminescence Dating and Archaeology of Holocene Fluvio-lacustrine Sediments of Abu Tartur, Eastern Sahara', in *Quaternary Geochronology* 2.1, pp. 314–321.

Buchanan, B. and M. Collard (2007), 'Investigating the Peopling of North America Through Cladistic Analyses of early Paleoindian Projectile Points', in *Journal of Anthropological Archaeology* 26.3, pp. 366–393.

Buchanan, B. and M. Collard (2008), 'Phenetics, Cladistics, and the Search for the Alaskan Ancestors of the Paleoindians: A Reassessment of Relationships Among the Clovis, Nenana, and Denali Archaeological Complexes', in *Journal of Archaeological Science* 35.6, pp. 1683–1694.

Buchez, N. (2007), 'Chronologie et Transformations Structurelles de l'Habitat au cours du prédynastique. Apports des mobiliers céramiques funéraires et domestiques du site d'Adaïma (Haute-Égypte)', PhD thesis, INRAP, Toulouse.

Buchez, N. (2011), 'Chalcolithique Final (ou Moyen?), Nagada IIC-D/IIIA', in *Archéo-Nil* 21, pp. 51–64.

Buck, C.E. (2005), 'Applications of the Bayesian Statistical Paradigm', in *Handbook of Archaeological Sciences*, ed. D.R. Brothwell and A.M. Pollard (Chichester: Wiley), pp. 695–702.

Buckley, S.A., K.A. Clark, and R.P. Evershed (2004), 'Complex organic chemical balms of Pharaonic animal mummies', in *Nature* 431.7006, pp. 294–299.

Budka, J. and E.M. Engel (2015), 'Pot Marks from Ancient Egypt: The Multiple Function of Marking Ceramics', in *Non-textual Marking Systems in Ancient Egypt (and Elsewhere)*, ed. J. Budka, F. Kammerzell, and S. Rzepka (Hamburg: Widmaier Verlag), pp. 185–186.

Castaing, J., M. Girod, and A. Zink (2004), 'Radiation Background Due to Radioactivity in Palaces and Museums: Influence on TL/OSL Dating', in *Journal of Cultural Heritage* 5.4, pp. 393–397.

Caton-Thompson, G. and E. Whittle (1975), 'Thermoluminescence Dating of the Badarian', in *Antiquity* 49.194, pp. 89–97.

Chłodnicki, M. (1995), 'Some Remarks About Late Predynastic, Early Dynastic and Old Kingdom Bread Moulds', in *Études et Travauz* 17, pp. 23–27.

Chłodnicki, M., K.M. Ciałowicz, and A. Mączyńska (2012), *Tell el-Farkha I: Excavations 1998-2011* (Poznań: Poznań Archaeological Museum).

Clark-Balzan, L.A. (2012), 'Dating the Aterian Using Techniques of Luminescence Dating and Implications for Mapping the Dispersal of Modern Homo Sapiens', PhD thesis, Oxford: University of Oxford.

Clark-Balzan, L.A., I. Candy, J.-L. Schwenninger, A. Bouzouggar, S. Blockley, R. Nathan, and R.N.E. Barton (2012), 'Coupled U-series and OSL Dating of a Late Pleistocene Cave Sediment Sequence, Morocco, North Africa: Significance for Constructing Palaeolithic Chronologies', in *Quaternary Geochronology* 12, pp. 53–64.

Cochrane, E.E. (2008), 'Migration and Cultural Transmission: Investigating Human Movement as an Explanation for Fijian Ceramic Change', in *Cultural Transmission*

in Archaeology: Issues and Case Studies, ed. M.J. O'Brien (Washington D.C.: Society for American Archaeology), pp. 132–145.

Cochrane, E.E. (2009), 'Evolutionary Explanation and the Record of Interest', in *Pattern and Process in Cultural Evolution*, ed. S. Shennan (Berkeley.: University of California Press), pp. 113–132.

Cochrane, E.E. and C.P. Lipo (2010), 'Phylogenetic Analyses of Lapita Decoration Do Not Support Branching Evolution or Regional Population Structure During Colonization of Remote Oceania', in *Philosophical Transactions of The Royal Society B* 365, pp. 3889–3902.

Collard, M. and S.J. Shennan (2000), 'Processes of Culture Change in Prehistory: A Case Study from the European Neolithic', in *Archaeogenetics: DNA and the Population Prehistory of Europe* (Cambridge: McDonald Institute for Archaeological Research), pp. 89–97.

Collard, M., S.J. Shennan, and J.J. Tehrani (2006), 'Branching, Blending and the Evolution of CUltural Similarities and Differences Among Human Populations', in *Evolution and Human Behaviour* 27, pp. 169–184.

Colombini, M.P., G. Giachi, F. Modugno, and E.. Ribechini (2005), 'Characterisation of Organic Residues in Pottery Vessels of the Roman Age from Antinoe (Egypt)', in *Microchemical Journal* 79.1, pp. 83–90.

Colombini, M.P., F. Modugno, F. Silvano, and M. Onor (2000), 'Characterization of the Balm of an Egyptian Mummy from the Seventh Century BC', in *Studies in Conservation* 45.1, pp. 19–29.

Coward, F., S. Shennan, S. Colledge, J. Conolly, and M. Collard (2008), 'The Spread of Neolithic Plant Economies from the Near East to Northwest Europe: A Phylogenetic Analysis', in *Journal of Archaeological Science* 35.1, pp. 42–56.

Cunningham, A.C., M. Evans, and J. Knight (2015), 'Quantifying Bleaching for Zero-age Fluvial Sediment: A Bayesian Approach', in *Radiation Measurements* 81, pp. 55–61.

Daniels, F., C.A. Boyd, and D.F. Sanders (1953), 'Thermoluminescence as a Research Tool', in *Science* 117, pp. 343–349.

Darwent, J. and M.J. O'Brien (2006), 'Using Cladistics to Construct Lineages of Projectile Points from Northeastern Missouri', in *Mapping Our Ancestors: Phylogenetic Approaches in Anthropology and Prehistory*, ed. C. Lipo, M.J. O'Brien, M. Collard, and S.J. Shennan (New York: Aldine), pp. 185–208.

Dee, M., D. Wengrow, A. Shortland, A. Stevenson, F. Brock, L. Girdland Flink, and C. Bronk Ramsey (2013), 'An Absolute Chronology for Early Egypt Using Radiocarbon Dating and Bayesian Statistical Modelling', in *Proceedings of the Royal Society A* 469.2159, p. 20130395.

Dee, M.W. (2013a), 'A Radiocarbon-based Chronology for the Middle Kingdom', in *Radiocarbon and the Chronologies of Ancient Egypt*, ed. A.J. Shortland and C. Bronk Ramsey (Oxford: Oxbow Books), pp. 174–181.

Dee, M.W. (2013b), 'A Radiocarbon-based Chronology for the New Kingdom', in *Radiocarbon and the Chronologies of Ancient Egypt*, ed. A.J. Shortland and C. Bronk Ramsey (Oxford: Oxbow Books), pp. 65–75.

Dee, M.W. (2013c), 'A Radiocarbon-based Chronology for the Old Kingdom', in *Radiocarbon and the Chronologies of Ancient Egypt*, ed. A.J. Shortland and C. Bronk Ramsey (Oxford: Oxbow Books), pp. 209–217.

Dee, M.W. (2013d), 'Investigating the Accuracy of Radiocarbon Dating in Egypt: Checks with Samples of Known Age', in *Radiocarbon and the Chronologies of Ancient Egypt*, ed. A.J. Shortland and C. Bronk Ramsey (Oxford: Oxbow Books), pp. 53–64.

Dee, M.W., C. Bronk Ramsey, A.J. Shortland, T.F.G. Higham, and J.M. Rowland (2009), 'Reanalysis of the Chronological Discrepancies Obtained by the Old and Middle Kingdom Monuments Project', in *Radiocarbon* 51.3, pp. 1061–1070.

Dee, M.W., J.M. Rowland, T.F.G. Higham, A.J. Shortland, F. Brock, S.A. Harris, and C. Bronk Ramsey (2012), 'Synchronising Radiocarbon Dating and the Egyptian Historical Chronology by Improved Sample Selection', in *Antiquity* 86.333, pp. 868–883.

Dee, M.W., A.J. Wengrow D. Shortland, A. Stevenson, F. Brock, and C. Bronk Ramsey (2016), 'Radiocarbon Dating of Early Egyptian Pot Residues', in *Vienna 2 – Ancient Egyptian Ceramics in the 21st Century*, ed. B. Bader, C.M. Knoblauch, and Köhler E.C., vol. 245, Orientalia Lovaniensia Analecta (Leuven: Peeters), pp. 119–125.

Dee, M.W., D. Wengrow, A.J. Shortland, A. Stevenson, F. Brock, and C. Bronk Ramsey (2014), 'Radiocarbon dating and the Naqada relative chronology', in *Journal of Archaeological Science* 46, pp. 319–323.

Dietze, M., S. Kreutzer, C. Burow, M.C. Fuchs, M. Fischer, and C. Schmidt (2016), 'The Abanico Plot: Visualising Chronometric Data with Individual Standard Errors', in *Quaternary Geochronology* 31, pp. 12–18.

Dreyer, G. (1987), 'Ein Siegel der frühzeitlichen Königsnekropole von Abydos', in *Mitteilungen des Deutschen Archäologischen Instituts, Kairo* 43, pp. 33–47.

Dreyer, G. (1996), 'Umm el-Qaab. Nachuntersuchungen im frühzeitlichen Königsfriedhof. 7/8 Vorbericht', in *Mitteilungen des Deutschen Archäologischen Instituts, Kairo* 52, pp. 11–81.

Dreyer, G. (2010), 'Report on the 22nd Campaign of Reexamining the Royal Tombs of Umm el-Qaab at Abydos 2007/2008', in *Annales du Service des Antiquités de l'Egypte* 84, pp. 143–155.

Dreyer, G., E.M. Engel, R. Hartmann, H. Köpp-Junk, P. Meyrat, V. Müller, and I. Regulski (2013), 'Umm el-Qaab. Nachuntersuchingen im Frühzeitlichen Köingsfriedhof

22./23./24. Vorbericht', in *Mitteilungen des Deutschen Archäologischen Instituts, Kairo* 69, pp. 17–71.

Dreyer, G., R. Hartmann, U. Hartung, H. Köpp, C. Lacher, V. Müller, and A. Nerlich A .and Zink (2003), 'Umm el-Qaab. Nachuntersuchungen im frühzeitlichen Königsfriedhof 13./14./15', in *Mitteilungen des Deutschen Archäologischen Institutes in Kairo* 59, pp. 49–64.

Duller, G.A.T. (1999), *Luminescence Analyst Computer Programme*, V4.12 (Aberystwyth).

Duller, G.A.T. (2003), 'Distinguishing Quartz and Feldspar in Single Grain Luminescence Measurements', in *Radiation Measurements* 37.2, pp. 161–165.

Duller, G.A.T. (2004), 'Luminescence Dating of Quaternary Sediments: Recent Advances', in *Journal of Quaternary Science* 19.2, pp. 183–192.

Duller, G.A.T. (2008), *Luminescence Dating: Guidelines on Using Luminescence Dating in Archaeology* (Swindon: English Heritage).

Durcan, J.A., G.E. King, and G.A.T. Duller (2015), 'DRAC: Dose Rate and Age Calculator for trapped charge dating', in *Quaternary Geochronology* 28, pp. 54–61.

Effland, U. and A. Effland (2006), 'Funde aus dem Mittleren Reich bis zur Mamlukenzeit aus Umm el-Qaab', in *Mitteilungen des Deutschen Archäologischen Instituts, Kairo* 62, pp. 131–150.

Efron, B. (1979), 'Bootstrap Methods: Another Look at the Jackknife', in *Annals of Statistics* 7, pp. 1–26.

Efron, B. (1981), 'Nonparametric Standard Errors and Confidence Intervals', in *Canadian Journal of Statistics* 9, pp. 139–172.

Efron, B. (1982), *The Jackknife, the Bootstrap and Other Resampling Plans* (Philidephia: Society for Industrial and Applied Math).

Eldredge N. Carcraft, J. (1980), *Phylogenetic Patterns and the Evolutionary Process* (New York: Columbia University Press).

Emery, W.B. (1949), *Excavations at Saqqara: Great Tombs of the First Dynasty I* (Cairo: Government Press).

Emery, W.B. (1954), *Excavations at Sakkara: Great Tombs of the First Dynasty II* (Cairo: Government Press).

Emery, W.B. (1958), *Excavations at Sakkara: Great Tombs of the First Dynasty III* (Cairo: Government Press).

Endler, J.A. (1986), *Natural Selection in the Wild*, 21 (Princeton: Princeton University Press).

Engel, E.M. (1997), 'Abydos: Umm el-Qa'ab, Grab des Chasechemui', in *Bulletin de Liaison du Groupe International D'étude de la Céramique Égyptienne* 20, pp. 25–26.

Engel, E.M. (2000), 'Abydos: Umm el-Qa'ab, Grab des Chasechemui', in *Bulletin de Liaison du Groupe International D'étude de la Céramique Égyptienne* 21, pp. 50–58.

Engel, E.M. (2005), 'Ein Weiterer Beleg für den Doppelfalken auf einem Serech', in *Bulletin of the Egyptian Museum* 2, pp. 65–68.

Engel, E.M. (2015), 'The Early Dynastic Pot Mark Project', in *Non-textual Marking Systems in Ancient Egypt (and Elsewhere)*, ed. J. Budka, F. Kammerzell, and S. Rzepka (Hamburg: Widmaier Verlag), pp. 215–228.

Evershed, R.P., S.N. Dudd, M.S. Copley, and A.J. Mukherjee (2002), 'Identification of Animal Fats via Compound Specific δ13C Values of Individual Fatty Acids: Assessments of Results for Reference Fats and Lipid Extracts of Archaeological Pottery Vessels', in *Documenta Praehistorica* 21, pp. 73–96.

Evershed, R.P., C. Heron, S. Charters, and J.L. Goad (1992), 'Chemical Analysis of Organic Residues in Ancient Pottery: Methodological Guidelines and Applications', in *Organic Residues in Archaeology: Their Identification and Analysis. Proceedings of the Conference Organised by the United Kingdom Institute for Conservations, Archaeology Section, held at York, May 10th 1990*, ed. R. White and H. Page (London: UKIC Archaeology Section), pp. 11–25.

Fahmi, N.M., A. El-Khatib, Y.M. Abd El-Salam, M.H. Shalaby, M.M. El-Gally, and M.A. Naim (2011), 'Study of the Environmental Impacts of the Natural Radioactivity Presents [*sic*] in Beach Sand and Lake Sediment samples Idku, Behara, Egypt', in *Tenth Radiation Physics and Protection Conference, 27-30 November 2010, Nasr City, Cairo, Egypt* (), pp. 391–402.

Feathers, J.K. (2003), 'Use of Luminescence Dating in Archaeology', in *Measurement Science and Technology* 14.9, pp. 1493–1509.

Feathers, J.K. and D. Rhode (1998), 'Luminescence Dating of Protohistoric Pottery from the Great Basin', in *Geoarchaeology* 13.3, pp. 287–308.

Felsenstein, J. (1981), 'A Likelihood Approach to Character Weighting and What it Tells Us About Parsimony and Compatibility', in *Biological Journal of the Linnean Society* 16, pp. 183–196.

El-Fiki, S.A., M.S. Abdel-Wahab, N. El-Faramawy, and M.A. El-Fiki (1994), 'Dating of Ancient Egyptian Pottery Using the Thermoluminescence Technique', in *Nuclear Instruments and Methods in Physics Research Section B: Beam Interactions with Materials and Atoms* 94.1, pp. 91–94.

Fitzpatrick, S.M., Q. Kaye, J. Feathers, J.A. Pavia, and K.M. Marsaglia (2009), 'Evidence for Inter-island Transport of Heirlooms: Luminescence Dating and Petrographic Analysis of Ceramic Inhaling Bowls from Carriacou, West Indies', in *Journal of Archaeological Science* 36.3, pp. 596–606.

Fleming, S.J. (1975), 'Supralinearity Corrections in Fine-grain Thermoluminescence Dating: A Re-appraisal', in *Archaeometry* 17.1, pp. 122–129.

Fleming, S.J. (1979), *Thermoluminescence Techniques in Archaeology* (Oxford: Clarendon Press).

Fleming, S.J., H. Jucker, and J. Riederer (1971), 'Etruscan Wall-Paintings on Terracotta: A Study in Authenticity', in *Archaeometry* 13.2, pp. 143–167.

Fleming, S.J., H.M. Moss, and A. Joseph (1970), 'Thermoluminescence Authenticity Testing of Some Six Dynasties Figures', in *Archaeometry* 12.1, pp. 57–63.

Fortey, R.A. and B.D.E. Chatterton (1988), 'Classification of the Trilobite Suborder Asaphina', in *Palaeontology* 31, pp. 165–222.

Frechen, M., U. Schweitzer, and A. Zander (1996), 'Improvements in Sample Preparation for the Fine Grain Technique', in *Ancient TL* 14.2, pp. 15–17.

Friedman, R.F. (1981), *Spatial Distribution in a Predynastic Cemetery: Naga Ed Der 7000* (Berkeley: University of California).

Gabora, L. (2006), 'The Fate of Evolutionary Archaeology: Survival or Extinction?', in *World Archaeology* 38.4, pp. 690–696.

Galbraith, R.F. and R.G. Roberts (2012), 'Statistical Aspects of Equivalent Dose and Error Calculation and Display in OSL Dating: An Overview and Some Recommendations', in *Quaternary Geochronology* 11, pp. 1–27.

El-Gamal, H., M.A. Farid, A.I. Abdel Mageed, M. Hasabelnaby, and H.M. Hassanien (2013), 'Assessment of natural radioactivity levels in soil samples from some areas in Assiut, Egypt', in *Environmental Science and Pollution Research* 20.12, pp. 8700–8708.

Gardiner, A.H. (1959), *The Royal Canon of Turin* (Oxford: Griffith institute).

Garstang, J. (1907), 'Excavations at Hierakonpolis, at Esna and in Nubia', in *Annales du Service des Antiquitiés de l'Égypte* 8, pp. 132–148.

Garstang, J. and K. Sethe (1903), *Mahâsna and Bêt Khallâf* (London: Quaritch).

Gillespie, R. (2002), 'Dating the First Australians', in *Radiocarbon* 44.2, pp. 455–472.

Gingerich, P.D. and M. Schoeninger (1977), 'The Fossil Record and Primate Phylogeny', in *Journal of Human Evolution* 6, pp. 483–505.

Godfrey-Smith, D.I., D.J. Huntley, and W.-H. Chen (1988), 'Optical Dating Studies of Quartz and Feldspar Sediment Extracts', in *Quaternary Science Reviews* 7.3, pp. 373–380.

Goedicke, C. (2006), 'Luminescence Dating of Egyptian Artefacts', in *Ancient Egyptian Chronology*, ed. E. Hornung, R. Krauss, and D. Warburton (Leiden: Brill), pp. 356–360.

Grajetzki, W. (2003), *Burial Customs in Ancient Egypt: Life in Death for Rich and Poor* (London: Duckworth).

Gray, R.D. and F.M. Jordan (2000), 'Language Trees Support the Express-train Sequence of Austronesian Expansion', in *Nature* 405.6790, pp. 1052–1055.

Grimal, N. (1992), *A History of Ancient Egypt* (Oxford: Blackwell).

Grogler, N., F.G. Houtermans, and H. Stauffer (1960), 'Ueber die Datierung von Keramik und Ziegel durch Thermolumineszenz', in *Helvetica Physica Acta* 33, pp. 595–596.

Guérin, G., B. Combès, C. Lahaye, K.J. Thomsen, C. Tribolo, P. Urbanova, P. Guibert, N. Mercier, and H. Valladas (2015), 'Testing the Accuracy of a Bayesian Central-Dose Model for Single-grain OSL Using Known-age Samples', in *Radiation Measurements* 81, pp. 62–70.

Guérin, G., N. Mercier, and G. Adamiec (2011), 'Dose-rate Conversion Factors: Update', in *Ancient TL* 29.1, pp. 5–8.

Guérin, G., N. Mercier, R. Nathan, G. Adamiec, and Y. Lefrais (2012), 'On the use of the infinite matrix assumption and associated concepts: a critical review', in *Radiation Measurements* 47.9, pp. 778–785.

Guibert, P., I.K. Bailiff, S. Blain, A.M. Gueli, M. Martini, E. Sibilia, G. Stella, and S.O. Troja (2009), 'Luminescence Dating of Architectural Ceramics from an Early Medieval Abbey: The St Philbert Intercomparison (Loire Atlantique, France)', in *Radiation Measurements* 44.5, pp. 488–493.

Hansen, V., A. Murray, J.-P. Buylaert, E.-Y. Yeo, and K. Thomsen (2015), 'A New Irradiated Quartz for Beta Source Calibration', in *Radiation Measurements* 81, pp. 123–127.

Harb, S.R.M., K.S. Din, A.E. Abbady, M.A.E. Ali, and R. Michel (2008), 'Measurements of Natural Radionuclides in Soil Samples from Upper Egypt', in *Nuclear Science and Techniques* 19.5, pp. 302–307.

Harper, C.W. (1976), 'Phylogenetic Inference in Paleontology', in *Journal of Palaeontology* 50, pp. 180–193.

Hart, J.P. and W. Engelbrecht (2012), 'Northern Iroquoian Ethnic Evolution: A Social Network Analysis', in *Journal of Archaeological Method and Theory* 19, pp. 322–349.

Hartmann, R. (2006), 'Grab des Peribsen: Funde', in Dreyer, G., A. Effland, E.M. Effland U. Engel, U. Hartmann R. Hartung, C. Lacher, V. Müller, and A. Pokorny, 'Umm el-Qaab – Nachuntersuchungen im frühzeitlichen Königsfriedhof', in *Mitteilungen des Deutschen Archäologischen Instituts, Kairo* 62, pp. 67–129.

Hartmann, R. (2015), 'Ein Corpus von Ritzmarken auf Weinkr'ugen aus dem Grab des Ninetjer in Saqqara', in *Non-textual Marking Systems in Ancient Egypt (and Elsewhere)*, ed. J. Budka, F. Kammerzell, and S. Rzepka (Hamburg: Widmaier Verlag), pp. 229–243.

Hartung, U., E.C. Köhler, V. Müller, and M.F. Ownby (2015), 'Imported Pottery from Abydos: a New Petrographic Perspective', in *Ägypten und Levante* 25, pp. 295–333.

Hassan, F.A. (1980), 'Radiocarbon Chronology of Archaic Egypt', in *Journal of Near Eastern Studies* 39.3, pp. 203–207.

Hassan, F.A. (1985), 'Radiocarbon Chronology of Neolithic and Predynastic Sites in Upper Egypt and the Delta', in *The African Archaeological Review* 3, pp. 95–116.

Hauser, D.L. and G. Boyajian (1997), 'Proportional Change and Patterns of Homoplasy: Sanderson and Donoghue Revisited', in *Cladistics* 13, pp. 97–100.

Hendrickx, S. (1989), 'De Grafvelden der Naqada-cultuur in Zuid-Egypte, met Bijzondere Aandacht voor het Naqada III Grafveld te Elkab. Interne Chronologie en Sociale Differentiatie', PhD thesis, Leuven: Katholieke Universiteit te Leuven.

Hendrickx, S. (1994), *Elkab V: The Naqada III Cemetery* (Brussels: Musée Royaux d'Art et d'Histoire–Koninklijke Musea voor Kunst en Geschiedenis).

Hendrickx, S. (1996), 'The Relative Chronology of the Naqada Culture. Problems and Possibilities', in *Aspects of Early Egypt*, ed. J. Spencer (London: British Museum Press), pp. 36–69.

Hendrickx, S. (1999), 'La Chronologie de la Préhistoire Tardive et des Débuts de L'histoire de L'Egypte', in *Archéo-Nil* 9, pp. 13–81.

Hendrickx, S. (2006), 'Predynastic–Early Dynastic Chronology', in *Ancient Egyptian Chronology*, ed. E. Hornung, R. Krauss, and D. Warburton (Leiden: Brill), pp. 55–93.

Hendrickx, S. (2011), 'Naqada IIIA-B, A Crucial Phase in the Relative Chronology of the Naqada Culture', in *Archéo-Nil* 21, pp. 65–80.

Hendrickx, S., D. Faltings, L. Op De Beeck, D. Raue, and C. Micheiels (2002), 'Milk, Beer and Bread Technology During the Early Dynastic Period', in *Mitteilungen des Deutschen Archäologischen Instituts. Abteilung Kairo* 58, pp. 277–304.

Hennig, W. (1950), *Grundzüge einer Theorie der Phylogenetischen Systematik* (Berlin: Deutscher Zentralverlag).

Hennig, W. (1966), *Phylogenetic Systematics* (Illinois: Urbana).

Holden, C.J (2002), 'Bantu Language Trees Reflect the Spread of Farming Across Sub-Saharan Africa: A Maximum-parsimony Analysis', in *Proceedings of the Royal Society of London B: Biological Sciences* 269.1493, pp. 793–799.

Hood, A.G.E. (2007), 'The Ceramic Assemblage of the Naqada IIID Period – A Tentative Analysis of the Ceramic Typological and Chronological Sequence from the End of the First Dynasty to the Early Old Kingdom: Problems, Possibilities and Priorities.', Honours Thesis, Sydney: Macquarie University.

Hood, A.G.E. (2010a), 'A Study of the Pottery', in Regulski, I., C. Lacher, and A. Hood, 'Preliminary Report on the Leiden Excavations in the Second Dynasty Necropolis at Saqqara, Season 2009', in *Jaarbericht "Ex Oriente Lux"* 42, pp. 37–44.

Hood, A.G.E. (2010b), 'Establishing a New Typology for the Ceramics of Southern Madagascar by Luminescence Dating', MA thesis, Oxford: University of Oxford.

Hood, A.G.E. (in press), 'A Brief Look at First and Second Dynasty Ceramics at Elephantine and their Chronological Implications', in *Funde und Befunde aus der Umge-*

bung des Satettempels. Grabungen von 2006-2009, Elephantine, ed. P. Kopp, vol. TBC, Archäologische Veröffentlichungen (Mainz: Verlag Philipp Von Zabern).

Hood, A.G.E and J-L. Schwenninger (2015), 'The Minimum Extraction Technique: A New Sampling Methodology for Optically Stimulated Luminescence Dating of Museum Ceramics', in *Quaternary Geochronology* 30, pp. 381–385.

Hood, A.G.E. and J.-L. Schwenninger (2016), 'Optically Stimulated Luminescence (OSL) Dating and its Application to Ancient Egyptian Ceramics in the 21st Century', in *Vienna 2 – Ancient Egyptian Ceramics in the 21st Century*, ed. B. Bader, C.M. Knoblauch, and Köhler E.C., vol. 245, Orientalia Lovaniensia Analecta (Leuven: Peeters), pp. 287–298.

Hood, A.G.E. and J.L. Valentine (2012), 'The Application of Cladistics to Early Dynastic Egyptian Ceramics: Applying a New Method', in *Egyptology in Australia and New Zealand 2009: Proceedings of the Conference Held in Melbourne, September 4th-6th*, ed. C.M. Knoblauch and J.C. Gill (Oxford: Archaeopress), pp. 47–59.

Hood, A.G.E., M.W. Woodworth M. Dee, J.-L. Schwenninger, C. Bronk Ramsey, and P.W. Ditchfield (in press), 'A Tale of Six Vessels: A Multidisciplinary Approach to the Analysis of Six Predynastic and Early Dynastic Vessels from Abydos, Ballas and Naqada – Preliminary Remarks', in *Egypt at its Origins 5: Proceedings of the Fifth International Conference "Origin of the State. Predynastic and Early Dynastic Egypt", Cairo, 2014*, vol. TBC, Orientalia Lovaniensia Analecta ().

Hornung, E., R. Krauss, and D. Warburton (2006), *Ancient Egyptian Chronology* (Leiden: Brill).

Huntley, D.J., D.I Godfrey-Smith, and M.L.W Thewalt (1985), 'Optical Dating of Sediments', in *Nature* 313, pp. 105–107.

Huyge, D., D.A.G. Vandenberghe, M. De Dapper, F. Mees, W. Claes, and J.C. Darnell (2011), 'First Evidence of Pleistocene Rock Art in North Africa: Securing the Age of the Qurta Petroglyphs (Egypt) through OSL Dating', in *Antiquity* 85.330, pp. 1184–1193.

Ikram, S. (2015), *Death and Burial in Ancient Egypt* (Cairo: AUC Press).

Jacquet-Gordon, H. (1981), 'A Tentative Typology of Egyptian Bread Moulds', in *Studien zur Altägyptischen Keramik*, ed. D. Arnold (Mainz: Verlag Phillip von Zabern), pp. 11–24.

Johnson, K. (2008), *Quantitative Methods in Linguistics* (Oxford: Wiley).

Jones, J., T.F.G Higham, R. Oldfield, T.P. O'Connor, and S.A Buckley (2014), 'Evidence for Prehistoric Origins of Egyptian Mummification in Late Neolithic Burials', in *PloS one* 9.8, e103608.

Jordan, P. and S. Shennan (2003), 'Cultural Transmission, Language, and Basketry Traditions Amongst the California Indians', in *Journal of Anthropological Archaeology* 22.1, pp. 42–74.

Jucha, M. (2001), 'Initial Results of Research on Predynastic and Early Dynastic Pottery from Tell El-Farkha 1998–1999', in *Proceedings of the First Central European Conference of Young Egyptologists. Egypt, 1999*, ed. J. Popielska-Grzybowska (Warsaw: Perspectives of Research), pp. 39–45.

Jucha, M. (2003), 'Tell el-Farkha 1998-1999: Pottery from Predynastic and Early Dynastic Strata', in *Egyptology at the Dawn of the Twenty-first Century: Proceedings of the Eighth International Congress of Egyptologists Cairo 2000*, ed. Z. Hawass, vol. 1 (Cairo: American University in Cairo Press), pp. 262–271.

Jucha, M. (2005), *Tell el-Farkha II: The Pottery of the Predynastic Settlement (Phases 2 to 5)* (Poznań: Poznań Archaeological Museum).

Junding, X. (1993), 'A Quick TL Authenticity Testing for the Tang Dynasty Tri-Coloured Pottery', in *Nuclear Techniques* 4, pp. 247–250.

Junker, H. (1913), *Bericht über die Grabungen der Kaiserl. Akademie der Wissenschaften in Wien auf dem Friedhof in Turah: Winter 1909-1910* (Vienna: Hölder).

Kahl, J. (2006), 'Inscriptional Evidence for the Relative Chronology of Dynasties 0–2', in *Ancient Egyptian Chronology*, ed. E. Hornung, R. Krauss, and D. Warburton (Leiden: Brill), pp. 94–115.

Kaiser, W. (1957), 'Zur Inneren Chronologie der Naqadakultur', in *Archaeologia Geographica* 6, pp. 69–77.

Kaiser, W. (1964), 'Einige Bemerkungen zur Ägyptischen Frühzeit', in *Zeitschrift für Ägyptische Sprache* 91, pp. 86–125.

Kaiser, W. (1990), 'Zur Entstehung des gesamtägyptischen Staates', in *Mitteilungen des Deutschen Archäologischen Instituts, Albeitung Kairo* 46, pp. 287–299.

Kemp, B.J. (1975), 'Dating Pharaonic Cemeteries. Part I: Non-mechanical Approaches to Seriation', in *Mitteilungen des Deutschen Archäologischen Instituts, Kairo* 31.2, pp. 259–291.

Kennedy, G.C. and L. Knopff (1960), 'Dating by Thermoluminescence', in *Archaeology* 13, pp. 147–148.

Kilikoglou, V., Y. Maniatis, and A.P. Grimanis (1988), 'The Effect of Purification and Firing of Clays on Trace Element Provenance Studies', in *Archaeometry* 30.1, pp. 37–46.

Kimpe, K., C. Drybooms, E. Schrevens, P.A. Jacobs, R. Degeest, and M. Waelkens (2004), 'Assessing the Relationship Between Form and Use of Different Kinds of Pottery from the Archaeological Site Sagalassos (Southwest Turkey) with Lipid Analysis', in *Journal of Archaeological Science* 31.11, pp. 1503–1510.

Kitchen, K.A. (1991), 'The Chronology of Ancient Egypt', in *World Archaeology* 23.2, pp. 201–208.

Kitching, I.J., P.L. Florey, C.J. Humphries, and D.M. Williams (1998), *Cladistics: The Theory and Practice of Parsimony Analysis* (Oxford: Oxford University Press).

Klasens, A. (1957), 'The Excavations of the Leiden Museum of Antiquities at Abu-Roash: Report of the First Season. Part I', in *Oudheidkundige Mededelingen uit het Rijksmusuen van Oudheden* 38, pp. 58–68.

Klasens, A. (1958), 'The Excavations of the Leiden Museum of Antiquities at Abu-Roash: Report of the First Season. Part II', in *Oudheidkundige Mededelingen uit het Rijksmusuen van Oudheden* 39, pp. 69–94.

Klasens, A. (1960), 'The Excavations of the Leiden Museum of Antiquities at Abu-Roash: Report of the Third Season 1959. Part I', in *Oudheidkundige Mededelingen uit het Rijksmusuen van Oudheden* 41, pp. 69–94.

Köhler, E.C. in prep, 'Auch die Letze Scherbe – More Thoughts on the 'Naqada Culture'', in prep.

Köhler, E.C. (1998), *Tell el-Fara'in-Buto III. Die Keramik von der späten Naqada-Kultur bis zum frühen Alten Reich (Schichten III bis VI)*, vol. 94, Archäologische Veröffentlichungen (Mainz: Verlag Philipp Von Zarbern).

Köhler, E.C. (2004), 'On the Origins of Memphis: The New Excavations in the Early Dynastic Necropolis at Helwan', in *Egypt at its Origins: Studies in Memory of Barbara Adams. Proceedings of the International Conference "Origin of the State. Predynastic and Early Dynastic Egypt", Kraków, 28th August–1st September 2002*, ed. S. Hendrickx, R.F. Friedman, K.M. Ciałwicz, and M. Chłodnicki, vol. 138, Orientalia Lovaniensia Analecta (Leuven: Peeters), pp. 295–315.

Köhler, E.C. (2005), *Helwan I: Excavations in Early Dynastic Cemetery, Season 1997/1998* (Heidelberg: Heidelberger Orientverlag).

Köhler, E.C. (2011), 'Introduction', in *Archéo-Nil* 21, pp. 5–11.

Köhler, E.C. (2013), 'Early Dynastic Egyptian Chronologies', in *Radiocarbon and the Chronologies of Ancient Egypt*, ed. A.J. Shortland and C. Bronk Ramsey (Oxford: Oxbow Books), pp. 224–234.

Köhler, E.C. (2014a), *Helwan III: Excavations in Operation 4, Tombs 1–50* (Leidorf: Rahden/Westf.).

Köhler, E.C. (2014b), 'Of Pots and Myths – Attempting a Comparative Study of Funerary Pottery Assemblages in the Egyptian Nile Valley During the Late 4th Millennium BC', in *The Nile Delta as a Centre of Cultural Interactions Between Upper Egypt and the Southern Levant in the 4th Millennium BC*, ed. A. Mączyńska, vol. 13, Studies in African Archaeology (Poznań: Poznań Archaeological Museum), pp. 155–180.

Köhler, E.C. and J.C. Smythe (2004), 'Early Dynastic Pottery from Helwan – Establishing a Ceramic Corpus of the Naqada III Period', in *Cahiers de la Céramique Égyptienne* 7, pp. 123–144.

Köhler, E.C., J.C. Smythe, and A.G.E. Hood (2011), 'Naqada IIIC-D - The End of the Naqada Culture?', in *Archéo-Nil* 21, pp. 101–110.

Köhler, E.C. and J.-P. Thalmann (2014), 'Synchronising Early Egyptian Chronologies and the Northern Levant', in *Egypt and the Southern Levant in the Early Bronze Age*, ed. F. Höflmayer and R. Eichmann, vol. 31, Orient-Archäologie (Leidorf: Rahden/Westf.), pp. 181–206.

Köhler, E.C. and E.C.M. Van Den Brink (2002), 'Four Jars with Incised Serekh-Signs from Helwan Recently Retrieved from the Cairo Museum', in *Göttinger Miszellen: Beiträge zur ägyptologischen Diskussion* 187, pp. 59–82.

Koller, J., U. Baumer, Y. Kaup, M. Schmid, and U. Weser (2003), 'Ancient Materials: Analysis of a Pharaonic Embalming Tar', in *Nature* 425.6960, pp. 784–784.

Köpp, H. (2011), 'Grab des Chasechemui: Keramik', in Dreyer, G., A.I. Blübaum, E.M. Engel, H. Köpp, and V. Müller, in *Mitteilungen des Deutschen Archäologischen Instituts, Kairo* 67, pp. 85–90.

Kroeper, K. (2003), 'Radiocarbon and Thermoluminescence Dates from the Pre/Early Dynastic Cemetery of Minshat Abu Omar (North-Eastern Nile Delta)', in *Cultural Markers in the Later Prehistory of Northeastern Africa and Recent Research*, vol. 8, Studies in African Archaeology (), pp. 227–244.

Kroeper, K. and D. Wildung (1994), *Minshat Abu Omar: ein vor- und frühgeschichtlicher Friedhof im Nildelta. Vol. 1 Gräber 1–114*, vol. 1 (Mainz: Verlag Philipp von Zabern).

Kroeper, K. and D. Wildung (2000), *Minshat Abu Omar: ein vor- und frühgeschichtlicher Friedhof im Nildelta. Vol. 2 Gräber 115–204*, vol. 2 (Mainz: Verlag Philipp von Zabern).

Kuksis, A., P. Child, J.J. Myher, L. Marai, I.M. Yousef, and P.K. Lewin (1978), 'Bile Acids of a 3200-Year-Old Egyptian Mummy', in *Canadian Journal of Biochemistry* 56.12, pp. 1141–1148.

Lacher, C.M. (2011), 'The Tomb of Ninetjer at Saqqara', in *Egypt at its Origins 3: Proceedings of the Third International Conference "Origin of the State. Predynastic and Early Dynastic Egypt", London, 27th July–1st August 2008*, ed. R.F. Friedman and P.N. Fiske, vol. 205, Orientalia Lovaniensia Analecta (Leuven: Peeters), pp. 213–231.

Lang, A., C. Hatté, D.-D. Rousseau, P. Antoine, M. Fontugne, L. Zöller, and U. Hambach (2003), 'High-resolution Chronologies for Loess: Comparing AMS 14C and Optical Dating Results', in *Quaternary Science Reviews* 22.10, pp. 953–959.

Lang, A.R. and V.F. Miuscov (1967), 'Dislocations and Fault Surfaces in Synthetic Quartz', in *Journal of Applied Physics* 38.6, pp. 2477–2483.

Larsen, H. (1939), 'Three Shaft Tombs with Chambers at Maassara, Egypt', in *Acta Archaeologica* 10, pp. 161–206.

Larsen, H. (1940), 'Tomb Six at Maassara: An Egyptian Second Dynasty Tomb', in *Acta Archaeologica* 11, pp. 103–124.

Lian, O.B. and R.G. Roberts (2006), 'Dating the Quaternary: Progress in Luminescence Dating of Sediments', in *Quaternary Science Reviews* 25.19, pp. 2449–2468.

Libby, W.F. (1980), 'Archaeology and Radiocarbon Dating', in *Radiocarbon* 22.4, pp. 1017–1020.

Lipo, C., M.J. O'Brien, M. Collard, and S.J. Shennan, eds. (2006), *Mapping Our Ancestors: Phylogenetic Approaches in Anthropology and Prehistory* (New York: Aldine).

Lipscomb, D. (1998), *Basics of Cladistic Analysis* (Washington DC: George Washington University).

Liritzis, I, D. Katsanopoulou, S. Soter, and R.B. Galloway (2001), 'In Search of Ancient Helike, Gulf of Corinth, Greece', in *Journal of Costal Research* 17.1, pp. 118–128.

Liritzis, I., C. Sideris, A. Vafiadou, and J. Mitsis (2008), 'Mineralogical, Petrological and Radioactivity Aspects of Some Building Material from Egyptian Old Kingdom Monuments', in *Journal of Cultural Heritage* 9.1, pp. 1–13.

Liritzis, I., A. Vafiadou, N. Zacharias, G.S. Polymeris, and R.G. Bednarik (2013), 'Advances in Surface Luminescence Dating: New Data from Selected Monuments', in *Mediterranean Archaeology and Archaeometry* 13.3, pp. 105–115.

Long, H., Z.P. Lai, N.A. Wang, and J.R. Zhang (2011), 'A Combined Luminescence and Radiocarbon Dating Study of Holocene Lacustrine Sediments from Arid Northern China', in *Quaternary Geochronology* 6.1, pp. 1–9.

Lycett, S.J. (2007), 'Why is there a lack of Mode 3 Levallois technologies in East Asia? A phylogenetic test of the Movius–Schick hypothesis', in *Journal of Anthropological Archaeology* 26.4, pp. 541–575.

Lycett, S.J. (2009), 'Understanding Ancient Hominin Dispersals Using Artefactual Data: A Phylogeographic Analysis of Acheulean Handaxes', in *PLoS One* 4.10, e7404.

Lyman, R.L. and M.J. O'Brien (1997), 'The Concept of Evolution in Early Twentieth Century Americanist Archaeology', in *Rediscovering Darwin: Evolutionary theory and archeological explanation*, ed. C.M. Barton, G.A. Clark, and D.B. Bamforth, vol. 7, Archaeological Papers of the American Anthropological Association 1 (Virginia: American Anthropological Association), pp. 21–48.

Lyman, R.L. and M.J. O'Brien (2006a), 'Evolutionary Archaeology is Unlikely to Go Extinct: Response to Gabora', in *World Archaeology* 38.4, pp. 697–703.

Lyman, R.L. and M.J. O'Brien (2006b), 'Seriation and Cladistics: the Difference Between Anagenetic and Cladogenetic Evolution', in *Mapping Our Ancestors: Phylogenetic Ap-*

proaches in Anthropology and Prehistory, ed. C. Lipo, M.J. O'Brien, M. Collard, and S.J. Shennan (New Brunswick: Aldine Transaction), pp. 65–88.

Lyons-Weiler, J., G.A. Hoelzer, and R.J. Tausch (1998), 'Optimal Outgroup Analysis', in *Biological Journal of the Linnean Society* 64, pp. 493–511.

Mace, A.C., G.A. Reisner, and A.M. Lythgoe (1909), *The Early Dynastic Cemeteries of Naga-ed-Dêr, Part II* (Leipzig: JC Hinrichs).

Mączyńska, A. (2004), 'Pottery Tradition at Tell el-Farkha', in *Egypt at its Origins: Studies in Memory of Barbara Adams. Proceedings of the International Conference "Origin of the State. Predynastic and Early Dynastic Egypt", Kraków, 28th August–1st September 2002*, ed. S. Hendrickx, R.F. Friedman, K.M. Ciałwicz, and M. Chłodnicki, vol. 138, Orientalia Lovaniensia Analecta (Leuven: Peeters), pp. 421–442.

Mallory-Grennough, L.M. and J.D. Greenough (1998), 'New Data for Old Pots: Trace-Element Characterizatio of Ancient Egyptian Pottery Using ICP-MS', in *Journal of Archaeological Science* 25, pp. 85–97.

Manning, S. (2006), 'Radiocarbon Dating and Egyptian Chronology', in *Ancient Egyptian Chronology*, ed. E. Hornung, R. Krauss, and D. Warburton (Leiden: Brill), pp. 327–355.

Manning, S. (2010), 'Radiocarbon and the Dating of Pre- and Proto History in the East Mediterranean (first date to decades later): a late-blooming romcom?', Radiocarbon Dating and the Egyptian Chronology, unpublished conference abstract booklet. Oxford.

Martin, L., S. Incerti, and N. Mercier (2015), 'DosiVox: Implementing Geant 4-based Software for Dosimetry Simulations Relevant to Luminescence and ESR Dating Techniques', in *Ancient TL* 33 (1), pp. 1–10.

Martin, L. and N. Mercier (2015), *DosiVox Manual* (Bordeaux).

Mauz, B. and A. Lang (2004), 'Removal of the Feldspar-derived Luminescence Component from Polymineral Fine Silt Samples for Optical Dating Applications: Evaluation of Chemical Treatment Protocols and Quality Control Procedures', in *Ancient TL* 22.1, pp. 1–8.

McCarthy, I., K. Ridgway, M. Leseure, and N. Fieller (2000), 'Organisational Diversity, Evolution and Cladistic Classifications', in *Omega* 28.1, pp. 77–95.

McCarthy, I.P. (2005), 'Toward a Phylogenetic Reconstruction of Organizational Life', in *Journal of Bioeconomics* 7.3, pp. 271–307.

McGovern, P.E. (1997), 'Wine of Egypt's Golden Age: An Archaeochemical Perspective', in *Journal of Egyptian Archaeology* 83, pp. 69–108.

Miller, D. (1985), *Artefacts as Categories: A Study of Ceramic Variability in Central India* (Cambridge: Cambridge University Press).

Mindant-Reynes, B. and P. Sabatier (1999), 'Préhistoire Egytianne et Radiocarbone', in *Archéo-Nil* 9, pp. 83–107.

Morgan, J. de (1896), *Recherches sur les Origines de l'Egypte, I. L'Age de la Pierre et les Métaux* (Paris: Ernest Leroux).

Morgenstein, M.E. and C.A Redmount (2005), 'Using Portable Energy Dispersive X-ray Fluorescence (EDXRF) Analysis for On-site Study of Ceramic Sherds at El Hibeh, Egypt', in *Journal of Archaeological Science* 32.11, pp. 1613–1623.

Morwood, M.J., R.P. Soejono, R.G. Roberts, T. Sutikna, C.S.M. Turney, K.E. Westaway, W.J. Rink, J.-X. Zhao, G.D. van den Bergh, A.D. Rokus, D.R. Hobbs, M.W. Moore, M.I. Bird, and L.K. Fifield (2004), 'Archaeology and Age of a New Hominin from Flores in eastern Indonesia', in *Nature* 431.7012, pp. 1087–1091.

Mottram, H.R., S.N. Dudd, G.J. Lawrence, A.W Stott, and R.P. Evershed (1999), 'New Chromatographic, Mass Spectrometric and Stable Isotope Approaches to the Classification of Degraded Animal Fats Preserved in Archaeological Pottery', in *Journal of Chromatography A* 833.2, pp. 209–221.

Müller, V. (2004), 'The Chronological Implication of Seal Impressions: Further Evidence for Cultic Activities in the Middle Kingdom in the Early Dynastic Royal Necropolis at Umm el-Qaab/Abydos', in *Scarabs of the Second Millennium BB from Egypt, Nubia, Crete and the Levant. Chronological and Historical Implications*, ed. M. Bietak and E. Czerny (Vienna: Verlag der Österreichischen Akademie der Wissenschaften), pp. 141–159.

Murnane, W.J. (1981), 'The Sed Festival: A Problem in Historical Method', in *Mitteilungen des Deutschen Archäologischen Instituts, Albeitung Kairo* 37, pp. 369–376.

Murray, A.S. and J.M. Olley (2002), 'Precision and Accuracy in the Optically Stimulated Luminescence Dating of Sedimentary Quartz: A Status Review', in *Geochronometria* 21.1, pp. 1–16.

Murray, A.S. and A.G. Wintle (2000), 'Luminescence Dating of Quartz Using an Improved Single-Aliquot Regenerative-Dose Protocol', in *Radiation Measurements* 32.1, pp. 57–73.

Murray, T. (2002), 'Evaluating Evolutionary Archaeology', in *World Archaeology* 34.1, pp. 47–59.

Nada, A., T.M. Abd-El Maksoud, M. Abu-Zeid Hosnia, T. El-Nagar, and S. Awad (2009), 'Distribution of Radionuclides in Soil Samples from a Petrified Wood Forest in El-Qattamia, Cairo, Egypt', in *Applied Radiation and Isotopes* 67.4, pp. 643–649.

Needham, S., C. Bronk Ramsey, D. Coombs, C. Cartwright, and P. Pettitt (1997), 'An Independent Chronology for British Bronze Age Metalwork: The Results of the Oxford Radiocarbon Accelerator Programme', in *Archaeological Journal* 154.1, pp. 55–107.

Neff, H. and D.O. Larson (1997), 'Methodology of Comparison in Evolutionary Archaeology', in *Rediscovering Darwin: Evolutionary Theory and Archaeological Explanation*,

ed. Barton C.M. and G.A. Clark, vol. 7, Archaeological Papers of the American Anthropological Associations 1 (), pp. 75–94.

Nicholson, P.T. (1993), 'The Firing of Pottery', in *An Introduction to Ancient Egyptian Pottery*, ed. D. Arnold and J. Bourriau (Mainz: von Zabern), pp. 103–120.

Nicholson, P.T. and H.L. Patterson (1985a), 'Ethnoarchaeology in Egypt: The Ballâs Pottery Project', in *Archaeology* 38.3, pp. 52–59.

Nicholson, P.T. and H.L. Patterson (1985b), 'Pottery Making in Upper Egypt: An Ethnoarchaeological Study', in *World Archaeology* 17.2, pp. 222–239.

Nicholson, P.T. and H.L. Patterson (1989), 'Ceramic Technology in Upper Egypt: A Study of Pottery Firing', in *World Archaeology* 21.1, pp. 71–85.

Nixon, K.C. and J.M. Carpenter (1993), 'On Outgroups', in *Cladistics* 9, pp. 413–426.

O'Brien, M.J. (2001), 'Cladistics and Archaeological Phylogeny', in *The Missouri Archaeologist* 63, pp. 31–52.

O'Brien, M.J., J. Darwent, and R.L. Lyman (2001), 'Cladistics is Useful for Reconstructing Archaeological Phylogenies: Palaeoindian Points from the Southeastern United States', in *Journal of Archaeological Science* 28.10, pp. 1115–1136.

O'Brien, M.J. and R. L. Lyman (2003), *Cladistics and Archaeology* (Salt Lake City: University of Utah Press).

O'Brien, M.J. and R.L. Lyman (1999), *Seriation, Stratigraphy, and Index Fossils: The Backbone of Archaeological Dating* (New York: Kluwer Academic/Plenum Publishers).

O'Brien, M.J. and R.L. Lyman (2000), 'Darwinian Evolutionism is Applicable to Historical Archaeology', in *International Journal of Historical Archaeology* 4.1, pp. 71–112.

O'Brien, M.J. and R.L. Lyman (2002), 'Evolutionary Archeology: Current Status and Future Prospects', in *Evolutionary Anthropology* 11.1, pp. 26–35.

O'Brien, M.J. and R.L. Lyman (2009), 'Darwinism and Historical Archaeology', in *International Handbook of Historical Archaeology*, ed. T. Majewski and D. Gaimster (), pp. 227–252.

O'Brien, M.J., R.L. Lyman, and J.A. Darwent (2002), 'Cladistics and Archaeological Phylogeny', in *Perspectivas Integradoras entre Arqueología y Evolución. Teoría, Método y Casos de Aplicación* (), pp. 175–86.

O'Brien, M.J., R.L. Lyman, Y. Saab, E. Saab, J Darwent, and D.S. Glover (2002), 'Two Issue in Archaeological Phylogenetics: Taxon Construction and Outgroup Selection', in *Journal of Theoretical Biology* 215, pp. 133–150.

Olley, J., G. Caitcheon, and A. Murray (1998), 'The Distribution of Apparent Dose as Determined by Optically Stimulated Luminescence in Small Aliquots of Fluvial Quartz: Implications for Dating Young Sediments', in *Quaternary Science Reviews* 17.11, pp. 1033–1040.

Olley, J.M., P. De Deckker, R.G. Roberts, L.K. Fifield, H. Yoshida, and G. Hancock (2004), 'Optical Dating of Deep-sea Sediments Using Single Grains of Quartz: A Comparison with Radiocarbon', in *Sedimentary Geology* 169.3, pp. 175–189.

Olley, Jon M, Richard G Roberts, Hiroyuki Yoshida, and James M Bowler (2006), 'Single-grain Optical Dating of Grave-infill Associated with Human Burials at Lake Mungo, Australia', in *Quaternary Science Reviews* 25.19, pp. 2469–2474.

Op de Beeck, L. (2004), 'Possibilities and Restrictions for the Use of Maidum-bowls as Chronological Indicators', in *Cahiers de la céramique égyptienne* 7, pp. 239–274.

Orton, C., P. Tyers, and A. Vince (1993), *Pottery in Archaeology*, Cambridge Manuals in Archaeology (Cambridge: Cambridge University Press).

Ownby, M. (2009), 'Petrographic and Chemical Analysis of Select 4th Dynasty Pottery Fabrics from the Giza Plateau', in *Studies on Old Kingdom Pottery*, ed. T.I. Rzeuska and A. Wodzińska (Warsaw: Wydawnictwo Neriton), pp. 113–137.

Ownby, M. and J. Bourriau (2009), 'The Movement of Middle Bronze Age Transport Jars: A Provenance Study Based on Petrographic and Chemical Analysis of Canaanite Jars from Memphis, Egypt', in *Interpreting Silent Artefacts: Petrographic Approaches to Archaeological Ceramics*, ed. P.S. Quinn (Oxford: Archaeopress), pp. 173–188.

Ownby, M. and D. Griffiths (2009), 'Issues of Scum: Technical Analyses of Egyptian Marl C to Answer Technological Questions', in *Ägypten und Levante* 19, pp. 229–239.

Parkinson, R. (1997), *The Tale of Sinuhe and Other Ancient Egyptian Poems 1940–1640 B.C.* (Oxford: Oxford University Press).

Parsche, F. and A. Nerlich (1995), 'Presence of Drugs in Different Tissues of an Egyptian Mummy', in *Fresenius' Journal of Analytical Chemistry* 352.3-4, pp. 380–384.

Paterson, A.M., G.P. Wallis, and R.D. Gray (1995), 'Penguins, Petrels, and Parsimony: Does Cladistic Analysis of Behavior Reflect Seabird Phylogeny?', in *Evolution*, pp. 974–989.

Payne, J.C. (1992), 'Predynastic chronology at Naqada', in *The Followers of Horus: Studies dedicated to Michael Allen Hoffman* (Oxford: Oxbow Books), pp. 185–192.

Payne, J.C., A. Kaczmarczyk, and S.J. Fleming (1977), 'Forged Decoration on Predynastic Pots', in *Journal of Egyptian Archaeology*, pp. 5–12.

Petrie, W.M.F. (1899), 'Sequences in Prehistoric Remains', in *Journal of the Royal Anthropological Institute of Great Britain and Ireland* 29, pp. 295–301.

Petrie, W.M.F. (1900), *The Royal Tombs of the First Dynasty: Part I* (London: Egypt Exploration Fund).

Petrie, W.M.F. (1901a), *Diospolis Parva* (London: Egypt Exploration Fund).

Petrie, W.M.F. (1901b), *The Royal Tombs of the First Dynasty* (London: Egypt Exploration Fund).

Petrie, W.M.F. (1920), *Prehistoric Egypt* (London: British School of Archaeology in Egypt).

Petrie, W.M.F. (1921), *Corpus of Prehistoric Pottery and Palettes* (London: British School of Archaeology in Egypt).

Petrie, W.M.F., M.A. Murray, and H. Petrie (1953), *Ceremonial Slate Palettes: Corpus of Proto-Dynastic Pottery: Thirty Plates of Drawings* (London: British School of Egyptian Archaeology).

Petrie, W.M.F. and J.E. Quibell (1896), *Naqada and Ballas* (London: Quaritch).

Petrie, W.M.F., G.A. Wainwright, and A.H. Gardiner (1913), *Tarkhan I and Memphis V*, vol. 23 (London: School of Archaeology in Egypt).

Petrie, W.M.F., G.A. Wainwright, and EJ.H. Mackay (1912), *The Labyrinth Gerzeh and Mazghuneh* (London: School of Archaeology in Egypt).

Pietsch, T.J., J.M. Olley, and G.C. Nanson (2008), 'Fluvial Transport as a Natural Luminescence Sensitiser of Quartz', in *Quaternary Geochronology* 3.4, pp. 365–376.

Polikreti, K., C.T. Michael, and Y. Maniatis (2002), 'Authenticating Marble Sculpture with Thermoluminescence', in *Ancient TL* 20.1, pp. 11–18.

Pollard, M., C. Batt, B. Stern, and S.M.M. Young (2007), *Analytical Chemistry in Archaeology* (Cambridge: Cambridge University Press).

Prescott, J.R. and J.T. Hutton (1988), 'Cosmic Ray and Gamma Ray Dosimetry for TL and ESR', in *International Journal of Radiation Applications and Instrumentation. Part D. Nuclear Tracks and Radiation Measurements* 14.1-2, pp. 223–227.

Prescott, J.R. and J.T. Hutton (1994), 'Cosmic Ray Contributions to Dose Rates for Luminescence and ESR Dating: Large Depths and Long-term Time Variations', in *Radiation Measurements* 23.2, pp. 497–500.

Prescott, JR and LG Stephan (1982), 'The Contribution of Cosmic radiation to the environmental dose for thermoluminescence dating. Latitude, altitude and depth dependences', in *PACT: Second Specialist Seminar on Thermoluminesence Dating, Oxford, Research Laboratory for Archaeology and the History of Art, July 1980*, ed. V. Mejdahl and M.J. Aitken, vol. 6 (), pp. 17–25.

Preucel, R.W. (1999), 'Review of Evolutionary Archaeology: Theory and Application', in *Journal of Field Archaeology* 26, pp. 93–99.

Preusser, F., M.L. Chithambo, T. Götte, M. Martini, K. Ramseyer, E.J. Sendezera, G.J. Susino, and A.G. Wintle (2009), 'Quartz as a Natural Luminescence Dosimeter', in *Earth-Science Reviews* 97.1, pp. 184–214.

Preusser, F., D. Degering, M. Fuchs, A. Hilgers, A. Kadereit, N. Klasen, M. Krbetschek, D. Richter, and J.Q.G. Spencer (2008), 'Luminescence Dating: Basics, Methods and Applications', in *Quaternary Science Journal* 57.1-2, pp. 95–149.

Preusser, F. and H.U. Kasper (2001), 'Comparison of Dose Rate Determination Using High-resolution Gamma Spectrometry and Inductively Coupled Plasma–Mass Spectrometry', in *Ancient TL* 19.1, pp. 19–23.

Preusser, F., K. Ramseyer, and C. Schlüchter (2006), 'Characterisation of Low OSL Intensity Quartz from the New Zealand Alps', in *Radiation Measurements* 41.7, pp. 871–877.

Proctor, H.C. (1992), 'Sensory Exploitation and the Evolution of Male Mating Behaviour: A Cladistic Test Using Water Mites (Acari Parasitengona)', in *Animal Behaviour* 44.4, pp. 745–752.

Ramadan, A.B. and S.A. El-Mongy (2001), 'Overview of the Egyptian Radiation Monitoring Network and Radioactivity Levels of the Egyptian Territories', in *Assessment and Management of Environmental Risks: Proceedings of the NATO Advanced Research Workshop on Assessment and Management of Environmental Risks: Methods and Applications in Eastern European and Developing Countries Lisbon, Portugal October 1–4, 2000*, vol. 4, Nato Science Series (Dordrecht: Springer Netherlands), pp. 317–324.

Randall-MacIver, D, A.C. Mace, and F.L. Griffith (1902), *El Amrah and Abydos, 1899-1901* (London: The Egypt Exploration Fund).

Raue, D. (1999), 'Ägyptische und Nubische Keramik der 1–4 Dynastie', in Kaiser, W., F. Arnold, M. Bomma, T. Hikade, F. Hoffmann, H. Jaritz, P. Kopp, W. Niederberger, J.-P. Paetznick, C. von Pilgrim, B. von Pilgrim, D. Raue, T. Rzeiska, S. Schaten, A. Seiler, L. Stalder, and M. Ziermann, 'Stadt und Tempel von Elephantine 25/26/27 Grabungsbericht', in *Mitteilungen des Deutschen Archäologischen Instituts, Kairo* 55, pp. 173–189.

Redford, D.B. (1986), *Pharaonic King-Lists, Annals, and Day-Books: A Contribution to the Study of the Egyptian Sense of History* (Mississauga: Benben Publications).

Redmount, C.A. and M.E. Morgenstein (1996), 'Major and Trace Element Analysis of Modern Egyptian Pottery', in *Journal of Archaeological Science* 23.5, pp. 741–762.

Rees-Jones, J. (1995), 'Optical Dating of Young Sediments Using Fine-grain Quartz', in *Ancient TL* 13.2, pp. 9–14.

Regert, M., H.A. Bland, S.N. Dudd, P.F. van Bergen, and R.P. Evershed (1998), 'Free and Bound Fatty Acid Oxidation Products in Archaeological Ceramic Vessels', in *Proceedings of the Royal Society of London B: Biological Sciences* 265.1409, pp. 2027–2032.

Renfrew, C. and P. Bahn (2008), *Archaeology: Theories, Methods and Practice. Fifth Edition* (London: Thames and Hudson).

Rexová, K., D. Frynta, and J. Zrzavỳ (2003), 'Cladistic Analysis of Languages: Indo-European Classification Based on Lexicostatistical Data', in *Cladistics* 19.2, pp. 120–127.

Rhodes, Edward J (2011), 'Optically Stimulated Luminescence Dating of Sediments Over the Past 200,000 years', in *Annual Review of Earth and Planetary Sciences* 39, pp. 461–488.

Rhodes, E.J., C. Bronk Ramsey, Z. Outram, C. Batt, L. Willis, S. Dockrill, and J. Bond (2003), 'Bayesian Methods Applied to the Interpretation of Multiple OSL Dates: High Precision Sediment Ages from Old Scatness Broch Excavations, Shetland Isles', in *Quaternary Science Reviews* 22.10, pp. 1231–1244.

Rhodes, E.J., P. Fanning, Holdaway S., and Bolton C. (2009), 'Archaeological Surfaces in Western NSW: Stratigraphic Contexts and Preliminary OSL Dating of Hearths', in *New Directions in Archaeological Science*, ed. A. Fairbairn, S. O'Connor, and B. Marwick (Canberra: ANU press), pp. 189–202.

Ribechini, E., M.P. Colombini, G. Giachi, F. Modugno, and P. Pallecchi (2009), 'A Multi-Analytical Approach for the Characterization of Commodities in a Ceramic Jar from Antinoe)Egypt)', in *Archaeometry* 51.3, pp. 480–494.

Rice, P.M. (2005), *Pottery Analysis: A Sourcebook* (Chicago: The University of Chicago Press).

Richards, J. (2002), 'Text and Context in Late Old Kingdom Egypt: The Archaeology and Historiography of Weni the Elder', in *Journal of the American Research Center in Egypt* 39, pp. 75–102.

Riederer, J. (1978), 'Die Datierung Ägyptischer Bronzehohlgüsse mit Hilfe der Thermolumineszenz-Analyse', in *Studien zur Altägyptischen Kultur* 6, pp. 163–168.

Riso, TUD (2007), *Guide to "The Riso Single grain laser OSL system"*, tech. rep., Riso National Laboratory.

Rittenour, T.M. (2008), 'Luminescence Dating of Fluvial Deposits: Applications to Geomorphic, Palaeoseismic and Archaeological Research', in *Boreas* 37.4, pp. 613–635.

Roberts, R., M. Bird, J. Olley, R. Galbraith, E. Lawson, G. Laslett, H. Yoshida, R. Jones, R. Fullagar, G. Jacobsen, and Q. Hua (1998), 'Optical and Radiocarbon Dating at Jinmium Rock Shelter in Northern Australia', in *Nature* 393.6683, pp. 358–362.

Roberts, R.G. (1997), 'Luminescence Dating in Archaeology: From Origins to Optical', in *Radiation Measurements* 27.5, pp. 819–892.

Roberts, R.G., R.F. Galbraith, J.M. Olley, H. Yoshida, and G.M. Laslett (1999), 'Optical Dating of Single and Multiple Grains of Quartz from Jinmium Rock Shelter, Northern Australia: Part II, Results and Implications', in *Archaeometry* 41.2, pp. 365–395.

Robinson, P.M.W. and R.J. O'Hara (1996), 'Cladistic Analysis of an Old Norse Manuscript Tradition', in *Research in Humanities Computing* 4, pp. 115–137.

Romanus, K., J. Poblome, K. Verbeke, A. Luypaerts, P. Jacobs, D. De Vos, and M. Waelkens (2007), 'An Evaluation of Analytical and Interprative Methodologies for the Extraction and Identification of Lipds Associated with Pottery Sherds from the Site of Sagalassos', in *Archaeometry* 49.4, pp. 729–747.

Rowland, J.M. (2008), 'Building Bridges Between Radiocarbon, Relative and Historical Chronologies: The Case of Early Egypt', in *Chronology and Archaeology in Ancient*

Egypt (the Third Millennium B.C.) Ed. H. Vymazalová and M. Bárta (Prague: Czech Institute of Egyptology), pp. 10–22.

Ryholt, K. (2004), 'The Turin King-List', in *Ägypten und Levante* 14, pp. 135–155.

Sanderson, M.J. and M.J. Donoghue (1989), 'Patterns of Variation in Levels of Homoplasy', in *Evolution* 43, pp. 1781–1795.

Savage, S.H. (2001), 'Towards an AMS Radiocarbon Chronology of Predynastic Egyptian Ceramics', in *Radiocarbon* 43.3, pp. 1255–1278.

Sawakuchi, A.O., M.W. Blair, R. DeWitt, F.M. Faleiros, T. Hyppolito, and C.C.F. Guedes (2011), 'Thermal History Versus Sedimentary History: OSL Sensitivity of Quartz Grains Extracted from Rocks and Sediments', in *Quaternary Geochronology* 6.2, pp. 261–272.

Scharff, A. (1927), *Grundzüge der Ägyptischen Vorgeschichte* (Leipzig: JC Hinrichs).

Schultz, D.J. (1980), 'The Effect of Hydrofluoric Acid on Quartz Shape – Fourier Grain Shape Analysis', in *Journal of Sedimentary Research* 50.2, pp. 644–645.

Schvoerer, M., M.-C. Delavergne, and R. Chapoulie (1988), 'The Thermoluminescence (TL) of Egyptian Blue', in *International Journal of Radiation Applications and Instrumentation. Part D. Nuclear Tracks and Radiation Measurements* 14.1-2, pp. 321–327.

Scott, D.A., S. Warmlander, J. Mazurek, and S. Quirke (2009), 'Examination of Some Pigments, Grounds and Media from Egyptian Cartonnage Fragments in the Petrie Museum, University College London', in *Journal of Archaeological Science* 36.3, pp. 923–932.

Sekkina, M., M.A. El Fiki, S.A. Nossair, and N.R. Khalil (2003), 'Thermoluminescence Archaeological Dating of Pottery in the Egyptian Pyramids Zone', in *Ceramics-Silikaty* 47.3, pp. 94–99.

Serpico, M. and B. Stern (2011), 'The Contents of Jars in Hatshepsut's Foundation Deposit at Deir el-Bahri and their Significance for Trade', in *Under the Potter's Tree: Studies on Ancient Egypt Presented to Janine Bourriau on the Occasion of her 70th Birthday*, ed. D. Aston, B. Bader, C. Gallorini, P. Nicholson, and S. Buckingham (Leuven: Peeters), pp. 843–885.

Serpico, M. and R. White (1996), 'A Report on the Analysis of the Contents of a Cache of Jars from the Tomb of Djer', in *Aspects of Early Egypt*, ed. J. Spencer (London: British Museum Press), pp. 128–39.

Serpico, M. and R. White (2000), 'Appendix 9: Summary of the Results of Chemical Analysis of the Contents of Wavy-Handled Jars', in *Catalogue of the Predynastic Egyptian Collection in the Ashmolean Museum, with Addenda (Revised Edition)*, ed. J.C. Payne (Oxford: Griffith Institute), pp. 302–303.

Shaw, I., ed. (2000), *The Oxford History of Ancient Egypt.* (Oxford: Oxford University Press).

Shaw, I. and P. Nicholson (2002), *The British Museum Dictionary of Ancient Egypt* (London: The British Museum Press).

Shortland, A.J. (2000), 'When, How and Where-The Application of Science to Egyptology', in *Current Research in Egyptology 2000*, ed. A. Mcdonald and C. Riggs, vol. 909, British Archaeological Reports (Oxford: Archaeopress), pp. 91–95.

Shortland, A.J. (2013), 'An Introduction to Egyptian Historical Chronology', in *Radiocarbon and the Chronologies of Ancient Egypt*, ed. A.J. Shortland and C. Bronk Ramsey (Oxford: Oxbow Books), pp. 19–28.

Shortland, A.J. and C. Bronk Ramsey, eds. (2013), *Radiocarbon and the Chronologies of Ancient Egypt* (Oxford: Oxbow Books).

Smith, A.B. (1994), *Systematics and the Fossil Record: Documenting Evolutionary Patterns* (Oxford: Blackwell Scientific).

Smith, B.W., M.J. Aitken, E.J. Rhodes, P.D. Robinson, and D.M. Geldard (1986), 'Optical Dating: Methodological Aspects', in *Radiation Protection Dosimetry* 17.1-4, pp. 229–233.

Smythe, J.C. (2004), 'The Pottery from Operation 3/Tomb 1 at Helwan', in *Egypt at its Origins: Studies in Memory of Barbara Adams. Proceedings of the International Conference "Origin of the State. Predynastic and Early Dynastic Egypt", Kraków, 28th August–1st September 2002*, ed. S. Hendrickx, R.F. Friedman, K.M. Ciałowicz, and M. Chłodnicki, vol. 138, Orientalia Lovaniensia Analecta (Leuven: Peeters), pp. 317–335.

Smythe, J.C. (2008), 'New Results from a Second Storage Tomb at Helwan. Implications for the Naqada III Period in the Memphite Region', in *Egypt at its Origins 2: Proceedings of the Third International Conference "Origin of the State. Predynastic and Early Dynastic Egypt", Toulouse, France 5th–8th September, 2005*, ed. B. Midant-Reynes and Y. Tristant, vol. 172, Orientalia Lovaniensia Analecta (Leuven: Peeters), pp. 151–185.

Sroor, A., S.Y. Afifi, A.S. Abdel-Haleem, A.B. Salman, and M. Abdel-Sammad (2002), 'Environmental Pollutant Isotope Measurements and Natural Radioactivity Assessment for North Tushki Area, South Western Desert, Egypt', in *Applied Radiation and Isotopes* 57.3, pp. 427–436.

Stern, B., C. Heron, L. Corr, M. Serpico, and J. Bourriau (2003), 'Compositional variations in aged and heated Pistacia resin found in Late Bronze Age Canaanite amphorae and bowls from Amarna, Egypt', in *Archaeometry* 45, pp. 457–469.

Stern, B., C. Heron, M. Serpico, and J. Bourriau (2000), 'A Comparison of Methods for Establishing Fatty Acid Concentration Gradients Across Pot Sherds: A Case Study Using Late Bronze Age Canaanite Amphorae', in *Archaeometry* 42.2, pp. 399–414.

Stern, B., C. Heron, T. Tellefsen, and M. Serpico (2008), 'New Investigations into the Uluburun Resin Cargo', in *Journal of Archaeological Science* 35.8, pp. 2188–2203.

Suter, S.J. (1994), 'Cladistic Analysis of the LIving Cassiduloids (Echinoidea), and the Effects of Character Ordering and Successive Approximations Weighting', in *Zoological Journal of the Linnean Society* 112, pp. 363–387.

Swofford, D.L.. (2002), *PAUP*: Phylogenetic Analysis Using Parsimony (*and other methods). Version 4.* (Sunderland).

El-Taher, A. and A.G.E. Abbady (2012), 'Natural Radioactivity Levels and Associated Radiation Hazards in Nile River Sediments from Aswan to El-Minia, Upper Egypt', in *Indian Journal of Pure and Applied Physics* 50.4, pp. 224–230.

Tehrani, J. and M. Collard (2002), 'Investigating Cultural Evolution Through Biological Phylogenetic Analyses of Turkmen Textiles', in *Journal of Anthropological Archaeology* 21.4, pp. 443–463.

Tehrani, J.J. and M. Collard (2009), 'On the Relationship Between Interindividual Cultural Transmission and Population-level Cultural Diversity: A Case Study of Weaving in Iranian Tribal Populations', in *Evolution and Human Behavior* 30.4, pp. 286–300.

Tobia, S.K. and E.V. Sayre (1974), 'An Analytical Comparison of Various Egyptian Soils, Clays, Shales and Some Ancient Pottery by Neutron Activation', in *Recent Advances in Science and Technology of Materials* 3, pp. 99–128.

Uosif, M.A., S.A.M. Issa, K.Y. Abuel-Fadl, M.A.M. Taha, and A.M. Mostafa (2013), 'The Status of Natural Radioactivity and Heavy Metals Pollution on Soil at Assiut Zone in Central Upper Egypt', in *Radiation Protection and Environment* 36.1, pp. 20–26.

Uosif, M.A.M. (2007), 'Gamma-ray Spectroscopic Analysis of Selected Samples from Nile River Sediments in Upper Egypt', in *Radiation Protection Dosimetry* 123.2, pp. 215–220.

Van Den Brink, E.C.M. (1992), 'Corpus and Numerical Evaluation of the "Thinite" Potmarks', in *The Followers of Horus. Studies Dedicated to The Memory of Michael Allen Hoffman*, ed. R. Friedman and B. Adams (Oxford: Oxbow Books), pp. 265–296.

Van Den Brink, E.C.M. (1996), 'The Incised Serekh-Signs of Dynasties 0-1, Part I: Complete Vessels', in *Aspects of Early Egypt*, ed. J. Spencer (London: British Museum Press), pp. 140–58.

Van Den Brink, E.C.M. (2001), 'The Pottery-Incised Serekh-Signs of Dynasties 0-1 Part 11: Fragments and Additional Complete Vessels', in *Archéo-Nil* 11, pp. 23–100.

Vermeersch, P.M., E. Paulissen, P. van Peer, S. Stokes, C. Charlier, C. Stringer, and W. Lindsay (1998), 'A Middle Palaeolithic Burial of a Modern Human at Taramsa Hill, Egypt', in *Antiquity* 72.277, pp. 475–484.

Vogt, C., G. Bourgeois, M. Schvoerer, P. Gouin, M. Girard, and S. Thiébault (2002), 'Notes on some of the Abbasid amphorae of Istabl 'Antar-Fustat (Egypt)', in *Bulletin of the American Schools of Oriental Research*, pp. 65–80.

Vreeze, M. de (2016), ''A Strange Bird will Breed in the Delta Marsh': The Evolution of Tell el Yahudiya Juglets and the Role of Tell el-Dab'a as a Hybrid Zone', in *Vienna 2 – Ancient Egyptian Ceramics in the 21st Century*, ed. B. Bader, C.M. Knoblauch, and Köhler E.C., vol. 245, Orientalia Lovaniensia Analecta (Leuven: Peeters), pp. 155–177.

Walker, M. (2005), *Quaternary Dating Methods* (Chichester: Wiley).

Waters, M.R., S.L. Forman, T.A. Jennings, L.C. Nordt, S.G. Driese, J.M. Feinberg, J.L. Keene, J. Halligan, A. Lindquist, J. Pierson, C.T. Hallmark, M.B. Collins, and J.E. Wiederhold (2011), 'The Buttermilk Creek Complex and the Origins of Clovis at the Debra L. Friedkin Site, Texas', in *Science* 331.6024, pp. 1599–1603.

Whittle, A.W.R., F.M.A. Healy, and A. Bayliss (2011), *Gathering Time: Dating the Early Neolithic Enclosures of Southern Britain and Ireland* (Oxford: Oxbow Books).

Whittle, E.H. (1975), 'Thermoluminescent Dating of Egyptian Predynastic Pottery from Hemamieh and Qurna-Tarif', in *Archaeometry* 17.1, pp. 119–122.

Wiley, E.O., D. Siegel-Causey, D.R. Brooks, and V.A. Funk (1991), *The Complete Cladist: A Primer of Phylogenetic Procedures* (Kansas: The University of Kansas Museum of Natural History).

Wilkinson, E.M. (1974), 'Techniques of Data Analysis: Seriation Theory', in *Archaeo-Physika* 5, pp. 1–142.

Wilkinson, T.A.H. (1995), 'A new comparative chronology for the Predynastic-Early Dynastic transition', in *The Journal of the Ancient Chronology Forum* 7, pp. 5–26.

Wilkinson, T.A.H. (1999), *Early Dynastic Egypt* (Abingdon: Routledge).

Wilkinson, T.A.H. (2000), *Royal Annals of Ancient Egypt: The Palermo Stone and its Associated Fragments* (London: Routledge).

Wintle, A.G. (2008), 'Fifty Years of Luminescence Dating', in *Archaeometry* 50.2, pp. 276–312.

Wintle, A.G. and A.S. Murray (2006), 'A Review of Quartz Optically Stimulated Luminescence Characteristics and Their Relevance in Single-Aliquot Regeneration Dating Protocols', in *Radiation Measurements* 41.4, pp. 369–391.

Wintle, Ann G and AS Murray (1999), 'Luminescence Sensitivity Changes in Quartz', in *Radiation Measurements* 30.1, pp. 107–118.

Wodzińska, A. (2009), *A Manual of Egyptian Pottery – Volume 2: Naqada III–Middle Kingdom* (Boston: Ancient Egypt Research Associates).

Zimmerman, D.W. (1967), 'Thermoluminescence from Fine Grains from Ancient Pottery', in *Archaeometry* 10.1, pp. 26–28.

Zimmerman, D.W. (1971), 'Thermoluminescent Dating Using Fine Grains from Pottery', in *Archaeometry* 13.1, pp. 29–52.

Zink, A. (2013), 'A Coarse Bayesian Approach to Evaluate Luminescence Ages', in *Geochronometria* 40.2, pp. 90–100.

Zink, A. and E. Porto (2005), 'Luminescence Dating of the Tanagra Terracottas of the Louvre Collections', in *Geochronometria* 24.2, pp. 21–26.

Zink, A.J.C. (2002), 'Bayesian Approach Applied to Authenticity Testing by Luminescence', in *Archeologia e Calcolatori* 13, pp. 211–216.

Zink, A.J.C. (2015), 'Bayesian Analysis of Luminescence Measurements', in *Radiation Measurements* 81, pp. 71–77.

Zink, A.J.C., G.J. Susino, E. Porto, and T.N. Huffman (2012), 'Direct OSL Dating of Iron Age Pottery from South Africa: Preliminary Dosimetry Investigations', in *Quaternary Geochronology* 8, pp. 1–9.

Part VII

Appendices

Appendix A

ICP-MS analysis of the ceramic samples

During this project, an additional analytical method, inductively coupled plasma mass spectrometry (ICP-MS), which was a by-product of the OSL measurements, yielded interesting preliminary results, which, although not central to the original project design, still warrant brief disclosure, as they add to the goal of advocating a multidisciplinary approach to the study of Egyptian ceramics put forward in this thesis. The benefit of examining ICP-MS results on clay fabrics is that they can lend themselves to clay provenancing studies.

As is discussed in Section 5.3.3, the quantification of radioisotopes present in the ceramic fabric of the vessel being subjected to OSL dating is essential in order to accurately determine the internal dose rate and hence age of a vessel. Of specific importance to OSL dating is the determination of the quantities of uranium (U), thorium (Th), and potassium (K) present and this is generally achieved by inductively coupled plasma mass spectrometry (ICP-MS). ICP-MS is a method for determining the concentrations of a suite of trace elements within an inorganic sample, and detects elements down to parts per billion (and sometimes even parts per trillion) levels (Pollard et al. 2007: 195). Although ICP-MS analysis can use either laser ablation or solution analysis to introduce the sample into the plasma, solution analysis (preparation using acid digestion), is the most commonly employed (Pollard et al. 2007: 197), and was how the majority of ICP-MS analyses were carried out upon the samples presented in this thesis (a description of the ICP-MS preparation and sampling for work carried out during this project is given in Section 5.3.3). This analysis was carried out by the Department of Earth Sciences, University of Oxford. It should be noted that, in addition to ICP-MS, neutron activation analysis (NAA), x-ray diffraction (XRF), and, to a lesser extent, ICP-OES(AES) (optical emissions spectroscopy/atomic emission spectroscopy), can be used for quantifying elemental concentrations within a sample, but ICP-MS is now considered the industry standard and choice protocol for such work (Pollard et al. 2007: 195). Furthermore, on a

more practical level, the quantity of sample required for ICP-MS is significantly smaller than what is required for NAA, which is of pivotal importance when dealing with museum material.

Although ICP-MS analysis (or similar techniques such as neutron activation analysis (NAA) or x-ray diffraction (XRF)) has long been used as a clay provenancing tool in archaeology and in Egyptian archaeology (see discussion below), for the purpose of this project it was initially only to be used as an age calculation tool for OSL dating. In general, the quantity of material used for an ICP-MS sample in conjunction with a standard pottery OSL sample is sufficient to produce a comprehensive elemental analysis of the ceramic material. However, due to the incredibly small quantities of sample obtained for the MET, and the need to calibrate the ICP-MS machinery correctly in order to get the best precision for determining the quantities of U, Th and K, it was only possible to do a specific analysis of these three elements. As a result, a comprehensive elemental analysis was not achieved for the majority of samples.[63]

It was initially expected that the ICP-MS results would only contribute to the OSL data, owing to our inability to do a full elemental analysis. This was of course regrettable (but necessary) as a full elemental analysis of a large number of ceramic vessels would have led to a better understanding of the patterns of trace element concentrations found within the material, which in turn has the potential to shed light upon the origin of clay sources and thus the possible provenance of certain types, wares, and individual vessels. However, it was encouraging to see that even with only three elements quantified (one major/minor element (potassium) and two trace elements (uranium and thorium)), some patterns emerged within the data set presented here. Nonetheless, it is necessary to clearly state that these three elements can offer very limited insight into clay provenancing, particularly given that the presence of uranium can often be more indicative of ground water movement than provenance. In further studies, it would be necessary to focus upon characterisation of other occurring minor and trace elements within the samples, to assist in further discussing potential clay sources. In particular, minor elements examined in clay provenancing studies tend to be calcium, iron, potassium, titanium, magnesium, manganese, sodium, chromium, and nickel; and trace elements of interest

[63] This was not so much to do with lack of material as with the cost involved with specifically calibrating the machine to detect such small quantities in such small concentrations. It was already necessary to run two sets of samples, one looking solely at K and the other at both Th and U. They could not be run together based on the significant variation between the concentrations of these elements: for accurate concentration determination they had to be done separately. To have introduced additional elements into the analysis would have required far greater machine time than funding that was available for the project, and so it was decided to limit the elemental analysis to U, Th, and K as these were the three elements required to finalise the OSL dates. However, additional material solution is left over from these analyses which can be used in future studies to assess other informative trace elements within the samples (see below for further details).

include caesium, rubidium, vanadium, uranium, tantalum, scandium, lithium, gold, selenium, antimony, strontium, cobalt, and thorium (to name only the most common) (Rice 2005: 390; Kilikoglou et al. 1988). Any such study would be further strengthened by identifying a range of potential natural clay sources existing in the expected regions of production, should such information be available and obtainable (Kilikoglou et al. 1988).

The samples subjected to ICP-MS analysis in this project were those same samples subjected to OSL analysis, so ICP-MS values for ^{238}U, ^{232}Th, and ^{40}K are available for each of the samples from Bêt Khallaf, Turah, Abydos (Tomb of Djer), Naqada, and Ballas. As already discussed, the analyses were carried out by the Department of Earth Sciences, University of Oxford.[64] From a provenancing perspective, examination of the three elements obtained in this study is of limited usefulness.

Table A.1: ICP-MS data from Egyptian samples.

ID	U	Th	K	ID	U	Th	K
X4113	1.34	5.20	1.19	X5477	1.93	10.57	1.00
X4114	1.03	4.32	0.98	X5478	3.46	8.75	0.85
X4115	1.45	5.83	1.26	X5479	3.20	7.99	1.00
X4116	1.99	7.30	0.98	X5482	1.95	6.51	1.18
X4117	1.85	7.50	1.25	X5484	1.89	5.62	1.22
X5458	1.81	6.70	0.97	X5486	3.68	10.45	0.65
X5459	2.45	7.69	1.01	X5488	2.29	8.51	0.89
X5461	1.31	5.56	1.51	X5489	2.06	7.61	1.25
X5462	1.19	4.90	1.32	X5490	2.15	7.82	0.98
X5463	1.24	5.95	1.45	X4120	2.18	6.78	0.93
X5464	1.27	5.78	1.33	X5466	3.78	17.58	1.59
X5465	1.70	7.06	1.41	X5469	2.26	7.87	1.19
X5467	1.15	5.63	1.48	X5471	1.34	5.82	1.76
X5468	1.88	6.95	1.04	X5474	3.75	8.15	0.87
X5470	1.14	6.05	1.27	X5476	3.39	14.19	1.21
X5472	1.43	5.15	1.37	X5483	1.48	4.81	1.16
X5473	1.77	5.64	1.22	X5485	1.55	5.86	2.09
X5475	4.21	9.03	1.08	X5487	2.04	7.22	0.95

[64] It is necessary to note here again, that the samples X4112, X4118, X4119 and X5460 were analysed by a commercial company who were unable to complete additional analyses on the ceramic material as they were not confident in the results due to the small sample sizes.

Nevertheless, based on the observations of concentrations of U, Th, and K, it was possible to produce a hierarchical cluster analysis based on principle components (Figure A.1), which showed a relationship between the isotopic concentrations present in each sample and the visual clay analysis carried out for each sample, that is, that an observable correlation existed between clay types (as discussed in the captions for Figure A.1). Although these preliminary observations are interesting, it would be unwise to make any further statements regarding their potential implications for clay provenancing of Egyptian ceramics. Their main purpose here is to acknowledge that ICP-MS as a by-product of OSL analysis has the potential to also assist in the discussion of clay provenancing questions. In the future, when funding is obtained to complete an elemental analysis of these samples by further ICP-MS work, it will be fascinating to see what the results will enable us to say about this data set, and the results in turn will lend themselves to furthering the application of a multidisciplinary approach to the study of Egyptian ceramics.

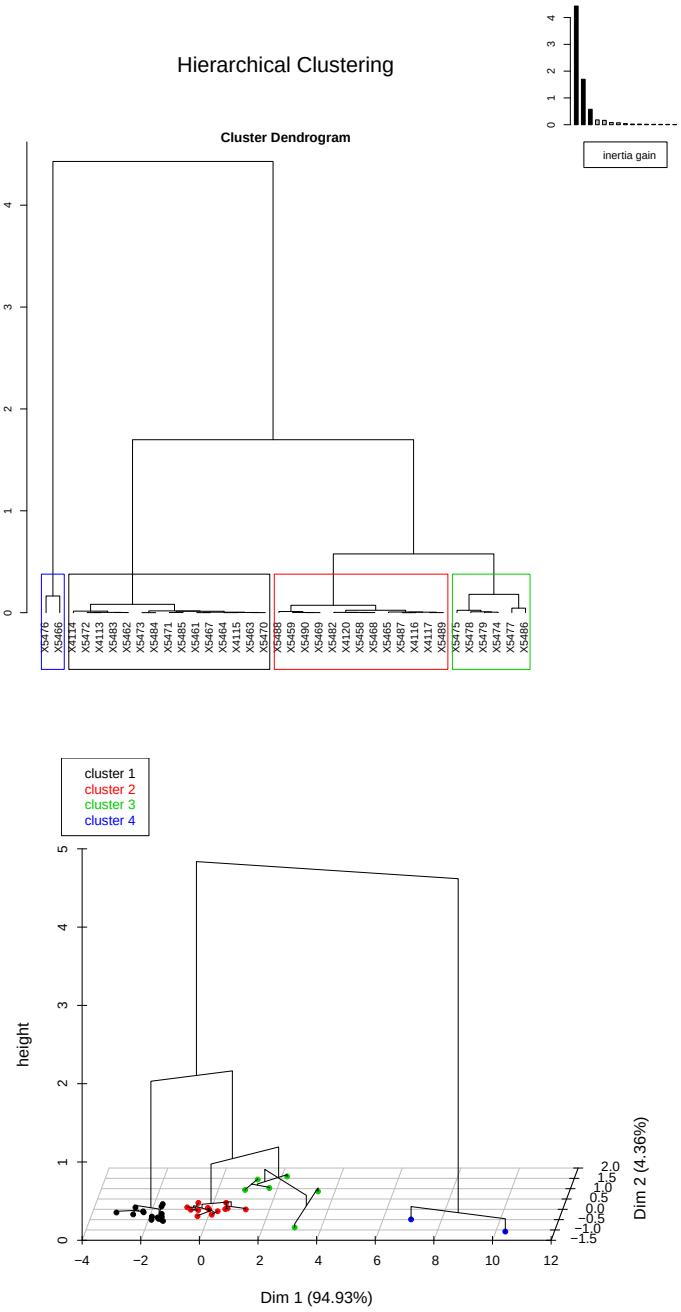

Figure A.1: Above: A dendrogram illustrating the results of the cluster analysis. Inset: A plot of the inertia gain as a function of the number of clusters. Below: A three-dimensional representation of the cluster analysis, illustrating how the clustering has interpreted the results of the principal component analysis. While, as discussed in the text, there is insufficient data to make any firm conclusions, it is interesting to note that cluster 1 is composed of medium to coarse Nile silt clays, cluster 2 is dominated by marl clays and fine Nile clays (primarily cylindrical vessels and wine jars), cluster 3 is made up of marl clays originating in Abydos and Wavy-Handled vessels, and cluster 4 is composed of the imported vessels at Abydos and the Islamic sherd.

Appendix B

GC-MS analysis of the pot contents

In addition to the chronological value of the ceramic samples found in the Tomb of Djer, it was also acknowledged that the samples taken for dating purposes could also be subjected to gas chromatography mass spectrometry analysis (GC-MS). Such analysis was possible because there was sufficient sample material available for GC-MS analysis, which remained after OSL sampling of the six vessels from the Ashmolean Museum yielding pot contents which were both organic and minerogenic in composition (presented in Chapter 9). GC-MS analysis would further the scope of the study of these vessels by providing an indication as to the contents of the vessels and thus the potential use of the vessel. It should of course be acknowledged that the contents of the vessels might not necessarily be the original contents of the vessels, since they may have been reused at some point. However, as discussed in Section 9.6, the radiocarbon date obtained for the material was consistent with the First Dynasty (see also Dee et al. 2016), so it is likely that either the contents still present were original to the vessel or were contemporary with the time of burial. The benefit of belonging to a multidisciplinary laboratory meant that, given the latter opportunity, we were able to seek the assistance of our colleagues to do some preliminary GC-MS analyses. However, funding was not available to conduct a full analysis of the material and this will have to wait for a future funding source. Nonetheless, preliminary findings have indicated that further research along these lines would be of significant interest and value, and are therefore presented here.

GC-MS is well known in Egyptian archaeology, and this technique has been applied previously to the study of pot contents/residues (e.g. McGovern 1997, Ribechini et al. 2009; Serpico and Stern 2011; Serpico and White 1996; Serpico and White 2000; Stern et al. 2000; Stern et al. 2003; Vogt et al. 2002), as well as to the study of both human and animal mummies (e.g. Buckley et al. 2004; Jones et al. 2014; Kuksis et al. 1978; Parsche and Nerlich 1995, Colombini et al. 2000), and a variety of other artefacts containing or-

ganic component such as cartonnage pigments (e.g. Scott et al. 2009), resins from the Uluburun shipwreck (Stern et al. 2008), embalming tars (e.g. Koller et al. 2003) to name but a select few. Indeed, of the six vessels presented within this study, five have previously been analysed by Serpico and White (Serpico and White 1996; Serpico and White 2000). Using GC-MS analysis, vessel AN1895.533 from Ballas was identified as containing lipid-based contents, possibly a mixture of oil and fat, whereas it was only possible to conclude that the contents were lipid-based for vessel 1895.525 (from Naqada), although this latter analysis was carried out using Fourier Transport Infrared Spectroscopy (FT-IR) analysis, not GC-MS (Serpico and White 2000). In 1996, Serpico and White carried out a series of GC-MS analyses upon 14 vessels from the Tomb of Djer, though only presenting finalised results for eight of these. Of these eight, three were also used in the study presented here: 1896–1908 E. 3158, 1896–1908 E. 4065, 1896–1908 E. 4066 (i.e. 1896–1908 E. 4034 was not analysed by the team). For 1896–1908 E. 3158, their analyses indicated that a vegetable oil was present in the contents. In contrast, 1896–1908 E. 4065 and E. 4066 seemed to exhibit signatures of an animal fat component.

The GC-MS aspect of this project was, as already stated, not in the original research design of this thesis and the GC-MS analysis was opportunistic as the material sampled for GC-MS analysis was the discarded material of the OSL sample. Although the Serpico and White data was available for five of the six vessels, after further discussion with GC-MS practitioners M. Woodworth and P. Ditchfield at the Research Laboratory for Archaeology and the History of Art (RLAHA), University of Oxford, it was felt that re-analysis of these samples using GC-MS could improve upon the original analyses of Serpico and White. However, our results at present remain preliminary as funding was not available to complete analyses and only preliminary data could be obtained from our collaborators at RLAHA. Initial GC-MS analysis was carried out by M. Woodworth and P. Ditchfield; however, as will be discussed below, initial analyses did not yield conclusive results and additional analyses have been suggested by Mr Woodworth and Dr Ditchfield in order to gain a more comprehensive understanding of the material present in these vessels. These additional analyses could not be carried out at RLAHA, and thus require additional financial resources which will be sought in the future. However, a preliminary report was still produced by Mr Woodworth.[65]

For the new analyses undertaken for this project, sample extraction was carried out at the Ashmolean Museum, Oxford, and samples were removed using a scalpel. All sample preparation and analysis were subsequently carried out at RLAHA. Each sample was twice solvent extracted using standard protocols used at RLAHA (based upon Mottram

[65] Section B is paraphrased from the original report from Mr Woodworth, which can be read in full in Hood et al. in press. The author would like to extend her sincere thanks to Mr Woodworth and Dr Ditchfield for carrying out these analyses and for producing this report.

et al. 1999). All samples

> 'were analysed by GC-MS using an Agilent 7820A gas chromatograph equipped with a Restek Rxi-5ms column (30 m length × 0.25 mm ID × 0.25 µm film thickness, 5% diphenyl/95% dimethylpolysiloxane stationary phase). The mass spectrometer was an Agilent 5975 quadropole, operated in electron ionization mode (70 eV) and the mass scan range was 40–650 m/z. The gas chromatograph conditions were as follows: inlet temperature 300℃, flow rate 1.2 ml/min, transfer line temperature 280℃. Helium was used as the carrier gas. The temperature program for the GC oven was a 50℃ hold for 2 minutes, 50–300℃ at 10℃/min with a 10-minute isothermal hold at 300℃. Injection was made by an Agilent 7693A autosampler and sample injection volume was 1 µl in splitless mode' (Hood et al. in press).

Of the six samples analysed, a single sample, AN1896–1908 E.4066, yielded only trace organic material, and GC-MS results were not forthcoming for this sample. The remaining samples all produced similar lipid profiles, with Figure B.1 providing a representative sample of this profile. These samples contained saturated fatty acids (with a chain length between 9 and 26 carbons), and were typified by a prevalence of C16:0 and, secondarily, C18:0. Trace amounts of C18:1 were the only unsaturated fatty acids observed. Additionally, the samples yielded a variety of α,ω-dicarboxylic acids ('diacids') with a chain length ranging between C4 and C11 for sample AN1895.525 and AN1895.533, and between C4 and C12 for samples AN1896–1908 E.3158 and AN1896–1908 E.4034. Glycerol was also present.

The profiles of the analysed samples present severely degraded lipids. Glycerol is present owing to the degradation of triglycerides to free fatty acids. That diacids are also present is suggestive of the cleavage of the double bond of unsaturated fatty acids, and is in keeping with the observation that only trace amounts of any unsaturated fatty acids (i.e. C18:1) were identified in the samples (Evershed et al. 1992). The presence of a significant quantity of C9 diacid is indicative of double bond fracturing at position 9, probably owing to the degradation of oleic acid (C18:1 n-9). That diacids and glycerol were observable in these samples is illustrative of the arid environment in which the samples were found as both are vulnerable to leaching in archaeological samples as they are highly water soluble. Indeed, high concentrations of diacids are infrequently seen in archaeological samples, except when recovered from depositional environments with favourable conditions such as highly arid environments (e.g. Barnard 2008; Regert et al. 1998; Colombini et al. 2005).

Woodward further concludes that

> 'these samples present a rare opportunity to study such highly degraded and environmentally fragile samples. The range of diacids present is in-

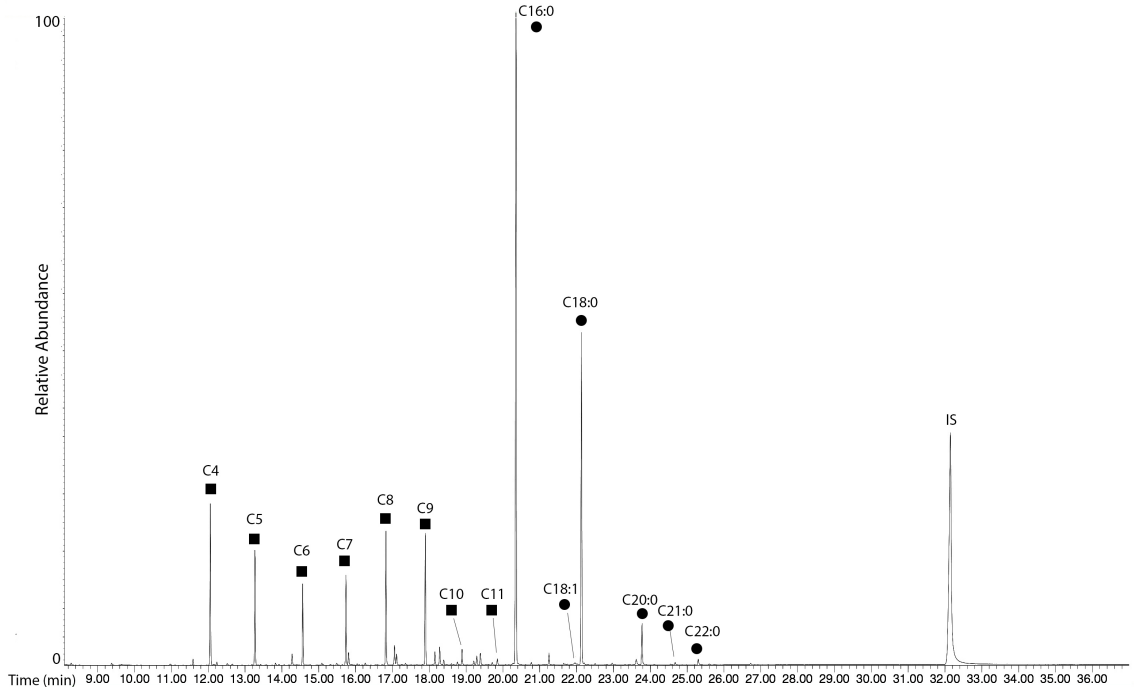

Figure B.1: Partial total ion chromatograph of sample AN1896–1908 E.4034, identifying primary analytes. Diacids are denoted by a square and identified by carbon number. Fatty acids are denoted by a circle and identified using the formula Cx:y (where x indicates the number of carbons and y indicates the number of double bonds). IS denotes the internal standard. Diacids and fatty acids are present as their trimethylsilyl esters (Hood et al. in press)

dicative of a range of unsaturated fatty acids with different double bond positions. The unsaturated fatty acids from which these degradation compounds formed would be expected to have had a wide variety of double bond positions due to fatty acids of different chain lengths and, possible, positional isomers. Diacids with a chain length of more than 10 carbons do not frequently occur in nature and are associated with plant waxes, although typically in association with long-chain waxes, which were not observed in these samples (Colombini et al. 2005). Odd chain-length fatty acids (C15:0 and C17:0) were observed in the samples in trace quantities. While such fatty acids have been associated with fats from ruminant animals, the quantities observed are at background levels and may be the result of depositional or post-depositional microbial contribution (Romanus et al. 2007). The presence of long-chain fatty acids (i.e. C20:0 and above) indicates a plant source for at least part of the lipid contribution. The ratio of C16:0 to C18:0 fatty acids is also consistent with a plant source (Kimpe et al. 2004). While preliminary analyses are yet unable to determine the specific origin of the residues unequivocally, it has provided an insight into some elements of the residue's composition as well as a starting point for further examination' (Hood et al. in press).

Although we must here reiterate that the samples are significantly degraded with respect to the lipids, which in turn makes it at present impossible to assign an origin of the lipid based upon their biomarkers (molecular compounds specific to an individual source), it has been suggested that a promising next step in the analysis of the contents of these six vessels is to carry out Gas Chromatography-Combustion-Isotope Ratio Mass Spectrometry (GC-C-IRMS) of C16:0 and C18:0 fatty acids for the 13C/12C ratios (M. Woodworth, Pers. Comm. 2016, cf. Evershed et al. 2002). GC-C-IRMS has previously been seen to be an effective proxy for establishing the origin of lipids, and its primary advantage is that the technique utilises the stable C16:0 and C18:0 components of the sample, which our samples have in abundance. This analysis can differentiate between terrestrial and marine sources, ruminants and non-ruminants, as well as C3 and C4 plants, and it is thought that this will be the best way forward for further analysis of these samples.

In conclusion, although preliminary analyses can offer insight into the components of the pot contents, they have not yet been able to offer any detailed information that might pertain to the origin of the vessels. In order to achieve this, it will be necessary to engage in GC-C-IRMS analysis. Through this further analysis, it is very probable that we will be able to identify broadly the contents of the vessels, at least to a family/genus level, if not species level. It is thought that by using GC-C-IRMS the original results obtained by Serpico and White (Serpico and White 1996; Serpico and White 2000) could be improved upon to shed further light upon this assemblage of vessels. We look forward to continuing to work on this project in the future.

Appendix C

Ceramic catalogue for the Bêt Khallaf material

It should be noted that the ceramics within the following catalogue have two identification codes: a museum code (accession number) and a laboratory code. All discussions within the text of this thesis, when referring to a specific ceramic piece, use the laboratory code as the main identifying number.

The 5 digit warecode designation follows that developed by Köhler (Köhler 1998; Köhler 2005).

Table C.1: Catalogue entry for X4113

Collection	Garstang Museum
Museum Code	E.4224
Lab. Code	X4113
Provenance	Bêt Khallaf Tomb K2*
Provenance History	
Excavated by John Garstang, 1901.	
Vessel/Object Description	
Height	3.8 cm
Rim Diameter	17 cm
Fracture is brown; medium-low density, medium Nile silt clay. Exterior and interior are rough smoothed with turning marks near rim.	
Warecode	21201
Munsell	7.5YR 5/4
Fabric Description	
Coarse limestone $\geq$ 2.5 mm (1)	
Fine limestone $\leq$ 0.8 mm (1)	
Coarse sand $\geq$ 1 mm (1)	
Fine sand $\leq$ 0.5 mm (1-2)	
Coarse chaff $\leq$ 2 cm (1-2)	
Fine chaff $\leq$ 0.5 mm (2)	
Grit $\leq$ 0.1 mm (3)	
Mica $\leq$ 0.2 mm (1–2)	
Publication Records	
Likely Garstang (1903: Pl. XXX, 5 or 6)	
Additional Notes	
* Although museum records are incomplete, based on the published information, it is likely this piece comes from Tomb K2 (i.e. based upon the ceramic types presented in Garstang's publication).	

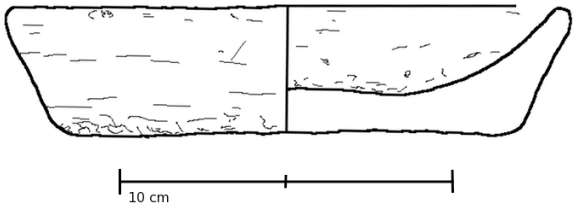

Table C.2: Catalogue entry for X4114

Collection	Garstang Museum
Museum Code	E.4228
Lab. Code	X4114
Provenance	Bêt Khallaf, Tomb K2*
Provenance History	
Excavated by John Garstang, 1901	
Vessel/Object Description	
Height	7.6 cm
Rim Diameter	20.5 cm
Fracture: reddy brown—black—reddy brown; low density, medium coarse Nile silt clay. Exterior and exterior surface rough-smoothed; turning marks around rim.	
Warecode	(1-2)1201
Munsell	Red Clay Body: 2.5YR 5/4-6 Clay Body: 5YR 5/4
Fabric Description	
Coarse limestone $\leq$ 5 mm (1)	
Fine limestone $\leq$ 1 mm (2-3)	
Coarse sand $\leq$ 4 mm (1-2)	
Fine sand $\leq$ 1 mm (2-3)	
Superfine sand $\leq$ 0.3 mm (2-3)	
Coarse chaff $\leq$ 1 cm (2)	
Fine chaff $\leq$ 5 mm (2)	
Grit $\leq$ 0.1 mm (2)	
Mica $\leq$ 0.1 mm (2)	
Publication Records	
Likely Garstang (1903: Pl. XXX, 13)	
Additional Notes	
* Although museum records are incomplete, based on the published information, it is likely this piece comes from Tomb K2 (i.e. based upon the ceramic types presented in Garstang's publication).	

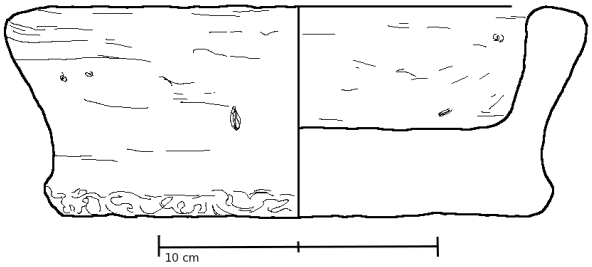

Table C.3: Catalogue entry for X4115

Collection	Garstang Museum
Museum Code	E.4610
Lab. Code	X4115
Provenance	Bêt Khallaf, Tomb K2*
Provenance History	
Excavated by John Garstang, 1901.	
Vessel/Object Description	
Height	6.5 cm
Rim Diameter	19.4 cm
No fracture details; low density, fairly coarse Nile silt clay. Exterior surface roughened; turning marks around rim. Interior surface rough-smoothed; turning marks around rim and base.	
Warecode	(1-2)1201
Munsell	7.5YR 5/3
Fabric Description	
Coarse limestone $\geq$ 7 mm (1)	
Fine limestone $\geq$ 0.8 mm (2)	
Coarse quartz $\geq$ 4 mm (1)	
Fine sand $\geq$ 0.3 mm (1-2)	
Sand $\geq$ 1 mm (1-2)	
Coarse chaff $\geq$ 2 mm (2)	
Grit $\geq$ 0.1 mm (2-3)	
Mica $\geq$ 0.1 mm (1)	
Publication Records	
Likely Garstang (1903: Pl. XXX, 4)	
Additional Notes	
* Although museum records are incomplete, based on the published information, it is likely this piece comes from Tomb K2 (i.e. based upon the ceramic types presented in Garstang's publication).	

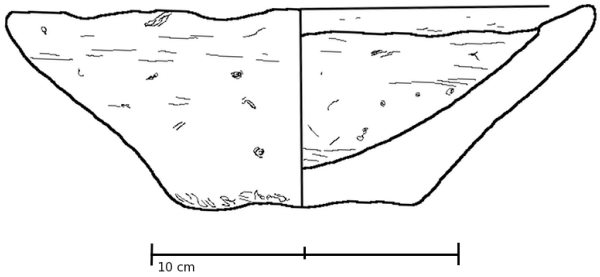

Table C.4: Catalogue entry for X4116

Collection	Garstang Museum
Museum Code	E.6103
Lab. Code	X4116
Provenance	Bêt Khallaf, Tomb K5*
Provenance History	
Excavated by John Garstang, 1901.	
Vessel/Object Description	
Height	43.1 cm
Rim Diameter	6.8 cm
Fracture is red—brown—red; medium-high density, medium marl clay. Exterior is wet smoothed, vertical scraping marks on body, applied band decoration turning marks on rim and neck. Interior is wet smoothed, turning marks near rim.	
Warecode	22201
Munsell	Red Clay Body: 10R 5/6-8 Yellow Clay Body: 10YR 6/4 White Clay Body: 10YR 7/3-4
Fabric Description	
Coarse limestone $\geq$ 2 mm (1–2)	
Fine limestone $\leq$ 0.8 mm (2)	
Coarse sand $\geq$ 0.6 mm (2)	
Fine sand $\leq$ 0.3 mm (2)	
Coarse chaff $\leq$ 1.5 cm (1)	
Fine chaff $\leq$ 0.5 mm (2)	
Grit $\leq$ 0.1 mm (2)	
Mica $\leq$ 0.1 mm (1)	
Publication Records	
Likely Garstang (1903: Pl. XXXI, 23)	
Additional Notes	
* Although museum records are incomplete, based on the published information, it is likely this piece comes from Tomb K5 (i.e. based upon the ceramic types presented in Garstang's publication).	

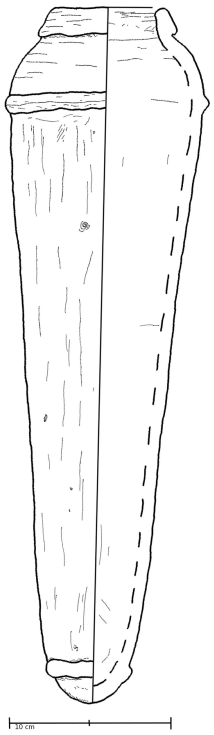

Table C.5: Catalogue entry for X4117

Collection	Garstang Museum
Museum Code	E.4079
Lab. Code	X4117
Provenance	Bêt Khallaf, Tomb K5*
Provenance History	
Excavated by John Garstang, 1901.	
Vessel/Object Description	
Height	49.6 cm
Rim Diameter	9.1 cm
Fracture unknown; medium-high density, medium marl clay. Exterior is wet smoothed, applied band decoration, vertical scraping marks on body, turning marks on rim and neck. Interior is wet smoothed, turning marks near rim.	
Warecode	22201
Munsell	Red Clay Body: 10R 5/4-6 Yellow Clay Body: 7.5YR 6/4
Fabric Description	
Coarse limestone $\geq$ 2 mm (1-2)	
Fine limestone $\leq$ 0.2 mm (2)	
Coarse sand $\geq$ 0.6 mm (1-2)	
Fine sand $\leq$ 0.3 mm (2)	
Chaff $\leq$ 5 mm (1)	
Large quartz $\leq$ 8 mm (1)	
Grit $\leq$ 0.1 mm (2)	
Mica $\leq$ 0.1 mm (2)	
Publication Records	
Likely Garstang (1903: Pl. XXXI, 24–26.	
Additional Notes	
* Although museum records are incomplete, based on the published information, it is likely this piece comes from Tomb K5 (i.e. based upon the ceramic types presented in Garstang's publication).	

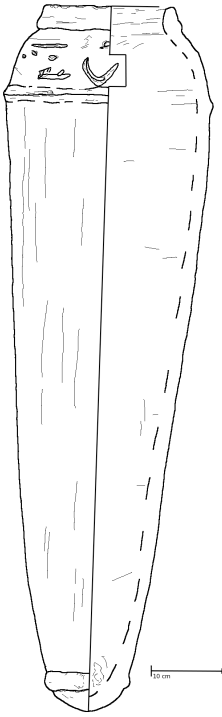

Table C.6: Catalogue entry for X4118

Collection	Garstang Museum
Museum Code	E.6445
Lab. Code	X4118
Provenance	Bêt Khallaf, Tomb K5.
Provenance History	
Excavated by John Garstang, 1901.	
Vessel/Object Description	
Height	32.3 cm
Rim Diameter	13.8 cm
Fracture: brown—red—black—red—brown; medium density, medium-coarse Nile silt clay. Exterior surface is very eroded, turning marks near both top and bottom rims. Interior is wet smoothed, turning marks near both top and bottom rims, roughened in between.	
Warecode	11201
Munsell	7.5YR 5/3-4
Fabric Description	
Coarse limestone $\leq$ 5 mm (1)	
Fine limestone $\leq$ 1 mm (2)	
Coarse sand $\leq$ 1.5 mm (1-2)	
Fine sand $\leq$ 0.8 mm (1-2)	
Coarse chaff $\leq$ 3 mm (2)	
Fine chaff $\leq$ 0.5 mm (3)	
Grit $\leq$ 0.1 mm (3)	
Mica $\leq$ 0.1 mm (1)	
Publication Records	
Garstang (1903: Pl. XXXI, 30)	
Additional Notes	
White painted/wash?	

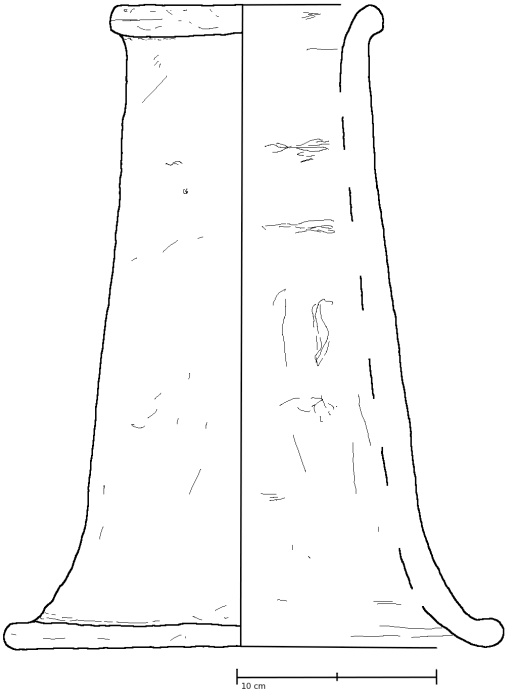

Table C.7: Catalogue entry for X4119

Collection	Garstang Museum
Museum Code	E.4260
Lab. Code	X4119
Provenance	Bêt Khallaf, Tomb K1.
Provenance History	
Excavated by John Garstang, 1901.	
Vessel/Object Description	
Height	28.8 cm
Rim Diameter	9.7 cm
Fracture: red—black—red; medium density, coarse-medium Nile silt clay. Exterior surface is quite eroded, possibly remains of red slip, turning marks on rim/neck, wet smoothed. Interior is wet smoothed, but very eroded.	
Warecode	(1-2)1201
Munsell	Clay Body: 5YR 4-3/2 Red Slip(?): 10R 4/4-6
Fabric Description	
Coarse limestone $\leq$ 3 mm (1)	
Fine limestone $\leq$ 0.8 mm (3)	
Coarse sand $\leq$ 4 mm (1-2)	
Fine sand $\leq$ 0.9 mm (2)	
Coarse chaff $\leq$ 3 mm (2)	
Fine chaff $\leq$ 1 mm (3)	
Grit $\leq$ 0.1 mm (2)	
Mica $\leq$ 0.1 mm (1)	
Publication Records	
Garstang (1903: Pl. XXX, 20)	
Additional Notes	
Similar vessel known from tomb of Djoser according to museum record cards.	

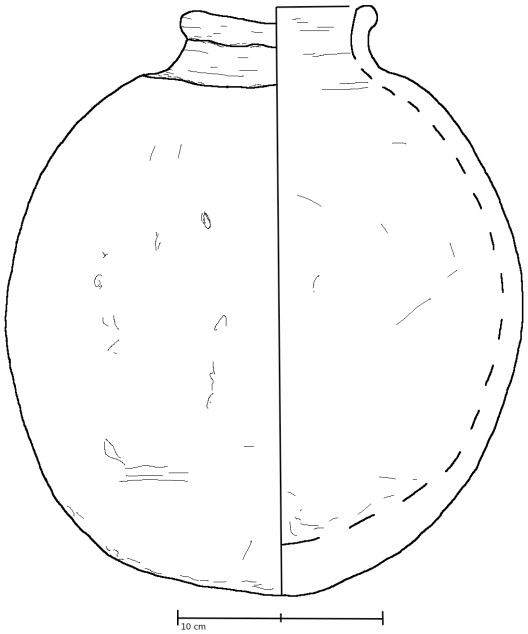

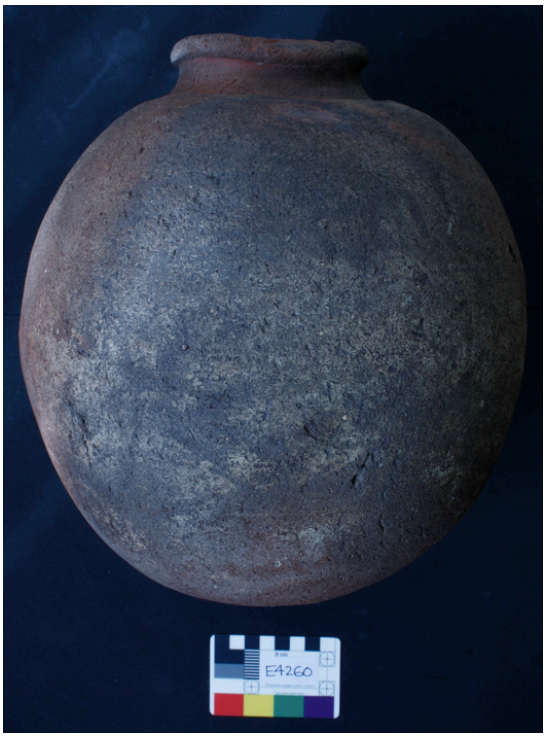

Table C.8: Catalogue entry for X4120

Collection	Garstang Museum
Museum Code	E.3080
Lab. Code	X4120
Provenance	Bêt Khallaf
Provenance History	
Excavated by John Garstang, 1901.	
Vessel/Object Description	
Height	11.2 cm
Rim Diameter	13.8 cm
No fracture details; medium-high density, fine marl clay. Exterior surface is smoothed, turning marks on neck, red slip at widest point of the vessel and on the rim. Interior smoothed with some turning marks.	
Warecode	32321
Munsell	Clay Body: 2.5YR 5-4/6 Red Slip: 10R 4/6
Fabric Description	
Coarse limestone $\leq$ 0.8 mm (1)	
Fine limestone $\leq$ 0.3 mm (1)	
Fine sand $\leq$ 0.2 mm (1)	
Coarse chaff $\leq$ 4 mm (1)	
Fine chaff $\leq$ 0.5 mm (2)	
Grit $\leq$ 0.1 mm (3)	
Mica $\leq$ 0.2 mm (1-2)	
Publication Records	
Additional Notes	
This piece does not appear in any of Garstang's publications. In the 1903 volume, Garstang specifically addresses 3rd, 5th and 6th ceramic forms, so it is likely that Garstang believed that this vessel was in a secondary context and did not include it in his final publication.	

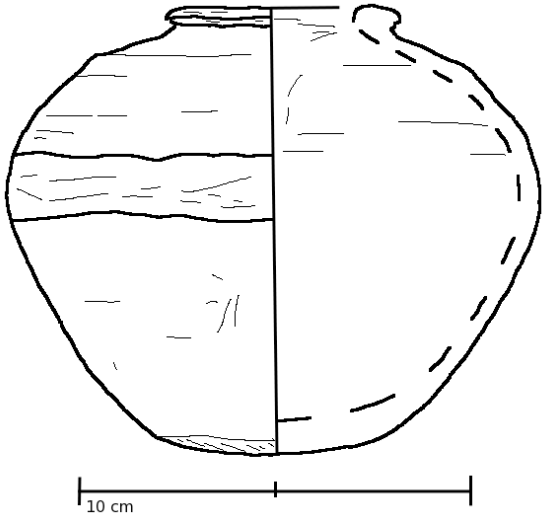

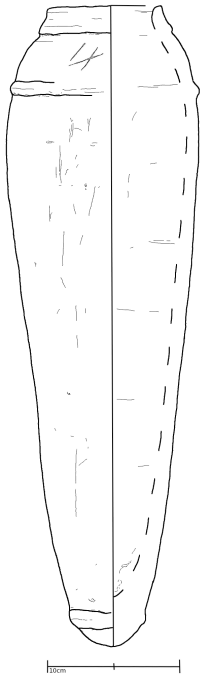

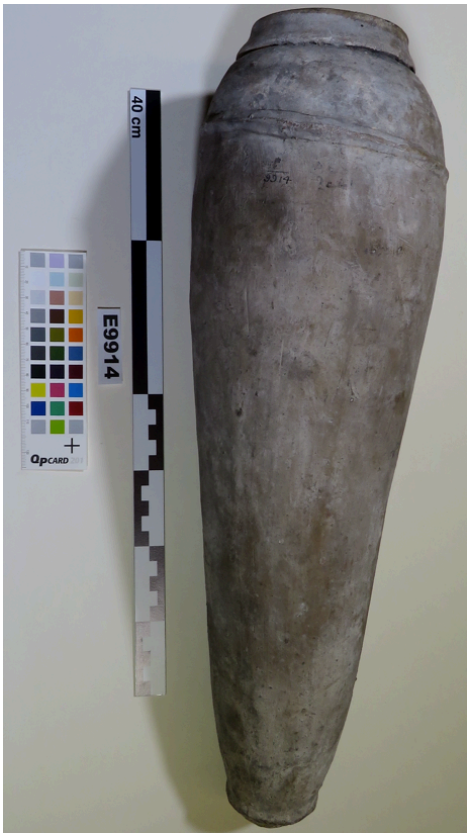

Table C.9: Catalogue entry for X5458

Collection	Penn Museum
Museum Code	E.9914
Lab. Code	X5458
Provenance	Bêt Khallaf, Tomb K1
Provenance History	
Excavated by John Garstang, 1901	
Vessel/Object Description	
Height	48.3 cm
Rim Diameter	8.7 cm
Fracture is unknown; medium density, medium marl clay. Exterior is wet smoothed, slightly scraped vertically, applied banded decoration. Pot mark on shoulder, turning marks around rim and shoulder. Some finger prints present on the body. Pot mark on shoulder. Interior is rough smoothed with wheel marks, and turning marks on rim.	
Warecode	22201
Munsell	5YR 5/2-3
Fabric Description	
Coarse limestone $\leq$ 5 mm (1)	
Limestone $\leq$ 1 mm (1)	
Fine limestone $\leq$ 0.2 mm (1)	
Sand $\geq$ 0.5 mm (1)	
Fine sand $\geq$ 0.2 mm (2)	
Chaff $\leq$ 1 mm (1)	
Grit $\leq$ 0.1 mm (2)	
Mica $\geq$ 0.1 mm (1)	
Publication Records	
Garstang (1903: Pl. XXXI, 22)	
Additional Notes	

Table C.10: Catalogue entry for X5459

Collection	Penn Museum
Museum Code	E.9915
Lab. Code	X5459
Provenance	Bêt Khallaf, Tomb K1*
Provenance History	
Excavated by John Garstang, 1901	
Vessel/Object Description	
Height	46.1 cm
Rim Diameter	8.2 cm
Fracture is unknown; high density, medium-coarse marl clay. Exterior is wet smoothed, slightly scraped vertically with several wet incised marks. Applied banded decoration. Pot mark on shoulder, turning marks around rim. Interior is wet smoothed with turning marks on rim and shoulder, and to around mid-way down the vessel. Very rough base.	
Warecode	22201
Munsell	5YR 5/3
Fabric Description	
Coarse limestone $\leq$ 4 mm (1)	
Limestone $\leq$ 1 mm (1)	
Fine limestone $\leq$ 0.2 mm (1)	
Sand $\geq$ 0.5 mm (1)	
Chaff $\leq$ 8 mm (2)	
Grit $\leq$ 0.1 mm (2)	
Publication Records	
Garstang (1903: Pl. XXXI, 21)*	
Additional Notes	
* Although Plate XXXI in Garstang (1903) only have two wine jars from Tomb K1 illustrated, both Penn and the Ashmolean state that their respective vessels are number 21 on Plate XXXI. It is likely therefore, that as was customary at this time, Garstang only drew a representative selection of vessels found. Cf. (X5469)	

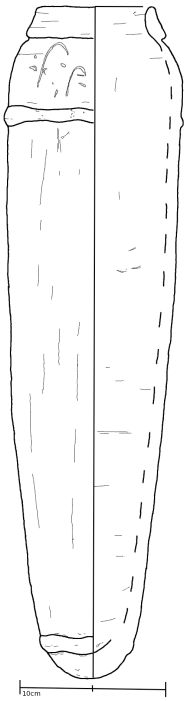

Table C.11: Catalogue entry for X5460

Collection	Penn Museum
Museum Code	E.9916
Lab. Code	X5460
Provenance	Bêt Khallaf, Tomb K2
Provenance History	
Excavated by John Garstang, 1901	
Vessel/Object Description	
Height	27.1 cm
Rim Diameter	10 cm
Fracture is brown—black—brown; low density, medium Nile silt clay. Exterior is wet smoothed, turning marks around rim and shoulder. Interior is wet smoothed with turning marks on shoulder.	
Warecode	21201
Munsell	2.5YR 5/4
Fabric Description	
Limestone $\leq$ 1 mm (1)	
Fine limestone $\leq$ 0.3 mm (1)	
Coarse sand $\geq$ 0.5 mm (2)	
Fine sand $\leq$ 0.1 mm (1)	
Chaff $\leq$ 1.5 mm (2)	
Fine chaff $\leq$ 1 mm (2)	
Grit $\leq$ 0.1 mm (2)	
Mica $\leq$ 0.1 mm (2)	
Publication Records	
Garstang (1903: Pl. XXX, 15)	
Additional Notes	

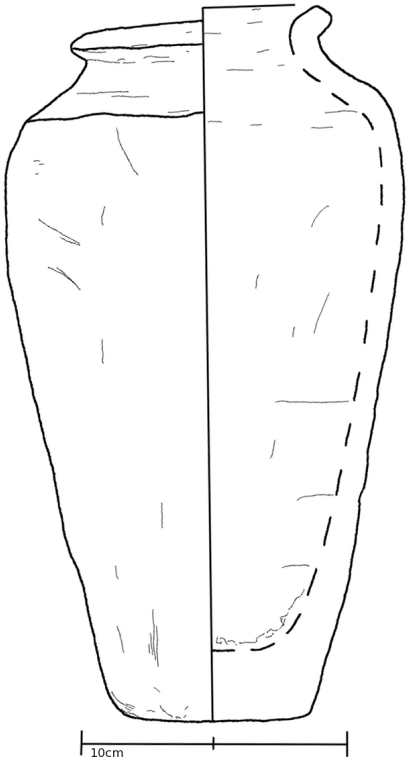

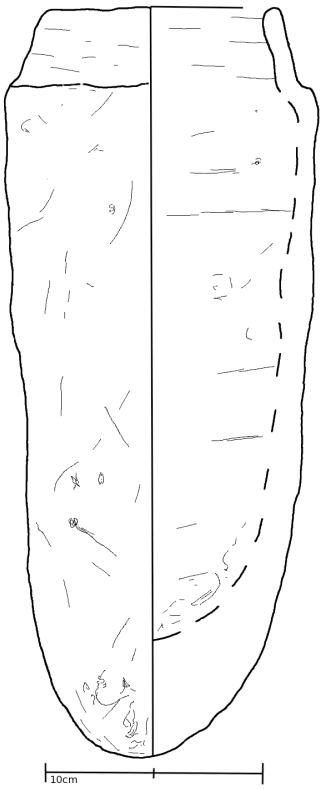

Table C.12: Catalogue entry for X5461

Collection	Penn Museum
Museum Code	E.9917
Lab. Code	X5461
Provenance	Bêt Khallaf, Tomb K2
Provenance History	
Excavated by John Garstang, 1901.	
Vessel/Object Description	
Height	34.5 cm
Rim Diameter	11.1 cm
Fracture is red-brown; low density, medium Nile silt clay. Exterior is roughly smoothed and lumpy from being hand worked, turning marks around rim. Interior is rough smoothed with heavy turning marks near rim.	
Warecode	21201
Munsell	5YR 5/3
Fabric Description	
Limestone $\leq$ 2 mm (1)	
Fine limestone $\leq$ 1 mm (1-2)	
Coarse sand $\geq$ 1.5 mm (2-3)	
Fine sand $\leq$ 0.2 mm (2-3)	
Chaff $\leq$ 1 cm (2)	
Fine chaff $\leq$ 4 mm (2)	
Grit $\leq$ 0.1 mm (2)	
Mica $\leq$ 0.1 mm (2)	
Publication Records	
Garstang (1903: Pl. XXXI, 33)	
Additional Notes	

Table C.13: Catalogue entry for X5462

Collection	Penn Museum
Museum Code	E.9919
Lab. Code	X5462
Provenance	Bêt Khallaf, Tomb K5
Provenance History	
Excavated by John Garstang, 1901	
Vessel/Object Description	
Height	24.4 cm
Rim Diameter	10.7 cm
Fracture is red—black—red; medium-low density, medium Nile silt clay. Exterior is roughly smoothed and lumpy from being hand worked, finger imprints around rim. Interior is rough smoothed with heavy turning marks.	
Warecode	21201
Munsell	10R 4/3-4
Fabric Description	
Limestone $\leq$ 2 mm (1)	
Fine limestone $\leq$ 0.5 mm (1)	
Coarse sand $\geq$ 1 mm (1-2)	
Fine sand $\leq$ 0.5 mm (2)	
Chaff $\leq$ 1 cm (2-3)	
Fine chaff $\leq$ 1 mm (2-3)	
Grit $\leq$ 0.1 mm (2)	
Mica $\leq$ 0.1 mm (2)	
Quartz $\leq$ 8 mm (1)	
Publication Records	
Garstang (1903: Pl. XXX, 10)	
Additional Notes	

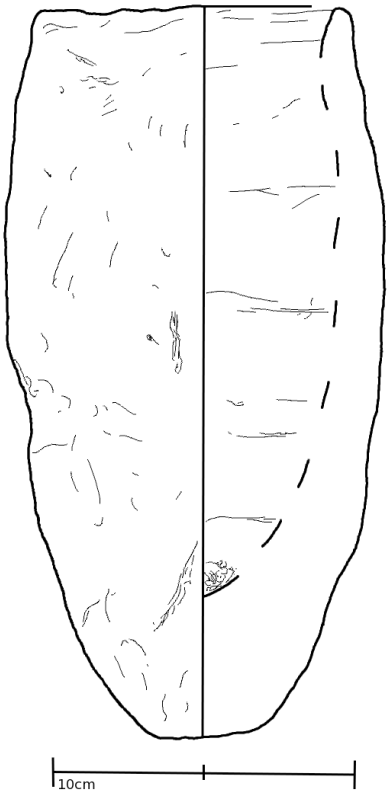

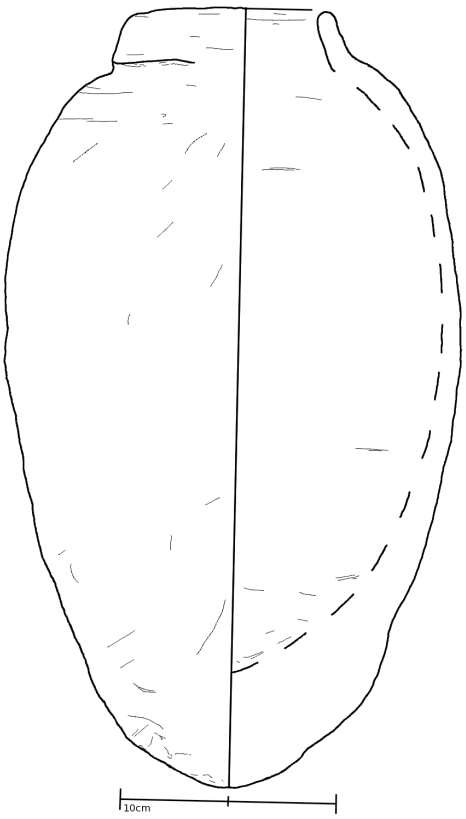

Table C.14: Catalogue entry for X5463

Collection	Penn Museum
Museum Code	E.9920
Lab. Code	X5463
Provenance	Bêt Khallaf, Tomb K2
Provenance History	
Excavated by John Garstang, 1901	
Vessel/Object Description	
Height	45.2 cm
Rim Diameter	10 cm
Fracture is red—grey-brown—red; medium density, medium Nile silt clay. Exterior is roughly smoothed, turning marks from rim to shoulder, very rough lower surface with finger impressions. Interior is wet smoothed with turning marks around rim. Made over hump?	
Warecode	21201
Munsell	Clay Body: 10R 5/8 Firing skin: 5YR 5/1-2
Fabric Description	
Limestone $\leq$ 1 mm (1)	
Coarse sand $\geq$ 1 mm (1-2)	
Fine sand $\leq$ 0.4 mm (2)	
Chaff $\leq$ 8 mm (2)	
Fine chaff $\leq$ 1 mm (2)	
Grit $\leq$ 0.1 mm (2)	
Mica $\leq$ 0.2 mm (2)	
Organic $\leq$ 0.5 mm (1)	
Large organic $\leq$ 1 mm (1)	
Publication Records	
Garstang (1903: Pl. XXXI, 31)	
Additional Notes	

Table C.15: Catalogue entry for X5464

Collection	Penn Museum
Museum Code	E.9921
Lab. Code	X5464
Provenance	Bêt Khallaf, Tomb K2
Provenance History	
Excavated by John Garstang, 1901	
Vessel/Object Description	
Height	9.1 cm
Rim Diameter	19.5 cm
Fracture unknown; medium density, medium Nile silt clay. Exterior is roughly smoothed, smoothing marks predominant around base, turning marks from rim to middle of the vessel. Interior is wet smoothed with working marks, heavy turning marks around the rim, internal rim looks like it has been hand moulded.	
Warecode	21201
Munsell	10R 5-4/6
Fabric Description	
Limestone $\leq$ 5 mm (1)	
Coarse sand $\geq$ 1 mm (1)	
Fine sand $\leq$ 0.5 mm (2)	
Chaff $\leq$ 5 mm (2)	
Fine chaff $\leq$ 1 mm (2-3)	
Grit $\leq$ 0.1 mm (2)	
Mica $\leq$ 0.2 mm (1)	
Organic $\leq$ 0.2 mm (1)	
Publication Records	
Garstang (1903: Pl. XXX, 3)	
Additional Notes	

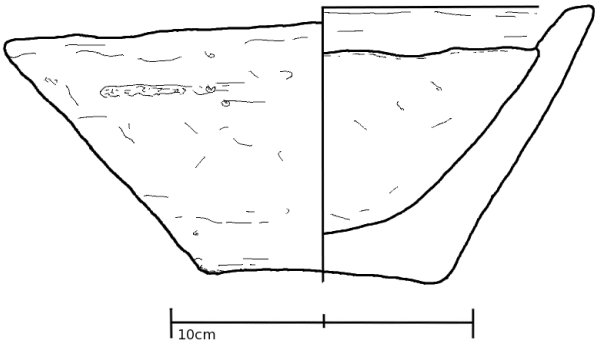

Table C.16: Catalogue entry for X5465

Collection	Ashmolean Museum
Museum Code	E.513
Lab. Code	X5465
Provenance	Bêt Khallaf, Tomb K2
Provenance History	
Excavated by John Garstang, 1901	
Vessel/Object Description	
Height	11.3 cm
Rim Diameter	17.5 cm
Fracture is brown—orange; medium density, medium Nile silt clay. Exterior is wet smoothed, turning marks around rim. Diagonal smoothing marks on body and base. Interior is same as exterior. Red slip on both interior and exterior.	
Warecode	21221
Munsell	Red Slip: 10R 5-4/6
Fabric Description	
Limestone $\leq$ 3 mm (1)	
Fine limestone $\leq$ 1.5 mm (2)	
Surface treatment makes fabric difficult to determine, but sand and chaff and grit present.	
Publication Records	
Garstang (1903: Pl. XXX, 7)	
Additional Notes	
Form 24 s in Petrie et al. 1953.	

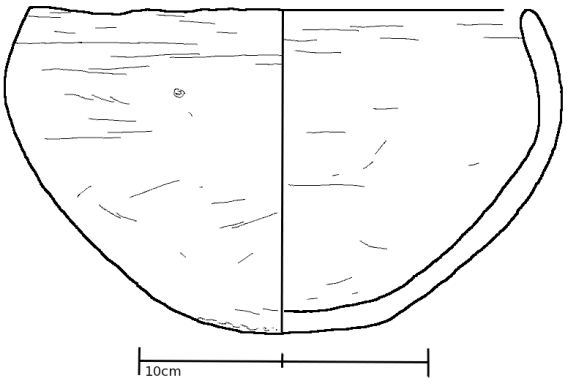

Table C.17: Catalogue entry for X5466

Collection	Ashmolean Museum
Museum Code	E.514
Lab. Code	X5466
Provenance	Bêt Khallaf, Tomb K2
Provenance History	
Excavated by John Garstang, 1901	
Vessel/Object Description	
Height	22.2 cm
Width	4.95 cm
Fracture is brown-red—dark brown; medium-high density, fine marl (?) clay. Fragment of a ceramic spoon. Ladle diameter c. 7-10 cm. Spoon interior is very well smoothed with turning marks. The handle is hand formed, wet smoothed, possibly polished. Possibly Aswan clay?	
Warecode	33201
Munsell	2.5YR 5/6-8
Fabric Description	
Sand $\leq$ 0.5 mm (1)	
Fine sand $\leq$ 0.2 mm (2)	
Chaff $\leq$ 0.5 mm (1)	
Limestone $\leq$ 1 mm (2-3)	
Mica $\leq$ 0.1 mm (2)	
Publication Records	
Additional Notes This piece does not appear in any of Garstang's publications. In the 1903 volume, Garstang specifically addresses 3rd, 5th and 6th ceramic forms, so it is likely that Garstang believed that this vessel was in a secondary context and did not include it in his final publication.	
Additional Notes	
Form 24 s in Petrie et al. 1953.	

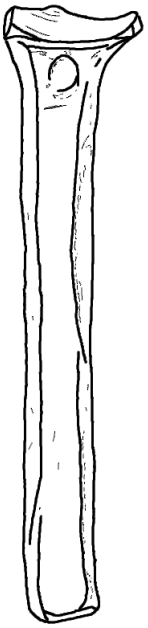

Table C.18: Catalogue entry for X5467

Collection	Ashmolean Museum
Museum Code	E.515
Lab. Code	X5467
Provenance	Bêt Khallaf, Tomb K5
Provenance History	
Excavated by John Garstang, 1901	
Vessel/Object Description	
Height	13.9 cm
Rim Diameter	16.5 cm
Fracture is unknown; medium density, medium-fine Nile silt clay. Exterior is wet smoothed, turning marks around rim. On main body to base vertical smoothing marks are present made by finger prints. Some black ash on base and on one side of the vessel. Interior is wet smoothed with turning marks near rim, but rough base. Red slip on both interior and exterior.	
Warecode	21221
Munsell	Red Slip: 10R 4/4 Clay Body: 7.5YR 6/4-6
Fabric Description	
Limestone $\leq$ 0.3 mm (2)	
Sand $\geq$ 0.3 mm (2)	
Chaff $\leq$ 1 cm (1)	
Fine chaff $\geq$ 1.5 mm (2)	
Grit $\leq$ 0.1 mm (2)	
Mica $\leq$ 0.1 mm (2)	
Fibres $\leq$ 0.5 mm (2)	
Publication Records	
Garstang (1903: Pl. XXX, 8)	
Additional Notes	

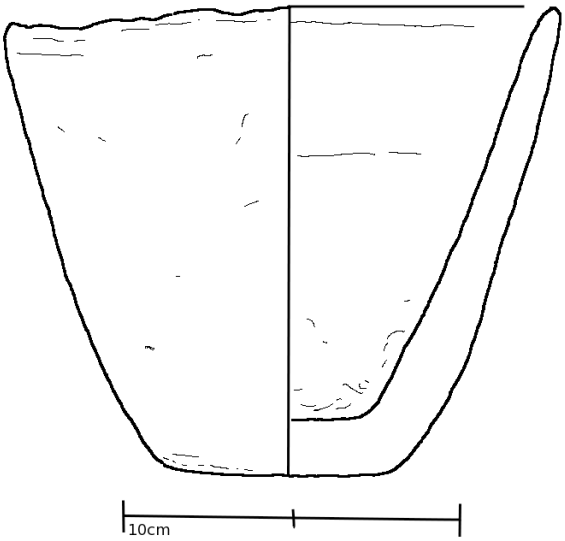

Table C.19: Catalogue entry for X5468

Collection	Ashmolean Museum
Museum Code	E.556
Lab. Code	X5468
Provenance	Bêt Khallaf, Tomb K3
Provenance History	
Excavated by John Garstang, 1901	
Vessel/Object Description	
Height	37 cm
Rim Diameter	10 cm
Fracture is unknown; medium-high density, medium-fine Nile silt clay (mixed?). Exterior is wet smoothed, white colour from rim to shoulder, with turning marks. Some fine diagonal scraping marks. Interior is wet smoothed with turning marks near rim.	
Warecode	((2-3)1201
Munsell	White body: 7.5YR 6/3-4 Clay Body: 2.5YR 5/6
Fabric Description	
Coarse limestone $\leq$ 1.5 mm (1)	
Limestone $\leq$ 1 mm (2)	
Fine limestone $\leq$ 0.5 mm (2)	
Sand $\geq$ 0.5 mm (3)	
Chaff $\leq$ 7 mm (1)	
Fine chaff $\geq$ 4 mm (2)	
Grit $\leq$ 1 mm (2)	
Publication Records	
Likely Garstang (1903: Pl. XXXI, 27)	
Additional Notes	
Form 81k in Brunton (1927).	

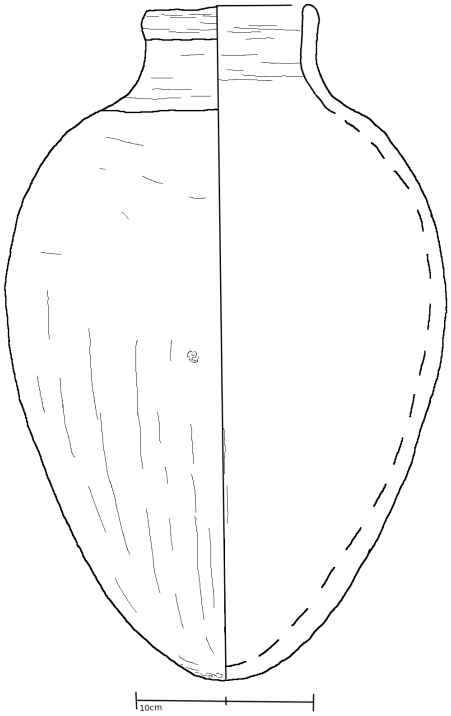

Table C.20: Catalogue entry for X5469

Collection	Ashmolean Museum
Museum Code	E.572
Lab. Code	X5469
Provenance	Bêt Khallaf, Tomb K1*
Provenance History	
Excavated by John Garstang, 1901	
Vessel/Object Description	
Height	40.5 cm
Rim Diameter	7 cm
Fracture is unknown; medium-high density, medium-fine marl silt clay. Exterior is wet smoothed with turning marks near rim. Applied band decoration. Interior is same as exterior (base fairly rough).	
Warecode	22201
Munsell	7.5YR 5/2-3
Fabric Description	
Coarse Limestone $\leq$ 4 mm (2)	
Limestone $\leq$ 1.5 mm (2)	
Fine limestone $\leq$ 0.5 mm (3)	
Grit $\leq$ 0.1 mm (1)	
Mica $\leq$ 0.1 mm (1)	
Sand and some chaff present as well.	
Publication Records	
Garstang (1903: Pl. XXXI, 21)*	
Additional Notes	
Although Plate XXXI in Garstang (1903) only have two wine jars from Tomb K1 illustrated, both Penn and the Ashmolean state that their respective vessels are number 21 on Plate XXXI. It is likely therefore, that as was customary at this time, Garstang only drew a representative selection of vessels found. Cf. (X5459) Form 76s in Petrie et al. 1953.	

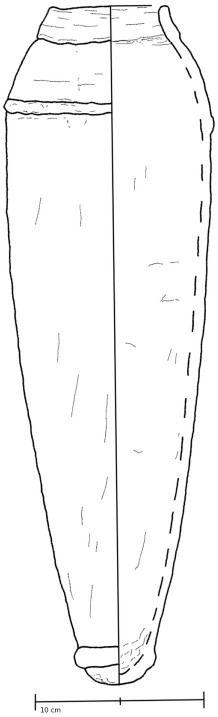

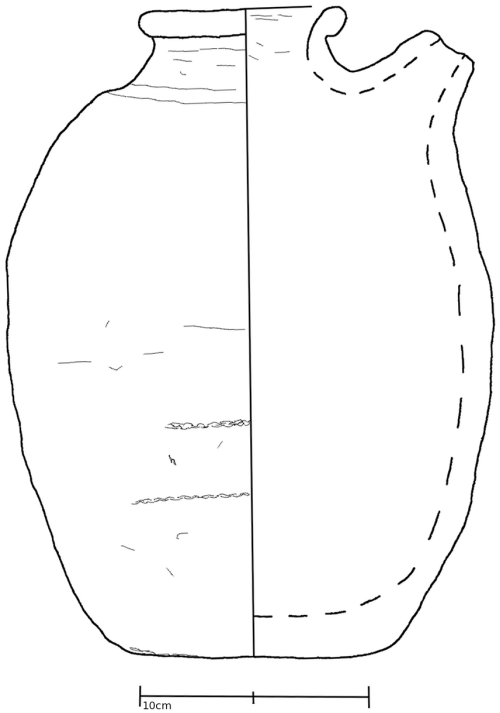

Table C.21: Catalogue entry for X5470

Collection	Ashmolean Museum
Museum Code	E.573
Lab. Code	X5470
Provenance	Bêt Khallaf, Tomb K2
Provenance History	
Excavated by John Garstang, 1901	
Vessel/Object Description	
Height	28.3 cm
Rim Diameter	9.1 cm
Fracture is brown-red—dark brown; medium-low density, medium-coarse Nile silt clay. Exterior is rough smoothed, with turning marks around rim. Firing skin/white was present on some areas. Remains of red slip. Formed spout. Interior is wet smoothed with turning marks around rim.	
Warecode	21222
Munsell	Clay Body: 7.5YR 5/6 Red Slip: 10R 5/6
Fabric Description	
Small rocks (quartz?) $\leq$ 4 mm (1)	
Sand $\leq$ 0.8 mm (2)	
Chaff $\leq$ 1 cm (1)	
Medium chaff $\leq$ 5 mm (3)	
Fine chaff $\leq$ 1 mm (3)	
Limestone $\leq$ 1 .1 mm (1)	
Mica $\leq$ 0.1 mm (1)	
Grit $\leq$ 0.1 mm (2)	
Shell $\leq$ 1 mm (3) – long angular white shards	
Publication Records	
Garstang (1903: Pl. XXX, 13)	
Additional Notes	
Form 99x in Petrie et al. 1953.	

Table C.22: Catalogue entry for X5471

Collection	Ashmolean Museum
Museum Code	E.4109
Lab. Code	X5471
Provenance	Bêt Khallaf, Tomb K2
Provenance History	
Excavated by John Garstang, 1901	
Vessel/Object Description	
Height	25.4 cm
Rim Diameter	8.7 cm
Fracture is brown—dark brown—red-brown—brown; low density, coarse-medium Nile silt clay. Exterior is rough smoothed, with turning marks around rim. Interior is wet smoothed with turning marks around rim, very rough base.	
Warecode	21201
Munsell	Clay Body: combination of 10R 4/6, 5YR 6/6, 10YR 7/3-4.
Fabric Description	
Large quartz $\leq$ 1 cm (1)	
Sand $\leq$ 1 mm (1)	
Fine sand $\leq$ 0.5 mm ()	
Chaff $\leq$ 1.5 cm (2)	
Fine chaff $\leq$ 2 mm (2)	
Limestone $\leq$ 1 mm (1)	
Mica $\leq$ 0.1 mm (2)	
Grit $\leq$ 0.1 mm (2)	
Publication Records	
Garstang (1903: Pl. XXX, 9)	
Additional Notes	

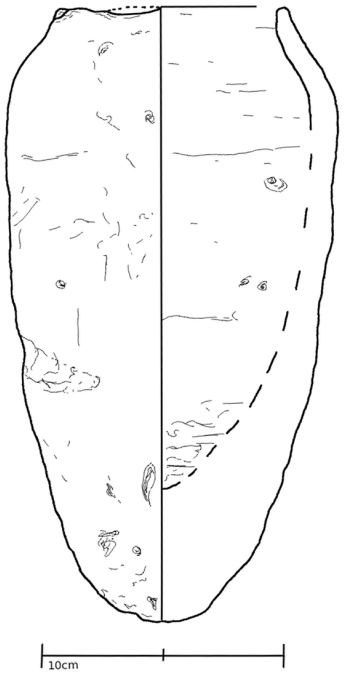

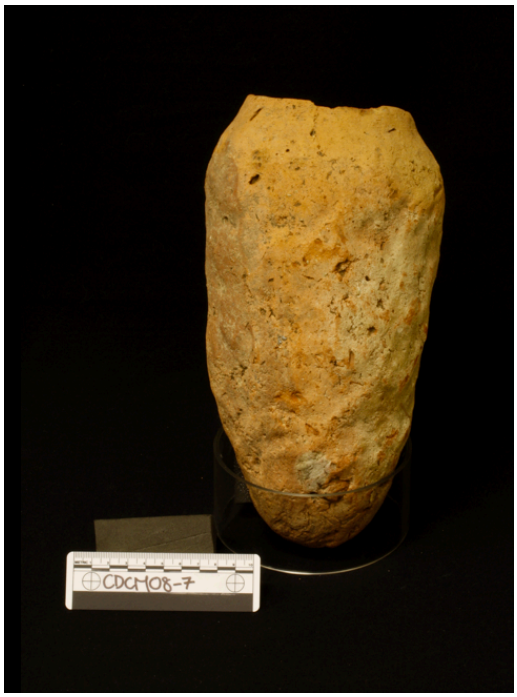

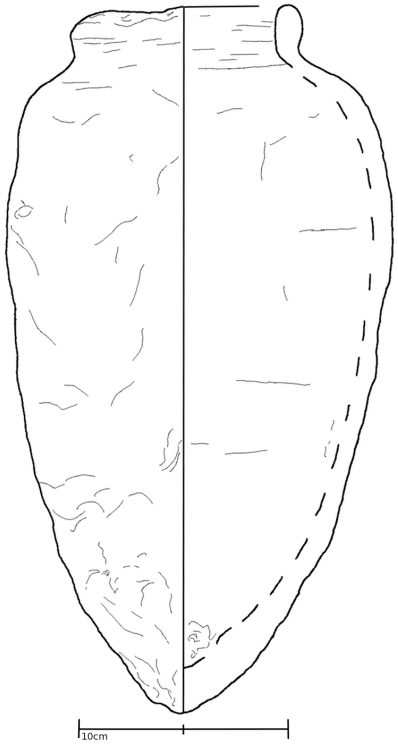

Table C.23: Catalogue entry for X5472

Collection	Ashmolean Museum
Museum Code	E.4110
Lab. Code	X5472
Provenance	Bêt Khallaf, Tomb K2
Provenance History	
Excavated by John Garstang, 1901	
Vessel/Object Description	
Height	c. 33.7 cm
Max Diameter	18.9 cm
Fracture is unknown; medium density, medium-coarse Nile silt clay. Exterior is rough smoothed with turning marks near rim. Interior is same as exterior.	
Warecode	21201
Munsell	7.5YR 6-5/4
Fabric Description	
Sand $\leq$ 0.5 mm (2-3)	
Fine chaff $\leq$ 2 mm (3)	
Chaff $\leq$ 1 cm (2-3)	
Limestone $\leq$ 1 mm (1)	
grit $\leq$ 0.2 mm (1)	
Publication Records	
Garstang (!903: Pl. XXXI, 34)	
Additional Notes	

Table C.24: Catalogue entry for X5473

Collection	Ashmolean Museum
Museum Code	E.4117
Lab. Code	X5473
Provenance	Bêt Khallaf, Tomb K2
Provenance History	
Excavated by John Garstang, 1901	
Vessel/Object Description	
Height	20.1 cm
Rim Diameter	20.3 cm
Fracture is red-brown—pink-brown—red-brown; low density, medium-coarse Nile silt clay. Exterior is rough smoothed, turning marks around rim and upper body. Interior is wet smoothed with turning marks around rim.	
Warecode	(1-2)1201
Munsell	Clay Body: 7.5YR 5/4 Unfired base: 10YR 3/1
Fabric Description	
Coarse sand $\leq$ 5 mm (1)	
Sand $\leq$ 2 mm (2)	
Fine sand $\leq$ 0.5 mm (2-3)	
Chaff $\leq$ 1 cm (1)	
Fine chaff $\leq$ 0.5 mm (3)	
Limestone $\leq$ 1 mm (2)	
Mica $\leq$ 0.1 mm (2)	
Grit $\leq$ 0.2 mm (2)	
Fibres $\leq$ 3 mm (1)	
Publication Records	
Garstang (1903: Pl. XXX, 17)	
Additional Notes	

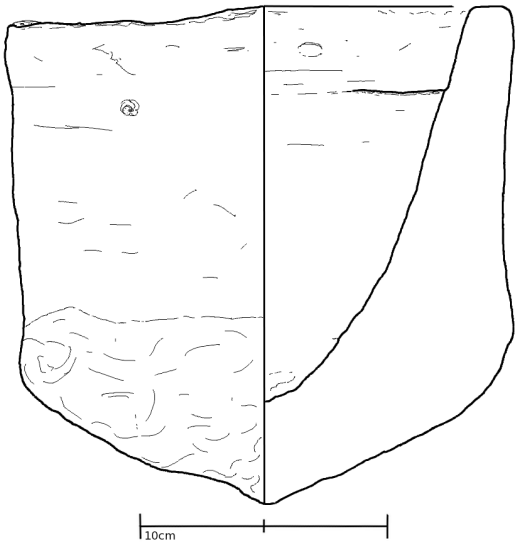

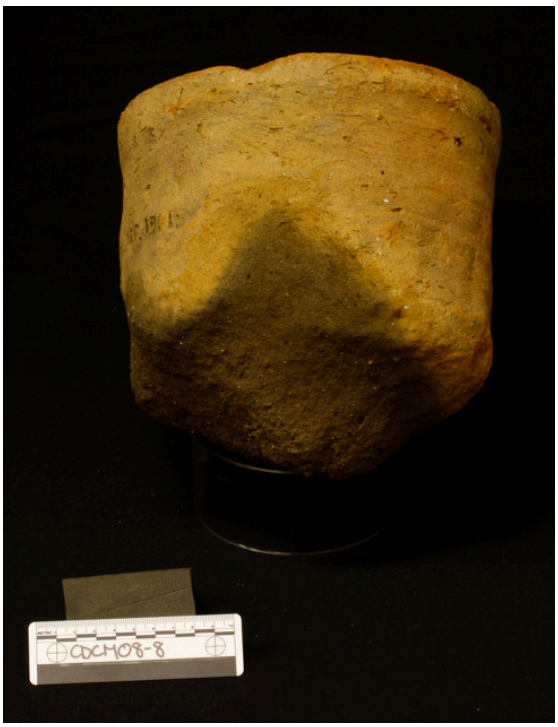

Appendix D

OSL aliquot data for the Bêt Khallaf ceramic assemblage

The following appendix presents the raw OSL data used to discuss the Bêt Khallaf OSL results presented in Chapter 5. For each sample, this appendix presents the following data:

1. A kernel density plot (KDE) (Galbraith and Roberts 2012: 9–11).[66] This plot illustrates the distribution of the aliquots which compose the final OSL equivalent dose measurement calculated using the central age model (CAM) (Galbraith and Roberts 2012: 15–16). The data displayed for coarse grains and fine grains are uncalibrated raw data, therefore the central age model figures presented in this Appendix need to be used in conjunction with Table 5.1.

2. A table presenting a detailed description of the measurements for each aliquot used in the calculation of the final OSL measurement for the sample and the rejection criteria used. This includes:

    a) D_e and D_e error– the palaeodose measurement and its corresponding error.

    b) Test dose error—a test dose is given to each aliquot after measurement of the natural and laboratory-induced luminescence signal (LN, L_1, L_2 etc). This test dose (TN, T_1, T_2 etc) allows the change in sensitivity of the quartz to be corrected for by examining the L_x/T_x ratio (e.g. Duller 2008: 11); Murray and Wintle 2000). The rejection criterion set for the test dose error is $\leq$ 20%.

    c) Recycling ratio—a repeat measurement is made on a selected dose step for each aliquot (usually 50s or 100s). This test checks that the SAR protocol is

[66] KDE plots in the appendix were made using the *R Shiny* Luminescence Package, available online: http://zerk.canopus.uberspace.de/R.Lum/

correcting for sensitivity changes in the aliquot by examining the ratio between the initial dose signal and its repeated dose step. Ideally, this ratio would be 1. However it is standard practice to allow for a 10% error on this ratio (i.e. 0.0 to 1.1) (e.g. Duller 2008: 11–12; Murray and Olley 2002: 3; Preusser et al. 2008: 112; Rhodes 2011: 472) For the samples in this thesis, we have in general adopted the standard $\leq$ 20% error on the recycling ratio. This is because the small number of aliquots available for each sample necessitates a larger degree of flexibility in the rejection criteria in order to ensure enough aliquots are available to determine a final age estimate. While the majority of aliquots adhered to standard rejection criteria percentages for most samples, in order to produce a more robust dataset for use alongside this first application of MET, the 10% rejection criteria limit was extended to 20% for the recycling ratio. This was a necessary compromise as it was not possible to increase the sample size extracted due to the unwillingness of museums to subject their vessels to larger-than-necessary sampling scars. As this is the first development of MET and its application to a large dataset, further experimentation would be required assess the effect on the precision of the D_e measurement of using a relaxed rejection criteria of 20% rather than 10% and to complement the experimental data presented in Figure 4.6 and Figure 4.7.

d) Recuperation—this occurs when a additional (and thus undesirable) luminescence signal is caused by any preheating that happens to the sample before measurement (Preusser et al. 2008: 112). To test whether this is occurring within a sample, a 0s dose step is given to the sample. The resulting signal measured should be zero, however usually a very small quantity of signal is still observed. The rejection criterion for the recuperation value is $\leq$ 5% (Murray and Olley 2002: 3; Murray and Wintle 2000).

e) IRSL/OSL ratio—in order to ensure that the OSL signal for each aliquot is not being contaminated with a feldspar signal component (feldspars also display luminescence properties although these vary greatly in character from quartz signals), it is necessary to examine the ratio between the IRSL (feldspar) and OSL (quartz) signal. Although no official standard rejection criteria exist for this ratio (Duller 2003), for the samples examined in the project, if a ratio of $\leq$ 15% was observed, the aliquot was accepted (i.e. the IRSL signal was $\leq$ 15% of the OSL signal). This was measured by dividing the IRSL signal by either the natural OSL signal or the signal from highest test dose, depending on

the individual sample.[67] Finally, a select number of fine grain aliquots were examined with an SEM to determine chemically whether a large quantity of the grains were in fact feldspars, in addition to quartz. Although only a small number of samples were screened (eight), using the SEM mapping feature it was observed that the vast majority of grains were quartz (∼90%) and the rest of the sample was composed of other minerals, including potassium feldspars, but also sodium and calcium feldspars (Figure A3.1). Therefore, the combination of an IRSL bleach prior to OSL measurement, incorporation of an IRSL/OSL ratio rejection criterion, in addition to confirmation of only a small quantity of feldspars being present renders our measurement protocol suitable for OSL dating of the quartz fraction.

3. OSL shine down curve—this graph is taken from a representative aliquot of the sample being measured. It shows the decay of the luminescence signal throughout laboratory stimulation. Graphs plotted using Analyst (Duller 1999).

4. OSL dose response curve—this graph is taken from a representative aliquot of the sample being measured. It shows the natural luminescence signal observed (red line), when plotted against the regenerative dose curve composed of a series of laboratory induced doses. Graphs plotted using Analyst (Duller 1999).

5. CAM (central age model) table—this table displays the final D_e used to calculate the age of a sample. This is calculated using the central age model (Galbraith and Roberts 2012) from the aliquots from each sample (i.e. after all rejection criteria were met). This table also presents the overdispersion (OD) values, and corresponding error, associated with the CAM determination, allowing an assessment of the statistical variability of the aliquot distribution to be made.

NB All aliquot data units presented in this appendix are in seconds (s). For final age calculations presented in Chapter 5, these units have been converted into the standard international unit for absorbed radiation, grays (Gy). The conversion of seconds to grays is achieved by multiplying the central dose (s) by the calibrated machine (Gy/s)—this gives the final D_e measurement in Gy.

NB In this appendix coarse grain (CG) data is denoted in black ink, whereas fine grain (FG) data is denoted by red ink.

[67] It is likely that, for every aliquot measured in this project, any IRSL signal present would have been removed by IR stimulation being carried out before measuring the OSL signal during each SAR cycle (i.e. a post-IR blue measurement was used) (cf. Mauz and Lang 2004).

Table D.1: OSL data for Sample X4113 – Coarse Grain and Fine Grain

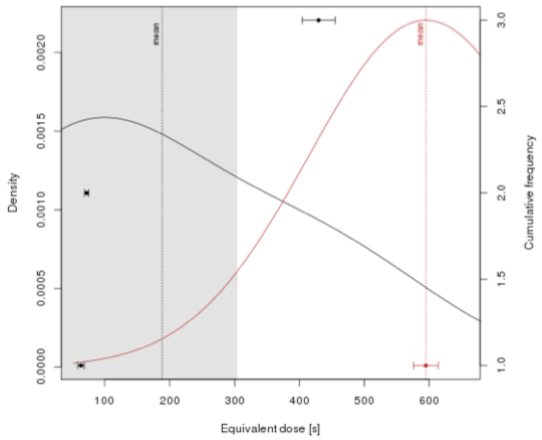

Figure D.1: Kernel Density Estimate Plot for Sample X4113

D_e (s)	D_e error (s)	Test Dose Error (%)	Recycling Ratio	Recup. (%)	IRSL/ OSL ratio (%)
72.31	6.64 (≤10%)	≤10	1.25±0.14 (12%)	3.3±1.5	6
63.56	10.14 (16%)	≤10	1.27±0.21 (≤10%)	8.9±3.7	2
429.58	50.64 (12%)	≤10	0.80±0.20 (≤10%)	3.0±2.2	3
594.83	37.95 (≤10%)	≤10	1.17±0.19 (≤10%)	0.4±0.7	2

Figure D.2: Primary Dataset for KDE plot for X4113. NB primary data set is comprised of 3 aliquots selected from a total of 9 aliquots (coarse grains) and 1 out of 6 aliquots (fine grains) after selection criteria were met.

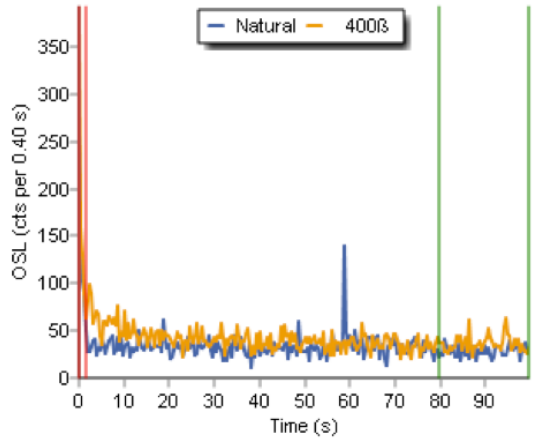

Figure D.3: OSL shine down curve for a representative aliquot of X4113

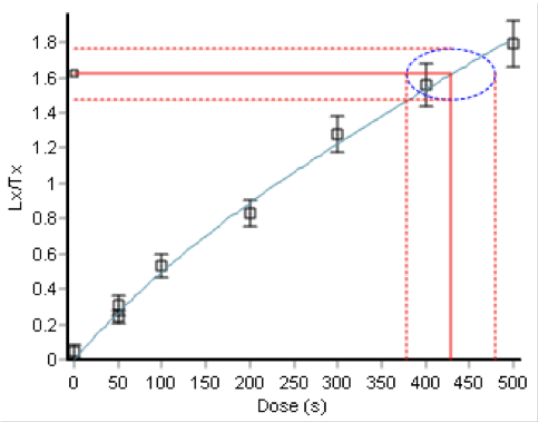

Figure D.4: OSL dose response curve for a representative aliquot of X4113

Figure D.5: Final OSL measurement (based on the CAM) and over dispersion value for X4113. Calibrated machine dose rates (Gy/s): 0.03849789 (CG), 0.03739700 (FG).

Central dose (s)	Central Dose Error (s)	OD (%)	OD error (%)
125.71	63.32	86.33	33.44
594.83	37.95	N/A	N/A

Table D.2: OSL data for Sample X4114 – Coarse Grain (No fine grain material was retrieved for this sample)

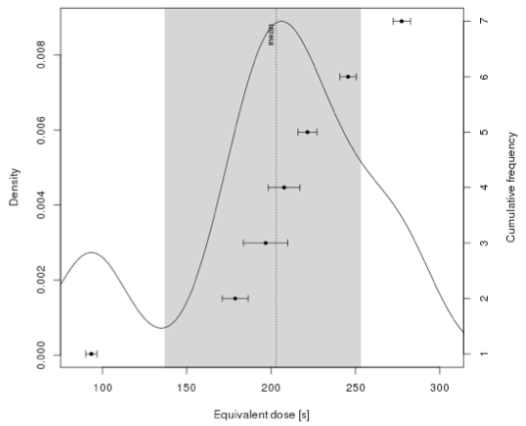

Figure D.6: Kernel Density Estimate Plot for Sample X4114

D_e (s)	D_e error (s)	Test Dose Error (%)	Recycling Ratio	Recup. (%)	IRSL/ OSL ratio (%)
93.42	6.65 (≤10%)	≤10	1.08±0.09 (≤10%)	5.1±1.2	2
207.80	18.90 (≤10%)	≤10	0.99±0.15 (≤10%)	5.2±1.6	3
277.41	10.22 (≤10%)	≤10	1.12±0.04 (≤10%)	0.6±0.0	≤1
245.63	9.79 (≤10%)	≤10	1.04±0.04 (≤10%)	0.5±0.1	2
221.61	11.35 (≤10%)	≤10	1.06±0.10 (≤10%)	2.3±0.4	4
196.83	26.28 (13%)	≤10	0.95±0.26 (≤10%)	3.4±2.8	3
178.81	15.42 (≤10%)	≤10	1.25±0.15 (≤10%)	3.1±0.9	2

Figure D.7: Primary Dataset for KDE plot for X4114. NB Primary data set is comprised of 7 aliquots (selected from a total of 7 aliquots after selection criteria were met).

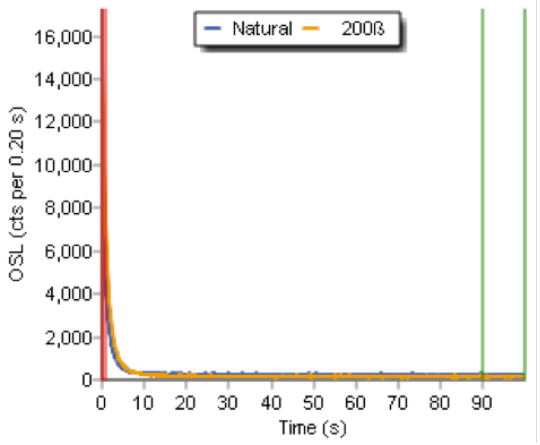

Figure D.8: OSL shine down curve for a representative aliquot of X4114

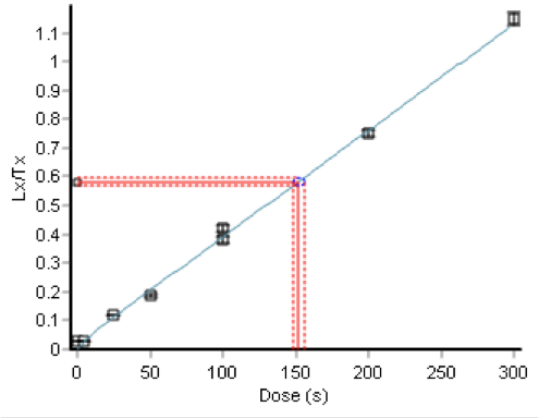

Figure D.9: OSL dose response curve for a representative aliquot of X4114

Figure D.10: Final OSL measurement (based on the CAM) and over dispersion value for X4114. Calibrated machine dose rates (Gy/s): 0.03842184 (CG).

Central dose (s)	Central Dose Error (s)	OD (%)	OD error (%)
194.45	24.44	32.32	5.19

Table D.3: OSL data for Sample X4115 – Coarse Grain and Fine Grain

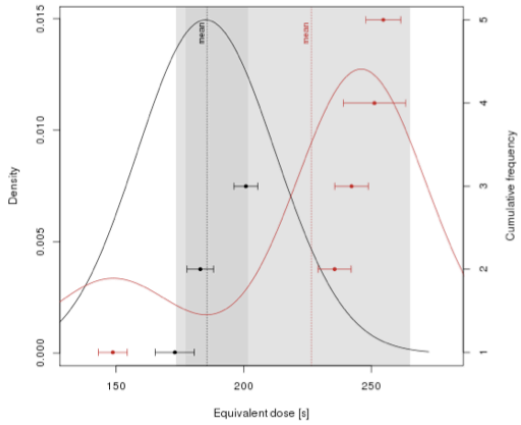

Figure D.11: Kernel Density Estimate Plot for Sample X4115

D_e (s)	D_e error (s)	Test Dose Error (%)	Recycling Ratio	Recup. (%)	IRSL/OSL ratio (%)
172.98	15.33 (≤10%)	≤10	0.98±0.10 (≤10%)	1.2±0.5	5
182.93	10.34 (≤10%)	≤10	1.21±0.08 (≤10%)	0.1±0.1	≤1
200.79	9.36 (≤10%)	≤10	1.12±0.06 (≤10%)	0.3±0.1	≤1
254.62	13.66 (≤10%)	≤10	1.02±0.09 (≤10%)	1.4±0.5	6
251.17	24.32 (≤10%)	≤10	1.16±0.19 (≤10%)	-1.3±-1.0	14
242.15	13.19 (≤10%)	≤10	1.06±0.10 (≤10%)	0.2±0.5	5
235.53	12.98 (≤10%)	≤10	1.07±0.09 (≤10%)	0.7±0.5	2
148.68	11.30 (≤10%)	≤10	1.03±0.12 (≤10%)	1.3±1.2	10

Figure D.12: Primary Dataset for KDE plot for X4115. NB Primary data set is comprised of 3 aliquots selected from a total of 7 aliquots (coarse grains) and 5 out of 5 aliquots (fine grains) after selection criteria were met.

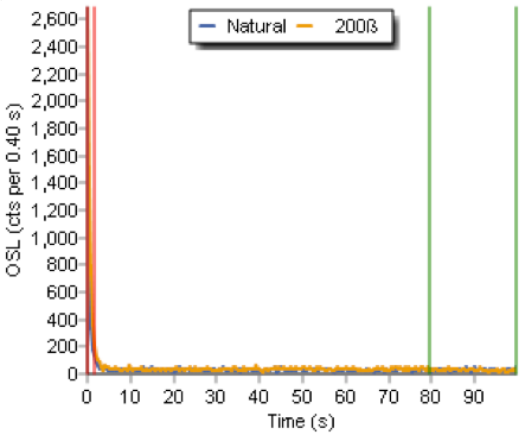

Figure D.13: OSL shine down curve for a representative aliquot of X4115

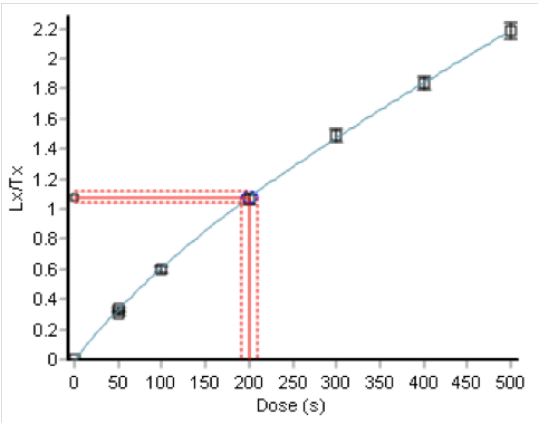

Figure D.14: OSL dose response curve for a representative aliquot of X4115

Figure D.15: Final OSL measurement (based on the CAM) and over dispersion value for X4115. Calibrated machine dose rates (Gy/s): 0.03842184 (CG), 0.03819457 (FG).

Central dose (s)	Central Dose Error (s)	OD (%)	OD error (%)
190.3	6.38	0.57	1.67
222.73	19.75	18.62	2.88

Table D.4: OSL data for Sample X4116 – Coarse Grain (No fine grain data available; of 6 aliquots, all failed to meet rejection criteria)

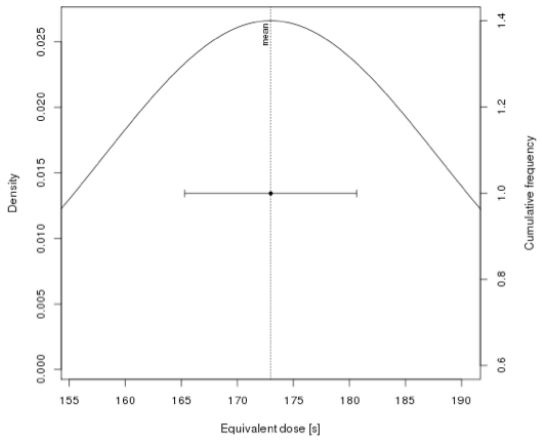

Figure D.16: Kernel Density Estimate Plot for Sample X4116

D_e (s)	D_e error (s)	Test Dose Error (%)	Recycling Ratio	Recup. (%)	IRSL/ OSL ratio (%)
172.98	15.33 (≤10%)	≤10	0.98±0.10 (≤10%)	1.2±0.5	5

Figure D.17: Primary Dataset for KDE plot for X4116. NB Primary data set is comprised of 1 aliquot selected from a total of 2 aliquots after selection criteria were met.

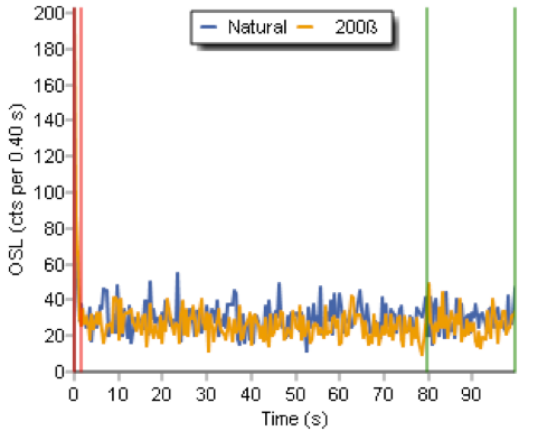

Figure D.18: OSL shine down curve for a representative aliquot of X4116

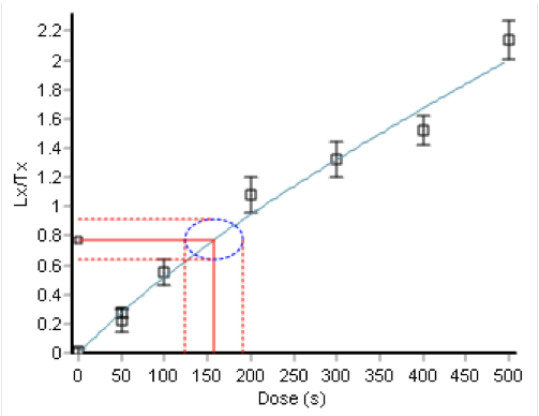

Figure D.19: OSL dose response curve for a representative aliquot of X4116

Figure D.20: Final OSL measurement (based on the CAM) and over dispersion value for X4116. Calibrated machine dose rates (Gy/s): 0.03849789 (CG).

Central dose (s)	Central Dose Error (s)	OD (%)	OD error (%)
172.98	15.33	N/A	N/A

Table D.5: OSL data for Sample X4117 – Fine Grain (No coarse grain data available; of 2 aliquots, all failed to meet rejection criteria)

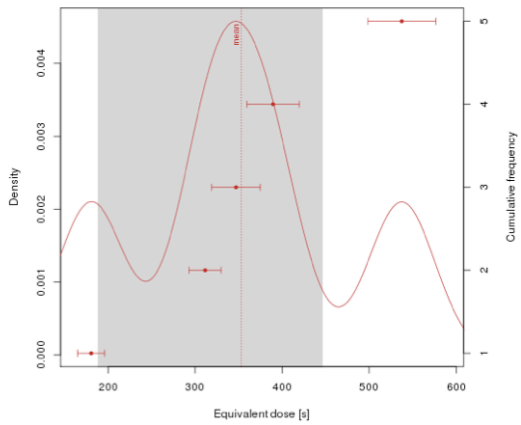

Figure D.21: Kernel Density Estimate Plot for Sample X4117

D_e (s)	D_e error (s)	Test Dose Error (%)	Recycling Ratio	Recup. (%)	IRSL signal (%)
311.62	36.73 (12%)	≤10	1.34±0.33 (≤10%)	4.4±1.8	6
347.04	55.80 (16%)	12	0.68±0.19 (13%)	-0.3±-2.1	11
537.38	77.84 (14%)	12	0.66±0.24 (≤10%)	7.1±2.4	10
389.72	60.15 (15%)	13	0.84±0.36 (≤10%)	2.9±2.5	7
180.47	31.23 (16%)	14	0.81±0.31 (≤10%)	0.2±4.9	11

Figure D.22: Primary Dataset for KDE plot for X4117. NB primary data set is comprised of 5 aliquots selected from a total of 6 aliquots after selection criteria were met.

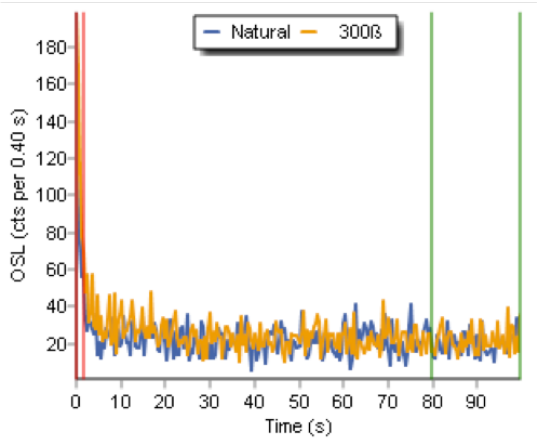

Figure D.23: OSL shine down curve for a representative aliquot of X4117

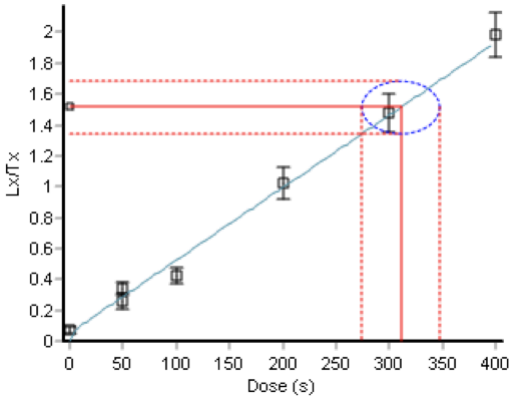

Figure D.24: OSL dose response curve for a representative aliquot of X4117

Figure D.25: Final OSL measurement (based on the CAM) and over dispersion value for X4117. Calibrated machine dose rates (Gy/s): 0.03819457 (FG).

Central dose (s)	Central Dose Error (s)	OD (%)	OD error (%)
335.16	51.9	31.18	6.78

Table D.6: OSL data for Sample X4118 – Coarse Grain and Fine Grain

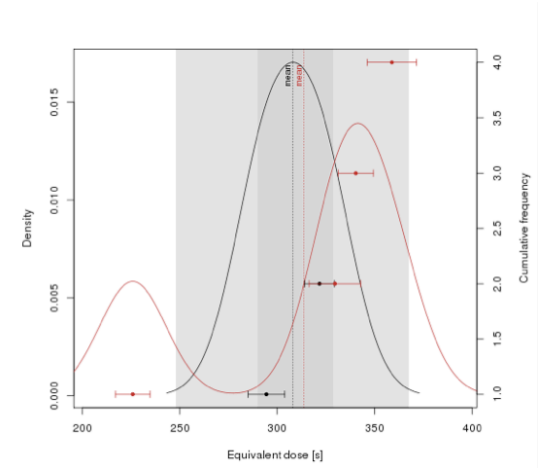

Figure D.26: Kernel Density Estimate Plot for Sample X4118

D_e (s)	D_e error (s)	Test Dose Error (%)	Recycling Ratio	Recup. (%)	IRSL / OSL ratio (%)
321.70	15.23 (≤10%)	≤10	1.19±0.08 (11%)	0.5±0.2	≤1
294.49	18.75 (≤10%)	≤10	1.11±0.12 (≤10%)	0.4±0.4	5
340.32	18.06 (≤10%)	≤10	1.20±0.13 (≤10%)	-0.1±-0.5	3
358.84	25.42 (≤10%)	≤10	1.04±0.14 (≤10%)	-1.0±-0.6	4
329.66	26.56 (≤10%)	≤10	0.94±0.14 (≤10%)	-0.3±-0.9	≤1
225.91	17.74 (≤10%)	≤10	1.18±0.17 (≤10%)	-0.2±-1.0	5

Figure D.27: Primary Dataset for KDE plot for X4118. NB Primary data set is comprised of 2 aliquots selected from a total of 5 aliquots (coarse grains) and 4 out of 4 aliquots (fine grains) after selection criteria were met.

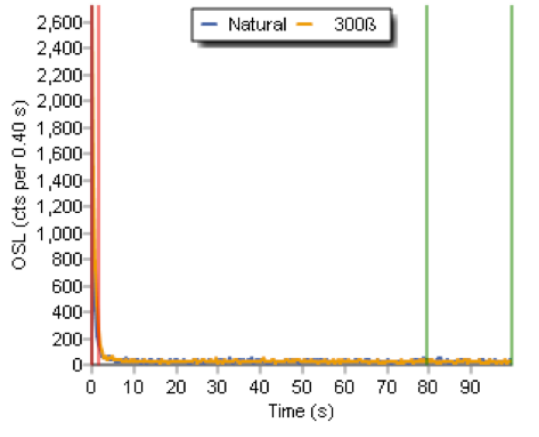

Figure D.28: OSL shine down curve for a representative aliquot of X4118

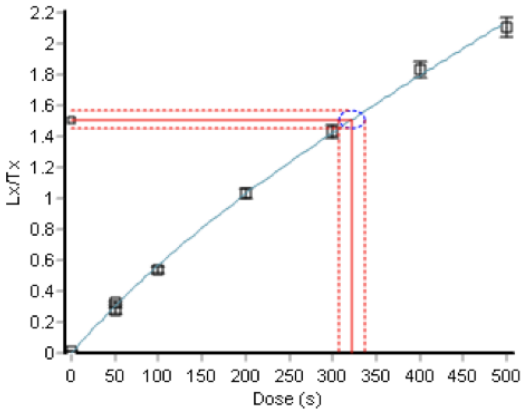

Figure D.29: OSL dose response curve for a representative aliquot of X4118

Figure D.30: Final OSL measurement (based on the CAM) and over dispersion value for X4118. Calibrated machine dose rates (Gy/s): 0.03849789 (CG), 0.03819457 (FG).

Central dose (s)	Central Dose Error (s)	OD (%)	OD error (%)
311.74	11.84	N/A	N/A
309.98	27.78	16.46	N/A

No OSL data is available for Sample X4119

- No data for coarse grain material. Of 6 aliquots, all failed to meet rejection criteria.
- No data for fine grain material. Of 6 aliquots, all failed to meet rejection criteria.

No OSL data is available for Sample X4120

- No data for coarse grain material. Of 3 aliquots, all failed to meet rejection criteria.
- No data for fine grain material. Of 6 aliquots, all failed to meet rejection criteria.

Table D.7: OSL data for Sample X5458 – Coarse Grain and Fine Grain

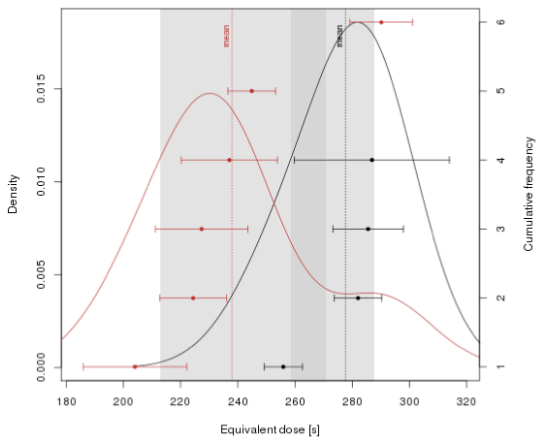

Figure D.31: Kernel Density Estimate Plot for Sample X5458

D_e (s)	D_e error (s)	Test Dose Error (%)	Recycling Ratio	Recup. (%)	IRSL signal (%)
281.99	16.56 (≤10%)	≤10	1.04±0.09 (≤10%)	2.5±0.7	3
285.58	24.63 (≤10%)	≤10	1.18±0.12 (≤10%)	5.4±1.5	7
255.92	13.4 (≤10%)	≤10	1.1±0.09 (12%)	2.3±0.7	3
39.97	1.97 (≤10%)	≤10	0.96±0.05 (≤10%)	0.8±2.1	4
286.85	54.95 (19%)	14	0.88±0.36 (≤10%)	0.3±2.2	8
227.40	32.33 (14%)	≤10	0.90±0.28 (≤10%)	0.5±3.4	10
204.03	36.23 (18%)	11	0.73±0.23 (≤10%)	7.9±4.5	7
224.41	23.39 (11%)	≤10	1.38±0.2 (16%)	6.8±1.5	2
237.06	33.59 (14%)	11	0.89±0.29 (≤10%)	-1.0±-3.1	10
244.88	16.62 (≤10%)	≤10	0.92±0.12 (≤10%)	2.7±1.1	5
290.10	21.92 (18%)	≤10	1.37±0.20 (≤10%)	3.3±1.1	4

Figure D.32: Primary Dataset for KDE plot for X5458. NB Primary data set is comprised of 5 aliquots selected from a total of 7 aliquots (coarse grains) and 6 out of 6 aliquots (fine grains) after selection criteria were met.

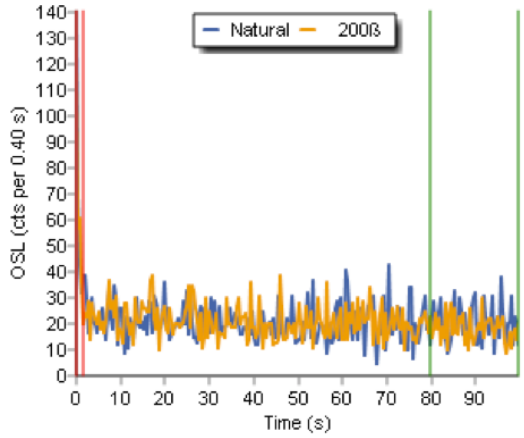

Figure D.33: OSL shine down curve for a representative aliquot of X5458

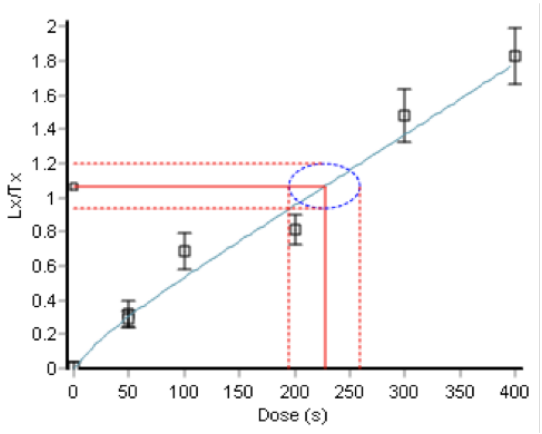

Figure D.34: OSL dose response curve for a representative aliquot of X5458

Figure D.35: Final OSL measurement (based on the CAM) and over dispersion value for X5458. Calibrated machine dose rates (Gy/s): 0.03877326 (CG), 0.03819457 (FG).

Central dose (s)	Central Dose Error (s)	OD (%)	OD error (%)
270.74	9.47	0	N/A
246.66	11.91	5.59	1.5

Table D.8: OSL data for Sample X5459 – Coarse Grain (No fine grain data available; of 6 aliquots, all failed to meet rejection criteria)

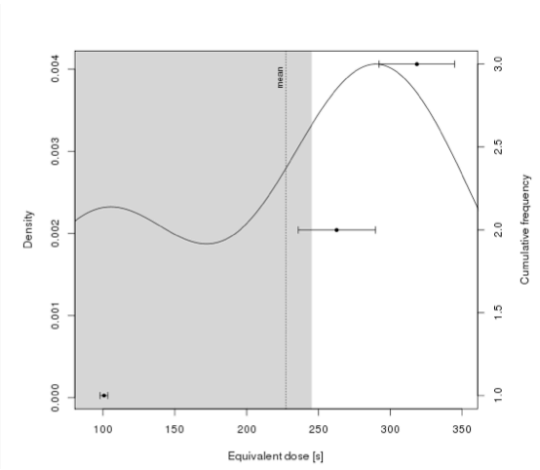

Figure D.36: Kernel Density Estimate Plot for Sample X5459

D_e (s)	D_e error (s)	Test Dose Error (%)	Recycling Ratio	Recup. (%)	IRSL signal (%)
318.47	52.47 (16%)	≤10	1.25±0.29 (≤10%)	1.4±2.5	3
262.78	53.47 (20%)	≤10	1.30±0.21 (≤10%)_	-1.2±0.9	≤1
100.66	5.29 (≤10%)	≤10	1.24±0.07 (18%)	0.8±0.4	≤1

Figure D.37: Primary Dataset for KDE plot for X5459. NB Primary data set is comprised of 3 aliquots selected from a total of 10 aliquots after selection criteria were met.

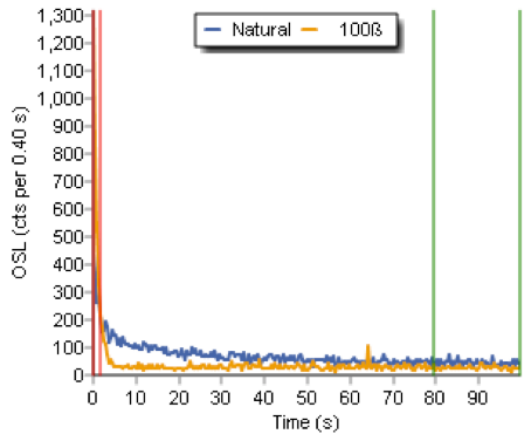

Figure D.38: OSL shine down curve for a representative aliquot of X5459

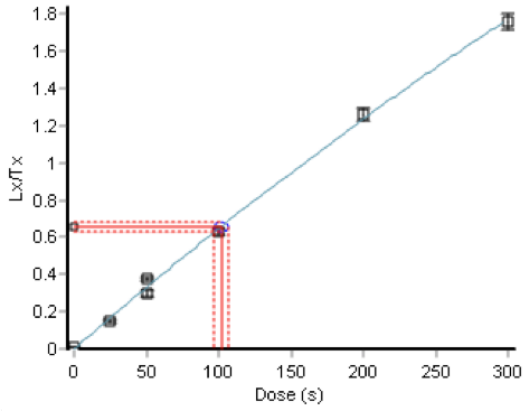

Figure D.39: OSL dose response curve for a representative aliquot of X5459

Figure D.40: Final OSL measurement (based on the CAM) and over dispersion value for X5459. Calibrated machine dose rates (Gy/s): 0.03877326 (CG).

Central dose (s)	Central Dose Error (s)	OD (%)	OD error (%)
198.2	59.91	50.12	15.78

Table D.9: OSL data for Sample X5460 – Coarse Grain and Fine Grain

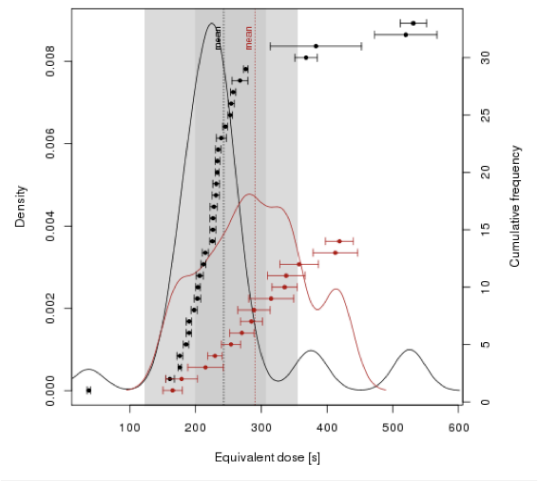

Figure D.41: Kernel Density Estimate Plot for Sample X5460

Figure D.42: Primary Dataset for KDE plot for X5460. (Shown Overleaf). NB Primary data set is comprised of 23 aliquots selected from a total of 30 aliquots (coarse grains) and 14 out of 16 aliquots (fine grains) after selection criteria were met.

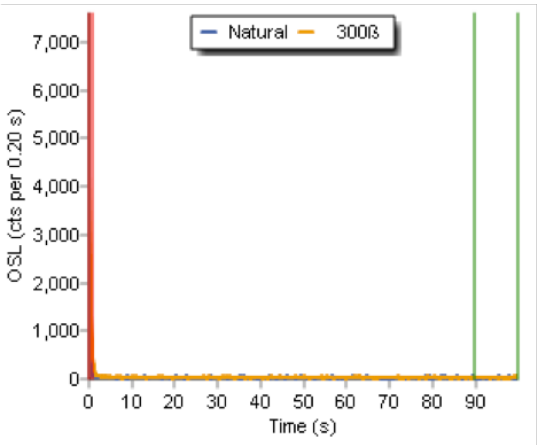

Figure D.43: OSL shine down curve for a representative aliquot of X5460

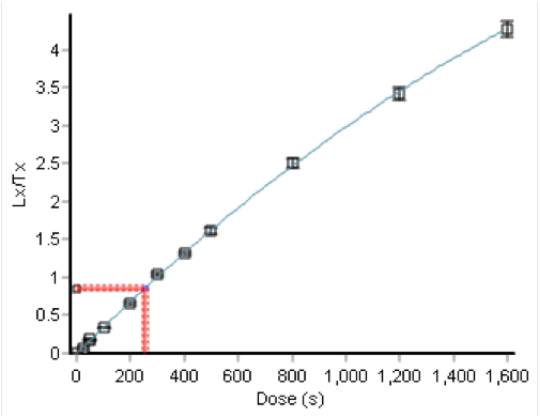

Figure D.44: OSL dose response curve for a representative aliquot of X5460

Figure D.45: Final OSL measurement (based on the CAM) and over dispersion value for X5460. Calibrated machine dose rates (Gy/s): 0.04007744 (CG), 0.03842184 (FG).

Central dose (s)	Central Dose Error (s)	OD (%)	OD error (%)
224.06	14.89	37.41	2.92
286.97	19.82	20.49	2.72

Figure D.42: Primary data set for X5460.

D_e (s)	D_e error (s)	Test Dose Error (%)	Recycling Ratio	Recup. (%)	IRSL signal (%)	Grain Size (µm) & treatment
276.29	7.02 (≤10%)	≤10	1.04±0.03 (≤10%)	0.5±0.0	≤1	90 – 250 µm TE: HCl +30 min HF
208.52	6.62 (≤10%)	≤10	1.09±0.04 (≤10%)	0.6±0.1	≤1	90 – 250 µm TE: HCl + 30 min HF
233.17	7.61 (≤10%)	≤10	1.09±0.04 (≤10%)	0.4±0.0	≤1	90 – 250 µm TE: HCl + 30 min HF
160.98	13.23 (≤10%)	≤10	1.08±0.11 (≤10%)	1.7±0.6	9	90 – 250 µm TE: HCl + 30 min HF
230.80	11.22 (≤10%)	≤10	1.22±0.07 (15%)	1.0±0.2	≤1	90 – 250 µm TE: HCl + 30 min HF
254.17	9.45 (≤10%)	≤10	1.09±0.07 (≤10%)	0.7±0.1	≤1	90 – 250 µm TE: HCl + 30 min HF
234.32	8.53 (≤10%)	≤10	1.14±0.15 (≤10%)	3.2±0.2	2	90 – 250 µm TE: HCl + 30 min HF
180.89	7.92 (≤10%)	≤10	1.20±0.05 (≤10%)	0.9±0.1	5	90 – 250 µm TE: HCl + 30 min HF
252.54	7.30 (≤10%)	≤10	1.10±0.04 (≤10%)	0.7±0.1	≤1	90 – 250 µm TE: HCl + 30 min HF
257.24	8.07 (≤10%)	≤10	1.22±0.06 (17%)	0.4±0.1	≤1	90 – 250 µm TE: HCl + 30 min HF
245.03	7.21 (≤10%)	≤10	1.15±0.04 (11%)	0.4±0.0	≤1	90 – 250 µm TE: HCl + 30 min HF
531.32	39.97 (≤10%)	≤10	1.06±0.05 (≤10%)	0.6±0.1	≤1	90 – 250 µm TE: HCl + 30 min HF
232.95	6.22 (≤10%)	≤10	1.14±0.03 (11%)	0.7±0.0	≤1	90 – 250 µm TE: HCl + 30 min HF
214.70	9.57 (≤10%)	≤10	1.12±0.06 (≤10%)	1.3±0.2	4	90 – 250 µm TE: HCl only
202.78	10.18 (≤10%)	≤10	1.21±0.08 (13%)	1.0±0.3	5	90 – 250 µm TE: HCl only
227.65	10.90 (≤10%)	≤10	1.16±0.08 (≤10%)	1.4±0.3	4	90 – 250 µm TE: HCl only
231.24	10.50 (≤10%)	≤10	1.20±0.06 (14%)	0.1±0.1	3	90 – 250 µm TE: HCl only
197.76	9.60 (≤10%)	≤10	1.02±0.06 (≤10%)	0.9±0.3	12	90 – 250 µm TE: HCl only
225.49	8.30 (≤10%)	≤10	0.9±0.1 (≤10%)	0.9±0.1	4	90 – 250 µm TE: HCl only
211.71	7.46 (≤10%)	≤10	1.16±0.05 (≤10%)	1.1±0.1	3	90 – 250 µm TE: HCl only
175.75	5.62 (≤10%)	≤10	1.13±0.06 (≤10%)	0.8±0.2	4	90 – 250 µm TE: HCl only
165.40	8.01 (≤10%)	≤10	1.08±0.06 (≤10%)	0.7±0.3	3	90 – 250 µm TE: no treatment
206.18	10.63 (≤10%)	≤10	1.08±0.07 (≤10%)	0.8±0.2	6	90 – 250 µm TE: no treatment
189.96	7.89 (≤10%)	≤10	1.13±0.06 (≤10%)	0.3±0.2	5	90 – 250 µm TE: no treatment
239.01	14.82 (≤10%)	≤10	1.29±0.13 (17%)	0.6±0.5	12	90 – 250 µm TE: no treatment

D_e (s)	D_e error (s)	Test Dose Error (%)	Recycling Ratio	Recup. (%)	IRSL signal (%)	Grain Size (µm) & treatment
368.13	33.96 (≤10%)	≤10	1.11±0.09 (≤10%)	-0.5±-0.2	≤1	90 – 250 µm MET HCl +30 sec HF
175.84	9.23 (≤10%)	≤10	1.12±0.07 (≤10%)	0.9±0.3	2	90 – 250 µm MET HCl +30 sec HF
225.03	9.09 (≤10%)	≤10	1.07±0.05 (≤10%)	0.6±0.1	≤1	90 – 250 µm MET HCl +30 sec HF
37.17	5.12 (≤10%)	≤10	1.25±0.09 (16%)	2.0±1.7	13	90 – 250 µm MET HCl +30 sec HF
226.25	8.73 (≤10%)	≤10	1.16±0.05 (11%)	0.8±0.1	≤1	90 – 250 µm MET HCl +30 sec HF
519.93	94.85 (19%)	14	0.58±0.37 (≤10%)	-6.3±-3.6	11	90 – 250 µm MET HCl +30 sec HF
267.39	23.92 (≤10%)	≤10	1.05±0.12 (≤10%)	1.4±0.6	5	90 – 250 µm MET HCl +30 sec HF
383.10	138.93 (37%)	≤10	1.22±0.29 (≤10%)	-1.2±-1.3	13	90 – 250 µm MET HCl +30 sec HF

D_e (s)	D_e error (s)	Test Dose Error (%)	Recycling Ratio	Recup. (%)	IRSL signal (%)
418.77	42.29 (11%)	≤10	1.37±0.33 (≤10%)	-2.7±-1.0	4
315.05	68.56 (22%)	≤10	1.35±0.39 (≤10%)	-0.6±-1.9	8
253.88	28.55 (12%)	≤10	0.72±0.13 (16%)	-0.1±-1.7	6
288.87	49.10 (17%)	≤10	1.20±0.33 (≤10%)	-0.3±-1.8	12
229.29	21.89 (≤10%)	≤10	0.82±0.18 (≤10%)	1.5±1.6	12
284.73	33.26 (12%)	≤10	1.26±0.26 (≤10%)	0.0±1.1	10
165.12	29.62 (18%)	11	2.22±1.67 (≤10%)	6.3±4.5	13
335.61	38.41 (12%)	≤10	1.05±0.21 (≤10%)	1.4±1.3	10
412.73	67.68 (17%)	13	0.75±0.20 (≤10%)	-1.0±-1.4	10
337.88	57.36 (17%)	12	1.43±0.47 (≤10%)	5.0±2.1	8
214.96	53.97 (26%)	14	0.68±0.30 (≤10%)	3.5±5.0	10
178.69	49.15 (28%)	16	0.67±0.24 (≤10%)	5.6±7.0	9
357.55	58.60 (17%)	16	1.47±0.53 (≤10%)	6.2±2.6	9
270.24	36.72 (14%)	≤10	1.30±0.34 (≤10%)	0.7±2.0	11

Table D.10: OSL data for Sample X5461 – Coarse Grain and Fine Grain

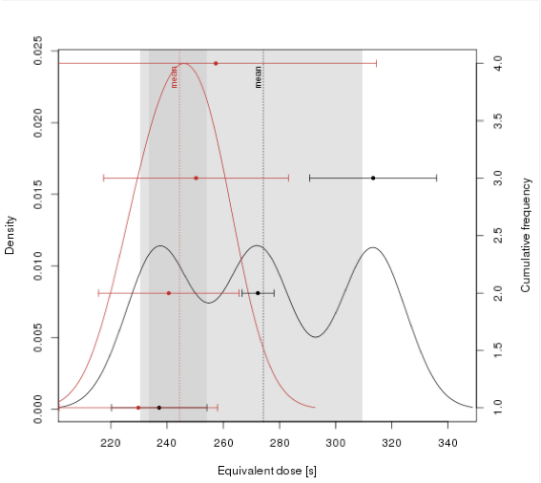

Figure D.46: Kernel Density Estimate Plot for Sample X5461

D_e (s)	D_e error (s)	Test Dose Error (%)	Recycling Ratio	Recup. (%)	IRSL signal (%)
313.34	45.21 (14%)	≤10	1.35±0.24 (11%)	2.7±2.2	4
237.16	34.00 (14%)	≤10	1.32±0.18 (≤10%)	-2.5±-1.4	2
272.38	11.25 (≤10%)	≤10	1.17±0.05 (12%)	0.2±0.1	≤1
257.30	114.37 (45%)	20	1.16±0.29 (≤10%)	11.9±7.4	8
250.30	65.80 (26%)	18	0.65±0.29 (≤10%)	-7.5±-4.6	11
240.63	50.00 (21%)	20	0.82±0.36 (≤10%)	-5.0±-6.5	6
229.72	56.44 (25%)	20	0.91±0.35 (≤10%)	9.5±6.1	3

Figure D.47: Primary Dataset for KDE plot for X5461. NB Primary data set is comprised of 3 aliquots selected from a total of 6 aliquots (coarse grains) and 4 out of 6 aliquots (fine grains) after selection criteria were met.

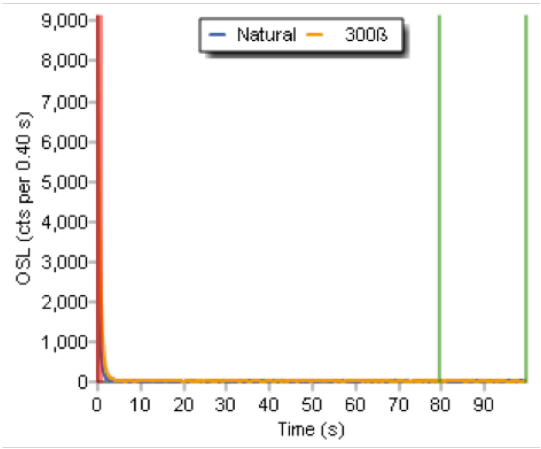

Figure D.48: OSL shine down curve for a representative aliquot of X5461

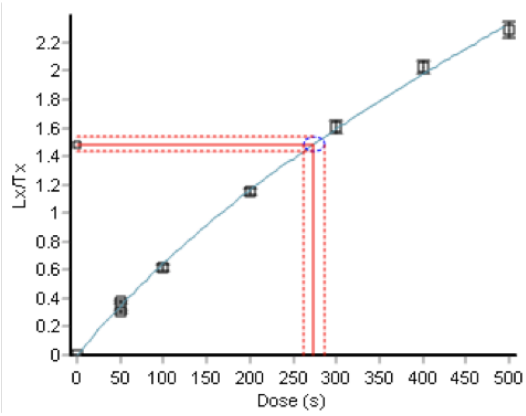

Figure D.49: OSL dose response curve for a representative aliquot of X5461

Figure D.50: Final OSL measurement (based on the CAM) and over dispersion value for X5461. Calibrated machine dose rates (Gy/s): 0.03877326 (CG), 0.03819457 (FG).

Central dose (s)	Central Dose Error (s)	OD (%)	OD error (%)
272.38	10.42	0	N/A
241.20	31.33	0	N/A

Table D.11: OSL data for Sample X5462 – Coarse Grain (No fine grain data available; of 6 aliquots, all failed to meet rejection criteria)

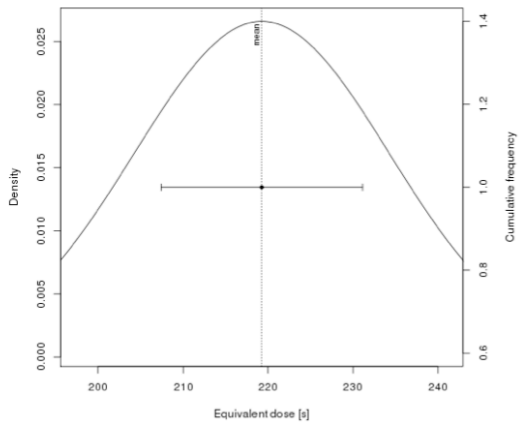

Figure D.51: Kernel Density Estimate Plot for Sample X5462

D_e (s)	D_e error (s)	Test Dose Error (%)	Recycling Ratio	Recup. (%)	IRSL signal (%)
219.25	23.69 (11%)	≤ 10	1.28±0.17 (≤10%)	20.9±2.5	5

Figure D.52: Primary Dataset for KDE plot for X5462. NB Primary data set is comprised of 1 aliquot selected from a total of 10 aliquots after selection criteria were met.

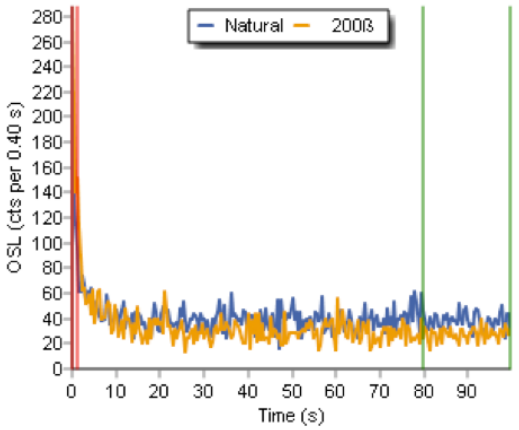

Figure D.53: OSL shine down curve for a representative aliquot of X5462

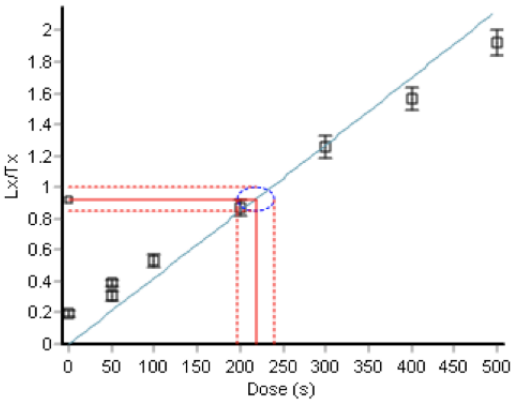

Figure D.54: OSL dose response curve for a representative aliquot of X5462

Figure D.55: Final OSL measurement (based on the CAM) and over dispersion value for X5462. Calibrated machine dose rates (Gy/s): 0.03819457 (FG).

Central dose (s)	Central Dose Error (s)	OD (%)	OD error (%)
219.25	23.69	N/A	N/A

Table D.12: OSL data for Sample X5463 – Coarse Grain and Fine Grain

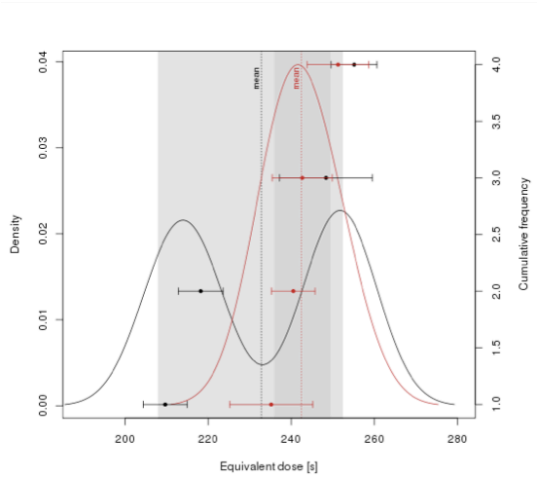

Figure D.56: Kernel Density Estimate Plot for Sample X5463

D_e (s)	D_e error (s)	Test Dose Error (%)	Recycling Ratio	Recup. (%)	IRSL signal (%)
218.18	10.74 (≤10%)	≤10	1.07±0.07 (≤10%)	0.0±0.4	4
255.11	11.07 (≤10%)	≤10	115±0.06 (≤10%)	0.8±0.3	4
209.67	10.57 (≤10%)	≤10	1.01±0.07 (≤10%)	-0.2±-0.5	5
248.36	22.34 (≤10%)	≤10	1.30±0.16 (14%)	0.9±0.6	1
240.50	10.50 (≤10%)	≤10	1.11±0.09 (≤10%)	0.6±0.3	2
235.19	20.08 (≤10%)	≤10	1.03 ±0.15 (≤10%)	-0.1±-1.1	3
242.64	14.4 (≤10%)	≤10	1.13±0.11 (≤10%)	0.4±0.5	4
251.24	14.84 (≤10%)	≤10	1.24±0.13 (≤10%)	1.8±0.6	2

Figure D.57: Primary Dataset for KDE plot for X5463. NB Primary data set is comprised of 4 aliquots selected from a total of 10 aliquots (coarse grains) and 4 out of 6 aliquots (fine grains) after selection criteria were met.

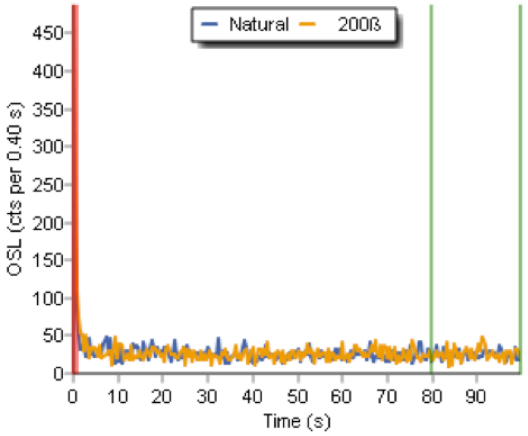

Figure D.58: OSL shine down curve for a representative aliquot of X5463

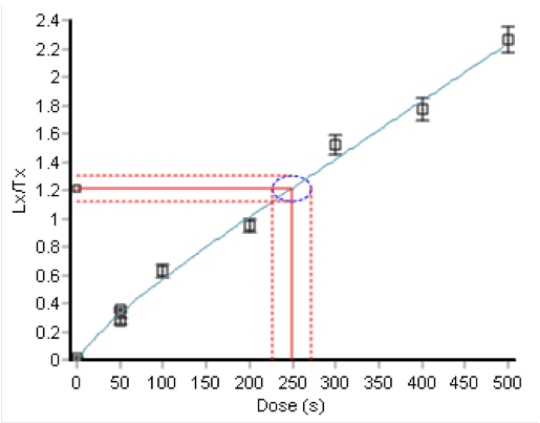

Figure D.59: OSL dose response curve for a representative aliquot of X5463

Figure D.60: Final OSL measurement (based on the CAM) and over dispersion value for X5463. Calibrated machine dose rates (Gy/s): 0.03877326 (CG), 0.03819457 (FG).

Central dose (s)	Central Dose Error (s)	OD (%)	OD error (%)
230.70	10.17	6.79	N/A
242.85	6.92	0	N/A

Table D.13: OSL data for Sample X5464 – Coarse Grain and Fine Grain

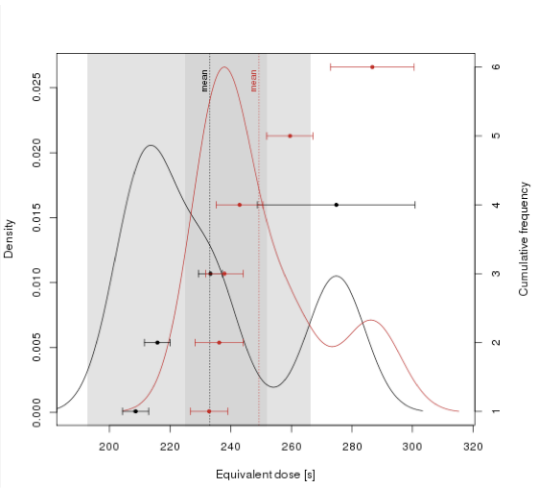

Figure D.61: Kernel Density Estimate Plot for Sample X5464

D_e (s)	D_e error (s)	Test Dose Error (%)	Recycling Ratio	Recup. (%)	IRSL signal (%)
215.73	8.51 (≤10%)	≤10	1.17±0.05 (≤10%)	1.3±0.1	≤1
274.83	52.04 (19%)	12	1.05±0.23 (≤10%)	-8.3±4.1	9
208.54	8.60 (≤10%)	≤10	1.10±0.05 (≤10%)	3.6±0.3	2
233.32	7.92 (≤10%)	≤10	1.18±0.06 (13%)	0.9±0.1	≤1
242.97	15.42 (≤10%)	≤10	1.23±0.15 (≤10%)	5.5±1.1	9
286.74	27.62 (≤10%)	≤10	1.01±0.16 (≤10%)	4.3±1.6	3
232.86	12.29 (≤10%)	≤10	1.03±0.09 (≤10%)	4.1±0.7	5
235.20	15.98 (≤10%)	≤10	1.25±0.14 (11%)	2.9±1.0	8
237.96	12.37 (≤10%)	≤10	0.99±0.09 (≤10%)	4.2±0.8	4
259.50	15.16 (≤10%)	≤10	1.19±0.11 (≤10%)	3.1±0.6	3

Figure D.62: Primary Dataset for KDE plot for X5464. NB Primary data set is comprised of 4 aliquots selected from a total of 6 aliquots (coarse grains) and 6 out of 6 aliquots (fine grains) after selection criteria were met.

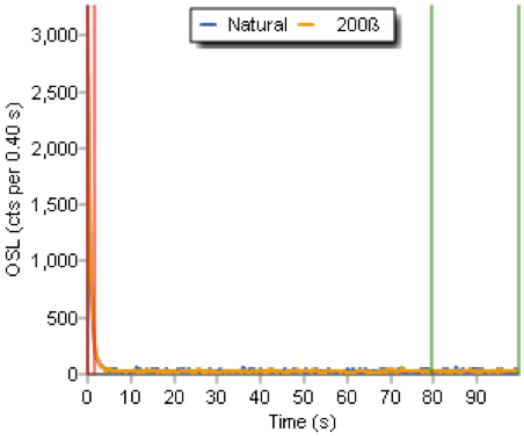

Figure D.63: OSL shine down curve for a representative aliquot of X5464

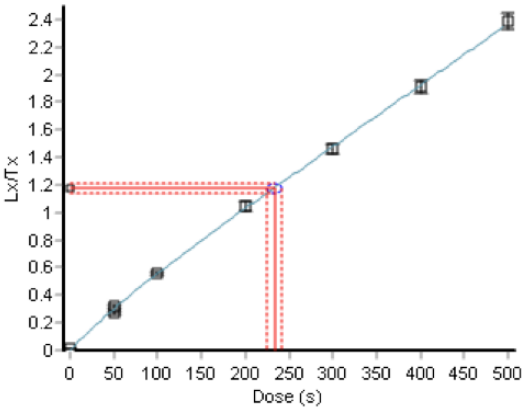

Figure D.64: OSL dose response curve for a representative aliquot of X5464

Figure D.65: Final OSL measurement (based on the CAM) and over dispersion value for X5464. Calibrated machine dose rates (Gy/s): 0.03877326 (CG), 0.03819457 (FG).

Central dose (s)	Central Dose Error (s)	OD (%)	OD error (%)
221.04	6.17	3.06	0.55
244.19	6.11	0	N/A

Table D.14: OSL data for Sample X5465 – Coarse Grain and Fine Grain

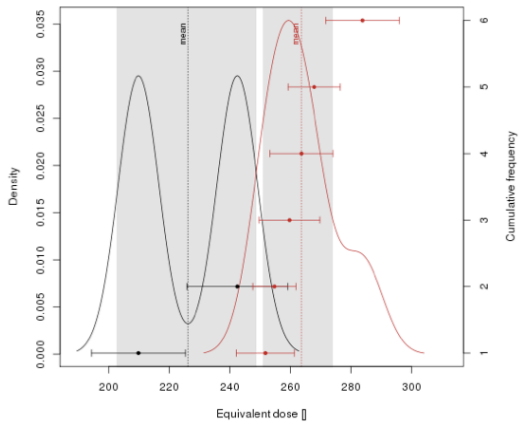

Figure D.66: Kernel Density Estimate Plot for Sample X5465

D_e (s)	D_e error (s)	Test Dose Error (%)	Recycling Ratio	Recup. (%)	IRSL signal (%)
209.88	30.99 (15%)	≤10	1.01±0.18 (≤10%)	7.7±5.3	10
242.49	33.35 (14%)	≤10	0.91±0.22 (≤10%)	-0.1±-2.8	7
259.72	20.01 (≤10%)	≤10	0.92±0.17 (≤10%)	0.6±1.4	5
254.73	14.30 (≤10%)	≤10	1.15±0.13 (≤10%)	1.7±0.8	3
251.76	19.14 (≤10%)	≤10	0.83±0.12 (≤10%)	2.6±1.2	10
263.64	20.79 (≤10%)	≤10	1.08±0.19 (≤10%)	5.0±1.5	7
267.85	17.17 (≤10%)	≤10	0.89±0.12 (≤10%)	2.6±1.0	6
283.90	24.22 (≤10%)	≤10	1.06±0.17 (≤10%)	3.4±1.36	9

Figure D.67: Primary Dataset for KDE plot for X5465. NB Primary data set is comprised of 2 aliquots selected from a total of 6 aliquots (coarse grains) and 6 out of 6 aliquots (fine grains) after selection criteria were met.

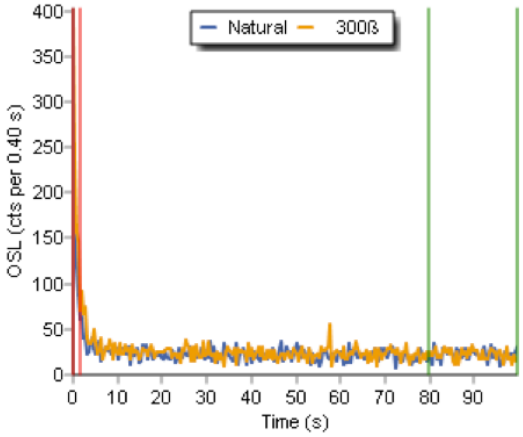

Figure D.68: OSL shine down curve for a representative aliquot of X5465

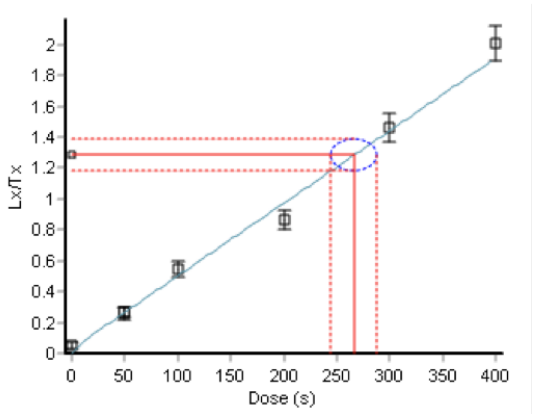

Figure D.69: OSL dose response curve for a representative aliquot of X5465

Figure D.70: Final OSL measurement (based on the CAM) and over dispersion value for X5465. Calibrated machine dose rates (Gy/s): 0.03877326 (CG), 0.03819457 (FG).

Central dose (s)	Central Dose Error (s)	OD (%)	OD error (%)
226.75	22.82	0	N/A
262.01	7.56	0	N/A

Table D.15: OSL data for Sample X5466 – Coarse Grain (No fine grain data available; of 6 aliquots, all failed to meet rejection criteria)

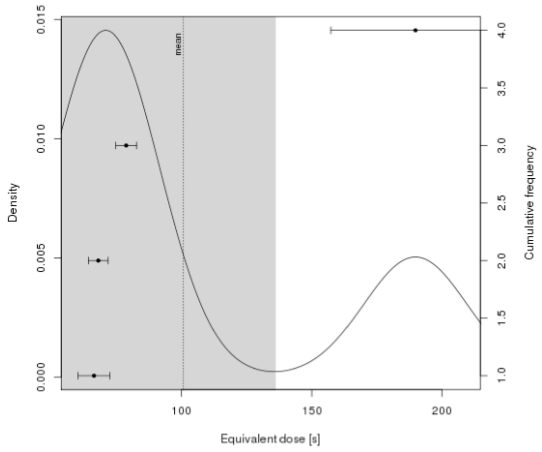

Figure D.71: Kernel Density Estimate Plot for Sample X5466

D_e (s)	D_e error (s)	Test Dose Error (%)	Recycling Ratio	Recup. (%)	IRSL signal (%)
68.01	7.99 (11%)	≤10	0.97±0.09 (≤10%)	7.3±3.7	4
66.35	12.18 (18.5%)	≤10	1.17±0.16 (≤10%)	2.3±5.5	3
78.73	7.99 (11%)	≤10	1.27±0.13 (15%)	-3.3±-3.2	2
189.76	64.83 (34%)	16	1.17±0.45 (≤10%)	1.7±3.3	5

Figure D.72: Primary Dataset for KDE plot for X5466. NB Primary data set is comprised of 3 aliquots selected from a total of 7 aliquots after selection criteria were met.

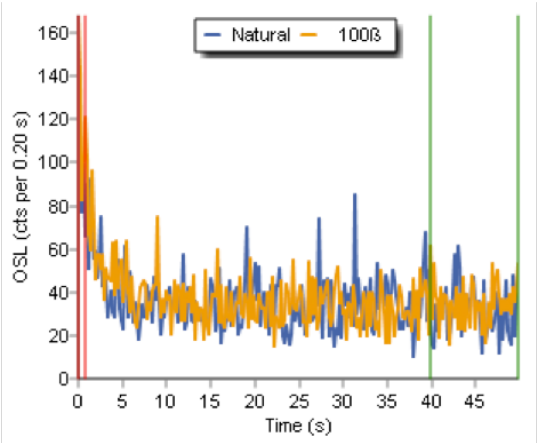

Figure D.73: OSL shine down curve for a representative aliquot of X5466

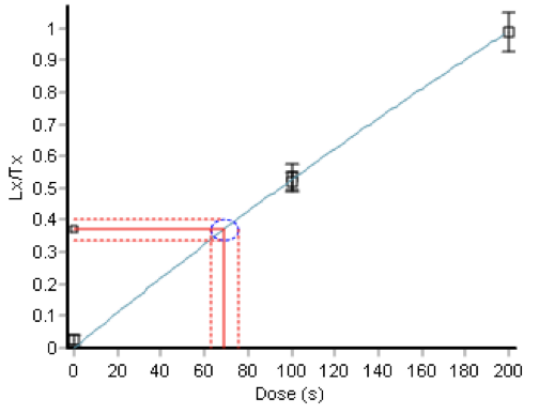

Figure D.74: OSL dose response curve for a representative aliquot of X5466

Figure D.75: Final OSL measurement (based on the CAM) and over dispersion value for X5466. Calibrated machine dose rates (Gy/s): 0.03877326 (CG).

Central dose (s)	Central Dose Error (s)	OD (%)	OD error (%)
75.41	5.14	0	N/A

Table D.16: OSL data for Sample X5467 – Coarse Grain and Fine Grain

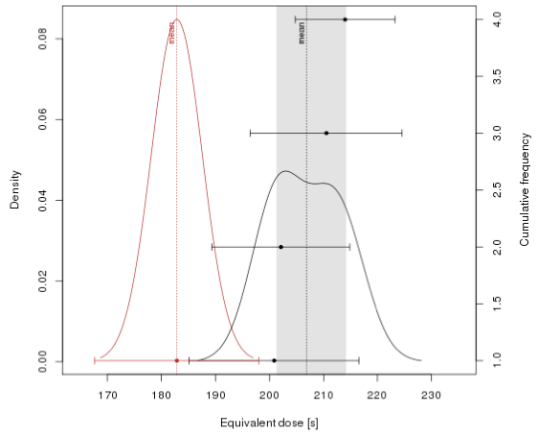

Figure D.76: Kernel Density Estimate Plot for Sample X5467

D_e (s)	D_e error (s)	Test Dose Error (%)	Recycling Ratio	Recup. (%)	IRSL signal (%)
214.01	18.47 (≤10%)	≤10	1.07±0.14 (≤10%)	-4.0±-1.6	2
210.50	28.11 (13%)	≤10	1.02±0.14 (≤10%)	-2.3±-2.6	4
202.09	25.55 (13%)	≤10	0.87±0.11 (≤10%)	2.7±2.0	≤1
200.84	31.48 (16%)	≤10	1.34±0.31 (≤10%)	0.0±0.0	2
182.84	30.34 (17%)	12	2.87±2.23 (≤10%)	7.2±8.5	7

Figure D.77: Primary Dataset for KDE plot for X5467. NB Primary data set is comprised of 4 aliquots selected from a total of 16 aliquots (coarse grains) and 1 out of 6 aliquots (fine grains) after selection criteria were met.

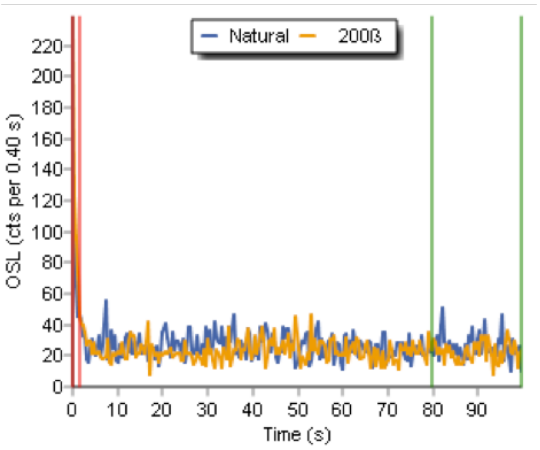

Figure D.78: OSL shine down curve for a representative aliquot of X5467

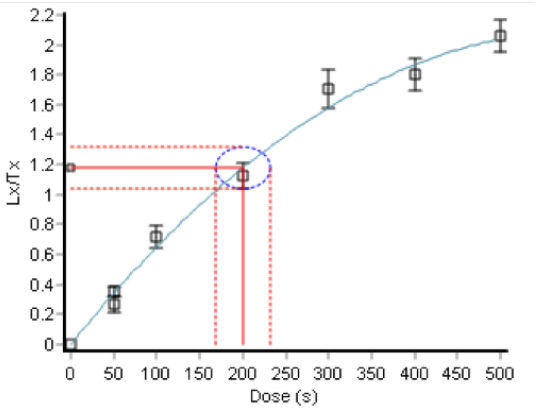

Figure D.79: OSL dose response curve for a representative aliquot of X5467

Figure D.80: Final OSL measurement (based on the CAM) and over dispersion value for X5467. Calibrated machine dose rates (Gy/s): 0.03877326 (CG), 0.03819457 (FG).

Central dose (s)	Central Dose Error (s)	OD (%)	OD error (%)
208.90	12.19	0	N/A
182.84	30.34	N/A	N/A

Table D.17: OSL data for Sample X5468 – Coarse Grain and Fine Grain

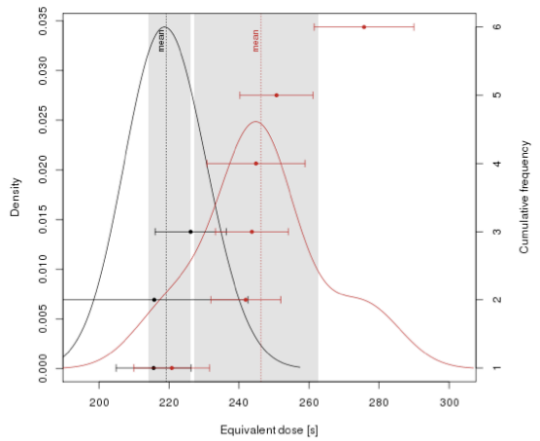

Figure D.81: Kernel Density Estimate Plot for Sample X5468

D_e (s)	D_e error (s)	Test Dose Error (%)	Recycling Ratio	Recup. (%)	IRSL signal (%)
215.77	53.51 (25%)	≤10	1.35±0.26 (≤10%)	-6.4±-3.7	9
226.19	20.24 (≤10%)	≤10	1.03±0.16 (≤10%)	2.6±2.9	4
215.61	21.45 (≤10%)	≤10	1.34±0.21 (14%)	-8.4±-2.6	7
241.91	19.97 (≤10%)	≤10	0.83±0.13 (≤10%)	6.5±1.8	5
220.79	21.57 (≤10%)	≤10	1.4±0.24 (≤10%)	4.4±2.1	5
243.66	20.84 (≤10%)	≤10	1.41±0.29 (13%)	-1.2±-2.3	2
250.70	20.88 (≤10%)	≤10	1.07±0.21 (≤10%)	4.1±1.9	5
244.84	28.06 (12%)	≤10	1.54±0.41 (13%)	-1.3±-2.1	5
275.73	28.45 (11%)	≤10	0.81±0.17 (≤10%)	2.2±1.7	7

Figure D.82: Primary Dataset for KDE plot for X5468. NB Primary data set is comprised of 3 aliquots selected from a total of 12 aliquots (coarse grains) and 6 out of 6 aliquots (fine grains) after selection criteria were met.

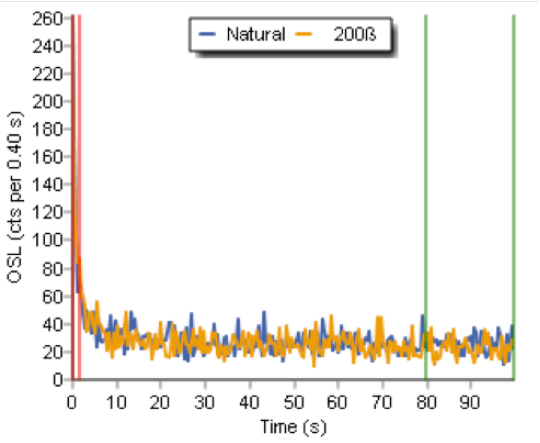

Figure D.83: OSL shine down curve for a representative aliquot of X5468

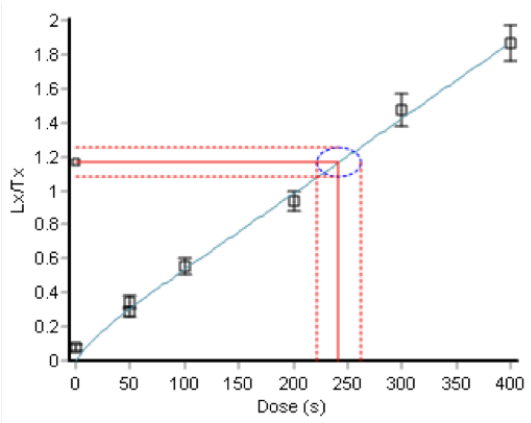

Figure D.84: OSL dose response curve for a representative aliquot of X5468

Figure D.85: Final OSL measurement (based on the CAM) and over dispersion value for X5468. Calibrated machine dose rates (Gy/s): 0.03912468 (CG), 0.03819457 (FG).

Central dose (s)	Central Dose Error (s)	OD (%)	OD error (%)
221.01	14.20	0	N/A
245.30	9.26	0	N/A

No OSL data is available for Sample X5469

- No data for coarse grain material. Of 12 aliquots, all failed to meet rejection criteria.
- No data for fine grain material. Of 6 aliquots, all failed to meet rejection criteria.

Table D.18: OSL data for Sample X5470 – Coarse Grain and Fine Grain

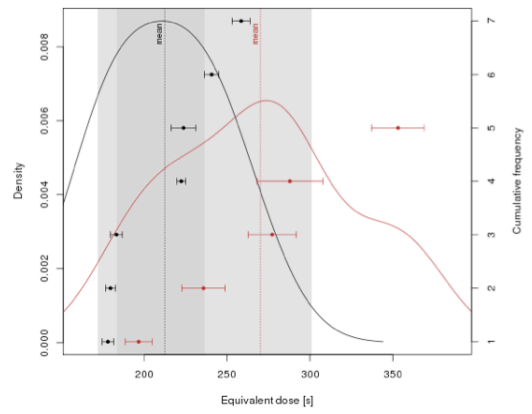

Figure D.86: Kernel Density Estimate Plot for Sample X5470

D_e (s)	D_e error (s)	Test Dose Error (%)	Recycling Ratio	Recup. (%)	IRSL signal (%)
240.67	8.46 (≤10%)	≤10	1.12±0.05 (≤10%)	0.01±-0.1	≤1
178.18	7.07 (≤10%)	≤10	1.02±0.08 (≤10%)	0.1±0.4	≤1
223.78	14.87 (≤10%)	≤10	1.26±0.12 (15%)	-0.3±-0.4	3
258.58	10.86 (≤10%)	≤10	1.20±0.07 (13%)	0.1±0.1	≤1
183.31	7.13 (≤10%)	≥10	1.12±0.07 (≤10%)	0.3±0.3	≤1
222.43	5.33 (≤10%)	≤10	1.05±0.04 (≤10%)	0.4±0.0	≤1
179.74	5.85 (≤10%)	≤10	1.11±0.05 (≤10%)	0.2±0.1	≤1
196.72	16.29 (≤10%)	≤10	1.29±0.23 (≤10%)	2.6±1.6	3
353.04	31.58 (≤10%)	≤10	1.43±0.27 (16%)	-1.8±-0.8	3
287.92	39.78 (14%)	≤10	0.83±0.17 (≤10%)	-0.5±-1.9	4
235.81	26.01 (12%)	≤10	1.11±0.23 (≤10%)	-4.5±-1.9	4
277.25	29.00 (11%)	≤10	0.82±0.20 (≤10%)	-2.0±1.8	5

Figure D.87: Primary Dataset for KDE plot for X5470. NB Primary data set is comprised of 7 aliquots selected from 10 aliquots (coarse grains) and 6 out of 6 aliquots (fine grains) after selection criteria were met.

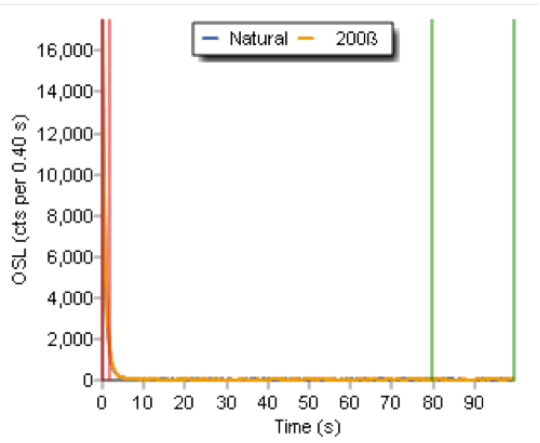

Figure D.88: OSL shine down curve for a representative aliquot of X5470

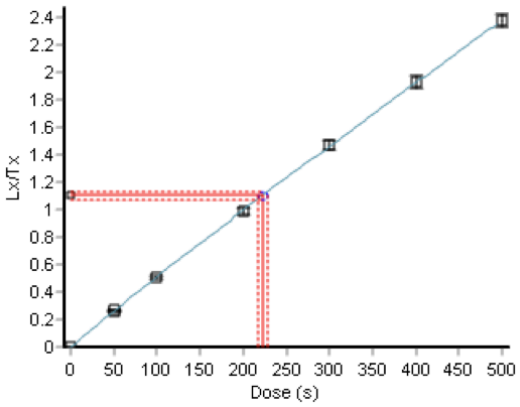

Figure D.89: OSL dose response curve for a representative aliquot of X5470

Figure D.90: Final OSL measurement (based on the CAM) and over dispersion value for X5470. Calibrated machine dose rates (Gy/s): 0.03877326 (CG), 0.03819457 (FG).

Central dose (s)	Central Dose Error (s)	OD (%)	OD error (%)
210.02	11.26	13.59	1.46
263.98	24.90	18.30	3.28

No OSL data is available for Sample X5471

- No data for coarse grain material. Of 5 aliquots, all failed to meet rejection criteria.
- No data for fine grain material. Of 6 aliquots, all failed to meet rejection criteria.

Table D.19: OSL data for Sample X5472 – Coarse Grain and Fine Grain

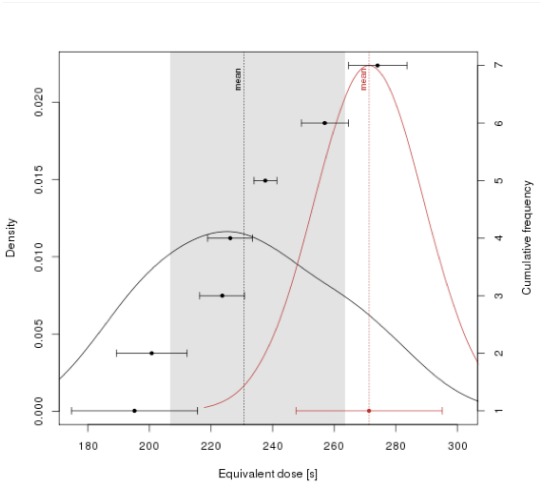

Figure D.91: Kernel Density Estimate Plot for Sample X5472

D_e (s)	D_e error (s)	Test Dose Error (%)	Recycling Ratio	Recup. (%)	IRSL signal (%)
274.16	18.97 (≤10%)	≤10	1.22±0.10 (13%)	-0.3±-0.5	5
256.98	15.20 (≤10%)	≤10	0.90±0.07 (≤10%)	-2.9±-0.5	3
200.75	22.94 (12%)	≤10	1.12±0.11 (≤10%)	2.0±1.2	5
225.19	14.55 (≤10%)	≤10	1.08±0.08 (≤10%)	1.2±0.6	2
195.15	41.01 (22%)	≤10	1.60±0.66 (≤10%)	-0.7±-1.3	≤1
237.67	7.38 (≤10%)	≤10	1.19±0.04 (≤10%)	0.2±0.0	≤1
223.60	14.52 (≤10%)	≤10	1.27±0.13 (15%)	0.2±0.5	≤1
271.37	47.55 (18%)	16	0.45±0.39 (17%)	8.0±6.6	13

Figure D.92: Primary Dataset for KDE plot for X5472. NB Primary data set is comprised of 7 aliquots selected from a total of 9 aliquots (coarse grains) and 1 out of 6 aliquots (fine grains) after selection criteria were met.

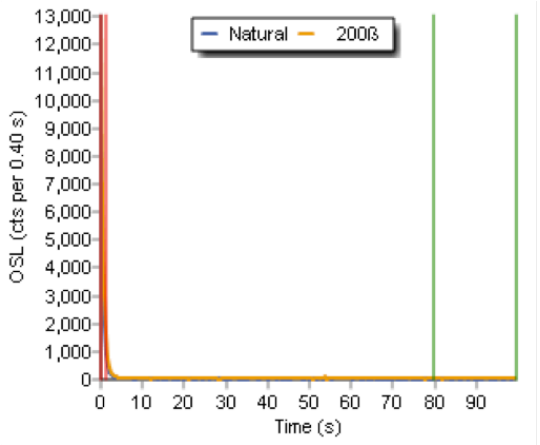

Figure D.93: OSL shine down curve for a representative aliquot of X5472

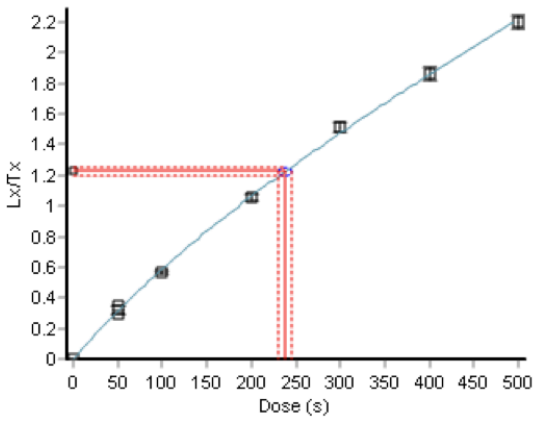

Figure D.94: OSL dose response curve for a representative aliquot of X5472

Figure D.95: Final OSL measurement (based on the CAM) and over dispersion value for X5472. Calibrated machine dose rates (Gy/s): 0.03877326 (CG), 0.03819457 (FG).

Central dose (s)	Central Dose Error (s)	OD (%)	OD error (%)
238.61	5.19	0	28.62
271.37	47.55	N/A	N/A

Table D.20: OSL data for Sample X5473 – Coarse Grain and Fine Grain

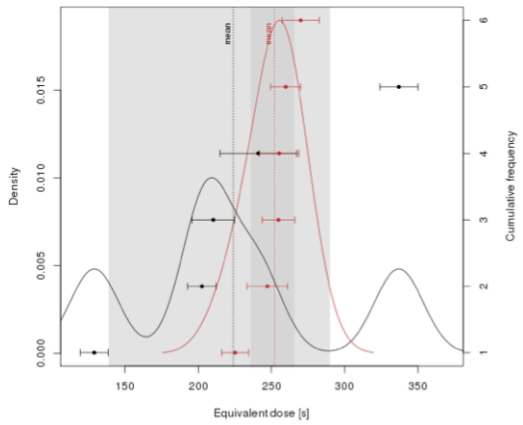

Figure D.96: Kernel Density Estimate Plot for Sample X5473

D_e (s)	D_e error (s)	Test Dose Error (%)	Recycling Ratio	Recup. (%)	IRSL signal (%)
241.04	52.28 (22%)	11	0.88±0.22 (≤10%)	3.0±4.5	7
129.05	18.94 (15%)	≤10	0.91±0.14 (≤10%)	0.8±3.3	4
210.26	29.05 (14%)	≤10	1.31±0.21 (≤10%)	-6.7±-2.1	5
202.47	19.42 (≤10%)	≤10	1.22±0.11 (13%)	0.8±0.4	≤1
336.95	25.76 (≤10%)	≤10	0.84±0.13 (≤10%)	0.7±0.8	≤1
254.78	22.13 (≤10%)	≤10	1.38±0.33 (≤10%)	-3.9±-1.6	2
259.76	20.62 (≤10%)	≤10	1.03±0.15 (≤10%)	-0.6±-0.9	≤1
269.99	25.41 (≤10%)	≤10	1.30±0.18 (12%)	-0.5±-0.8	≤1
255.31	26.94 (11%)	≤10	0.88±0.22 (≤10%)	-2.0±-2.0	3
247.22	27.52 (12%)	≤10	0.90±0.17 (≤10%)	2.3±1.5	≤1
225.21	18.70 (≤10%)	≤10	0.91±0.14 (≤10%)	0.2±1.2	≤1

Figure D.97: Primary Dataset for KDE plot for X5473. NB Primary data set is comprised of 3 aliquots selected from a total of 12 aliquots (coarse grains) and 6 out of 6 aliquots (fine grains) after selection criteria were met.

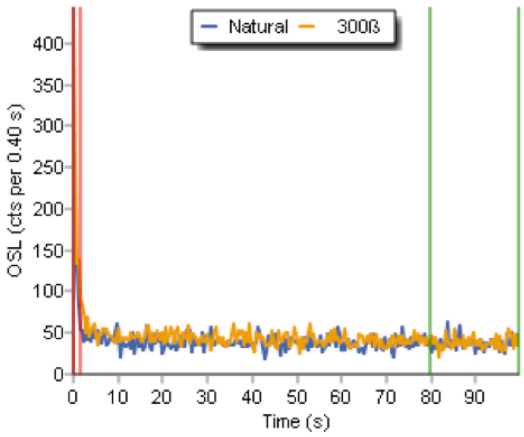

Figure D.98: OSL shine down curve for a representative aliquot of X5473

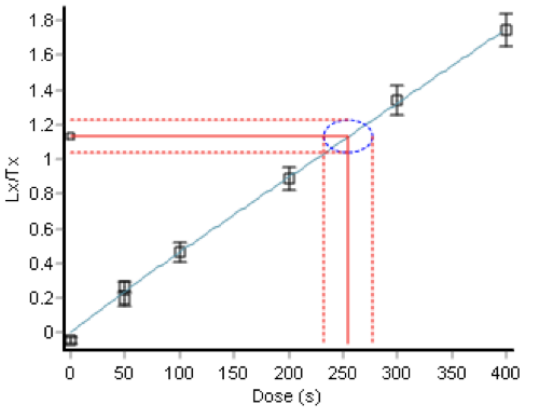

Figure D.99: OSL dose response curve for a representative aliquot of X5473

Figure D.100: Final OSL measurement (based on the CAM) and over dispersion value for X5473. Calibrated machine dose rates (Gy/s): 0.03877326 (CG), 0.03819457 (FG).

Central dose (s)	Central Dose Error (s)	OD (%)	OD error (%)
215.74	31.19	29.28	N/A
251.08	9.36	0	N/A

Appendix E

DRAC input and output data for material from Bêt Khallaf

Table E.1: Input Data for DRAC for material from Bêt Khallaf

Sample ID	FG/CG	Mineral	Conversion factors	ExternalU (ppm)	errExternal U (ppm)	External Th (ppm)	errExternal Th (ppm)	External K (%)	errExternal K (%)	Calculate external Rb from K conc?	Grain size min (microns)	Grain size max (microns)
X4113	CG	Q	Guerinetal2011	1.34	0.075	5.2	0.2912	1.19	0.06664	Y	90	180
X4114	CG	Q	Guerinetal2011	1.03	0.058	4.32	0.24192	0.98	0.05488	Y	90	250
X4115	CG	Q	Guerinetal2011	1.45	0.081	5.83	0.32648	1.26	0.07056	Y	90	180
X4116	CG	Q	Guerinetal2011	1.99	0.111	7.3	0.4088	0.98	0.05488	Y	90	180
X4113	FG	PM	Guerinetal2011	1.34	0.075	5.2	0.2912	1.19	0.06664	Y	4	11
X4115	FG	PM	Guerinetal2011	1.45	0.081	5.83	0.32648	1.26	0.07056	Y	4	11
X4117	FG	PM	Guerinetal2011	1.85	0.104	7.5	0.42	1.25	0.07	Y	4	11
X4118	FG	PM	Guerinetal2011	2.3	0.129	6.3	0.3528	1.54	0.08624	Y	4	11
X5458	CG	Q	Guerinetal2011	1.82	0.102	6.7	0.3752	0.97	0.05432	Y	90	180
X5459	CG	Q	Guerinetal2011	2.45	0.137	7.69	0.43064	1.01	0.05656	Y	90	250
X5461	CG	Q	Guerinetal2011	1.31	0.073	5.56	0.31136	1.51	0.08456	Y	90	180
X5462	CG	Q	Guerinetal2011	1.19	0.067	4.9	0.2744	1.32	0.07392	Y	180	250
X5463	CG	Q	Guerinetal2011	1.24	0.069	5.95	0.3332	1.45	0.0812	Y	90	250
X5464	CG	Q	Guerinetal2011	1.27	0.07112	5.78	0.32368	1.33	0.07448	Y	90	180
X5458	FG	PM	Guerinetal2011	1.81	0.10136	6.7	0.3752	0.97	0.05432	Y	4	11
X5460	FG	PM	Guerinetal2011	1.9	0.1064	6.2	0.3472	1.83	0.10248	Y	4	11
X5461	FG	PM	Guerinetal2011	1.31	0.07336	5.56	0.31136	1.51	0.08456	Y	4	11
X5463	FG	PM	Guerinetal2011	1.24	0.06944	5.95	0.3332	1.45	0.0812	Y	4	11
X5464	FG	PM	Guerinetal2011	1.27	0.07112	5.78	0.32368	1.33	0.07448	Y	4	11
X5465	CG	Q	Guerinetal2011	1.7	0.0952	7.06	0.39536	1.41	0.07896	Y	90	180
X5466	CG	Q	Guerinetal2011	3.68	0.20608	17.58	0.98448	1.59	0.08904	Y	90	250
X5467	CG	Q	Guerinetal2011	1.15	0.0644	5.63	0.31528	1.48	0.08288	Y	90	250
X5468	CG	Q	Guerinetal2011	1.88	0.10528	6.95	0.3892	1.04	0.05824	Y	90	180
X5470	CG	Q	Guerinetal2011	1.14	0.06384	6.05	0.3388	1.27	0.07112	Y	90	250
X5472	CG	Q	Guerinetal2011	1.43	0.08008	5.15	0.2884	1.37	0.07672	Y	90	250
X5473	CG	Q	Guerinetal2011	1.77	0.09912	5.64	0.31584	1.22	0.06832	Y	90	180
X5465	FG	PM	Guerinetal2011	1.7	0.0952	7.06	0.39536	1.41	0.07896	Y	4	11
X5467	FG	PM	Guerinetal2011	1.15	0.0644	5.63	0.31528	1.48	0.08288	Y	4	11
X5468	FG	PM	Guerinetal2011	1.88	0.10528	6.95	0.3892	1.04	0.05824	Y	4	11
X5470	FG	PM	Guerinetal2011	1.14	0.06384	6.05	0.3388	1.27	0.07112	Y	4	11
X5472	FG	PM	Guerinetal2011	1.43	0.08008	5.15	0.2884	1.37	0.07672	Y	4	11
X5473	FG	PM	Guerinetal2011	1.77	0.09912	5.64	0.31584	1.22	0.06832	Y	4	11
X5460(3)	CG	Q	Guerinetal2011	1.42	0.07952	5.79	0.32424	1.48	0.08288	Y	90	250
X5460(3)	FG	PM	Guerinetal2011	1.42	0.0795	5.79	0.3242	1.48	0.0829	Y	4	11
X4118(3)	CG	Q	Guerinetal2011	1.42	0.0795	5.79	0.3242	1.48	0.0829	Y	90	180
X4118(3)	FG	PM	Guerinetal2011	1.42	0.0795	5.79	0.3242	1.48	0.0829	Y	4	11

Table E.2: Input Data for DRAC for material from Bêt Khallaf continued

Sample ID	alpha-Grain size attenuation	beta-Grain size attenuation	Etch depth min (microns)	Etch depth max (microns)	beta-Etch depth attenuation factor	a-value	erra-value	Water content ((wet weight - dry weight)/dry weight) %	errWater content %
X4113	Brennanetal1991	Guerinetal2012-Q	0	0	X	0.1	0.02	3	2
X4114	Brennanetal1991	Guerinetal2012-Q	0	0	X	0.1	0.02	3	2
X4115	Brennanetal1991	Guerinetal2012-Q	0	0	X	0.1	0.02	3	2
X4116	Brennanetal1991	Guerinetal2012-Q	0	0	X	0.1	0.02	3	2
X4113	Brennanetal1991	Guerinetal2012-Q	0	0	X	0.038	0.002	3	2
X4115	Brennanetal1991	Guerinetal2012-Q	0	0	X	0.038	0.002	3	2
X4117	Brennanetal1991	Guerinetal2012-Q	0	0	X	0.038	0.002	3	2
X4118	Brennanetal1991	Guerinetal2012-Q	0	0	X	0.038	0.002	3	2
X5458	Brennanetal1991	Guerinetal2012-Q	0	0	X	0.1	0.02	3	2
X5459	Brennanetal1991	Guerinetal2012-Q	0	0	X	0.1	0.02	3	2
X5461	Brennanetal1991	Guerinetal2012-Q	0	0	X	0.1	0.02	3	2
X5462	Brennanetal1991	Guerinetal2012-Q	0	0	X	0.1	0.02	3	2
X5463	Brennanetal1991	Guerinetal2012-Q	0	0	X	0.1	0.02	3	2
X5464	Brennanetal1991	Guerinetal2012-Q	0	0	X	0.1	0.02	3	2
X5458	Brennanetal1991	Guerinetal2012-Q	0	0	X	0.038	0.002	3	2
X5460	Brennanetal1991	Guerinetal2012-Q	0	0	X	0.038	0.002	3	2
X5461	Brennanetal1991	Guerinetal2012-Q	0	0	X	0.038	0.002	3	2
X5463	Brennanetal1991	Guerinetal2012-Q	0	0	X	0.038	0.002	3	2
X5464	Brennanetal1991	Guerinetal2012-Q	0	0	X	0.038	0.002	3	2
X5465	Brennanetal1991	Guerinetal2012-Q	0	0	X	0.1	0.02	3	2
X5466	Brennanetal1991	Guerinetal2012-Q	0	0	X	0.1	0.02	3	2
X5467	Brennanetal1991	Guerinetal2012-Q	0	0	X	0.1	0.02	3	2
X5468	Brennanetal1991	Guerinetal2012-Q	0	0	X	0.1	0.02	3	2
X5470	Brennanetal1991	Guerinetal2012-Q	0	0	X	0.1	0.02	3	2
X5472	Brennanetal1991	Guerinetal2012-Q	0	0	X	0.1	0.02	3	2
X5473	Brennanetal1991	Guerinetal2012-Q	0	0	X	0.1	0.02	3	2
X5465	Brennanetal1991	Guerinetal2012-Q	0	0	X	0.038	0.002	3	2
X5467	Brennanetal1991	Guerinetal2012-Q	0	0	X	0.038	0.002	3	2
X5468	Brennanetal1991	Guerinetal2012-Q	0	0	X	0.038	0.002	3	2
X5470	Brennanetal1991	Guerinetal2012-Q	0	0	X	0.038	0.002	3	2
X5472	Brennanetal1991	Guerinetal2012-Q	0	0	X	0.038	0.002	3	2
X5473	Brennanetal1991	Guerinetal2012-Q	0	0	X	0.038	0.002	3	2
X5460(3)	Brennanetal1991	Guerinetal2012-Q	0	0	X	0.1	0.02	3	2
X5460(3)	Brennanetal1991	Guerinetal2012-Q	0	0	X	0.038	0.002	3	2
X4118(3)	Brennanetal1991	Guerinetal2012-Q	0	0	X	0.1	0.02	3	2
X4118(3)	Brennanetal1991	Guerinetal2012-Q	0	0	X	0.038	0.002	3	2

Table E.3: Input Data for DRAC for material from Bêt Khallaf continued

Sample ID	Depth (m)	errDepth (m)	Overburden density (g cm-3)	errOverburden density (g cm-3)	Latitude (decimal degrees)	Longitude (decimal degrees)	Altitude (m)
X4113	12	1	2	0.2	26.295483	31.7717979	94
X4114	12	1	2	0.2	26.295483	31.7717979	94
X4115	12	1	2	0.2	26.295483	31.7717979	94
X4116	11	1	2	0.2	26.295483	31.7717979	94
X4113	12	1	2	0.2	26.295483	31.7717979	94
X4115	12	1	2	0.2	26.295483	31.7717979	94
X4117	12	1	2	0.2	26.295483	31.7717979	94
X4118	12	1	2	0.2	26.295483	31.7717979	94
X5458	27	1	2	0.2	26.295483	31.7717979	94
X5459	27	1	2	0.2	26.295483	31.7717979	94
X5461	12	1	2	0.2	26.295483	31.7717979	94
X5462	11	1	2	0.2	26.295483	31.7717979	94
X5463	12	1	2	0.2	26.295483	31.7717979	94
X5464	12	1	2	0.2	26.295483	31.7717979	94
X5458	27	1	2	0.2	26.295483	31.7717979	94
X5460	12	1	2	0.2	26.295483	31.7717979	94
X5461	12	1	2	0.2	26.295483	31.7717979	94
X5463	12	1	2	0.2	26.295483	31.7717979	94
X5464	12	1	2	0.2	26.295483	31.7717979	94
X5465	12	1	2	0.2	26.295483	31.7717979	94
X5466	12	1	2	0.2	26.295483	31.7717979	94
X5467	11	1	2	0.2	26.295483	31.7717979	94
X5468	12	1	2	0.2	26.295483	31.7717979	94
X5470	12	1	2	0.2	26.295483	31.7717979	94
X5472	12	1	2	0.2	26.295483	31.7717979	94
X5473	12	1	2	0.2	26.295483	31.7717979	94
X5465	12	1	2	0.2	26.295483	31.7717979	94
X5467	11	1	2	0.2	26.295483	31.7717979	94
X5468	12	1	2	0.2	26.295483	31.7717979	94
X5470	12	1	2	0.2	26.295483	31.7717979	94
X5472	12	1	2	0.2	26.295483	31.7717979	94
X5473	12	1	2	0.2	26.295483	31.7717979	94
X5460(3)	12	1	2	0.2	26.295483	31.7717979	94
X5460(3)	12	1	2	0.2	26.295483	31.7717979	94
X4118(3)	11	1	2	0.2	26.295483	31.7717979	94
X4118(3)	12	1	2	0.2	26.295483	31.7717979	94

Table E.4: DRAC outputs for material from Bêt Khallaf

Sample ID	FG/CG	Mineral	Water corrected alpha-doserate	Water corrected erralpha-doserate	Water corrected betadoser-ate	Water corrected errbeta-doserate	Cosmic-doserate (Gy.ka-1)	errCosmic-doserate (Gy.ka-1)
X4113	CG	Q	0.1	0.027	1.16	0.06	0.051	0.005
X4114	CG	Q	0.072	0.026	0.931	0.053	0.051	0.005
X4115	CG	Q	0.11	0.03	1.239	0.064	0.051	0.005
X4116	CG	Q	0.143	0.039	1.133	0.054	0.056	0.006
X4113	FG	PM	0.236	0.02	1.247	0.061	0.051	0.005
X4115	FG	PM	0.26	0.022	1.333	0.065	0.051	0.005
X4117	FG	PM	0.333	0.028	1.424	0.067	0.051	0.005
X4118	FG	PM	0.343	0.029	1.681	0.081	0.051	0.005
X5458	CG	Q	0.131	0.035	1.091	0.053	0.018	0.002
X5459	CG	Q	0.147	0.052	1.201	0.062	0.018	0.002
X5461	CG	Q	0.102	0.028	1.4	0.075	0.051	0.005
X5462	CG	Q	0.054	0.01	1.184	0.063	0.056	0.006
X5463	CG	Q	0.094	0.034	1.334	0.077	0.051	0.005
X5464	CG	Q	0.103	0.029	1.267	0.067	0.051	0.005
X5458	FG	PM	0.311	0.026	1.179	0.054	0.018	0.002
X5460	FG	PM	0.307	0.026	1.85	0.093	0.051	0.005
X5461	FG	PM	0.241	0.02	1.502	0.076	0.051	0.005
X5463	FG	PM	0.245	0.02	1.456	0.074	0.051	0.005
X5464	FG	PM	0.243	0.02	1.362	0.068	0.051	0.005
X5465	CG	Q	0.131	0.036	1.408	0.072	0.051	0.005
X5466	CG	Q	0.278	0.102	1.991	0.101	0.051	0.005
X5467	CG	Q	0.088	0.032	1.338	0.078	0.056	0.006
X5468	CG	Q	0.136	0.037	1.156	0.056	0.051	0.005
X5470	CG	Q	0.092	0.034	1.193	0.068	0.051	0.005
X5472	CG	Q	0.092	0.033	1.282	0.073	0.051	0.005
X5473	CG	Q	0.119	0.032	1.245	0.063	0.051	0.005
X5465	FG	PM	0.31	0.026	1.517	0.074	0.051	0.005
X5467	FG	PM	0.229	0.019	1.458	0.075	0.056	0.006
X5468	FG	PM	0.323	0.027	1.25	0.058	0.051	0.005
X5470	FG	PM	0.238	0.02	1.304	0.065	0.051	0.005
X5472	FG	PM	0.242	0.02	1.398	0.07	0.051	0.005
X5473	FG	PM	0.283	0.024	1.341	0.064	0.051	0.005
X5460(3)	CG	Q	0.098	0.035	1.374	0.079	0.051	0.005
X5460(3)	FG	PM	0.256	0.021	1.5	0.075	0.051	0.005
X4118(3)	CG	Q	0.108	0.03	1.397	0.074	0.056	0.006
X4118(3)	FG	PM	0.256	0.021	1.5	0.075	0.051	0.005

Appendix F

Mineralogy of ceramics samples

Another factor which can potentially impact on $\dot{D}$ is inclusions of additional minerals, or, more specifically, the potential dose received by the sample from radiogenic minerals contained within the sample's clay fabric. Inclusions found in ceramic fabrics are often a mixture of minerals, many of which can have their own radiogenic properties that can affect the dose rate received by the quartz grains within the sample.

To determine which minerals may be present in a sample in addition to quartz, it is possible to examine sample material, after OSL measurement, under an SEM. It was beyond the scope of this project to examine every aliquot measured, thus only two representative samples of each Nile and marl clay from Bêt Khallaf were examined. In addition to this a literature review was also done to determine the extent of additional minerals commonly found within Egyptian clays.

For the two marl and two Nile silt samples selected from the Bêt Khallaf data set, an SEM mineral map was made of ∼50% of a fine grain aliquot of each sample.[68] Figures F.1 and F.2 present two example images of the SEM mapping process carried out.

The mineral maps provide a brief, but informative overview of a selection of grains

[68] Unfortunately SEM analysis could only be carried out upon the fine grain fraction of the samples. This is because prior to OSL measurement, the coarse mineral grains must be held fast on to the surface of the grain (i.e. so that they do not detach during measurement). This is done using a silicon gel. Due to the small number of grains measured on each disc however, the silicon gel was found to coat the grains in a very thick layer of silicon which is difficult to see through on an SEM and the quantity of silica present could potentially make further analysis more difficult. In contrast, the fine grain fraction is settled onto the discs and as such requires no silicon gel as a holding agent. Furthermore, more fine grain material was available for analysis (several thousand grains rather than ∼20 grains), and also no HF acid etch had been carried out upon the sample, thus a more representative mineral fraction would be examined. Of course, fine grain aliquot preparation induces its own biases. In particular, only a 4–11 μm is represented, thus minerals outside this size range will be excluded from analysis. Additionally, the fine grain aliquots were prepared using a settling technique based upon Stokes' law. The settling process was set up to select for quartz grains specifically (i.e. with a density of 2.65g/cm^3) and thus minerals with a significantly different density may not have been obtained during the settling process, thus producing a sampling bias in the final observed material.

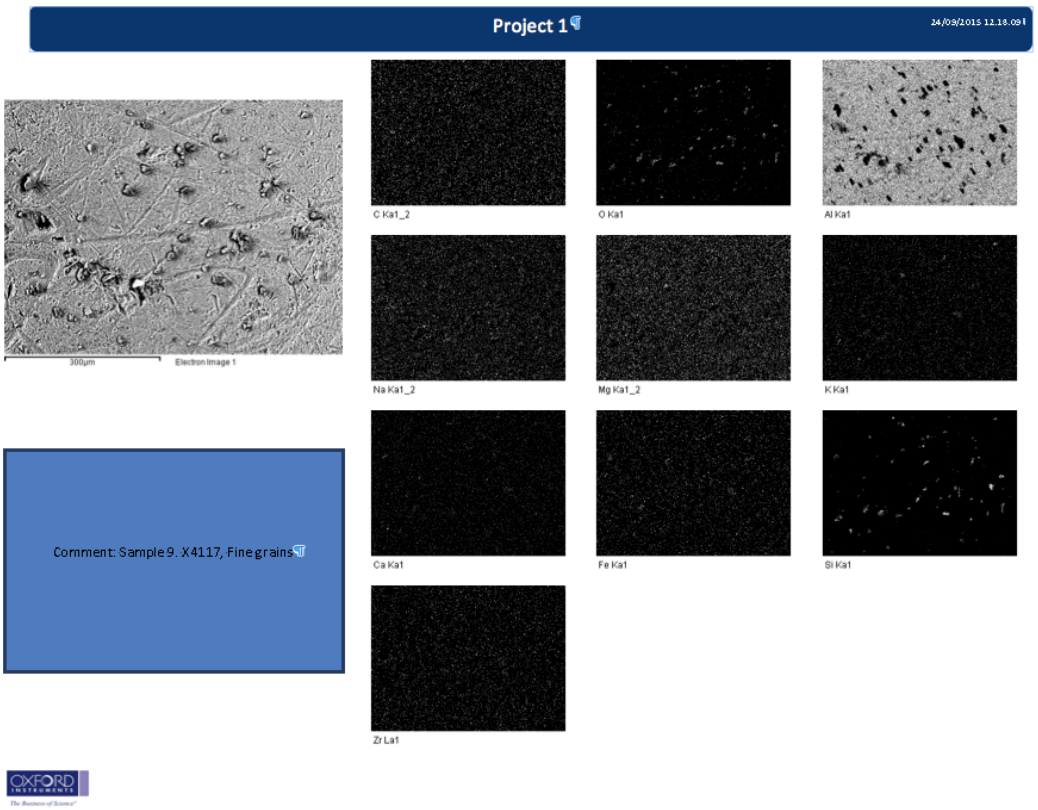

Figure F.1: SEM mineral map of sample X4117, a marl clay sample from Bêt Khallaf.

based upon their elemental composition, where specific elements can be screened for which allow identification of minerals known to potentially affect the dose of the sample. Secondly, SEM mapping allowed a basic understanding of the quantity of specific elements (and thus minerals) to be achieved.

For the purposes of this project, we were particularly interested in determining whether the sample had any zircon inclusions as zircon has properties that can greatly affect the dose rate of a sample, as well as having a luminescence signal of its own (Fleming 1979: 116, Smith et al. 1986: 229).

From analysis of ∼50% of the surface of each aliquot, it was found that the dominant mineral within the grain population was quartz (∼90%), although some feldspars (both Ca, Na, and K feldspars) and some primarily calcium-based minerals (possibly apatite or amphiboles, a more detailed analysis was not possible). In sample X5460 a single zircon was also present. These numbers are approximate only as a full quantitive analysis was not possible due to time restrictions. Therefore, these values are mainly qualitative values. Furthermore, a small quantity of other different types of minerals are likely to be present, as seen in the literature, but only those known to affect the OSL analysis of a sample were actively looked for.

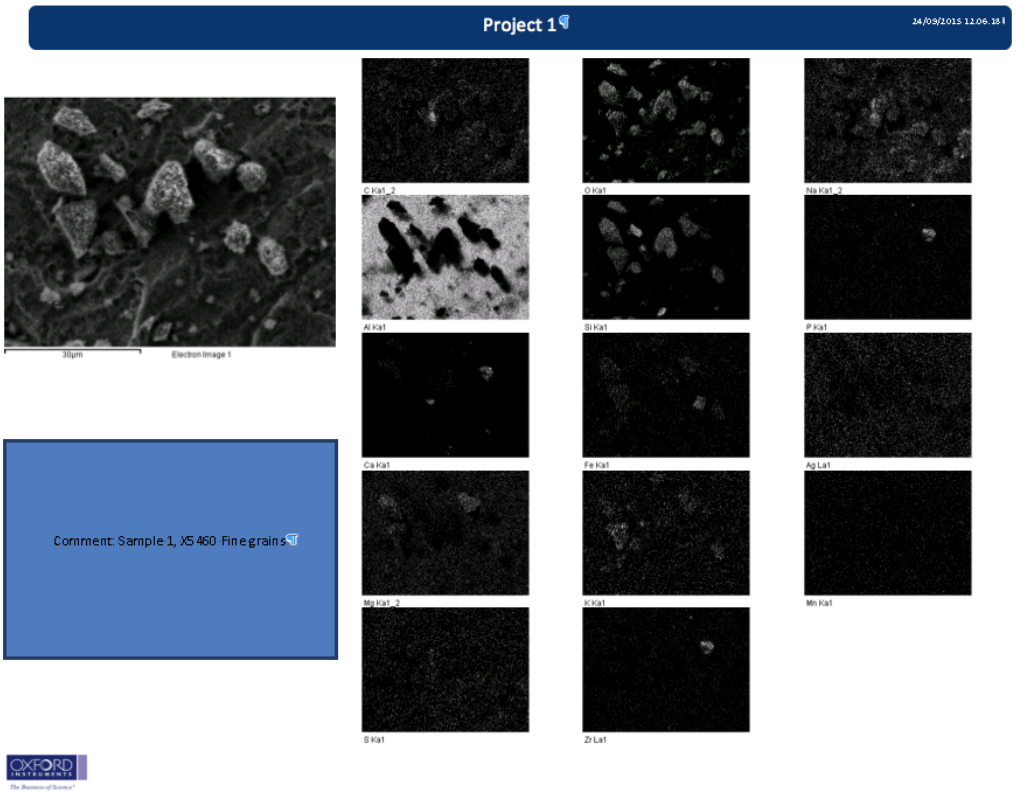

Figure F.2: SEM mineral map of sample X5460, a Nile silt clay sample from Bêt Khallaf.

Of course, given the potential biases of a fine grain fraction with regard to mineral presence/absence, it is difficult to determine absolute occurrence of heavy minerals within the fabric. However, Fleming 1979 does note that we expect to see heavy minerals such as zircon and apatite within most clay fabrics, although these are usually less than < 1%, so again they are not necessarily going to be present in a very small sample size, and, furthermore, it is unlikely that such small concentrations will affect the overall dose rate for this project (only a single zircon was seen out of several thousand grains).

To aid the limited SEM analysis presented here, a literature review for Egyptian petrographic studies was also carried out. Although the literature surrounding petrographic studies is limited, it is still possible to gauge a fairly comprehensive assessment of the typical components found in both Egyptian Nile silt and marl clays for late Naqada III/Old Kingdom ceramics.[69] In a study by Ownby (Ownby 2009) a selection of Old Kingdom pottery was found to have a fairly uniform distribution of clay inclusions across the analysed data set. Marl clay fabrics consistently yielded inclusions of quartz, poly-

[69] A larger corpus of petrographic analysis exists for ceramics dating to other periods of Egyptian history (especially the Middle and New Kingdoms). However, it was decided to limit the material used as a comparative resource to the material which was approximately contemporary with the Bêt Khallaf data set, thus not permitting a temporal bias for clay provenance to affect comparisons too extensively.

crystalline quartz, k-feldspars, plagioclase, mica (muscovite and biotite), limestone, red iron oxides, serpentine, amphiboles, chaff, clay pellets, and chert. Additionally, in some samples, marls were also seen to include pyroxenes, microfossils and epidote, and Nile silts were seen to include garnet and bone. Ownby also includes tentative inclusions (which cannot be verified optically), of marls having tourmaline and zircon present, and the possibility of Niles having epidote, quartzite, volcanic glass, chalcedony, kyanite, grog, zircon, olivines, tourmaline, and zoisite.

Of these inclusions identified by Ownby, the only inclusion found which could potentially affect the $\dot{D}$ of OSL samples was zircon. Yet again, within Ownby's work, zircons seem to be infrequent enough, when coupled with the SEM results presented here, to indicate that zircons are not a significant cause for concern within this project. Furthermore, should zircons be a contributing factor within the Bêt Khallaf samples, it is likely that this would be evidenced by a significantly elevated uranium concentration of well over 100 ppm and as high as several thousand ppm (Fleming 1979: 116).

Another contributing factor to the impacts of additional mineral grains in the clay fabric upon OSL dating is the question of sample homogeneity. In an ideal situation, to accurately determine $\dot{D}_{int}$, one would need to determine the composition and thus the natural radiation emission of the entire matrix, that is, the whole pot. This would of course result in the destruction of the vessel. Obviously, this is not possible for museum material (nor indeed is it desirable for any sample, even from recently excavated fieldwork site)—the sacrifice of an entire ancient object for scientific gain is not a permissible compromise. Thus, the full extent of the clay composition of a vessel can never be fully reconstructed, nor is it guaranteed that the sample taken for analysis is necessarily representative of the entire vessel, though it may be more representative of the material surrounding the D_e sample – only the nearby material matters for $\dot{D}_\alpha$ and $\dot{D}_\beta$. This is unfortunately an unavoidable issue in OSL dating: the only possibility is to acknowledge that $\dot{D}_{int}$ is based on an assumption of a representative sample.

In summary, the elemental and petrographic information allows us to make several necessary, but informed, assumptions as to the nature of the composition of the ceramic material, which in turn assists in understanding the intricacies of accurately constructing $\dot{D}$ for OSL dating:

1. that the majority of the samples are composed mainly of quartz

2. feldspars, zircons, and other minerals which may give rise to an internal dose are present, but in quantities small enough not to necessitate major consideration for the purpose of this project.

3. that the $\dot{D}_{int}$ sample measured is assumed to be representative of the actual $\dot{D}_{int}$ of the vessel.

Appendix G

Sample DosiVox input files for Bêt Khallaf

In this appendix we list an example of the DosiVox input files used for simulation of the external dose rates in Bêt Khallaf. The sections of the file which specify the dosimetry are omitted for brevity as they add no new information. They can easily be recreated by copying the contents of the preceding cartography section and replacing the material indices with the appropriate relative radionucleide concentrations, given at the start of each section.

An example input file for ^{238}U. The file is listed below, with dosimetry information removed for brevity. Radionucleide concentrations are given in Table G.1.

Material Name	Material Index	Radionucleide Concentration (ppm)
Clay	0	1.43
Fill	1	1.51
Gebel	2	1.51
Air	3	0.0
Residue	4	Not Present
ClayBase	5	1.43

Table G.1: Radionucleide concentrations for sample Bêt Khallaf DosiVox input file.

```
 v_emitter_U_npart_8000_id_13 #
    result file name

8000 1. # ( x 1000 ) emitted
   particles, clock value (%)
3 0 0 0 #particle emitted: 1 for
   alpha, 2 for beta, 3 for gamma ;
    momentum of emission in X,Y,Z
   directions (0 0 0 for random
   direction)
1 0.01 #element emitter (1 for
   uranium series, 2 for thorium
   series, 3 for potassium, 0 for
   User Defined), cut in range
   value (mm)
1 3142 5 0 #index for detector
   definition, detector voxel,
   material for mapping, emission
   from grains
7 1 50. 50. #number of probe cells,
    probe diam (mm), probe offset
   in X and Y (in % of voxel X,Y
   sizes)
4  #number of new components
   defined
6  #number of materials used

18 _TiO 1 2 Ti 1 O 1

19 _MnO 1 2 Mn 1 O 1

20 _P2O5 1 2 P 2 O 5

21 _Org 1 3 C 55 H 98 O 6

0  # material index
Clay  # material name
1.6  # dry density (g/cm3)
3  # water content, % of dry mass
11  # number of components
1 60 2 15 9 10 11 2.5 12 4 13 2 14
   2 18 1.5 19 0.5 16 1.5 20 1 #
   component index, % of dry mass
### granulometry ###
2 2.65 5 2 #grain component index,
   density, compacity (%), number
   of granulometric fractions
### diameter in mm, volumetric
   fraction (%) of the total grains
    mass (sum must be equal to 100)
    ###
0.15 70
0.05 30
```

```
1  # material index
Fill  # material name
1.2  # dry density (g/cm3)
3  # water content, % of dry mass
11  # number of components
1 55 2 7.5 9 4.5 11 2 12 10.0 13
    1.5 14 1.5 18 1 20 1 19 0.5 16
    15.5 # component index, % of dry
     mass
### granulometry ###
0 0 0 0 #grain component index,
    density, compacity (%), number
    of granulometric fractions
### diameter in mm, volumetric
    fraction (%) of the total grains
     mass (sum must be equal to 100)
     ###

2  # material index
Gebel  # material name
2.6  # dry density (g/cm3)
3  # water content, % of dry mass
11  # number of components
1 55 2 7.5 9 4.5 11 2 12 10.0 13
    1.5 14 1.5 18 1 20 1 19 0.5 16
    15.5 # component index, % of dry
     mass
### granulometry ###
0 0 0 0 #grain component index,
    density, compacity (%), number
    of granulometric fractions
### diameter in mm, volumetric
    fraction (%) of the total grains
     mass (sum must be equal to 100)
     ###

3  # material index
_Air  # material name
0.001  # dry density (g/cm3)
3.5 # water content, % of dry mass
1  # number of components
15 100 # component index, % of dry
    mass
### granulometry ###
0 0 0 0 #grain component index,
    density, compacity (%), number
    of granulometric fractions
### diameter in mm, volumetric
    fraction (%) of the total grains
     mass (sum must be equal to 100)
     ###

4  # material index
_Residue # material name
1.0  # dry density (g/cm3)
10  # water content, % of dry mass
11  # number of components
1 13 2 3.5 9 1.5 11 0.5 12 3.5 13 1
     14 0.5 18 0.5 20 0.5 19 0.5 21
    75 # component index, % of dry
    mass
### granulometry ###
0 0 0 0 #grain component index,
    density, compacity (%), number
    of granulometric fractions
### diameter in mm, volumetric
    fraction (%) of the total grains
     mass (sum must be equal to 100)
     ###

5  # material index
ClayBase # material name
1.6  # dry density (g/cm3)
3  # water content, % of dry mass
11  # number of components
1 60 2 15 9 10 11 2.5 12 4 13 2 14
    2 18 1.5 19 0.5 16 1.5 20 1 #
    component index, % of dry mass
### granulometry ###
2 2.65 5 2 #grain component index,
    density, compacity (%), number
    of granulometric fractions
### diameter in mm, volumetric
    fraction (%) of the total grains
     mass (sum must be equal to 100)
     ###
0.15 70
0.05 30

15    12   20 # voxels number along
     X,Y and Z axes
300   300   150 #voxels size along X
    ,Y and Z axes (mm)

### MEDIUM COMPOSITION -
    cartography of materials with
    their index

2 2 2 2 2 2 2 2 2 2 2 2 2 2 2
2 2 2 2 2 2 2 2 2 2 2 2 2 2 2
2 2 2 2 2 2 2 2 2 2 2 2 2 2 2
2 2 2 2 2 2 2 2 2 2 2 2 2 2 2
2 2 2 2 2 2 2 2 2 2 2 2 2 2 2
2 2 2 2 2 2 2 2 2 2 2 2 2 2 2
2 2 2 2 2 2 2 2 2 2 2 2 2 2 2
2 2 2 2 2 2 2 2 2 2 2 2 2 2 2
2 2 2 2 2 2 2 2 2 2 2 2 2 2 2
2 2 2 2 2 2 2 2 2 2 2 2 2 2 2
```

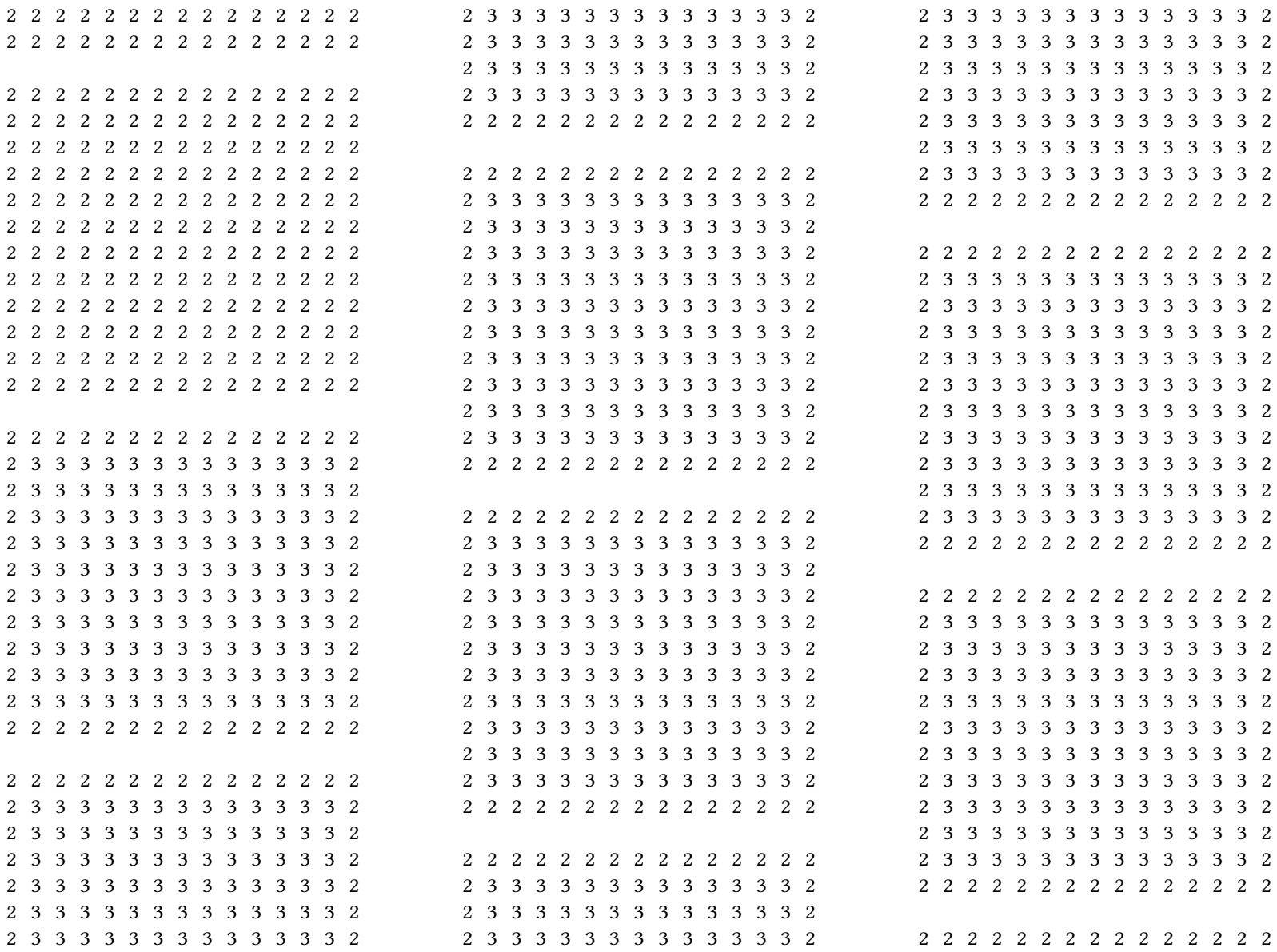

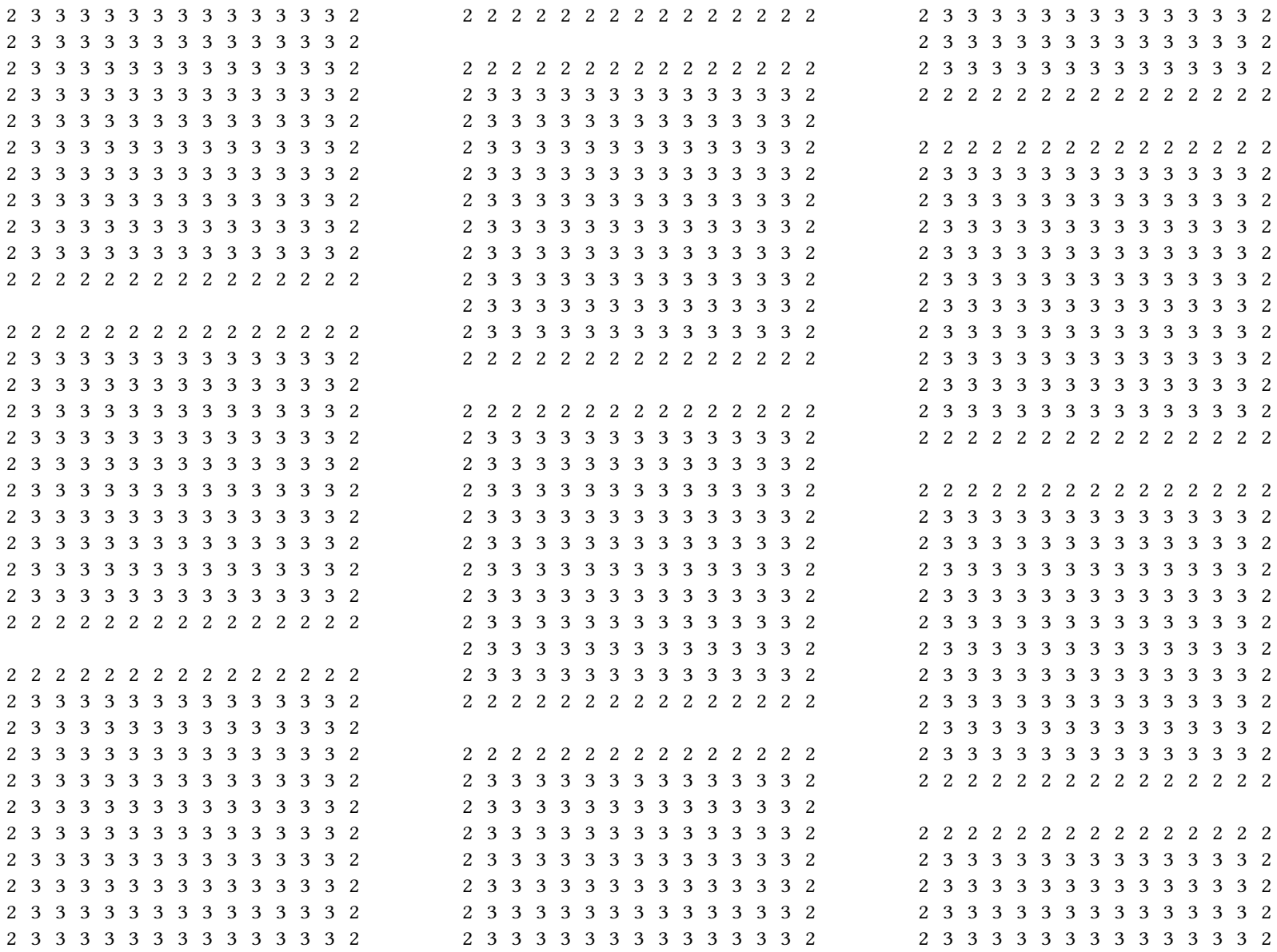

```
2 3 3 3 3 3 3 3 3 3 3 3 3 3 2
2 3 3 3 3 3 3 3 3 3 3 3 3 3 2
2 3 3 3 3 3 3 3 3 3 3 3 3 3 2
2 3 3 3 3 3 3 3 3 3 3 3 3 3 2
2 3 3 3 3 3 3 3 3 3 3 3 3 3 2
2 3 3 3 3 3 3 3 3 3 3 3 3 3 2
2 2 2 2 2 2 2 2 2 2 2 2 2 2 2

2 2 2 2 2 2 2 2 2 2 2 2 2 2 2
2 1 1 1 1 1 1 1 1 1 1 1 1 1 2
2 1 1 1 1 1 1 1 1 1 1 1 1 1 2
2 1 1 1 1 1 1 1 1 1 1 1 1 1 2
2 1 1 1 1 1 1 1 1 1 1 1 1 1 2
```

```
2 1 1 1 1 1 1 1 1 1 1 1 1 1 2
2 1 1 1 1 1 1 1 1 1 1 1 1 1 2
2 1 1 1 1 1 1 1 1 1 1 1 1 1 2
2 1 1 1 1 1 1 1 1 1 1 1 1 1 2
2 1 1 1 1 1 1 1 1 1 1 1 1 1 2
2 1 1 1 1 1 1 1 1 1 1 1 1 1 2
2 2 2 2 2 2 2 2 2 2 2 2 2 2 2

2 2 2 2 2 2 2 2 2 2 2 2 2 2 2
2 1 1 1 1 1 1 1 1 1 1 1 1 1 2
2 1 1 1 1 1 1 1 1 1 1 1 1 1 2
2 1 1 1 1 1 1 1 1 1 1 1 1 1 2
2 1 1 1 1 1 1 1 1 1 1 1 1 1 2
```

```
2 1 1 1 1 1 1 1 1 1 1 1 1 1 2
2 1 1 1 1 1 1 1 1 1 1 1 1 1 2
2 1 1 1 1 1 1 1 1 1 1 1 1 1 2
2 1 1 1 1 1 1 1 1 1 1 1 1 1 2
2 1 1 1 1 1 1 1 1 1 1 1 1 1 2
2 1 1 1 1 1 1 1 1 1 1 1 1 1 2
2 2 2 2 2 2 2 2 2 2 2 2 2 2 2

### Cartography of U, Th or K for
    the external medium :

---Removed for brevity---
```

(Continued Overleaf)

```
### Define detector size ###

30 30 15 # voxels number along X,Y and Z axes

### INTERNAL VOXEL COMPOSITION - cartography of
   materials with their index

3 3 3 3 3 3 3 3 3 3 3 3 3 3 3 3 3 3 3 3 3 3 3 3 3 3 3
   3 3 3
3 3 3 3 3 3 3 3 3 3 3 3 3 3 3 3 3 3 3 3 3 3 3 3 3 3 3
   3 3 3
3 3 3 3 3 3 3 3 3 3 3 3 3 3 3 3 3 3 3 3 3 3 3 3 3 3 3
   3 3 3
3 3 3 3 3 3 3 3 3 3 3 3 3 3 3 3 3 3 3 3 3 3 3 3 3 3 3
   3 3 3
3 3 3 3 3 3 3 3 3 3 3 3 3 3 3 3 3 3 3 3 3 3 3 3 3 3 3
   3 3 3
3 3 3 3 3 3 3 3 3 3 3 3 3 3 3 3 3 3 3 3 3 3 3 3 3 3 3
   3 3 3
3 3 3 3 3 3 3 3 3 3 3 3 3 3 3 3 3 3 3 3 3 3 3 3 3 3 3
   3 3 3
3 3 3 3 3 3 3 3 3 3 3 3 3 3 3 3 3 3 3 3 3 3 3 3 3 3 3
   3 3 3
3 3 3 3 3 3 3 3 3 3 3 3 3 3 3 3 3 3 3 3 3 3 3 3 3 3 3
   3 3 3
3 3 3 3 3 3 3 3 3 0 0 0 0 0 0 0 0 0 0 0 0 3 3 3 3 3 3
   3 3 3
3 3 3 3 3 3 3 3 3 0 3 3 3 3 3 3 3 3 3 3 0 3 3 3 3 3 3
   3 3 3
3 3 3 3 3 3 3 3 3 0 3 3 3 3 3 3 3 3 3 3 0 3 3 3 3 3 3
   3 3 3
3 3 3 3 3 3 3 3 3 0 3 3 3 3 3 3 3 3 3 3 0 3 3 3 3 3 3
   3 3 3
3 3 3 3 3 3 3 3 3 0 3 3 3 3 3 3 3 3 3 3 0 3 3 3 3 3 3
   3 3 3
3 3 3 3 3 3 3 3 3 0 3 3 3 3 3 3 3 3 3 3 0 3 3 3 3 3 3
   3 3 3
3 3 3 3 3 3 3 3 3 0 3 3 3 3 3 3 3 3 3 3 0 3 3 3 3 3 3
   3 3 3
3 3 3 3 3 3 3 3 3 0 3 3 3 3 3 3 3 3 3 3 0 3 3 3 3 3 3
   3 3 3
3 3 3 3 3 3 3 3 3 0 3 3 3 3 3 3 3 3 3 3 0 3 3 3 3 3 3
   3 3 3
3 3 3 3 3 3 3 3 3 0 3 3 3 3 3 3 3 3 3 3 0 3 3 3 3 3 3
   3 3 3
3 3 3 3 3 3 3 3 3 0 3 3 3 3 3 3 3 3 3 3 0 3 3 3 3 3 3
   3 3 3
3 3 3 3 3 3 3 3 3 0 0 0 0 0 0 0 0 0 0 0 0 3 3 3 3 3 3
   3 3 3
3 3 3 3 3 3 3 3 3 3 3 3 3 3 3 3 3 3 3 3 3 3 3 3 3 3 3
   3 3 3
3 3 3 3 3 3 3 3 3 3 3 3 3 3 3 3 3 3 3 3 3 3 3 3 3 3 3
   3 3 3
3 3 3 3 3 3 3 3 3 3 3 3 3 3 3 3 3 3 3 3 3 3 3 3 3 3 3
   3 3 3
3 3 3 3 3 3 3 3 3 3 3 3 3 3 3 3 3 3 3 3 3 3 3 3 3 3 3
   3 3 3
3 3 3 3 3 3 3 3 3 3 3 3 3 3 3 3 3 3 3 3 3 3 3 3 3 3 3
   3 3 3
3 3 3 3 3 3 3 3 3 3 3 3 3 3 3 3 3 3 3 3 3 3 3 3 3 3 3
   3 3 3
3 3 3 3 3 3 3 3 3 3 3 3 3 3 3 3 3 3 3 3 3 3 3 3 3 3 3
   3 3 3
3 3 3 3 3 3 3 3 3 3 3 3 3 3 3 3 3 3 3 3 3 3 3 3 3 3 3
   3 3 3
3 3 3 3 3 3 3 3 3 3 3 3 3 3 3 3 3 3 3 3 3 3 3 3 3 3 3
   3 3 3

3 3 3 3 3 3 3 3 3 3 3 3 3 3 3 3 3 3 3 3 3 3 3 3 3 3 3
   3 3 3
3 3 3 3 3 3 3 3 3 3 3 3 3 3 3 3 3 3 3 3 3 3 3 3 3 3 3
   3 3 3
```

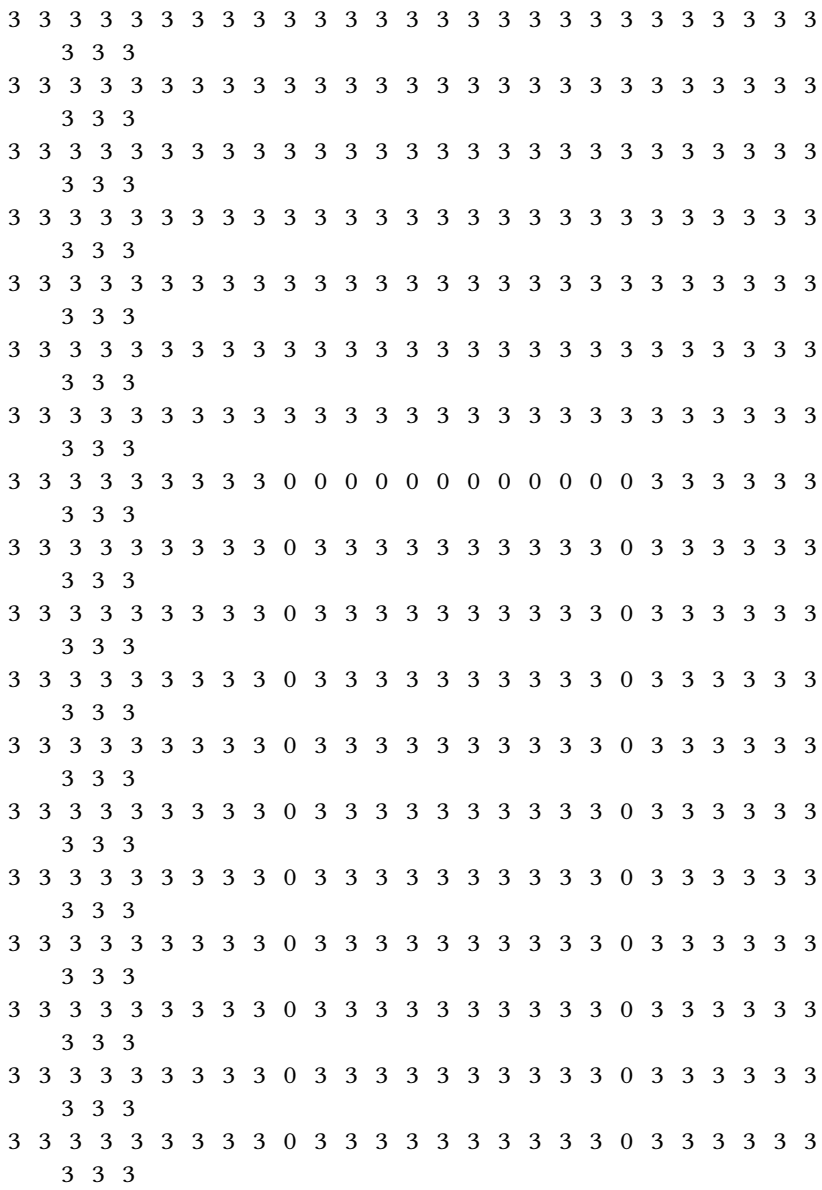

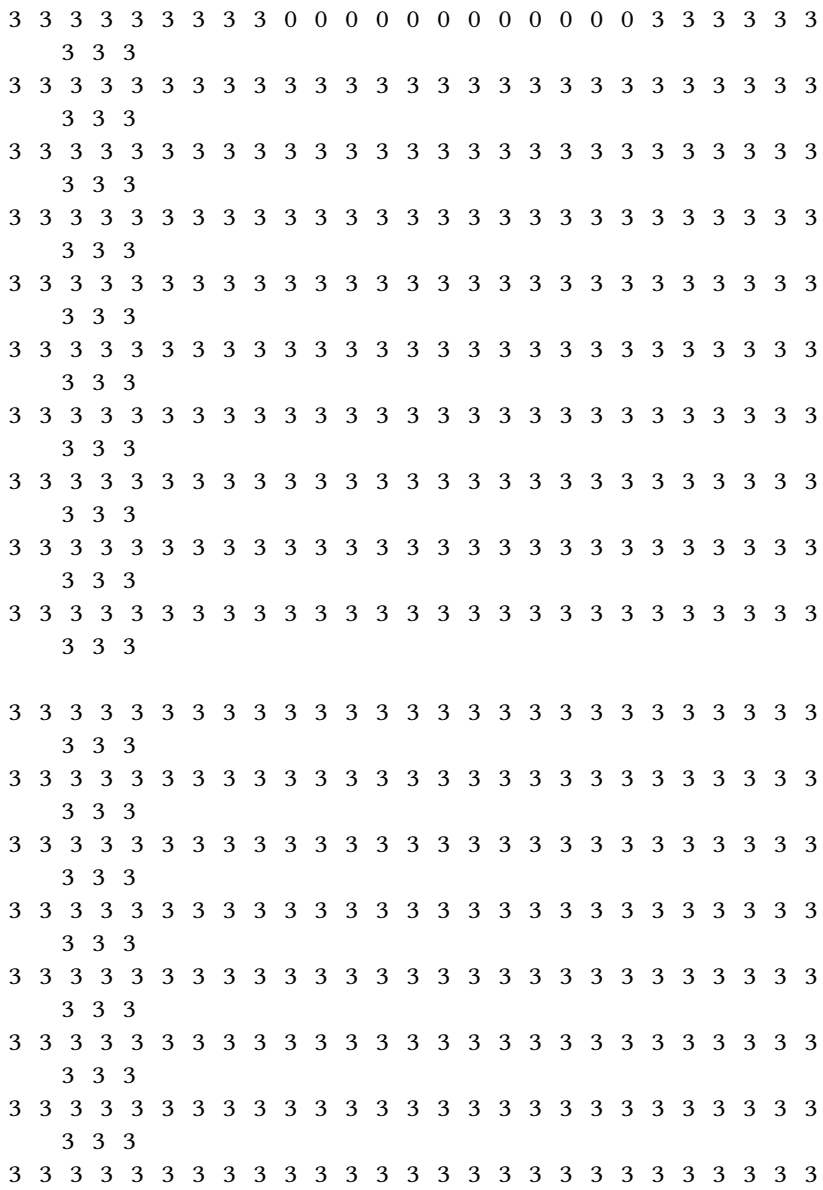

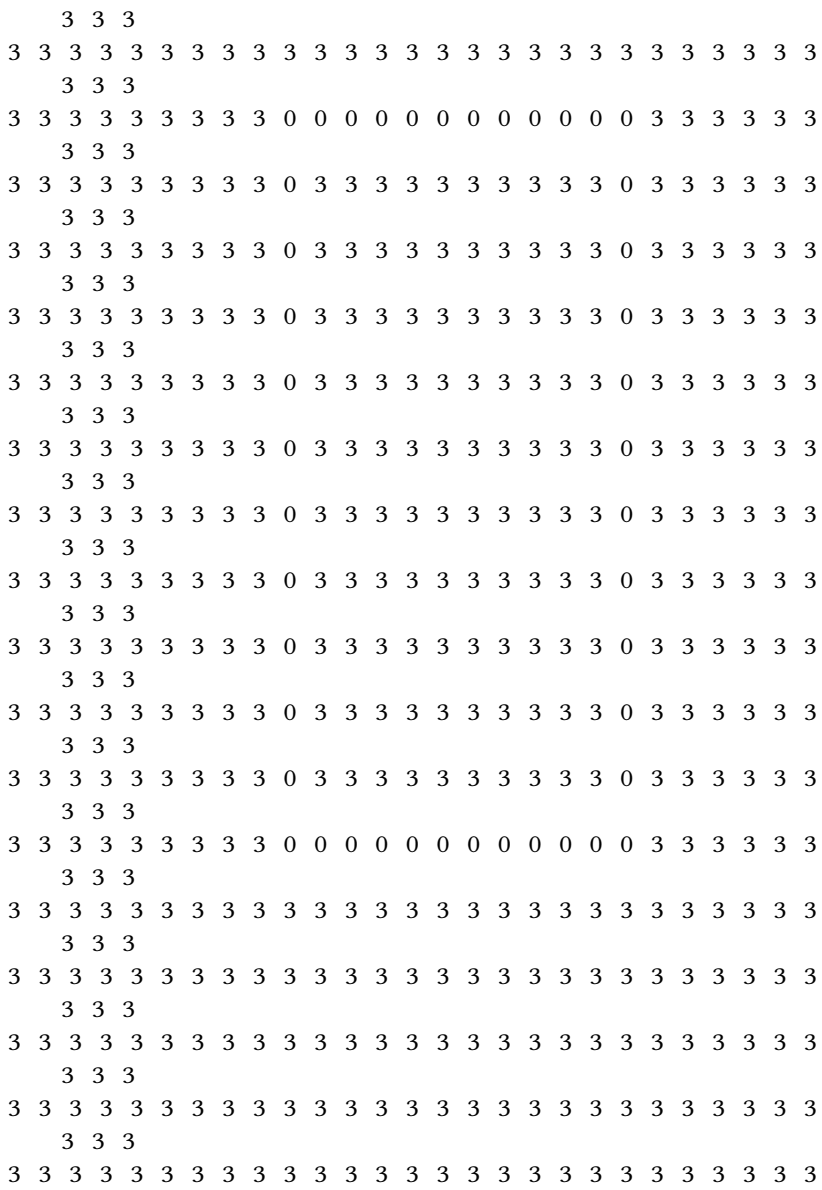

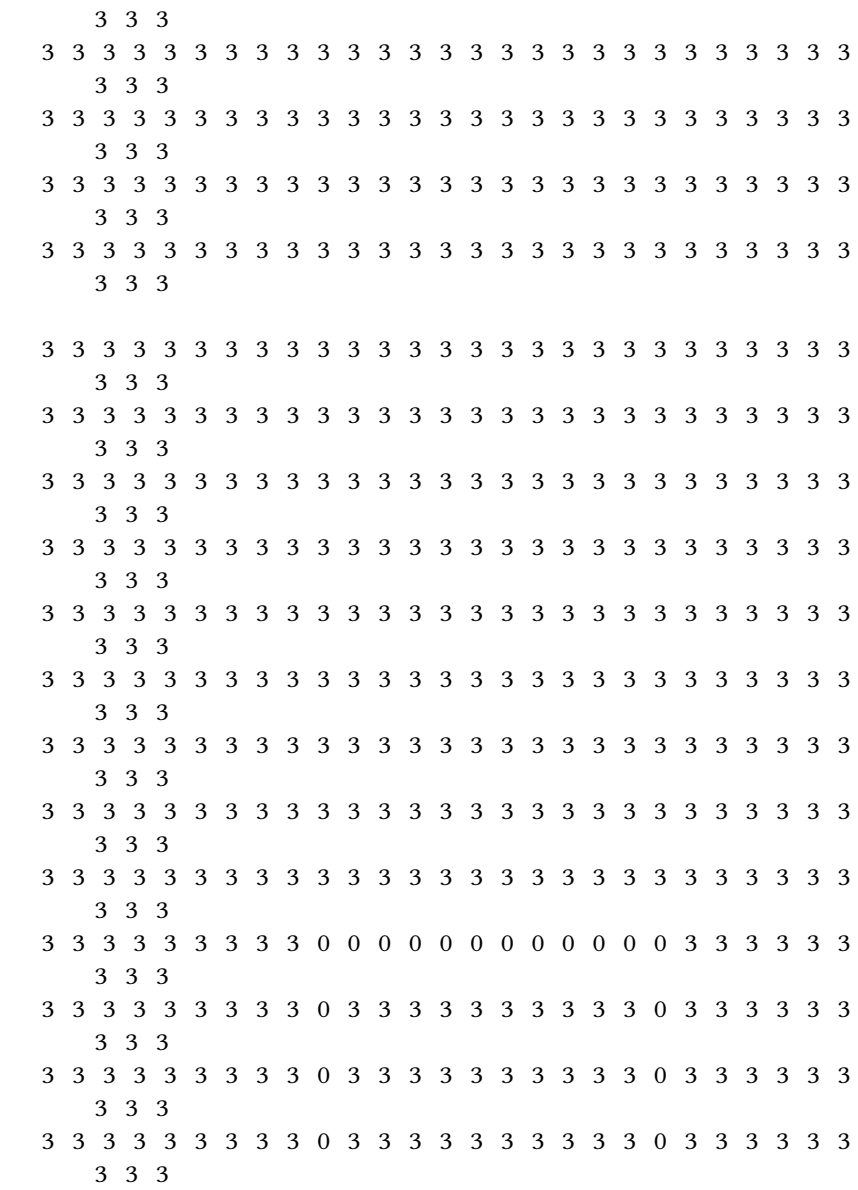

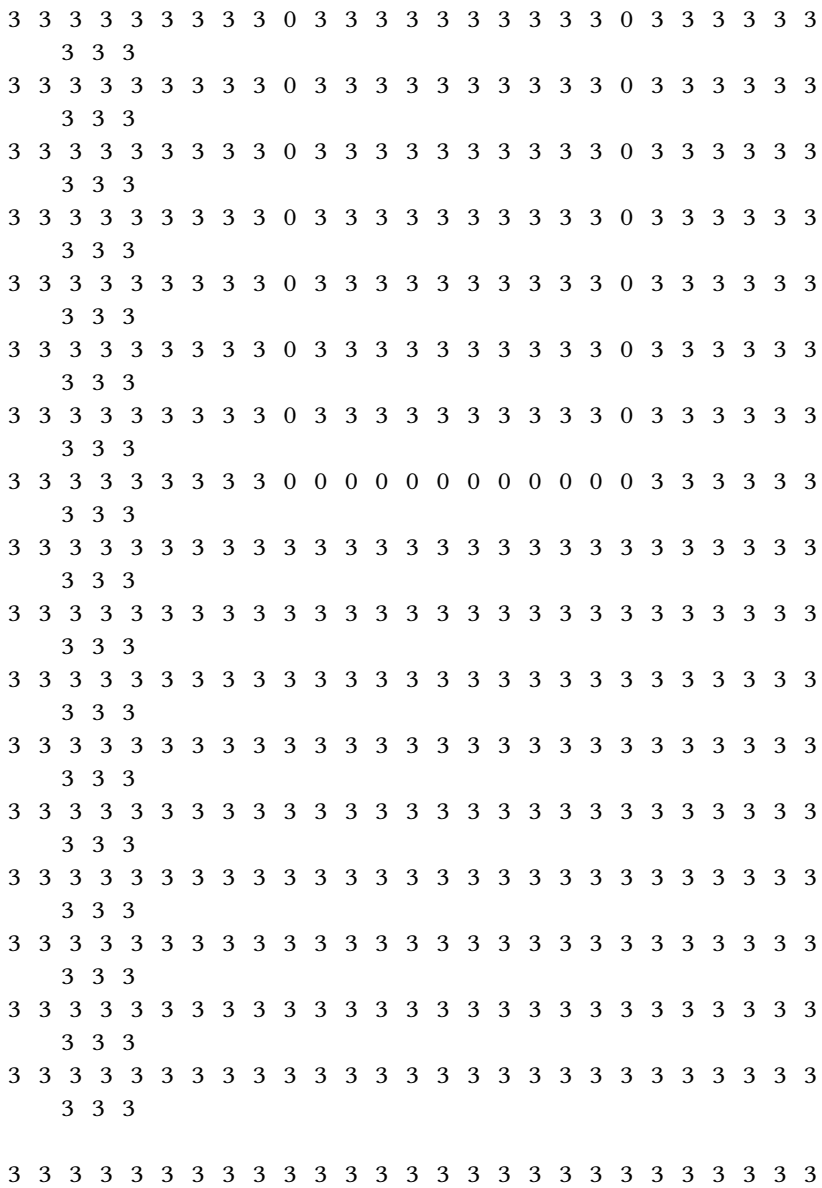

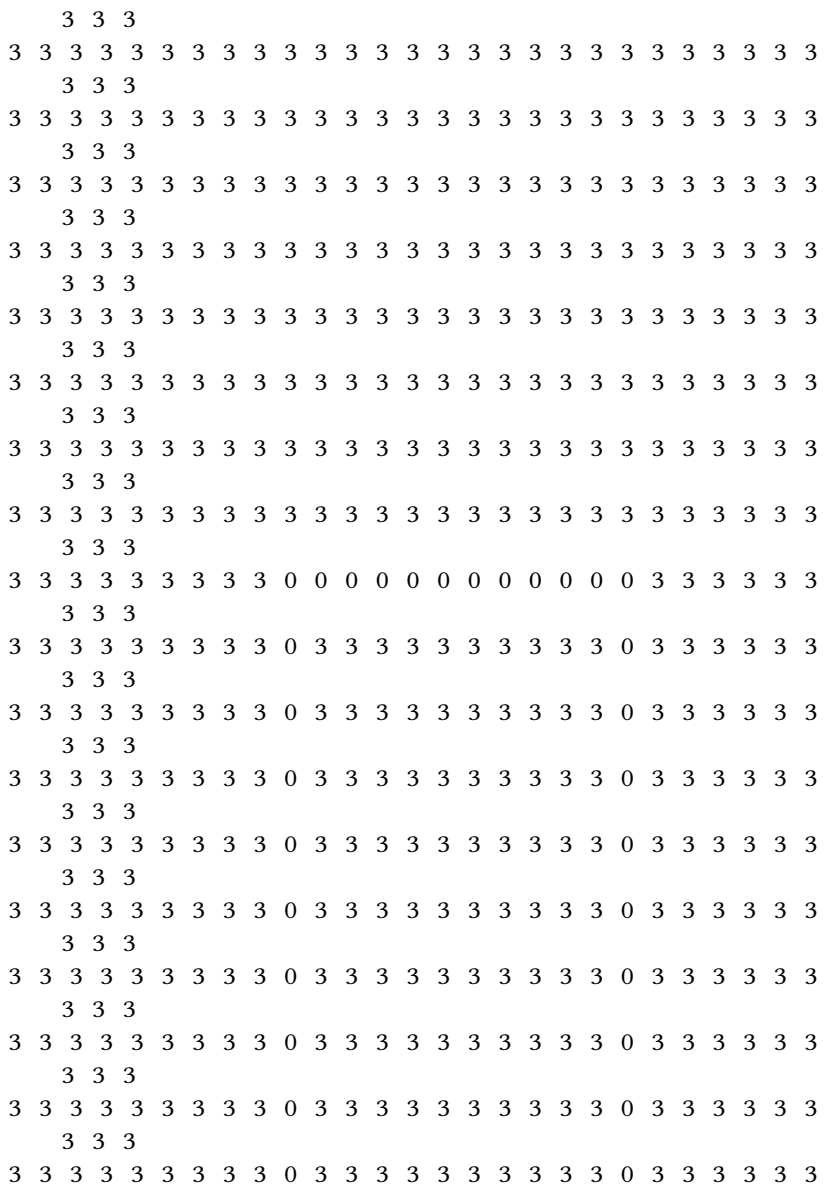

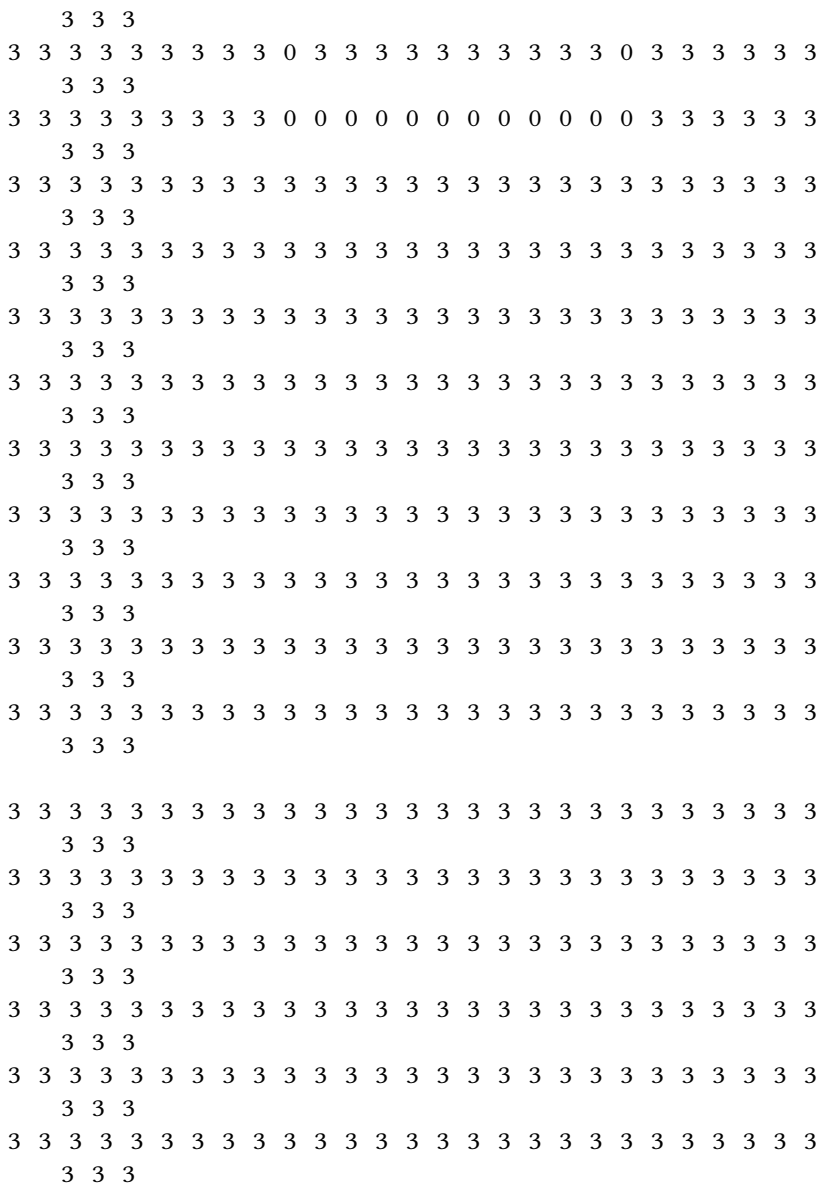

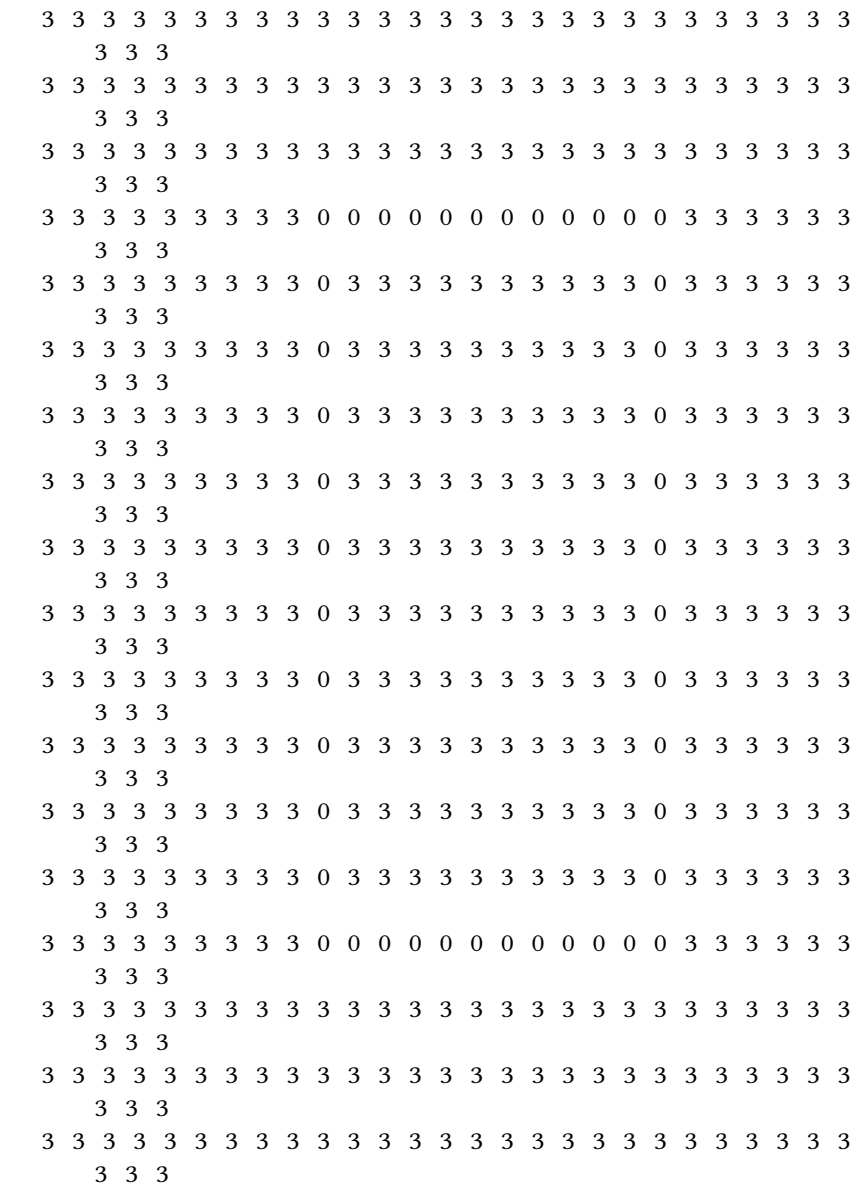

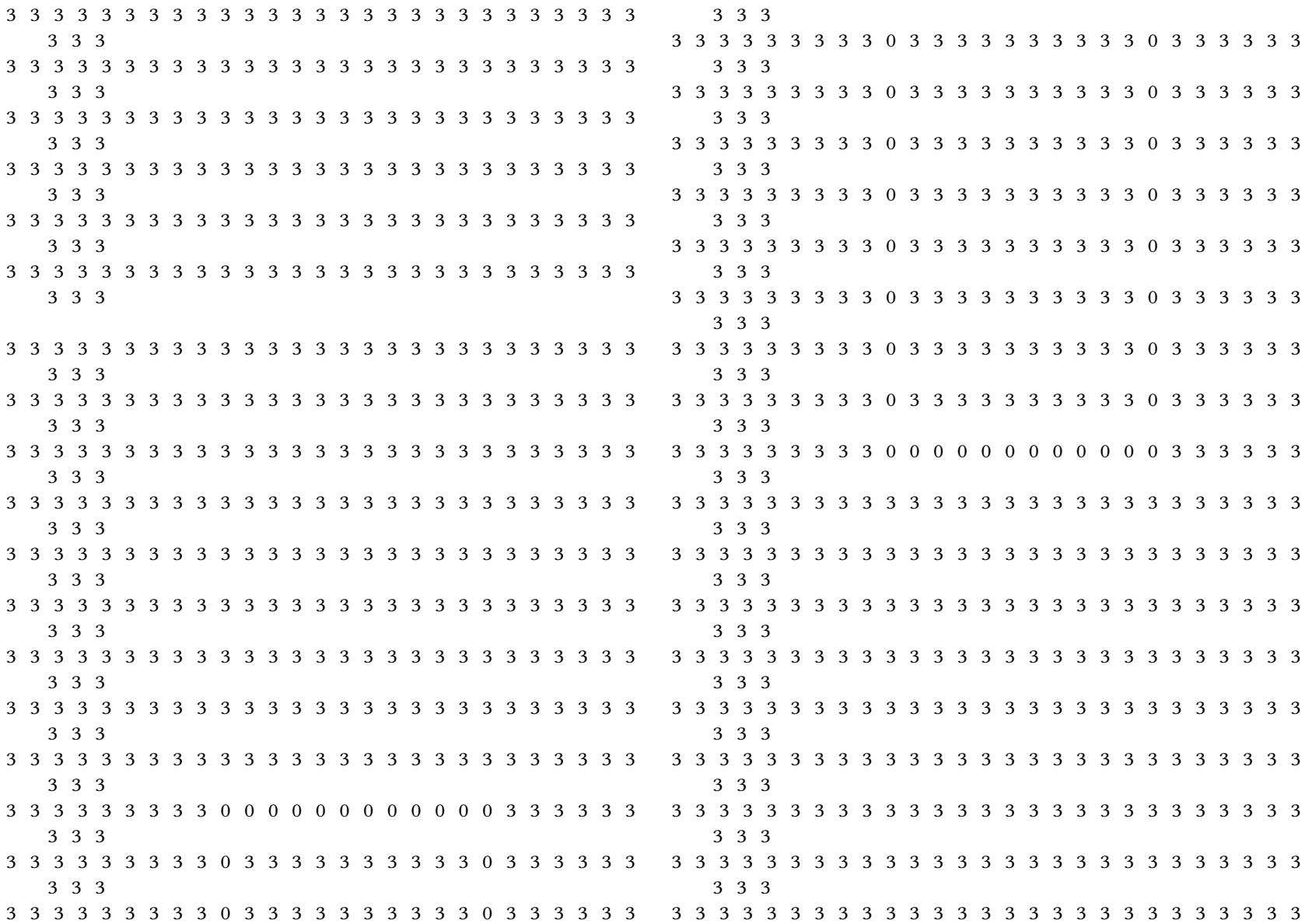

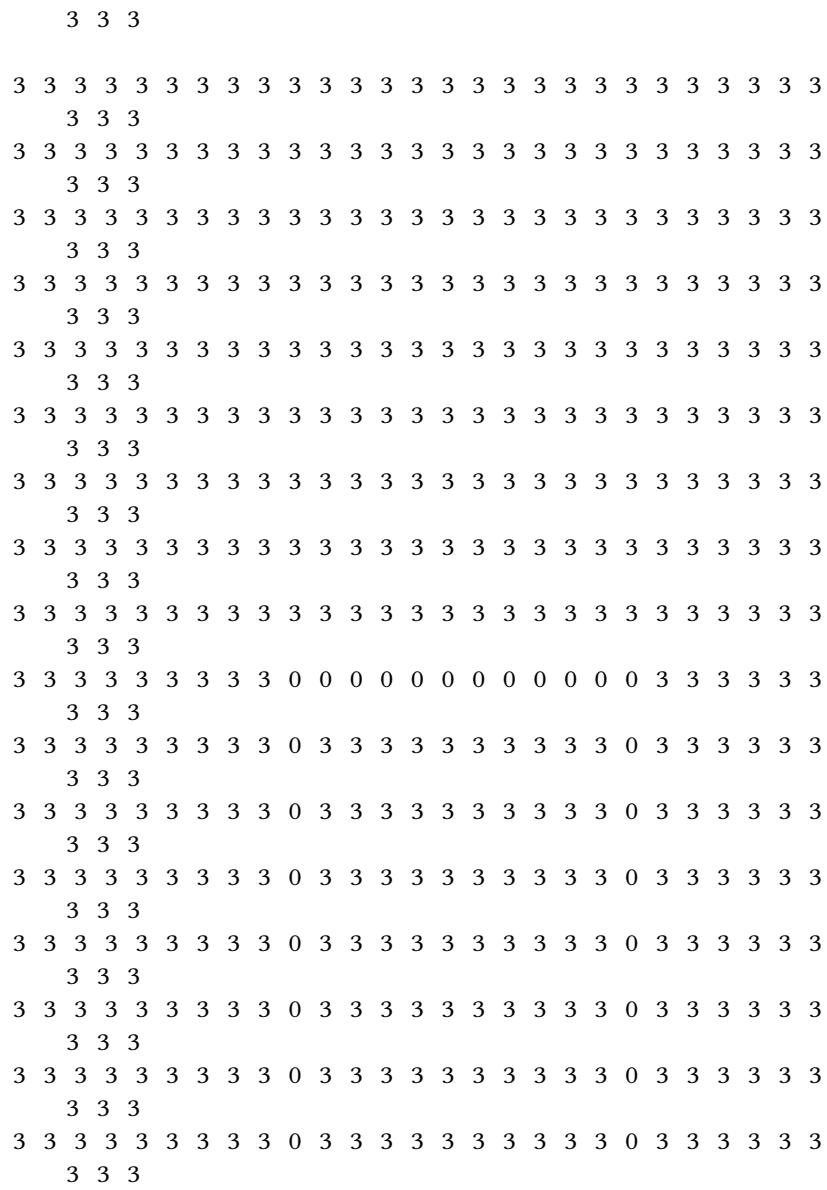

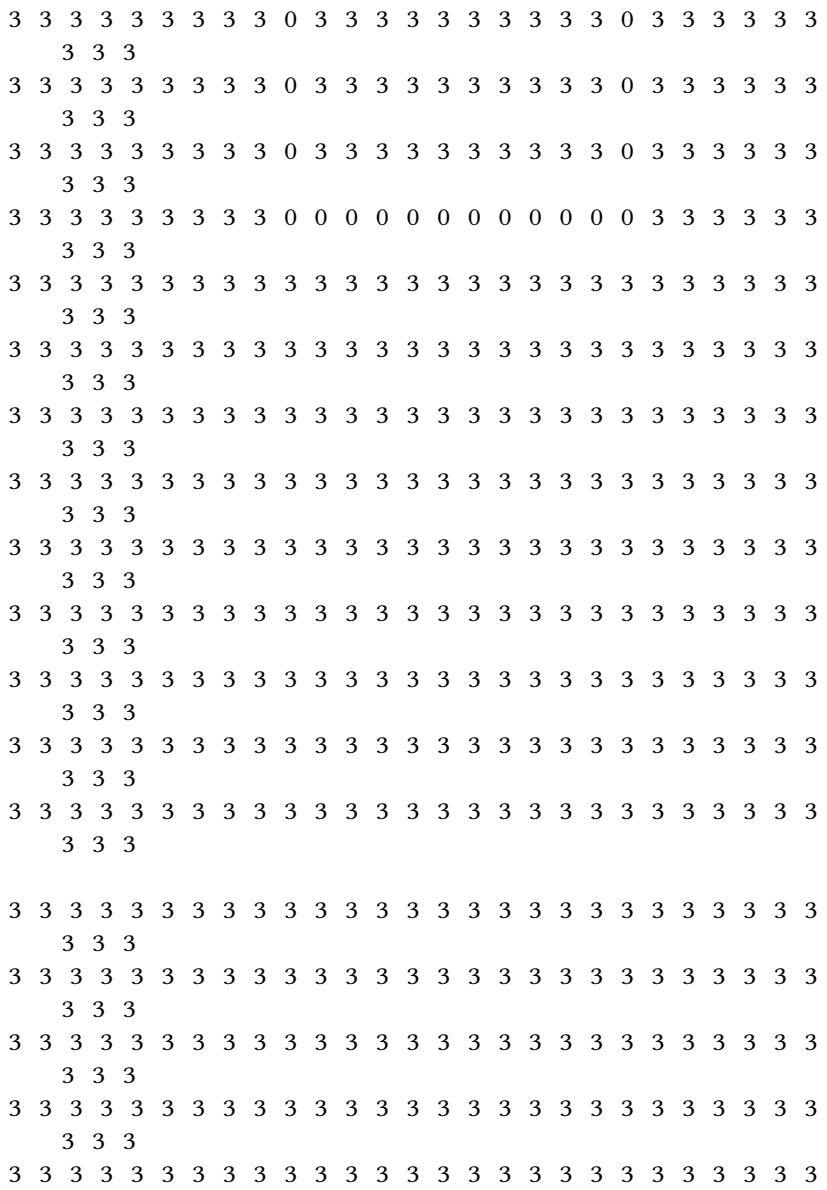

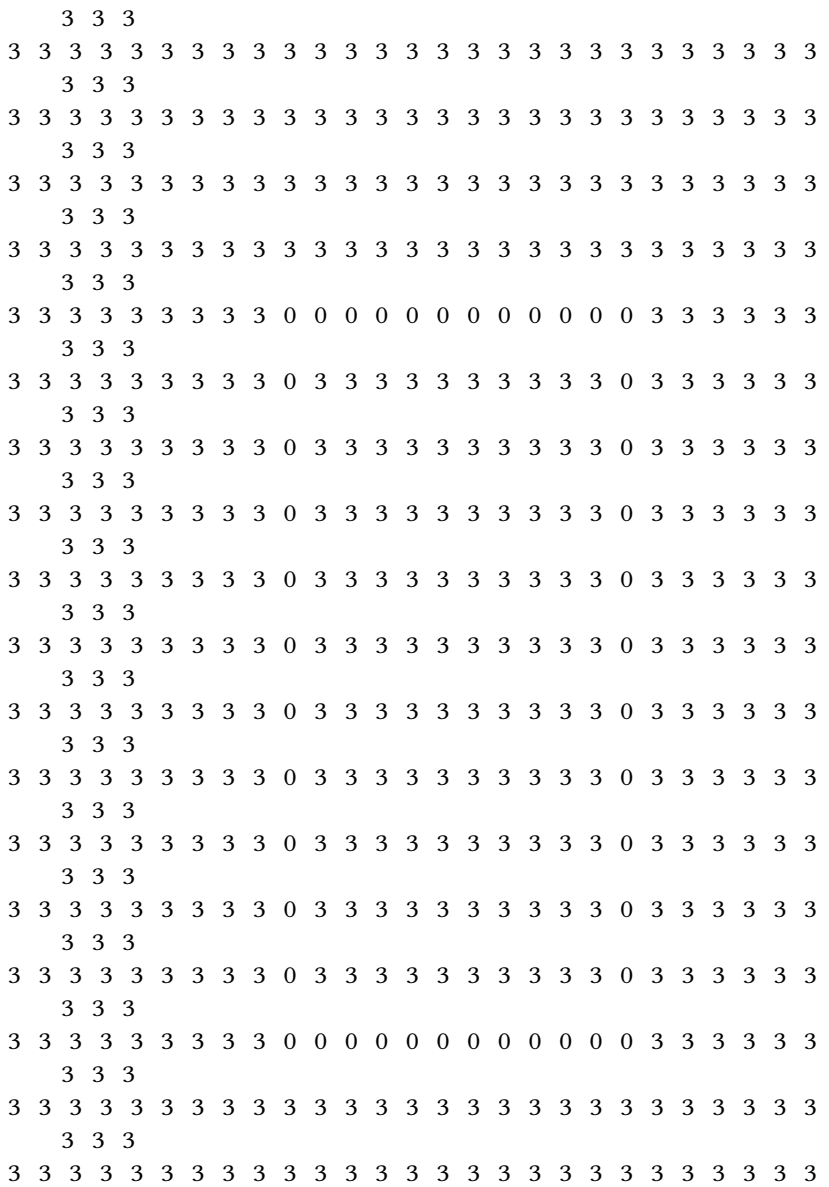

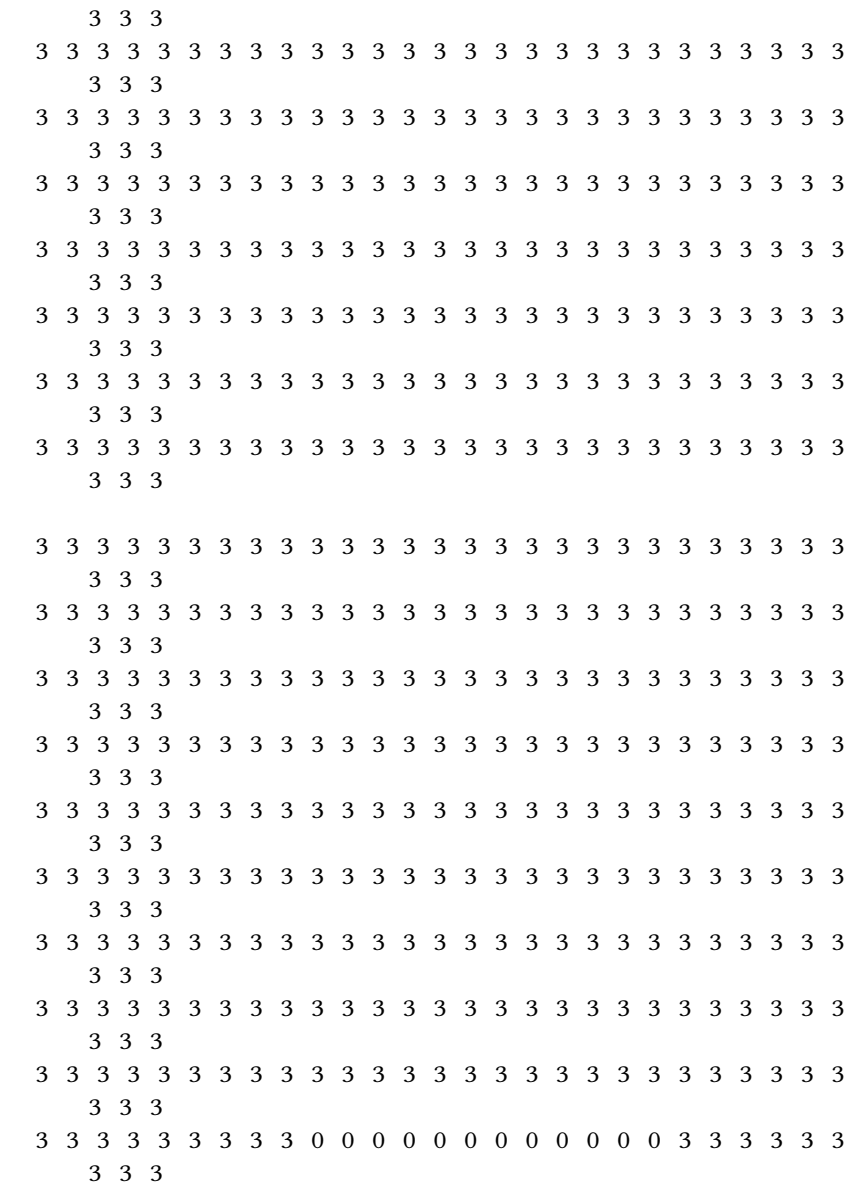

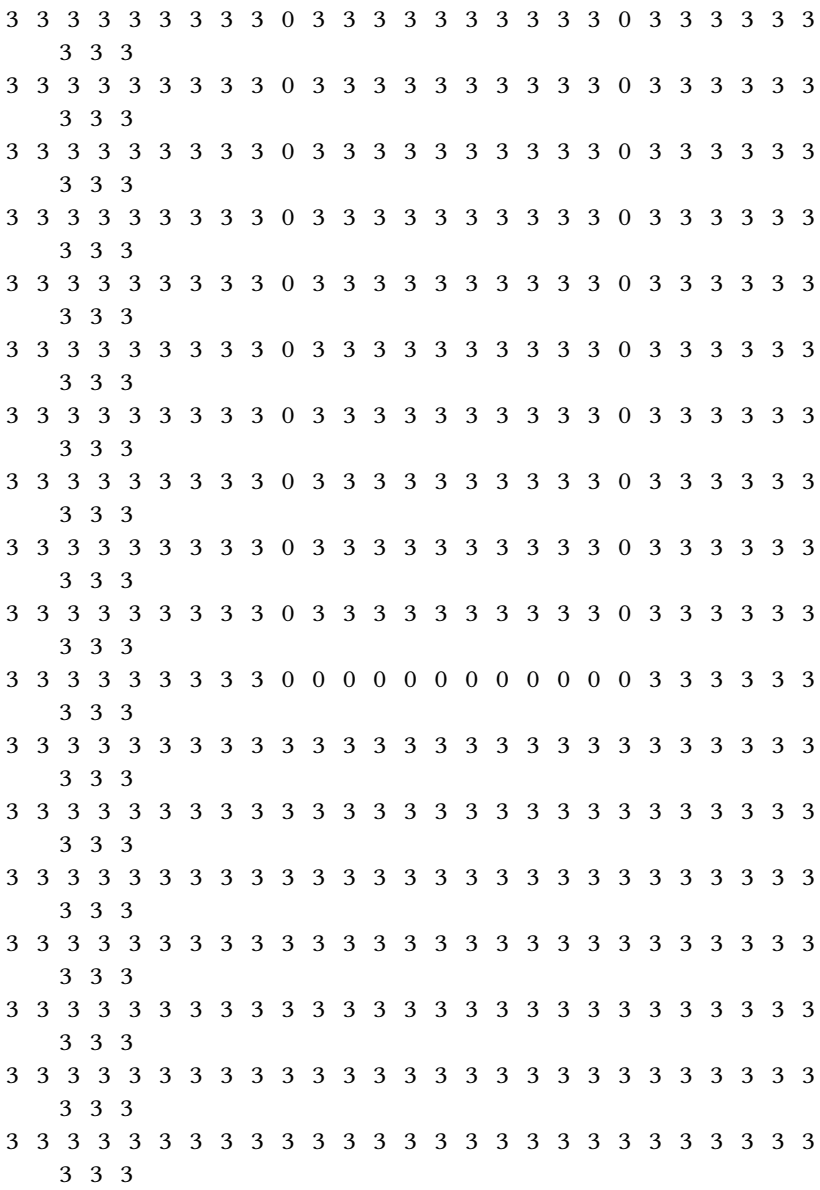

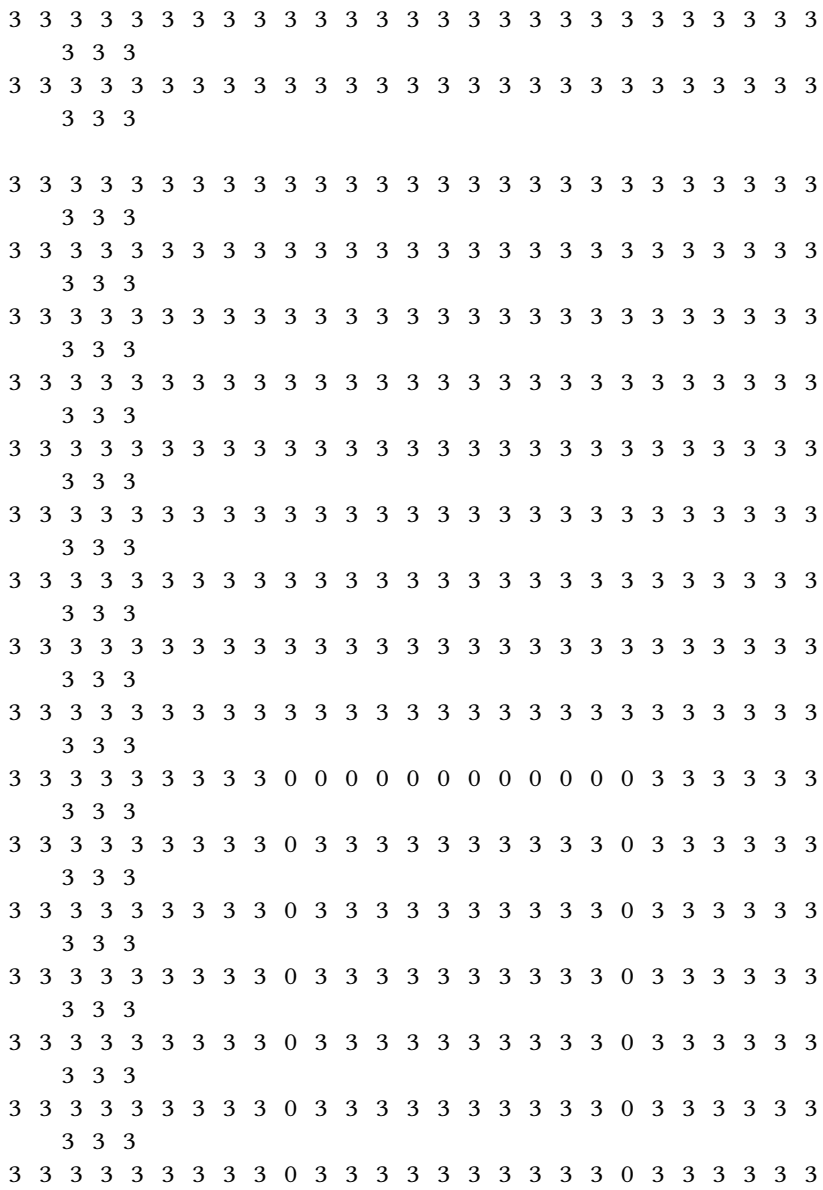

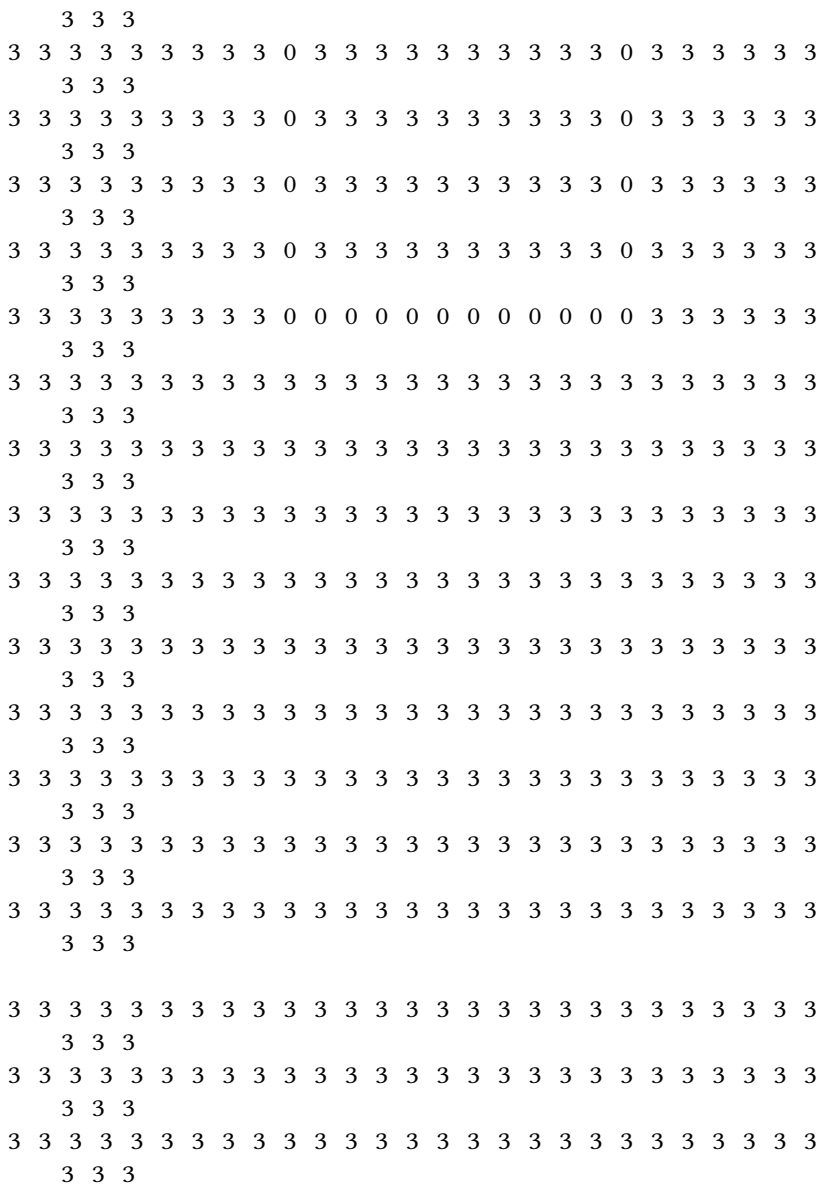

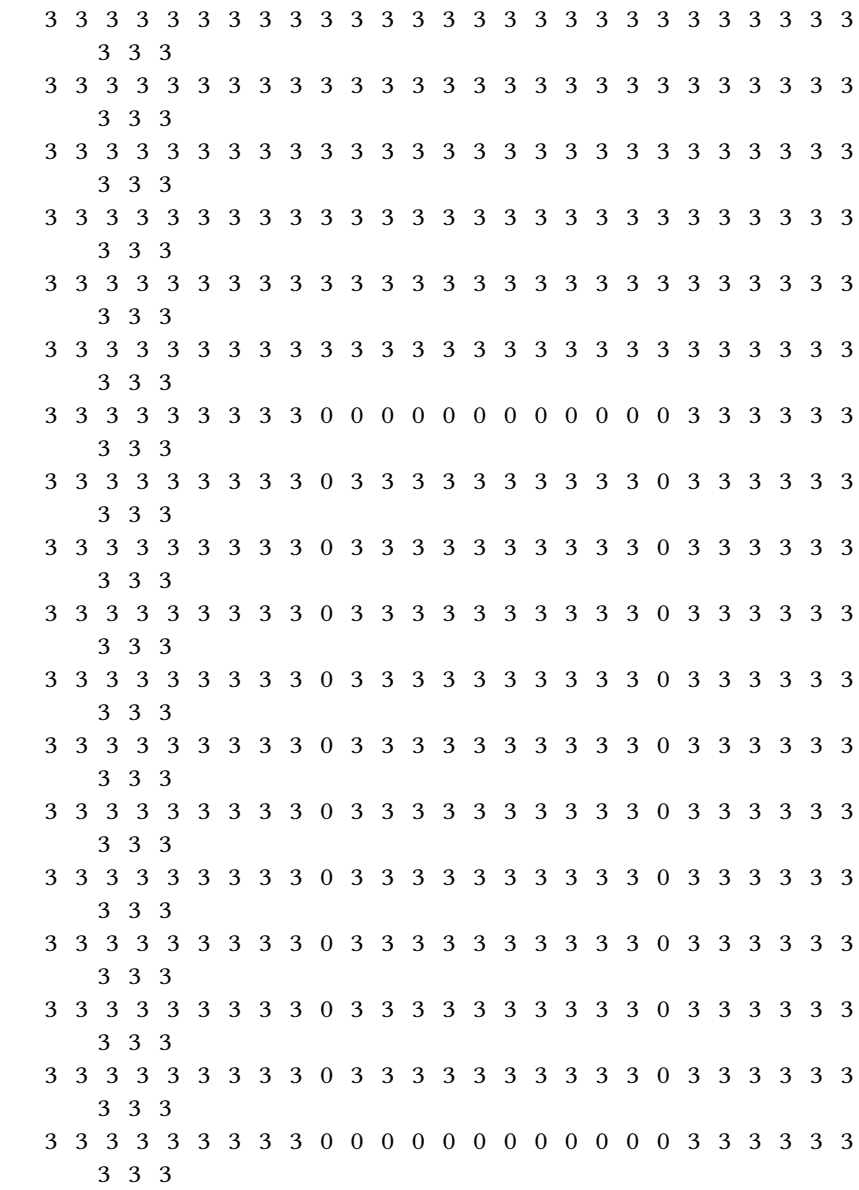

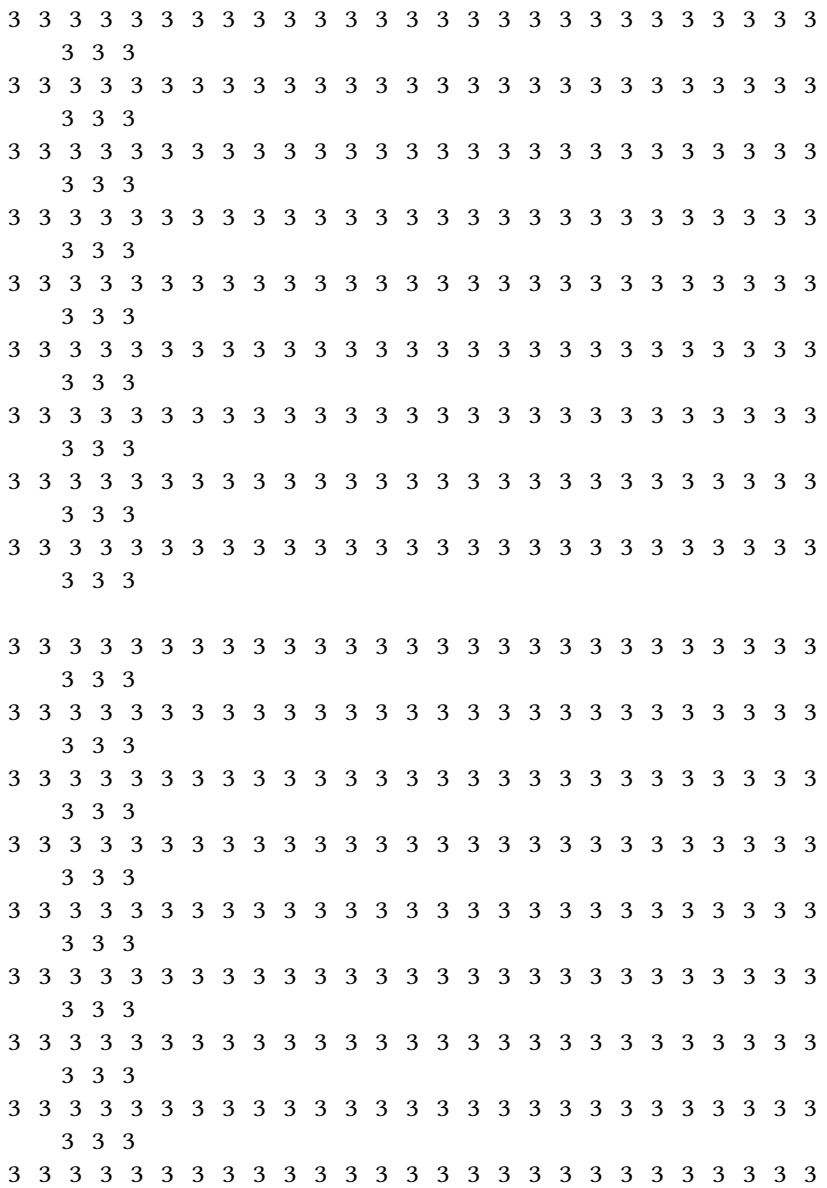

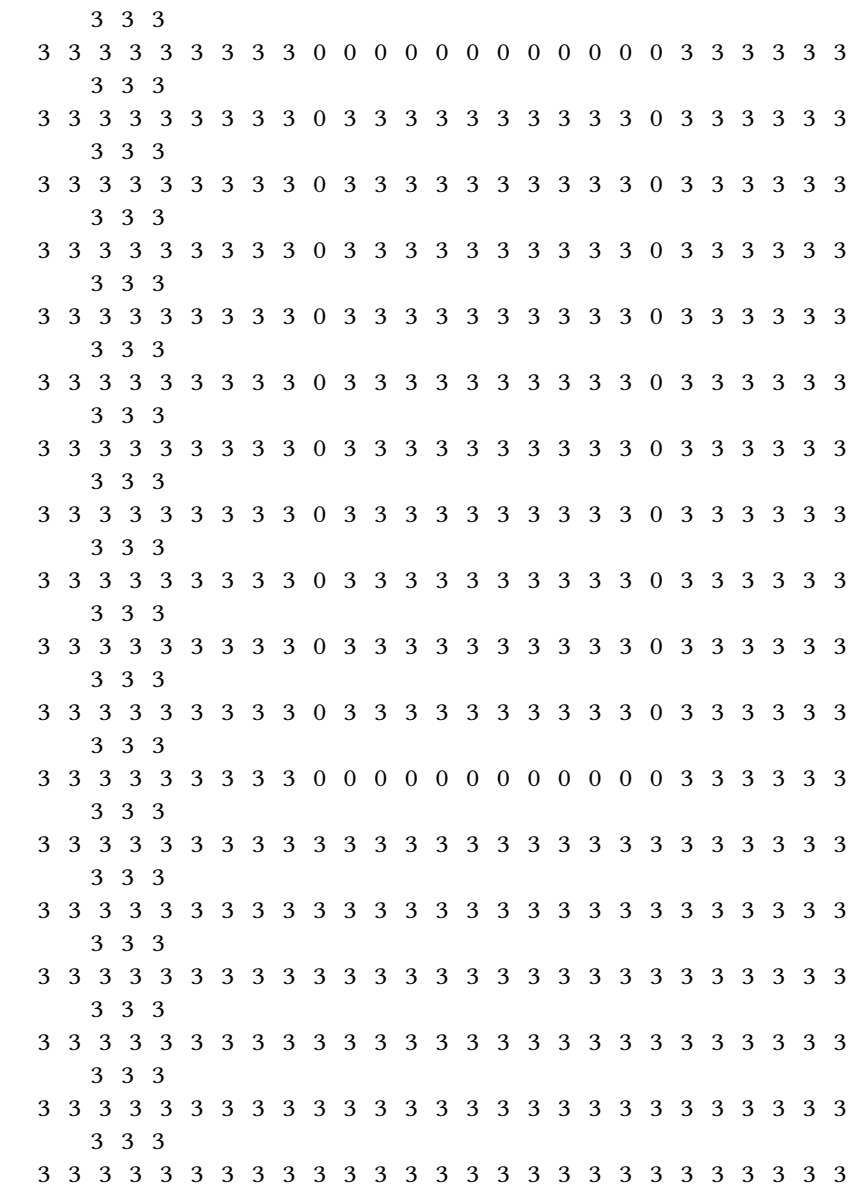

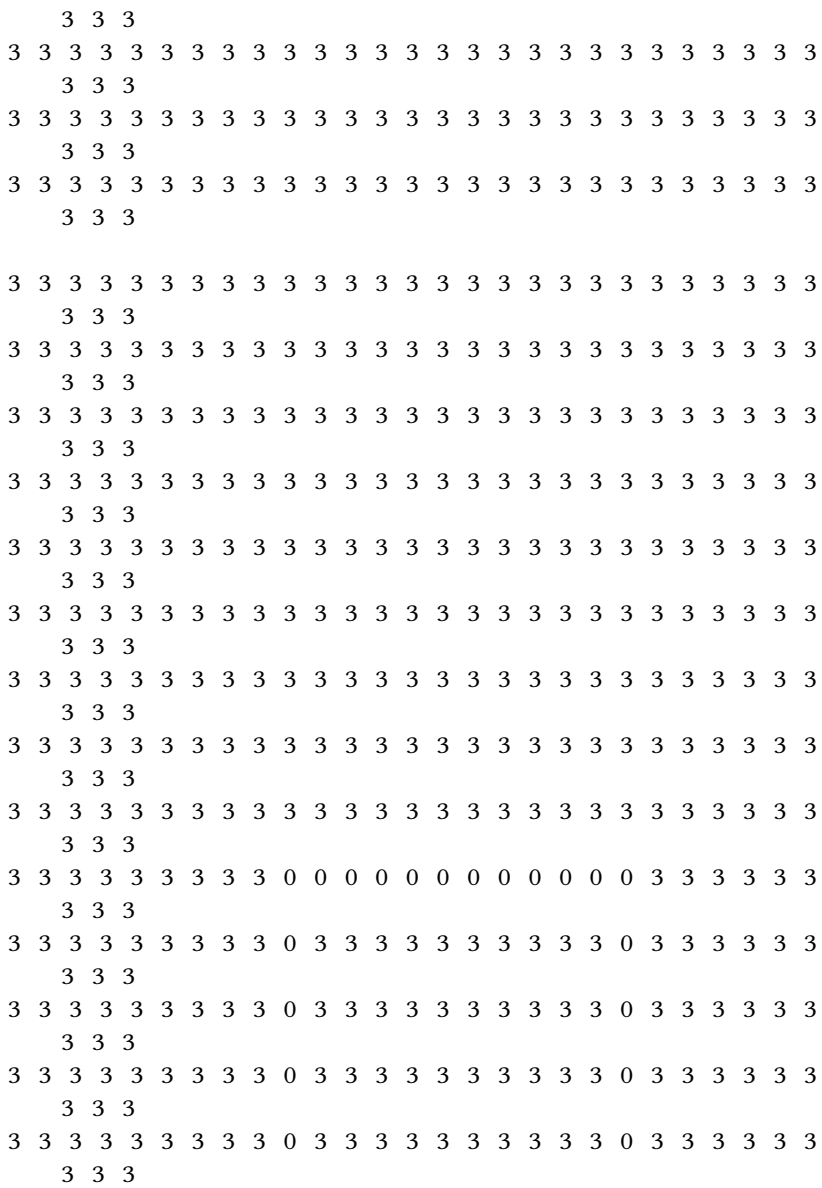

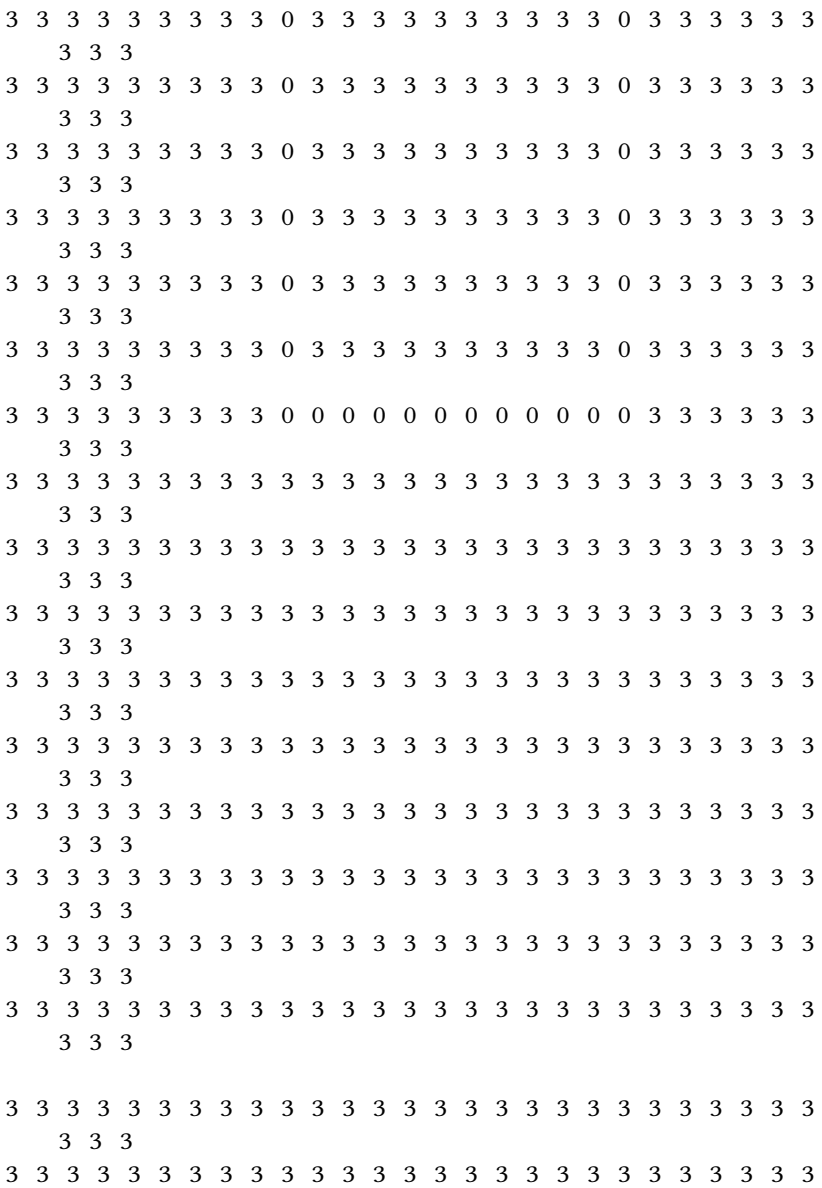

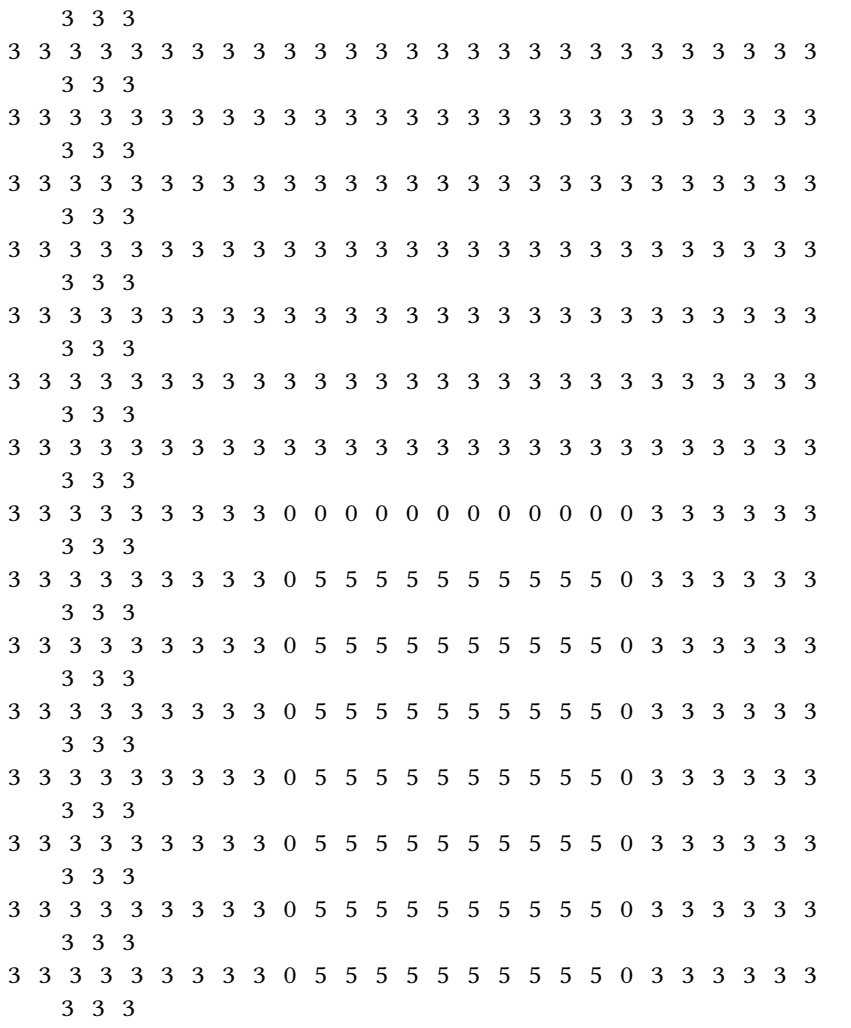

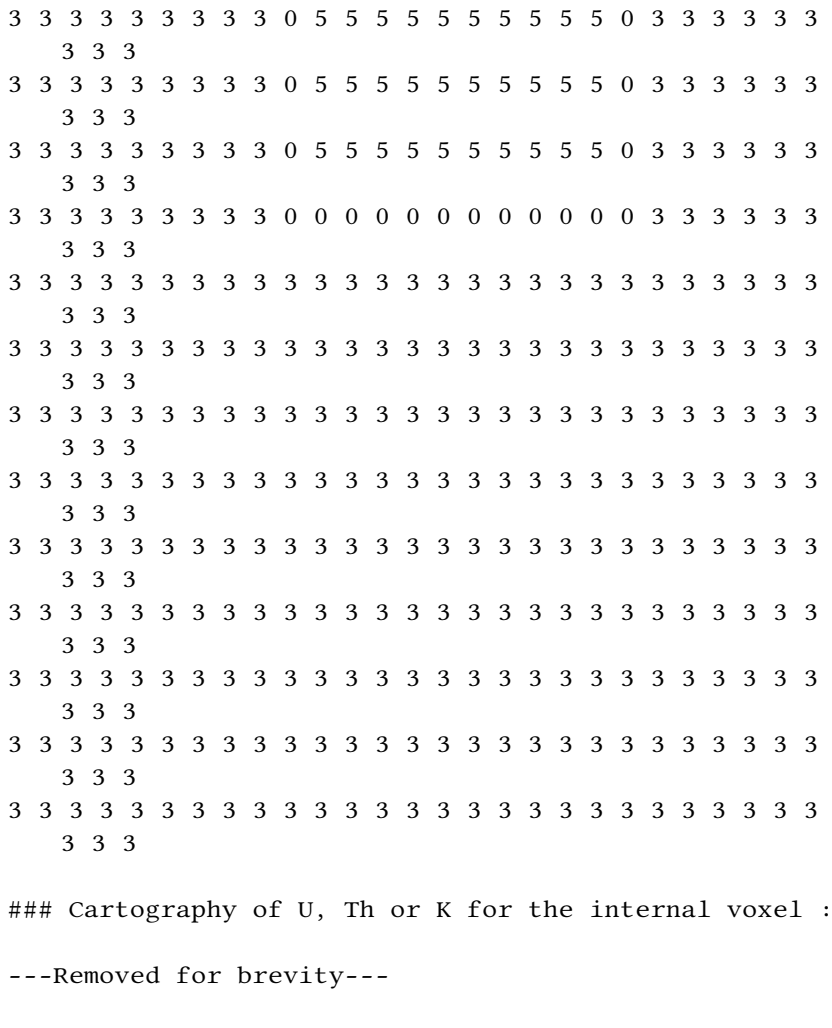

Cartography of U, Th or K for the internal voxel :

---Removed for brevity---

Appendix H

Input data for OxCal modelling of Bêt Khallaf Case 1

This appendix presents the OxCal input file for the Bêt Khallaf Case 1 model.

```
Plot()
{
Outlier_Model("General",T(5),U
    (0,4),"t");
Sequence("Bet Khallaf")
{
 Boundary("Start ED")
 {
  U(BC(4000),BC(2000));
  color="red";
 };
 Phase("BK ED")
 {
  Date("X5462", N(AD(2015)
      -4502,553))
  {
   Outlier(0.05);
  };
  Date("X4114CG", N(AD(2015)
      -4773,698))
  {
   Outlier(0.05);
  };
  Date("X5461", N(AD(2015)
      -4639,316))
  {
   Outlier(0.05);
  };
  Date("X4118", N(AD(2015)
      -5435,309))
  {
   Outlier(0.05);
  };
  Date("X5472", N(AD(2015)
      -4663,293))
  {
   Outlier(0.05);
  };
  Date("X4115", N(AD(2015)
      -3675,243))
  {
   Outlier(0.05);
  };
  Date("X5460", N(AD(2015)
      -4747,291))
  {
   Outlier(0.05);
  };
  Date("X5464", N(AD(2015)
      -4282,198))
  {
   Outlier(0.05);
  };
  Date("X5458", N(AD(2015)
      -5134,490))
  {
   Outlier(0.05);
  };
  Date("X5459", N(AD(2015)
      -3996,1231))
  {
   Outlier(0.05);
  };
```

```
 Date("X4116", N(AD(2015)
    -3480,715))
 {
  Outlier(0.05);
 };
 Date("X4117", N(AD(2015)
    -5258,852))
 {
  Outlier(0.05);
 };
 Date("X5468", N(AD(2015)
    -4340,228))
 {
  Outlier(0.05);
 };
 Date("X5473", N(AD(2015)
    -4250,246))
 {
  Outlier(0.05);
 };
};
Boundary("End ED")
{
 color="orange";
};
Boundary("Start FIP")
{
 color="yellow";
};
Phase("BK FIP")
{
 Date("X5463", N(AD(2015)
    -4096,186))
 {
  Outlier(0.05);
 };
 Date("X5467", N(AD(2015)
    -3732,281))
 {
  Outlier(0.05);
 };
 Date("X5465", N(AD(2015)
    -4042,204))
 {
  Outlier(0.05);
 };
 Date("X5470", N(AD(2015)
    -4443,303))
 {
  Outlier(0.05);
 };
};
Boundary("End FIP")
{
 color="green";
};
Boundary("Start Islamic")
{
 color="blue";
};
Phase("BKIslamic")
{
 Date("X5466", N(AD(2015)-987,91))
 {
  Outlier(0.05);
 };
};
Boundary("End Islamic")
{
 U(AD(500),AD(1900));
 color="violet";
};
};
```

Appendix I

Input data for OxCal modelling of Bêt Khallaf Case 2

This appendix presents the OxCal input file for the Bêt Khallaf Case 2 model.

```
Plot()
 {
  Outlier_Model("General",T(5),U
      (0,4),"t");
  Sequence("Bet Khallaf")
  {
   Boundary("Start ED")
   {
   U(BC(4000),BC(2000));
   color="red";
   };
   Phase("BK ED")
   {
   Date("X5462", N(AD(2015)
       -4502,553))
   {
    Outlier(0.05);
   };
   Date("X4114CG", N(AD(2015)
       -4773,698))
   {
    Outlier(0.05);
   };
   Date("X5461", N(AD(2015)
       -4639,316))
   {
    Outlier(0.05);
   };
   Date("X4118", N(AD(2015)
       -5435,309))
   {
    Outlier(0.05);
   };
   Date("X5472", N(AD(2015)
       -4663,293))
   {
    Outlier(0.05);
   };
   Date("X4115", N(AD(2015)
       -3675,243))
   {
    Outlier();
   };
   Date("X5460", N(AD(2015)
       -4747,291))
   {
    Outlier(0.05);
   };
   Date("X5464", N(AD(2015)
       -4282,198))
   {
    Outlier(0.05);
   };
   Date("X5458", N(AD(2015)
       -5134,490))
   {
    Outlier(0.05);
   };
   Date("X5459", N(AD(2015)
       -3996,1231))
   {
    Outlier(0.05);
```

```
 };
 Date("X4116", N(AD(2015)
     -3480,715))
 {
  Outlier(0.05);
 };
 Date("X4117", N(AD(2015)
     -5258,852))
 {
  Outlier(0.05);
 };
 Date("X5468", N(AD(2015)
     -4340,228))
 {
  Outlier(0.05);
 };
 Date("X5473", N(AD(2015)
     -4250,246))
 {
  Outlier(0.05);
 };
};
Boundary("End ED")
{
 color="orange";
};
Boundary("Start FIP")
{
 color="yellow";
};
Phase("BK FIP")
{
 Date("X5463", N(AD(2015)
     -4096,186))
 {
  Outlier(0.05);
 };
 Date("X5467", N(AD(2015)
     -3732,281))
 {
  Outlier(0.05);
 };
 Date("X5465", N(AD(2015)
     -4042,204))
 {
  Outlier(0.05);
 };
 Date("X5470", N(AD(2015)
     -4443,303))
 {
  Outlier(0.05);
 };
};
Boundary("End FIP")
{
 color="green";
};
Boundary("Start Islamic")
{
 color="blue";
};
Phase("BKIslamic")
{
 Date("X5466", N(AD(2015)-987,91))
 {
  Outlier(0.05);
 };
};
Boundary("End Islamic")
{
 U(AD(500),AD(1900));
 color="violet";
};
};
};
```

Appendix J

Ceramic catalogue for the Turah and Hierakonpolis material

It should be noted that the ceramics within the following catalogue have two identification codes: a museum code (accession number) and a laboratory code. All discussions within the text of this thesis, when refereeing to a specific ceramic piece, using the laboratory code as the main identifying number.

The 5 digit warecode designation follows that developed by Köhler (Köhler 1998; Köhler 2005).

Table J.1: Catalogue entry for X4112

Collection	Garstang Museum
Museum Code	E.5248
Lab. Code	X4112
Provenance	Hierakonpolis, Tomb 306*
Provenance History	
Excavated by John Garstang, 1906	
Vessel/Object Description	
Height	13.5 cm
Width	17.2 cm
Fracture: grey-red—grey—grey-red; medium-high density, medium -fine nile silt clay (maybe some mixing?). Exterior is wet smoothed with some diagonal scraping marks; pot mark depicting *serekh* of Narmer; Interior is wet smoothed.	
Warecode	21201
Munsell	7.5YR 5/4
Fabric Description	
Coarse limestone $\leq$ 3 mm (1)	
Fine limestone $\leq$ 0.3 mm (2)	
Coarse sand $\leq$ 2 mm (1-2)	
Fine sand $\leq$ 0.4 mm (1-2)	
Coarse chaff $\leq$ 0.5 mm (1)	
Fine chaff $\leq$ 0.2 mm (1-2)	
Grit $\leq$ 0.1 mm (2)	
Mica $\leq$ 0.1 mm (1)	
Publication Records	
Garstang (1907: 135; Pl. III)	
Additional Notes	
* Excavation notes, (published in ASAE), indicate this piece was excavated at the Temenos in HK, under a structure excavated initially by Green and Quibell, priod to Garstang's excavations. However the museum card says Tomb 306, HK. It is likely that the museum catalogue in wrong with respect to the information contained on its card.	

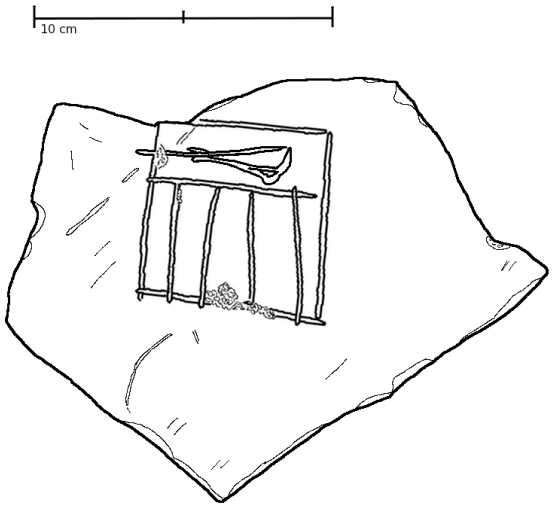

Table J.2: Catalogue entry for X5482

Collection	University of Vienna
Museum Code	Vienna 16
Lab. Code	X5482
Provenance	Turah

Provenance History

Excavated by Junker, 1901 from Turah. Provenance unknown.

Vessel/Object Description

Height	20.9 cm
Diameter	10.3 cm

No fracture details; high density, medium-fine marl clay.

Exterior surface smoothed with some fingerprint turning marks present. Incised band (wavy handle) decoration, done in an upwards motion; possibly some white slip, or else firing skin. Interior surface rough-smoothed; turning marks.

Warecode	32301
Munsell	CB: 2.5YR 5/6 WS/FS: 10YR 7/2

Fabric Description

Coarse limestone $\geq$ 4 mm (2)
Fine limestone $\geq$ 1 mm (2-3)
Fine sand $\geq$ 0.3 mm (2)
Sand $\geq$ 1 mm (2-3)
Coarse chaff $\geq$ 3 mm (2)
Fine chaff $\geq$ 1 mm (2-3)
Grit $\geq$ 0.1 mm (2)
Mica $\geq$ 0.1 mm (2)

Publication Records

Additional Notes

Slightly abnormal large limestone inclusions (not a fabric from Abydos)

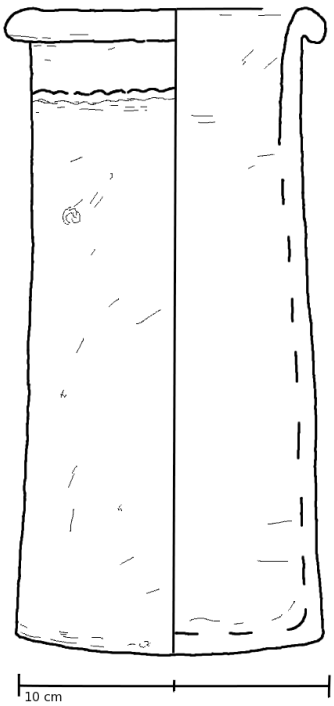

Table J.3: Catalogue entry for X5483

Collection	University of Vienna
Museum Code	Vienna 4
Lab. Code	X5483
Provenance	Turah
Provenance History	
Excavated by Junker, 1901 from Turah. Provenance unknown.	
Vessel/Object Description	
Height	28.6 cm
Diameter	11.6 cm
Pinky-brown fracture; high density, medium marl clay, possibly mixed. Exterior surface roughly smoothed with turning marks on rim to neck and some scraping marks on body. Painted red net design and wavy handle; turning marks around rim. Interior surface rough, with many working marks on body and turning marks around rim.	
Warecode	22201 + red paint
Munsell	CB: 10YR 6/3 RP: 2.5YR 4/2-3
Fabric Description	
Coarse limestone $\geq$ 2.5 mm (1)	
Fine limestone $\geq$ 0.2 mm (3)	
Fine sand $\geq$ 0.2 mm (2-3)	
Sand $\geq$ 1 mm (1)	
Coarse chaff $\geq$ 5 mm (1)	
Fine chaff $\geq$ 1 mm (2)	
Grit $\geq$ 0.1 mm (2)	
Mica $\geq$ 0.1 mm (2)	
Organic (?) $\geq$ 1 mm (1)	
Publication Records	
Additional Notes	
Poorly mixed clay, might have a little bit of nile in it. Definitely not similar to Abydos fabric.	

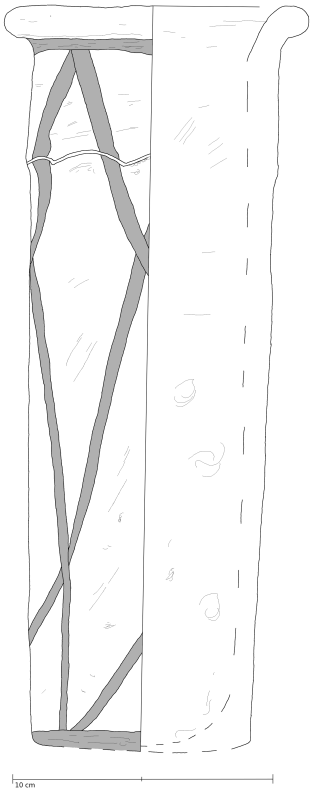

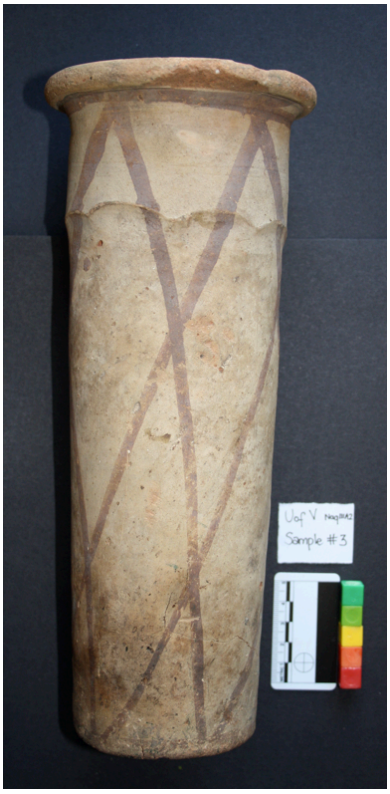

Table J.4: Catalogue entry for X5484

Collection	University of Vienna
Museum Code	Vienna 21
Lab. Code	X5484
Provenance	Turah
Provenance History	
Excavated by Junker, 1901 from Turah. Provenance unknown.	
Vessel/Object Description	
Height	12.9 cm
Diameter	7.5 cm
No fracture details; medium density, medium marl clay. Exterior surface roughly smoothed, but perhaps once very smooth but now very eroded; turning marks on base and rim. Interior surface smoothed with working marks.	
Warecode	22(3?)01
Munsell	5YR 6–5/4
Fabric Description	
Coarse limestone $\geq$ 2 mm (1)	
Fine limestone $\geq$ 0.5 mm (2-3)	
Fine sand $\geq$ 0.2 mm (1-2)	
Sand $\geq$ 0.5 mm (2)	
Coarse chaff $\geq$ 3 mm (1)	
Fine chaff $\geq$ 0.5 mm (1-2)	
Grit $\geq$ 0.1 mm (2)	
Mica $\geq$ 0.1 mm (2)	
Publication Records	
Additional Notes	
Very sandy, large limestone inclusions, would have originally been quite fine but now erroded	

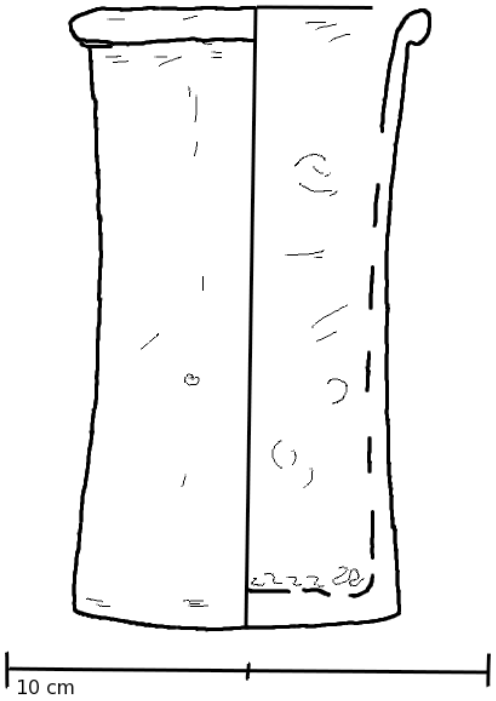

Table J.5: Catalogue entry for X5485

Collection	University of Vienna
Museum Code	Vienna 19
Lab. Code	X5485
Provenance	Turah
Provenance History	
Excavated by Junker, 1901 from Turah. Provenance unknown.	
Vessel/Object Description	
Height	17.5 cm
Diameter	6.2 cm
No fracture details; medium density, medium Nile silt clay. Exterior surface rough smoothed with turning marks around rim; seems to have been shaped by natural shape of hand. Interior surface rough-smoothed; turning marks around rim.	
Warecode	21201
Munsell	10R 4/4-6
Fabric Description	
Coarse limestone $\geq$ 3 mm (1)	
Fine limestone $\geq$ 0.3 mm (1-2)	
Fine sand $\geq$ 0.3 mm (2)	
Sand $\geq$ 1 mm (1-2)	
Coarse chaff $\geq$ 5 mm (1-2)	
Fine chaff $\geq$ 1 mm (1-2)	
Grit $\geq$ 0.1 mm (2)	
Mica $\geq$ 0.1 mm (2)	
Publication Records	
Additional Notes	

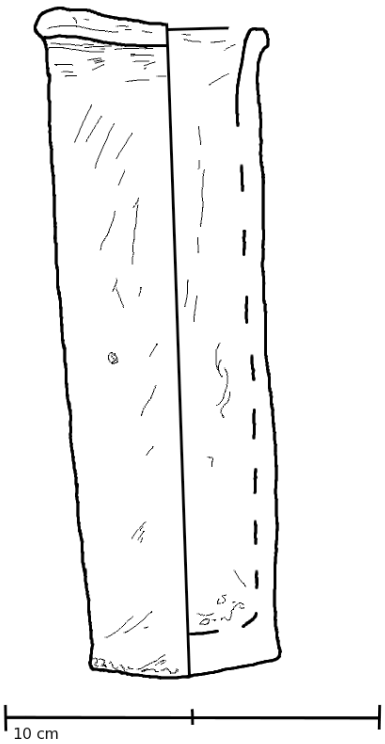

Table J.6: Catalogue entry for X5486

Collection	University of Vienna
Museum Code	Vienna 3
Lab. Code	X5486
Provenance	Turah
Provenance History	
Excavated by Junker, 1901 from Turah. Provenance unknown.	
Vessel/Object Description	
Height	29.9 cm
Diameter	11 cm
No fracture details; medium-high density, medium-fine marl clay. Exterior surface roughly smoothed; scraping marks all over body. Turning marks on neck and rim. Interior surface same as exterior, but rough (not roughly smoothed).	
Warecode	22(2-3)01
Munsell	2.5YR 6/4-6
Fabric Description	
Coarse limestone $\geq$ 1.5 mm (1) Fine limestone $\geq$ 0.3 mm (2) Fine sand $\geq$ 0.2 mm (2-3) Sand $\geq$ 0.6 mm (2) Coarse chaff $\geq$ 4 mm (1) Fine chaff $\geq$ 1 mm (2) Grit $\geq$ 0.1 mm (2) Mica $\geq$ 0.1 mm (2)	
Publication Records	
Additional Notes	
Very sandy, not as much coarse imestone, slightly finer fabric than others in assemblage.	

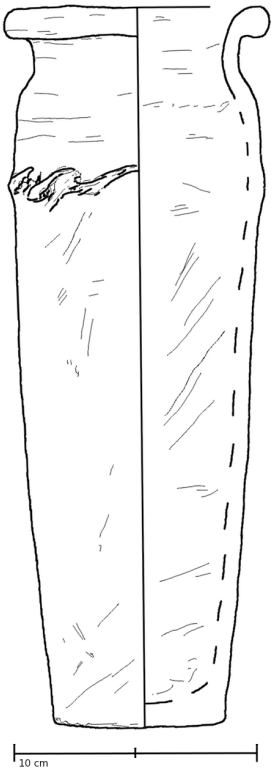

Table J.7: Catalogue entry for X5487

Collection	University of Vienna
Museum Code	Vienna 104
Lab. Code	X5487
Provenance	Turah
Provenance History	
Excavated by Junker, 1901 from Turah. Provenance unknown.	
Vessel/Object Description	
Height	23.9 cm
Diameter	9.9 cm
No fracture details; high density, medium marl clay. Exterior surface roughly smoothed with many slightly oblique working marks over body. Many working marks near base; pot mark. Interior surface rough, with turning marks around rim.	
Warecode	22201
Munsell	7.5YR 6/2-3
Fabric Description	
Coarse limestone $\geq$ 4 mm (1) Fine limestone $\geq$ 0.5 mm (1-2) Fine sand $\geq$ 0.1 mm (2-3) Sand $\geq$ 0.4 mm (2-3) Coarse chaff $\geq$ 4 mm (1) Fine chaff $\geq$ 0.1 mm (2) Grit $\geq$ 0.1 mm (2) Mica $\geq$ 0.1 mm (2)	
Publication Records	
Additional Notes	
More like a wine jar marl (cf. ICP-MS), possibly later cylindrical vessel imitation.	

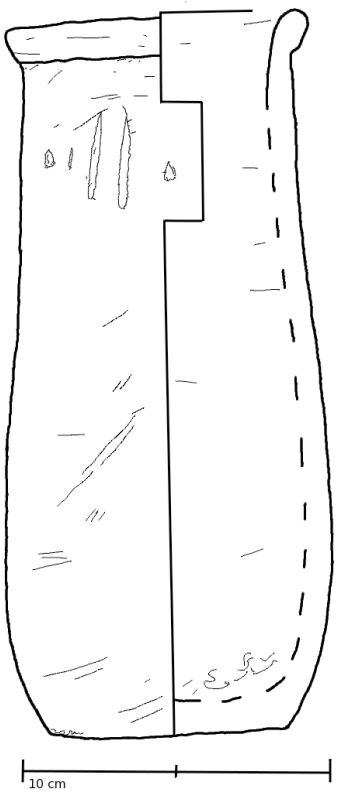

Table J.8: Catalogue entry for X5488

Collection	University of Vienna
Museum Code	Vienna 103
Lab. Code	X5488
Provenance	Turah
Provenance History	
Excavated by Junker, 1901 from Turah. Provenance unknown.	
Vessel/Object Description	
Height	24.9 cm
Diameter	11.4 cm
Red-brown fracture; high density, medium-fine marl clay. Exterior surface very well smoothed, some working marks on base and body; rim and neck fairly eroded; wavy handle decoration. Interior surface rough-smoothed; many working/turning marks.	
Warecode	(2-3)2305
Munsell	CB: 7.5YR 6/3-4 Smooth clay: 2.5YR 7-6/3
Fabric Description	
Coarse limestone $\geq$ 3 mm (1) Fine limestone $\geq$ 0.2mm (1) Fine sand $\geq$ 0.2 mm (1-2) Fine chaff $\geq$ 1 mm (1) Grit $\geq$ 0.1 mm (2) Mica $\geq$ 0.1 mm (2)	
Publication Records	
Additional Notes	
Very similar to the Abydos material. Very fine (i.e. 5 designation),	

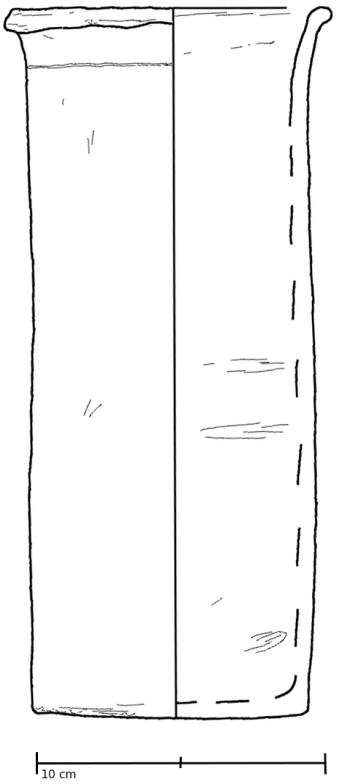

Table J.9: Catalogue entry for X5489

Collection	University of Vienna
Museum Code	Vienna WJB
Lab. Code	X5489
Provenance	Turah
Provenance History	
Excavated by Junker, 1901 from Turah. Provenance unknown.	
Vessel/Object Description	
Height	
Diameter	
Red—grey—red fracture; medium density, medium-fine Nile silt clay (slightly mixed?). Exterior surface rough smoothed; some working marks; pot mark; banded decoration; very eroded near rim. Interior surface rough-smoothed; some working marks.	
Warecode	21201
Munsell	2.5YR 5-4/4
Fabric Description	
Coarse limestone $\geq$ 5 mm (2) Fine limestone $\geq$ 1 mm (3) Fine sand $\geq$ 0.5 mm (2) Sand $\geq$ 1 mm (2) Coarse chaff $\geq$ 4 mm (1) Grit $\geq$ 0.1 mm (2) Mica $\geq$ 0.1 mm (2)	
Publication Records	
Additional Notes	

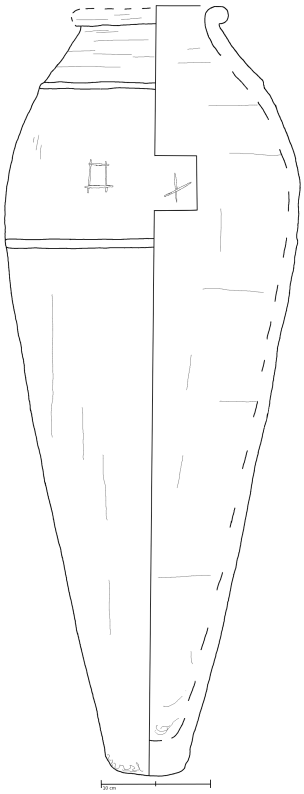

Table J.10: Catalogue entry for X5490

Collection	University of Vienna
Museum Code	Vienna WJS
Lab. Code	X5490
Provenance	Turah
Provenance History	
Excavated by Junker, 1901 from Turah. Provenance unknown.	
Vessel/Object Description	
Height	59.8 cm
Diameter	14.6 cm
No fracture details; high density, medium-fine Nile silt clay (slightly mixed?). Exterior surface well smoothed and polished; turning marks around rim to shoulder, and some near base. Interior surface rough-smoothed.	
Warecode	21301
Munsell	2.5YR 4/4
Fabric Description	
Limestone $\geq$ 3 mm (1-2) Fine limestone $\geq$ 0.2 mm (2) Fine sand $\geq$ 0.3 mm (2) Sand $\geq$ 1 mm (1) Coarse chaff $\geq$ 3 mm (1) Chaff $\geq$ 0.5 mm (1-2) Grit $\geq$ 0.1 mm (2) Mica $\geq$ 0.1 mm (2)	
Publication Records	
Additional Notes	

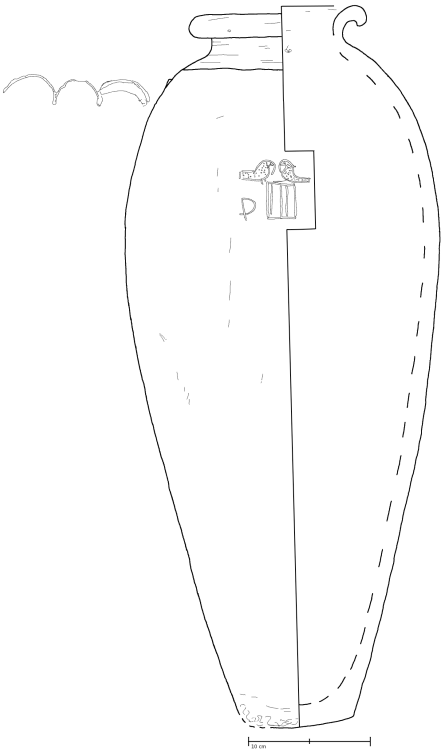

Appendix K

OSL aliquot data for the Turah and Hierakonpolis ceramic assemblage

The following appendix presents the raw OSL data used to discuss the Turah OSL results presented in Chapter 8.

It should be noted that The discussion of the rejection/acceptance criteria given in Appendix D is also applied to the following OSL raw data.

NB All aliquot data units presented in this appendix are in seconds (s). For final age calculations presented in Chapter 8, these units have been converted into the standard international unit for absorbed radiation, Grays (Gy). The conversion of seconds to grays is achieved by multiplying the central dose (s) by the calibrated machine (Gy/s)—this gives the final D_e measurement in Gy.

NB In this appendix coarse grain (CG) data is denoted in black ink, whereas fine grain (FG) data is denoted by red ink.

Table K.1: OSL data for Sample X4112 – Coarse Grain (No fine grain data was retrieved for this sample)

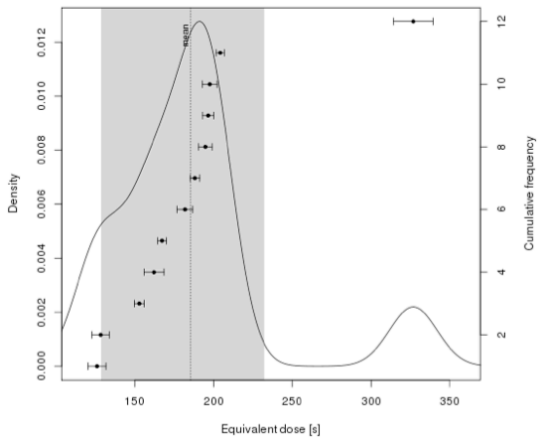

Figure K.1: Kernel Density Estimate Plot for Sample X4112

D_e (s)	D_e error (s)	Test Dose Error (%)	Recycling Ratio	Recup. (%)	IRSL/ OSL ratio (%)
326.81	25.26 (≤10%)	≤10	0.87±0.10 (≤10%)	2.1±0.6	≤1
204.18	5.13 (≤10%)	≤10	1.09±0.03 (≤10%)	0.4±0.0	≤1
197.57	9.3 (≤10%)	≤10	1.19±0.07 (12%)	0.4±0.5	≤1
196.58	7.16 (≤10%)	≤10	1.08±0.05 (≤10%)	0.4±0.2	≤1
194.8	8.62 (≤10%)	≤10	1.09±0.06 (≤10%)	0.7±0.3	≤1
188.16	6.05 (≤10%)	≤10	1.10±0.04 (≤10%)	0.1±0.1	≤1
181.78	10.06 (≤10%)	≤10	0.98±0.06 (≤10%)	2.1±0.6	2
167.27	5.64 (≤10%)	≤10	1.02±0.05 (≤10%)	0.4±0.5	≤1
162.16	12.7 (≤10%)	≤10	0.94±0.09 (≤10%)	-2.1±1.3	≤1
152.82	6.11 (≤10%)	≤10	1.07±0.5 (≤10%)	0.5±0.2	≤1
128.31	11.11 (≤10%)	≤10	1.17±0.11 (≤10%)	-3.0±-1.4	≤1

Figure K.2: Primary Dataset for KDE plot for X4112. NB primary data set is comprised of 11 aliquots (selected from a total of 18 aliquots after selection criteria were met).

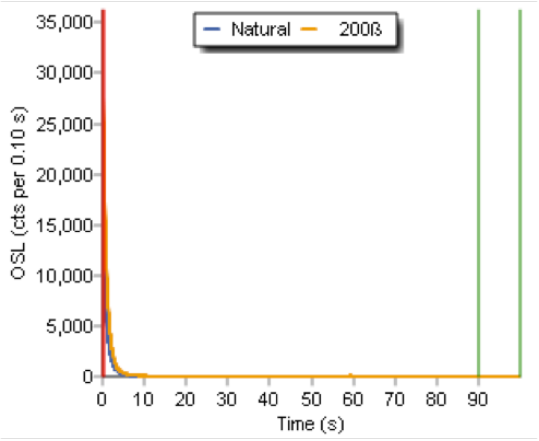

Figure K.3: OSL shine down curve for a representative aliquot of X4112

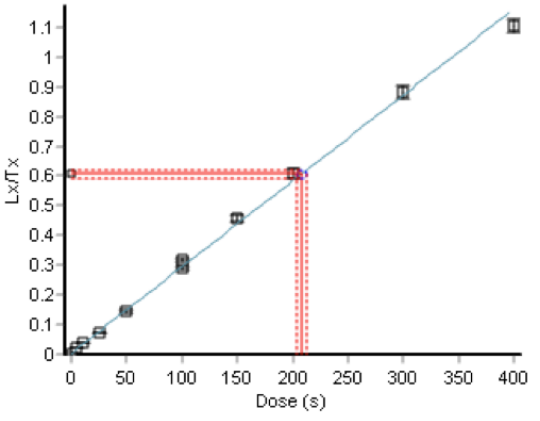

Figure K.4: OSL dose response curve for a representative aliquot of X4112

Figure K.5: Final OSL measurement (based on the CAM) and over dispersion value for X4112. Calibrated machine dose rates (Gy/s): 0.04113196 (CG).

Central dose (s)	Central Dose Error (s)	OD (%)	OD error (%)
180.61	11.78	21.85	2.22

Table K.2: OSL data for Sample X5482 – Fine Grain (No coarse grain data available; of 5 aliquots, all failed to meet rejection criteria)

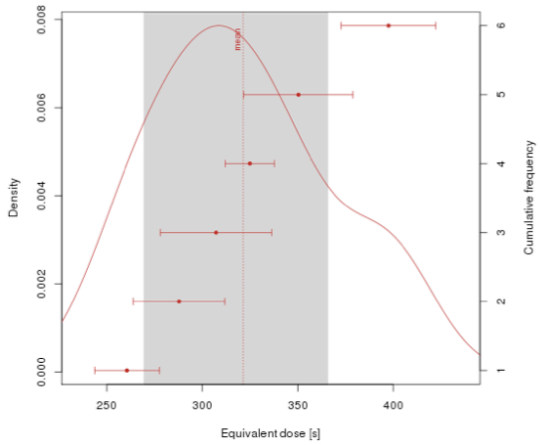

Figure K.6: Kernel Density Estimate Plot for Sample X5482

D_e (s)	D_e error (s)	Test Dose Error (%)	Recycling Ratio	Recup. (%)	IRSL signal (%)
350.33	57.35 (16%)	13	3.59±13.45 (≤10%)	-5.1±-5.7	12
287.82	48.01 (17%)	12	0.77±0.24 (19%)	-0.2±-2.9	4
324.88	25.65 (≤10%)	≤10	0.89±0.17 (≤10%)	1.4±1.3	3
397.62	49.51 (13%)	≤10	1.27±0.44 (≤10%)	3.9±2.8	7
307.20	58.44 (20%)	12	1.87±0.96 (≤10%)	1.4±3.3	6
260.56	33.88 (14%)	≤10	1.21±0.40 (≤10)	-1.9±-3.5	11

Figure K.7: Primary Dataset for KDE plot for X5482. NB primary data set is comprised of 6 out of 6 aliquots after selection criteria were met.

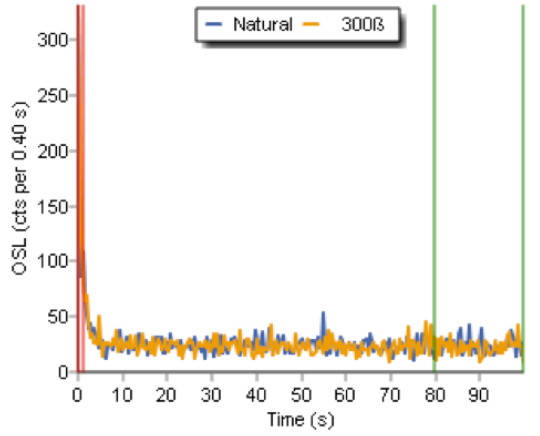

Figure K.8: OSL shine down curve for a representative aliquot of X5482

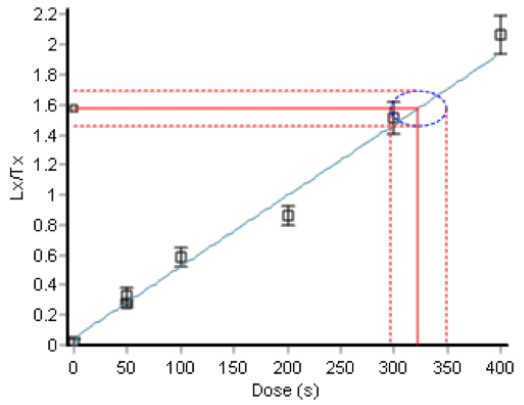

Figure K.9: OSL dose response curve for a representative aliquot of X5482

Figure K.10: Final OSL measurement (based on the CAM) and over dispersion value for X5482. Calibrated machine dose rates (Gy/s): 0.03819457 (CG).

Central dose (s)	Central Dose Error (s)	OD (%)	OD error (%)
322.27	16.43	0.09	12.17

No OSL data is available for Sample X5483

- No coarse grain material was recovered from this sample as it did not survive the HF treatment.
- No data for fine grain material. Of 6 aliquots, all failed to meet rejection criteria.

Table K.3: OSL data for Sample X5484 – Coarse Grain (No fine grain data available; of 5 aliquots, all failed to meet rejection criteria)

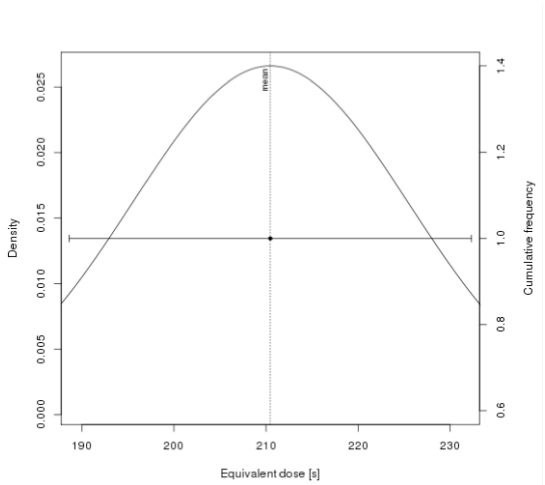

Figure K.11: Kernel Density Estimate Plot for Sample X5484

D_e (s)	D_e error (s)	Test Dose Error (%)	Recycling Ratio	Recup. (%)	IRSL signal (%)
210.47	43.71 (21%)	12	0.83±0.29 (≤10%)	6.5±6.0	≤1

Figure K.12: Primary Dataset for KDE plot for X5484. NB primary data set is comprised of 1 aliquot selected from a total of 8 aliquots after selection criteria were met.

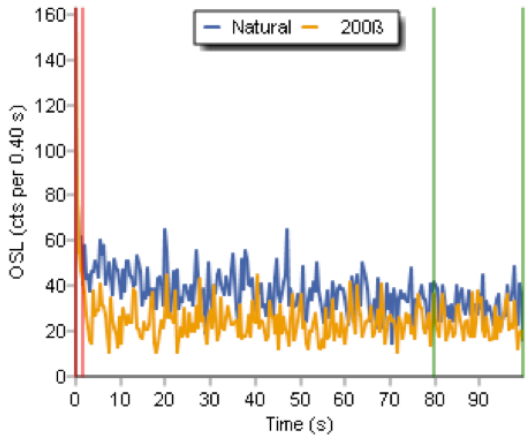

Figure K.13: OSL shine down curve for a representative aliquot of X5484

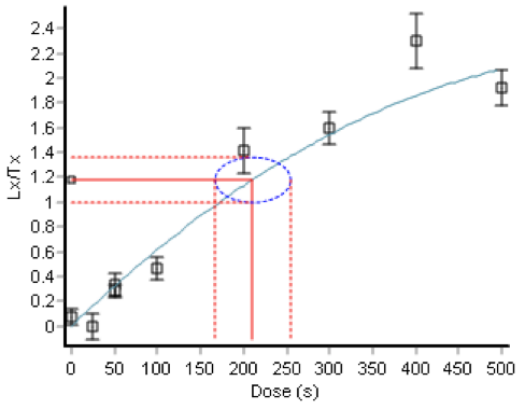

Figure K.14: OSL dose response curve for a representative aliquot of X5484

Figure K.15: Final OSL measurement (based on the CAM) and over dispersion value for X5484. Calibrated machine dose rates (Gy/s): 0.03842184(CG).

Central dose (s)	Central Dose Error (s)	OD (%)	OD error (%)
210.47	43.71	N/A	N/A

No OSL data is available for Sample X5485

- No data for coarse grain material. Of 13 aliquots, all failed to meet rejection criteria.
- No data for fine grain material. Of 6 aliquots, all failed to meet rejection criteria.

Table K.4: OSL data for Sample X5486 – Coarse Grain and Fine Grain

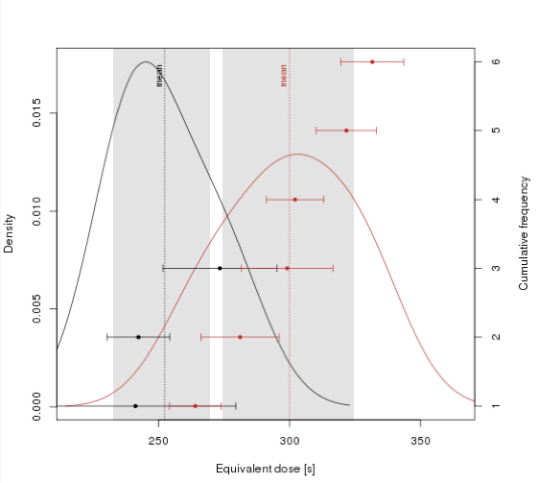

Figure K.16: Kernel Density Estimate Plot for Sample X5486

D_e (s)	D_e error (s)	Test Dose Error (%)	Recycling Ratio	Recup. (%)	IRSL signal (%)
242.29	23.84 (≤10%)	≤10	0.93±0.17 (≤10%)	-2.1±-1.6	≤1
241.16	76.79 (32%)	16	1.46±0.51 (≤10%)	3.9±4.1	2
273.40	43.58 (16%)	11	0.87±0.22 (≤10%)	1.2±2.1	2
§	23.06 (≤10%)	≤10	0.95±0.14 (≤10%)	-0.4±-0.9	5
281.15	29.86 (11%)	(≤10%)	1.28±0.23 (≤10%)	3.5±1.4	6
302.12	21.79 (≤10%)	(≤10%)	1.24±0.23 (≤10%)	1.4±1.1	5
263.97	19.72 (≤10%)	(≤10%)	1.14±0.19 (≤10%)	4.8±1.2	4
331.59	24.17 (≤10%)	(≤10%)	1.32±0.22 (≤10%)	2.4±0.9	6
299.11	34.84 (12%)	(≤10%)	1.22±0.22 (≤10%)	3.4±1.4	7

Figure K.17: Primary Dataset for KDE plot for X5486. NB primary data set is comprised of 3 aliquots selected from a total of 7 aliquots (coarse grains) and 6 out of 6 aliquots (fine grains) after selection criteria were met.

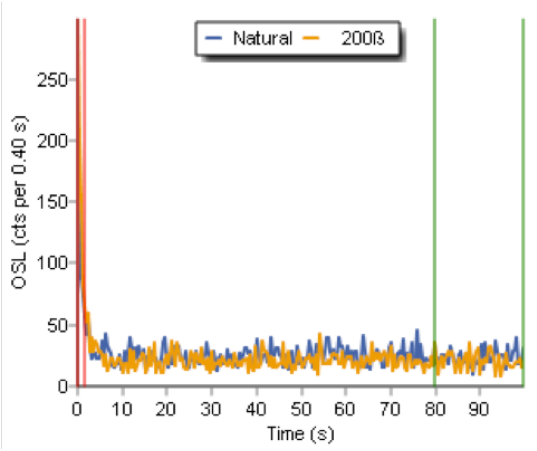

Figure K.18: OSL shine down curve for a representative aliquot of X5486

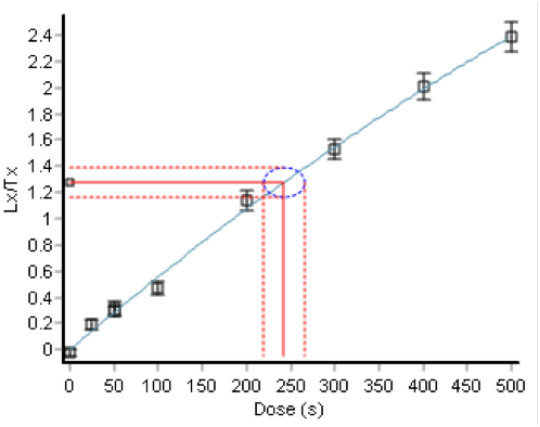

Figure K.19: OSL dose response curve for a representative aliquot of X5486

Figure K.20: Final OSL measurement (based on the CAM) and over dispersion value for X5486. Calibrated machine dose rates (Gy/s): 0.03842184 (CG), 0.03819457 (FG).

Central dose (s)	Central Dose Error (s)	OD (%)	OD error (%)
249,89	20.23	0	N/A
301.32	10.73	0	N/A

No OSL data is available for Sample X5487

- No data for coarse grain material. Of 9 aliquots, all failed to meet rejection criteria.
- No data for fine grain material. Of 6 aliquots, all failed to meet rejection criteria.

Table K.5: OSL data for Sample X5488 – Coarse Grain and Fine Grain

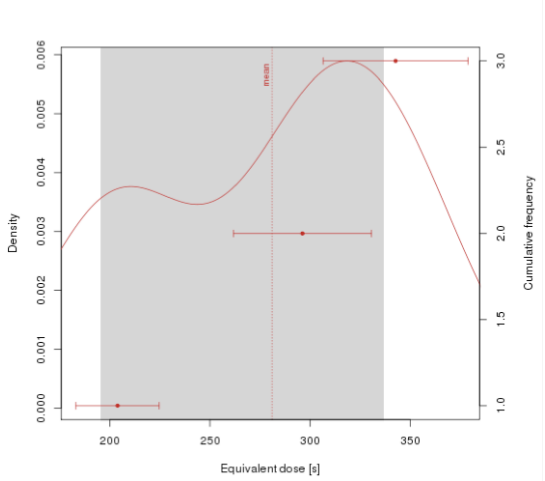

Figure K.21: Kernel Density Estimate Plot for Sample X5488

D_e (s)	D_e error (s)	Test Dose Error (%)	Recycling Ratio	Recup. (%)	IRSL signal (%)
295.18	68.78 (23%)	17	0.85±0.88 (≤10%)	11.5±5.6	15
342.69	72.45 (21%)	17	2.03±1.82 (≤10%)	6.7±6.9	11
203.89	41.74 (21%)	13	2.14±1.67 (≤10%)	10.4±8.8	14

Figure K.22: Primary Dataset for KDE plot for X5488. NB primary data set is comprised of 3 aliquots selected from a total of 6 aliquots after selection criteria were met.

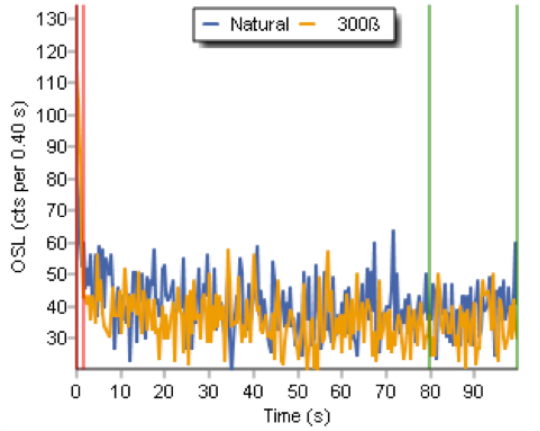

Figure K.23: OSL shine down curve for a representative aliquot of X5488

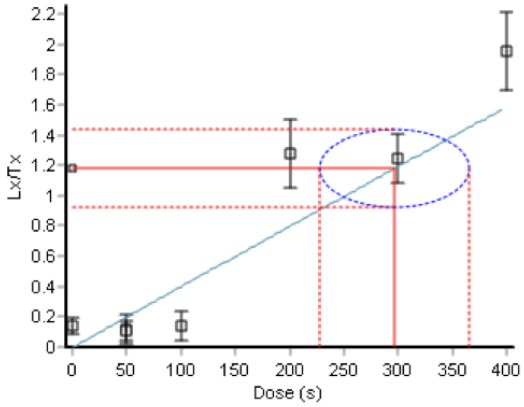

Figure K.24: OSL dose response curve for a representative aliquot of X5488

Figure K.25: Final OSL measurement (based on the CAM) and over dispersion value for X5488. Calibrated machine dose rates (Gy/s): 0.03819457 (FG).

Central dose (s)	Central Dose Error (s)	OD (%)	OD error (%)
271.89	36.4	8.59	7.46

Table K.6: OSL data for Sample X5489 – Coarse Grain and Fine Grain

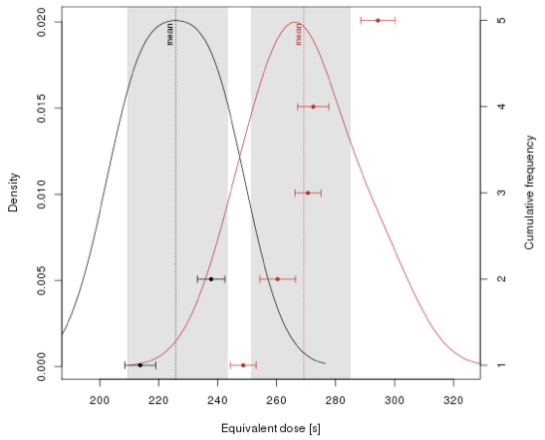

Figure K.26: Kernel Density Estimate Plot for Sample X5489

D_e (s)	D_e error (s)	Test Dose Error (%)	Recycling Ratio	Recup. (%)	IRSL signal (%)
237.78	9.28 (≤10%)	≤10	0.97±0.07 (≤10%)	0.2±0.3	6
213.77	10.41 (≤10%)	≤10	1.01±0.09 (≤10%)	-0.3±-0.4	≤1
272.39	10.40 (≤10%)	≤10	1.11±0.09 (≤10%)	0.8±0.3	≤1
270.58	8.83 (≤10%)	≤10	1.01±0.06 (≤10%)	0.9±0.2	≤1
248.66	8.66 (≤10%)	≤10	1.05±0.07 (≤10%)	0.6±0.3	≤1
294.30	11.57 (<10%)	≤10	1.03±0.07 (≤10%)	0.6±0.3	≤1
260.30	12.08 (≤10%)	≤10	1.25±0.10 (16%)	1.0±0.5	2

Figure K.27: Primary Dataset for KDE plot for X5489.
NB primary data set is comprised of 2 aliquots selected from a total of 14 aliquots (coarse grains) and 5 out of 6 aliquots (fine grains) after selection criteria were met.

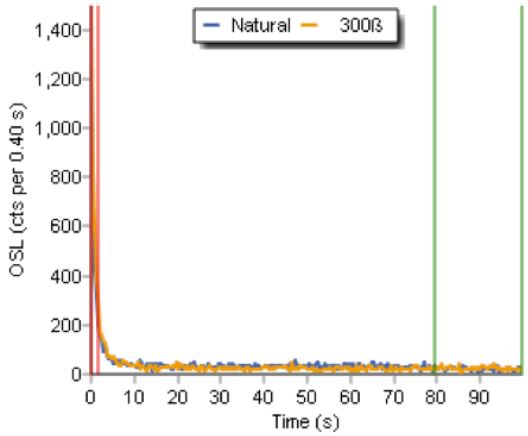

Figure K.28: OSL shine down curve for a representative aliquot of X5489

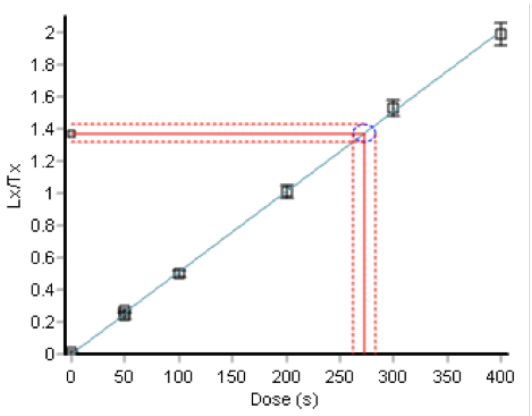

Figure K.29: OSL dose response curve for a representative aliquot of X5489

Figure K.30: Final OSL measurement (based on the CAM) and over dispersion value for X5489. Calibrated machine dose rates (Gy/s): 0.03842184 (CG), 0.03819457 (FG).

Central dose (s)	Central Dose Error (s)	OD (%)	OD error (%)
227.3	8.35	2.86	0.79
268.7	6.74	4.12	0.49

Table K.7: OSL data for Sample X5490 – Fine Grain (No coarse grain data available; of 12 aliquots, all failed to meet rejection criteria)

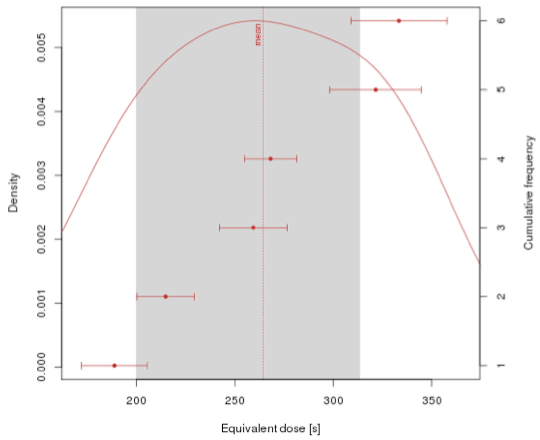

Figure K.31: Kernel Density Estimate Plot for Sample X5490

D_e (s)	D_e error (s)	Test Dose Error (%)	Recycling Ratio	Recup. (%)	IRSL signal (%)
268.17	26.59 (≤10%)	≤10	0.89±0.28 (≤10%)	7.2±2.9	14
259.41	34.41 (14%)	≤10	1.33±0.36 (≤10%)	2.5±2.5	13
188.78	33.50 (18%)	≤10	1.80±0.68 (13%)	-1.0±-4.4	14
333.42	48.94 (15%)	≤10	0.76±0.29 (≤10%)	0.0±2.6	12
214.86	29.31 (14%)	≤10	0.87±0.26 (≤10%)	-0.1±-3.3	5
321.58	46.60 (15%)	11	0.79±0.28 (≤10%)	-3.3±-5.2	6

Figure K.32: Primary Dataset for KDE plot for X5490. NB primary data set is comprised of 6 out of 6 aliquots (fine grains) after selection criteria were met.

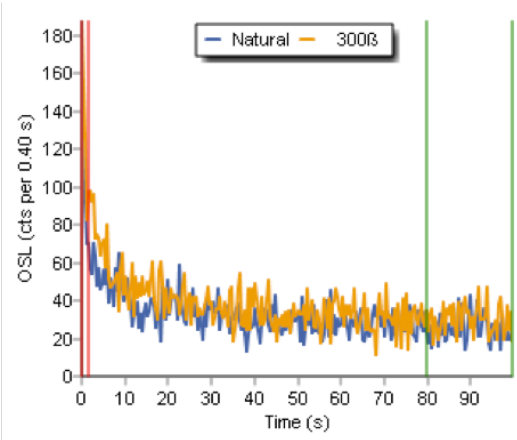

Figure K.33: OSL shine down curve for a representative aliquot of X5490

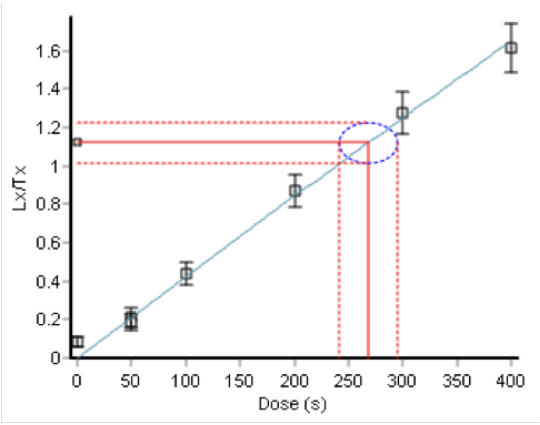

Figure K.34: OSL dose response curve for a representative aliquot of X5490

Figure K.35: Final OSL measurement (based on the CAM) and over dispersion value for X5490. Calibrated machine dose rates (Gy/s): 0.03819457 (FG).

Central dose (s)	Central Dose Error (s)	OD (%)	OD error (%)
262.23	18.39	10.41	2.58

Appendix L

Ceramic catalogue for the Abydos, Ballas, and Naqada material

It should be noted that the ceramics within the following catalogue have two identification codes: a museum code (accession number) and a laboratory code. All discussions within the text of this thesis, when referring to a specific ceramic piece, use the laboratory code as the main identifying number.

The 5 digit warecode designation follows that developed by Köhler (Köhler 1998; Köhler 2005).

Table L.1: Catalogue entry for X5474

Collection	Ashmolean Museum
Museum Code	AN 1895.525
Lab. Code	X5474
Provenance	Naqada, Grave T5
Provenance History	
Excavated by Flinders Petrie, 1895	
Vessel/Object Description	
Height	26.5 cm
Diameter	11.8 cm
Fracture is unknown; medium density, medium marl clay. Interior is badly eroded and filled with pot contents. Exterior is wet smoothes with lots of visible working marks, finger prints and scraping marks. Wavy handle decoration.	
Warecode	22201
Munsell	Clay Body: 7.5YR 6/4 Firing Skin: 2.5YR 6/3-4
Fabric Description	
Sand $\leq$ 0.5 mm (2)	
Fine sand $\leq$ 0.2 mm (2)	
Limestone $\leq$ 1 mm (1)	
Fine limestone $\leq$ 0.2 mm (2)	
Mica $\leq$ 0.1 mm (1)	
Chaff $\leq$ 4mm (1)	
Fine chaff $\leq$ 1 mm (1-2)	
Small black inclusions $\leq$ 0.2 mm (2-3)	
Publication Records	
Petrie and Quibell 1896: 19–20; Pl. LXXXII.	
Additional Notes	
Form W14–19 in Petrie 1921. Sequence Date 50.	

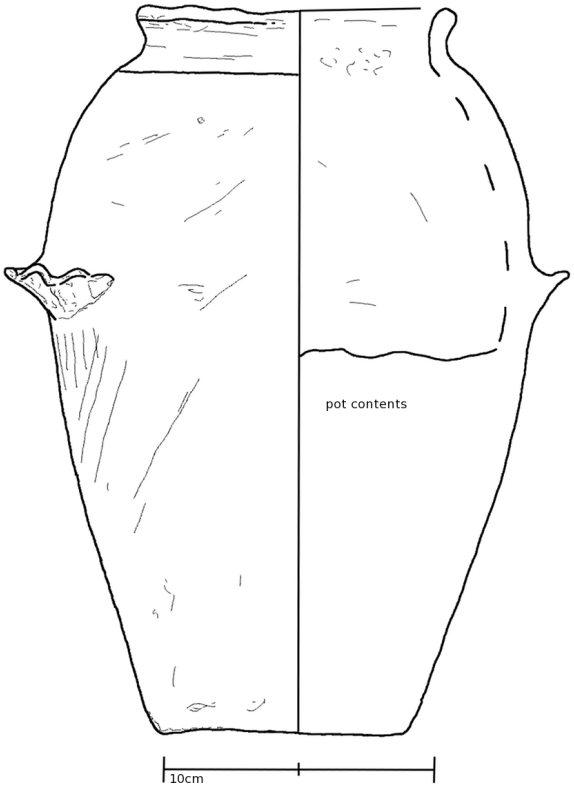

Table L.2: Catalogue entry for X5475

Collection	Ashmolean Museum
Museum Code	AN 1895.533
Lab. Code	X5475
Provenance	Ballas, Grave 588
Provenance History	
Excavated by Flinders Petrie, 1895	
Vessel/Object Description	
Height	28.2 cm
Diameter	11.2 cm
Fracture is unknown; medium density, medium marl clay. Interior surface is very eroded and filled with pot contents. Exterior surface is wet smoothes with visible working marks. Wavy handle decoration is applied. Rim eroded, discolouration from moisture visible.	
Warecode	22201
Munsell	7.5YR 5/4-6
Fabric Description	
Sand $\leq$ 0.5 mm (2-3)	
Fine sand $\leq$ 0.2 mm (2-3)	
Limestone $\leq$ 1 mm (1)	
Fine limestone $\leq$ 0.2 mm (2)	
Mica $\leq$ 0.1 mm (1)	
Chaff $\leq$ 5mm (1)	
Fine chaff $\leq$ 1 mm (2)	
Small black inclusions $\leq$ 0.2 mm (1-2)	
Fibres $\leq$ 0.3 mm (1)	
Grit $\leq$ 0.1 (2)	
Publication Records	
Additional Notes	

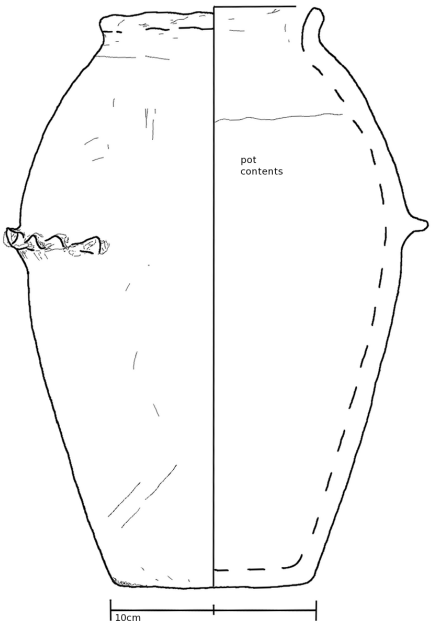

Table L.3: Catalogue entry for X5476

Collection	Ashmolean Museum
Museum Code	E.3158
Lab. Code	X5476
Provenance	Abydos, Tomb O (Djer)
Provenance History	
Excavated by Flinders Petrie 1899–1902.	
Vessel/Object Description	
Height	26.3 cm
Diameter	13.8 cm
Fracture is grey; no clean breaks so difficult to determine fabric characteristics, but likely imported clay (medium density). Exterior is smoothed, perhaps polished, but difficult to determine as covered with tar-like material and charred material. Slight evidence of vertical working marks on body. Where visible, surface seems well smoothed. Interior surface is covered in charred pot contents.	
Warecode	(2-3)3301
Munsell	Clay Body: 10YR 5/3
Fabric Description	
Sand $\leq$ 0.3 mm (2)	
Grit $\leq$ 0.1 mm (2)	
Small angular brown inclusions $\leq$ 0.6 mm (2)	
Large angular brown inclusions $\leq$ 1 mm (2)	
Fine limestone $\leq$ 0.1 mm (2)	
Mica $\leq$ 0.1 mm (2)	
Fine Chaff $\leq$ 0.2 mm (2)	
Charcoal (?) $\leq$ 1 mm (1)	
Publication Records	
Pet	
Additional Notes	

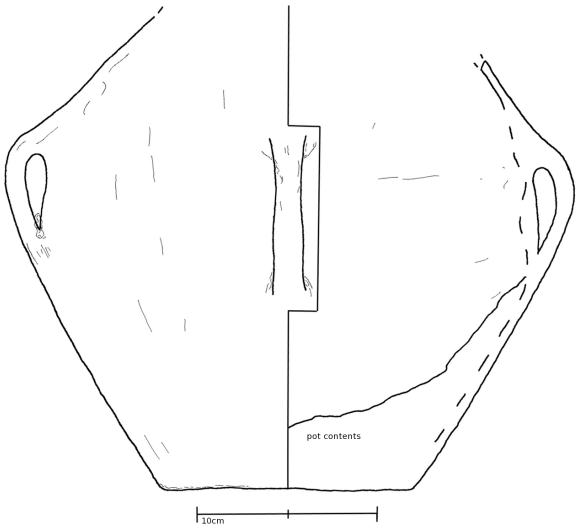

Table L.4: Catalogue entry for X5477

Collection	Ashmolean Museum
Museum Code	E.4034
Lab. Code	X5477
Provenance	Abydos, Tomb O (Djer)
Provenance History	
Excavated by Flinders Petrie 1899–1902.	
Vessel/Object Description	
Height	24.5 cm
Diameter	9.5 cm
Fracture is red in colour, but as no clean breaks; difficult to determine fabric characteristics, but likely imported clay (medium density). Exterior is coated in charred remains and sediment so can not get a clear view of surface. Possibly evidence of polishing, but unclear. Pot mark present near top of vessel. Likely smoothed exterior, with some vertical scrape marks. Interior is almost entirely covered in pot contents.	
Warecode	23201
Munsell	Clay Body: 5YR 4/4 “polished” area: 7.5YR 3/2-3
Fabric Description	
Sand $\leq$ 0.6 mm (2)	
Fine sand $\leq$ 0.2 mm (2)	
Grit $\leq$ 0.1 mm (2)	
Black/brown inclusions $\leq$ 0.2 mm (2)	
Limestone $\leq$ 0.5 mm (1)	
Fine limestone $\leq$ 0.1 mm (2)	
Mica $\leq$ 0.1 mm (2)	
Chaff $\leq$ 1mm (1)	
Fine Chaff $\leq$ 0.2 mm (2)	
Publication Records	
Additional Notes	

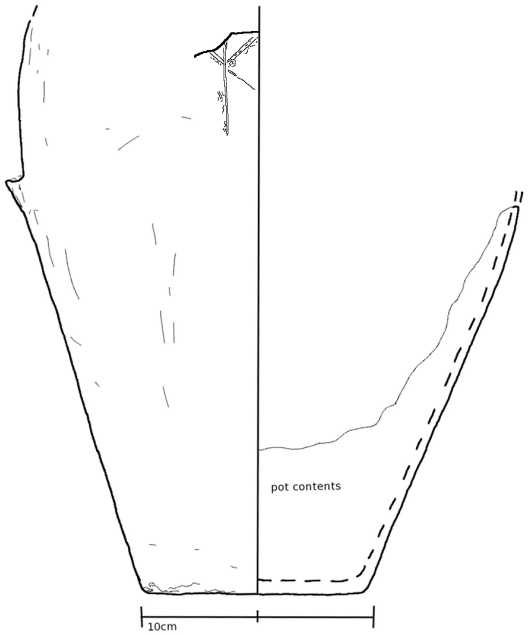

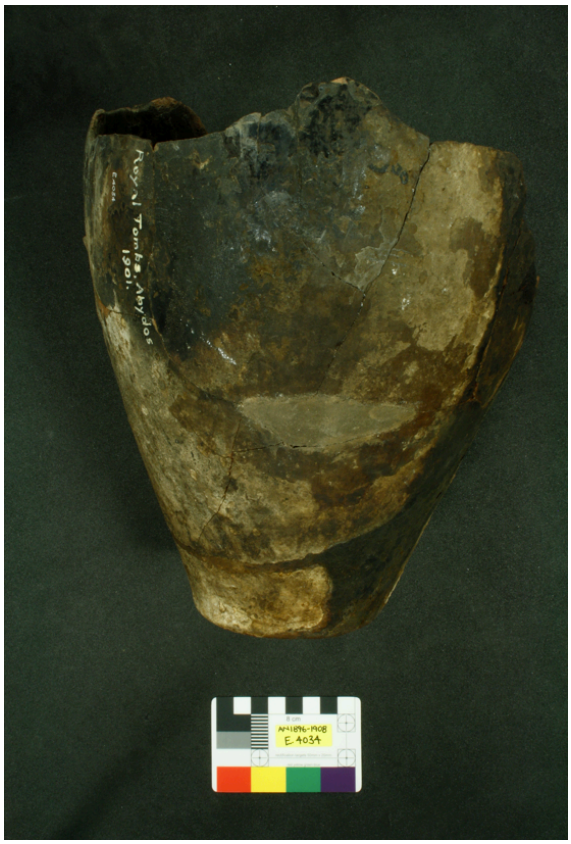

Table L.5: Catalogue entry for X5478

Collection	Ashmolean Museum
Museum Code	E.4065
Lab. Code	X5478
Provenance	Abydos, Tomb O (Djer)
Provenance History	
Excavated by Flinders Petrie 1899–1902.	
Vessel/Object Description	
Height	23.7 cm
Diameter	n/a
Fracture is brown; high density, medium-fine marl clay. N.b. very difficult to determine clay type as surface very burnt and no fresh break. Interior surface is eroded but fairly smooth. Pot contents in base. Exterior surface is wet smoothed with some vertical scraping and working marks.	
Warecode	22201
Munsell	5YR 5-4/3
Fabric Description	
Sand $\leq$ 0.5 mm (1-2)	
Fine sand $\leq$ 0.1 mm (1-2)	
Limestone $\leq$ 1 mm (1)	
Fine limestone $\leq$ 0.2 mm (1)	
Mica $\leq$ 0.1 mm (2)	
Fine chaff $\leq$ 0.5 mm (1)	
Organic $\leq$ 0.8 mm (1-2)	
Fibres $\leq$ 1.5 mm (1-2)	
Grit $\leq$ 0.1 (2-3)	
Publication Records	
Additional Notes	

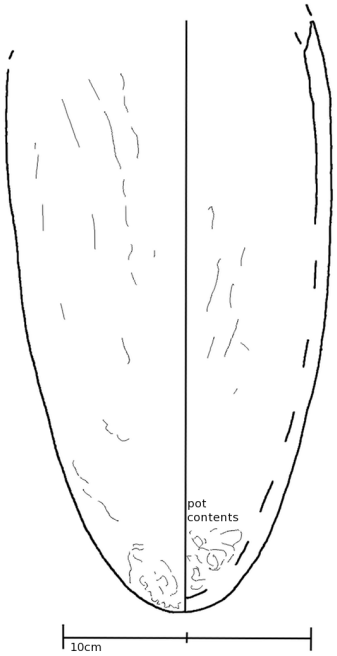

Table L.6: Catalogue entry for X5479

Collection	Ashmolean Museum
Museum Code	E.4066
Lab. Code	X5479
Provenance	Abydos, Tomb O (Djer)
Provenance History	
Excavated by Flinders Petrie 1899–1902.	
Vessel/Object Description	
Height	23.5 cm
Diameter	n/a
Fracture is brown; high density, medium-fine marl clay. N.b. very difficult to determine clay type as surface very burnt and no fresh break. Interior surface is eroded but fairly smooth. Pot contents in base. Exterior surface is wet smoothed with some vertical scraping and working marks.	
Warecode	(22201
Munsell	5YR 5-4/3
Fabric Description	
Sand $\leq$ 0.5 mm (1-2)	
Fine sand $\leq$ 0.1 mm (1-2)	
Limestone $\leq$ 1 mm (1)	
Fine limestone $\leq$ 0.2 mm (1)	
Mica $\leq$ 0.1 mm (2)	
Fine chaff $\leq$ 0.5 mm (1)	
Organic $\leq$ 0.8 mm (1-2)	
Fibres $\leq$ 1.5 mm (1-2)	
Grit $\leq$ 0.1 (2-3)	
Publication Records	
Additional Notes	

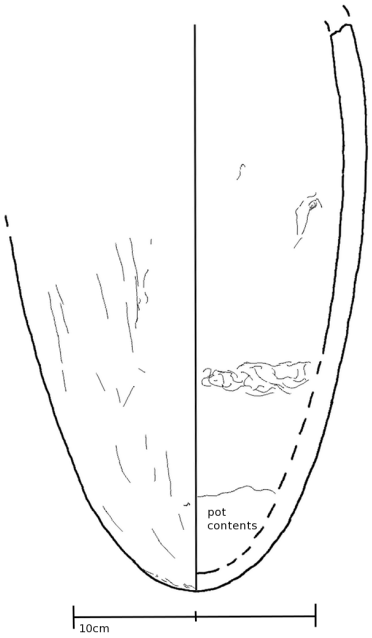

Appendix M

OSL aliquot data for the Abydos, Naqada, and Ballas ceramic assemblage (both ceramic data and residue data)

The following appendix presents the raw OSL data used to discuss the results presented in Chapter 9.

It should be noted that the discussion of the rejection/acceptance criteria given in Appendix D is also applied to the following OSL raw data.

NB All aliquot data units presented in this appendix are in seconds (s). For final age calculations presented in Chapter 9, these units have been converted into the standard international unit for absorbed radiation, Grays (Gy). The conversion of seconds to grays is achieved by multiplying the central dose (s) by the calibrated machine (Gy/s)—this gives the final D_e measurement in Gy.

NB In this appendix coarse grain (CG) data is denoted in black ink, whereas fine grain (FG) data is denoted by red ink.

No OSL data is available for Sample X5474

- No data for coarse grain material. Of 5 aliquots, all failed to meet rejection criteria.
- No data for fine grain material. Of 6 aliquots, all failed to meet rejection criteria.

Table M.1: OSL data for Sample X5475 – Coarse Grain (No fine grain data available; of 6 aliquots, all failed to meet rejection criteria)

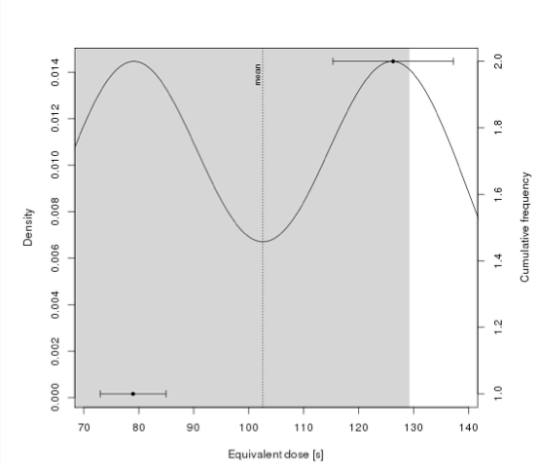

Figure M.1: Kernel Density Estimate Plot for Sample X5475

D_e (s)	D_e error (s)	Test Dose Error (%)	Recycling Ratio	Recup. (%)	IRSL signal (%)
78.95	12.01 (16%)	≤10	0.90±0.16 (≤10%)	11.0±5.2	≤1
126.26	21.85 (18%)	≤10	1.12±0.18 (≤10%)	-0.7±2.3	≤1

Figure M.2: Primary Dataset for KDE plot for X5475. NB primary data set is comprised of 2 aliquots selected from a total of 8 aliquots after selection criteria were met.

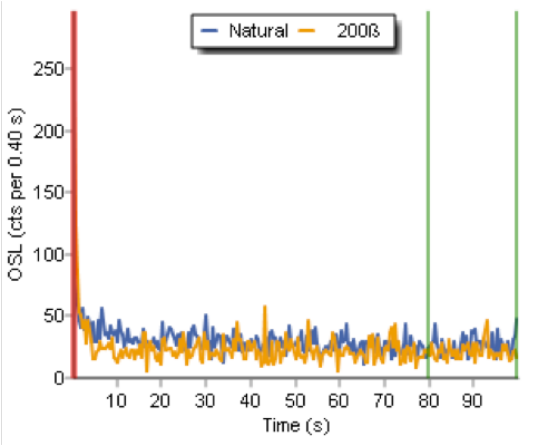

Figure M.3: OSL shine down curve for a representative aliquot of X5475

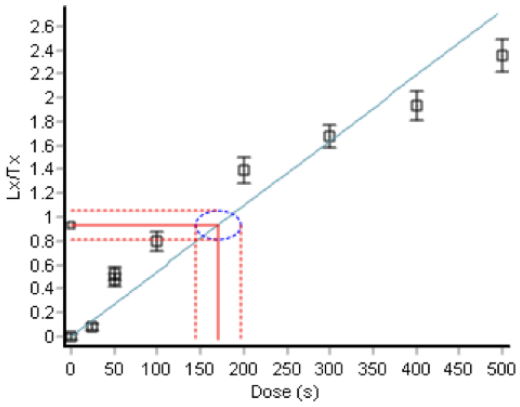

Figure M.4: OSL dose response curve for a representative aliquot of X5475

Figure M.5: Final OSL measurement (based on the CAM) and over dispersion value for X5475. Calibrated machine dose rates (Gy/s): 0.03849789 (CG).

Central dose (s)	Central Dose Error (s)	OD (%)	OD error (%)
98.4	16.27	16.84	6.65

No OSL data is available for Sample X5476

- No data for coarse grain material. Of 5 aliquots, all failed to meet rejection criteria.
- No data for fine grain material. Of 6 aliquots, all failed to meet rejection criteria.

Table M.2: OSL data for Sample X5477 – Fine Grain (No coarse grain data available; of 5 aliquots, all failed to meet rejection criteria)

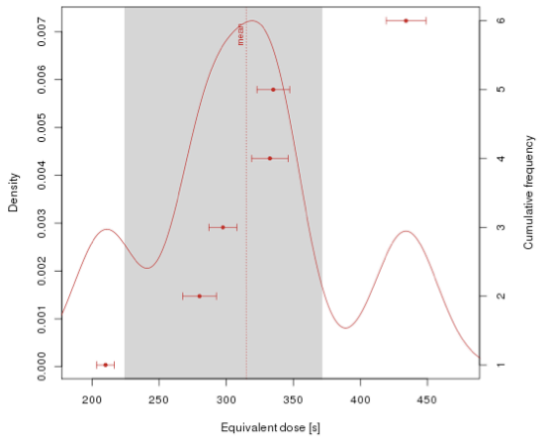

Figure M.6: Kernel Density Estimate Plot for Sample X5477

D_e (s)	D_e error (s)	Test Dose Error (%)	Recycling Ratio	Recup. (%)	IRSL signal (%)
332.55	27.12 (≤10%)	≤10	1.24±0.13 (12%)	1.8±0.8	≤1
280.08	25.02 (≤10%)	≤10	1.18±0.14 (≤10%)	2.0±1.0	≤1
297.56	20.86 (≤10%)	≤10	1.36±0.14 (22%)	0.0±0.8	≤1
335.03	24.39 (≤10%)	≤10	1.10±0.12 (≤10%)	2.6±0.9	≤1
210.08	13.22 (≤10%)	≤10	1.27±0.09 (18%)	2.2±0.6	≤1
434.06	29.79 (≤10%)	≤10	1.08±0.10 (≤10%)	0.9±0.6	≤1

Figure M.7: Primary Dataset for KDE plot for X5477. NB primary data set is comprised of 6 out of 6 aliquots after selection criteria were met.

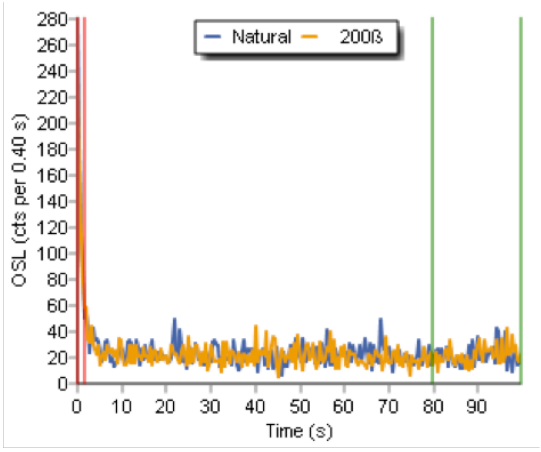

Figure M.8: OSL shine down curve for a representative aliquot of X5477

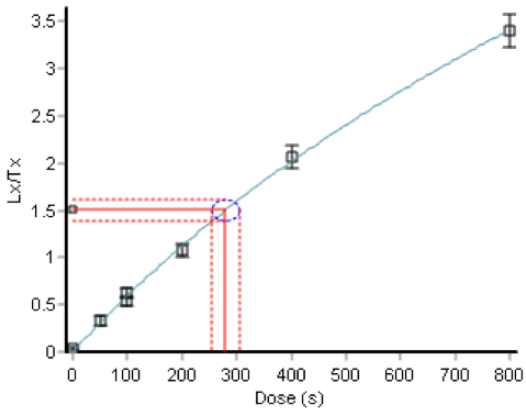

Figure M.9: OSL dose response curve for a representative aliquot of X5477

Figure M.10: Final OSL measurement (based on the CAM) and over dispersion value for X5477. Calibrated machine dose rates (Gy/s): 0.03842184 (FG).

Central dose (s)	Central Dose Error (s)	OD (%)	OD error (%)
307.37	28.06	21.09	3.14

Table M.3: OSL data for Sample X5478 – Coarse Grain (No fine grain data available; of 12 aliquots, all failed to meet rejection criteria)

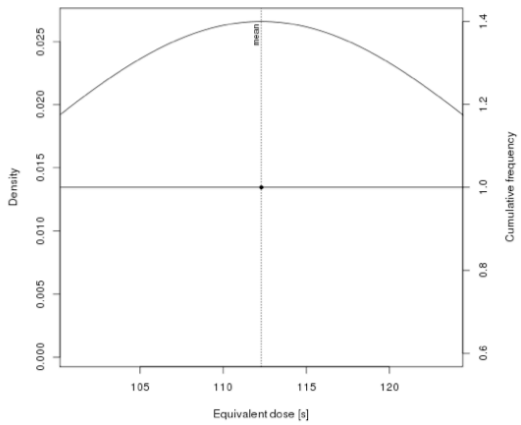

Figure M.11: Kernel Density Estimate Plot for Sample X5478

D_e (s)	D_e error (s)	Test Dose Error (%)	Recycling Ratio	Recup. (%)	IRSL signal (%)
112.29	48.69 (44%)	≤10	0.95±0.51 (≤10%)	-15.4±-22.3	10%

Figure M.12: Primary Dataset for KDE plot for X5478. NB primary data set is comprised of 1 aliquots selected from a total of 16 aliquots after selection criteria were met. . calibration

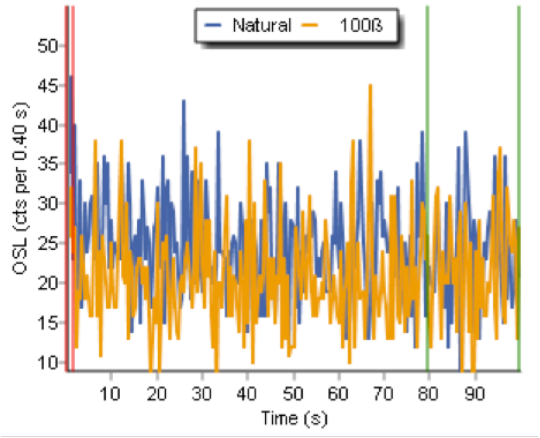

Figure M.13: OSL shine down curve for a representative aliquot of X5478

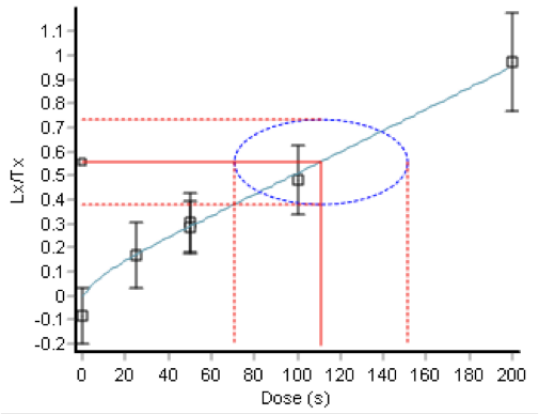

Figure M.14: OSL dose response curve for a representative aliquot of X5478

Figure M.15: Final OSL measurement (based on the CAM) and over dispersion value for X5478. Calibrated machine dose rates (Gy/s): 0.03842184 (FG).

Central dose (s)	Central Dose Error (s)	OD (%)	OD error (%)
112.29	48.69	N/A	N/A

Table M.4: OSL data for Sample X5479 – Fine Grain (No coarse grain data available; of 5 aliquots, all failed to meet rejection criteria)

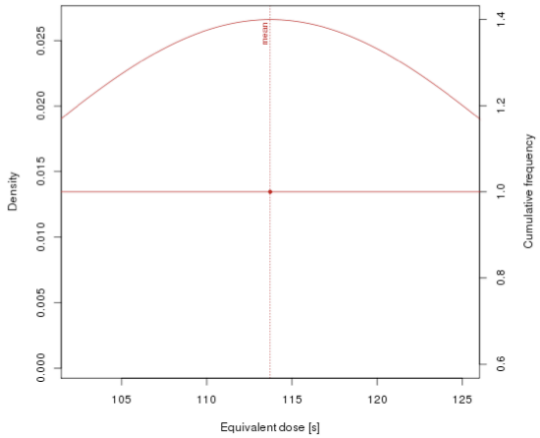

Figure M.16: Kernel Density Estimate Plot for Sample X5479

D_e (s)	D_e error (s)	Test Dose Error (%)	Recycling Ratio	Recup. (%)	IRSL signal (%)
113.73	39.75 (36%)	14	1.38±0.44 (≤10%)	15.8±11.2	3

Figure M.17: Primary Dataset for KDE plot for X5479. NB primary data set is comprised of 1 aliquots selected from a total of 16 aliquots after selection criteria were met.

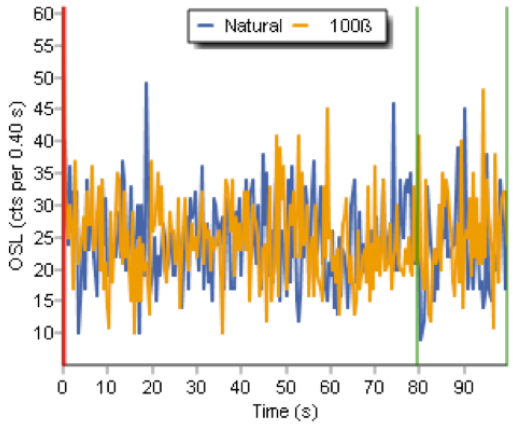

Figure M.18: OSL shine down curve for a representative aliquot of X5479

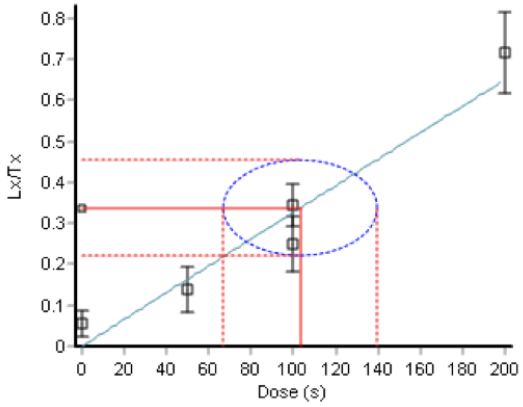

Figure M.19: OSL dose response curve for a representative aliquot of X5479

Figure M.20: Final OSL measurement (based on the CAM) and over dispersion value for X5479. Calibrated machine dose rates (Gy/s): 0.03842184 (CG).

Central dose (s)	Central Dose Error (s)	OD (%)	OD error (%)
113.73	39.75	N/A	N/A

No OSL data is available for Sample X6112

- No data for coarse grain material. Of 2 aliquots, all failed to meet rejection criteria.
- No fine grain material was retrieved from this sample.

No OSL data is available for Sample X6113

- No data for coarse grain material. Of 14 aliquots, all failed to meet rejection criteria.
- No fine grain material was retrieved from this sample.

Table M.5: OSL data for Sample X6114 – Coarse Grain (No fine grain material was retrieved for this sample)

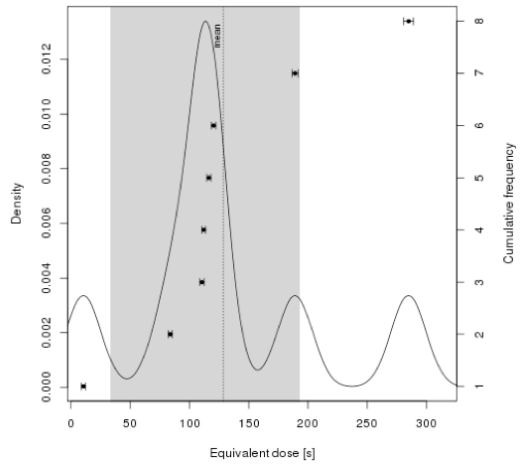

Figure M.21: Kernel Density Estimate Plot for Sample X6114

D_e (s)	D_e error (s)	Test Dose Error (%)	Recycling Ratio	Recup. (%)	IRSL signal (%)
120.39	3.70 (≤10%)	≤10	1.12±0.03 (≤10%)	2.3±0.1	≤1
284.72	8.02 (≤10%)	≤10	1.12±0.03 (≤10%)	1.3±0.0	≤1
189.02	5.10 (≤10%)	≤10	1.04±0.03 (≤10%)	2.2±0.1	≤1
10.58	3.61 (≤10%)	≤10	1.18±0.04 (15%)	1.1±0.1	≤1
110.68	3.96 (≤10%)	≤10	1.10±0..04 (≤10%)	4.6±0.3	≤1
83.93	3.06 (≤10%)	≤10	1.08±0.04 (≤10%)	0.7±0.1	≤1
116.40	3.44 (≤10%)	≤10	1.05±0.04 (≤10%)	1.8±0.1	≤1
112.10	3.19 (≤10%)	≤10	1.12±0.04 (≤10%)	2.1±0.1	≤1

Figure M.22: Primary Dataset for KDE plot for X6114. NB primary data set is comprised of 8 out of 8 aliquots after selection criteria were met.

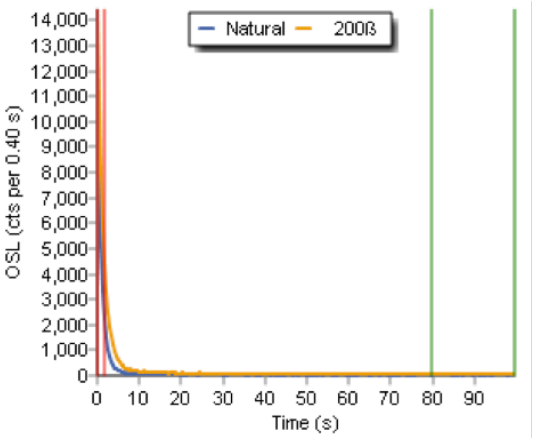

Figure M.23: OSL shine down curve for a representative aliquot of X6114

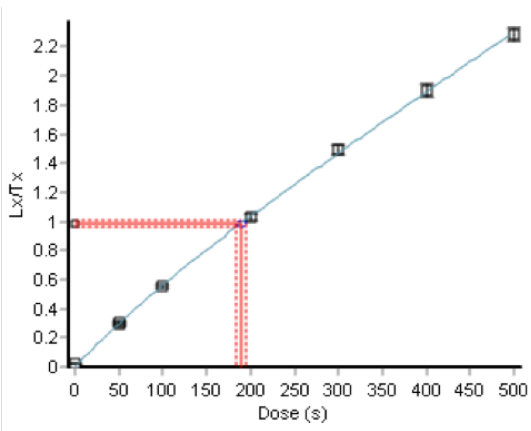

Figure M.24: OSL dose response curve for a representative aliquot of X6114

Figure M.25: Final OSL measurement (based on the CAM) and over dispersion value for X6114. Calibrated machine dose rates (Gy/s): 0.03912468 (CG, aliquots 1–2), 0.03799368 (CG, aliquots 3–8).

Central dose (s)	Central Dose Error (s)	OD (%)	OD error (%)
101.86	29.78	81.88	18.87

Table M.6: OSL data for Sample X6115 – Coarse Grain (No fine grain material was retrieved for this sample)

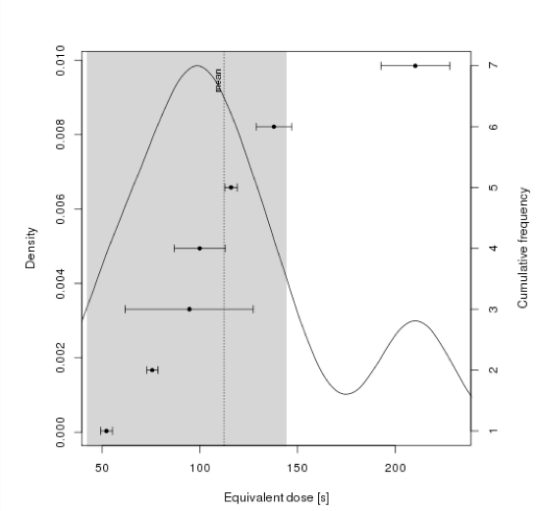

Figure M.26: Kernel Density Estimate Plot for Sample X6115

D_e (s)	D_e error (s)	Test Dose Error (%)	Recycling Ratio	Recup. (%)	IRSL signal (%)
75.67	5.77 (≤10%)	≤10	1.00±0.07 (≤10%)	5.6±1.8	≤1
52.25	6.08 (12%)	≤10	1.26±0.12 (20%)	-8.3±-2.5	≤1
115.99	6.23 (≤10%)	≤10	0.99±0.08 (≤10%)	2.0±0.08	≤1
137.95	18.04 (15%)	≤10	1.33±0.23 (≤10%)	4.6±1.2	≤1
99.93	26.11 (27%)	≤10	1.48±0.50 (≤10%)	14.3±8.6	6
94.62	65.56 (69%)	≤10	0.76±0.34 (≤10%)	-23.3±-28.7	7
210.26	35.33 (17%)	≤10	1.28±0.29 (≤10%)	0.3±2.0	3

Figure M.27: Primary Dataset for KDE plot for X6115. NB primary data set is comprised of 7 out of 8 aliquots after selection criteria were met.

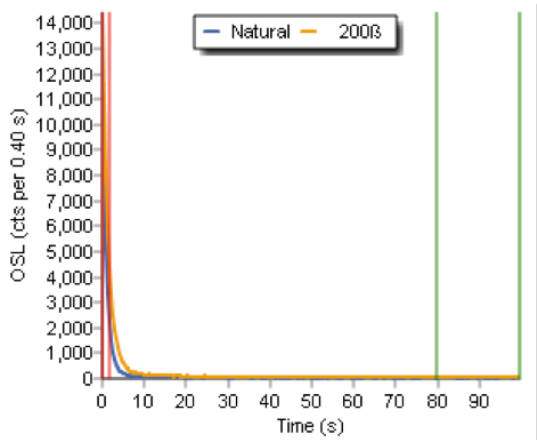

Figure M.28: OSL shine down curve for a representative aliquot of X6115

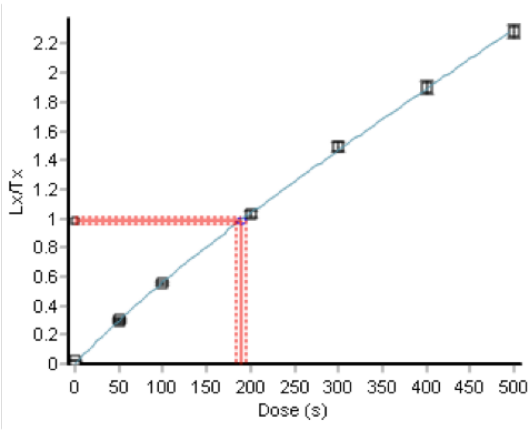

Figure M.29: OSL dose response curve for a representative aliquot of X6115

Figure M.30: Final OSL measurement (based on the CAM) and over dispersion value for X6115. Calibrated machine dose rates (Gy/s): 0.03912468 (CG, aliquots 1–2), 0.03799368 (CG, aliquots 3–7).

Central dose (s)	Central Dose Error (s)	OD (%)	OD error (%)
103.43	17.89	40.97	8.39

Table M.7: OSL data for Sample X6116 – Coarse Grain (No fine grain material was retrieved for this sample)

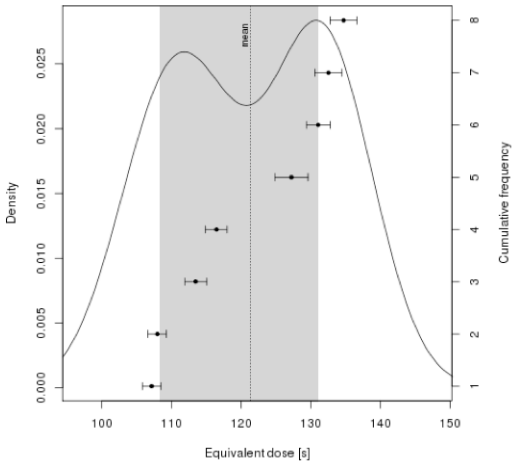

Figure M.31: Kernel Density Estimate Plot for Sample X6116

D_e (s)	D_e error (s)	Test Dose Error (%)	Recycling Ratio	Recup. (%)	IRSL signal (%)
107.18	2.66 (≤10%)	≤10	1.03±0.03 (≤10%)	0.1±0.1	≤1
107.98	2.64 (≤10%)	≤10	1.00±0.03 (≤10%)	0.1±0.1	≤1
113.50	3.18 (≤10%)	≤10	1.00±0.04 (≤10%)	2.0±0.3	≤1
134.72	3.84 (≤10%)	≤10	0.95±0.03 (≤10%)	0.4±0.2	≤1
132.55	3.84 (≤10%)	≤10	0.95±0.03 (≤10%)	0.8±0.2	≤1
131.10	3.40 (≤10%)	≤10	0.95±0.03 (≤10%)	0.6±0.1	≤1
127.24	4.78 (≤10%)	≤10	0.95±0.04 (≤10%)	1.8±0.4	≤1
116.46	3.10 (≤10%)	≤10	0.93±0.03 (≤10%)	0.7±0.2	≤1

Figure M.32: Primary Dataset for KDE plot for X6116. NB primary data set is comprised of 8 out of 8 aliquots after selection criteria were met.

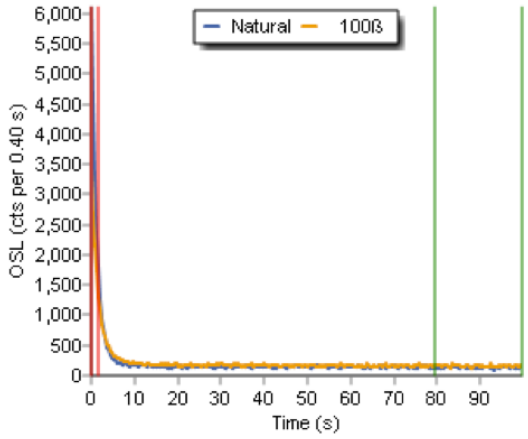

Figure M.33: OSL shine down curve for a representative aliquot of X6116

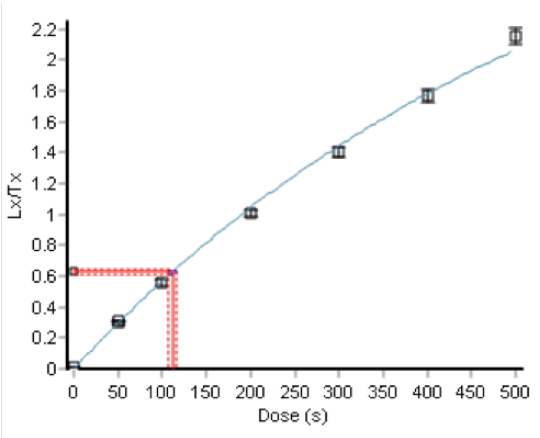

Figure M.34: OSL dose response curve for a representative aliquot of X6116

Figure M.35: Final OSL measurement (based on the CAM) and over dispersion value for X6116. Calibrated machine dose rates (Gy/s): 0.03912468 (CG, aliquots 1–2), 0.03799368 (CG, aliquots 3–8).

Central dose (s)	Central Dose Error (s)	OD (%)	OD error (%)
120.73	3.79	8.42	0.68

Table M.8: OSL data for Sample X6120 – Coarse Grain (No fine grain material was retrieved for this sample)

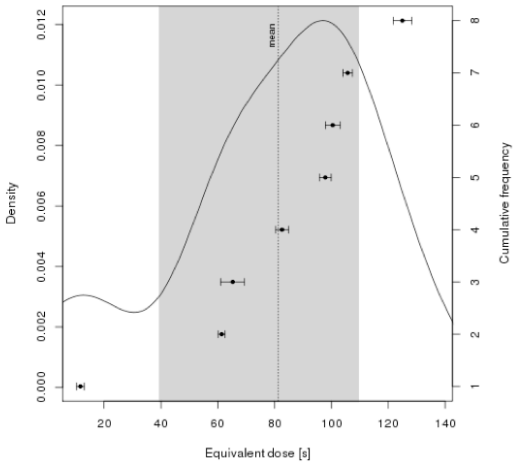

Figure M.36: Kernel Density Estimate Plot for Sample X6120

D_e (s)	D_e error (s)	Test Dose Error (%)	Recycling Ratio	Recup. (%)	IRSL signal (%)
65.20	8.40 (13%)	≤10	1.03±0.11 (≤10%)	13.5±6.5	3
11.65	2.69 (24%)	≤10	0.91±0.06 (11%)	4.7±15.2	9
105.73	3.32 (≤10%)	≤10	0.96±0.04 (≤10%)	2.1±0.6	≤1
61.38	2.48 (≤10%)	≤10	1.02±0.07 (≤10%)	4.4±2.8	≤1
97.81	4.21 (≤10%)	≤10	0.91±0.04 (≤10%)	0.4±0.5	≤1
82.62	4.45 (≤10%)	≤10	1.12±0.09 (≤10%)	2.8±1.9	≤1
100.47	5.19 (≤10%)	≤10	1.18±0.11 (≤10%)	6.8±2.0	3
125.00	6.52 (≤10%)	≤10	1.01±0.09 (≤10%)	3.4±1.4	≤1

Figure M.37: Primary Dataset for KDE plot for X6120. NB primary data set is comprised of 8 out of 8 aliquots after selection criteria were met.

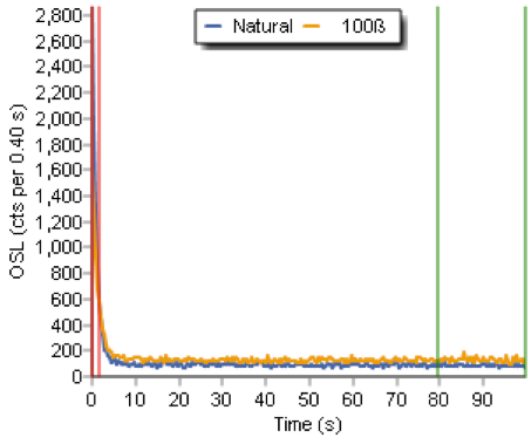

Figure M.38: OSL shine down curve for a representative aliquot of X6120

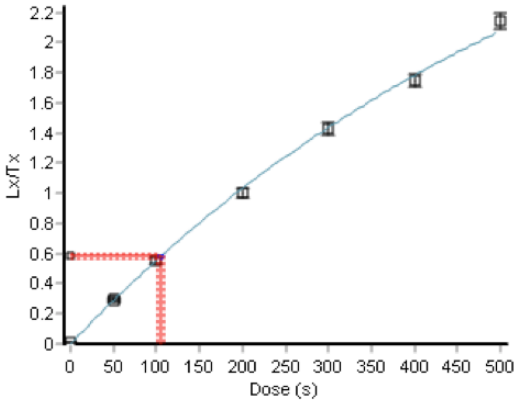

Figure M.39: OSL dose response curve for a representative aliquot of X6120

Figure M.40: Final OSL measurement (based on the CAM) and over dispersion value for X6120. Calibrated machine dose rates (Gy/s): 0.03912468 (CG, aliquots 1–2), 0.03799368 (CG, aliquots 3–8).

Central dose (s)	Central Dose Error (s)	OD (%)	OD error (%)
70.46	16.43	65.22	13.46

Appendix N

Input data for OxCal modelling of the Naqada, Ballas, and Tomb of Djer (Abydos) assemblage

The input file for the final OxCal model, which incorporates ages and model assumptions.

```
 Plot()
{
 Outlier_Model("General",T(5),U
     (0,4),"t");
 Sequence("Abydos")
 {
  Boundary("Start Naqada IIC or IID
      ")
  {
   color="blue";
  };
  Phase("Naqada IIC or IID")
  {
   R_Date("525a", 4577, 35)
   {
    Outlier(0.05);
   };
   R_Date("525b", 4543, 31)
   {
    Outlier(0.05);
   };
   R_Date("533a", 4625, 31)
   {
    Outlier(0.05);
   };
   R_Date("533b", 4582, 29)
   {
    Outlier(0.05);
   };
  };
  Boundary("End Naqada IID")
  {
   color="violet";
  };
  Boundary("Start Reign Djer")
  {
   color="red";
  };
  Phase("Reign of Djer")
  {
   R_Date("4034", 4344, 32)
   {
    Outlier(0.05);
   };
   R_Date("4066", 4397, 29)
   {
    Outlier(0.05);
   };
   Date("4034 (5477)pot", N(AD(2015)
       -5774,569))
   {
    Outlier(0.05);
   };
```

```
 R_Date("4065", 4307, 33)
 {
  Outlier(0.05);
 };
};
Boundary("End Reign Djer")
{
 color="orange";
};
Boundary("FireStart")
{
 color="yellow";
};
Phase("Tomb Fire")
{
 Date("6115(4034)res", N(AD(2015)
     -3625,668))
 {
  Outlier(0.05);
 };
 Date("6120(3158)sed", N(AD(2015)
     -2592,634))
 {
  Outlier(0.05);
 };
 Date("6116(4066)pot", N(AD(2015)
     -3606,245))
 {
  Outlier(0.05);
 };
 Date("6114(3158)res", N(AD(2015)
     -2914,868))
 {
  Outlier(0.05);
 };
 Date("5478", N(AD(2015)-2120,923)
     )
 {
  Outlier(0.05);
 };
 Date("5479", N(AD(2015)-1797,633)
     )
 {
  Outlier(0.05);
 };
};
Boundary("FireEnd")
{
 color="green";
};
Fire = (FireStart + FireEnd)/2;
};
```